Universidad Nacional Autónoma de México

Posgrado en Ciencias de la Tierra

Centro de Geociencias

Campus Juriquilla

Origen del cinturón de oro orogénico Caborca, Sonora, México

T E S I S

Que para optar por el grado de
Doctor en Ciencias de la Tierra

(Geología, depósitos minerales y sistemas hidrotermales)

Presenta

Aldo Izaguirre Pompa

Jurado examinador

1) Dr. Roberto Stanley Molina Garza (Centro de Geociencias, UNAM, presidente)
2) Dr. Carles Canet Miquel (Instituto de Geofísica, UNAM, vocal)
3) Dr. Alexander Iriondo Perrée (Centro de Geociencias, UNAM, secretario)
4) Dr. Gilles Pierre René Levresse (Centro de Geociencias, UNAM, suplente)
5) Dr. Lucas Hilario Ochoa Landín (Universidad de Sonora, UNAM, suplente)

Comité Tutoral

Dr. Alexander Iriondo Perrée (Director de tesis)
Dr. Antoni Camprubí Cano
Dr. Roberto Stanley Molina Garza

Juriquilla, Querétaro, México 22 de junio de 2017

Universidad Nacional Autónoma de México
UNAM
Biblioteca Central
Dirección General de Bibliotecas de la UNAM

UNAM – Dirección General de Bibliotecas
Tesis Digitales
Restricciones de uso

DERECHOS RESERVADOS ©
PROHIBIDA SU REPRODUCCIÓN TOTAL O PARCIAL

Todo el material contenido en esta tesis esta protegido por la Ley Federal del Derecho de Autor (LFDA) de los Estados Unidos Mexicanos (México).

El uso de imágenes, fragmentos de videos, y demás material que sea objeto de protección de los derechos de autor, será exclusivamente para fines educativos e informativos y deberá citar la fuente donde la obtuvo mencionando el autor o autores. Cualquier uso distinto como el lucro, reproducción, edición o modificación, será perseguido y sancionado por el respectivo titular de los Derechos de Autor.

Índice

Agradecimientos [*4*]

Declaratoria de ética [*8*]

Prólogo [*9*]

Resumen [*10*]

Abstract [*12*]

Capítulos

1. Introducción [*14*]

    1.1. Encuadre geológico del COGB [*18*]

    1.2. Características mineralógicas del COGB [*22*]

    1.3. Control estructural de la mineralización del COGB [*25*]

    1.4. Resumen tectónico durante del tiempo de mineralización del COGB [*32*]

2. Motivación del proyecto doctoral [*36*]

    2.1. Objetivos y métodos del estudio [*37*]

    2.2. Hipótesis del estudio [*37*]

    2.3. Técnicas analíticas [*37*]

3. Estudio geoquímico de balance masas del COGB [*39*]

4. Geocronología $^{40}Ar/^{39}Ar$ de las vetas auríferas del COGB [*76*]

5. Introducción a los depósitos de oro orogénico de México [*131*]

6. Encuadre tectónico de la mineralización aurífera del COGB [*144*]

7. Conclusiones [*221*]

8. Apéndices [*225*]

Apéndice A. Poster de estudios de isotopía estable δD, $\delta^{18}O$ y $\delta^{34}S$ de vetas auríferas del COGB [*225*]

Apéndice B. Técnicas empleadas en los estudios analíticos del COGB [*227*]

B.1. Preparación de muestras y análisis geoquímico en rocas encajonantes y vetas de cuarzo [*227*]

B.2. Método de balance de masas [*228*]

B.3. Método de correlación geoquímica bivariable [*230*]

B.4. Técnica de SEM-EDS [*230*]

B.5. Técnicas analíticas utilizadas para estudios de isótopos estables de azufre en sulfuros y oxígeno–hidrógeno en silicatos [*231*]

B.6. Métodos analíticos utilizados para estudios de geocronología por el método $^{40}Ar/^{39}Ar$ en mica blanca hidrotermal [*233*]

Referencias [*236*]

Agradecimientos

Primeramente, agradezco a **Alexander Iriondo** por ser el director de este trabajo doctoral, brindándome su asesoramiento, atención y apoyo durante las diferentes etapas de su elaboración. Especialmente, le agradezco por darme buenas enseñanzas y costumbres, dentro de lo académico y lo personal. También, le agradezco que me haya brindado su magnífica amistad.

Quiero agradecer al **CONACyT** por la ayuda económica brindada a través de una beca para realizar mis estudios de doctorado; también al fondo de becas mixtas por otorgar una extensión, de la misma, durante una estancia realizada en el U.S. Geological Survey en Denver, Colorado, Estados Unidos. Gracias a los proyectos **PAPIIT-UNAM (IN-116709)** y **CONACYT (CB-82518 y CB-129370)** por aportar parte del financiamiento de las campañas de campo y de los estudios analíticos que permitieron realizar este trabajo.

Agradezco enormemente a **Daniel Miggins** por haberme asistido y apoyado con sus consejos durante la estancia en Denver, Colorado. Igualmente, le agradezco por su grandiosa amistad. De igual forma, agradezco a **Erin Marsh** y **Richard Goldfarb** por apoyarme parcialmente en la financiación y brindarme asesoría en parte de los estudios analíticos realizados en la estancia en Denver. También, gracias a **Leonid Neymark, Craig Johnson, Loretta Kwak, James Paces, Ryan Taylor, William Christiansen, Cayce Gulbransen** y **Heather Lowers** por sus enseñanzas técnicas y científicas durante la elaboración de los estudios analíticos en esta estancia.

Se agradece a **Thierry Calmus** y **Pablo Peñaflor** por facilitar el uso de las instalaciones de laboratorio de la Estación Regional del Noroeste de la UNAM (Hermosillo). Agradezco a **Francisco Paz Moreno** (UNISON) y **Shannon Mahon** (U.S.

Geological Survey) por el préstamo de equipo de laboratorio y por su ayuda en el transporte del mismo.

Se agradece a **Michael Kunk** y **Ryan McAleer** (U.S. Geological Survey) por todo el apoyo brindado durante una estancia en los Laboratorios de Termocronología de Argón del U.S. Geological Survey en Reston, Virgina, Estados Unidos. También por otorgarme manutención y alimentación sin ningún interés más que el de apoyarme.

Agradezco al Servicio Geológico Mexicano (SGM), en especial, a **Enrique Espinosa Arámburu**, **Antonio Caballero Martínez, Javier Hernández Rojas, Francisco Cendejas Cruz, Basilio Cervantes López** y **Jaime Castro Escárrega**, por el apoyo técnico y logístico brindado durante la campaña de campo y en el manejo de muestras de roca y vetas de cuarzo.

Me encuentro agradecido con las compañías mineras: Fresnillo plc **(Luis Novelo)**; Minera Penmont S. de R.L. de C.V. **(Enrique García Reimbert)**; Granmin S.A. de C.V. (**Miguel Marín Payán** y **Ariel Navarro Herrera**) por permitirme muestrear en sus distintos proyectos mineros y por la logística prestada en algunos casos. Además, agradezco a los gambusinos del poblado la Ciénega, Sonora, México por brindar información de los accesos del área estudiada y la disponibilidad de algunos de ellos para acompañarme durante el muestreo de rocas y vetas mineralizadas con oro.

Agradezco a todos los miembros de la **Familia Vázquez** que residen en Sonoyta, Sonora, y en Ajo, Arizona, por su ayuda y amistad durante el muestreo de las vetas auríferas colectadas en ambas regiones de la frontera (México-Estados Unidos).

Se agradece a las autoridades de la **CONANP** y al personal de la **Reserva de la Biosfera El Pinacate y Gran Desierto de Altar** por permitir la recolección de muestras

para este estudio científico. Su autorización se realizó a través de un permiso especial otorgado a **Alexander Iriondo** y a su equipo de trabajo "**Los Amigos de Precámbrico"**. Se agradece a las autoridades de **Cabeza Prieta National Wildlife Refuge** por permitir hacer muestreo en zonas del área protegida que administran en el suroeste de Arizona.

Gracias a mi comité tutoral **Alexander Iriondo**, **Antoni Camprubí** y **Roberto Molina Garza** por todo el apoyo brindado a lo largo del desarrollo de mi proyecto doctoral. Agradezco los comentarios realizados durante las lecturas de los distintos apartados que componen esta tesis. Estoy agradecido con el trabajo realizado por los miembros del comité evaluador de esta tesis (**Roberto Molina Garza, Carles Canet, Alexander Iriondo, Gilles Levresse** y **Lucas Ochoa Landín)**.

Agradezco a todos los coautores participantes de las publicaciones científicas que componen esta tesis por aportar su conocimiento y trabajo intelectual mismo que ha permitido el desarrollado de la temática de este estudio (**Alexander Iriondo, Antoni Camprubí, Michael Kunk, Ryan McAleer, William Atkinson Jr., Luis Martínez Torres, Antonio Caballero Martínez, Enrique Espinoza Arámburu, Francisco Moreira Rivera**).

Gracias al experto en laminación de rocas **Juan Vásquez Ramírez (Juanito)** (CGEO) por la asistencia y atención en el corte de rocas para la preparación de láminas delgadas. Agradezco al colega **Luis Martínez Torres (Koldo)** (Universidad del País Vasco) por apoyarme con la preparación de secciones delgadas de rocas.

Agradezco a **Marta Pereda Miranda** por su disponibilidad y por la ayuda brindada durante su tiempo como asistente en el posgrado del Centro de Geociencias.

Mil gracias también a todos mis compañeros y colegas de trabajo en especial a **Harim Arvizu “el Guapo de Santa Rosa”** y a todos los estudiantes del CGEO que se involucraron en este trabajo.

Declaratoria de ética

"Declaro conocer el Código de Ética de la Universidad Nacional Autónoma de México, plasmado en la Legislación Universitaria. Con base en las definiciones de integridad y honestidad ahí especificadas, aseguro mediante mi firma al calce que el presente trabajo es original y enteramente de mi autoría. Todas las citas de, o referencias a, la obra de otros autores aparece debida y adecuadamente señaladas, así como acreditadas mediante los recursos editoriales convencionales."

M.C. Aldo Izaguirre Pompa

Alumno

Dr. Alexander Iriondo

Tutor y director de tesis

Prólogo

Esta tesis ha sido enfocada en encontrar el origen del cinturón de oro orogénico Caborca (COGB), provincia que se caracteriza por contener mineralización de tipo oro orogénico en vetas de cuarzo a lo largo del noroeste de Sonora. Con este objetivo, se han elaborado varios estudios geológicos científicos que fueron sometidos, aceptados y publicados en revistas científicas y/o en congresos científicos. La tesis incluye (1) un estudio geoquímico de alteración hidrotermal orogénica (balance de masas) que ayuda a determinar el grado de homogeneidad de los fluidos mineralizantes; (2) un estudio de geocronología $^{40}Ar/^{39}Ar$ en mica blanca hidrotermal (sericita) enfocado en la obtención de edades de la mineralización aurífera orogénica del COGB; (3) una caracterización isotópica estable (oxígeno, deuterio y azufre) usando distintos minerales de la paragénesis mineral (*e.g.*, pirita, galena, cuarzo, mica blanca, turmalina) para obtener temperatura y tipo de agua que constituyó el fluido hidrotermal generador de las vetas de cuarzo aurífero del COGB (4) un trabajo que introduce a los depósitos minerales de oro orogénico de México haciendo especial énfasis con las ocurrencias minerales del COGB; y por último (5) se concluyó planteando un encuadre tectónico de la mineralización.

Resumen

Diversos estudios multidisciplinarios se realizaron empleando un muestreo representativo de vetas de cuarzo aurífero y rocas encajonantes del cinturón de oro orogénico Caborca (COGB, por sus siglas en inglés) con el objetivo de encontrar el origen de la mineralización. (1) Un estudio de balance de masas en combinación a varios estudios convencionales (*e.g.*, análisis bivariable de Au y Ag, caracterización mineral usando microscopía SEM, petrografía) han permitido establecer un alto grado de homogeneidad geoquímico de los fluidos mineralizantes, caracterizándose por aportar K_2O, W, Cu, Pb, Mo, Tl, Be, Zn, V, Sb, Ag, Sn, SiO_2, Se, Ni y FeO durante la formación de las vetas de cuarzo y durante la alteración de rocas encajonantes. (2) Con un estudio de geocronología $^{40}Ar/^{39}Ar$ en micas blancas hidrotermales, asociadas a las vetas de cuarzo aurífero, se propone que la mineralización tuvo un inicio súbito y rápido (~69 Ma) con un clímax de mineralización a los ~61 Ma y un declive paulatino entre 58–36 Ma. (3) Mediante un estudio de isotopía estable de oxígeno, hidrógeno y azufre ($\delta^{18}O$, δD, $\delta^{34}S$), usando pares minerales (*e.g.*, cuarzo-mica blanca, pirita-galena) de las vetas de cuarzo hidrotermal, se pudo determinar la temperatura promedio (~327º C) de formación de las vetas auríferas. Además, utilizando un diagrama de discriminación (δD *vs.* $\delta^{18}O$) se logró obtener que las vetas auríferas fueron originadas a partir de fluidos con una fuerte afinidad a aguas metamórficas, quizás generadas a profundidades significativas (>20 km) debido a procesos de deshidratación en rocas en facies metamórficas de anfibolita o inclusive de facies metamórficas de mayor grado (*e.g.*, granulita).

El encuadre tectónico de la mineralización del COGB establece que un proceso de engrosamiento cortical ocurrido durante una etapa temprana (~90–70 Ma) de la orogenia

Larámide fue la principal causa de generación de los fluidos mineralizantes. En respuesta a una subducción planar repentina ocurrida durante la orogenia Larámide, un proceso de extensión cortical sinconvergente inició a los ~70 Ma afectando la región que comprende el antearco cordillerano en el noroeste de México. Esta extensión cortical sinconvergente generó un considerable enfriamiento de la corteza adelgazada, la cual permitió generar una región frágil sobre la corteza que facilitó el ascenso y precipitación de los fluidos mineralizantes cargados en metales preciosos y que formaron vetas de cuarzo aurífero a lo largo del COGB. Otra consecuencia debido a la subducción plana durante el larámide fue una migración hacia el Este del arco magmático causando la generación contemporánea de los depósitos de pórfidos de Cu-Mo en el noroeste de México y el suroeste de los Estados Unidos. Este escenario, supondría que los depósitos de oro orogénico fueron generados en un artearco sin magmatismo, mientras que los pórfidos Cu-Mo se generarían alejados hacia el Este en la región del arco magmático.

En este modelo de mineralización, se ha interpretado que el área del COGB fue mayormente levantada tectónicamente y, por tanto, presenta un mayor grado de denudación (vetas formadas a profundidades mínimas de ~4–6 km) con respecto a la región de pórfidos Cu-Mo que fue formada a menor profundidad (~1–2 km). En otras palabras, estos cinturones minerales contemporáneos han sido expuestos uno junto a otro a pesar de representar diferentes niveles corticales originalmente. Esta diferencia de niveles corticales pudiera ser explicada con un periodo de extensión cortical intenso Eoceno-Oligoceno causando denudación preferencial y afectando la zona del antearco previamente engrosada. También, quizás pueda ser explicado debido a que ocurrió un rebote isostático generando que al menos ~4–6 km de material de la corteza, de la región

del antearco, fueran removidos hasta lograr la exhumación de las vetas auríferas del COGB presentes en la superficie desde el Oligoceno.

Abstract

Multidisciplinary studies were performed on a representative sampling collection of gold-bearing quartz veins and host rocks from the caborca orogenic gold belt (COGB) in order to found the origin of mineralization. (1) A geochemical mass balance study using hydrothermally altered hosts rocks and combining conventional studies (e.g., bivariate Au and Ag analysis, SEM microscopy, petrography) suggest a high degree of geochemical homogeneity of the mineralizing fluids, mainly enriched in K_2O, W, Cu, Pb, Mo, Tl, Be, Zn, V, Sb, Ag, Sn, SiO_2, Se, Ni and FeO. (2) New $^{40}Ar/^{39}Ar$ geochronology of white micas associated with gold-bearing quartz veins suggests that mineralization developed rapidly after ~69 Ma, peaked at ~61 Ma and decreased more slowly from 58 to 36 Ma. (3) An oxygen, hydrogen, and sulfur ($\delta^{18}O$, δD, and $\delta^{34}S$) isotopic study was undertaken on a variety of hydrothermal minerals determining an estimated mean temperature of ~327° C for the ore forming process. A discrimination diagram (δD vs. $\delta^{18}O$) suggest that the quartz veins were derived from fluids with strong affinity to metamorphic waters, perhaps generated at significant crustal depths (>20 km) due to a process of metamorphic dehydration of water-rich minerals (e.g., amphibole) or even higher metamorphic facies (e.g., granulite).

The tectonic framework for COGB mineralization establishes that crustal thickening during the early compressive stage (~90–70 Ma) of the Laramide orogeny was the main cause to generate the mineralizing fluids. As a response to a sudden flat

subduction during the Laramide orogeny a process of synconvergent crustal extension started at ~70 Ma affecting the Cordillera forearc region in northwestern Mexico. This Laramide synconvergent extension produce a marked cooling of the thinned crust which in turn generated regional brittle conditions that facilitated the ascent and precipitation of metal-laden metamorphic fluids that formed the quartz-gold vein mineralization along the COGB. Another consequence due to the Laramide flat subduction was an eastward arc migration that was the cause of generation of contemporaneous Late Cretaceous-Eocene Cu-Mo porphyry deposits in northwestern Mexico and southwestern United States. In this scenario, orogenic gold deposits would have been formed in the amagmatic forearc region, whereas the porphyries were generated further to the east in the magmatic arc region.

In this mineralization model, it was interpreted that the COGB area was more uplifted, and suffered higher degrees of denudation (veins formed at minimum depths of ~4–6 km), than the region of Cu-Mo porphyries that formed at shallower crustal depths (~1–2 km). In other words, both coeval mineral belts were exposed next to each other even though they represent very different crustal levels. This crustal level disparity could be explained by a period of intense Eocene to Oligocene tectonic/crustal denudation that preferentially affected the previously over thickened forearc region. Perhaps due to isostatic rebound, at least 4–6 km of crustal material from the forearc region were removed until the final exhumation of the COGB veins occurred, most likely, by the Oligocene.

Capítulo 1. Introducción

La existencia de depósitos de tipo oro orogénico se debe a procesos compresivos entre márgenes tectónicos que, a su vez, son los causantes de la construcción orogénica y la formación de cadenas de montañas (Bierlein *et al*., 2009; Tomkins, 2013). Concretamente, el tiempo de formación de estos depósitos se asocia a una etapa tardía y/o postpico metamórfico dentro de la construcción orogénica (Goldfarb y Groves, 2015), manifestándose con la formación de vetas cuarzosas auríferas. Esta fase tardía metamórfica implica necesariamente la existencia de un proceso ulterior de metamorfismo prograd o que generalmente ocurre a niveles profundos de la corteza (Tomkins, 2013; Fu y Touret, 2014). La formación del COGB no es la excepción y su génesis encaja con el modelo general de oro orogénico a nivel global (Tabla 1), presentado en un encuadre tectónico compresivo (Izaguirre *et al.*, en prensa); sin embargo, presenta singularidades que mencionaremos a lo largo de este compendio.

El cinturón de oro orogénico Caborca (COGB) es una extensa provincia metalogenética que contiene mineralización de oro tipo orogénico y se sitúa dentro del dominio orográfico de la Cordillera de América del Norte (Figura 1). Presenta una forma alargada que se extiende (~600 km de largo y ~80 km de ancho) en el noroeste de Sonora, México (~80% de su área) y cubre una pequeña porción del sur de Arizona y California, Estados Unidos. Posee numerosos depósitos minerales constituidos por vetas de cuarzo aurífero que se encuentran en explotación minera (*e.g*., La Herradura, San Francisco-Llano, El Chanate, Noche Buena; Figura 2). Estos minados son principalmente a cielo abierto, pero también existen algunos subterráneos de menor escala. En total entre

Tabla 1. Características de la mineralización del cinturón de oro orogénico Caborca versus el conocimineto general de los depósitos de oro orogénico.

	***Cinturón de oro orogénico Caborca*[1]** vs.	***Oro orogénico a nivel global*[2]**
Rocas encajonantes de la mineralización	Rocas de basamento paleoproterozoicas: Gneises en facies de esquistos verdes, esquistos y granitoides. Rocas carbonatadas neoproterozoicas y paleozoicas. Rocas gnéisicas, granitoides, sedimentarias y volacánicas del Pérmico, Triásico, Jurásico, Cretácico y Paleoceno asociadas a la actividad de la Cordillera de América del Norte.	Terrenos deformados de todas las edades (rocas en facies de esquistos verdes) asociadas a arcos. Predominan las rocas de edad arqueana y las originadas en momentos de mayor intensidad orogénica durante el fanerozoico.
Temperatura de la mineralización	260–390ºC; con un promedio de ~327°C.	300 ± 50ºC.
Presiones y profundidades de formación	0.5–1.2 kbars, ~2 a 4–6 km.	1–3 kbars; epizonal-mesozonal (2–12 km).
Morfología de los depósitos	Vetas cuarzo-cabonato y *stock-work* localizados en zonas de cizalla (mayormente fallas de cabalgaduras). Oro diseminado y vetas. Con presencia de alteración supergénica en sulfuros y carbonatos frecuentemente observados como óxidos de hierro, haluros y caliche.	Vetas de cuarzo-carbonato en estructuras de cizalla (milonitas) estructuras formadas en condiciones dúctiles-frágiles, sin aparente zoneación mineral.
Minerales hidrotermales	Cuarzo, carbonatos (calcita, ankerita y siderita), mica blanca, pirite, galena, esfalerita, scheelita, turmalina, molibdenita, teluros y oro nativo.	Cuarzo, carbonatos (calcita, ankerita y siderita), mica blanca, pirita, galena, esfalerita, calcopirita, pirrotita, marcasita, arsenopirita (mayormente sulfuros de Fe), albita, clorita, scheelita, y turmalina.
Tipos de alteración y minerales de alteración originados en la roca encajonante	Silicificación, carbonatización, sericitización, piritización, cloritización.	Carbonatos (calcita, ankerita, dolomita, siderita), pirita, cuarzo, pirrotita o arsenopirita, sericita o fuchsita, albita, feldespato K y clorita.
Elementos químicos de enriquecimiento	K, W, Cu, Pb, Mo, Tl, Be, Zn, V, Sb, Ag, Sn, Si, Se, Ni y Fe (As y Te en menor medida).	K, As, B, Bi, Hg, Sb, Te, W, Cu, Pb y Zn.
Características de los fluidos	Una fuente metamórfica con baja salinidad (2–11% eq. peso % NaCl), ricos en H_2O, N_2, CO_2 (1–11 mol %), valores de $\delta^{18}O$ = 7 a 17‰ y $\delta^{2}H$ de -39 a -107‰.	Una fuente metamórfica con baja salinidad (~3–10% eq. peso % NaCl), ricos en H_2O, H_2O–$CO_2 \geq$ 5mol%, ± CH_4 y N_2. valores de $\delta^{18}O$ = 5 a 8‰ y de $\delta^{2}H$ = -10 to -40‰.
Valores de: Volumen rocas mineralizadas (Mt); producción (Moz); ley mineral (g/t) de las minas más importantes	La Herradura: 200/6.0/1.0; El Chanate: 52/1.5/0.9; San Francisco-Llano: 113/2.4/0.7; Noche Buena: 35/0.6/0.5, y La Choya: 8.3/0.4/1.3.	Golden Mile (Yilgram Craton): 1000/64.0/2.0; Homestake: > 150/40.0/8.3; Grass-Valley-Nevada: 40/21.4/16.9; Bendingo Goldfield (Tasman Orogen): 41/17.0/12.9; Brasilia: 725/10.0/0.4, y Alaska-Juneau: 198/9.0/1.4.
Otras características importantes	Bajo contenido en sulfuros (~3%), estructuralmente controlados por roca encajonante. Alteración mineral por oxidación presenta minerales secundarios (hematita, goethita, wulfenita, jarosita, plumbojarosita, anglesita y chlorargirita). Leyes de bajo grado (Au = ~1 gr/ton), Au/Ag = 1:9. Depositación controlada por estructuras regionales y de cizalla local.	Bajo contenido de sulfuros (3–5%), depositación estructuralmente controlada, leyes moderadas (Au = 5–30 gr/ton), Au/Ag = 10:1. Depositación asociada a estructuras de cizalla.

1. Datos compilados de: Albinson (1989); Pérez-Segura *et al.* (1996); Iriondo y Atkinson (2000); Araux-Sánchez *et al*. (2001); Noriega-Martínez (2006); Quintanar-Ruíz (2008); De la Torre-Carlos (2009); Izaguirre *et al*. (2012); Izaguirre e Iriondo (2014).
2. Datos de Groves *et al*. (1998) y Goldfarb *et al*. (2005).

Figura 1. Localización del cinturón de oro orogénico Caborca (COGB) en la Cordillera de América del Norte**.**

Figura 2. Localización del cinturón de oro orogénico Caborca (COGB) ubicado en el noroeste de Sonora y suroeste de Estados Unidos. Se presentan las minas más importantes económicamente o con relevancia histórica. En puntos rojos se señalan ocurrencias de vetas de cuarzo con la paragénesis mineral del oro orogénico.

explotación y reservas probables suman más de ~22 millones en onzas de oro (Izaguirre *et al.*, en prensa).

1.1. Encuadre geológico del COGB

La mineralización del cinturón de oro orogénico Caborca ocurrió durante el periodo Cretácico tardío al Eoceno generando gran cantidad de vetas de cuarzo con oro a lo largo de la región (~69–36 Ma, Figura 3A y 4). Estas se encuentran hospedadas en una gran variedad de litologías con edades desde el proterozoico hasta el cuaternario. La ocurrencia de vetas de cuarzo aurífero es común a lo largo de rocas del basamento ígneo-metamórfico que constituye a la región (Figura 3). El basamento se compone por ortogneises, paragneises, gneises bandeados, esquistos de edad Paleoproterozoico (~1800–1600 Ma) y metagranitos y anortositas del Mesoproterozoico (~1400–1100 Ma) que en conjunto se clasifican como rocas premineralización (Figura 5). Las vetas cuarcíferas se presentan en menor medida sobre rocas de plataforma calcárea y de cuenca de edades del Neoproterozoico y Paleozoico superpuestas sobre las rocas antiguas del basamento ígneo-metamórfico paleoproterozoico y mezoproterozoico. La mineralización aurífera también ocurre en rocas calcáreas y detríticas con edades del Jurásico y Cretácico. Regionalmente las vetas del COGB son muy abundantes en afloramientos de rocas graníticas, volcánicas, volcanosedimentarias, gnéisicas y esquistosas relacionadas a la larga actividad de la margen activa Cordillerana con edades del Pérmico hasta el Paleoceno (McDowell *et al.*, 2001; Arvizu *et al.*, 2009; Mauel *et al*. 2011; Valencia-Moreno y Ortega-Rivera, 2011).

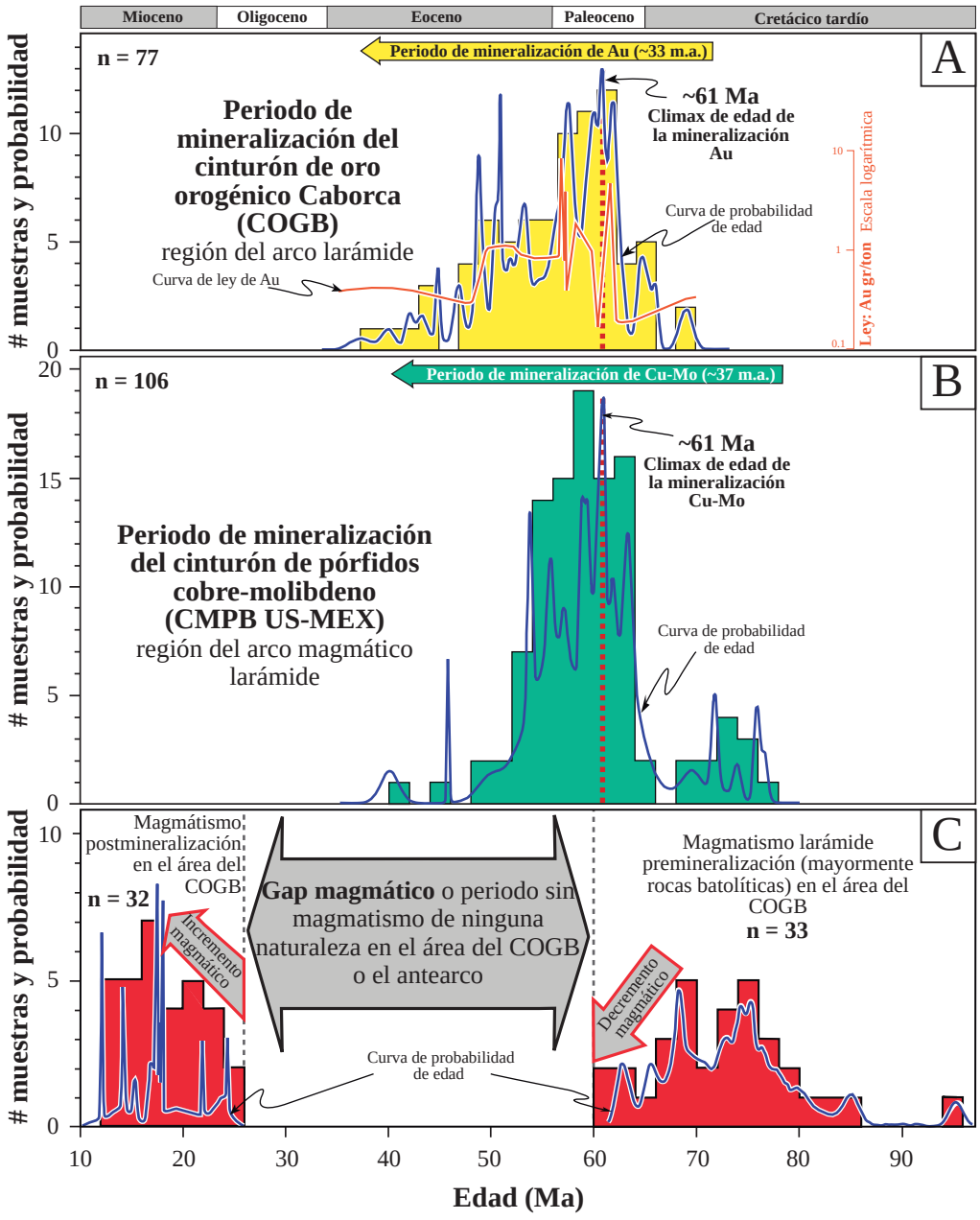

Figura 3. Histogramas de edades y curvas de probabilidad de A) vetas de cuarzo aurífero (n = 77) del cinturón de oro orogénico Caborca (COGB) con un pico de ~61 Ma que representa el clímax de mineralización (Paleoceno medio); B) de pórfidos de Cu-Mo del cinturón de cobre-molibdeno de Estados Unidos y México (CMPB US-MEX; clímax de mineralización a ~61 Ma); C) de edades de cristalización de rocas ígneas premineralización y postmineralización (Oligoceno al presente) a lo largo del área del COGB**.**

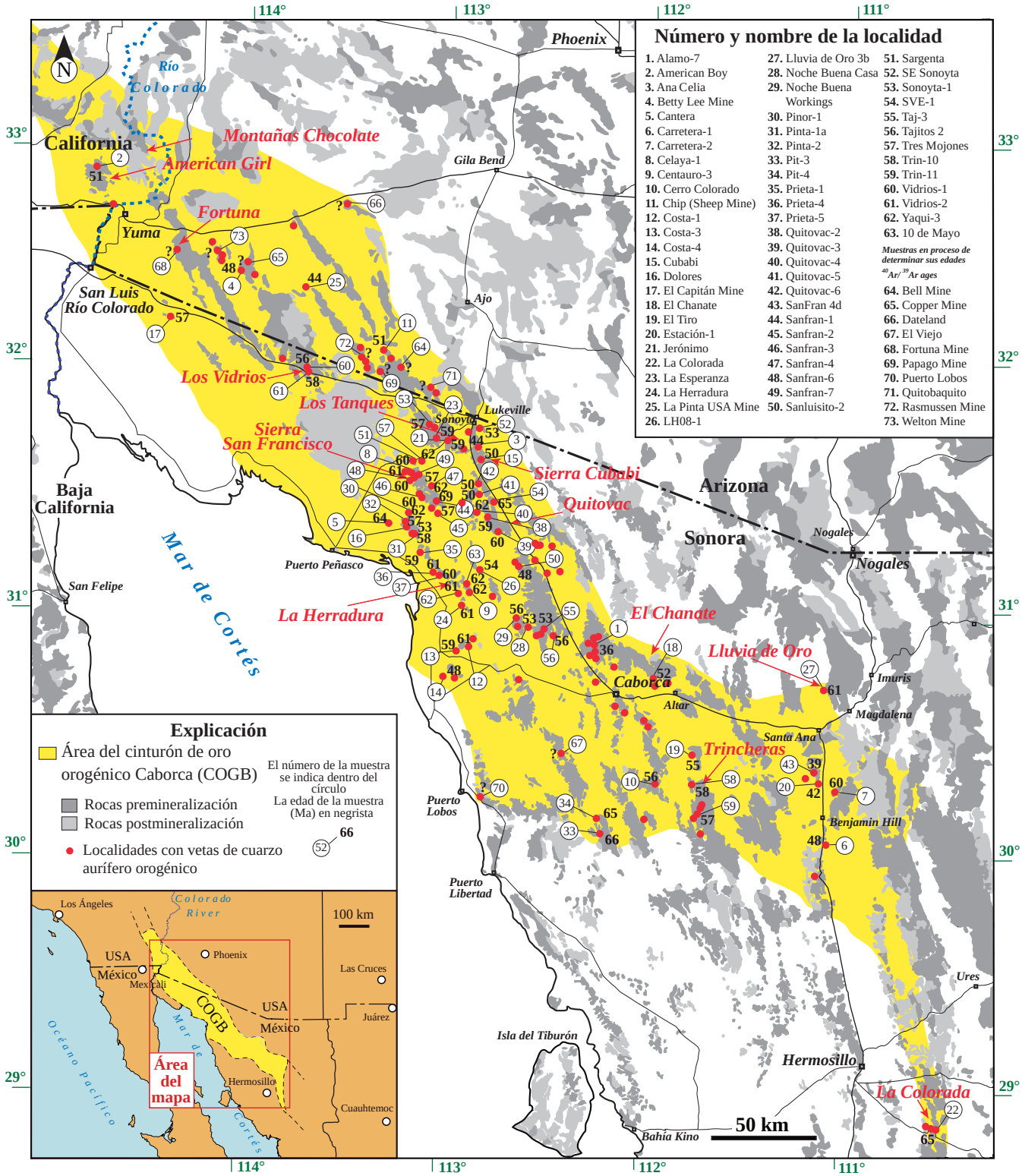

Figura 4. Mapa del noroeste de Sonora y suroeste de Arizona mostrando las 63 localidades del cinturón de oro orogénico Caborca (COGB) con vetas de cuarzo aurífero datas con la técnica $^{40}Ar/^{39}Ar$ usando micas blancas hidrotermales. Localidades en rojo muestran sitios con vetas de oro orogénico determinadas usando la paragénesis mineral. El área amarilla muestra la extensión estimada del COGB. Los dominios en gris oscuro sugieren afloramientos de rocas premineralización con edades mayores que ~60 Ma y los dominios en gris claro rocas postmineralización con edades de ~25 Ma hasta la actualidad.

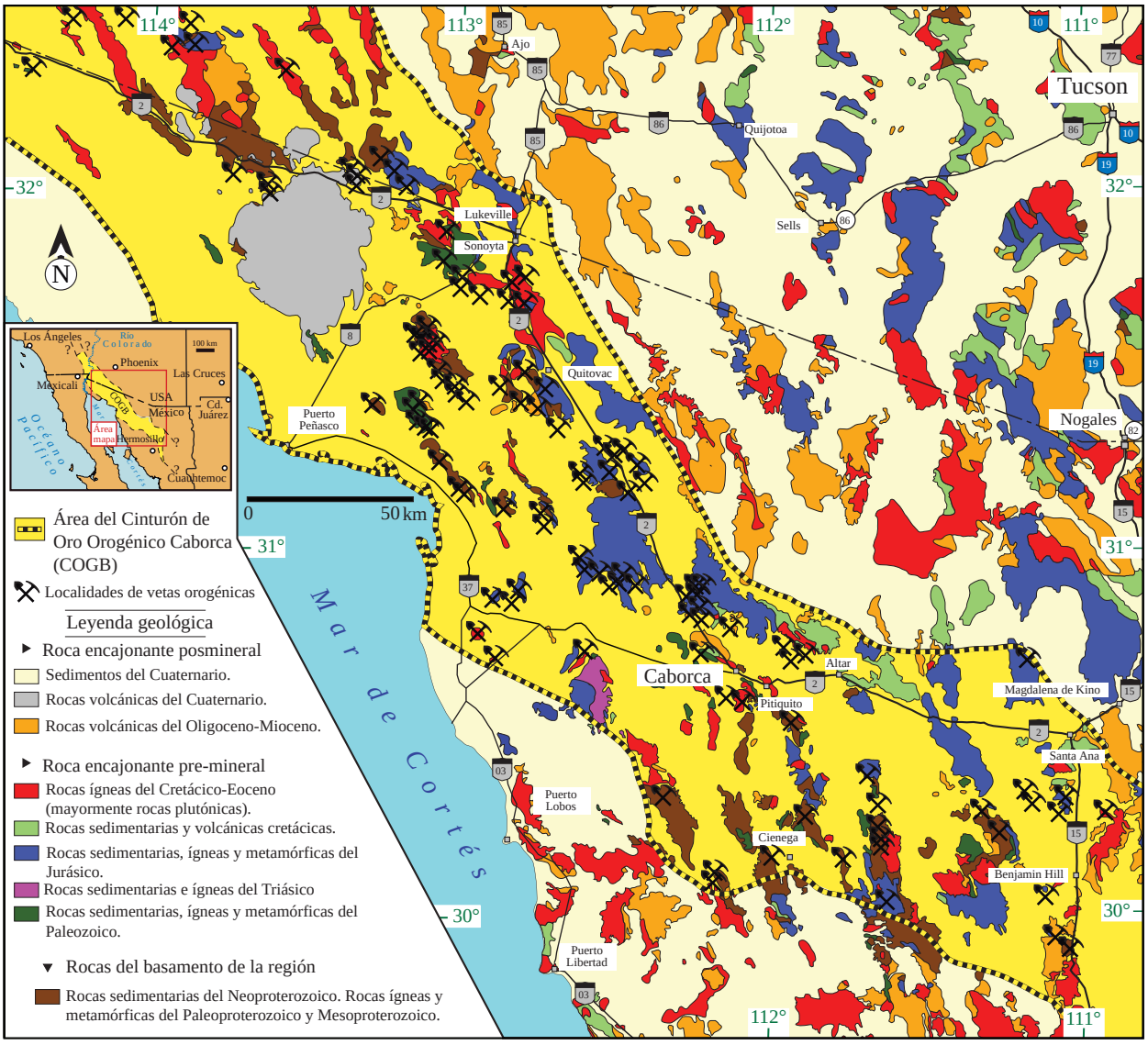

Figura 5. Plano geológico del noroeste de Sonora y suroeste de Arizona (modificado de Iriondo *et al*., 2005). Adicionalmente se muestra el área del cinturón de oro orogénico Caborca (COGB) en color amarillo (modificado de Izaguirre *el al*., 2017). La presencia de ocurrencias de mineralización orogénica es señalada con símbolos de mina.

Por otro lado, rocas consideradas como postmineralización (Figura 5) son principalmente rocas volcánicas lávicas y piroclásticas originadas durante el periodo Oligoceno-Mioceno y rocas volcánicas de composición basáltica más recientes del Plioceno al Cuaternario. También existen un gran número de depósitos sedimentarios postmineralización rellenando cuencas intermontanas y asociados a erosión de bloques levantados durante el periodo extensional Basin and Range en el Cenozoico tardío (Henry y Aranda-Gómez, 2000). Sin embargo, estas cuencas y sedimentos albergan mineralización relevante de tipo oro de placer (*e.g.*, Tajitos y El Boludo; Figura 2) y que, como fuente principal, han sido propuestas las vetas de cuarzo aurífero del COGB (*e.g.*, Wilson *et al.*, 2009)

1.2. Características mineralógicas del COGB

La mineralización aurífera del COGB se caracteriza por vetas de cuarzo hidrotermal, masivo, lechoso y translucido que contienen una paragénesis mineral de cristales megascópicos de carbonato de calcio-hierro (mayormente calcita, siderita y ankerita), mica blanca gruesa y fina (sericita), pirita, galena, oro nativo y oro-plata incluido en sulfuros (Figura 6). Observadas con detalle, se pueden discriminar minerales microscópicos de esfalerita, covelita, turmalina, scheelita, sulfuros de telurio y teluros de Au–Ag (Pérez-Segura, 2009; Izaguirre *et al.*, 2012). Comúnmente, a lo largo del cinturón de oro, las vetas auríferas presentan pocos sulfuros (~3%) y una gran mayoría presentan oxidación mostrándose como seudomorfos de hierro (goethita, Figura 7) y espacios vacíos donde yacían estos minerales (oquedades). En términos generales, la mineralización aurífera presenta una ley baja que en promedio muestra una relación

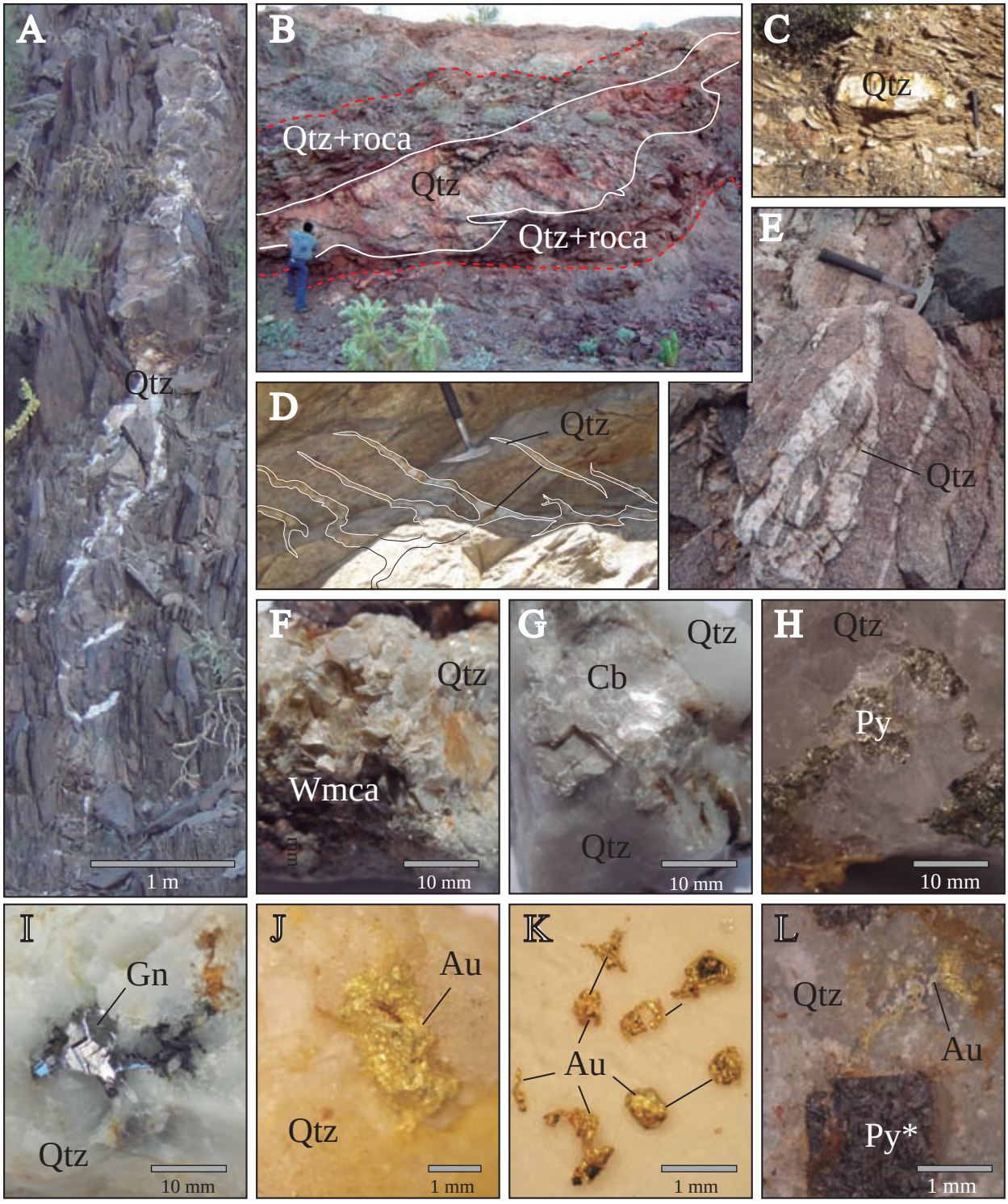

Figura 6. Vetas de cuarzo hidrotermal y minerales de la paragénesis del cinturón de oro orogénico Caborca (COGB). A-D) Vetas de cuarzo con arreglos en echelon asociadas a cizallas. E) Veta en forma trenzada. F) Mica blanca y cuarzo. G) Carbonato (calcita) en vetas de cuarzo. H) Pirita en cuarzo. I) Galena en cuarzo. J) Oro en cuarzo. K) Pepitas de oro (mina San Francisco-Llano veta con ~134 g/t de Au). L) Cuarzo con pseudomorfos de goethita y oro, después de pirita. Au = oro; Cb = carbonato (comúnmente calcita); Gn = Galena; Py = Pirita; Py* = Pseudomorfo de pirita; Qtz = cuarzo; Wmca = mica blanca.

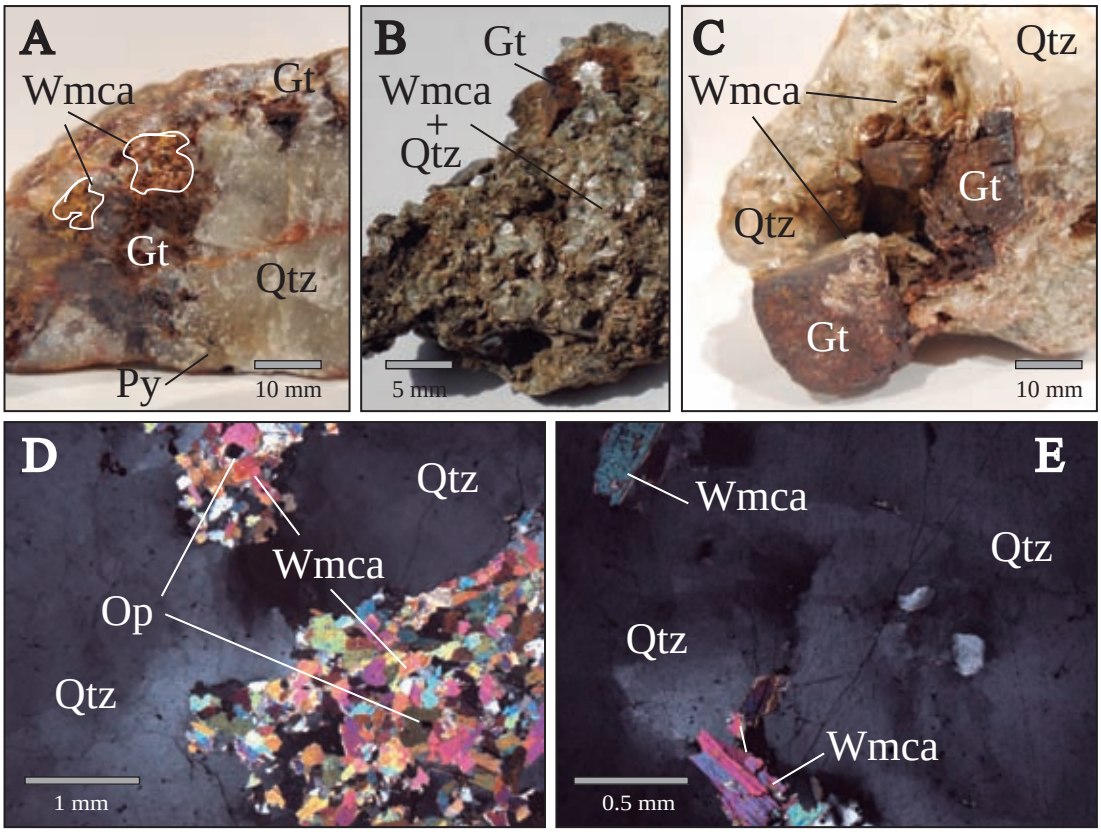

Figura 7. Muestras de vetas de cuarzo del cinturón de oro orogénico Caborca. A) Cuarzo hidrotermal con pseudomorfos de goethita, después de pirita, y parches de mica blanca hidrotermal. B-C) Cuarzo hidrotermal, mica blanca y pseudomorfos de goethita. D-E) Microfotografías de secciones delgadas usando microscopio petrográfico, en luz polarizada analizada, de vetas de cuarzo hidrotermal con parches de mica blanca con intercrecimientos de minerales opacos (posiblemente pirita o goethita). Gt = Goethita; Op = minerales opacos; Qtz = cuarzo; Wmca = mica blanca.

Au/Ag = 1:9 (Izaguirre *et al.*, 2012). Las alteraciones generadas por los fluidos hidrotermales sobre las rocas encajonantes son intensas en zonas de stock-work y menos penetrantes en vetas únicas; típicamente, las alteraciones consisten en silicificación, carbonatización, seritización, piritización y cloritización (Izaguirre *et al.*, 2012). Los fluidos de alteración han dejado firmas geoquímicas homogéneas de enriquecimiento a lo largo del cinturón en elementos como: K, W, Cu, Pb, Mo, Tl, Be, Zn, V, Sb, Ag, Sn, Si, Se, Ni y Fe, As y Th (Figura 8). Las temperaturas de formación de las vetas auríferas para todo el COGB fueron obtenidas a partir de estudios de termometría de pares minerales de la paragénesis mineral (Figura 9) y oscilan entre ~180–550°C, aunque ~80% se encuentra entre ~200–400°C; el promedio ponderado indica ~327ºC, que es moderadamente más elevado que las obtenidas en estudios previos (*e.g.*, Albinson, 1989; Pérez-Segura *et al.*, 1996; Araux-Sánchez *et al*., 2001; Noriega-Martínez, 2006). Los estudios de inclusiones evidencian que los fluidos hidrotermales mineralizantes presentan baja salinidad (~2–11% eq. wt% al NaCl) y contenidos altos de H_2O, N_2, CO_2 (1–11 mol%). Por último, estudios de isótopos estables han revelado que los fluidos hidrotermales con valores de $\delta^{18}O$ entre 7–17‰ y de δD entre –39 a –107‰ (Figura 10) obtenidos de cuarzo y mica blanca, respectivamente, presentan una fuerte afinidad a aguas derivadas de reacciones metamórficas; como explicación se ha sugerido que han derivado por metamorfismo de rocas profundas de >20 km (Izaguirre e Iriondo, 2014)

1.3. Control estructural de la mineralización del COGB

Por un largo tiempo, el modelo de control estructural de la mineralización del COGB fue asociado a la hipotética megacizalla Mojave-Sonora (hMSM, Anderson y

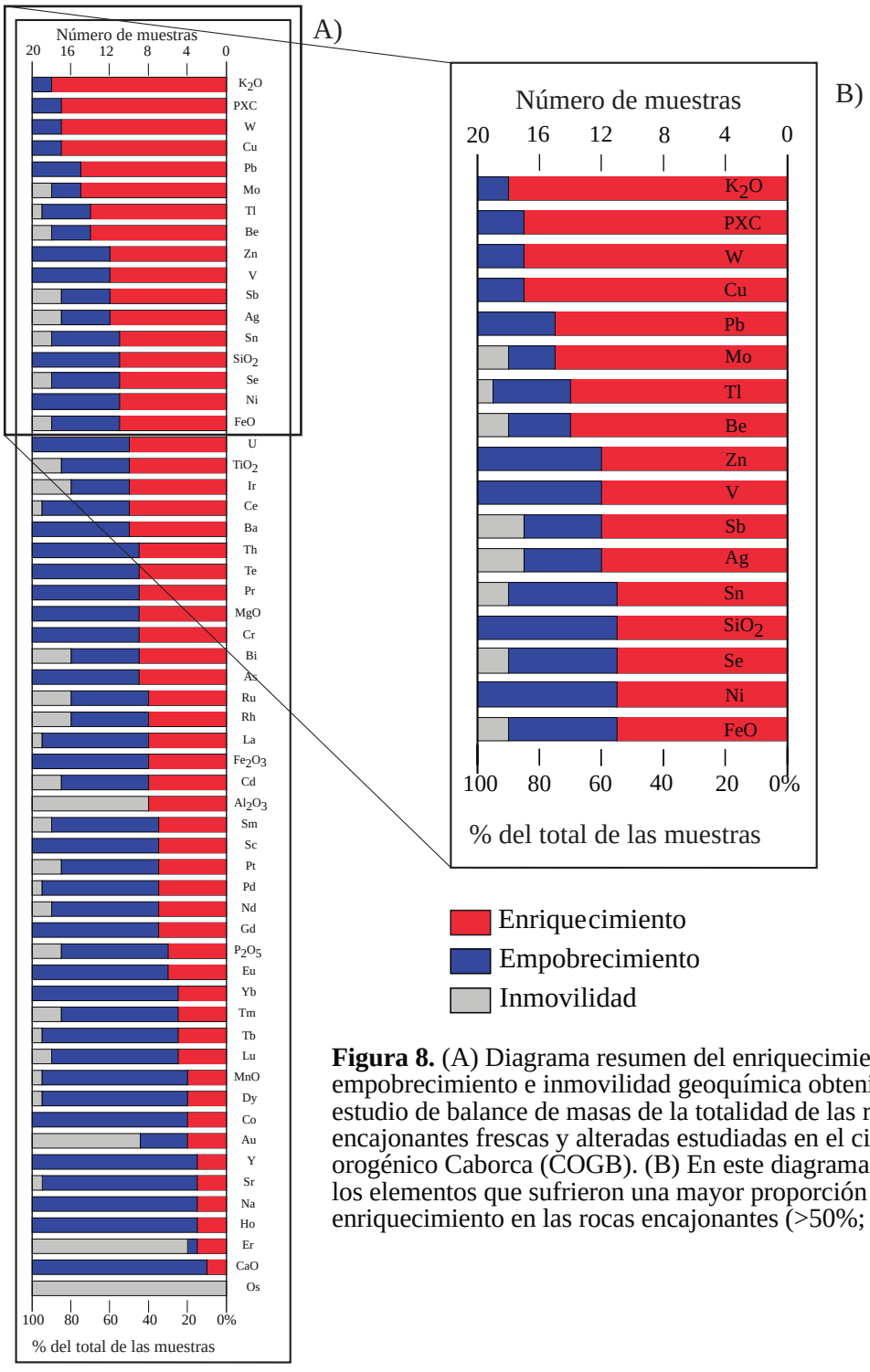

Figura 8. (A) Diagrama resumen del enriquecimiento, empobrecimiento e inmovilidad geoquímica obtenidos en el estudio de balance de masas de la totalidad de las rocas encajonantes frescas y alteradas estudiadas en el cinturón de oro orogénico Caborca (COGB). (B) En este diagrama se enfatiza en los elementos que sufrieron una mayor proporción o grado de enriquecimiento en las rocas encajonantes (>50%; barras rojas).

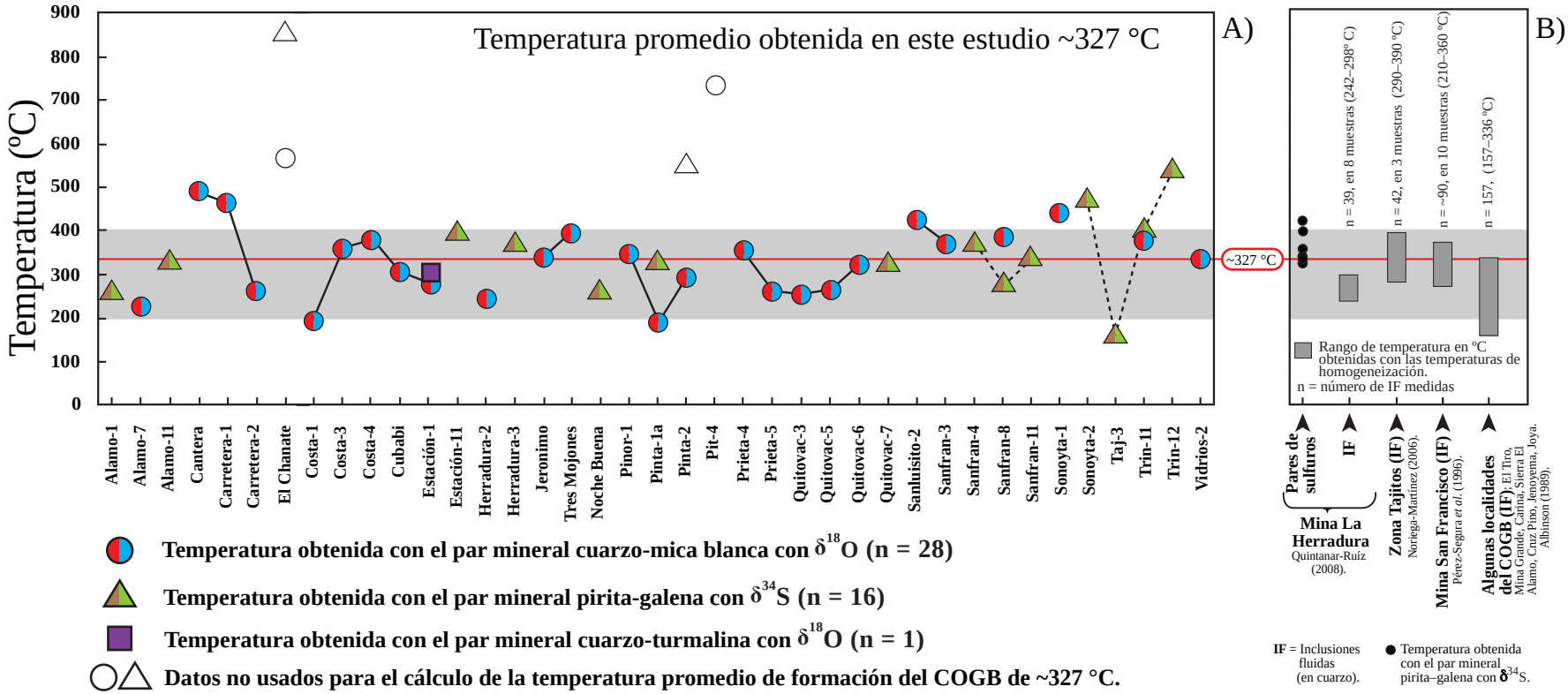

Figura 9. Temperaturas de formación de las vetas auríferas del cinturón de oro orogénico Caborca (COGB). A) Temperaturas de formación obtenidas asumiendo equilibrio isotópico de pares minerales y calculado según las ecuaciones teóricas establecidas para cuarzo-mica blanca (Chacko *et al*., 1996; Zheng, 1999), galena-pirita (Ohmoto y Rye 1979; Li y Liu, 2006) y cuarzo-turmalina (Zheng, 1993) usando isótopos de oxígeno y azufre. La temperatura promedio de formación de ~327ºC fue obtenida utilizando las muestras rellenas con color. Las muestras vacías fueron descartadas debido a que se consideró que las temperaturas eran muy elevadas y se interpretó que no se encontraban bajo equilibrio isotópico durante su formación. B) A manera comparativa se muestran las temperaturas de trabajos previos en algunas localidades del COGB y que fueron obtenidas mayormente por estudios de inclusiones fluidas; estas muestran temperaturas menores de formación al presente estudio.

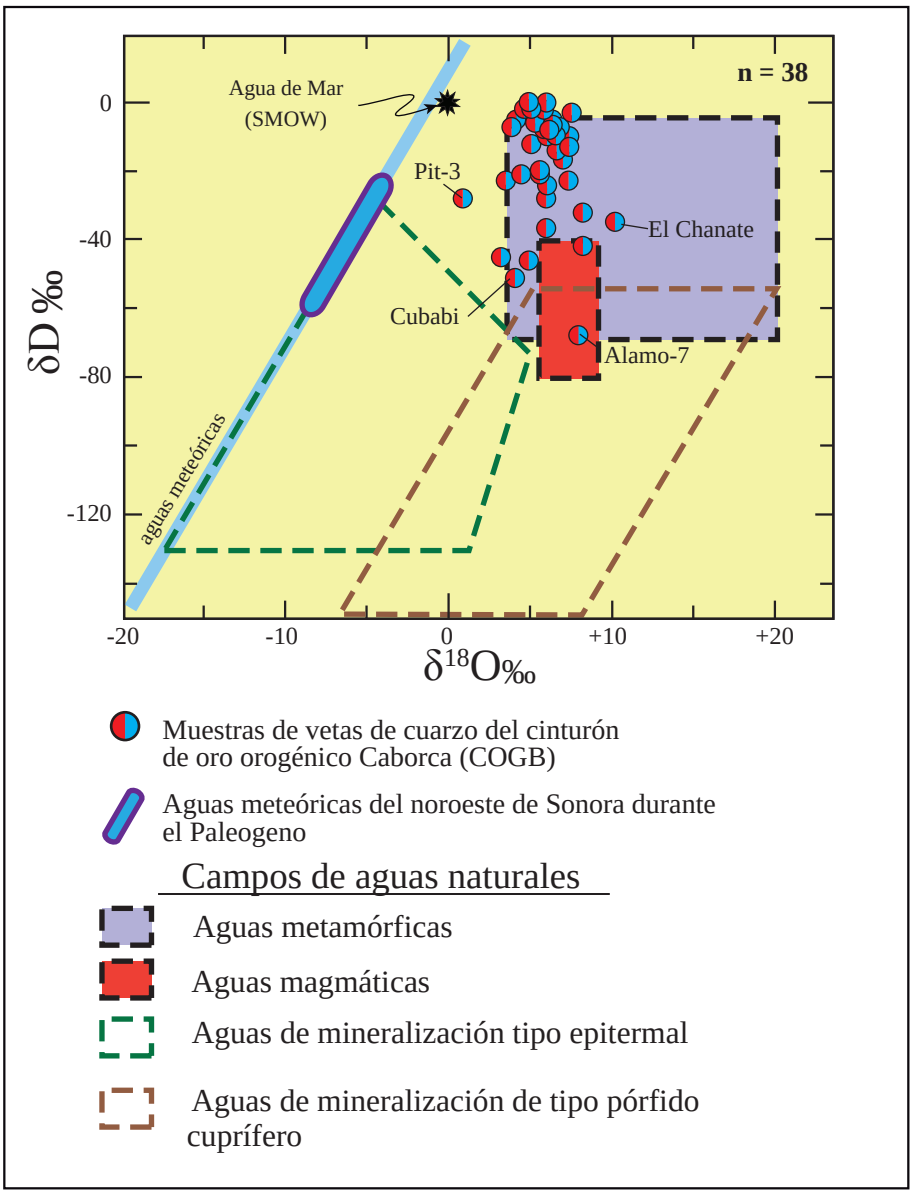

Figura 10. (A) Diagrama discriminatorio de isótopos estables δD versus $\delta^{18}O$ de las muestras de vetas de cuarzo aurífero del cinturón de oro orogénico Caborca (COGB) utilizando el par mineral cuarzo-mica blanca (n = 38). Los datos fueron recalculados a la temperatura del fluido hidrotermal a ~327° C usando las ecuaciones de Zhang *et al.* (1989) para el oxígeno y Suzuoki y Epstein (1976) para el deuterio. Los campos de aguas naturales de depósitos tipo epitermal y pórfidos Cu-Mo se obtuvieron a partir de Taylor (1997); los de aguas metamórficas a partir de Sheppard (1986) y los de aguas magmáticas y aguas meteóricas de noroeste de Sonora a partir de Taylor (1974).

Silver, 1979, 2005; Campbell y Anderson, 2003). Este modelo fue aceptado por compañías mineras, geólogos de exploración y por algunos estudios geológicos (*e.g.*, Quintanar-Ruíz, 2008; De la Torre-Carlos, 2009). Este sugería que el origen y/o localización de las vetas auríferas fueron debilitadas a la presencia de una debilidad cortical creada por la hMSM. Esta hipotética falla sugiere un desplazamiento lateral izquierdo de ~800–1000 km ocurrido durante el Jurásico tardío, afectando a profundidad rocas del basamento paleoproterozoico y sus rocas de cobertera depositadas desde el Paleozoico hasta el Jurásico. Sin embargo, la existencia de esta falla es un asunto controvertido en la comunidad geológica ya que muchos estudios desaprueban la hipótesis poniendo en duda su existencia debido a que gran parte de la deformación presente en la región no puede ser de edad jurásica (*e.g.*, Molina-Garza y Geissman, 1999; Iriondo *et al.*, 2005; Molina-Garza e Iriondo *et al.*, 2005; Poole *et al.*, 2005; Izaguirre-Pompa, 2009; Jacques-Ayala y García-Barragán, 2014).

Estudios más afines con el encuadre geológico de la región y la mineralización del COGB sugieren un modelo para el control estructural asociado a cizallas de bajo ángulo, cabalgamientos y bandas de esquistosidad de edad Larámide (*e.g.*, Iriondo, 2001; Poulsen *et al.*, 2008; Nourse e Irwin, 2010; Izaguirre *et al.*, 2017). Las morfologías de las vetas de cuarzo aurífero generadas a lo largo de estas estructuras presentan arreglos en echelón (Figura 6A-D) o en forma trenzada (Figura 6E). Las orientaciones conocidas de las vetas orogénicas sugieren un predominio regional NW-SE (330–340°, Figura 11).

Por otro lado, se sugiere que buena parte de la extensión que abarca el COGB coincide espacialmente con el basamento ígneo metamórfico precámbrico denominado provincia Yavapai (Iriondo y Premo, 2011, Figura 12A). Como explicación a esta

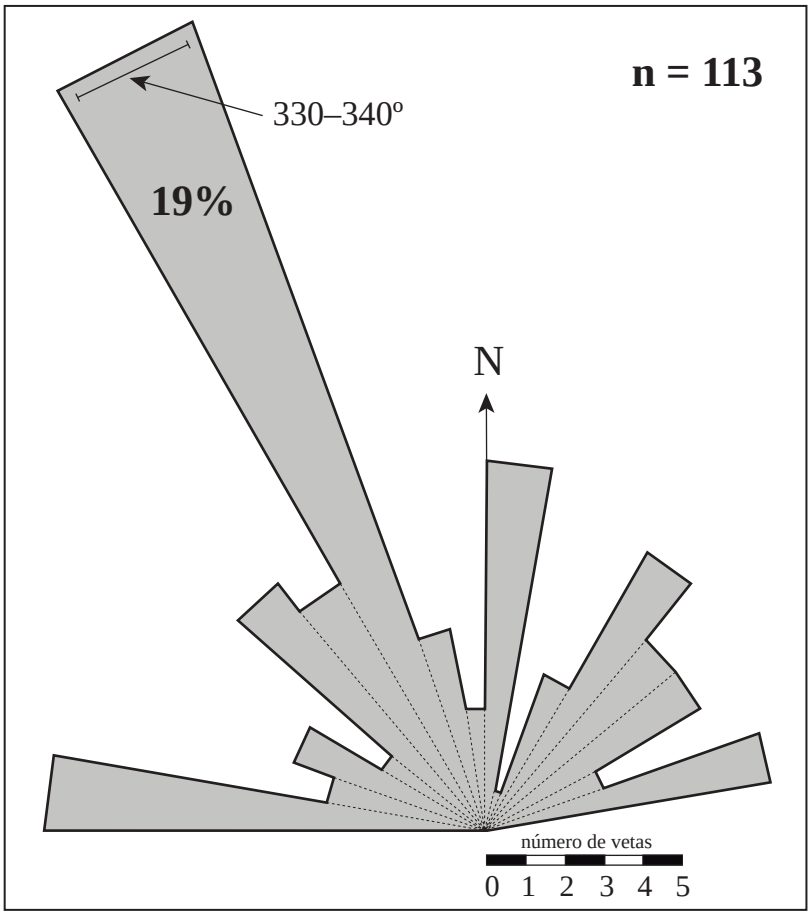

Figura 11. Diagrama de roseta que muestra la orientación de 113 planos medidos en vetas orogénicas a lo largo del cinturón de oro orogénico Caborca (COGB). La mayor frecuencia de orientaciones corresponde a ~19% en dirección 330–340°.

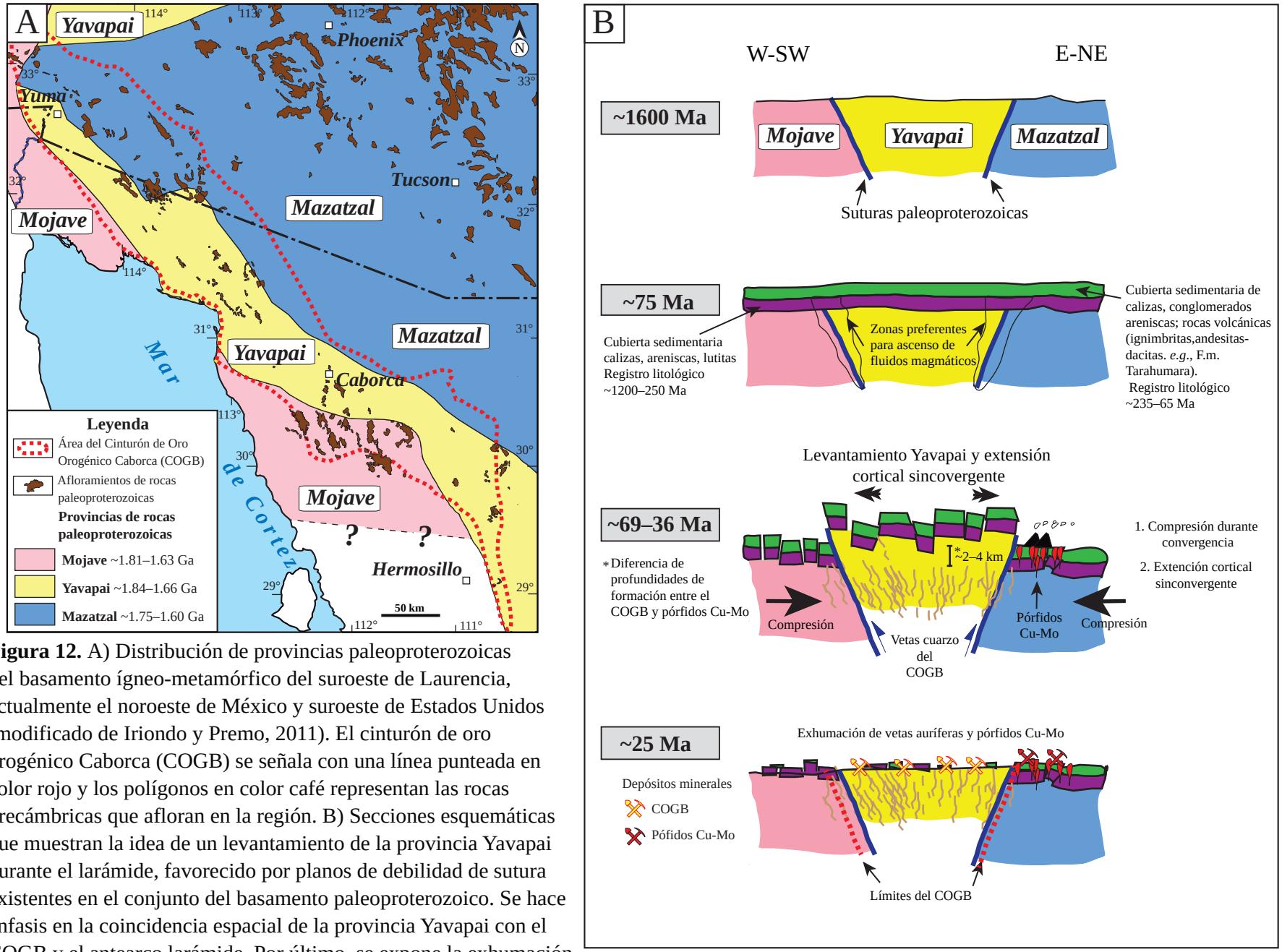

Figura 12. A) Distribución de provincias paleoproterozoicas del basamento ígneo-metamórfico del suroeste de Laurencia, actualmente el noroeste de México y suroeste de Estados Unidos (modificado de Iriondo y Premo, 2011). El cinturón de oro orogénico Caborca (COGB) se señala con una línea punteada en color rojo y los polígonos en color café representan las rocas precámbricas que afloran en la región. B) Secciones esquemáticas que muestran la idea de un levantamiento de la provincia Yavapai durante el larámide, favorecido por planos de debilidad de sutura existentes en el conjunto del basamento paleoproterozoico. Se hace énfasis en la coincidencia espacial de la provincia Yavapai con el COGB y el antearco larámide. Por último, se expone la exhumación a finales del periodo Oligoceno del COGB y los pórfidos de Cu-Mo.

coincidencia se propone que la provincia Yavapai presenta un alto grado de debilitamiento estructural que propicio la canalización de los fluidos mineralizantes. Esta debilidad cortical ha sido asociada a un levantamiento preferencial de esta zona durante el periodo Larámide (Iriondo e Izaguirre, 2016; Figura 12B).

1.4. Resumen tectónico y tiempo de mineralización del COGB

El establecimiento de la orogenia Larámide en el noroeste de México y suroeste de Estados Unidos sucedió a los ~95–90 Ma (Damon *et al*., 1983), poco después de finalizar la acreción del arco de islas Alisitos contra la margen occidental Cordillerana (~110–100 Ma; Figura 13A), ahora al occidente de Baja California y el suroeste de California, Estados Unidos (*e.g.,* Johnson *et al*., 1999; Wetmore *et al*., 2003). En un inicio, la orogenia Larámide se caracterizó por una etapa de subducción que generó actividad magmática y deformación con un ángulo de subducción elevado de la placa oceánica Farallón (Figura 14A). Durante este periodo de compresión ocurrió el metamorfismo en rocas profundas (>20 km) que generó los fluidos mineralizantes del COGB (Figura 14A). No obstante, después ocurrió un cambió en el proceso convergente que generó una reducción del ángulo de subducción de la placa Farallón creando una subducción plana a partir de los ~75 Ma (*e.g.,* Coney and Reynolds, 1977; Bird, 1988; Usui et al., 2003; Wells and Hoisch, 2008). Este hecho ocasionó una migración del arco magmático larámide hacia el Este, posicionando el eje de generación de rocas ígneas en una región un poco más apartada a la trinchera (Figura 13B y 14B).

La consecuencia más importante de la subducción plana fue la generación de un proceso de extensión cortical sinconvergente, asociada a un levantamiento isostático que

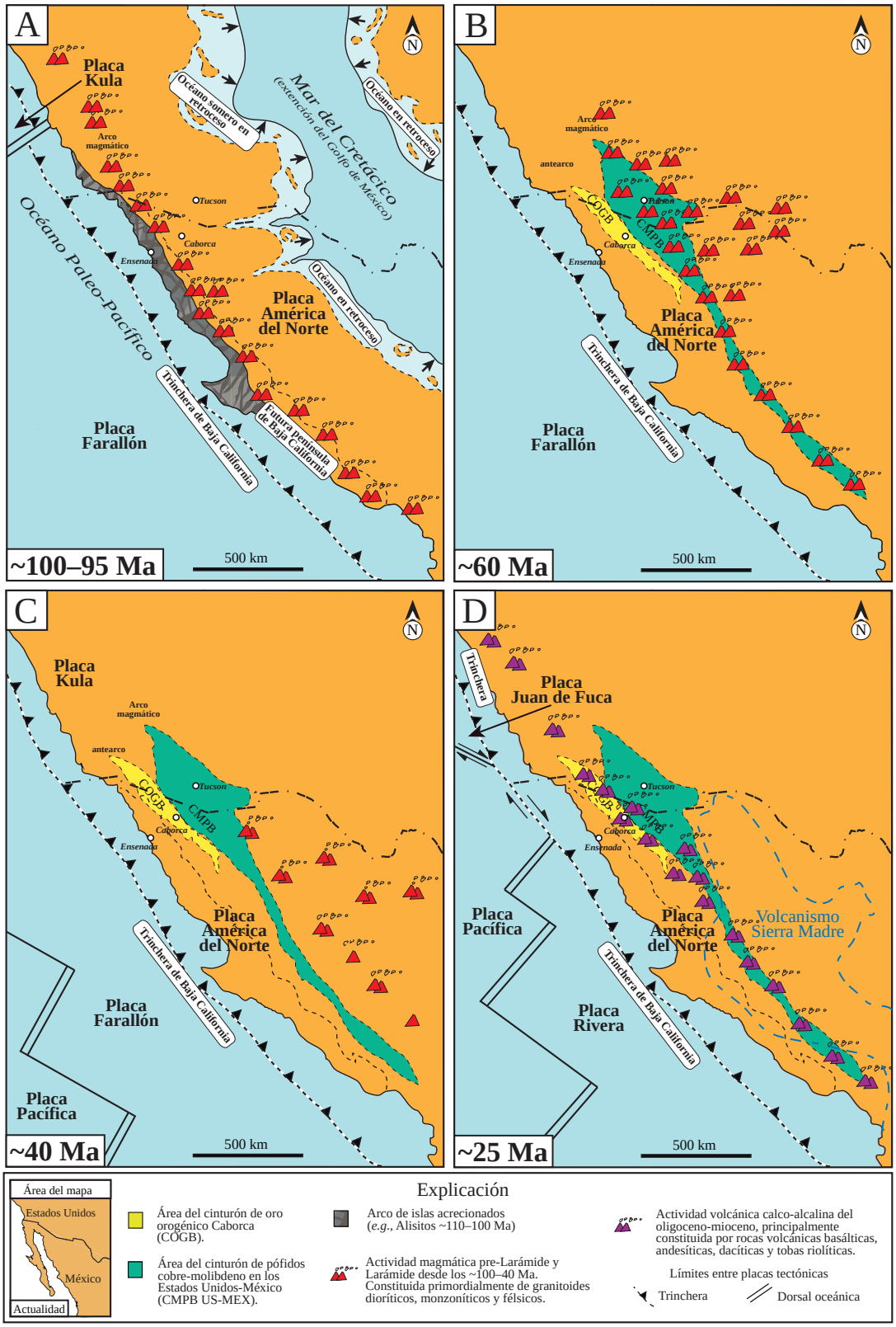

Figura 13. Paleogeografía de la Cordillera de América del Norte enfocada en ilustrar la evolución tectónica que afectó al cinturón de oro orogénico Caborca (COGB) y al cinturón de pórfidos de Cu-Mo de Estados Unidos y México (CMPB US-MX). A) Inicio de la orogenia Larámide. B) Clímax de mineralización del COGB y CMPB US-MX. C) Cese de la mineralización del COGB y CMPB US-MX. D) Magmatismo oligiceno-mioceno depositado sobre vetas de cuarzo aurífero exhumadas. Paleotectónica y paleogeografía sintetizada a partir de Gastil, 1975; Bird, 1988; Bennett *et al.*, 2013; http://plate-tectonic.narod.ru.

Compresión téctonica del Cretácico temprano al Eoceno margen cordillerana de América del Norte (sección a lo largo del noroeste de México al suroeste de Estados Unidos)

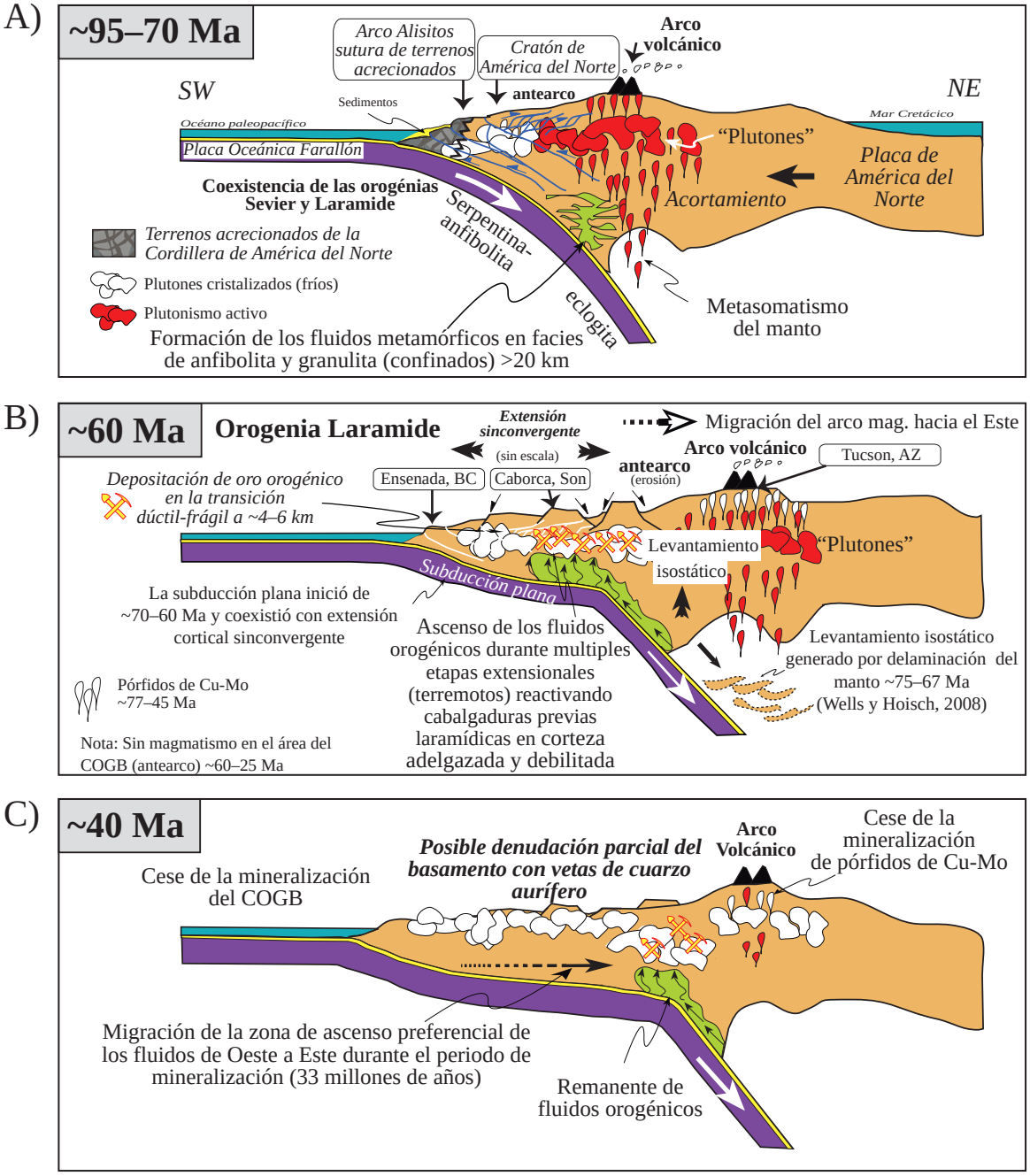

Figura 14. Secciones tectónicas para documentar el cinturón de oro orogénico Caborca (COGB). A) Sección que muestra la formación de los fluidos mineralizantes debido a metamórfismo profundo durante la subducción en un elevado ángulo de la placa Farallón. B) La formación de las vetas auríferas inició (~70 Ma) durante un periodo de subducción planar larámide que como resultado generó un evento de extensión cortical sinconvergente a lo largo de la zona del antearco, que primero fue engrosada y después levantada isostáticamente. Como otra consecuencia, la subducción planar generó migración del arco magmático, hacia el Este, permitiendo la generación contemporánea entre el COGB y los depósitos de pórfidos de Cu-Mo que ocurrieron en el noroeste de México y el suroeste de los Estados Unidos. Este escenario, supone que los depósitos de oro orogénico fueron generados en un artearco sin magmatismo mientras que los pórfidos Cu-Mo se generaron en la región del arco magmático. C) Se pone en evidencia un rejuvenecimiento de las vetas orogénicas hacia la porción Este del COGB, posiblemente debido a una migración de la zona de ascenso de los fluidos mineralizantes. La mineralización cesaría a los ~36 Ma, y un proceso de denudación permitiría la exposición de algunas de las vetas auríferas a finales del Oligoceno.

habría afectectado la región del antearco a partir de ~70 Ma (Izaguirre *et al*., en prensa). Esto generaría una corteza adelgazada, fría y frágil donde los fluidos orogénicos, ricos en metales preciosos, ascendieron con mayor facilidad (Figura 14B) teniendo como consecuencia el inicio de la formación de vetas auríferas (~69–36 Ma), que alcanzaron un clímax de la mineralización a ~61 Ma (Figura 3A). Este punto de mayor generación de vetas coincidiría con el menor ángulo alcanzado de la placa en subducción. La migración del arco magmático, hacia el Este, permitió la generación contemporánea entre el COGB y los depósitos de pórfidos de Cu-Mo que ocurrieron en el noroeste de México y el suroeste de los Estados Unidos (Figura 3A y 3B). Este escenario, supondría que los depósitos de oro orogénico fueron generados en un artearco sin magmatismo (Figura 3C), mientras que los pórfidos Cu-Mo se generarían en la región del arco magmático (Figura 14B). Finalmente, a finales del Eoceno la mineralización de oro orogénico y de los pórfidos Cu-Mo cesó (~36 Ma, Figura 13C y 14C). La placa en subducción Farallón paulatinamente recupero un ángulo elevado de subducción, generando su retroceso y actividad volcánica (~25 Ma) que cubrió discordantemente las vetas auríferas exhumadas para finales del Oligoceno (Figura 13D).

El modelo de mineralización exige que el área del COGB tuvo que haber sufrido un mayor grado de denudación con respecto a la región de pórfidos Cu-Mo. Esto debido a que los cinturones minerales son contemporáneos y han sido expuestos en superficie a pesar de representar diferentes niveles corticales originalmente (Figura 12B). Esta diferencia de niveles corticales (~2–5 km) se explicaría con los diversos eventos tectónicos que afectaron principalmente el antearco (*e.g.*, levantamiento isostático, extensión cortical sinconvergente).

Capítulo 2. Motivación del proyecto doctoral

La principal motivación para realizar este trabajo de tesis doctoral ha sido un interés legítimo mutuo tutor-estudiante por encontrar respuestas a múltiples cuestionamientos geológicos derivados de la presencia de las vetas auríferas en el noroeste de Sonora (Figura 2 y 4). Interés magnificado durante algunos años de trabajo geológico regional por parte del tutor y el estudiante, mismo que facilitó el establecimiento de un plan de trabajo para esta tesis. La problemática fue la inexistencia de trabajos sistemáticos de carácter geológico regional que comprendieran esfuerzos multidisciplinarios (geoquímica, geocronología, isotopía estable, análisis tectónico) y que plantearan respuestas al origen del COGB. Esta necesidad derivó en un proyecto que tomó en cuenta los estudios pioneros de reconocimiento de las principales zonas auríferas de la región (Silberman *et al.*, 1988; Albinson, 1989). También, se consultaron los estudios con resultados de geocronología, descriptiva mineral y mostrando algunas condiciones de formación de las vetas, referentes solo a algunas zonas mineralizadas como son Tajitos (Pérez-Segura, 1993; Noriega-Martínez, 2006; Figura 2), San Francisco-Llano (Changkuon, 1990; Pérez-Segura *et al.*, 1996; Poulsen et al., 2008), Quitovac (Iriondo y Atkinson, 2000; Iriondo, 2001), La Pinta (Araux Sánchez *et al.*, 2001), La Herradura-Cerro Prieto (Quintanar-Ruíz, 2008; Ornelas-Macías y Verdugo-Noriega, 2009).

2.1. Objetivos y métodos del estudio

Algunos objetivos fueron planteados para hallar respuesta a la principal motivación de este estudio que era encontrar el origen del cinturón de oro orogénico Caborca (COGB). Se realizaron diferentes estudios con resultados que han ayudado a dar respuesta a este propósito (Capítulos 3–6; Apéndice A1).

2.2. Hipótesis del estudio

Varias hipótesis se plantearon durante el plan de trabajo inicial y durante la evolución del mismo. Estas convergieron en una misma idea general que es el poner a prueba la supuesta homogeneidad geoquímica, geocronológica e isotópica de los fluidos mineralizantes debido a un solo pulso de mineralización.

2.3. Técnicas analíticas

En la primera fase de este estudio, se realizó un muestreo regional que en principio ayudó a delimitar la extensión conocida del COGB por medio de la identificación y confirmación de ocurrencias de mineralización de oro orogénico (Figura 2). Se muestrearon más de un centenar de muestras diversas, vetas de cuarzo, roca fresca encajonante de la mineralización y roca con alteración mineral. El muestreo se realizó de forma sistemática tomando las mismas cantidades (5–10 kg) de material (roca encajonate, vetas de cuarzo) y realizando los mismos procedimientos en una extensa campaña de campo, que duró un mes, seguida de múltiples visitas (1–2 semanas) al área de estudio. Asimismo, la preparación de muestras para realizar los diversos estudios analíticos presentados se hizo utilizando las instalaciones de laboratorio SepLab del Centro de

Geociencias UNAM y del Instituto de Geología (ERNO) usando las técnicas establecidas y descritas en el Apéndice B1-B6.

Capítulo 3. Estudio geoquímico de balance masas del COGB

Homogeneidad geoquímica de los fluidos mineralizantes del cinturón de oro orogénico Caborca, NW de Sonora, México: Estudio de balance de masas de la alteración hidrotermal en rocas encajonantes (*Geochemical homogeneity of the mineralizing fluids from the Caborca Orogenic Gold Belt, NW Sonora, México: Mass balance study of hydrothermal alteration in host rocks*) publicado: Boletín de la Sociedad Geológica Mexicana (2012) 64(1). Autores: Aldo Izaguirre, Alexander Iriondo, Juan A. Caballero-Martínez, Francisco Moreira-Rivera, Enrique Espinoza-Arámburu.

• Objetivos: Auxiliarse de este estudio para hacer una caracterización de la alteración hidrotermal orogénica presente en la roca encajonante a lo largo del COGB (Izaguirre et al., 2012). Determinar los elementos geoquímicos característicos de la alteración asociada a los depósitos de oro orogénico del COGB. Encontrar el grado de homogeneidad geoquímico de la mineralización. Delimitar la extensión areal del COGB usando las nuevas ocurrencias caracterizadas por el conjunto de estos estudios. Evaluar la idea de asociar el origen de la mineralización a un solo periodo tectónico compresivo y orogénico.

• Estudios: Se realizó un estudio geoquímico de balance de masas usando pares de roca fresa y roca alterada, con el objetivo de cuantificar geoquímicamente las concentraciones de elementos mayores, traza y preciosos que fueron adicionados (enriquecidos) a la roca encajonante durante el paso de fluidos mineralizantes, que formaron las vetas auríferas orogénicas. A la inversa, se obtuvo el cálculo geoquímico de elementos extraídos (empobrecidos) en la roca encajonante.

Este estudio se complementó con un análisis de correlación geoquímica bivariable de las vetas auríferas. Además, se realizó una caracterización de la paragénesis mineral usando la técnica de microscopía electrónica (SEM-EDS) en conjunto con petrografía y mineragrafía y con el uso de luz ultravioleta.

Boletín de la Sociedad Geológica Mexicana
Volumen 64, núm. 1, 2012, p. 119-153

Homogeneidad geoquímica de la alteración hidrotermal del cinturón de oro orogénico del NW de Sonora, México: Estudio de balance de masas en rocas encajonantes de la mineralización

Aldo Izaguirre[1,*], Alexander Iriondo[1, 2], Juan Antonio Caballero-Martínez[3], Francisco Moreira-Rivera[3], Enrique Espinosa-Arámburu[3]

[1] Centro de Geociencias, Universidad Nacional Autónoma de México, Campus Juriquilla, Boulevard Juriquilla 3001, Juriquilla, 76230, Querétaro, México
[2] Department of Geological Sciences, Jackson School of Geosciences, The University of Texas at Austin, Austin, 78712, Texas, EUA
[3] Servicio Geológico Mexicano, Boulevard Felipe Ángeles km 93.50-4, Colonia Venta Prieta Pachuca, 42080, Hidalgo, México

[*] aldoizapo@gmail.com

Resumen

Un estudio geoquímico de balance de masas, combinado con otros de carácter multidisciplinario (petrografía, correlación geoquímica bivariable de Au y Ag e inclusiones minerales en pirita y oro nativo) en rocas encajonantes alteradas y en vetas de cuarzo presentes a lo largo del Cinturón de Oro Orogénico Caborca (COOC), permitieron evaluar el grado de homogeneidad geoquímica de los fluidos que generaron la alteración hidrotermal y las vetas auríferas que componen la mineralización en el NW de Sonora, México.

Los resultados del estudio de balance de masas, realizado mediante el método de isocona combinando geoquímica de roca fresca y alterada de 20 localidades del COOC, muestran que la mayoría de las rocas encajonantes (> 50 %) se enriquecieron en los compuestos y elementos K_2O, W, Cu, Pb, Mo, Tl, Be, Zn, V, Sb, Ag, Sn, SiO_2, Se, Ni y FeO. Por lo contrario, el balance de masas muestra un empobrecimiento en los elementos Ca, Y, Na, Ho, Co, Sr, Yb, Mn, Dy, Er y Tb. Este consistente patrón de enriquecimiento y empobrecimiento encontrado en las muestras recolectadas en toda la extensión del COOC (~400 km de largo y ~60-80 km de ancho) sugiere un alto grado de homogeneidad de la alteración originada por los fluidos mineralizantes.

Los estudios petrográfícos de las rocas encajonantes frescas y alteradas sugieren que la alteración hidrotermal consistió principalmente en silicificación, sericitización, cloritización, epidotización y piritización. El estudio geoquímico bivariable de Au y Ag, realizado en vetas de cuarzo, indica una estrecha correlación (positiva) con los elementos que sufrieron mayor enriquecimiento en el estudio de balance de masas. De esta manera, estos pudieran proporcionar una guía geoquímica útil en la exploración mineral de Au en la región.

Por otro lado, en cristales de pirita y oro nativo de vetas de cuarzo se encontraron múltiples inclusiones minerales de oro y plata nativos, galena, covelita, esfalerita, molibdenita, scheelita y turmalina que explicarían, mineralógicamente, los enriquecimientos elementales detectados por los métodos geoquímicos empleados en este estudio.

Finalmente, la homogeneidad geoquímica del fluido mineralizante sugerida en este estudio permitiría proponer un evento coetáneo de mineralización de gran envergadura para gran parte del NW de Sonora (vetas de cuarzo con oro de tipo orogénico) durante el periodo compresivo laramídico que se desarrolló durante el Cretácico tardío al Terciario temprano.

Palabras clave: Balance de masas, homogeneidad, alteración hidrotermal, mineralización, oro orogénico, Sonora, México, método de isocona, vetas de cuarzo, microscopia electrónica, correlación bivariable.

Abstract

A geochemical mass balance study, combined with petrography, bivariate Au and Ag geochemical analysis, and inclusion study

in pyrites and native gold, was performed on a suite of hydrothermally altered host rocks and contemporaneous quartz veins from the Caborca Orogenic Gold Belt in NW Sonora, Mexico (COOC; by its abbreviations in Spanish: Cinturón de Oro Orogénico Caborca). These combined studies helped evaluating the geochemical homogeneity of the mineralizing fluids that formed the alteration envelopes and the auriferous quartz veins in the entire area occupying the COOC (~400 km long and ~60-80 km wide belt).

The isocon statistical technique used in the mass balance study was applied on 20 pairs of mayor and trace element geochemical data of altered and fresh rock samples. The results show that the majority (>50 %) of the altered host rocks are enriched in K_2O, W, Cu, Pb, Mo, Tl, Be, Zn, V, Sb, Ag, Sn, SiO_2, Se, Ni and FeO, and are clearly depleted in Ca, Y, Na, Ho, Co, Sr, Yb, Mn, Dy, Er and Tb. The similar pattern of enrichment and depletion was shown by most of the studied samples suggesting a high degree of geochemical homogeneity of the mineralizing fluids.

Petrography on both the altered and fresh rocks indicates that the hydrothermal alteration primarily consisted of silicification, sericitization, chloritization, epidotization and pyritization. The bivariate Au and Ag geochemical studies, done in auriferous quartz veins, show a strong positive correlation between these two elements and the enriched elements shown by the mass balance study on the altered host rocks. Therefore, these elements could be utilized as a geochemical exploration guide to targeting orogenic gold deposits in the region. Multiple inclusions of native gold and silver, galena, covellite, sphalerite, molybdenite, scheelite and tourmaline were encapsulated in pyrite and native gold grains in the quartz veins. Presence of these mineral occurrences explains most of the elemental anomalies obtained geochemically on the quartz veins and altered host rocks.

In conclusion, the geochemical homogeneity of the mineralizing fluid, proposed in this study, implies that the mineralization (Au-rich quartz veins) and associated alteration assemblages were part of a large-scale event synchronous with the Laramide orogeny when compressional tectonism was active during Late Cretaceous to Early Tertiary time.

Keywords: Mass balance, homogeneity, hydrothermal alteration, mineralization, orogenic gold, Sonora, México, isocon method, quartz veins, electron microscopy, bivariate correlaction.

1. Introducción

El siguiente trabajo presenta un estudio geoquímico de balance de masas de la alteración hidrotermal presente en las rocas encajonantes del Cinturón de Oro Orogénico Caborca (COOC), zona localizada al NW de Sonora, México (Figura 1). La denominación de COOC se presenta en este trabajo para comunicar y facilitar el manejo cuando se refiere a la mineralización aurífera de tipo oro orogénico en el NW de Sonora. El objetivo principal de este estudio ha sido el evaluar la hipótesis que asume una homogeneidad geoquímica de los fluidos hidrotermales mineralizantes durante la génesis de la mineralización de tipo orogénico a largo del COOC. Dicha homogeneidad será evaluada por medio de (1) un estudio geoquímico de balance de masas, (2) un análisis de correlación bivariable de los elementos químicos de las vetas de cuarzo del COOC, (3) petrografía de las rocas encajonantes frescas y alteradas (Figuras 2, 3 y 5; Tabla 1), y (4) la caracterización de microscopía electrónica de barrido con espectroscopía de energía dispersiva (SEM-EDS) de inclusiones minerales encapsuladas en granos de pirita y oro nativo.

Otro objetivo de este estudio de balance de masas es determinar la proporción de enriquecimiento, empobrecimiento e inmovilidad de elementos mayores, traza y preciosos de las muestras encajonantes de la mineralización utilizando pares de roca fresca y alterada. Esto se logra calculando los incrementos y decrementos en las concentraciones de cada elemento de la roca fresca (original) con respecto a la roca alterada por el proceso hidrotermal mineralizante. Para encontrar dichos cambios se usó el concepto de diagramas de isocona propuesto por Grant (1986) y que se presentará en este trabajo.

2. Estudios previos de la mineralización de tipo orogénico en el NW de Sonora

Los primeros estudios publicados en relación con el área que abarca el Cinturón de Oro Orogénico Caborca (COOC) fueron de carácter regional, con poco detalle, y consistieron en un reconocimiento de la geología estructural y geoquímica de la mineralización que sirvieron para delimitar la extensión y relaciones de Au-Ag entre las expresiones minerales de este cinturón (Silberman *et al.*, 1987, 1988). Sin embargo, en estos estudios se incluyeron depósitos epitermales u otras tipologías de yacimientos dentro de una inmensa área, mucho mayor a la actualmente propuesta en este estudio (Figura 1). Albinson (1989) realizó un estudio regional de inclusiones fluidas determinando que las vetas de cuarzo con Au son de tipo mesotermal, tipología que actualmente se conoce como oro orogénico. Estudios más recientes y de más detalle han permitido caracterizar temporal y geoquímicamente algunas zonas mineralizadas del COOC con el objetivo de contextualizar la mineralización y proponer su paragénesis. Estas zonas

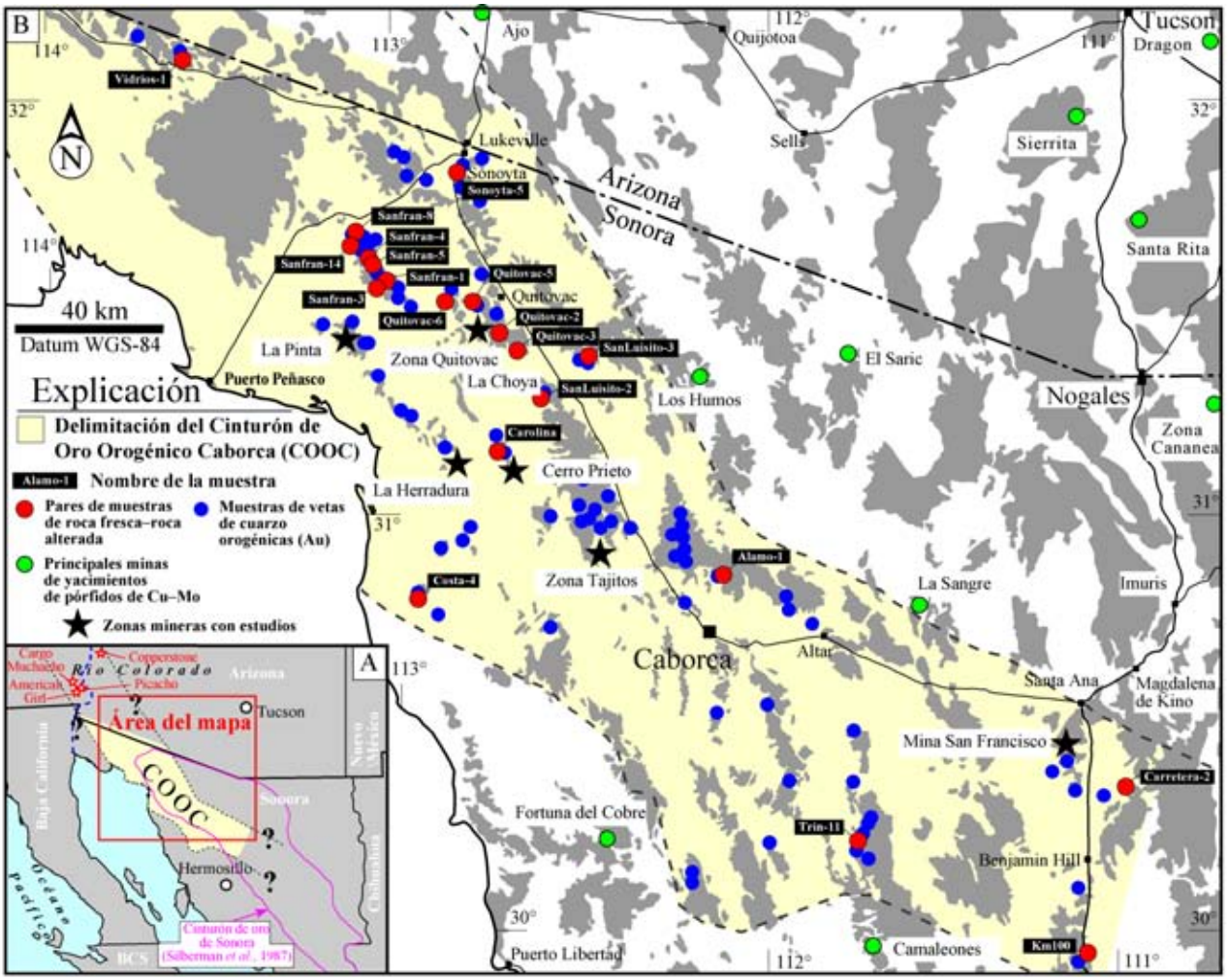

Figura 1. Localización de los pares de muestras de roca encajonante fresca y alterada para la realización del estudio de balance de masas en el Cinturón de Oro Orogénico Caborca (COOC), NW de Sonora, México. Afloramientos de cerros y sierras de roca firme en color gris y en blanco valles de sedimentos no consolidados. Polígonos del mapa tomados de Iriondo (2001).

mineralizadas (Figura 1) incluyen la Mina San Francisco-Llano (Changkuon, 1990; Pérez-Segura *et al*., 1996; Araiza-Martínez, 1998; Poulsen *et al*., 2008), Zona Quitovac-La Choya (Durgin y Terán, 1996; Iriondo y Atkinson, 2000; Iriondo, 2001), Zona Tajitos (Noriega-Martínez, 2006), La Pinta (Araux-Sánchez, 2000) y La Herradura-Cerro Prieto (Quintanar-Ruíz, 2008; Ornelas-Macías y Verdugo-Noriega, 2009). Esta región mineralizada de Au (COOC) presenta las siguientes características:

1. Edades de mineralización del Cretácico tardío-Terciario temprano obtenidas por medio de estudios geocronológicos en sericita o mica blanca (K-Ar y Ar-Ar; Pérez-Segura *et al*., 1996; Iriondo y Atkinson, 2000; Araux-Sánchez, 2000; Iriondo, 2001) y magnetita o pirita (Re-Os; Quintanar-Ruíz, 2008).
2. El estudio de los fluidos mineralizantes, mediante la medición de inclusiones fluidas atrapadas en el cuarzo de las vetas, indican temperaturas medias de precipitación de ~260-370 ºC, salinidades bajas (~3 % en peso equivalente de NaCl) y contenidos altos en CO_2 (*p.e.*, Albinson, 1989; Pérez-Segura *et al*., 1996; Noriega-Martínez, 2006; Quintanar-Ruíz, 2008).
3. Cálculos termobarométricos sugieren presiones litostáticas de ~1.1 kbar que han permitido calcular profundidades medias de precipitación de las vetas de ~3.5-4.5 km (Noriega-Martínez, 2006).
4. Las firmas isotópicas (O, H, S y C) indican que los fluidos son de origen metamórfico, característico de la tipología de yacimientos minerales de oro orogénico (Quintanar-Ruíz, 2008).

En general, estos estudios también sugieren que este tipo de mineralización se precipitó, preferentemente, a lo largo de fallamientos y fracturas bien establecidas (zonas de debilidad). Por último, recientemente Iriondo y Premo (2010) sugirieron que los fluidos de mineralización de Au en el NW de Sonora se canalizaron precisamente por una zona de debilidad estructural que coincide espacialmente con los límites de la provincia de basamento paleoproterozoica

Yavapai.

3. Muestreo de las rocas encajonantes y vetas de cuarzo del COOC

El muestreo consistió en colectar los pares de roca encajonate fresca y alterada y las vetas de cuarzo del Cinturón de Oro Orogénico Caborca (COOC) (Figura 1). Los puntos estratégicos a muestrear se seleccionaron empleando información de las publicaciones previas y las cartas geológico-mineras del Servicio Geológico Mexicano (SGM) a escala 1:250,000 del NW de Sonora. También los reportes en texto publicados por el SGM, donde se han ubicado minas o zonas mineralizadas con las características paragenéticas comunes del oro orogénico (vetas de cuarzo, carbonatos de calcio y/o hierro, sericita, mica blanca, clorita, epidota, pirita y galena, principalmente). Durante el muestreo se cubrió una proporción amplia de ocurrencias de la mineralización del COOC, permitiendo un muestreo espacialmente representativo (Figura 1) colectando 20 pares de muestras de roca encajonante fresca y alterada, que fueran representativos de la mineralización. También se colectaron muestras en 102 vetas de cuarzo (Figura 1), que incluyeron algunos fragmentos de la roca encajonante alterada, como comúnmente se hace en el muestreo de tipo canal-esquirla. Las muestras de roca alterada se colectaron en los halos de alteración generados por los fluidos precursores de las vetas de Au del COOC. Las rocas frescas fueron colectadas alejadas de dicha zona alterada hasta encontrar roca visualmente fresca, que en promedio resultó comúnmente ~10 m a partir del fin del halo de alteración generado por las vetas de cuarzo. Cabe aclarar que en algunos de estos puntos de muestreo existe cierto grado de enriquecimiento supergénico, producto, principalmente, del intemperismo de pirita. Este proceso pudo ser debido a variaciones del nivel freático, seguramente originadas durante procesos de oxidación-reducción en el periodo extensional (basculamientos) desde el Mioceno a la actualidad y que generó mineralogías secundarias como carbonatos y silicatos de cobre (*p.e.*, malaquita, azurita, crisocola), wulfenita y óxidos de hierro (*p.e.*, goethita).

Las observaciones de campo, realizadas durante el muestreo, permitieron trazar el perímetro aproximado que presenta geográficamente el Cinturón de Oro Orogénico Caborca (COOC; Figura 1). El COOC tiene dimensiones aproximadas de 400 km de largo y 60-80 km de ancho con una orientación NW-SE. El límite del muestreo, hacia la porción norte, fue la frontera política con los Estados Unidos (Arizona). Sin embargo, la mineralización de tipo orogénico aparentemente continúa, en dirección NW, hacia el estado de California, donde se han reportado ocurrencias de oro orogénico en la zona minera de Cargo Muchacho, American Girl y, posiblemente, Picacho y Copperstone (Branham, 1988; Figura 1A). El límite hacia el sureste del COOC se localiza a ~50 km al SE del poblado de Benjamín Hill donde terminan las ocurrencias de mineralización de esta tipología debido a la presencia de rocas volcánicas oligoceno-miocénicas que las cubren. Finalmente, hacia el NE y SW del cinturón, el límite está estimado por la presencia de otras tipologías de yacimientos (*p.e.*, pórfidos cupríferos) con paragénesis minerales diferentes a las presentes en el COOC (Figura 1B).

4. Técnicas analíticas

4.1. Preparación de las muestras

La preparación de rocas encajonantes y vetas de cuarzo consistió en triturar ~3 kg de muestra representativa de cada localidad a estudiar (Figura 1). Para el triturado se empleó una quebradora de gran capacidad marca *Chipmuck* que fue previamente limpiada con cada una de las muestras para evitar al máximo la contaminación entre muestras. Del material quebrado resultante se realizó un cuarteo para obtener ~150 g de gravilla que se utilizó en el proceso final de pulverizado usando el sistema de pulverizado *Shatter Box* con contenedores de alúmina para evitar contaminación metálica. Sin embargo, para el pulverizado de las muestras de vetas de cuarzo se utilizó un contenedor de carburo de tungsteno con anillo interno para agilizar el proceso. De cada muestra se obtuvieron ~100 g de polvo con un tamaño de partícula inferior a las ~74 micras, el cual se envió para su análisis a los laboratorios del Centro Experimental Chihuahua pertenecientes al Servicio Geológico Mexicano.

Las muestras se analizaron por medio de diferentes técnicas analíticas para determinar las concentraciones de elementos mayores, traza y preciosos (Tablas A1 y A2 del Apéndice A). Se usaron las técnicas analíticas de espectrometría de emisión atómica con fuente de plasma de acoplamiento inductivo (ICP–AES, por sus siglas en inglés) para analizar Al, Al_2O_3, As, Ba, Be, Bi, CaO, Co, Cr, Cu, FeO, Fe_2O_3, K_2O, MgO, MnO, Mo, Na_2O, Ni, P_2O_5, Pb, Sb, SiO_2, Se, Sn, Sr, Te, TiO_2, Tl, V, W, Zn. También se empleó la espectrometría de masas con fuente de plasma de acoplamiento inductivo (ICP–MS, por sus siglas en inglés) para obtener Ag, Ce, Dy, Eu, Gd, Ho, Ir, La, Lu, Nd, Os, Pd, Pr, Pt, Rh, Ru, Sc, Sm, Tb, Th, Tm, U, Y, Yb. Por otro lado, la pérdida por calcinación (probablemente, y en mayor medida, se componga de H_2O, contenidos orgánicos, carbonato de calcio y dióxido de carbono) se obtuvo al calentar la muestra a 950 ºC. Para el caso de la medición del Au se realizó copelación al fuego (*fire assay*) para obtener mejores resultados. Esto debido a que el oro de esta región se caracteriza por ser de grano fino, o criptocristalino, esta característica lo hace invisible, e inclusive cuando se emplea lupa de aumento.

4.2. Método de balance de masas

El estudio de balance de masas se elaboró utilizando

el método de isocona propuesto por Grant (1986, 2005), técnica basada en los estudios pioneros de Gresens (1967). Esta consiste en emplear un simple gráfico binario "x–y" donde, por costumbre universal, el eje "x" es igual a la concentración de elementos químicos medidos en la roca fresca y el eje "y" es igual a la concentración de elementos medidos en la roca alterada. Sobre este gráfico, se busca visualmente, o por medios estadísticos, una correlación entre los elementos que han tenido inmovilidad o que fueron inertes (argumento principal del método) durante el fenómeno geológico de alteración. De esta forma se elige la línea de isocona que se traza a través del origen (0,0) y los elementos inertes elegidos (*p.e*., Figura 5). El campo por encima de la línea de isocona incluye o abarca los elementos que sufrieron enriquecimiento elemental, mientras que los del campo inferior a la isocona indican empobrecimiento. Este método ha sido útil en los estudios de balance de masas y de movilidad de elementos mayores, traza y preciosos en depósitos minerales de oro orogénico en Nueva Zelanda (Pitcairn *et al*., 2006) y China (Wei *et al*., 2001). En estos estudios, se han determinado los elementos característicos de la alteración hidrotermal que han servido como una guía de exploración y en el cálculo de predicción de volúmenes de roca mineralizada de Au. Así mismo, otras tipologías de yacimientos (*p.e*., skarn) también han sido estudiadas con este método, en donde se ha tratado de determinar los mismos aspectos antes mencionados (Lentz, 2005).

El estudio de balance de masas se realizó enteramente con el programa computacional GEOISO (Coelho, 2006) y se generaron gráficos binarios de la geoquímica de la roca fresca versus la roca alterada (Figura 5) para cada par de las muestras estudiadas. En la elaboración de estos gráficos, las concentraciones químicas de los elementos expresadas en diferentes unidades (*p.e*., ppm; % en peso) se escalaron de forma arbitraria para conseguir treinta unidades en cada eje, multiplicando cada elemento por factores de normalización incluidos en el programa computacional. Cabe aclarar que cuando los valores de las concentraciones elementales de las muestras se encontraron por debajo del nivel de detección, se utilizó la mitad de ese valor (N.D.) para poder incluirlos en los diagramas de isocona (Tabla A1 del Apéndice A). Con ayuda de los algoritmos del programa se seleccionó la mejor isocona posible (línea de inmovilidad elemental), según los parámetros de correlación y error (Figura 5; línea en color verde). Por medio de estos algoritmos se obtuvieron las estimaciones de empobrecimiento, enriquecimiento e inmovilidad elemental que se muestran en las Figuras 6, 7, 8 y Tablas A3 a A5 del Apéndice A.

4.3. Método de correlación geoquímica bivariable

Con los datos geoquímicos obtenidos de las vetas se realizó un estudio de análisis de correlación geoquímica bivariable utilizando el paquete computacional *Statistical Package for Social Sciencies* (SPSS v19) para determinar el coeficiente de correlación "r" entre el elemento clave Au y los otros elementos traza y preciosos (Figura 9 y Tablas A6 del Apéndice A). Los coeficientes de correlación varían entre -1 y +1, y cuando r = 0, significa una completa independencia entre dos elementos analizados; o bien, cuando r = +1, indica una relación funcional directa. Por último, cuando r = -1 representa una correlación funcional inversa (*p.e*., Davis, 1986). Cabe aclarar que al momento de realizar los cálculos para algunas de las muestras, se utilizó el valor del límite de detección de los elementos. Los valores de los límites de detección se encuentran listados en la Tabla A2 del Apéndice A.

4.4. Técnica de SEM-EDS

Los estudios de microscopía electrónica de barrido con detector de espectroscopía de rayos X de energía dispersiva (SEM-EDS, por sus siglas en inglés) se realizaron en granos milimétricos de pirita, oro y galena de algunas muestras de vetas de cuarzo del Cinturón de Oro Orogénico Caborca (COOC). El procedimiento consistió en la elaboración de probetas de resina epóxica, montando cristales de pirita y galena de algunas de las muestras estudiadas en cinta doble cara, para posteriormente verter la resina epóxica en un molde y capturar los granos. Después del endurecimiento de las probetas se desbastó y pulió hasta llegar aproximadamente a la mitad de los granos para obtener un área máxima de exposición de los mismos. Por otro lado, los granos de oro de las muestras observadas se adhirieron con pintura de carbón conductora de electrones en unas pequeñas pastillas metálicas que sirven para su transporte y análisis dentro del SEM.

Para la obtención de imágenes y espectros de energía dispersiva por medio de análisis puntual de las muestras de pirita y galena se utilizó un SEM-EDS de marca JEOL5800LV. Para las muestras de oro se empleó un FEI Quanta 450 FEG, ambos, equipos del laboratorio de microsonda y microscopia electrónica del *U.S. Geological Survey, Federal Center*, en Denver, Colorado, Estados Unidos. Los datos fueron reducidos con el paquete computacional NSS 2.3 *Microbeam X-ray analysis* de Thermo Scientific, del cual se obtuvieron espectros de elementos químicos y composiciones de los análisis puntuales realizados sobre las superficies de los minerales.

5. Resultados

5.1. Estudios petrográficos de luz transmitida en la roca encajonante

Mediante un estudio petrográfico de las 20 muestras de roca encajonante fresca y alterada se detectó que la alteración cuarzo-sericítica que solo se observa en algunas de las muestras megascópicamente, en el campo, se encuentra presente microscópicamente en la totalidad de las rocas estudiadas (Tabla 1 y Figuras 2 a 4). Algunos ejemplos

Tabla 1. Resumen petrográfico de la mineralogía de las rocas encajonantes frescas y alteradas del Cinturón de Oro Orogénico Caborca, NW Sonora, México.

Muestra Localidad	Tipo de roca	Edad	Roca fresca Mineralogía primaria	Roca alterada Mineralogía de alteraración
Alamo-1	Arenisca	Jurásico temprano	Qtz+Pl+Bt	Ser+Ep+Clr
Carolina-1	Ortogneis	Paleoproterozoico	Kfs+Qtz+Pl+Bt	Ser+Qtz
Carretera-2	Granito	Cretácico-Terciario	Kfs+Pl+Qtz+Bt±Op	Ser±Op
Costa-4	Granito	Terciario temprano	Kfs+Pl+Qtz+Bt	Ser+Qtz
km100	Ortogneis	Mesoproterozoico	Kfs+Pl+Qtz+Bt	Ser+Qtz±Op
Quitovac-2	Granito	Jurásico temprano	Kfs+Pl+Qtz+Bt±Op	Ser+Qtz±Op
Quitovac-3	Granito	Jurásico temprano	Kfs+Pl+Qtz+Bt±Ttn±Apt±Op	Ser+Qtz±Op
Quitovac-5	Granodiorita	Cretácico tardío	Pl+Kfs+Qtz+Bt+Hbl±Op	Ser+Qtz±Op
Quitovac-6	Granito	Cretácico tardío	Kfs+Pl+Qtz+Bt	Ser+Qtz
Sanfran-1	Granito	Cretácico tardío	Kfs+Pl+Qtz+Bt±Apt±Ttn	Ser+Qtz+Clr±Op
Sanfran-3	Granito	Cretácico tardío	Kfs+Pl+Qtz+Bt±Apt±Op	Ser+Qtz±Op
Sanfran-4	Granito	Cretácico tardío	Kfs+Pl+Qtz+Bt±Apt±Op	Ser±Op
Sanfran-5	Granodiorita	Cretácico tardío	Pl+Kfs+Qtz+Bt±Op	Ser+Qtz±Op
Sanfran-8	Ortogneis	Paleoproterozoico	Pl+Qtz+Kfs+Hbl+Bt	Ser+Qtz
Sanfran-14	Ortogneis	Paleoproterozoico	Pl+Qtz+Kfs+Hbl+Bt±Op	Ser+Qtz±Op
Sanluisito-2	Granito	Jurásico temprano	Kfs+Pl+Qtz+Bt±Apt±Op	Ser+Qtz±Op
Sanluisito-3	Granodiorita	Jurásico temprano	Pl+Qtz+Kfs+Bt±Ttn	Ser+Qtz
Sonoyta-5	Granito	Cretácico tardío	Kfs+Pl+Qtz+Bt	Ser+Qtz+Ep+Clr±Op
Trin-11	Ortogneis	Paleoproterozoico	Kfs+Pl+Qtz+Bt	Ser+Qtz
Vidrios-1	Ortogneis	Paleoproterozoico	Kfs+Pl+Qtz+Bt±Op	Ser+Qtz±Op

Ap = apatito, Bt = biotita, Clr = clorita, Ep = epidota, Hbl = hornblenda, Kfs = feldespato, Op = opaco, Pl = plagioclasa, Qtz = cuarzo, Ser = sericita (mica blanca), Ttn = titanita. Signo +: Mineral componente, signo ±: Mineral accesorio.

de los minerales de alteración hidrotermal (sericita, cuarzo, epidota, clorita y minerales opacos) se pueden apreciar en las fotografías de las figuras antes mencionadas. Así mismo, se pueden ver los fantasmas o relictos de mineral desaparecidos asociados a la pérdida (destrucción), principalmente de los minerales ferromagnesianos y plagioclasas en los ejemplares de roca alterada. Esta alteración no es propiamente homogénea ya que se observan, en la mayoría de las muestras, parches de sericita y mosaicos de cuarzo. En la Tabla 1 se presenta un resumen de la mineralogía primaria en la roca fresca (original) y de la mineralogía de alteración presente en la roca alterada como resultado del hidrotermalismo. También se señala una clasificación litológica general y la edad del protolito definida a partir de estudios geocronológicos y de correlaciones con otras rocas similares fechadas en otros lugares del NW de Sonora.

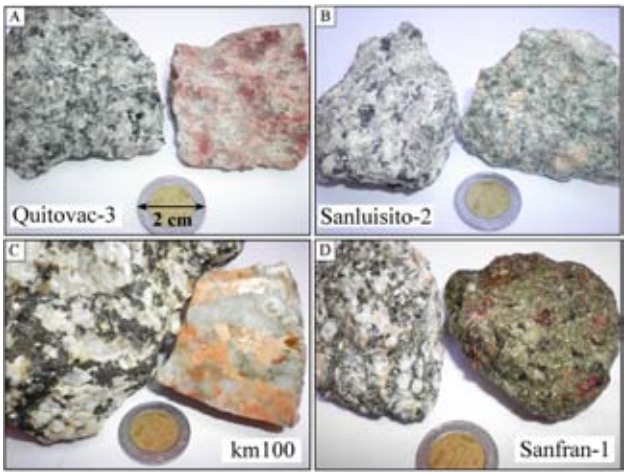

Figura 2. Fotografías de rocas encajonantes graníticas frescas (lado izquierdo de cada fotografía) y alteradas (lado derecho de cada fotografía) representativas del Cinturón de Oro Orogénico Caborca (COOC). En la fotografía A (muestra Quitovac-3) se puede observar una coloración rojiza de la roca alterada que indica la oxidación de los ferromagnesianos; también se observa mica blanca de color verde (sericita) que es producto de alteración mineral asociada al hidrotermalismo. En la fotografía B (muestra Sanluisito-2) se puede ver una coloración verdosa que indica la presencia de mica blanca, como mineral de alteración. En la fotografía C (muestra km100) se pueden ver, en la roca fresca, ferromagnesianos (oscuros) y feldespatos frescos (gris claro) y en contraparte alterados en el ejemplar de roca alterada. Finalmente, en la fotografía D (muestra Sanfran-1) se puede ver abundante mica blanca color verdosa en la muestra alterada comparando con su correspondiente ejemplar de roca fresca.

5.2. Estudio geoquímico de balance de masas

Los 20 pares de muestras de roca encajonante fresca y alterada por los fluidos mineralizantes del Cinturón de Oro Orogénico Caborca (Figuras 1 y 2; Tabla A1 del Apéndice A) se analizaron geoquímicamente para cuantificar las concentraciones de elementos mayores, traza y preciosos. De esta manera se pudo realizar un estudio de balance de masas usando la técnica de diagramas de isocona propuesta

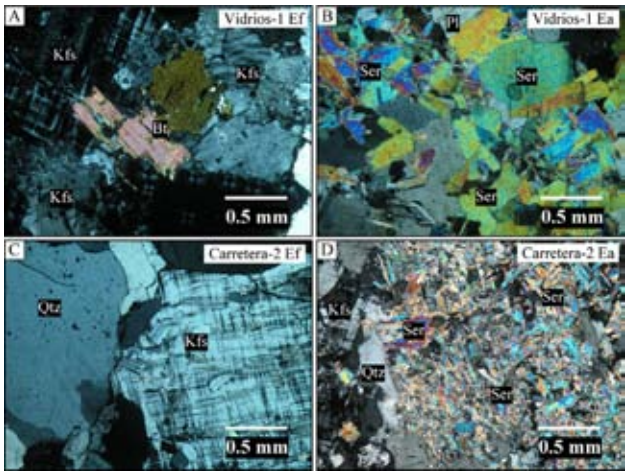

Figura 3. Fotomicrografías en luz polarizada analizada en sección delgada de rocas encajonantes frescas y alteradas por el hidrotermalismo en el Cinturón de Oro Orogénico Caborca (COOC). (A) Roca fresca gnéisica Vidrios-1 y (B) su contraparte alterada. (C) Roca fresca granítica Carretera-2 y (D) su contraparte alterada. Bt = biotita, Kfs = feldespato potásico (microclina), Pl = plagioclasa, Qtz = cuarzo, Ser = sericita (mica blanca).

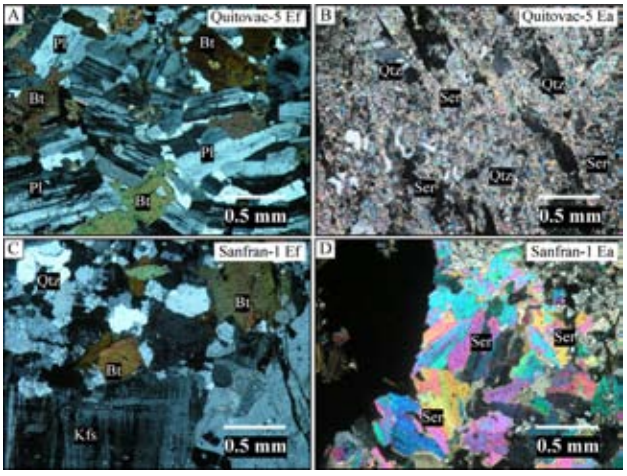

Figura 4. Fotomicrografías en luz polarizada analizada en sección delgada de rocas encajonantes frescas y alteradas por el hidrotermalismo en el Cinturón de Oro Orogénico Caborca (COOC). (A) Roca fresca microdiorítica Quitovac-5 y (B) su contraparte alterada. (C) Roca fresca granítica Sanfran-1 (D) su contraparte alterada. Bt = biotita, Kfs = feldespato potásico (microclina), Pl = plagioclasa, Qtz = cuarzo, Ser = sericita (mica blanca).

por Grant (1986).

En la Figura 5A-D, se muestran 4 ejemplos representativos de estos diagramas de isocona con sus correspondientes diagramas de barras (Figuras 6A–D) con los elementos más útiles para evaluar el fenómeno de alteración hidrotermal en el COOC. En estos diagramas, los elementos que grafican por encima de la isocona (campo sombreado de color gris) indican que fueron enriquecidos durante el proceso de alteración hidrotermal. Los elementos y compuestos K_2O, Cu, W, Mo, Pb, Be, Ag, Sb, V y Zn, y la pérdida por calcinación, señalados con una flecha punteada color rojo (Figura 5A), sufrieron un enriquecimiento de mayor envergadura en el total de las muestras del estudio. Por otro lado, los elementos que graficaron por debajo de la línea de isocona son los elementos que fueron empobrecidos durante el proceso de alteración hidrotermal, y están señalados con una línea punteada de color azul (Ca, Y, Na, Sr, Co, Mn y Dy).

El primer ejemplo de la Figura 5A corresponde a la muestra Sanfran-1 que es una roca granítica del Cretácico tardío (Tabla 1) que se localiza en la porción norte del COOC (Figura 1). En este ejemplo, la isocona se generó considerando los elementos Al_2O_3, Pd y Sn (elementos señalados en color verde como inmóviles) y forman un arreglo lineal con una muy buena correlación entre si (1.00 ± 0.041; Tabla A3 del Apéndice A). La línea de isocona también coincide con la constante de aluminio, elemento que por su baja solubilidad se considera como un elemento básicamente inerte en los estudios de balance de masas (Baumgartner y Olsen, 1995; Grant, 1986) y que es ideal para trazar, incluso por sí solo, la línea de isocona a través del origen. Sin embargo, de la totalidad de las muestras de este estudio, solo en un 60 % de los casos el Al_2O_3 muestra un comportamiento inerte, posiblemente debido a que la línea de isocona fue elegida por medios estadísticos, sin influencia del usuario, como sugieren Baumgartner y Olsen (1995) y Coelho (2006)

Los resultados de balance de masa indican que la muestra original (fresca) de la localidad Sanfran-1 tuvo una pérdida de masa de 21.3 % en la zona alterada (Tabla A3 del Apéndice A). El óxido mayor K_2O en la muestra Sanfran-1 se enriqueció y los fluidos incorporaron ~2.48 % de K_2O, lo que representa un incremento de ~0.87 veces o ~87 % su concentración con respecto al contenido en la roca fresca original (Tabla A3 del Apéndice A). El elemento Cu también fue enriquecido en ~621 ppm, lo que representa ~26 veces la concentración original de la roca fresca (Figura 6A). En contrapartida, el óxido mayor CaO se empobreció en 2.37 %, lo que representa casi el doble (~91 %) del CaO presente en la roca original. El elemento Y se empobreció en 2.38 ppm representando un poco más de la mitad (~54 %) del contenido inicial en la roca fresca. Por otro lado, la inmovilidad geoquímica para los elementos inertes es expresada como cero (Tabla A3 del Apéndice A). Sin embargo, en algunos elementos (*p.e.*, Os) puede que esta inmovilidad no sea representativa porque podría ser el resultado de la falta de precisión en las técnicas analíticas empleadas en su cuantificación. De esta manera, y sucesivamente, el empobrecimiento, enriquecimiento e inmovilidad se pueden leer con el resto de los elementos presentados en la Tabla A3 del Apéndice A.

La muestra granítica del Jurásico temprano Sanluisito-2 (Figuras 5B y 6B) se localiza hacia la zona centro del Cinturón de Oro Orogénico Caborca (Figura 1). De esta muestra se determinó estadísticamente una isocona con FeO, Sm y P_2O_5 (señalados en color verde). Éstos forman

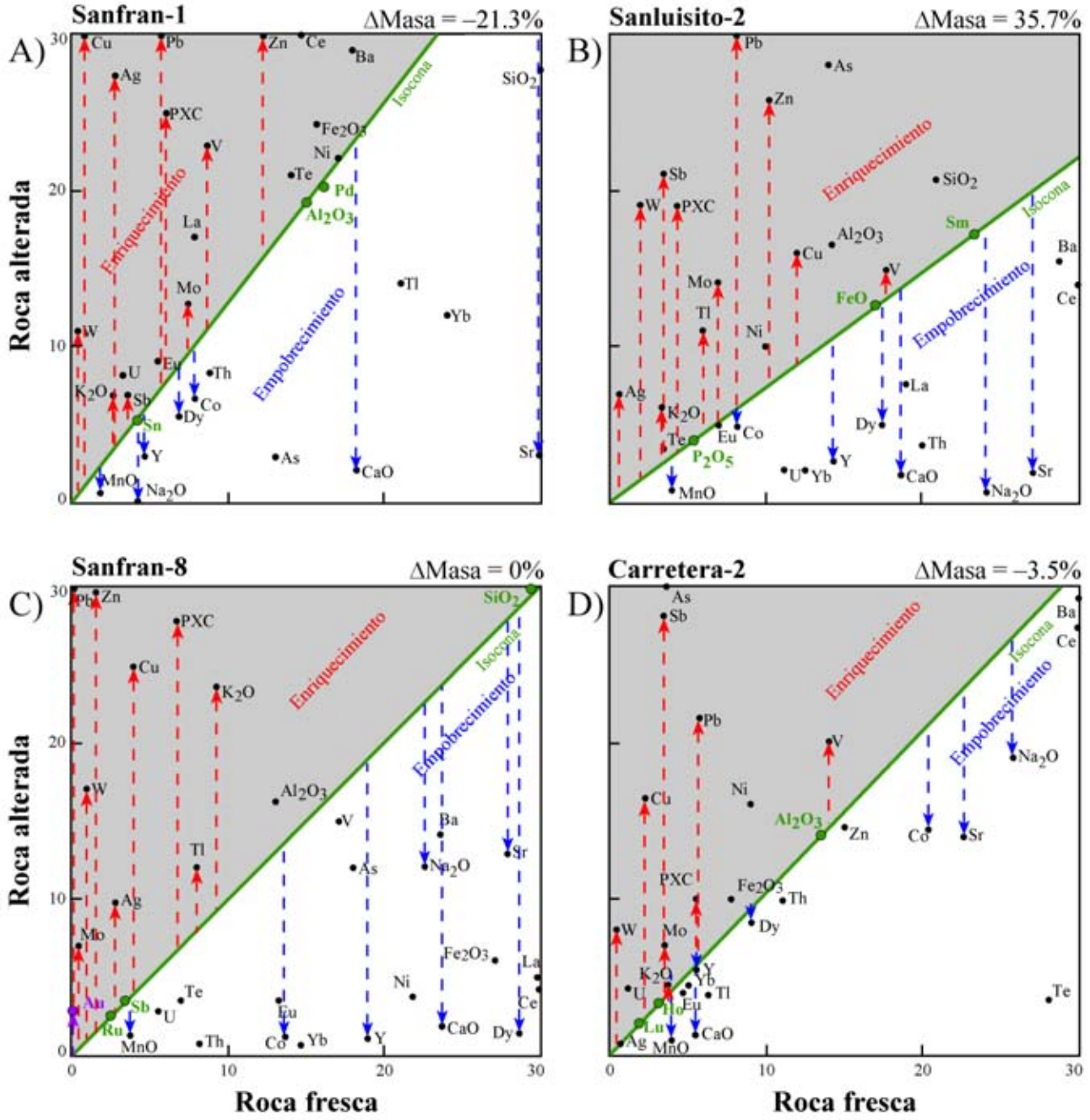

Figura 5. Diagramas de isocona de cuatro localidades representativas de zonas de alteración hidrotermal construidos a partir de elementos mayores y traza obtenidos en la roca encajonante fresca y alterada. La línea de isocona (línea de inmovilidad elemental en color verde) se encuentra dividiendo la tendencia de enriquecimiento (campo en gris) y empobrecimiento geoquímico (campo en blanco). Los elementos en verde fueron empleados para definir la línea de isocona. Las flechas rojas indican algunos de los elementos más característicos del enriquecimiento (K_2O, W, Cu, Pb, Mo, Tl, Zn, V, Sb y Ag), y la pérdida por calcinación (PXC). Por otra parte, las flechas azules indican los elementos más característicos del empobrecimiento elemental a lo largo del COOC (CaO, Na_2O, Sr, Y, Co, Dy, MnO). El punto y la flecha morada en el diagrama C indican enriquecimiento en Au. Diagramas graficados con el programa computacional GEOISO (Coelho, 2006).

un arreglo lineal con un coeficiente de correlación de 1.00 ± 0.003 (Tabla A3 del Apéndice A). En este caso, el aluminio no se comportó de forma inerte y presenta un pequeño grado de enriquecimiento que imposibilita usarlo en el cálculo de la isocona. De igual forma que en la descriptiva de la muestra anterior, se señalan con flechas punteadas en color rojo a los elementos que experimentaron una mayor proporción de enriquecimiento en el estudio, mientras que los elementos empobrecidos se señalan con flechas punteadas en color azul (Figura 5B). El elemento Tl se encuentra enriquecido ilustrándose que es uno de los elementos principales y representativos del enriquecimiento en las muestras del

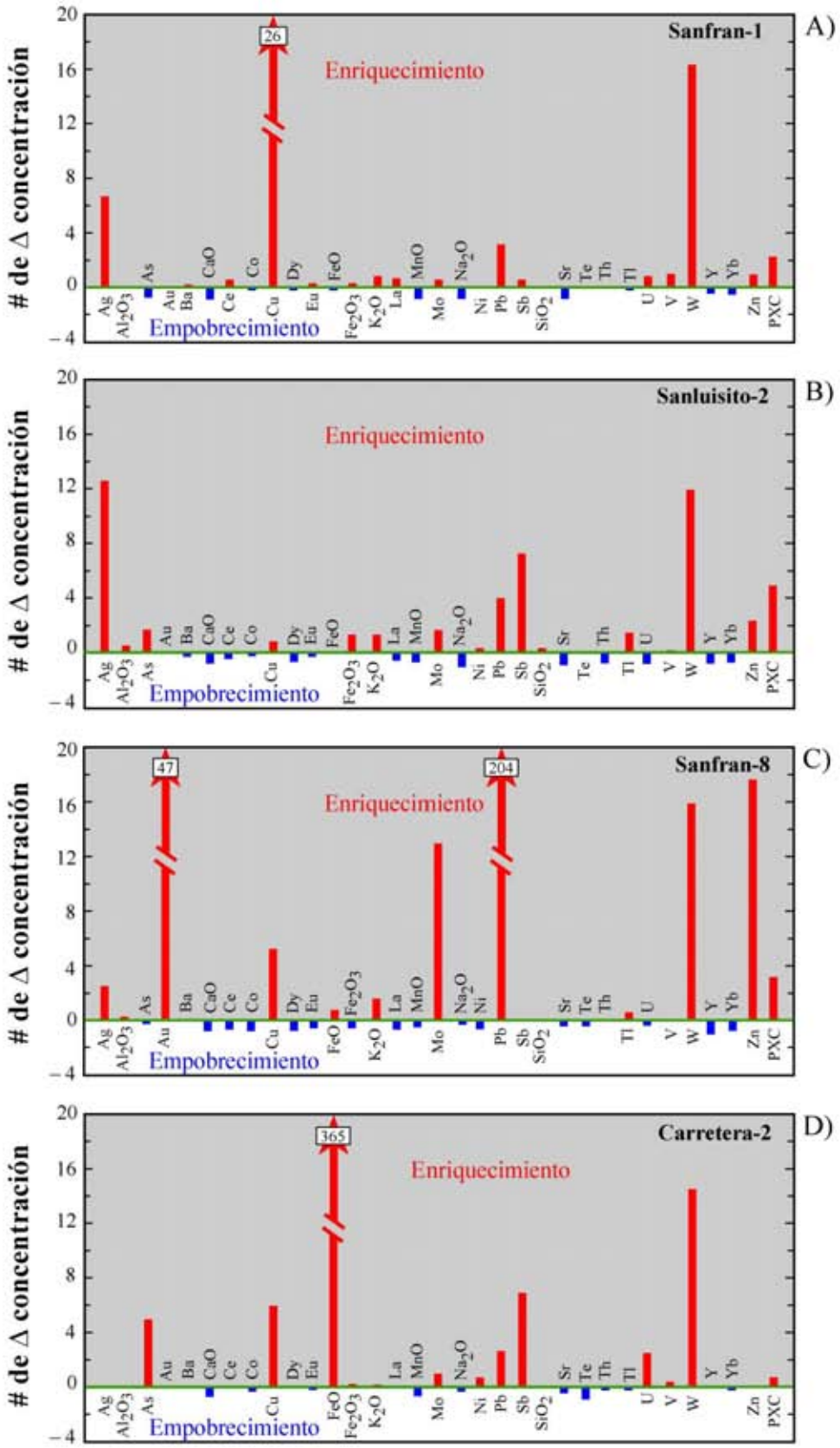

Figura 6. Histogramas A, B, C y D, correspondientes a los cuatro diagramas de isocona de la Figura 5A, B, C y D, respectivamente. Estos diagramas fueron construidos con el programa computacional GEOISO (Coelho, 2006). # de Δ concentración = número de veces que se enriqueció o empobreció cada elemento con respecto a su concentración original (roca fresca). Las barras con flecha roja indican el número de veces que se enriqueció ese elemento en particular.

conjunto de este estudio. Esta muestra alterada presenta una ganancia de 35.7 % con respecto al total de la masa de la roca fresca (Tabla A3 del Apéndice A). El óxido mayor K_2O se enriqueció en una mayor proporción que en la muestra anterior; en el orden de ~4.82 %, que implica ~1.5 veces (141 %) el contenido original en la roca (Figura 6B). En este caso, el enriquecimiento del Cu fue menor que en la muestra anterior ya que solo tuvo 9.71 ppm de aumento, que representa casi el doble del contenido (~80 %) en la roca fresca original. Por otra parte, el óxido mayor CaO se empobreció en 1.94 %, lo que representa ~77 % del CaO contenido en la roca fresca. También el Y se empobreció en 10.24 ppm, representando una disminución de ~76 % del contenido inicial.

La muestra Sanfran-8 (Figuras 5C y 6C) es una roca encajonante ortognéisica de edad paleoproterozoica localizada al norte del COOC (Figura 1) y de la cual se determinó una isocona con Ru, SiO_2 y Sb, con un coeficiente de correlación de 1.00 ± 0.0003 (Tabla A3 del Apéndice A). En esta muestra, el aluminio no se comportó de forma inerte presentando enriquecimiento, por lo que no fue seleccionado para formar parte de la isocona. También presenta enriquecimiento y empobrecimiento elemental en común con las otras muestras de este estudio (líneas punteadas en rojo y azul, respectivamente) y no presenta un cambio de masa considerable durante la alteración. Entre los elementos más enriquecidos se encuentran el Pb, que se presenta ~204 veces (Figura 6C) más concentrado que en la roca fresca (Tabla A3 del Apéndice A), el Au con ~47 veces (~ 4700 %) más de su concentración original, el Zn con ~18 veces más de su concentración original, y el W con 16 veces más de su concentración original. Por otro lado, los elementos más empobrecidos que presentó esta muestra fueron el Y, con un 97 % de pérdida con respecto a la roca original, y el Er y Pt, con un 96 % de pérdida con respecto a la roca original (fresca).

El último diagrama de isocona que se ejemplifica en la Figura 5 corresponde a la muestra Carretera-2 que es una muestra granítica de edad Cretácico tardío localizada al sur del Cinturón de Oro Orogénico Caborca (Figura 1). La línea de isocona de esta muestra se trazó con los elementos y compuestos con comportamiento inerte Al_2O_3, Lu y Ho, obteniendo un coeficiente de correlación de 1.00 ± 0.003 (Tabla A3 del Apéndice A). El aluminio, en este caso, se comportó como inerte y forma parte de la línea de isocona (Figura 5D). Esta muestra presenta un decremento de masa de ~3.5 % y un enriquecimiento y empobrecimiento elemental similar al de otras muestras de este estudio (líneas punteadas en rojo y azul, respectivamente). Entre los más enriquecidos se encuentran FeO, W, Sb, Cu y As, y entre los más empobrecidos, Te, MnO y CaO (Figura 6D).

Por su parte, en la Tabla 2 y Figura 7A se presenta un resumen de la totalidad de las muestras analizadas mediante este estudio geoquímico de balance de masas con un recuento semicuantitativo de la proporción de enriquecimiento, empobrecimiento e inmovilidad

Tabla 2. Resumen del balance de masas de la alteración hidrotermal en el Cinturón de Oro Orogénico Caborca, NW Sonora, México.

Elemento	Enriquecimiento %	Empobrecimiento %	Inmovilidad %
K_2O	90	10	0
PXC	85	15	0
W	85	15	0
Cu	85	15	0
Pb	75	25	0
Mo	75	15	10
Tl	70	25	5
Be	70	20	10
Zn	60	40	0
V	60	40	0
Sb	60	25	15
Ag	60	25	15
Sn	55	35	10
SiO_2	55	45	0
Se	55	35	10
Ni	55	45	0
FeO	55	35	10
U	50	50	0
TiO_2	50	35	15
Ir	50	30	20
Ce	50	45	5
Ba	50	50	0
Th	45	55	0
Te	45	55	0
Pr	45	55	0
MgO	45	55	0
Cr	45	55	0
Bi	45	35	20
As	45	55	0
Ru	40	40	20
Rh	40	40	20
La	40	55	5
Fe_2O_3	40	60	0
Cd	40	45	15
Al_2O_3	40	0	60
Sm	35	55	10
Sc	35	65	0
Pt	35	50	15
Pd	35	60	5
Nd	35	55	10
Gd	35	65	0
P_2O_5	30	55	15
Eu	30	70	0
Yb	25	75	0
Tm	25	60	15
Tb	25	70	5
Lu	25	65	10
MnO	20	75	5
Dy	20	75	5
Co	20	80	0
Au	20	25	55
Y	15	85	0
Sr	15	80	5
Na	15	85	0
Ho	15	85	0
Er	15	5	80
CaO	10	90	0
Os	0	0	100

Resumen porcentual obtenido con los resultados de Δ conc (Tabla A3 del Apéndice A).

*La inmovilidad elemental puede no ser representativa debido a las limitantes en las técnicas analíticas para la medición de la concentración de algunos elementos. Los datos sobre el área en color gris se pueden observar graficados en la Figura 7B.

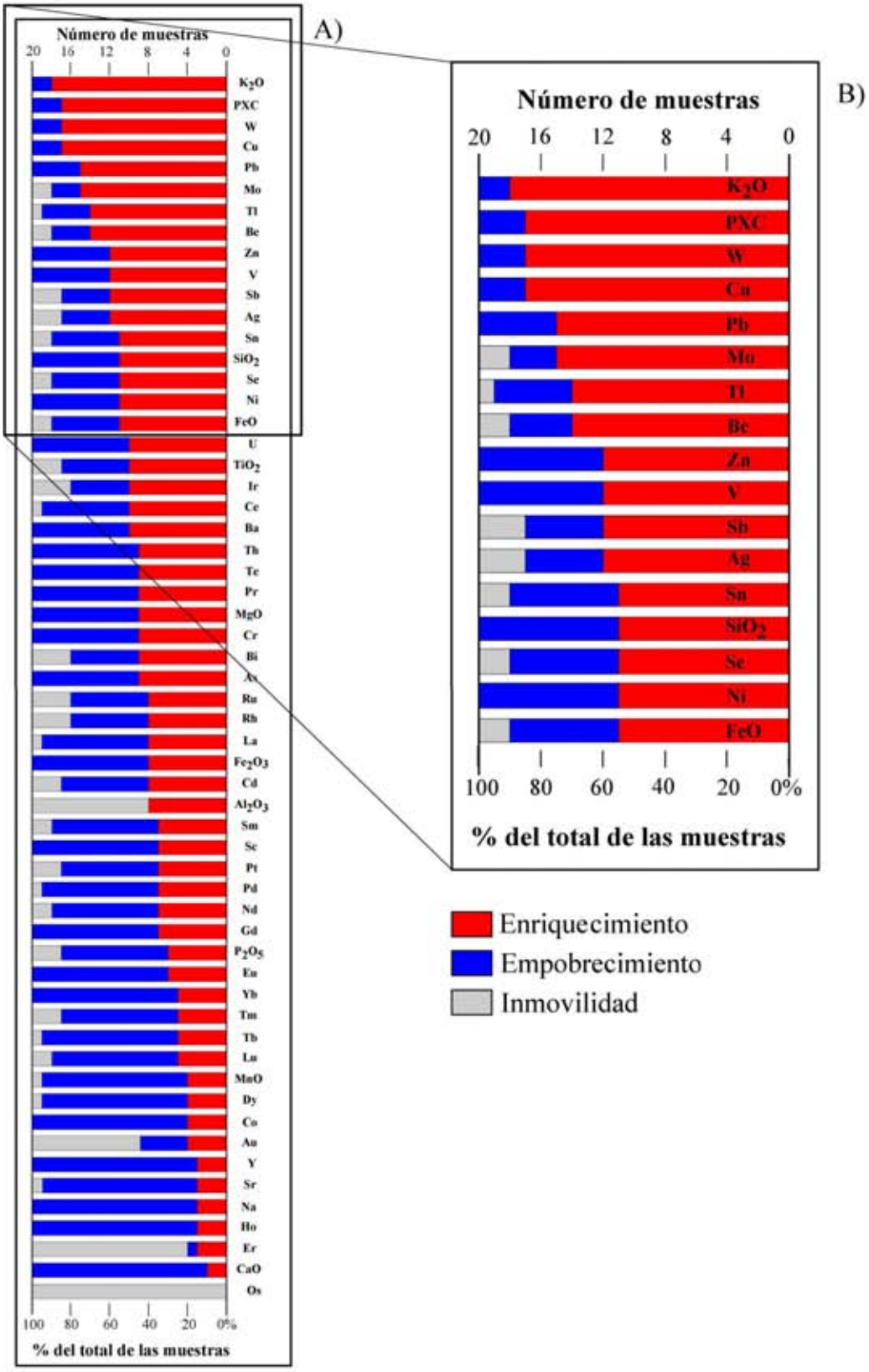

Figura 7. (A) Diagrama resumen del enriquecimiento, empobrecimiento e inmovilidad geoquímica obtenidos en el estudio de balance de masas de la totalidad de las rocas encajonantes frescas y alteradas estudiadas en el Cinturón de Oro Orogénico Caborca (COOC). (B) En este diagrama se enfatizan los elementos que sufrieron una mayor proporción o grado de enriquecimiento en las rocas encajonantes (> 50 %; barras rojas). Estos diagramas se construyeron con los datos presentados en la Tabla 1. Nota: La inmovilidad elemental en algunos casos pudiera ser artefacto de las limitantes en las técnicas analíticas con las que se obtuvieron los resultados geoquímicos de las rocas (*p.e.*, el Os).

elemental. Estos conceptos indican qué elementos han sido modificados o han permanecido sin cambios en sus concentraciones de la roca fresca (original) con respecto a la roca alterada. Los elementos y compuestos con una proporción de enriquecimiento > 50 % de la totalidad de las muestras, o mayormente enriquecidos en las rocas encajonantes alteradas, son el K_2O, W, Cu, Pb, Mo, Tl, Be, Zn, V, Sb, Ag, Sn, SiO_2, Se, Ni y FeO, y la pérdida por calcinación. Igualmente, los elementos con una proporción de empobrecimiento > 60 % en las rocas encajonantes alteradas son el Ca, Y, Na, Ho, Co, Sr, Yb, Mn, Dy, Eu y Tb (Figura 7A). Cabe destacar que las concentraciones de CO_2, S, Cl no han sido medidas para este estudio de balance de masas, pero sin duda estos elementos se encuentran presentes en los minerales de la paragénesis de la alteración de las rocas del COOC (*p.e.*, carbonatos de calcio y/o hierro, y pirita). También el S y Cl deberían haber tenido un papel importante en la disolución, transporte y precipitación del Au, en tanto en cuanto constituyen moléculas complejantes, como sugieren algunos estudios en yacimientos de oro orogénico (*p.e.*, Mernagh y Bierlein, 2008). Por último, las Figuras 8A y 8B presentan a los elementos y compuestos más importantes que fueron enriquecidos hasta más de 200 % (barras en color rojo) y empobrecidos en más de 50 % (barras en color azul) con respecto a la concentración de la roca fresca, respectivamente (Tablas A4 y A5 del Apéndice

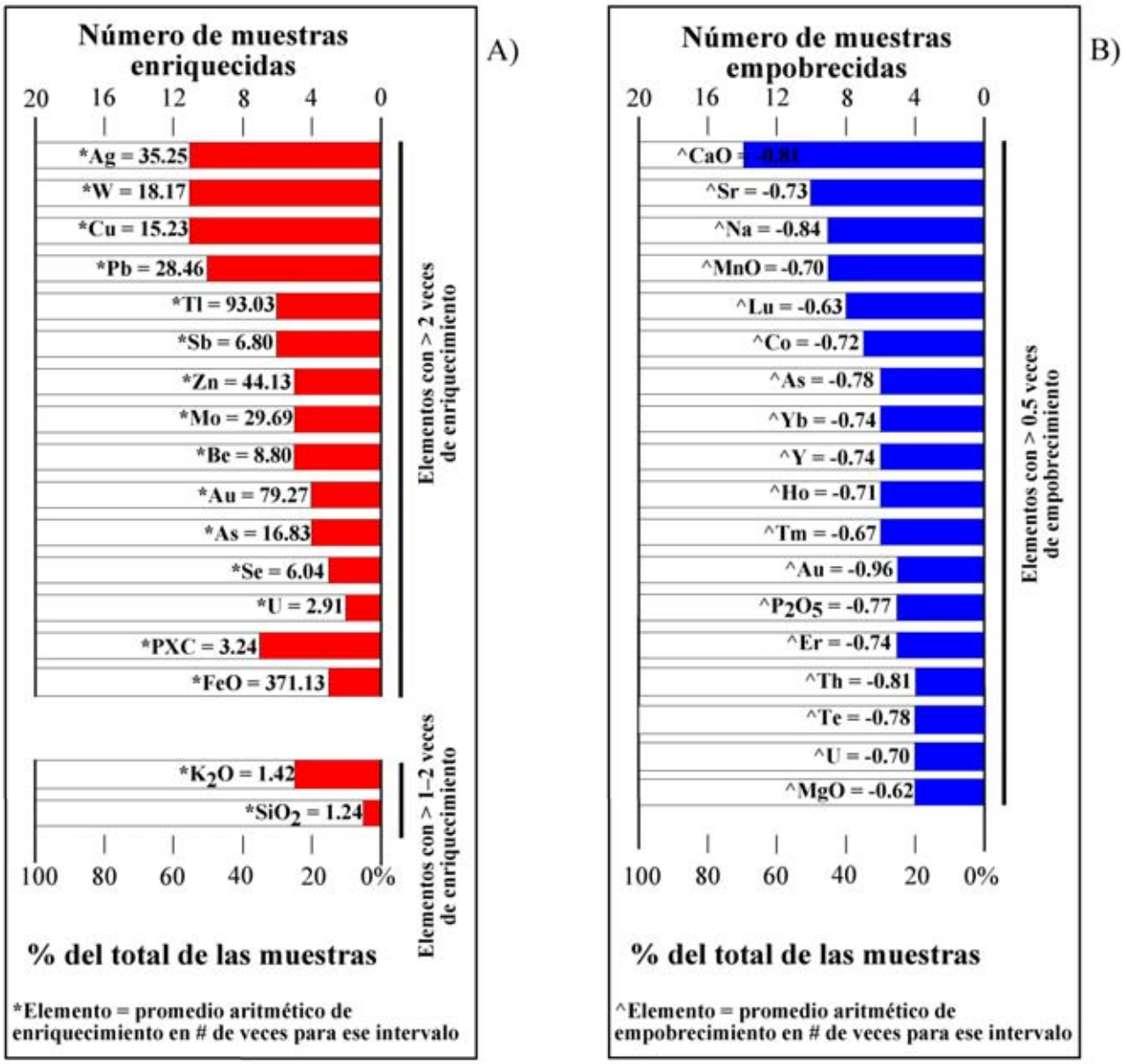

Figura 8. Diagramas de elementos con el mayor empobrecimiento y enriquecimiento geoquímico por unidad de veces con respecto a la roca fresca (original). El resto de los elementos y compuestos se muestran en la Tabla A5 del Apéndice. Los valores de los elementos mayores de esta figura se obtuvieron basándose en unidades de % en peso. Los valores de los elementos traza se obtuvieron usando unidades de partes por millón (ppm).

A). En las barras de cada elemento se muestra la media aritmética del cambio de concentración en número de veces con respecto a la roca fresca original para cada elemento. Los datos que se muestran en las Tablas A4 y A5, del Apéndice A, se obtuvieron al hacer un ordenamiento por rangos de los resultados de enriquecimiento y empobrecimiento que presenta cada elemento con respecto a la concentración original (Δ conc–C^A, Tabla A3 del Apéndice A).

5.3. Resultados del estudio geoquímico de correlación bivariable en vetas de cuarzo

En este estudio se analizaron 102 muestras de esquirlas de vetas de cuarzo representativas de la mineralización del Cinturón de Oro Orogénico Caborca para cuantificar las concentraciones de elementos traza y preciosos (Figura 1; Tabla A2 del Apéndice A). Cabe destacar que 20 de esas muestras coinciden con las 20 localidades del estudio de balance de masas presentado anteriormente.

Los resultados de este estudio de correlación geoquímica bivariable quedan ilustrados en un gráfico binario de coeficiente de correlación del Au *vs.* los elementos traza y elementos preciosos de las vetas de cuarzo (Figura 9A) dispuestos en orden de mayor a menor correlación. La correlación bivariable de la geoquímica de las vetas con el Au muestran que el Pb, Ag, Zn y Fe presentan una correlación positiva moderada (0.604 a 0.510). Los elementos As, Cu, Ni, Bi, Cr, Mo, Sr y Sb presentan una correlación positiva (0.377 a 0.225) la cual se puede considerar baja. Por lo contrario, los elementos Na, Y, Yb, Er y Pr presentan una correlación negativa muy baja (-0.073 a -0.022), y de los elementos como el Dy y Ca es casi nula (0.001 a 0.017).

La correlación geoquímica bivariable de Ag (Figura 9B) con la geoquímica de las vetas indica que el Pb presenta una correlación positiva alta (0.703), mientras que los elementos Zn, Au, Sb, As y Cu presentan un correlación positiva moderada (0.565 a 0.432). Una correlación positiva baja (0.305 a 0.219) es representada por el Mo, Sr, Fe, Bi, Ba y Cr. Por lo contrario, los elementos Na, Ca, Y, Yb, Dy, Ti, Mg, Th, Mn, Gd y Sm presentan correlación negativa muy baja (-0.173 a -0.004). Además, el elemento Er presenta una correlación negativa baja (-0.240), siendo más intensa que en el resto de los elementos.

5.4. Resultados de SEM-EDS en piritas y oro nativo

Granos milimétricos de pirita, galena y oro nativo de algunas muestras de vetas de cuarzo del COOC se seleccionaron para realizar estudios de microscopía electrónica de barrido con espectroscopía de energía dispersiva (SEM-EDS). El propósito es determinar los minerales incluidos y asociados a los sulfuros que pudieran explicar las anomalías geoquímicas elementales obtenidas en los estudios geoquímicos de las vetas de cuarzo. Esto, debido a que no se pudieron encontrar minerales en tamaños

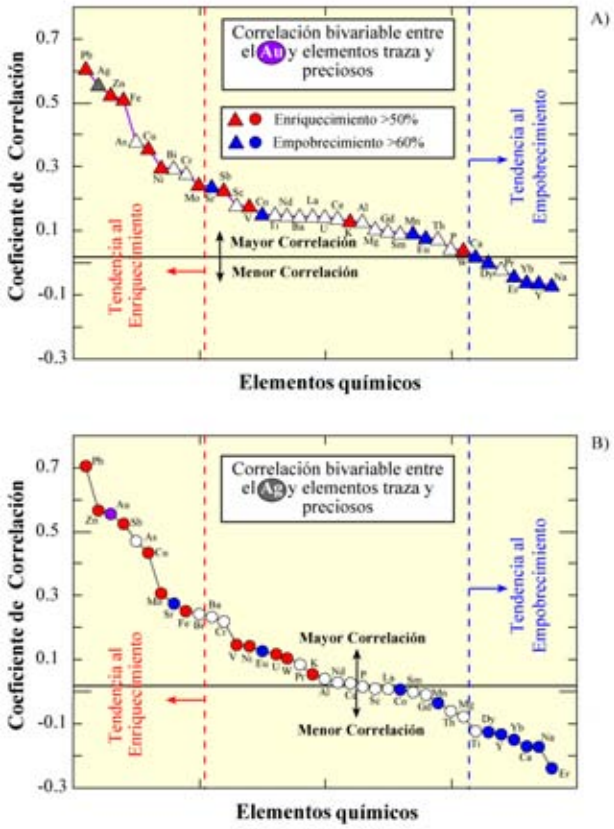

Figura 9. Coeficientes de correlación bivariable del Au (A) y Ag (B) con respecto a otros elementos traza y preciosos de 102 muestras de vetas de cuarzo del Cinturón de Oro Orogénico Caborca (COOC). Las muestras de vetas de cuarzo contenían, en algunos casos, parte del encajonante alterado por el hidrotermalismo. Las tendencias de enriquecimiento (triángulos y círculos en rojo) y de empobrecimiento (triángulos y círculos en azul) son las observadas a partir del estudio de balance de masas (Figura 6; Tabla A2 del Apéndice A).

megascópicos en los agregados de cuarzo que pudieran explicar dichas anomalías geoquímicas. De esta manera, se pretende interpretar mejor la presencia y origen de los elementos y compuestos geoquímicos analizados en el estudio de balance de masas de las rocas encajonantes de la mineralización del COOC.

Los resultados obtenidos consisten en imágenes SEM (Figuras 10, 11 y 12) con análisis puntuales espectrales EDS donde se obtuvo espectros de elementos y compuestos que sugieren un gran número de pequeñas inclusiones minerales (~10-50 µm) en los granos de pirita y oro nativo, resultando negativa la búsqueda en los granos de galena. Las inclusiones minerales encontradas en pirita mostraron en los espectros de energía dispersiva elementos como el Au, Ag, Pb, S, Cu, Zn, Fe, Mo, Te, Bi, K, W y Ti. En la inspección de granos de Au se pudo encontrar inclusiones minerales con W y Ca los cuales se puede interpretar como scheelita [$CaWO_4$] (Figura 12). Mediante el análisis de pirita con un microscopio óptico se dedujo que las inclusiones minerales pueden corresponder a oro nativo, telururos de plata, galena,

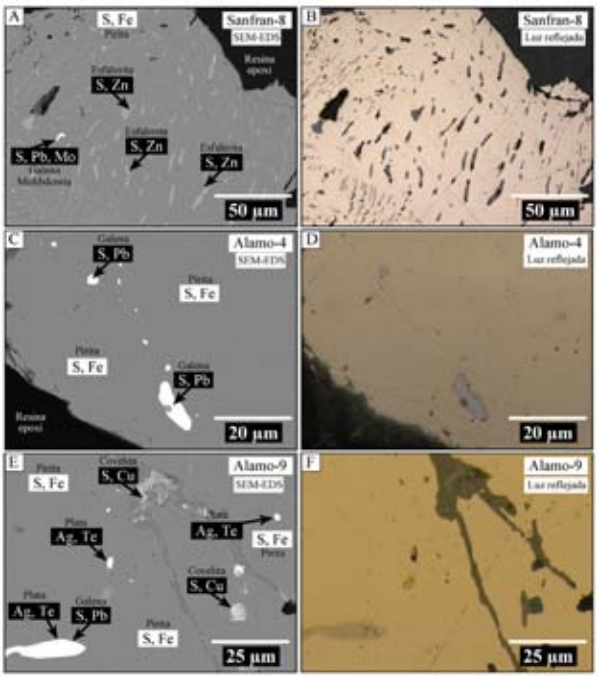

Figura 10. Microfotografías de piritas provenientes de vetas de cuarzo del Cinturón de Oro Orogénico Caborca (COOC). En el lado izquierdo se muestran imágenes de microscopio electrónico de barrido (SEM). Del lado derecho se pueden observar imágenes correspondientes a la misma área anterior pero obtenidas mediante un microscopio óptico de luz reflejada. Los elementos químicos señalados se obtuvieron mediante espectroscopía de energía dispersiva (EDS) conectado al SEM.

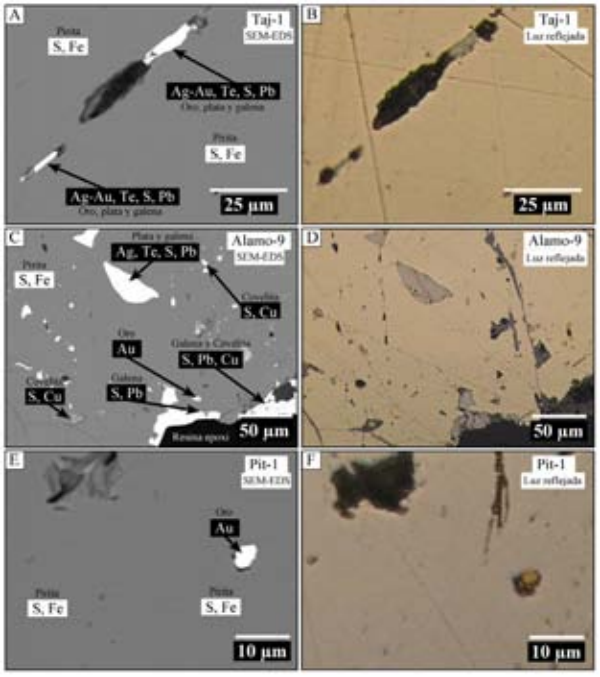

Figura 11. Fotomicrografías de muestras de pirita provenientes de vetas de cuarzo del Cinturón de Oro Orogénico Caborca (COOC). En el lado izquierdo se muestra nimágenes de microscopio electrónico de barrido (SEM). Del lado derecho se pueden observar imágenes correspondientes a la misma área anterior pero obtenidas mediante un microscopio óptico de luz reflejada. Los elementos químicos señalados se obtuvieron mediante espectroscopía de energía dispersiva (EDS) conectado al SEM.

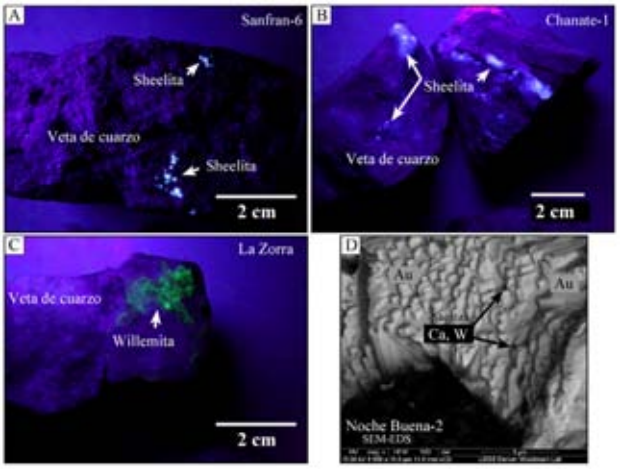

Figura 12. Fotografías de vetas de cuarzo con exposición de luz ultravioleta (A-C) e imagen de un grano de oro (D) obtenida con microscopio electrónico de barrido (SEM) en muestras del Cinturón de Oro Orogénico de Caborca (COOC). Las fotografías de vetas de cuarzo muestran los colores característicos de los minerales señalados (scheelita, azul, y willemita, verde). La imagen del grano de oro muestra elementos químicos que se obtuvieron con la técnica puntual de espectroscopía de energía dispersiva (EDS) conectado al SEM.

covelita, esfalerita, molibdenita y scheelita. Los posibles minerales de telururos, incluidos en las piritas, pudieran ser silvanita [$(Au,Ag)Te_2$], calaverita [$AuTe_2$] y altaíta [PbTe], como los encontrados en el depósito de tipo orogénico de San Francisco, en Estación Llano (Figura 1, Pérez-Segura *et al*., 1996). También con una lupa binocular se pudieron detectar inclusiones de turmalina dentro de algunos granos de pirita y, aplicando luz ultravioleta de onda corta en vetas de cuarzo, scheelita y willemita [Zn_2SiO_4] (Figura 12).

6. Discusión y conclusiones

Los estudios petrográficos de las rocas encajonantes alteradas en el COOC indican que la alteración hidrotermal generó silicificación, sericitización, cloritización, epidotización y piritización, aunque estas alteraciones no siempre son visibles megascópicamente. Por otra parte, la alteración presente no siempre es homogénea, y frecuentemente se observa formando parches; sin embargo, a pesar de tener una alteración hidrotermal heterogénea, los resultados del análisis de balance masas sugieren que existió una movilidad elemental considerable.

Los resultados del estudio de balance de masas (Tabla 2, Tabla A3 del Apéndice, Figura 7) permiten, de una manera semicuantitativa y rápida, la discriminación del cambio de masa total en la roca y del enriquecimiento, empobrecimiento e inmovilidad elemental asociado al proceso de mineralización hidrotermal a lo largo del COOC. El balance de masa total en cada roca encajonante, representadas mayormente por rocas graníticas, sugiere que las rocas que contienen más abundancia de feldespato

potásico fueron más susceptibles a la alteración hidrotermal y, en consecuencia, más susceptibles a cambiar su masa. Las muestras que aumentaron su masa en más de un 50 % (*p.e*., km100 y Quitovac 3) presentan un contenido elevado en SiO_2 y alta pérdida por calcinación, lo que explicaría el aumento de volumen. Por otro lado, en las rocas que perdieron masa en más de un 10 % (*p.e*., Sanfran-1 y Sanfran-3), la alteración mineral pudiera haber reducido su densidad.

Por su parte, el enriquecimiento elemental obtenido en este estudio indica que la mayoría de las rocas alteradas (> 50 %) presentan un enriquecimiento en K_2O, W, Cu, Pb, Mo, Tl, Be, Zn, V, Sb, Ag, Sn, SiO_2, Se, Ni y FeO, y alta pérdida por calcinación, a una escala mucho mayor con respecto a los elementos en que éstas se empobrecieron, como se observa en la Figura 8A y 8B. Esto también coincide en los porcentajes altos de aumento de masa con respecto a los porcentajes bajos de disminución de masa total en la roca.

En la Figura 8A y B se puede observar que el cambio de concentración elemental ocurrido en el enriquecimiento (*p.e*., en K_2O, Ag, W, Cu y Pb) y en el empobrecimiento (*p.e*., en CaO, Sr, Na, MnO), con respecto a la roca fresca, ha sido importante en número de veces o en porcentaje. De este modo, el enriquecimiento y empobrecimiento no es únicamente proporcional como se muestra en la Figura 7 e implica que los fluidos que originaron la alteración en el COOC tenían altas concentraciones en los elementos enriquecidos y capacidad de incorporar elementos de las rocas encajonantes.

Los resultados del estudio de correlación geoquímica bivariable realizados sobre las vetas de cuarzo del COOC sugieren que los elementos que presentaron una mayor proporción de enriquecimiento en el análisis de balance de masas (Pb, Ag, Zn, Fe, Cu, Ni, Mo Sb y V) coinciden con los elementos de mayor coeficiente de correlación positiva (triángulos rojos). Por el contrario, los elementos que presentaron una mayor proporción de empobrecimiento (Ca, Y, Na, Yb, Mn y Dy; triángulos azules) coinciden con los elementos con coeficientes de correlación negativa o nula (Figura 9A). Sin embargo, existen excepciones con algunos elementos que no coinciden con este comportamiento, como son el W y K para el caso del enriquecimiento, y el Sr y Eu para el caso del empobrecimiento. Por su parte, este mismo agrupamiento general de enriquecimiento y empobrecimiento elemental con respecto al Au también se observa para el caso de la Ag (Figura 9B; Tabla A6 del Apéndice A). Esta observación explica que el análisis realizado sobre las vetas de cuarzo, en conjunto con los fragmentos de la roca encajonante alterada, apoyan el resultado del estudio de balance de masas de una manera consistente. Es importante destacar que lo que sugieren los resultados de este estudio es que existe una correlación en el comportamiento de los elementos y compuestos con el estudio de balance masas, inclusive sin considerar los grados de correlación geoquímica bivariable.

Los estudios de SEM-EDS en combinación de la microscopía de luz reflejada y luz ultravioleta muestran la presencia de inclusiones minerales de oro nativo, telururos de plata, galena, covelita, esfalerita, molibdenita, scheelita, willemita y turmalina dentro de los cristales de pirita y en vetas de cuarzo (Figuras 10, 11 y 12). Estas inclusiones minerales concilian la existencia de los elementos enriquecidos durante el proceso de alteración hidrotermal, determinados a partir de los estudios geoquímicos de balance de masa y del análisis de correlación geoquímica del Au y Ag. Sin embargo, las inclusiones minerales no explicarían en su totalidad la presencia de algunos elementos que muestran un enriquecimiento según el balance de masas (*p.e*., Tl, V, Be, Sn, Se), y que aún siguen sin explicarse en la paragénesis mineral de las vetas de oro orogénico en el COOC. Por otra parte, algunos autores (Groves *et al*., 1998) sugieren que ciertos elementos contenidos en la mineralización y alteración orogénica pueden ser inexplicables, por lo que sugieren que estos elementos se encuentran sujetos a la disponibilidad en la corteza local y que son lixiviados durante el ascenso de los fluidos hidrotermales orogénicos.

En conclusión, los resultados obtenidos en este estudio sugieren que los fluidos que generaron la alteración hidrotermal en las rocas encajonantes de las vetas auríferas presentes en el Cinturón de Oro Orogénico Caborca (COOC) son muy homogéneos a lo largo del NW de Sonora. Esta homogeneidad es propuesta a pesar de las grandes distancias de centenares de kilómetros entre las muestras estudiadas (Figura 1) y sugiere que los fluidos posiblemente tuvieron un mismo origen de formación (metamorfismo) y también un mismo periodo de emplazamiento (coetaneidad). Todo esto indica que el evento mineralizante en el COOC tuvo lugar durante el periodo compresivo asociado a la orogenia Larámide del Cretácico tardío-Terciario temprano como ya ha sido sugerido anteriormente (Pérez-Segura *et al*., 1996; Iriondo y Atkinson, 2000; Iriondo, 2001; Poulsen *et al*., 2008; Quintanar-Ruíz, 2008). Este estudio también permite proponer que el COOC es un cinturón metalogenético de oro orogénico que es comparable, en su dimensión areal y en características geológicas con otras ocurrencias existentes alrededor del mundo como en Australia (Groves *et al*., 1998), Alaska y California (Goldfarb *et al*., 1991, 2008; Marsh *et al*., 2008). De igual forma, la geometría elongada del COOC (orientación general NW-SE) sugiere que debió existir una disposición estructural regional previa para la canalización y acenso de los fluidos (*p.e*., la coincidencia espacial del COOC con los límites de la provincia de basamento paleoproterozoica Yavapai) como lo sugieren Iriondo y Premo (2010). Cabe destacar que los elementos (K_2O, W, Cu, Pb, Mo, Tl, Be, Zn, V, Sb, Ag, Sn, SiO_2, Se, Ni y FeO) que se introdujeron a partir del fluido mineralizante en las rocas encajonates de este estudio (COOC) podrían emplearse como guía para la exploración mineral de Au en la región, incluyendo partes del SW de Arizona y SE de California. Por último, destacar que esta homogeneidad propuesta para los fluidos mineralizantes debería esperase

también en futuros estudios regionales de isotopía estable (H, O, S y C) y radiogénicos (Pb-Pb y Rb-Sr) a realizarse en minerales de la paragénesis del COOC (*p.e*., cuarzo, sericita o mica blanca, calcita, siderita, ankerita, pirita, galena, clorita, epidota).

Agradecimientos

Primeramente, agradecemos a las instituciones que otorgaron los proyectos de investigación PAPIIT/UNAM (clave IN-116709) y CONACYT (claves CB-82518 y CB-129370) por aportar parte del financiamiento para la campaña de campo de este estudio. También se agradece a la Coordinación de Estudios de Posgrado de la UNAM por su ayuda económica para realizar esta campaña de campo. Se agradece al CONACYT por otorgarle al primer autor una beca para una estancia de investigación en el *U.S. Geological Survey*, Denver, Colorado. Gracias al Servicio Geológico Mexicano (SGM), Gerencia Hermosillo, en Sonora, en especial a Francisco Cendejas-Cruz, Basilio Cervantes-López y Jaime Castro-Escarrega, por el apoyo logístico otorgado durante la campaña de campo y en el manejo de las muestras. Se agradece a Javier Hernández-Rojas, geólogo del SGM, por su compañía profesional durante el muestreo. Queremos expresar nuestros agradecimientos a Thierry Calmus y Pablo Peñaflor por permitir el acceso a los laboratorios de molienda y pulverizado de rocas del Instituto de Geología de la UNAM en la Estación Regional Noroeste en Hermosillo, Sonora. También se da las gracias a Montserrat Hernández-Ramírez por la ayuda brindada durante la molienda y pulverizado de las muestras. Agradecimientos a Luis Miguel Martínez-Torres de la Universidad del País Vasco, España, por elaborar desinteresadamente las secciones delgadas para el estudio petrográfico. Gracias a Shannon Mahan del *U.S. Geological Survey*, Denver, por el préstamo de contenedores de alúmina para el pulverizado de las muestras; así mismo se agradece a Dan Miggins (*U.S. Geological Survey* en Denver) y Francisco Paz-Moreno (Universidad de Sonora) por organizar el transporte de dichos contenedores. Agradecemos a Erin Marsh y Heather Lowers por facilitar y asesorar en el uso del microscopio electrónico de barrido (SEM) en el *U.S. Geological Survey* en Denver. También se agradece a José Solorio Munguía y Gilles Levresse por su ayuda en la obtención de imágenes de vetas de cuarzo con luz ultravioleta. Por último, se agradece a los revisores del manuscrito Ruth Esther Villanueva Estrada y Efrén Pérez Segura, así como a los editores del Boletín de la Sociedad Geológica Mexicana, Antoni Camprubí i Cano y Carles Canet Miquel, por sus comentarios críticos, constructivos y sugerencias que contribuyeron a mejorar y enriquecer el presente trabajo.

Referencias

Albinson, T.F., 1989, Vetas mesotermales auríferas del sector norte del Estado de Sonora, Memorias Técnicas, XVIII Convención Nacional AIMMGM, Acapulco, Guerrero, México, Asociación de Ingenieros de Minas, Metalurgistas y Geólogos de México, 20–40.

Araiza-Martínez, H., 1998, Geology and Mineralization of the San Francisco Gold Deposit, *en* Clark. K.F., (ed.), Gold Deposits of Northern Sonora, México: Society of Economic Geologists, Guidebook Series, 30, 49–58.

Araux-Sánchez, E., 2000, Geología y yacimientos minerales de la Sierra Pinta, municipio de Puerto Peñasco, Sonora: Departamento de Geología, Universidad de Sonora, tesis de maestría, 121 p.

Baumgartner, L.P., Olsen, S.N., 1995, A least-squares approach to mass transport calculations using the isocon method: Economic Geology, 90, 1261–1270.

Branham, A.D., 1988, Gold mineralization in low angle faults American Girl Valley, Cargo Muchacho Mountains, California: Department of Geology, Washington State University, tesis de maestría, 144 p.

Changkuon, L., 1990, Genesis of gold mineralization: San Francisco Mine, Sonora, Mexico: New Mexico Institute of Mining and Technology, Socorro, New Mexico, tesis de maestría, 129 p.

Coelho, J., 2006, GEOISO–A Windows program to calculate and plot mass balances and volume changes occurring in a variety of geologic processes: Computers and Geosciences, 32, 1523–1528.

Davis, J.C., 1986, Statistics and Data Analysis in Geology: Jonh Wiley & Sons Inc., New York, 2646 p.

Durgin, D.C., Terán, P.I., 1996, La Choya Au deposit, NW Sonora, Mexico, *en* Coyner, A.R., Fahey, P.L., (eds.), Geology and ore deposits of the American Cordillera: Geological Society of Nevada Symposium, Proceedings, Reno/Sparks, Nevada, 1369–1373.

Goldfarb, R.J., Newberry, R.J., Pickthorn, W.J., Gent, C.A., 1991, Oxygen, hydrogen and sulfur isotope studies in the Juneau gold belt, southeastern Alaska: Constraints on the origin of hydrothermal fluids: Economic Geology, 86, 66–88.

Goldfarb, R.J., Hart, C.J., Marsh, E.E., 2008, Orogenic gold and evolution of the Cordilleran orogen, *en* Spencer, J.E., Titley S.R. (eds.), Ores and orogenesis: Circum-Pacific tectonics, geologic evolution, and ore deposits: Arizona Geological Society Digest, 22, 311–323.

Grant, J.A., 1986, The isocon diagram–a simple solution to Gresens' ecuation for metasomatic alteration: Economic Geology, 81, 1976–1982.

Grant, J.A., 2005, Isocon analysis: A brief review of the method and applications: Physics and Chemistry of the Earth, 30, 997–1004.

Gresens, R.L., 1967, Composition–volume relationships of metasomatism: Chemical Geology, 2, 47–65.

Groves, D.I., Goldfarb, R.J., Grebre-Meriam, M., Hagemann, S.G., Robert, F., 1998, Orogenic gold deposits: A proposed classification in the context of their crustal distribution and relationship to other gold deposit types: Ore Geology Reviews, 13, 7–27.

Iriondo, A., 2001, Proterozoic basements and their laramide juxtaposition in NW Sonora, Mexico: Tectonic constraints on the SW margin of Laurentia: Boulder, Colorado, University of Colorado, tesis de doctorado, 222 p.

Iriondo, A., Atkinson, W.W., Jr., 2000, Orogenic gold mineralization along the proposed trace of the Mojave-Sonora megashear: Evidence for the Laramide Orogeny in NW Sonora, Mexico: Geological Society of America, Abstracts with Programs, 32, 393 p.

Iriondo, A., Premo, W.R., 2010, Las rocas cristalinas proterozoicas de Sonora y su importancia para la reconstrucción del margen continental SW de Laurencia–la pieza mexicana del rompecabezas de Rodinia, *en* Calmus, T., (ed.), Panorama sobre la geología de Sonora, México: Universidad Nacional Autónoma de México, Instituto de Geología, Boletín, 118, 25–55.

Lentz, D.R., 2005, Mass-balance analysis of mineralized skarn systems: Implications for eplacement processes, carbonate mobility, and permeability evolution, en Mao, J., Bierlein, F.P., (eds.), Mineral Deposit Research: Meeting the Global Challenge, Proceedings of the Biennial SGA Meeting, Beijing, China, 4, 421–424.

Marsh, E.E., Goldfarb, R.J., Kunk, M.J., Groves, D.I., Bierlein, F.P., Creaser R.A., 2008, New constraints on the timing of gold formation in the Sierra Foothills province, central California, *en* Spencer, J.E., Titley S.R. (eds.), Ores and orogenesis: Circum-Pacific tectonics, geologic evolution, and ore deposits: Arizona Geological Society Digest, 22, 369–388.

Mernagh, T.P., Bierlein, F.P., 2008, Transport and precipitation of gold in Phanerozoic metamorphic terranes from chemical modeling of fluid-rock interaction: Economic Geology, 103, 1613–1640.

Noriega-Martínez, O., 2006, Evidencias de dos etapas de mineralización de oro mesotermal en las áreas de Tajitos, Juárez-San Francisco, en la región de Caborca, Sonora México: Hermosillo, Sonora, Departamento de Geología, Universidad de Sonora, tesis de maestría, 85 p.

Ornelas-Macías, A., Verdugo-Noriega, G., 2009, Caracterización geológica, estructural y de mineralización en el área Karina, municipio de Caborca, Sonora, México: Hermosillo, Sonora, Departamento de Geología, Universidad de Sonora, tesis de licenciatura, 110 p.

Pérez-Segura, E., Cheilletz, A., Herrera-Urbina, S., Hanes, Y.J., 1996, Geología, mineralización, alteración hidrotermal y edad del yacimiento de oro de San Francisco, Sonora–Un depósito mesotermal en el Noroeste de México: Revista Mexicana de Ciencias Geológicas, 13, 65–89.

Pitcairn, I.K., Teagle, D.A., Craw, D., Olivo, G.R., Kerrich, R., Brewer, T.S., 2006, Sources of metals and fluids in orogenic gold deposits: Insights from the Ontago and Alpine Schists, New Zealand: Economic Geology, 101, 1525–1546.

Poulsen, K.H., Mortensen J.K., Walford, P.C., 2008, San Francisco gold deposit, Santa Ana region, Sonora, Mexico: Laramide orogenic, intrusion-related mineralization?, *en* Spencer, J.E., Titley S.R. (eds.), Ores and orogenesis: Circum-Pacific tectonics, geologic evolution, and ore deposits: Arizona Geological Society Digest, 22, 547–559.

Quintanar-Ruíz, F.J., 2008, La Herradura ore deposit: An orogenic gold deposit in northwestern Mexico: Tucson, Arizona, University of Arizona, tesis de maestría 97 p.

Silberman, M.L., Staude, J.M., Cox, D.P., 1987, Reconnaissance of gold prospects in northern Sonora, Mexico: U.S. Geological Survey, Administrative Report, 23 p.

Silberman, M.L., Giles D.A., Graubard, C., 1988, Characteristics of gold deposits in Northern Sonora, Mexico: A preliminary report: Economic Geology, 83, 1966–1974.

Wei, J.H., Liu, C.Q., Li, Z.D., Zhao, Y.X., 2001, Simulation of rock mass balance of two typical altered rocks in Wulong gold deposit of Liaoning, China: Journal of Central South University of Technology, China, 8, 197–202

Manuscrito recibido: Agosto 30, 2011.
Manuscrito corregido recibido: Enero 27, 2012.
Manuscrito aceptado: Enero 31, 2012.

Apéndice

Tabla A1. Elementos mayores y trazas de las rocas encajonantes frescas (Ef) y alteradas (Ea) del Cintur–n de Oro OrogŽnico Caborca, NW de Sonora, MŽxico.

Muestra	Niv. det.	Alamo1Ef	Alamo1Ea	Carolina1Ef	Carolina1Ea	Carretera2Ef	Carretera2Ea	Costa4Ef	Costa4Ea
Coordenadas		112¡ 0' 59.8"		112¡ 44' 2.5"		110¡ 57' 3.2"		112¡ 56' 52.5"	
		30¡ 50' 13.1"		31¡ 9' 12.8"		30¡ 18' 14.4"		30¡ 48' 33.2"	
Elementos mayores									
SiO_2	0.001	58.62	57.46	56.35	59.20	72.87	73.27	73.59	71.20
TiO_2	0.001	0.73	0.60	1.27	1.43	0.14	0.16	0.10	0.13
Al_2O_3	0.001	15.98	16.81	14.68	15.71	13.60	14.10	14.23	14.79
FeO	0.001	0.72	1.43	2.79	3.80	N.D.	0.19	N.D.	0.14
Fe_2O_3	0.001	5.68	3.43	5.62	5.20	1.11	1.41	1.08	1.08
MnO	0.001	0.10	0.11	0.16	0.09	0.07	0.02	0.04	0.04
MgO	0.001	3.10	3.54	1.99	2.12	0.35	0.36	0.24	0.28
CaO	0.001	5.03	6.15	3.14	1.17	0.78	0.18	1.68	1.07
Na_2O	0.001	3.11	2.52	1.69	0.12	3.68	2.71	3.63	3.85
K_2O	0.001	1.62	1.64	3.92	4.85	3.78	4.45	3.15	3.62
P_2O_5	0.001	0.20	0.21	0.52	0.55	0.05	0.06	0.03	0.04
PXC	0.010	3.68	3.96	4.08	3.45	0.79	1.42	0.74	1.42
Total		98.57	97.86	96.21	97.69	97.22	98.33	98.51	97.66
Elementos trazas									
Ag	0.100	N.D.	0.20	N.D.	N.D.	0.60	N.D.	N.D.	1.10
Al	1.000	85720.00	84758.00	76504.00	83523.00	72202.00	74355.00	76652.00	76103.00
As	1.000	23.00	7.00	5.00	20.00	7.00	58.00	5.00	9.00
Au	**0.001**	N.D.	N.D.	**0.03**	N.D.	N.D.	N.D.	**0.01**	N.D.
Ba	1.000	660.00	621.00	1693.00	1037.00	559.00	544.00	901.00	1044.00
Be	1.000	N.D.	N.D.	N.D.	N.D.	1.00	2.00	1.00	1.00
Bi	1.000	N.D.	N.D.	N.D.	N.D.	N.D.	N.D.	N.D.	N.D.
Cd	1.000	N.D.	N.D.	N.D.	N.D.	N.D.	N.D.	N.D.	N.D.
Ce	0.100	51.30	70.00	173.00	193.10	34.50	31.40	29.10	30.80
Co	1.000	22.00	19.00	19.00	23.00	3.00	2.00	2.00	1.00
Cr	1.000	36.00	26.00	21.00	23.00	5.00	7.00	6.00	6.00
Cu	1.000	26.00	90.00	24.00	26.00	5.00	36.00	29.00	8.00
Dy	0.100	3.60	2.90	9.50	10.50	1.30	1.20	3.00	1.80
Er	0.100	1.90	1.50	5.10	5.60	0.60	0.60	1.90	0.90
Eu	0.100	1.70	1.40	4.30	4.80	0.60	0.50	1.00	0.90
Gd	0.100	5.30	5.30	15.60	17.30	2.80	2.50	3.10	2.80
Ho	0.100	0.60	0.50	1.70	1.90	0.20	0.20	0.60	0.30
Ir	0.100	0.10	0.20	N.D.	N.D.	N.D.	N.D.	N.D.	N.D.
K	1.000	13562.00	13528.00	32271.00	40464.00	30931.00	36100.00	25926.00	30033.00
La	0.100	25.90	36.30	70.40	81.50	16.00	15.00	14.80	15.20
Lu	0.100	0.20	0.10	0.50	0.50	0.10	0.10	0.20	0.10
Mg	1.000	17370.00	19587.00	11195.00	11754.00	2124.00	2174.00	1465.00	1636.00
Mn	1.000	731.00	797.00	1196.00	621.00	517.00	185.00	314.00	271.00
Mo	1.000	N.D.	N.D.	1.00	1.00	N.D.	1.00	N.D.	1.00
Na	1.000	23157.00	18823.00	12590.00	855.00	27667.00	20359.00	26351.00	28156.00
Nd	0.100	26.10	28.60	82.60	92.60	14.10	12.70	13.20	13.20
Ni	1.000	41.00	40.00	22.00	28.00	9.00	16.00	7.00	8.00
Os	0.100	0.40	2.80	N.D.	N.D.	N.D.	N.D.	N.D.	N.D.
P	1.000	890.00	930.00	2290.00	2499.00	275.00	289.00	181.00	143.00
Pb	1.000	12.00	20.00	24.00	1.00	20.00	76.00	24.00	25.00
Pd	0.100	1.80	1.50	0.40	0.50	0.60	0.50	0.30	0.20
Pr	0.100	6.30	7.70	19.30	21.70	3.90	3.50	3.40	3.40
Pt	0.100	0.10	0.10	N.D.	N.D.	0.20	0.20	N.D.	0.20
Rh	0.100	N.D.	N.D.	N.D.	N.D.	N.D.	N.D.	N.D.	N.D.
Ru	0.100	0.10	0.10	N.D.	N.D.	N.D.	N.D.	N.D.	N.D.
Sb	1.000	N.D.	N.D.	N.D.	N.D.	N.D.	4.00	N.D.	N.D.
Sc	0.100	13.00	8.50	20.90	22.20	6.30	6.00	3.90	2.30
Se	1.000	N.D.	N.D.	N.D.	N.D.	N.D.	N.D.	8.00	N.D.
Sm	0.100	5.00	4.80	15.10	16.50	3.10	2.60	2.90	2.70
Sn	1.000	N.D.	N.D.	N.D.	N.D.	1.00	2.00	2.00	1.00
Sr	1.000	803.00	1077.00	132.00	32.00	91.00	56.00	315.00	272.00
Tb	0.100	0.70	0.60	1.90	2.10	0.30	0.30	0.50	0.30
Te	1.000	10.00	6.00	13.00	16.00	4.00	N.D.	N.D.	1.00
Th	0.100	5.80	13.60	7.30	8.50	11.10	9.80	5.80	4.90
Ti	0.010	4104.00	3400.00	5919.00	7720.00	787.00	753.00	734.00	649.00
Tl	0.100	N.D.	N.D.	N.D.	N.D.	5.00	4.00	3.00	6.00
Tm	0.100	0.20	0.20	0.60	0.60	0.10	0.10	0.30	0.10
U	1.000	1.00	2.60	2.00	2.40	1.20	4.30	1.40	1.00
V	0.100	103.00	120.00	62.00	63.00	14.00	20.00	10.00	10.00
W	1.000	ND	2.00	4.00	3.00	ND	8.00	1.00	1.00
Y	0.001	16.60	13.40	44.20	47.40	5.50	5.60	17.20	7.90
Yb	0.100	1.40	1.20	3.90	4.20	0.70	0.60	2.00	0.90
Zn	1.000	79.00	95.00	180.00	95.00	30.00	29.00	50.00	57.00

Continua en la siguiente p‡gina

Tabla A1. Continuación

Muestra	**Km100Ef**	**Km100Ea**	**Quitovac2Ef**	**Quitovac2Ea**	**Quitovac3Ef**	**Quitovac3Ea**	**Quitovac5Ef**	**Quitovac5Ea**
Coordenadas	111° 6' 36.8" 29° 58' 40.6"		112° 43' 38.1" 31° 26' 5.9"		112° 41' 51.1" 31° 25' 6.6"		112° 50' 23.6" 31° 30' 34.2"	
Elementos mayores								
SiO_2	58.45	74.45	65.93	68.74	64.42	75.90	54.02	55.28
TiO_2	1.18	0.34	0.38	0.38	0.50	0.14	0.89	0.92
Al_2O_3	16.06	11.53	15.30	15.64	15.64	12.08	17.59	17.58
FeO	4.58	0.14	0.26	0.19	1.09	0.00	0.58	1.43
Fe_2O_3	3.28	1.52	3.45	2.52	3.18	0.80	6.80	4.57
MnO	0.15	0.01	0.04	0.02	0.09	0.01	0.09	0.07
MgO	1.79	0.53	0.97	0.46	1.56	0.16	4.01	3.51
CaO	3.86	0.04	1.97	0.63	3.62	0.40	6.55	2.86
Na_2O	3.57	0.12	4.24	3.42	3.46	2.10	4.08	3.43
K_2O	3.67	6.20	3.59	4.09	3.71	5.21	2.06	3.24
P_2O_5	0.42	0.07	0.13	0.12	0.18	0.02	0.25	0.25
PXC	1.11	2.11	1.45	2.08	1.24	1.23	1.07	4.77
Total	98.12	97.06	97.71	98.29	98.69	98.05	97.99	97.91
Elementos trazas								
Ag	N.D.	8.80	N.D.	N.D.	N.D.	0.10	0.90	0.80
Al	85184.00	61591.00	78619.00	85605.00	83664.00	63914.00	94075.00	94257.00
As	7.00	4.00	15.00	N.D.	N.D.	N.D.	17.00	5.00
Au	N.D.	N.D.	N.D.	N.D.	**4.57**	N.D.	**0.02**	N.D.
Ba	1421.00	927.00	1477.00	1671.00	1188.00	372.00	923.00	940.00
Be	N.D.	N.D.	N.D.	N.D.	N.D.	N.D.	N.D.	N.D.
Bi	N.D.	N.D.	N.D.	N.D.	N.D.	N.D.	N.D.	N.D.
Cd	N.D.	N.D.	N.D.	N.D.	N.D.	N.D.	N.D.	1.00
Ce	138.70	163.60	58.80	49.20	91.30	76.80	44.20	44.60
Co	24.00	3.00	8.00	6.00	12.00	2.00	29.00	24.00
Cr	17.00	6.00	5.00	6.00	8.00	5.00	52.00	49.00
Cu	26.00	44.00	19.00	73.00	34.00	30.00	104.00	385.00
Dy	10.00	2.30	2.80	2.70	4.00	1.90	2.20	1.80
Er	5.50	1.10	1.70	1.70	2.50	1.30	1.10	0.90
Eu	3.60	1.40	1.60	1.70	1.80	0.60	1.60	1.50
Gd	15.10	8.50	4.60	4.10	6.70	4.30	4.40	4.00
Ho	1.80	0.30	0.50	0.50	0.80	0.40	0.40	0.30
Ir	N.D.	0.10	N.D.	N.D.	N.D.	N.D.	N.D.	N.D.
K	30350.00	51317.00	29253.00	33333.00	3331.00	43139.00	17015.00	26453.00
La	61.70	69.90	30.40	27.60	47.80	41.80	21.10	20.90
Lu	0.60	0.10	0.20	0.20	0.30	0.20	0.10	0.10
Mg	10122.00	3222.00	5527.00	2752.00	8718.00	976.00	22555.00	19708.00
Mn	1087.00	88.00	310.00	125.00	616.00	113.00	678.00	525.00
Mo	1.00	1.00	N.D.	N.D.	1.00	1.00	N.D.	N.D.
Na	26410.00	860.00	30788.00	25366.00	25232.00	15556.00	30088.00	24956.00
Nd	77.20	57.60	23.10	20.80	35.60	24.50	23.20	22.20
Ni	23.00	18.00	14.00	13.00	10.00	11.00	37.00	36.00
Os	0.20	2.90	N.D.	N.D.	N.D.	N.D.	N.D.	N.D.
P	1893.00	306.00	565.00	445.00	785.00	94.00	1048.00	1033.00
Pb	29.00	769.00	11.00	10.00	11.00	20.00	10.00	49.00
Pd	0.80	0.50	0.90	0.50	0.60	0.50	0.60	0.50
Pr	17.50	16.30	6.10	5.80	9.60	7.50	5.50	5.30
Pt	0.20	0.10	0.10	N.D.	0.30	0.10	N.D.	N.D.
Rh	N.D.	N.D.	N.D.	N.D.	N.D.	N.D.	N.D.	N.D.
Ru	N.D.	N.D.	N.D.	N.D.	N.D.	N.D.	N.D.	N.D.
Sb	N.D.	1.00	N.D.	N.D.	N.D.	N.D.	N.D.	N.D.
Sc	18.80	8.00	8.40	8.30	9.80	2.40	13.80	13.40
Se	N.D.	N.D.	3.00	N.D.	N.D.	N.D.	N.D.	N.D.
Sm	14.80	8.40	4.00	3.60	5.90	3.80	4.40	4.00
Sn	N.D.	1.00	N.D.	N.D.	N.D.	N.D.	N.D.	N.D.
Sr	251.00	45.00	247.00	178.00	355.00	81.00	751.00	198.00
Tb	1.90	0.70	0.50	0.50	0.80	0.40	0.50	0.40
Te	13.00	6.00	4.00	3.00	4.00	N.D.	13.00	9.00
Th	10.20	10.40	9.30	12.90	18.00	31.20	3.60	3.30
Ti	6784.00	1648.00	2096.00	1916.00	2956.00	657.00	5080.00	3146.00
Tl	N.D.	7.00	N.D.	1.00	5.00	9.00	N.D.	1.00
Tm	0.60	0.10	0.20	0.20	0.30	0.20	0.10	0.10
U	2.80	0.70	1.40	2.50	4.40	2.40	1.20	0.90
V	68.00	24.00	32.00	34.00	65.00	16.00	146.00	145.00
W	1.00	16.00	2.00	3.00	1.00	6.00	1.00	8.00
Y	47.40	8.30	13.90	13.00	22.10	11.10	10.10	8.00
Yb	4.40	0.70	1.50	1.60	2.40	1.40	0.90	0.70
Zn	211.00	46.00	79.00	36.00	56.00	26.00	111.00	122.00

Continua en la siguiente página

Tabla A1. Continuaci—n

Muestra	Quitovac6Ef	Quitovac6Ea	Sanfran1Ef	Sanfran1Ea	Sanfran3Ef	Sanfran3Ea	Sanfran4Ef	Sanfran4Ea
Coordenadas	112¡ 51' 55.3" 31¡ 29' 54.2"		113¡ 3' 56.0" 31¡ 32' 22.6"		113¡ 4' 44.1" 31¡ 31' 21.7"		113¡ 6' 42.4" 31¡ 37' 37.0"	
Elementos mayores								
SiO_2	71.92	68.93	68.48	63.40	74.02	72.50	72.31	71.31
TiO_2	0.19	0.21	0.34	0.62	0.28	0.07	0.04	0.06
Al_2O_3	15.09	16.33	14.98	19.23	11.81	13.77	14.20	15.39
FeO	0.00	0.26	0.15	0.15	0.19	0.14	0.00	N.D.
Fe_2O_3	1.33	1.95	2.24	3.46	2.59	0.65	0.67	0.75
MnO	0.03	0.03	0.04	0.01	0.02	0.01	0.01	0.01
MgO	0.32	0.35	0.97	1.47	0.26	0.15	0.08	0.11
CaO	1.57	0.04	2.60	0.30	1.55	0.19	0.70	0.20
Na_2O	3.99	0.16	4.31	0.09	2.18	1.06	4.07	1.59
K_2O	3.67	6.89	2.86	6.86	3.74	8.82	4.68	8.99
P_2O_5	0.05	0.07	0.14	0.15	0.04	0.00	0.01	0.06
PXC	0.78	3.46	0.87	3.56	0.49	0.56	0.37	0.77
Total	98.94	98.68	97.98	99.30	97.17	97.92	97.14	99.24
Elementos trazas								
Ag	0.50	0.40	0.40	3.90	N.D.	N.D.	0.40	2.10
Al	80237.00	87660.00	77980.00	102801.00	62770.00	73602.00	75959.00	80844.00
As	4.00	4.00	13.00	3.00	N.D.	N.D.	ND	7.00
Au	N.D.	N.D.	N.D.	N.D.	N.D.	N.D.	N.D.	**0.06**
Ba	1456.00	1396.00	486.00	785.00	1605.00	3826.00	910.00	2424.00
Be	N.D.	2.00	N.D.	11.00	ND	1.00	6.00	3.00
Bi	N.D.	N.D.	N.D.	N.D.	N.D.	N.D.	N.D.	1.00
Cd	N.D.	N.D.	N.D.	N.D.	N.D.	N.D.	N.D.	N.D.
Ce	67.40	42.60	36.20	74.20	71.50	15.60	8.90	22.20
Co	2.00	1.00	8.00	7.00	5.00	N.D.	N.D.	N.D.
Cr	4.00	8.00	10.00	14.00	8.00	6.00	6.00	6.00
Cu	29.00	42.00	24.00	829.00	26.00	531.00	11.00	333.00
Dy	1.60	0.20	1.00	0.80	1.40	1.00	0.90	1.10
Er	0.70	0.10	0.50	0.40	0.60	0.70	0.80	0.70
Eu	1.60	0.80	0.80	1.30	2.50	1.90	0.60	1.30
Gd	4.40	1.60	2.40	4.00	4.30	1.40	0.80	2.20
Ho	0.20	N.D.	0.20	0.10	0.20	0.20	0.20	0.20
Ir	0.10	N.D.	N.D.	N.D.	N.D.	N.D.	N.D.	0.10
K	30404.00	57143.00	23290.00	55025.00	30665.00	73247.00	38723.00	76983.00
La	35.00	22.90	18.10	38.90	39.50	9.40	5.50	11.20
Lu	0.10	N.D.	0.10	N.D.	0.10	0.10	0.20	0.10
Mg	1994.00	2105.00	5484.00	8197.00	1618.00	894.00	495.00	611.00
Mn	200.00	197.00	267.00	74.00	177.00	66.00	106.00	41.00
Mo	N.D.	7.00	N.D.	1.00	N.D.	41.00	N.D.	26.00
Na	29329.00	1179.00	31844.00	650.00	16366.00	7859.00	29955.00	11422.00
Nd	26.10	10.90	15.30	27.70	28.70	5.70	2.70	12.30
Ni	15.00	5.00	17.00	22.00	7.00	6.00	13.00	11.00
Os	2.10	N.D.	N.D.	N.D.	N.D.	N.D.	N.D.	3.30
P	242.00	309.00	608.00	565.00	181.00	142.00	43.00	190.00
Pb	28.00	331.00	21.00	110.00	27.00	51.00	74.00	479.00
Pd	0.40	0.30	0.30	0.30	0.20	0.20	1.10	0.70
Pr	7.40	3.70	4.10	7.90	7.50	1.60	0.90	3.00
Pt	N.D.	N.D.	0.20	N.D.	N.D.	N.D.	N.D.	N.D.
Rh	N.D.	N.D.	N.D.	N.D.	N.D.	N.D.	N.D.	N.D.
Ru	N.D.	N.D.	N.D.	N.D.	N.D.	N.D.	N.D.	N.D.
Sb	N.D.	5.00	N.D.	1.00	N.D.	2.00	N.D.	N.D.
Sc	3.30	3.10	2.80	7.50	2.60	2.30	1.00	2.00
Se	N.D.	N.D.	N.D.	N.D.	4.00	N.D.	N.D.	2.00
Sm	4.20	1.30	2.40	3.90	4.00	0.90	0.50	2.30
Sn	1.00	N.D.	N.D.	N.D.	N.D.	N.D.	2.00	1.00
Sr	433.00	188.00	527.00	54.00	154.00	331.00	352.00	320.00
Tb	0.40	0.10	0.20	0.30	0.40	0.20	0.10	0.30
Te	1.00	2.00	2.00	3.00	6.00	N.D.	N.D.	N.D.
Th	19.10	6.20	8.90	8.40	9.30	1.10	5.30	4.40
Ti	1174.00	851.00	2019.00	3342.00	1646.00	400.00	228.00	274.00
Tl	11.00	3.00	3.00	2.00	9.00	6.00	7.00	13.00
Tm	0.10	N.D.	0.10	N.D.	0.10	0.10	0.10	0.10
U	4.10	0.50	3.40	8.10	0.50	0.70	4.90	2.10
V	15.00	15.00	35.00	91.00	21.00	22.00	16.00	18.00
W	1.00	12.00	ND	11.00	ND	1.00	ND	33.00
Y	6.30	0.70	4.40	2.60	5.70	5.40	5.90	6.20
Yb	0.50	0.10	0.40	0.20	0.40	0.70	1.10	0.60
Zn	70.00	71.00	60.00	147.00	39.00	40.00	12.00	2212.00

Continua en la siguiente p‡gina

Tabla A1. Continuación

Muestra	Sanfran5Ef	Sanfran5Ea	Sanfran8Ef	Sanfran8Ea	Sanfran14Ef	Sanfran14Ea	Sanluisito2Ef	Sanluisito2Ea
Coordenadas	113° 6' 51.3"		113° 8' 11.4"		113° 7' 56.7"		112° 37' 31.0"	
	31° 37' 25.4"		31° 40' 19.8"		31° 39' 53.0"		31° 17' 2.0"	
Elementos mayores								
SiO_2	61.46	66.38	69.31	70.06	52.26	46.53	69.74	68.35
TiO_2	0.82	0.75	0.35	0.08	0.90	0.64	0.26	0.27
Al_2O_3	16.26	16.32	13.06	16.24	14.52	11.81	14.26	16.43
FeO	5.00	1.00	0.15	0.26	5.72	7.17	0.19	0.14
Fe_2O_3	2.62	3.81	3.88	0.86	3.49	4.66	2.43	1.81
MnO	0.07	0.04	0.06	0.02	0.16	0.22	0.06	0.02
MgO	3.03	1.48	2.56	1.04	7.16	11.38	0.96	0.94
CaO	1.05	0.22	3.39	0.26	7.26	9.30	2.52	0.43
Na_2O	1.11	0.42	3.24	1.72	2.65	1.27	3.45	0.09
K_2O	3.70	4.75	1.33	3.36	2.32	2.11	3.42	6.07
P_2O_5	0.05	0.03	0.08	0.02	0.26	0.12	0.08	0.06
PXC	2.61	3.11	0.96	3.97	2.63	3.77	0.62	2.71
Total	97.78	98.31	98.37	97.89	99.33	98.98	97.99	97.32
Elementos trazas								
Ag	N.D.	0.20	0.40	1.40	0.80	1.40	0.10	1.00
Al	84390.00	85858.00	66296.00	83778.00	73788.00	60624.00	75928.00	84882.00
As	10.00	13.00	18.00	12.00	11.00	N.D.	2.00	4.00
Au	N.D.	**0.02**	N.D.	**0.02**	**0.01**	N.D.	N.D.	N.D.
Ba	1131.00	1250.00	752.00	766.00	807.00	351.00	731.00	391.00
Be	N.D.	N.D.	N.D.	7.00	N.D.	N.D.	N.D.	3.00
Bi	N.D.	N.D.	N.D.	N.D.	N.D.	N.D.	N.D.	N.D.
Cd	N.D.	N.D.	N.D.	N.D.	N.D.	N.D.	N.D.	1.00
Ce	109.60	111.90	62.70	8.90	44.20	29.20	88.00	41.00
Co	25.00	23.00	14.00	1.00	40.00	52.00	8.00	5.00
Cr	99.00	100.00	51.00	8.00	279.00	678.00	8.00	8.00
Cu	32.00	94.00	23.00	144.00	19.00	7.00	12.00	16.00
Dy	5.60	4.80	4.10	0.20	10.30	8.70	2.50	0.70
Er	2.60	2.20	2.40	0.10	6.30	5.90	1.70	0.40
Eu	2.00	2.00	1.90	0.50	1.90	1.50	1.00	0.70
Gd	9.00	8.70	5.70	0.70	8.90	6.80	4.40	2.50
Ho	1.00	0.80	0.80	N.D.	2.00	1.90	0.50	0.10
Ir	N.D.	N.D.	N.D.	N.D.	N.D.	0.10	N.D.	N.D.
K	30104.00	39288.00	11390.00	27483.00	19128.00	17539.00	28300.00	50111.00
La	54.90	52.70	31.60	5.30	17.20	11.40	51.70	20.70
Lu	0.30	0.30	0.30	N.D.	0.90	0.90	0.30	N.D.
Mg	17926.00	8391.00	14355.00	5938.00	38676.00	67634.00	5472.00	5543.00
Mn	545.00	280.00	417.00	129.00	1110.00	1505.00	453.00	143.00
Mo	1.00	2.00	N.D.	7.00	N.D.	N.D.	1.00	2.00
Na	8175.00	3174.00	23105.00	12647.00	18769.00	8817.00	25379.00	745.00
Nd	45.40	45.20	28.50	3.60	29.80	21.90	24.30	16.00
Ni	60.00	54.00	81.00	14.00	161.00	182.00	10.00	10.00
Os	N.D.	N.D.	N.D.	N.D.	N.D.	0.10	N.D.	N.D.
P	207.00	138.00	344.00	87.00	1125.00	472.00	353.00	270.00
Pb	20.00	57.00	2.00	411.00	11.00	0.00	15.00	55.00
Pd	0.20	0.30	0.30	0.10	0.70	0.70	0.30	0.10
Pr	12.60	12.40	7.40	1.00	6.50	4.60	8.10	4.50
Pt	N.D.	N.D.	1.20	N.D.	N.D.	N.D.	N.D.	N.D.
Rh	N.D.	N.D.	N.D.	N.D.	N.D.	N.D.	N.D.	N.D.
Ru	N.D.	N.D.	N.D.	N.D.	N.D.	N.D.	N.D.	N.D.
Sb	N.D.	N.D.	N.D.	N.D.	N.D.	6.00	N.D.	3.00
Sc	17.60	16.10	9.90	3.20	30.60	49.90	5.80	3.10
Se	N.D.	N.D.	N.D.	1.00	N.D.	N.D.	N.D.	2.00
Sm	8.10	8.30	5.00	0.60	7.80	6.10	3.40	2.60
Sn	N.D.	N.D.	N.D.	1.00	N.D.	N.D.	N.D.	N.D.
Sr	127.00	47.00	401.00	185.00	342.00	145.00	268.00	19.00
Tb	1.10	1.00	0.80	N.D.	1.60	1.30	0.50	0.20
Te	13.00	6.00	1.00	N.D.	13.00	13.00	N.D.	N.D.
Th	15.20	16.40	8.20	0.80	0.40	0.80	59.80	11.00
Ti	4936.00	3974.00	2086.00	345.00	5058.00	3540.00	1649.00	1481.00
Tl	N.D.	4.00	8.00	12.00	N.D.	N.D.	6.00	11.00
Tm	0.30	0.30	0.30	N.D.	0.90	0.90	0.20	N.D.
U	1.60	6.70	0.80	0.40	0.40	0.40	11.30	2.00
V	108.00	107.00	40.00	35.00	133.00	202.00	43.00	36.00
W	1.00	26.00	1.00	17.00	1.00	1.00	2.00	19.00
Y	22.20	18.50	19.00	0.60	49.40	46.20	13.50	2.40
Yb	2.20	1.90	2.10	0.10	6.00	6.20	1.80	0.30
Zn	141.00	199.00	118.00	2221.00	137.00	318.00	71.00	177.00

Continua en la siguiente página

Tabla A1. Continuaci–n

Muestra	Sanluisito3Ef	Sanluisito3Ea	Sonoyta5Ef	Sonoyta5Ea	Trin11Ef	Trin11Ea	Vidrios1Ef	Vidrios1Ea
Coordenadas	112¡ 29' 18.1" 31¡ 22' 57.0"		112¡ 52' 3.5" 31¡ 49' 3.5"		111¡ 40' 57.8" 30¡ 11' 2.1"		113¡ 40' 45.2" 32¡ 5' 6.8"	
Elementos mayores								
SiO_2	60.07	62.90	73.27	71.35	68.24	70.17	64.61	60.76
TiO_2	0.59	0.59	0.09	0.16	0.52	0.39	0.71	0.70
Al_2O_3	16.36	15.79	14.85	16.50	14.14	13.41	15.86	17.59
FeO	0.84	1.00	0.00	0.14	0.27	0.26	0.28	0.27
Fe_2O_3	4.49	3.90	0.78	1.21	3.62	3.34	3.84	3.42
MnO	0.10	0.14	0.02	0.02	0.04	0.01	0.07	0.07
MgO	2.62	2.50	0.15	0.39	1.17	0.82	1.31	1.13
CaO	4.76	3.11	1.15	0.10	0.89	0.54	2.69	2.10
Na_2O	3.35	2.09	3.84	0.22	2.66	5.29	2.98	3.77
K_2O	2.78	4.12	3.39	6.16	4.32	1.24	4.95	7.33
P_2O_5	0.16	0.07	0.04	0.04	0.13	0.10	0.30	0.27
PXC	2.12	2.47	0.46	2.08	1.15	2.48	1.03	1.32
Total	98.24	98.68	98.04	98.37	97.15	98.05	98.63	98.73
Elementos trazas								
Ag	5.50	5.80	0.40	7.00	0.10	0.90	N.D.	N.D.
Al	84806.00	80283.00	80670.00	88271.00	76609.00	69590.00	85081.00	91594.00
As	12.00	6.00	9.00	4.00	ND	22.00	6.00	5.00
Au	N.D.	N.D.	N.D.	N.D.	N.D.	**0.06**	N.D.	N.D.
Ba	935.00	1163.00	1423.00	823.00	974.00	134.00	2711.00	2634.00
Be	N.D.	N.D.	N.D.	3.00	N.D.	N.D.	N.D.	N.D.
Bi	N.D.	N.D.	N.D.	N.D.	N.D.	N.D.	N.D.	N.D.
Cd	5.00	3.00	N.D.	N.D.	N.D.	N.D.	N.D.	N.D.
Ce	95.10	85.40	52.10	66.10	214.40	147.90	250.00	301.90
Co	19.00	21.00	1.00	2.00	11.00	8.00	15.00	6.00
Cr	30.00	33.00	7.00	5.00	24.00	22.00	12.00	8.00
Cu	28.00	1935.00	18.00	7.00	60.00	432.00	12.00	12.00
Dy	4.10	4.30	1.60	1.60	7.50	4.00	11.20	10.60
Er	2.30	2.30	0.70	0.60	2.50	1.90	6.60	6.10
Eu	2.00	2.10	1.30	0.90	3.30	1.20	5.30	4.90
Gd	6.90	6.70	3.40	4.00	16.70	11.00	18.80	19.70
Ho	0.70	0.80	0.30	0.20	1.00	0.60	2.10	1.90
Ir	N.D.	N.D.	N.D.	N.D.	N.D.	N.D.	N.D.	N.D.
K	22907.00	34208.00	28107.00	51002.00	35874.00	10381.00	40787.00	60477.00
La	51.00	44.70	26.10	33.40	89.20	62.10	111.40	140.70
Lu	0.30	0.30	0.10	N.D.	0.20	0.20	0.90	0.80
Mg	14995.00	14984.00	939.00	2360.00	6827.00	4780.00	7919.00	6807.00
Mn	736.00	1046.00	124.00	120.00	315.00	101.00	561.00	538.00
Mo	N.D.	N.D.	1.00	N.D.	1.00	1.00	3.00	24.00
Na	24167.00	15214.00	28831.00	1648.00	19378.00	38946.00	21690.00	27027.00
Nd	35.50	33.20	18.90	24.10	87.60	78.30	111.60	117.90
Ni	24.00	25.00	29.00	8.00	36.00	44.00	14.00	14.00
Os	N.D.	N.D.	N.D.	N.D.	N.D.	N.D.	N.D.	N.D.
P	717.00	314.00	170.00	190.00	558.00	450.00	1347.00	1115.00
Pb	246.00	773.00	74.00	12.00	15.00	66.00	54.00	41.00
Pd	0.50	0.50	0.20	0.40	0.20	0.40	0.80	0.50
Pr	10.30	9.30	5.60	7.10	23.10	21.60	30.30	33.20
Pt	N.D.	N.D.	N.D.	N.D.	N.D.	N.D.	N.D.	N.D.
Rh	N.D.	0.10	N.D.	N.D.	N.D.	N.D.	N.D.	N.D.
Ru	N.D.	N.D.	N.D.	N.D.	N.D.	N.D.	N.D.	N.D.
Sb	N.D.	N.D.	2.00	N.D.	N.D.	N.D.	N.D.	N.D.
Sc	13.60	11.90	2.20	3.40	9.00	10.10	12.50	14.50
Se	N.D.	N.D.	N.D.	6.00	N.D.	N.D.	N.D.	N.D.
Sm	5.90	5.90	3.10	3.90	17.20	11.10	18.40	18.10
Sn	N.D.	N.D.	N.D.	1.00	N.D.	N.D.	N.D.	N.D.
Sr	464.00	383.00	413.00	45.00	123.00	117.00	607.00	426.00
Tb	0.80	0.80	0.40	0.40	1.90	1.10	2.30	2.30
Te	4.00	4.00	N.D.	1.00	4.00	2.00	7.00	7.00
Th	19.90	17.60	12.30	16.40	49.60	53.00	30.60	29.50
Ti	3565.00	3461.00	628.00	798.00	3071.00	2069.00	4349.00	3217.00
Tl	N.D.	9.00	8.00	13.00	1.00	8.00	3.00	6.00
Tm	0.30	0.30	0.10	0.10	0.20	0.20	0.90	0.80
U	5.10	4.60	1.50	1.10	2.70	3.10	5.40	5.40
V	87.00	85.00	7.00	9.00	37.00	26.00	63.00	65.00
W	2.00	ND	1.00	2.00	ND	1.00	1.00	2.00
Y	18.80	20.40	6.60	5.70	21.00	12.50	52.80	48.90
Yb	2.00	2.00	0.60	0.40	1.70	1.40	6.00	5.50
Zn	234.00	6848.00	40.00	122.00	33.00	27.00	83.00	145.00

Los valores de los elementos mayores se encuentran expresados en % y los elemento trazas en partes por mill–n (ppm). La conversi–n a gramos por tonelada (g/t = ppm). N.D. = valor menor o igual a la capacidad de detecci–n anal'tica instrumental. Niv. det. = Nivel de detecci–n m'nimo. PXC = PŽrdida por calcinaci–n a 950 ¡C. Elementos mayores analizados por medio de la tŽcnica ICP-AES. Elementos traza analizados por la tŽcnica ICP-MS. Para el an‡lisis del Au se implement—la tŽcnica de an‡lisis al fuego. Datum de las coordenadas: WGS84.

Tabla A2. Elementos trazas y metales preciosos de 102 muestras de vetas de cuarzo del Cinturón de Oro Orogénico Caborca, NW de Sonora, México.

Muestra	**Niv. det.**	**Alamo-1**	**Alamo-2**	**Alamo-3**	**Alamo-4**	**Alamo-5**	**Alamo-6**	**Alamo-7**	**Alamo-8**	**Alamo-9**	**Alamo-10**	**Alamo-11**	**Antimonio-1**	**Carina-1**	**Carina-2**	**Carolina-1**	**Carretera-1**	**Carretera-2**
Coordena.		112° 0' 59.8"	112° 9' 15.6"	112° 9' 15.0"	112° 9' 15.3"	112° 9' 19.0"	112° 10' 58.8"	112° 12' 15.8"	112° 12' 9.3"	112° 12' 11.9"	112° 12' 10.7"	112° 12' 13.8"	112° 35' 50.8"	112° 44' 25.8"	112° 44' 25.8"	112° 44' 2.5"	111° 5' 49.0"	110° 57' 3.2"
		30° 50' 13.1"	30° 54' 29.4"	30° 54' 34.0"	30° 54' 34.7"	30° 54' 37.8"	30° 54' 2.3"	30° 55' 45.8"	30° 56' 4.5"	30° 56' 5.9"	30° 56' 4.5"	30° 56' 4.3"	30° 44' 10.9"	31° 10' 0.3"	31° 10' 0.3"	31° 9' 12.8"	30° 4' 54.1"	30° 18' 14.4"
Ag	1.000	1.00	6.00	3.00	104.00	24.00	1.00	10.00	24.00	27.00	16.00	41.00	8.00	1.00	5.00	2.00	N.D.	2.00
Al	1.000	5011.00	4189.00	23508.00	2165.00	5711.00	257.00	13978.00	5661.00	1286.00	2671.00	1967.00	17610.00	7762.00	9697.00	7182.00	5541.00	679.00
As	1.000	N.D.	347.00	4338.00	1774.00	1121.00	17.00	3.00	1.00	3.00	9.00	2.00	419.00	1.00	N.D.	27.00	N.D.	36.00
Au	**0.001**	N.D.	N.D.	**0.40**	**12.27**	**2.27**	**0.01**	**0.40**	**0.27**	**2.23**	**0.13**	**3.00**	**0.53**	**0.03**	**1.00**	**3.07**	N.D.	**0.40**
Ba	1.000	48.00	56.00	193.00	81.00	95.00	24.00	240.00	84.00	47.00	40.00	45.00	260.00	200.00	95.00	263.00	11.00	6.00
Be	1.000	N.D.	N.D.	N.D.	N.D.	N.D.	N.D.	N.D.	N.D.	N.D.	N.D.	N.D.	1.00	N.D.	N.D.	N.D.	1.00	N.D.
Bi	1.000	N.D.	N.D.	N.D.	N.D.	N.D.	1.00	N.D.	N.D.	2.00	N.D.	1.00	N.D.	N.D.	5.00	4.00	N.D.	7.00
Ca	0.001	72840.00	3330.00	25510.00	460.00	5510.00	220.00	430.00	790.00	460.00	1470.00	60.00	47460.00	19060.00	4030.00	90780.00	480.00	160.00
Cd	1.000	N.D.	1.00	11.00	7.00	6.00	N.D.	1.00	N.D.	52.00	1.00	24.00	2.00	N.D.	N.D.	N.D.	N.D.	N.D.
Ce	0.100	6.00	4.70	28.60	1.10	6.50	0.40	56.70	13.70	2.00	5.30	1.40	15.80	20.10	27.60	74.60	28.70	0.80
Co	1.000	2.00	2.00	7.00	1.00	2.00	1.00	1.00	2.00	4.00	1.00	2.00	3.00	83.00	5.00	59.00	1.00	1.00
Cr	1.000	273.00	341.00	223.00	390.00	375.00	466.00	261.00	339.00	404.00	396.00	372.00	257.00	11.00	360.00	3.00	1.00	393.00
Cu	1.000	90.00	21.00	216.00	411.00	349.00	10.00	18.00	4367.00	283.00	5384.00	232.00	27.00	14.00	67.00	258.00	11.00	13.00
Dy	0.100	0.50	0.30	1.00	0.10	0.30	0.10	1.00	0.60	0.10	0.30	N.D.	1.00	0.80	0.60	4.50	1.80	N.D.
Er	0.100	0.30	0.10	0.50	N.D.	0.10	0.10	0.50	0.30	0.10	0.10	N.D.	0.50	0.40	0.30	2.30	1.20	N.D.
Eu	0.100	0.20	0.10	0.60	0.10	0.20	N.D.	0.50	0.30	N.D.	0.10	N.D.	0.40	0.50	0.30	3.70	0.20	N.D.
Fe	0.001	6600.00	11990.00	30340.00	55510.00	13990.00	7780.00	9230.00	7160.00	6420.00	6550.00	8630.00	21970.00	13044.00	13110.00	60830.00	4530.00	6170.00
Gd	0.100	0.60	0.50	2.50	0.10	0.60	0.10	3.10	1.30	0.20	0.50	0.10	1.50	1.70	2.00	6.60	2.30	0.10
Ho	0.100	0.10	N.D.	0.20	N.D.	0.10	N.D.	0.10	0.10	N.D.	N.D.	N.D.	0.20	0.10	0.10	0.80	0.40	N.D.
Ir	0.100	N.D.	N.D.	N.D.	N.D.	N.D.	N.D.	N.D.	N.D.	N.D.	N.D.	N.D.	N.D.	N.D.	N.D.	N.D.	N.D.	N.D.
K	1.000	1066.00	2018.00	10067.00	1025.00	2926.00	73.00	8045.00	2694.00	749.00	1590.00	1133.00	7162.00	4067.00	5077.00	8584.00	3179.00	376.00
La	0.100	3.30	2.30	13.90	0.50	3.20	0.20	29.40	6.70	1.00	2.50	0.70	9.50	9.20	12.90	37.70	14.70	0.40
Lu	0.100	N.D.	N.D.	N.D.	N.D.	N.D.	N.D.	0.10	N.D.	N.D.	N.D.	N.D.	0.10	N.D.	N.D.	0.30	0.20	N.D.
Mg	1.000	2265.00	644.00	2182.00	128.00	1562.00	58.00	585.00	345.00	99.00	170.00	105.00	4259.00	6848.00	2637.00	736.00	384.00	74.00
Mn	1.000	1013.00	205.00	462.00	34.00	122.00	138.00	284.00	205.00	107.00	136.00	32.00	212.00	492.00	223.00	1595.00	90.00	38.00
Mo	1.000	1.00	2.00	3.00	5.00	2.00	2.00	1.00	1.00	35.00	1.00	4.00	3.00	7.00	9.00	11.00	1.00	4.00
Na	1.000	194.00	102.00	968.00	128.00	154.00	66.00	493.00	662.00	97.00	179.00	56.00	1065.00	194.00	205.00	2084.00	827.00	48.00
Nd	0.100	2.70	2.20	12.70	0.60	3.10	0.20	17.80	6.30	0.80	2.40	0.60	7.20	9.20	11.20	27.70	10.40	0.30
Ni	1.000	6.00	9.00	12.00	7.00	8.00	7.00	5.00	5.00	7.00	6.00	6.00	18.00	3.00	9.00	1.00	N.D.	7.00
Os	0.100	N.D.	N.D.	N.D.	N.D.	N.D.	N.D.	N.D.	N.D.	N.D.	N.D.	N.D.	N.D.	N.D.	N.D.	0.10	N.D.	N.D.
P	1.000	206.00	168.00	378.00	89.00	134.00	54.00	153.00	180.00	13.00	N.D.	13.00	474.00	237.00	131.00	846.00	39.00	26.00
Pb	1.000	12.00	6.00	30.00	311.00	176.00	6.00	98.00	17.00	4181.00	28.00	1062.00	82.00	18.00	453.00	17.00	17.00	654.00
Pd	0.100	N.D.	N.D.	N.D.	N.D.	N.D.	N.D.	N.D.	N.D.	N.D.	N.D.	N.D.	0.10	N.D.	N.D.	0.20	0.10	N.D.
Pr	0.100	0.70	0.60	3.40	0.10	0.80	0.10	5.60	1.70	0.20	0.60	0.20	1.90	2.40	3.10	7.60	3.10	0.10
Pt	0.100	N.D.	N.D.	N.D.	N.D.	N.D.	N.D.	N.D.	N.D.	N.D.	N.D.	N.D.	N.D.	N.D.	N.D.	N.D.	0.30	0.10
Rh	0.100	N.D.	N.D.	N.D.	N.D.	N.D.	N.D.	N.D.	N.D.	N.D.	0.10	N.D.	N.D.	N.D.	N.D.	N.D.	N.D.	N.D.
Ru	0.100	0.10	N.D.	N.D.	N.D.	N.D.	N.D.	N.D.	N.D.	N.D.	N.D.	N.D.	0.10	N.D.	N.D.	0.10	N.D.	N.D.
Sb	1.000	2.00	5.00	64.00	114.00	127.00	5.00	3.00	26.00	3.00	64.00	4.00	11295.00	7.00	6.00	2.00	1.00	11.00
Sc	0.100	2.40	1.30	4.70	0.90	1.70	0.30	2.00	1.90	0.50	1.00	0.90	4.00	3.20	2.10	4.60	1.00	0.20
Se	1.000	N.D.	N.D.	N.D.	10.00	2.00	N.D.	N.D.	1.00	8.00	1.00	3.00	N.D.	N.D.	N.D.	1.00	N.D.	N.D.
Sm	0.100	0.50	0.40	2.50	0.10	0.60	0.10	2.80	1.20	0.20	0.50	0.10	1.40	1.70	2.00	5.60	2.10	0.10
Sn	1.000	N.D.	N.D.	1.00	N.D.	N.D.	N.D.	1.00	N.D.	N.D.	N.D.	N.D.	1.00	N.D.	1.00	1.00	1.00	1.00
Sr	1.000	192.00	13.00	101.00	122.00	144.00	3.00	7.00	6.00	3.00	3.00	3.00	135.00	24.00	10.00	428.00	5.00	6.00
Tb	0.100	0.10	0.10	0.30	N.D.	0.10	N.D.	0.30	0.20	N.D.	0.10	N.D.	0.20	0.20	0.20	0.90	0.30	N.D.
Te	1.000	N.D.	N.D.	N.D.	N.D.	N.D.	N.D.	9.00	1.00	30.00	1.00	30.00	N.D.	1.00	7.00	2.00	N.D.	4.00
Th	0.100	0.70	0.60	3.80	0.40	0.70	0.10	12.10	2.10	0.40	0.50	0.10	2.00	1.30	5.00	2.80	32.80	0.70
Ti	1.000	201.00	33.00	120.00	17.00	45.00	8.00	152.00	70.00	22.00	44.00	39.00	84.00	110.00	145.00	361.00	48.00	11.00
Tl	1.000	N.D.	N.D.	N.D.	N.D.	N.D.	N.D.	N.D.	N.D.	N.D.	N.D.	N.D.	1.00	N.D.	N.D.	N.D.	N.D.	N.D.
Tm	0.100	N.D.	N.D.	N.D.	N.D.	N.D.	N.D.	N.D.	N.D.	N.D.	N.D.	N.D.	0.10	N.D.	N.D.	0.30	0.20	N.D.
U	0.100	0.20	0.10	1.10	0.40	0.20	0.10	0.60	0.30	0.40	0.10	0.10	1.80	1.20	0.60	0.50	7.30	2.70
V	1.000	17.00	17.00	86.00	11.00	12.00	6.00	11.00	10.00	6.00	5.00	11.00	40.00	17.00	18.00	7.00	5.00	8.00
W	1.000	1.00	1.00	1.00	1.00	1.00	N.D.	1.00	N.D.	N.D.	N.D.	1.00	59.00	603.00	10.00	453.00	6.00	2.00
Y	0.100	3.20	1.20	4.40	0.30	1.30	0.40	3.70	2.60	0.40	1.10	0.20	5.30	3.90	2.30	27.80	9.90	0.20
Yb	0.100	0.30	0.10	0.30	N.D.	0.10	0.10	0.40	0.20	0.10	0.10	N.D.	0.50	0.30	0.20	2.00	1.40	N.D.
Zn	1.000	12.00	19.00	189.00	196.00	280.00	7.00	54.00	18.00	1393.00	23.00	522.00	107.00	19.00	11.00	12.00	17.00	11.00

Continua en la siguiente página

Tabla A2. Continuaci–n

Muestra	Chanate-1	Chanate-2	Costa-1	Costa-2	Costa-3	Costa-4	Costa-5	EstaLlano-10	Km100	La Herradura	La Zorra	Las Animas	Libertad-1	Nochebuena-1	Nochebuena-2	Pinta-1	Pinta-1a
Coordena.	111¡ 55' 13.2"	111¡ 55' 13.1"	112¡ 52' 47.8"	112¡ 53' 24.0"	112¡ 53' 49.8"	112¡ 56' 52.5"	112¡ 54' 8.2"	111¡ 7' 8.5"	111¡ 6' 36.8"	112¡ 51' 49.0"	112¡ 11' 39.8"	111¡ 23' 21.7"	112¡ 22' 37.8"	112¡ 38' 47.4"	112¡ 37' 51.9"	113¡ 7' 21.7"	113¡ 7' 23.4"
	30¡ 48' 8.8"	30¡ 48' 6.6"	30¡ 56' 9.3"	30¡ 55' 17.2"	30¡ 55' 0.3"	30¡ 48' 33.2"	30¡ 45' 2.7"	30¡ 21' 4.9"	29¡ 58' 40.6"	31¡ 8' 41.8"	30¡ 45' 38.9"	30¡ 14' 16.9"	30¡ 10' 8.3"	31¡ 1' 50.2"	31¡ 1' 16.7"	31¡ 24' 17.6"	31¡ 24' 19.3"
Ag	2.00	30.00	N.D.	N.D.	8.00	N.D.	N.D.	3.00	7.00	N.D.	177.00	N.D.	N.D.	38.00	2.00	N.D.	10.00
Al	12310.00	3226.00	757.00	6425.00	3180.00	10812.00	2173.00	2012.00	2485.00	6470.00	2250.00	107.00	2363.00	8227.00	4529.00	3391.00	3072.00
As	55.00	886.00	N.D.	N.D.	3.00	15.00	17.00	N.D.	1.00	N.D.	113.00	N.D.	N.D.	771.00	1.00	N.D.	N.D.
Au	**0.83**	**25.06**	N.D.	N.D.	**0.04**	**0.01**	N.D.	**4.93**	**0.03**	N.D.	**0.05**	N.D.	N.D.	**0.20**	**18.43**	**0.30**	**1.90**
Ba	762.00	130.00	39.00	121.00	40.00	193.00	27.00	66.00	14.00	59.00	6008.00	3.00	91.00	109.00	75.00	26.00	41.00
Be	1.00	N.D.	N.D.	N.D.	N.D.	1.00	N.D.	N.D.	N.D.	N.D.	N.D.	N.D.	N.D.	N.D.	N.D.	N.D.	N.D.
Bi	N.D.	7.00	N.D.	N.D.	57.00	N.D.	8.00	4.00	N.D.	N.D.	N.D.	N.D.	N.D.	2.00	N.D.	3.00	14.00
Ca	28850.00	38730.00	280.00	4750.00	22890.00	7970.00	1360.00	1290.00	380.00	23810.00	820.00	210.00	420.00	8230.00	760.00	2160.00	700.00
Cd	4.00	14.00	N.D.	N.D.	1.00	1.00	N.D.	N.D.	N.D.	1.00	10.00	N.D.	N.D.	2.00	N.D.	N.D.	5.00
Ce	23.70	5.50	1.00	9.00	2.20	23.20	7.20	6.60	7.10	29.40	3.40	0.30	7.70	14.80	22.00	1.20	0.90
Co	97.00	12.00	1.00	2.00	203.00	1.00	277.00	5.00	1.00	3.00	N.D.	1.00	3.00	1.00	170.00	2.00	6.00
Cr	7.00	319.00	1.00	1.00	7.00	1.00	2.00	342.00	412.00	2.00	334.00	408.00	2.00	314.00	2.00	417.00	383.00
Cu	38.00	27.00	5.00	5.00	5.00	8.00	3.00	21.00	7.00	3.00	881.00	12.00	15.00	36.00	6.00	118.00	58.00
Dy	1.00	0.70	0.10	0.40	0.40	1.00	0.50	0.30	0.20	1.30	0.20	0.10	0.40	0.20	0.40	N.D.	0.10
Er	0.40	0.30	0.10	0.30	0.30	0.50	0.30	0.20	0.10	0.70	0.10	0.10	0.20	0.10	0.20	N.D.	N.D.
Eu	0.90	0.60	N.D.	0.20	0.20	0.30	N.D.	0.10	0.10	0.50	2.30	N.D.	0.10	0.20	0.20	N.D.	N.D.
Fe	17780.00	51720.00	3420.00	4750.00	8950.00	4600.00	2610.00	8480.00	10030.00	11880.00	9220.00	7410.00	25520.00	19270.00	9660.00	6420.00	8240.00
Gd	2.20	0.80	0.10	0.70	0.40	1.80	0.60	0.50	0.50	2.60	0.40	0.10	0.60	0.90	1.20	0.10	0.10
Ho	0.20	0.10	N.D.	0.10	0.10	0.20	0.10	0.10	N.D.	0.20	N.D.	N.D.	0.10	N.D.	0.10	N.D.	N.D.
Ir	N.D.	N.D.	N.D.	N.D.	N.D.	N.D.	N.D.	N.D.	N.D.	N.D.	N.D.	N.D.	N.D.	N.D.	N.D.	N.D.	N.D.
K	6710.00	1733.00	319.00	3244.00	1584.00	5729.00	1406.00	751.00	1668.00	3597.00	1023.00	41.00	1194.00	6290.00	2703.00	1517.00	1915.00
La	11.70	2.80	0.80	4.50	0.90	11.40	3.70	3.60	3.70	14.40	1.90	0.10	3.90	8.00	11.80	0.50	0.50
Lu	0.10	N.D.	N.D.	N.D.	N.D.	0.10	N.D.	N.D.	N.D.	0.10	0.20	N.D.	N.D.	N.D.	N.D.	N.D.	N.D.
Mg	6038.00	1857.00	130.00	946.00	959.00	647.00	239.00	492.00	291.00	11674.00	150.00	32.00	235.00	224.00	205.00	200.00	142.00
Mn	488.00	768.00	42.00	131.00	442.00	225.00	80.00	66.00	40.00	278.00	52.00	35.00	106.00	54.00	299.00	409.00	87.00
Mo	N.D.	4.00	1.00	1.00	24.00	1.00	18.00	4.00	3.00	1.00	7.00	1.00	1.00	137.00	1.00	4.00	8.00
Na	382.00	135.00	62.00	315.00	103.00	593.00	469.00	281.00	153.00	504.00	165.00	77.00	270.00	299.00	639.00	73.00	85.00
Nd	10.90	2.70	0.50	3.70	1.30	9.10	2.50	2.40	2.80	12.80	1.60	0.20	3.10	5.10	7.20	0.20	0.30
Ni	6.00	10.00	N.D.	1.00	4.00	1.00	2.00	7.00	7.00	4.00	7.00	7.00	5.00	7.00	2.00	19.00	7.00
Os	N.D.	N.D.	N.D.	N.D.	N.D.	N.D.	N.D.	N.D.	N.D.	N.D.	N.D.	N.D.	N.D.	N.D.	N.D.	N.D.	0.10
P	394.00	198.00	25.00	191.00	114.00	131.00	129.00	50.00	38.00	53.00	113.00	9.00	131.00	202.00	177.00	19.00	27.00
Pb	218.00	4002.00	6.00	3.00	219.00	20.00	11.00	50.00	249.00	10.00	5935.00	11.00	14.00	3088.00	259.00	431.00	366.00
Pd	N.D.	N.D.	N.D.	N.D.	N.D.	N.D.	N.D.	N.D.	N.D.	N.D.	N.D.	N.D.	N.D.	N.D.	0.10	N.D.	N.D.
Pr	2.90	0.70	0.10	1.00	0.30	2.60	0.80	0.70	0.80	3.40	0.40	N.D.	0.90	1.60	2.20	0.10	0.10
Pt	0.10	N.D.	N.D.	N.D.	N.D.	N.D.	N.D.	N.D.	N.D.	N.D.	N.D.	N.D.	N.D.	N.D.	0.10	0.20	N.D.
Rh	N.D.	N.D.	N.D.	N.D.	N.D.	N.D.	N.D.	N.D.	N.D.	N.D.	N.D.	N.D.	N.D.	N.D.	N.D.	N.D.	N.D.
Ru	N.D.	N.D.	N.D.	N.D.	N.D.	N.D.	N.D.	N.D.	N.D.	N.D.	N.D.	N.D.	N.D.	N.D.	N.D.	N.D.	N.D.
Sb	2.00	17.00	1.00	N.D.	N.D.	N.D.	N.D.	8.00	145.00	2.00	504.00	5.00	1.00	133.00	2.00	3.00	2.00
Sc	4.30	1.10	0.20	1.30	1.40	0.90	0.50	0.30	0.70	2.60	0.40	0.20	0.60	1.30	0.90	0.40	0.60
Se	N.D.	1.00	N.D.	N.D.	N.D.	N.D.	N.D.	N.D.	N.D.	N.D.	5.00	N.D.	N.D.	1.00	1.00	N.D.	1.00
Sm	2.20	0.70	0.10	0.70	0.40	1.70	0.50	0.40	0.40	2.50	0.40	0.10	0.60	0.80	1.10	N.D.	0.10
Sn	1.00	N.D.	N.D.	N.D.	N.D.	1.00	N.D.	N.D.	N.D.	1.00	N.D.	N.D.	N.D.	1.00	N.D.	N.D.	N.D.
Sr	182.00	293.00	3.00	6.00	22.00	15.00	5.00	4.00	4.00	35.00	233.00	1.00	5.00	78.00	9.00	9.00	8.00
Tb	0.30	0.10	N.D.	0.10	0.10	0.20	0.10	0.10	N.D.	0.30	N.D.	N.D.	0.10	0.10	0.10	N.D.	N.D.
Te	N.D.	1.00	N.D.	N.D.	1.00	N.D.	N.D.	9.00	8.00	N.D.	N.D.	N.D.	N.D.	3.00	N.D.	N.D.	1.00
Th	1.80	0.70	0.10	2.10	0.20	3.80	1.70	1.50	0.90	9.30	0.50	N.D.	4.00	4.90	4.90	0.50	0.40
Ti	64.00	27.00	14.00	103.00	41.00	41.00	37.00	21.00	35.00	28.00	11.00	3.00	22.00	38.00	32.00	11.00	19.00
Tl	N.D.	N.D.	N.D.	N.D.	N.D.	N.D.	N.D.	N.D.	N.D.	N.D.	N.D.	N.D.	N.D.	N.D.	N.D.	N.D.	N.D.
Tm	N.D.	N.D.	N.D.	N.D.	N.D.	0.10	N.D.	N.D.	N.D.	0.10	N.D.	N.D.	N.D.	N.D.	N.D.	N.D.	N.D.
U	0.20	0.10	0.10	0.60	0.20	1.00	0.70	0.10	0.40	0.80	0.90	0.10	0.60	1.70	1.80	0.90	0.30
V	19.00	8.00	3.00	11.00	22.00	5.00	5.00	7.00	14.00	5.00	204.00	5.00	12.00	15.00	7.00	6.00	4.00
W	746.00	191.00	5.00	2.00	708.00	10.00	942.00	6.00	3.00	2.00	1172.00	14.00	13.00	3.00	1052.00	13.00	5.00
Y	4.10	3.00	0.40	2.40	2.40	4.50	4.00	1.40	0.70	6.50	0.70	0.80	2.20	0.80	1.80	0.20	0.40
Yb	0.40	0.20	0.10	0.30	0.20	0.50	0.20	0.10	0.10	0.60	0.60	0.10	0.20	0.10	0.20	N.D.	N.D.
Zn	195.00	604.00	5.00	8.00	46.00	29.00	5.00	6.00	40.00	20.00	337.00	4.00	27.00	193.00	125.00	240.00	427.00

Continua en la siguiente p‡gina

Tabla A2. Continuación

Muestra	Pinta-2	Pit-1	Pit-2	Pit-3	Pit-4	Prieta-1	Prieta-3	Prieta-4	Prieta-5	Prieta-6	Quitovac-1	Quitovac-2	Quitovac-3	Quitovac-4	Quitovac-5	Quitovac-6	Sanluisito-1
Coordena.	113° 7' 17.3" 31° 24' 27.4"	112° 6' 57.5" 30° 31' 53.2"	112° 1' 52.0" 30° 22' 43.4"	112° 10' 48.2" 30° 4' 42.3"	112° 11' 2.8" 30° 4' 47.8"	113° 4' 7.1" 31° 18' 46.5"	113° 4' 28.1" 31° 19' 39.2"	113° 1' 12.9" 31° 14' 46.3"	113° 0' 51.9" 31° 14' 2.9"	113° 0' 51.7" 31° 14' 4.0"	112° 43' 37.3" 31° 25' 56.8"	112° 43' 38.1" 31° 26' 5.9"	112° 41' 51.1" 31° 25' 6.6"	112° 46' 6.1" 31° 29' 25.4"	112° 50' 23.6" 31° 30' 34.2"	112° 51' 55.3" 31° 29' 54.2"	112° 29' 43.0" 31° 4' 5.3"
Ag	5.00	33.00	N.D.	N.D.	N.D.	N.D.	N.D.	N.D.	N.D.	2.00	N.D.	1.00	8.00	1.00	1.00	1.00	1.00
Al	10329.00	536.00	77.00	1665.00	708.00	5388.00	7169.00	5252.00	7047.00	2861.00	2073.00	1361.00	7685.00	8711.00	1632.00	2635.00	1209.00
As	N.D.	N.D.	N.D.	N.D.	N.D.	2.00	1.00	2.00	2.00	17.00	N.D.	1.00	27.00	2.00	4.00	7.00	2.00
Au	**0.90**	**0.01**	N.D.	N.D.	N.D.	N.D.	N.D.	**0.03**	N.D.	**0.02**	**0.83**	**0.03**	**0.06**	**0.27**	**1.00**	**0.04**	**0.40**
Ba	93.00	88.00	4.00	16.00	4.00	64.00	169.00	102.00	69.00	138.00	37.00	36.00	88.00	130.00	30.00	49.00	19.00
Be	N.D.	N.D.	N.D.	N.D.	N.D.	N.D.	N.D.	N.D.	N.D.	N.D.	N.D.	N.D.	N.D.	N.D.	N.D.	N.D.	N.D.
Bi	N.D.	N.D.	N.D.	N.D.	1.00	N.D.	1.00	1.00	1.00	4.00	N.D.	1.00	10.00	1.00	5.00	5.00	N.D.
Ca	6700.00	140.00	350.00	3055.00	143.00	1406.00	2594.00	2403.00	18263.00	93304.00	1448.00	103.00	11314.00	2541.00	1456.00	684.00	857.00
Cd	5.00	N.D.	N.D.	N.D.	N.D.	N.D.	N.D.	N.D.	N.D.	N.D.	N.D.	N.D.	N.D.	N.D.	N.D.	N.D.	N.D.
Ce	7.90	1.60	0.10	0.50	1.80	6.80	6.60	79.70	5.70	5.60	9.20	1.40	6.50	30.00	1.50	2.70	1.90
Co	1.00	328.00	1.00	1.00	1.00	1.00	1.00	1.00	5.00	8.00	4.00	1.00	1.00	3.00	1.00	1.00	1.00
Cr	309.00	2.00	451.00	406.00	427.00	264.00	245.00	311.00	316.00	210.00	335.00	423.00	371.00	344.00	398.00	380.00	382.00
Cu	164.00	46.00	10.00	18.00	23.00	6.00	9.00	13.00	29.00	1002.00	6.00	15.00	151.00	121.00	16.00	12.00	7.00
Dy	0.30	0.10	N.D.	N.D.	N.D.	0.30	0.50	2.90	0.50	1.30	0.60	N.D.	0.50	0.90	N.D.	0.10	0.10
Er	0.20	0.10	N.D.	N.D.	N.D.	0.10	0.30	1.40	0.30	0.80	0.50	N.D.	0.30	0.50	N.D.	N.D.	N.D.
Eu	0.30	N.D.	N.D.	N.D.	N.D.	0.30	0.50	0.60	0.30	1.30	0.10	N.D.	0.20	0.40	N.D.	N.D.	N.D.
Fe	6380.00	2210.00	4200.00	4043.00	3464.00	3111.00	3528.00	5404.00	11539.00	27641.00	30248.00	4529.00	15910.00	11746.00	5568.00	9822.00	3512.00
Gd	0.60	0.10	N.D.	N.D.	0.10	0.60	0.50	6.30	0.70	1.10	0.70	0.10	0.70	2.40	0.10	0.20	0.10
Ho	0.10	N.D.	N.D.	N.D.	N.D.	0.10	0.10	0.50	0.10	0.30	0.10	N.D.	0.10	0.10	N.D.	N.D.	N.D.
Ir	N.D.	N.D.	N.D.	N.D.	N.D.	N.D.	N.D.	N.D.	N.D.	N.D.	N.D.	N.D.	N.D.	N.D.	N.D.	N.D.	N.D.
K	5681.00	305.00	43.00	767.00	338.00	3073.00	4072.00	1822.00	2053.00	495.00	1146.00	822.00	3493.00	4881.00	929.00	1839.00	742.00
La	4.00	0.60	0.10	0.40	1.20	3.80	3.90	33.80	2.40	2.40	4.60	0.70	3.60	14.10	1.00	1.70	1.00
Lu	N.D.	N.D.	N.D.	N.D.	N.D.	N.D.	N.D.	0.20	N.D.	0.10	0.10	N.D.	N.D.	0.10	N.D.	N.D.	N.D.
Mg	474.00	52.00	31.00	221.00	38.00	231.00	362.00	862.00	2347.00	1652.00	298.00	120.00	584.00	497.00	115.00	112.00	109.00
Mn	521.00	27.00	43.00	65.00	31.00	56.00	43.00	109.00	239.00	891.00	103.00	30.00	723.00	175.00	43.00	89.00	68.00
Mo	6.00	1.00	1.00	1.00	1.00	1.00	1.00	1.00	1.00	2.00	1.00	4.00	22.00	4.00	2.00	3.00	1.00
Na	215.00	63.00	129.00	348.00	211.00	481.00	850.00	619.00	468.00	133.00	256.00	57.00	105.00	336.00	67.00	117.00	58.00
Nd	3.10	0.50	0.10	0.20	0.60	2.60	2.30	32.00	3.00	3.20	3.50	0.60	3.40	13.20	0.60	0.90	0.70
Ni	7.00	1.00	8.00	6.00	7.00	5.00	5.00	7.00	17.00	18.00	9.00	9.00	7.00	7.00	7.00	7.00	8.00
Os	N.D.	N.D.	N.D.	N.D.	N.D.	N.D.	N.D.	N.D.	N.D.	N.D.	N.D.	0.10	N.D.	N.D.	N.D.	N.D.	N.D.
P	89.00	56.00	12.00	37.00	19.00	228.00	557.00	265.00	394.00	88.00	59.00	20.00	144.00	80.00	23.00	60.00	23.00
Pb	2085.00	224.00	5.00	4.00	4.00	6.00	19.00	9.00	7.00	12.00	7.00	9.00	859.00	127.00	89.00	132.00	14.00
Pd	N.D.	N.D.	N.D.	N.D.	N.D.	N.D.	N.D.	N.D.	N.D.	N.D.	N.D.	N.D.	N.D.	N.D.	N.D.	N.D.	N.D.
Pr	0.90	0.10	N.D.	0.10	0.20	0.70	0.70	8.80	0.70	0.70	1.00	0.20	0.90	3.50	0.20	0.30	0.20
Pt	N.D.	0.10	N.D.	N.D.	N.D.	N.D.	0.10	0.10	N.D.	N.D.	N.D.	N.D.	N.D.	N.D.	N.D.	N.D.	N.D.
Rh	N.D.	N.D.	N.D.	N.D.	N.D.	N.D.	N.D.	N.D.	N.D.	N.D.	N.D.	N.D.	N.D.	N.D.	N.D.	N.D.	N.D.
Ru	N.D.	N.D.	N.D.	N.D.	N.D.	N.D.	N.D.	N.D.	N.D.	0.10	N.D.	N.D.	N.D.	N.D.	N.D.	N.D.	N.D.
Sb	3.00	44.00	3.00	3.00	2.00	1.00	1.00	1.00	1.00	1.00	1.00	3.00	5.00	2.00	6.00	10.00	3.00
Sc	0.90	0.20	0.10	0.20	0.10	0.30	0.50	0.60	1.40	1.90	4.50	0.60	1.40	1.50	0.40	0.50	0.30
Se	N.D.	N.D.	N.D.	N.D.	N.D.	N.D.	N.D.	N.D.	N.D.	N.D.	N.D.	N.D.	1.00	9.00	N.D.	N.D.	N.D.
Sm	0.60	0.10	N.D.	N.D.	0.10	0.50	0.50	6.70	0.70	0.90	0.70	0.10	0.70	2.60	0.10	0.10	0.10
Sn	N.D.	N.D.	N.D.	N.D.	N.D.	N.D.	N.D.	N.D.	N.D.	N.D.	1.00	N.D.	N.D.	1.00	N.D.	N.D.	N.D.
Sr	34.00	3.00	1.00	12.00	2.00	7.00	11.00	14.00	25.00	63.00	3.00	1.00	77.00	18.00	4.00	16.00	2.00
Tb	0.10	N.D.	N.D.	N.D.	N.D.	0.10	0.10	0.70	0.10	0.20	0.10	N.D.	0.10	0.20	N.D.	N.D.	N.D.
Te	N.D.	N.D.	N.D.	N.D.	N.D.	N.D.	N.D.	N.D.	N.D.	1.00	N.D.	N.D.	1.00	N.D.	4.00	9.00	1.00
Th	1.40	0.20	N.D.	3.90	2.10	1.10	1.30	26.90	0.50	0.10	2.80	0.60	1.30	4.00	0.20	0.50	0.60
Ti	39.00	11.00	5.00	9.00	12.00	23.00	23.00	23.00	29.00	13.00	1347.00	32.00	116.00	88.00	25.00	37.00	22.00
Tl	N.D.	N.D.	N.D.	N.D.	N.D.	N.D.	N.D.	N.D.	N.D.	N.D.	N.D.	N.D.	N.D.	N.D.	N.D.	N.D.	N.D.
Tm	N.D.	N.D.	N.D.	N.D.	N.D.	N.D.	N.D.	0.20	N.D.	0.10	0.10	N.D.	N.D.	0.10	N.D.	N.D.	N.D.
U	3.00	0.40	N.D.	0.70	0.60	0.10	0.20	2.40	0.30	0.30	0.80	0.20	1.90	1.10	0.10	0.40	0.10
V	53.00	2.00	4.00	3.00	3.00	2.00	4.00	6.00	15.00	22.00	42.00	5.00	129.00	7.00	7.00	4.00	3.00
W	23.00	601.00	3.00	1.00	N.D.	N.D.	1.00	1.00	1.00	2.00	1.00	1.00	11.00	10.00	5.00	51.00	1.00
Y	1.50	0.70	0.10	0.30	0.20	1.30	2.50	10.80	2.50	7.30	4.20	0.20	2.50	3.30	0.10	0.60	0.20
Yb	0.20	0.10	N.D.	N.D.	N.D.	0.10	0.30	1.30	0.20	0.60	0.70	N.D.	0.30	0.40	N.D.	N.D.	N.D.
Zn	461.00	7.00	2.00	2.00	3.00	4.00	6.00	10.00	15.00	23.00	8.00	4.00	85.00	12.00	54.00	11.00	5.00

Continua en la siguiente página

Tabla A2. Continuaci~~ó~~n

Muestra	Sanluisito-2	Sanluisito-3	Sanfran-1	Sanfran-2	Sanfran-3	Sanfran-4a	Sanfran-4b	Sanfran-4c	Sanfran-5a	Sanfran-5b	Sanfran-6	Sanfran-7	Sanfran-8	Sanfran-8a	Sanfran-9	Sanfran-10	Sanfran-11
Coordena.	112¡ 37' 31.0"	112¡ 29' 18.1"	113¡ 3' 56.0"	113¡ 5' 3.7"	113¡ 4' 44.1"	113¡ 6' 42.4"	113¡ 6' 39.0"	113¡ 6' 35.5"	113¡ 6' 51.3"	113¡ 6' 51.9"	113¡ 6' 33.7"	113¡ 6' 34.5"	113¡ 8' 11.4"	113¡ 8' 11.0"	113¡ 8' 11.4"	113¡ 8' 14.3"	113¡ 8' 19.8"
	31¡ 17' 2.0"	31¡ 22' 57.0"	31¡ 32' 22.6"	31¡ 31' 59.0"	31¡ 31' 21.7"	31¡ 37' 37.0"	31¡ 37' 37.2"	31¡ 37' 36.4"	31¡ 37' 25.4"	31¡ 37' 25.7"	31¡ 37' 57.5"	31¡ 38' 23.3"	31¡ 40' 19.8"	31¡ 40' 20.2"	31¡ 40' 20.3"	31¡ 40' 15.5"	31¡ 40' 16.4"
Ag	1.00	8.00	13.00	8.00	1.00	28.00	10.00	36.00	5.00	5.00	8.00	4.00	19.00	3.00	4.00	4.00	58.00
Al	3359.00	10319.00	10999.00	2681.00	559.00	303.00	4338.00	7517.00	2973.00	5338.00	4838.00	3108.00	2103.00	84.00	7362.00	1357.00	10753.00
As	2.00	3.00	65.00	6.00	N.D.	N.D.	3.00	9.00	5.00	4.00	3.00	N.D.	20.00	13.00	57.00	85.00	39.00
Au	**0.30**	**0.80**	**0.33**	**0.80**	N.D.	**4.87**	**0.47**	**4.90**	**0.09**	**1.20**	**0.17**	**0.01**	**1.00**	**5.50**	**4.67**	**17.26**	**2.67**
Ba	131.00	51.00	907.00	89.00	23.00	57.00	181.00	193.00	52.00	109.00	66.00	60.00	33.00	7.00	69.00	254.00	443.00
Be	N.D.	N.D.	2.00	N.D.	N.D.	N.D.	3.00	5.00	N.D.	1.00	3.00	N.D.	N.D.	N.D.	2.00	N.D.	2.00
Bi	1.00	N.D.	231.00	9.00	2.00	4.00	62.00	3.00	14.00	1.00	39.00	8.00	16.00	3.00	4.00	1.00	42.00
Ca	440.00	2590.00	4280.00	16220.00	690.00	338.00	5766.00	824.00	796.00	1194.00	365.00	362.00	434.00	79.00	1881.00	28620.00	2780.00
Cd	N.D.	1.00	N.D.	N.D.	N.D.	19.00	1.00	1.00	N.D.	N.D.	N.D.	N.D.	9.00	N.D.	N.D.	N.D.	8.00
Ce	6.10	14.60	10.20	2.40	0.50	0.80	7.00	22.60	10.00	5.70	4.70	1.60	2.10	0.10	11.00	1.50	12.40
Co	4.00	4.00	4.00	5.00	1.00	1.00	5.00	8.00	1.00	3.00	2.00	1.00	2.00	1.00	1.00	1.00	14.00
Cr	418.00	364.00	317.00	341.00	257.00	357.00	302.00	236.00	261.00	346.00	296.00	317.00	332.00	321.00	321.00	308.00	377.00
Cu	18.00	2665.00	5703.00	67.00	311.00	358.00	328.00	75.00	15.00	39.00	33.00	9.00	170.00	9.00	179.00	31.00	991.00
Dy	0.10	0.50	0.20	0.20	N.D.	N.D.	0.40	0.40	0.20	0.10	0.10	0.10	0.10	N.D.	0.30	0.10	0.60
Er	0.10	0.30	0.10	0.10	N.D.	N.D.	0.30	0.20	0.10	0.10	0.10	N.D.	N.D.	N.D.	0.10	N.D.	0.30
Eu	0.20	0.20	0.50	0.10	N.D.	N.D.	0.20	0.40	0.10	0.10	0.10	0.10	N.D.	N.D.	0.20	0.10	0.40
Fe	13720.00	13990.00	22580.00	8353.00	7081.00	8957.00	14356.00	48262.00	11017.00	17067.00	12794.00	7977.00	11641.00	8701.00	22730.00	34360.00	24830.00
Gd	0.40	1.00	0.70	0.20	N.D.	0.10	0.60	1.40	0.70	0.40	0.30	0.10	0.20	N.D.	0.80	0.10	1.20
Ho	N.D.	0.10	N.D.	N.D.	N.D.	N.D.	0.10	0.10	N.D.	N.D.	N.D.	N.D.	N.D.	N.D.	N.D.	N.D.	0.10
Ir	N.D.	N.D.	N.D.	N.D.	N.D.	N.D.	N.D.	N.D.	N.D.	N.D.	N.D.	N.D.	N.D.	N.D.	N.D.	N.D.	N.D.
K	1954.00	2773.00	5802.00	1718.00	377.00	161.00	3026.00	5159.00	2640.00	2781.00	3475.00	1716.00	1053.00	65.00	3025.00	641.00	5350.00
La	3.20	8.10	5.30	1.30	0.30	0.20	5.00	11.80	5.40	3.00	3.50	1.00	1.10	0.10	5.60	0.80	6.40
Lu	N.D.	N.D.	N.D.	N.D.	N.D.	N.D.	N.D.	N.D.	N.D.	N.D.	N.D.	N.D.	N.D.	N.D.	N.D.	N.D.	N.D.
Mg	411.00	3854.00	1029.00	425.00	49.00	41.00	2020.00	1281.00	367.00	694.00	1124.00	424.00	174.00	20.00	988.00	1803.00	1230.00
Mn	59.00	335.00	84.00	546.00	30.00	45.00	386.00	101.00	22.00	44.00	64.00	41.00	58.00	28.00	35.00	33.00	325.00
Mo	85.00	7.00	333.00	16.00	102.00	27.00	509.00	27.00	21.00	44.00	33.00	17.00	89.00	45.00	14.00	32.00	53.00
Na	150.00	181.00	210.00	98.00	48.00	50.00	151.00	159.00	491.00	153.00	159.00	118.00	65.00	50.00	952.00	97.00	195.00
Nd	2.50	5.30	4.20	1.20	0.20	0.20	2.20	8.80	3.70	2.10	1.70	0.70	1.00	0.10	4.60	0.70	5.80
Ni	8.00	12.00	11.00	8.00	6.00	7.00	17.00	13.00	16.00	11.00	8.00	7.00	9.00	6.00	7.00	7.00	19.00
Os	N.D.	N.D.	N.D.	0.10	N.D.	N.D.	N.D.	N.D.	N.D.	N.D.	N.D.	N.D.	N.D.	0.10	N.D.	0.10	N.D.
P	61.00	167.00	ND	65.00	33.00	23.00	107.00	429.00	51.00	101.00	98.00	77.00	49.00	16.00	56.00	155.00	124.00
Pb	154.00	643.00	1154.00	15.00	10.00	2681.00	2333.00	2434.00	162.00	80.00	712.00	90.00	1416.00	366.00	873.00	622.00	9807.00
Pd	N.D.	N.D.	N.D.	N.D.	N.D.	N.D.	N.D.	N.D.	N.D.	N.D.	N.D.	N.D.	N.D.	N.D.	N.D.	N.D.	N.D.
Pr	0.70	1.50	1.20	0.30	0.10	N.D.	0.60	2.50	1.10	0.60	0.50	0.20	0.30	N.D.	1.20	0.20	1.60
Pt	N.D.	N.D.	N.D.	N.D.	N.D.	N.D.	N.D.	N.D.	N.D.	N.D.	N.D.	N.D.	N.D.	N.D.	N.D.	N.D.	N.D.
Rh	N.D.	N.D.	0.10	N.D.	N.D.	N.D.	N.D.	N.D.	N.D.	N.D.	N.D.	N.D.	N.D.	N.D.	N.D.	N.D.	0.10
Ru	N.D.	N.D.	N.D.	N.D.	N.D.	N.D.	N.D.	N.D.	N.D.	N.D.	N.D.	N.D.	N.D.	N.D.	N.D.	N.D.	N.D.
Sb	14.00	3.00	43.00	11.00	N.D.	3.00	N.D.	1.00	1.00	2.00	3.00	1.00	2.00	1.00	2.00	3.00	16.00
Sc	0.90	2.20	1.60	0.70	0.10	0.10	1.30	2.00	0.70	1.50	1.10	0.60	0.40	0.20	0.90	0.80	1.90
Se	1.00	3.00	1.00	N.D.	1.00	1.00	N.D.	6.00	4.00	1.00	N.D.	N.D.	3.00	1.00	1.00	14.00	6.00
Sm	0.40	0.90	0.70	0.20	N.D.	0.10	0.50	1.40	0.60	0.40	0.30	0.10	0.20	N.D.	0.80	0.10	1.10
Sn	N.D.	N.D.	N.D.	N.D.	N.D.	N.D.	N.D.	N.D.	N.D.	N.D.	N.D.	N.D.	N.D.	N.D.	N.D.	N.D.	1.00
Sr	21.00	23.00	138.00	37.00	4.00	6.00	13.00	67.00	12.00	56.00	25.00	25.00	33.00	3.00	37.00	49.00	18.00
Tb	N.D.	0.10	0.10	N.D.	N.D.	N.D.	0.10	0.10	0.10	N.D.	N.D.	N.D.	N.D.	N.D.	0.10	N.D.	0.10
Te	N.D.	10.00	1.00	1.00	N.D.	2.00	3.00	2.00	2.00	1.00	2.00	1.00	1.00	N.D.	N.D.	N.D.	8.00
Th	0.70	3.90	0.90	0.70	0.10	0.10	3.10	2.20	1.90	0.80	0.80	0.10	0.30	0.20	1.10	0.40	1.20
Ti	54.00	122.00	141.00	41.00	14.00	3.00	108.00	58.00	31.00	47.00	62.00	24.00	15.00	7.00	53.00	54.00	151.00
Tl	N.D.	N.D.	N.D.	N.D.	N.D.	N.D.	N.D.	N.D.	N.D.	N.D.	N.D.	N.D.	N.D.	N.D.	N.D.	N.D.	N.D.
Tm	N.D.	N.D.	N.D.	N.D.	N.D.	N.D.	N.D.	N.D.	N.D.	N.D.	N.D.	N.D.	N.D.	N.D.	N.D.	N.D.	N.D.
U	1.20	0.60	23.10	0.90	0.20	0.60	1.50	7.40	1.30	16.10	0.90	0.20	0.20	0.10	0.10	0.20	1.30
V	25.00	46.00	36.00	10.00	8.00	2.00	24.00	50.00	20.00	23.00	82.00	11.00	9.00	3.00	160.00	12.00	27.00
W	3.00	1.00	2.00	5.00	4.00	343.00	525.00	136.00	178.00	401.00	349.00	174.00	26.00	6.00	8.00	9.00	7.00
Y	0.40	2.60	0.80	1.00	0.30	0.20	2.40	1.30	0.60	0.50	0.90	0.20	0.30	N.D.	0.80	0.50	2.50
Yb	N.D.	0.30	0.10	0.10	N.D.	N.D.	0.30	0.20	0.10	0.10	0.10	N.D.	N.D.	N.D.	0.10	0.10	0.30
Zn	62.00	1615.00	41.00	6.00	6.00	729.00	684.00	441.00	15.00	28.00	22.00	7.00	315.00	8.00	145.00	29.00	1587.00

Continua en la siguiente p~~á~~gina

Tabla A2. Continuación

Muestra	Sanfran-12	Sanfran-13	Sanfran-14	Sanfran-15	SanfLlano-1	SanfLlano-2	SanfLlano-2a	SanfLlano-11	Sonoyta-1	Sonoyta-2	Sonoyta-3	Sonoyta-4	Sonoyta-5	Taj-1	Taj-2	Taj-3	Taj-4
Coordena.	113° 8' 22.0"	113° 8' 5.1"	113° 7' 56.7"	113° 7' 41.6"	111° 6' 53.5"	111° 8' 16.6"	111° 8' 23.8"	111° 7' 5.2"	113° 0' 36.5"	112° 59' 32.8"	112° 49' 29.3"	112° 59' 50.2"	112° 52' 3.5"	112° 22' 0.2"	112° 22' 2.6"	112° 22' 6.4"	112° 22' 7.8"
	31° 40' 10.1"	31° 40' 11.6"	31° 39' 53.0"	31° 40' 25.4"	30° 20' 35.1"	30° 21' 12.3"	30° 21' 10.6"	30° 21' 1.3"	31° 53' 20.2"	31° 52' 46.0"	31° 51' 0.2"	31° 52' 5.0"	31° 49' 3.5"	30° 57' 32.7"	30° 57' 34.2"	30° 57' 35.6"	30° 57' 40.8"
Ag	8.00	1.00	6.00	3.00	1.00	N.D.	N.D.	31.00	2.00	9.00	1.00	3.00	59.00	8.00	21.00	153.00	11.00
Al	15527.00	2569.00	3573.00	10092.00	10191.00	6171.00	10384.00	1775.00	796.00	1235.00	4037.00	14913.00	3093.00	1578.00	1360.00	199.00	641.00
As	24.00	N.D.	4.00	7.00	N.D.	6.00	4.00	N.D.	28.00	23.00	2.00	14.00	7.00	25.00	83.00	189.00	134.00
Au	**0.13**	**0.03**	**0.13**	**0.20**	**1.40**	**0.05**	**0.08**	**115.66**	**1.03**	**4.00**	N.D.	**1.40**	**0.09**	**0.43**	**6.90**	**0.33**	**1.27**
Ba	675.00	117.00	65.00	187.00	108.00	83.00	34.00	7.00	54.00	32.00	149.00	54.00	9638.00	32.00	43.00	4.00	5.00
Be	2.00	1.00	1.00	1.00	N.D.	N.D.	N.D.	N.D.	N.D.	N.D.	N.D.	N.D.	N.D.	N.D.	N.D.	N.D.	N.D.
Bi	23.00	1.00	3.00	7.00	N.D.	N.D.	N.D.	52.00	94.00	27.00	1.00	49.00	2.00	2.00	1.00	6.00	1.00
Ca	1010.00	1220.00	4290.00	3670.00	10004.00	5751.00	43801.00	246.00	5035.00	772.00	598.00	9870.00	259.00	173.00	507.00	46.00	2868.00
Cd	1.00	1.00	4.00	N.D.	N.D.	N.D.	N.D.	N.D.	1.00	N.D.	N.D.	3.00	1.00	1.00	6.00	N.D.	N.D.
Ce	9.20	1.60	1.60	0.90	27.60	18.70	4.00	0.70	2.30	0.90	4.40	15.70	4.30	5.50	7.90	0.30	1.20
Co	6.00	3.00	2.00	4.00	48.00	3.00	11.00	7.00	4.00	2.00	2.00	11.00	N.D.	1.00	1.00	1.00	2.00
Cr	371.00	401.00	347.00	373.00	330.00	354.00	235.00	391.00	338.00	368.00	366.00	277.00	388.00	381.00	316.00	385.00	347.00
Cu	81.00	32.00	293.00	665.00	13.00	66.00	49.00	279.00	1527.00	360.00	450.00	9709.00	483.00	41.00	10.00	12.00	31.00
Dy	0.30	0.20	0.30	0.10	1.40	1.30	0.40	0.20	0.20	0.10	0.40	0.70	0.10	0.10	0.10	N.D.	0.10
Er	0.10	0.20	0.20	0.10	0.80	0.80	0.40	0.10	0.10	N.D.	0.20	0.40	0.10	0.10	N.D.	N.D.	0.10
Eu	0.40	0.10	0.10	0.10	0.50	0.30	0.20	N.D.	0.10	N.D.	0.10	0.30	3.70	0.10	0.10	N.D.	0.10
Fe	25690.00	10310.00	7420.00	25010.00	36216.00	14159.00	16355.00	15239.00	10446.00	16615.00	6797.00	42998.00	6149.00	10881.00	6099.00	5118.00	7556.00
Gd	0.70	0.20	0.20	0.10	2.20	1.80	0.40	0.20	0.30	0.10	0.40	1.10	0.30	0.40	0.50	N.D.	0.10
Ho	N.D.	N.D.	0.10	N.D.	0.30	0.30	0.10	N.D.	N.D.	N.D.	0.10	0.10	N.D.	N.D.	N.D.	N.D.	N.D.
Ir	N.D.	N.D.	N.D.	N.D.	N.D.	N.D.	N.D.	N.D.	N.D.	N.D.	N.D.	N.D.	N.D.	N.D.	N.D.	N.D.	N.D.
K	9353.00	1484.00	1841.00	5524.00	4935.00	1380.00	802.00	305.00	303.00	637.00	2056.00	2193.00	1768.00	996.00	936.00	33.00	347.00
La	5.20	0.90	0.80	0.60	13.40	10.20	2.10	1.10	1.30	0.80	2.20	8.90	2.80	2.60	3.90	0.10	0.60
Lu	N.D.	N.D.	N.D.	N.D.	0.10	0.10	0.10	N.D.	N.D.	N.D.	N.D.	0.10	0.40	N.D.	N.D.	N.D.	N.D.
Mg	1388.00	425.00	297.00	586.00	6694.00	2282.00	8589.00	395.00	285.00	327.00	1241.00	9220.00	107.00	150.00	122.00	13.00	218.00
Mn	71.00	70.00	228.00	61.00	305.00	134.00	582.00	41.00	185.00	32.00	110.00	793.00	140.00	78.00	44.00	98.00	166.00
Mo	8.00	2.00	1.00	89.00	ND	2.00	1.00	4.00	6.00	22.00	4.00	3.00	141.00	8.00	4.00	4.00	6.00
Na	489.00	83.00	97.00	186.00	543.00	494.00	488.00	65.00	47.00	78.00	255.00	352.00	95.00	50.00	51.00	34.00	43.00
Nd	3.20	0.70	0.70	0.40	11.30	8.40	1.70	0.70	1.00	0.50	1.70	6.20	1.50	2.30	3.10	0.10	0.60
Ni	19.00	8.00	10.00	8.00	60.00	10.00	16.00	10.00	7.00	6.00	8.00	19.00	7.00	7.00	6.00	6.00	8.00
Os	N.D.	N.D.	N.D.	N.D.	N.D.	N.D.	N.D.	N.D.	N.D.	N.D.	N.D.	0.10	N.D.	N.D.	N.D.	N.D.	N.D.
P	167.00	45.00	N.D.	30.00	571.00	180.00	137.00	44.00	18.00	57.00	91.00	187.00	39.00	60.00	21.00	45.00	16.00
Pb	282.00	9.00	222.00	9.00	13.00	11.00	18.00	263.00	23.00	755.00	192.00	35.00	897.00	856.00	564.00	13201.00	139.00
Pd	N.D.	N.D.	N.D.	N.D.	N.D.	N.D.	N.D.	N.D.	N.D.	N.D.	N.D.	N.D.	N.D.	N.D.	N.D.	N.D.	N.D.
Pr	0.90	0.20	0.20	0.10	3.10	2.30	0.50	0.20	0.30	0.10	0.50	1.80	0.40	0.60	0.90	N.D.	0.10
Pt	N.D.	N.D.	N.D.	N.D.	N.D.	N.D.	N.D.	N.D.	N.D.	N.D.	N.D.	N.D.	N.D.	N.D.	N.D.	N.D.	N.D.
Rh	N.D.	N.D.	N.D.	N.D.	N.D.	N.D.	N.D.	N.D.	N.D.	N.D.	N.D.	0.10	N.D.	N.D.	N.D.	0.10	N.D.
Ru	N.D.	N.D.	N.D.	N.D.	N.D.	N.D.	N.D.	N.D.	N.D.	N.D.	N.D.	0.10	N.D.	N.D.	N.D.	N.D.	N.D.
Sb	3.00	2.00	17.00	2.00	1.00	1.00	N.D.	2.00	2.00	2.00	1.00	1.00	24.00	4.00	3.00	34.00	3.00
Sc	2.70	0.90	0.90	1.30	3.00	2.00	3.90	0.40	0.30	0.40	1.20	5.80	0.30	0.30	0.20	N.D.	0.30
Se	4.00	N.D.	N.D.	3.00	N.D.	N.D.	N.D.	N.D.	1.00	N.D.	N.D.	N.D.	N.D.	1.00	N.D.	1.00	N.D.
Sm	0.70	0.20	0.20	0.10	2.00	1.60	0.30	0.10	0.20	0.10	0.30	1.00	0.30	0.40	0.50	N.D.	0.10
Sn	1.00	N.D.	N.D.	5.00	N.D.	N.D.	N.D.	N.D.	N.D.	N.D.	N.D.	2.00	N.D.	N.D.	N.D.	N.D.	N.D.
Sr	37.00	5.00	5.00	9.00	29.00	15.00	33.00	10.00	18.00	7.00	5.00	281.00	177.00	5.00	3.00	44.00	5.00
Tb	0.10	N.D.	N.D.	N.D.	0.30	0.30	0.10	N.D.	N.D.	N.D.	0.10	0.10	N.D.	N.D.	N.D.	N.D.	N.D.
Te	7.00	N.D.	1.00	N.D.	3.00	1.00	N.D.	306.00	14.00	12.00	N.D.	1.00	N.D.	4.00	16.00	31.00	2.00
Th	1.00	0.10	0.10	0.10	4.80	7.20	0.90	0.50	0.20	0.20	1.10	2.70	0.90	0.60	0.80	0.10	0.10
Ti	156.00	66.00	31.00	111.00	887.00	351.00	671.00	48.00	36.00	34.00	93.00	671.00	14.00	17.00	15.00	5.00	6.00
Tl	N.D.	N.D.	N.D.	N.D.	N.D.	N.D.	N.D.	N.D.	N.D.	N.D.	N.D.	N.D.	N.D.	N.D.	N.D.	N.D.	N.D.
Tm	N.D.	N.D.	N.D.	N.D.	0.10	0.10	0.10	N.D.	N.D.	N.D.	N.D.	0.10	N.D.	N.D.	N.D.	N.D.	N.D.
U	0.50	0.10	0.30	0.80	0.30	0.30	0.20	0.70	15.40	1.40	0.90	11.00	3.10	0.10	0.40	1.30	0.20
V	22.00	7.00	10.00	21.00	24.00	25.00	29.00	10.00	17.00	128.00	39.00	59.00	32.00	5.00	8.00	2.00	4.00
W	69.00	5.00	6.00	26.00	10.00	5.00	2.00	128.00	3.00	3.00	1.00	85.00	2.00	1.00	1.00	1.00	1.00
Y	1.10	1.30	1.40	1.00	6.90	5.90	3.00	1.00	1.10	0.50	1.90	3.30	0.50	0.40	0.20	N.D.	0.50
Yb	0.10	0.20	0.20	0.10	0.70	0.70	0.50	0.20	0.10	N.D.	0.20	0.40	0.90	N.D.	N.D.	N.D.	0.10
Zn	214.00	78.00	167.00	61.00	37.00	20.00	36.00	17.00	20.00	6.00	22.00	71.00	257.00	30.00	89.00	26.00	73.00

Continua en la siguiente página

Tabla A2. Continuaci–n

Muestra	Taj-5	Taj-6	Taj-7	Taj-8	Taj-9	Taj-10	Trin-1	Trin-2	Trin-10	Trin-11	Trin-12	Trin-13	Trin-14	Vidrios-1	Vidrios-2	Vidrios-3	Vidrios-4
Coordena.	112¡ 22' 7.5"	112¡ 21' 56.4"	112¡ 25' 36.1"	112¡ 25' 43.4"	112¡ 25' 33.5"	112¡ 26' 5.1"	111¡ 43' 31.0"	111¡ 56' 28.0"	111¡ 41' 14.1"	111¡ 40' 57.8"	111¡ 42' 2.0"	111¡ 42' 45.3"	111¡ 42' 14.4"	113¡ 40' 45.2"	113¡ 40' 45.5"	113¡ 45' 16.2"	113¡ 59' 58.5"
	30¡ 57' 42.0"	30¡ 57' 43.9"	30¡ 57' 22.3"	30¡ 57' 26.3"	30¡ 57' 22.3"	30¡ 56' 49.6"	30¡ 19' 37.1"	30¡ 10' 44.2"	30¡ 10' 57.9"	30¡ 11' 2.1"	30¡ 11' 14.5"	30¡ 10' 21.1"	30¡ 9' 31.6"	32¡ 5' 6.8"	32¡ 5' 6.5"	32¡ 8' 1.7"	32¡ 10' 52.4"
Ag	3.00	2.00	771.00	3.00	13.00	11.00	3.00	2.00	12.00	12.00	7.00	10.00	8.00	N.D.	N.D.	2.00	1.00
Al	3381.00	5836.00	8566.00	747.00	6301.00	2225.00	194.00	226.00	1875.00	3103.00	966.00	320.00	6142.00	1251.00	1402.00	2266.00	1855.00
As	232.00	51.00	35.00	9.00	47.00	19.00	N.D.	4.00	126.00	7.00	48.00	20.00	6.00	N.D.	N.D.	2.00	2.00
Au	**0.17**	**0.05**	**4.27**	**0.77**	**0.93**	**3.27**	**0.02**	**0.03**	**0.04**	**8.77**	**0.40**	**0.30**	**1.37**	N.D.	N.D.	**0.04**	**0.02**
Ba	40.00	43.00	45.00	9.00	734.00	26.00	6.00	8.00	31.00	130.00	19.00	11.00	54.00	26.00	37.00	99.00	35.00
Be	1.00	1.00	1.00	N.D.	1.00	N.D.	N.D.	N.D.	N.D.	N.D.	N.D.	N.D.	N.D.	N.D.	N.D.	N.D.	N.D.
Bi	N.D.	1.00	N.D.	N.D.	N.D.	1.00	N.D.	N.D.	30.00	82.00	8.00	4.00	15.00	6.00	N.D.	20.00	1.00
Ca	17515.00	625.00	8776.00	6216.00	1530.00	10955.00	117.00	9756.00	106.00	237.00	52.00	73.00	215.00	2477.00	2073.00	927.00	2014.00
Cd	N.D.	N.D.	3.00	N.D.	N.D.	2.00	N.D.	N.D.	N.D.	N.D.	N.D.	2.00	N.D.	N.D.	N.D.	N.D.	N.D.
Ce	7.00	49.70	12.70	0.60	16.10	5.30	0.20	0.20	8.70	22.80	1.10	0.80	25.90	0.30	2.00	0.10	1.50
Co	4.00	1.00	4.00	1.00	2.00	2.00	1.00	1.00	1.00	58.00	240.00	1.00	180.00	217.00	1.00	ND	2.00
Cr	326.00	277.00	257.00	366.00	16.00	340.00	341.00	313.00	323.00	179.00	2.00	327.00	3.00	4.00	195.00	234.00	236.00
Cu	14.00	9.00	373.00	10.00	15.00	69.00	6.00	92.00	29.00	115.00	5.00	84.00	288.00	4.00	4.00	2658.00	2656.00
Dy	0.50	1.10	0.60	N.D.	0.30	0.20	N.D.	N.D.	0.20	0.80	0.10	0.10	0.70	0.10	0.10	N.D.	0.10
Er	0.30	0.50	0.30	N.D.	0.10	0.10	N.D.	N.D.	0.10	0.50	N.D.	N.D.	0.30	N.D.	0.10	N.D.	N.D.
Eu	0.20	0.40	0.30	N.D.	0.40	0.10	N.D.	N.D.	0.10	0.20	N.D.	N.D.	0.40	N.D.	N.D.	N.D.	N.D.
Fe	16371.00	8871.00	15985.00	4269.00	12750.00	6918.00	3696.00	4815.00	10872.00	39792.00	2679.00	7935.00	8109.00	6271.00	4700.00	2644.00	7320.00
Gd	0.70	3.30	1.00	0.10	1.10	0.40	N.D.	N.D.	0.70	1.50	0.10	0.10	2.00	N.D.	0.10	N.D.	0.10
Ho	0.10	0.20	0.10	N.D.	N.D.	N.D.	N.D.	N.D.	N.D.	0.20	N.D.	N.D.	0.10	N.D.	N.D.	N.D.	N.D.
Ir	N.D.	N.D.	N.D.	N.D.	N.D.	N.D.	N.D.	N.D.	N.D.	N.D.	N.D.	N.D.	N.D.	N.D.	N.D.	N.D.	N.D.
K	1839.00	3692.00	4179.00	322.00	3279.00	1256.00	63.00	90.00	1371.00	2395.00	647.00	179.00	2881.00	814.00	1080.00	2819.00	1631.00
La	3.20	21.70	6.10	0.30	8.20	2.50	0.10	0.20	4.10	12.70	0.80	0.30	12.00	0.20	1.10	0.10	0.90
Lu	N.D.	N.D.	N.D.	N.D.	N.D.	N.D.	N.D.	N.D.	N.D.	0.10	N.D.	N.D.	N.D.	N.D.	N.D.	N.D.	N.D.
Mg	593.00	511.00	3093.00	116.00	641.00	1601.00	18.00	2444.00	128.00	138.00	94.00	48.00	619.00	334.00	143.00	52.00	437.00
Mn	395.00	127.00	251.00	33.00	23.00	256.00	33.00	85.00	37.00	28.00	3.00	35.00	68.00	13.00	30.00	17.00	81.00
Mo	26.00	2.00	4.00	1.00	10.00	3.00	1.00	10.00	3.00	ND	1.00	3.00	1.00	105.00	19.00	1.00	30.00
Na	113.00	124.00	341.00	97.00	135.00	184.00	55.00	38.00	272.00	1549.00	53.00	38.00	114.00	47.00	87.00	256.00	274.00
Nd	3.00	18.60	5.70	0.30	6.60	2.20	0.10	0.20	3.90	7.10	0.60	0.40	11.30	0.10	0.70	0.10	0.60
Ni	8.00	6.00	8.00	6.00	8.00	6.00	7.00	10.00	6.00	6.00	3.00	7.00	3.00	3.00	4.00	5.00	6.00
Os	N.D.	N.D.	0.10	N.D.	N.D.	N.D.	N.D.	0.10	N.D.	N.D.	N.D.	N.D.	N.D.	N.D.	N.D.	N.D.	N.D.
P	111.00	143.00	229.00	41.00	315.00	33.00	29.00	28.00	196.00	221.00	102.00	23.00	154.00	70.00	32.00	N.D.	13.00
Pb	107.00	46.00	333.00	48.00	50.00	409.00	3.00	902.00	462.00	21.00	643.00	2621.00	568.00	1.00	3.00	6.00	11.00
Pd	N.D.	N.D.	N.D.	N.D.	N.D.	N.D.	N.D.	N.D.	N.D.	N.D.	N.D.	N.D.	N.D.	N.D.	N.D.	N.D.	N.D.
Pr	0.80	5.20	1.50	0.10	1.80	0.60	N.D.	N.D.	1.00	2.30	0.20	0.10	3.00	N.D.	0.20	N.D.	0.20
Pt	N.D.	N.D.	N.D.	N.D.	N.D.	N.D.	N.D.	N.D.	N.D.	N.D.	N.D.	N.D.	0.10	N.D.	N.D.	N.D.	N.D.
Rh	N.D.	N.D.	N.D.	N.D.	N.D.	N.D.	N.D.	N.D.	N.D.	N.D.	N.D.	N.D.	N.D.	N.D.	N.D.	N.D.	N.D.
Ru	N.D.	N.D.	N.D.	N.D.	N.D.	N.D.	N.D.	N.D.	N.D.	N.D.	N.D.	N.D.	N.D.	N.D.	N.D.	N.D.	N.D.
Sb	3.00	2.00	33.00	3.00	3.00	39.00	3.00	6.00	3.00	1.00	1.00	3.00	1.00	N.D.	N.D.	1.00	1.00
Sc	1.00	0.70	2.20	0.10	0.90	0.40	N.D.	0.20	0.20	0.60	0.10	N.D.	0.60	0.20	0.30	0.10	0.20
Se	N.D.	N.D.	1.00	N.D.	N.D.	N.D.	N.D.	N.D.	N.D.	1.00	N.D.	1.00	N.D.	N.D.	N.D.	N.D.	N.D.
Sm	0.60	3.40	1.10	0.10	1.10	0.40	N.D.	N.D.	0.70	1.10	0.10	0.10	2.10	N.D.	0.10	N.D.	0.10
Sn	N.D.	1.00	N.D.	N.D.	N.D.	N.D.	N.D.	N.D.	N.D.	N.D.	N.D.	N.D.	N.D.	N.D.	N.D.	N.D.	6.00
Sr	20.00	45.00	40.00	13.00	100.00	12.00	2.00	9.00	11.00	14.00	1.00	3.00	9.00	3.00	10.00	13.00	12.00
Tb	0.10	0.30	0.10	N.D.	0.10	N.D.	N.D.	N.D.	0.10	0.20	N.D.	N.D.	0.20	N.D.	N.D.	N.D.	N.D.
Te	3.00	1.00	8.00	1.00	5.00	7.00	N.D.	N.D.	3.00	41.00	4.00	4.00	N.D.	N.D.	N.D.	1.00	N.D.
Th	0.60	6.90	1.80	0.10	2.10	0.80	0.10	0.30	2.40	38.60	0.40	0.30	3.20	0.10	0.20	N.D.	0.20
Ti	32.00	31.00	45.00	9.00	28.00	16.00	5.00	6.00	23.00	121.00	18.00	15.00	38.00	42.00	40.00	4.00	105.00
Tl	N.D.	N.D.	N.D.	N.D.	N.D.	N.D.	N.D.	N.D.	N.D.	N.D.	N.D.	N.D.	N.D.	N.D.	N.D.	N.D.	N.D.
Tm	N.D.	N.D.	N.D.	N.D.	N.D.	N.D.	N.D.	N.D.	N.D.	0.10	N.D.	N.D.	N.D.	N.D.	N.D.	N.D.	N.D.
U	1.00	1.00	0.30	0.10	0.30	3.80	0.20	0.40	0.70	0.30	0.10	0.40	0.70	0.10	N.D.	2.20	1.30
V	22.00	4.00	16.00	4.00	13.00	9.00	2.00	107.00	4.00	8.00	2.00	7.00	3.00	11.00	4.00	20.00	23.00
W	4.00	5.00	2.00	1.00	2.00	2.00	N.D.	3.00	1.00	N.D.	628.00	8.00	1081.00	736.00	5.00	4.00	2.00
Y	2.40	3.30	2.50	0.20	1.00	0.80	0.20	0.30	0.60	3.80	0.30	0.50	2.50	0.50	0.80	N.D.	0.70
Yb	0.30	0.30	0.20	N.D.	0.10	0.10	N.D.	N.D.	0.10	0.50	N.D.	N.D.	0.30	N.D.	0.10	N.D.	N.D.
Zn	36.00	33.00	200.00	4.00	43.00	169.00	1.00	5.00	20.00	12.00	21.00	42.00	12.00	4.00	3.00	5.00	67.00

Los elementos se analizaron por medio de ICP-AES. Para el an‡lisis del Au se implement–la tŽcnica de an‡lisis al fuego. Todos los valores se encuentran expresados en partes por mill–n (ppm). La conversi–n a gramos por tonelada (g/t = ppm).

N.D. = valor menor o igual a la capacidad de detecci–n anal'tica instrumental. Niv. det. = Nivel de detecci–n m'nimo. Coordena. = coordenadas geogr‡ficas. Datum de las coordenadas: WGS84.

Tabla A3. Resultados del balance de masas de las rocas encajonantes frescas y alteradas de la mineralización del Cinturón de Oro Orogénico Caborca, NW de Sonora, México.

Elemento	Alamo-1		Carolina-1		Carretera-2		Costa-4		Km100	
	Δ conc	Δ conc–C^A	Δ conc	Δ conc–C^A	Δ conc	Δ conc–C^A	Δ conc	Δ conc–C^A	Δ conc	Δ conc–C^A
Ag	0.14	2.80	0.00	0.00	0.00	-0.04	1.01	20.17	15.46	309.10
Al_2O_3	0.00	0.00	1.03	0.07	0.00	0.00	0.00	0.00	4.26	0.27
As	-16.35	-0.71	15.00	3.00	48.94	6.99	3.66	0.73	0.05	0.01
Au	0.00	-0.05	-0.03	-0.98	0.00	-0.04	-0.01	-0.95	0.00	0.00
Ba	-69.66	-0.11	-656.00	-0.39	-34.29	-0.06	103.47	0.12	212.29	0.15
Be	-0.03	-0.05	0.00	0.00	0.93	0.93	-0.04	-0.04	0.38	0.76
Bi	-0.03	-0.05	0.00	0.00	-0.02	-0.04	-0.02	-0.04	0.38	0.76
CaO	0.82	0.16	-1.97	-0.63	-0.61	-0.78	-0.65	-0.39	-3.79	-0.98
Cd	-0.03	-0.05	0.00	0.00	-0.02	-0.04	-0.02	-0.04	0.38	0.76
Ce	15.24	0.30	20.10	0.12	-4.21	-0.12	0.53	0.02	149.55	1.08
Co	-3.94	-0.18	4.00	0.21	-1.07	-0.36	-1.04	-0.52	-18.71	-0.78
Cr	-11.28	-0.31	2.00	0.10	1.75	0.35	-0.23	-0.04	-6.43	-0.38
Cu	59.56	2.29	2.00	0.08	29.72	5.95	-21.30	-0.74	51.52	1.98
Dy	-0.84	-0.23	1.00	0.11	-0.14	-0.11	-1.27	-0.42	-5.95	-0.60
Er	-0.47	-0.25	0.50	0.10	-0.02	-0.04	-1.03	-0.54	-3.56	-0.65
Eu	-0.37	-0.22	0.50	0.12	-0.12	-0.20	-0.13	-0.13	-1.13	-0.32
FeO	0.64	0.89	1.01	0.36	0.18	365.53	0.13	268.40	-4.33	-0.95
Fe_2O_3	-2.42	-0.43	-0.42	-0.08	0.25	0.23	-0.04	-0.04	-0.60	-0.18
Gd	-0.26	-0.05	1.70	0.11	-0.39	-0.14	-0.41	-0.13	-0.12	-0.01
Ho	-0.13	-0.21	0.20	0.12	-0.01	-0.04	-0.31	-0.52	-1.27	-0.71
Ir	0.09	0.90	0.00	0.00	0.00	-0.04	0.00	-0.04	0.13	2.52
K_2O	-0.06	-0.04	0.93	0.24	0.51	0.14	0.33	0.11	7.25	1.98
La	8.61	0.33	11.10	0.16	-1.53	-0.10	-0.18	-0.01	61.46	1.00
Lu	-0.11	-0.53	0.00	0.00	0.00	-0.04	-0.10	-0.52	-0.42	-0.71
MgO	0.27	0.09	0.13	0.07	0.00	-0.01	0.03	0.12	-0.86	-0.48
MnO	0.01	0.05	-0.07	-0.44	-0.05	-0.72	0.00	-0.04	-0.13	-0.88
Mo	-0.03	-0.05	0.00	0.00	0.47	0.93	0.46	0.92	0.76	0.76
Na	-5263.39	-0.23	-1.57	-0.93	-1.07	-0.29	0.07	0.02	-3.36	-0.94
Nd	1.09	0.04	10.00	0.12	-1.85	-0.13	-0.50	-0.04	24.29	0.32
Ni	-2.98	-0.07	6.00	0.27	6.43	0.72	0.70	0.10	8.71	0.38
Os	0.00	0.00	0.00	0.00	0.00	-0.04	0.00	-0.04	0.00	0.00
Pb	7.01	0.58	-23.00	-0.96	53.31	2.67	0.05	0.00	1325.91	45.72
Pd	-0.37	-0.21	0.10	0.25	-0.12	-0.20	-0.11	-0.36	0.08	0.10
Pr	1.02	0.16	2.40	0.12	-0.52	-0.13	-0.13	-0.04	11.22	0.64
Pt	-0.01	-0.05	0.00	0.00	-0.01	-0.04	0.14	2.85	-0.02	-0.12
P_2O_5	0.00	0.00	0.03	0.06	0.01	0.16	0.01	0.28	-0.30	-0.71
Rh	0.00	-0.05	0.00	0.00	0.00	-0.04	0.00	-0.04	0.04	0.76
Ru	-0.01	-0.05	0.00	0.00	0.00	-0.04	0.00	-0.04	0.04	0.76
Sb	-0.03	-0.05	0.00	0.00	3.36	6.72	-0.02	-0.04	1.26	2.52
Sc	-4.92	-0.38	1.30	0.06	-0.51	-0.08	-1.69	-0.43	-4.71	-0.25
Se	-0.03	-0.05	0.00	0.00	-0.02	-0.04	-7.52	-0.94	0.38	0.76
SiO_2	-4.00	-0.07	2.85	0.05	-2.20	-0.03	-5.09	-0.07	72.72	1.24
Sm	-0.44	-0.09	1.40	0.09	-0.59	-0.19	-0.30	-0.10	0.00	0.00
Sn	-0.03	-0.05	0.00	0.00	0.93	0.93	-1.04	-0.52	1.26	2.52
Sr	220.82	0.28	-100.00	-0.76	-36.99	-0.41	-53.30	-0.17	-171.71	-0.68
Tb	-0.13	-0.19	0.20	0.11	-0.01	-0.04	-0.21	-0.42	-0.67	-0.35
Te	-4.30	-0.43	3.00	0.23	-3.52	-0.88	0.46	0.92	-2.43	-0.19
Th	7.13	1.23	1.20	0.16	-1.65	-0.15	-1.09	-0.19	8.12	0.80
TiO_2	-0.16	-0.22	0.16	0.13	0.01	0.10	0.03	0.25	-0.58	-0.49
Tl	0.00	-0.05	0.00	0.00	-1.14	-0.23	2.77	0.92	12.28	245.67
Tm	-0.01	-0.05	0.00	0.00	0.00	-0.04	-0.20	-0.68	-0.42	-0.71
U	1.47	1.47	0.40	0.20	2.95	2.46	-0.44	-0.31	-1.57	-0.56
V	11.08	0.11	1.00	0.02	5.29	0.38	-0.38	-0.04	-25.71	-0.38
W	1.40	2.80	-1.00	-0.25	7.22	14.43	-0.04	-0.04	27.19	27.19
Y	-3.86	-0.23	3.20	0.07	-0.10	-0.02	-9.60	-0.56	-32.78	-0.69
Yb	-0.26	-0.19	0.30	0.08	-0.12	-0.17	-1.13	-0.57	-3.17	-0.72
Zn	11.31	0.14	-85.00	-0.47	-2.03	-0.07	4.84	0.10	-129.95	-0.62
PXC	0.08	0.02	-0.63	-0.15	0.58	0.73	0.63	0.85	2.61	2.35
Isocona	Al_2O_3, TiO_2, Yb		Lu, La, Ho		Al_2O_3, Lu, Ho		Al_2O_3, Lu, Pd		Sm, Pd, As	
Correlación	1.00		1.00		1.00		1.00		1.00	
Error	0.081		0.007		0.003		0.003		0.001	
ΔMasa	-4.9		0.0		-3.5		-3.8		76.2	

Continua en la siguiente página

Tabla A3. Continuaci–n

Elemento	Quitovac 2		Quitovac 3		Quitovac 5		Quitovac 6		Sanfran-1	
	Δ conc	Δ concÐC[A]	Δ conc	Δ concÐC[A]	Δ conc	Δ concÐC[A]	Δ conc	Δ concÐC[A]	Δ conc	Δ concÐC[A]
Ag	0.00	-0.02	0.11	2.11	-0.10	-0.11	-0.13	-0.26	2.64	6.60
Al_2O_3	0.00	0.00	3.12	0.20	0.00	0.00	0.00	0.00	0.00	0.00
As	-14.51	-0.97	0.28	0.55	-12.00	-0.71	-0.30	-0.08	-10.66	-0.82
Au	0.00	-0.02	-4.57	-1.00	-0.01	-0.97	0.00	-0.08	0.00	-0.22
Ba	157.67	0.11	-610.42	-0.51	17.54	0.02	-166.00	-0.11	125.51	0.26
Be	-0.01	-0.02	0.28	0.55	0.00	0.00	1.35	2.70	8.07	16.14
Bi	-0.01	-0.02	0.28	0.55	0.00	0.00	-0.04	-0.08	-0.11	-0.22
CaO	-1.35	-0.69	-3.00	-0.83	-3.69	-0.56	-1.53	-0.98	-2.37	-0.91
Cd	-0.01	-0.02	0.28	0.55	0.50	1.00	-0.04	-0.08	-0.11	-0.22
Ce	-10.67	-0.18	27.94	0.31	0.43	0.01	-28.04	-0.42	21.60	0.60
Co	-2.13	-0.27	-8.90	-0.74	-4.99	-0.17	-1.08	-0.54	-2.55	-0.32
Cr	0.87	0.17	-0.24	-0.03	-2.97	-0.06	3.39	0.85	0.91	0.09
Cu	52.41	2.76	12.58	0.37	281.22	2.70	9.81	0.34	621.78	25.91
Dy	-0.16	-0.06	-1.05	-0.26	-0.40	-0.18	-1.42	-0.88	-0.38	-0.38
Er	-0.04	-0.02	-0.48	-0.19	-0.20	-0.18	-0.61	-0.87	-0.19	-0.38
Eu	0.06	0.04	-0.87	-0.48	-0.10	-0.06	-0.86	-0.54	0.21	0.27
FeO	-0.07	-0.29	-1.09	-1.00	0.85	1.47	0.24	479.51	-0.03	-0.22
Fe_2O_3	-0.99	-0.29	-1.94	-0.61	-2.23	-0.33	0.47	0.36	0.46	0.20
Gd	-0.59	-0.13	-0.02	0.00	-0.40	-0.09	-2.92	-0.66	0.72	0.30
Ho	-0.01	-0.02	-0.18	-0.22	-0.10	-0.25	-0.15	-0.77	-0.12	-0.61
Ir	0.00	-0.02	0.03	0.55	0.00	0.00	-0.05	-0.54	-0.01	-0.22
K_2O	0.41	0.12	4.38	1.18	1.18	0.57	2.70	0.74	2.48	0.87
La	-3.40	-0.11	17.10	0.36	-0.19	-0.01	-13.84	-0.40	12.20	0.67
Lu	0.00	-0.02	0.01	0.04	0.00	0.00	-0.05	-0.54	-0.06	-0.61
MgO	-0.52	-0.54	-1.31	-0.84	-0.50	-0.12	0.00	0.01	0.18	0.18
MnO	-0.02	-0.51	-0.07	-0.83	-0.02	-0.22	0.00	-0.08	-0.03	-0.81
Mo	-0.01	-0.02	0.55	0.55	0.00	0.00	5.97	11.94	0.28	0.56
Na	-0.89	-0.21	-0.20	-0.06	-0.65	-0.16	-3.84	-0.96	-4.24	-0.98
Nd	-2.75	-0.12	2.44	0.07	-0.99	-0.04	-16.03	-0.61	6.28	0.41
Ni	-1.28	-0.09	7.08	0.71	-0.98	-0.03	-10.38	-0.69	0.14	0.01
Os	0.00	-0.02	0.00	0.55	0.00	0.00	0.00	-0.98	0.00	-0.22
Pb	-1.22	-0.11	20.05	1.82	39.03	3.90	277.87	9.92	64.69	3.08
Pd	-0.41	-0.46	0.18	0.29	-0.10	-0.17	-0.12	-0.31	-0.07	-0.22
Pr	-0.43	-0.07	2.05	0.21	-0.20	-0.04	-3.98	-0.54	2.05	0.50
Pt	-0.05	-0.51	-0.15	-0.48	0.00	0.00	0.00	-0.08	-0.16	-0.81
P_2O_5	-0.01	-0.10	-0.15	-0.83	0.00	0.00	0.02	0.29	-0.02	-0.17
Rh	0.00	-0.02	0.03	0.55	0.00	0.00	0.00	-0.08	-0.01	-0.22
Ru	0.00	-0.02	0.03	0.55	0.00	0.00	0.00	-0.08	-0.01	-0.22
Sb	-0.01	-0.02	0.28	0.55	0.00	0.00	4.12	8.24	0.28	0.56
Sc	-0.28	-0.03	-6.07	-0.62	-0.39	-0.03	-0.44	-0.13	3.04	1.09
Se	-2.51	-0.84	0.28	0.55	0.00	0.00	-0.04	-0.08	-0.11	-0.22
SiO_2	1.32	0.02	53.43	0.83	1.29	0.02	-8.22	-0.11	-19.09	-0.28
Sm	-0.48	-0.12	0.00	0.00	-0.40	-0.09	-3.00	-0.71	0.64	0.27
Sn	-0.01	-0.02	0.28	0.55	0.00	0.00	-0.54	-0.54	-0.11	-0.22
Sr	-72.87	-0.30	-229.24	-0.65	-552.89	-0.74	-259.28	-0.60	-484.93	-0.92
Tb	-0.01	-0.02	-0.18	-0.22	-0.10	-0.20	-0.31	-0.77	0.03	0.17
Te	-1.07	-0.27	-3.22	-0.81	-4.00	-0.31	0.85	0.85	0.34	0.17
Th	3.32	0.36	30.44	1.69	-0.30	-0.08	-13.37	-0.70	-2.36	-0.27
TiO_2	-0.01	-0.02	-0.28	-0.57	0.03	0.03	0.00	0.02	0.14	0.42
Tl	0.93	18.57	8.97	1.80	0.95	19.01	-8.23	-0.75	-1.44	-0.48
Tm	0.00	-0.02	0.01	0.04	0.00	0.00	-0.05	-0.54	-0.06	-0.61
U	1.05	0.75	-0.67	-0.15	-0.30	-0.25	-3.64	-0.89	2.91	0.86
V	1.26	0.04	-40.16	-0.62	-0.92	-0.01	-1.14	-0.08	35.89	1.03
W	0.94	0.47	8.32	8.32	7.01	7.01	10.09	10.09	8.07	16.14
Y	-1.18	-0.09	-4.87	-0.22	-2.10	-0.21	-5.65	-0.90	-2.38	-0.54
Yb	0.07	0.04	-0.23	-0.09	-0.20	-0.22	-0.41	-0.82	-0.24	-0.61
Zn	-43.78	-0.55	-15.63	-0.28	11.07	0.10	-4.39	-0.06	54.51	0.91
PXC	0.59	0.40	-0.15	-0.83	3.70	3.46	2.42	3.10	1.90	2.19
Isocona	Al_2O_3, Lu, Ho		Sm, Gd, Pd		Al_2O_3, Pd, Ho		Al_2O_3, Ho, Pd		Al_2O_3, Pd, Sn	
Correlaci–n	1.00		1.00		1.00		1.00		1.00	
Error	0.005		0.001		0.001		0.022		0.041	
ΔMasa	-2.2		55.3		0.6		-7.6		-21.3	

Continua en la siguiente p‡gina

Tabla A3. Continuación

Elemento	Sanfran-3		Sanfran-4		Sanfran-5		Sanfran-8		Sanfran-14	
	Δ conc	Δ conc–C^A	Δ conc	Δ conc–C^A	Δ conc	Δ conc–C^A	Δ conc	Δ conc–C^A	Δ conc	Δ conc–C^A
Ag	-0.01	-0.14	1.54	3.84	0.16	3.17	1.00	2.50	0.92	1.15
Al_2O_3	0.00	0.00	0.00	0.00	0.74	0.05	3.18	0.24	0.00	0.00
As	-0.07	-0.14	5.96	11.92	3.54	0.35	-6.00	-0.33	-10.39	-0.94
Au	0.00	-0.14	0.05	106.03	0.02	44.84	0.02	47.00	-0.01	-0.92
Ba	1676.41	1.04	1326.57	1.46	171.18	0.15	14.00	0.02	-375.46	-0.47
Be	0.36	0.72	-3.23	-0.54	0.02	0.04	6.50	13.00	0.12	0.23
Bi	-0.07	-0.14	0.42	0.85	0.02	0.04	0.00	0.00	0.12	0.23
CaO	-1.39	-0.90	-0.52	-0.74	-0.82	-0.78	-3.13	-0.92	4.17	0.58
Cd	-0.07	-0.14	-0.04	-0.08	0.02	0.04	0.00	0.00	0.12	0.23
Ce	-58.12	-0.81	11.58	1.30	6.97	0.06	-53.80	-0.86	-8.30	-0.19
Co	-4.57	-0.91	-0.04	-0.08	-1.04	-0.04	-13.00	-0.93	23.93	0.60
Cr	-2.85	-0.36	-0.46	-0.08	5.18	0.05	-43.00	-0.84	554.58	1.99
Cu	429.42	16.52	296.25	26.93	65.92	2.06	121.00	5.26	-10.39	-0.55
Dy	-0.54	-0.39	0.12	0.13	-0.60	-0.11	-3.90	-0.95	0.40	0.04
Er	0.00	0.00	-0.15	-0.19	-0.31	-0.12	-2.30	-0.96	0.95	0.15
Eu	-0.87	-0.35	0.60	1.00	0.08	0.04	-1.40	-0.74	-0.06	-0.03
FeO	-0.07	-0.37	0.00	0.00	-3.96	-0.79	0.11	0.73	3.10	0.54
Fe_2O_3	-2.03	-0.79	0.02	0.03	1.35	0.52	-3.02	-0.78	2.24	0.64
Gd	-3.10	-0.72	1.23	1.54	0.06	0.01	-5.00	-0.88	-0.54	-0.06
Ho	-0.03	-0.14	-0.02	-0.08	-0.17	-0.17	-0.75	-0.94	0.34	0.17
Ir	-0.01	-0.14	0.04	0.85	0.00	0.04	0.00	0.00	0.07	1.46
K_2O	3.83	1.02	3.62	0.77	1.25	0.34	2.03	1.53	0.27	0.12
La	-31.44	-0.80	4.83	0.88	0.00	0.00	-26.30	-0.83	-3.18	-0.19
Lu	-0.01	-0.14	-0.11	-0.54	0.01	0.04	-0.25	-0.83	0.21	0.23
MgO	-0.13	-0.51	0.02	0.27	-1.49	-0.49	-1.52	-0.59	6.83	0.95
MnO	-0.01	-0.57	0.00	-0.08	-0.03	-0.41	-0.04	-0.67	0.11	0.69
Mo	34.66	69.33	23.49	46.98	1.08	1.08	6.50	13.00	0.12	0.23
Na	-1.27	-0.58	-2.60	-0.64	-0.67	-0.61	-1.52	-0.47	-1.09	-0.41
Nd	-23.81	-0.83	8.65	3.20	1.69	0.04	-24.90	-0.87	-2.88	-0.10
Ni	-1.85	-0.27	-2.85	-0.22	-3.75	-0.06	-67.00	-0.83	62.76	0.39
Os	0.00	-0.14	0.00	59.90	0.00	0.04	0.00	0.00	0.00	1.46
Pb	16.74	0.62	367.96	4.97	39.38	1.97	409.00	204.50	-11.00	-1.00
Pd	-0.03	-0.14	-0.45	-0.41	0.11	0.56	-0.20	-0.67	0.16	0.23
Pr	-6.13	-0.82	1.87	2.08	0.32	0.03	-6.40	-0.87	-0.84	-0.13
Pt	-0.01	-0.14	0.00	-0.08	0.00	0.04	-1.15	-0.96	0.01	0.23
P_2O_5	-0.04	-1.00	0.05	4.54	-0.02	-0.38	-0.06	-0.75	-0.11	-0.43
Rh	-0.01	-0.14	0.00	-0.08	0.00	0.04	0.00	0.00	0.01	0.23
Ru	-0.01	-0.14	0.00	-0.08	0.00	0.04	0.00	0.00	0.01	0.23
Sb	1.22	2.43	-0.04	-0.08	0.02	0.04	0.00	0.00	6.88	13.75
Sc	-0.63	-0.24	0.85	0.85	-0.83	-0.05	-6.70	-0.68	30.75	1.01
Se	-3.57	-0.89	1.35	2.69	0.02	0.04	0.50	1.00	0.12	0.23
SiO_2	-11.84	-0.16	-6.51	-0.09	7.69	0.13	0.75	0.01	4.95	0.10
Sm	-3.23	-0.81	1.62	3.24	0.55	0.07	-4.40	-0.88	-0.30	-0.04
Sn	-0.07	-0.14	-1.08	-0.54	0.02	0.04	0.50	1.00	0.12	0.23
Sr	129.89	0.84	-56.74	-0.16	-78.04	-0.61	-216.00	-0.54	-163.73	-0.48
Tb	-0.23	-0.57	0.18	1.77	-0.06	-0.05	-0.75	-0.94	0.00	0.00
Te	-5.57	-0.93	-0.04	-0.08	-6.75	-0.52	-0.50	-0.50	2.98	0.23
Th	-8.36	-0.90	-1.24	-0.23	1.89	0.12	-7.40	-0.90	0.58	1.46
TiO_2	-0.22	-0.79	0.02	0.38	-0.04	-0.05	-0.27	-0.77	-0.11	-0.13
Tl	-3.85	-0.43	5.00	0.71	4.12	82.34	4.00	0.50	0.01	0.23
Tm	-0.01	-0.14	-0.01	-0.08	0.01	0.04	-0.25	-0.83	0.21	0.23
U	0.10	0.20	-2.96	-0.61	5.38	3.36	-0.40	-0.50	0.09	0.23
V	-2.13	-0.10	0.61	0.04	3.47	0.03	-5.00	-0.13	115.35	0.87
W	0.36	0.72	29.95	59.90	26.09	26.09	16.00	16.00	0.23	0.23
Y	-1.07	-0.19	-0.18	-0.03	-2.93	-0.13	-18.40	-0.97	7.40	0.15
Yb	0.20	0.50	-0.55	-0.50	-0.22	-0.10	-2.00	-0.95	1.62	0.27
Zn	-4.69	-0.12	2028.96	169.08	66.31	0.47	2103.00	17.82	253.97	1.85
PXC	-0.01	-0.02	0.34	0.92	0.63	0.24	3.01	3.14	2.01	0.76

Isocona	Al_2O_3, Lu, Pd	Al_2O_3, FeO, Ho	La, Pd, Gd	Ru, SiO_2, Sb	Al_2O_3, Lu, Ho
Correlación	1.00	1.00	1.00	1.00	1.00
Error	0.012	0.012	0.023	0.0003	0.087
ΔMasa	-14.2	-7.7	4.2	0.0	22.9

Continua en la siguiente página

Tabla A3. Continuaci–n

Elemento	Sanluisito-2		Sanluisito-3		Sonoyta-5		Trin-11		Vidrios-1	
	Δ conc	Δ concD^{A}	Δ conc	Δ concD^{A}	Δ conc	Δ concD^{A}	Δ conc	Δ concD^{A}	Δ conc	Δ concD^{A}
Ag	1.26	12.57	0.51	0.09	6.60	16.50	0.85	8.49	0.00	0.01
Al_2O_3	8.04	0.56	0.00	0.00	1.65	0.11	0.00	0.00	1.98	0.13
As	3.43	1.71	-5.78	-0.48	-5.00	-0.56	22.70	45.40	-0.93	-0.16
Au	0.00	0.36	0.00	0.04	0.00	0.00	0.06	119.21	0.00	0.01
Ba	-200.36	-0.27	269.98	0.29	-600.00	-0.42	-832.71	-0.86	-39.37	-0.02
Be	3.57	7.14	0.02	0.04	2.50	5.00	0.03	0.05	0.01	0.01
Bi	0.18	0.36	0.02	0.04	0.00	0.00	0.03	0.05	0.01	0.01
CaO	-1.94	-0.77	-1.54	-0.32	-1.05	-0.91	-0.32	-0.36	-0.56	-0.21
Cd	0.86	1.71	-1.89	-0.38	0.00	0.00	0.03	0.05	0.01	0.01
Ce	-32.36	-0.37	-6.62	-0.07	14.00	0.27	-58.45	-0.27	56.21	0.23
Co	-1.21	-0.15	2.76	0.15	1.00	1.00	-2.57	-0.23	-8.91	-0.59
Cr	2.86	0.36	4.19	0.14	-2.00	-0.29	-0.80	-0.03	-3.89	-0.32
Cu	9.71	0.81	1976.85	70.60	-11.00	-0.61	395.52	6.59	0.17	0.01
Dy	-1.55	-0.62	0.36	0.09	0.00	0.00	-3.28	-0.44	-0.45	-0.04
Er	-1.16	-0.68	0.08	0.04	-0.10	-0.14	-0.50	-0.20	-0.41	-0.06
Eu	-0.05	-0.05	0.18	0.09	-0.40	-0.31	-2.04	-0.62	-0.33	-0.06
FeO	0.00	0.00	0.20	0.23	-0.36	-0.72	0.00	0.02	-0.01	-0.02
Fe_2O_3	0.03	0.01	-0.45	-0.10	0.43	0.55	-0.10	-0.03	-0.37	-0.10
Gd	-1.01	-0.23	0.04	0.01	0.60	0.18	-5.10	-0.31	1.18	0.06
Ho	-0.36	-0.73	0.13	0.18	-0.10	-0.33	-0.37	-0.37	-0.17	-0.08
Ir	0.02	0.36	0.00	0.04	0.00	0.00	0.00	0.05	0.00	0.01
K_2O	4.82	1.41	1.49	0.54	2.77	0.82	-3.01	-0.70	2.49	0.50
La	-23.61	-0.46	-4.69	-0.09	7.30	0.28	-23.72	-0.27	31.31	0.28
Lu	-0.23	-0.77	0.01	0.04	-0.05	-0.50	0.01	0.05	-0.09	-0.10
MgO	0.32	0.33	-0.03	-0.01	0.24	1.60	-0.31	-0.26	-0.16	-0.13
MnO	-0.03	-0.55	0.05	0.45	0.00	0.00	-0.03	-0.74	0.00	0.01
Mo	1.71	1.71	0.02	0.04	-0.50	-0.50	0.05	0.05	21.34	7.11
Na	-3.33	-0.97	-1.19	-0.35	-3.62	-0.94	2.92	1.10	0.84	0.28
Nd	-2.59	-0.11	-1.10	-0.03	5.20	0.28	-5.04	-0.06	7.98	0.07
Ni	3.57	0.36	1.90	0.08	-21.00	-0.72	10.40	0.29	0.20	0.01
Os	0.00	0.36	0.00	0.04	0.00	0.00	0.00	0.05	0.00	0.01
Pb	59.64	3.98	554.90	2.26	-62.00	-0.84	54.59	3.64	-12.41	-0.23
Pd	-0.16	-0.55	0.02	0.04	0.20	1.00	0.22	1.11	-0.29	-0.37
Pr	-1.99	-0.25	-0.66	-0.06	1.50	0.27	-0.32	-0.01	3.37	0.11
Pt	0.02	0.36	0.00	0.04	0.00	0.00	0.00	0.05	0.00	0.01
P_2O_5	0.00	0.02	-0.09	-0.55	0.00	0.00	-0.03	-0.19	-0.03	-0.09
Rh	0.02	0.36	0.05	1.07	0.00	0.00	0.00	0.05	0.00	0.01
Ru	0.02	0.36	0.00	0.04	0.00	0.00	0.00	0.05	0.00	0.01
Sb	3.57	7.14	0.02	0.04	-1.50	-0.75	0.03	0.05	0.01	0.01
Sc	-1.59	-0.28	-1.27	-0.09	1.20	0.55	1.65	0.18	2.21	0.18
Se	2.21	4.43	0.02	0.04	5.50	11.00	0.03	0.05	0.01	0.01
SiO_2	23.02	0.33	5.10	0.09	-1.92	-0.03	5.75	0.08	-2.98	-0.05
Sm	0.13	0.04	0.21	0.04	0.80	0.26	-5.50	-0.32	-0.04	0.00
Sn	0.18	0.36	0.02	0.04	0.50	1.00	0.03	0.05	0.01	0.01
Sr	-242.21	-0.90	-67.17	-0.15	-368.00	-0.89	0.37	0.00	-174.91	-0.29
Tb	-0.23	-0.46	0.03	0.04	0.00	0.00	-0.74	-0.39	0.03	0.01
Te	0.18	0.36	0.14	0.04	0.50	1.00	-1.89	-0.47	0.10	0.01
Th	-44.87	-0.75	-1.67	-0.08	4.10	0.33	6.29	0.13	-0.68	-0.02
TiO_2	0.11	0.41	0.02	0.04	0.07	0.78	-0.11	-0.21	0.00	0.00
Tl	8.93	1.49	9.28	185.50	5.00	0.63	7.44	7.44	3.09	1.03
Tm	-0.13	-0.66	0.01	0.04	0.00	0.00	0.01	0.05	-0.09	-0.10
U	-8.59	-0.76	-0.33	-0.07	-0.40	-0.27	0.57	0.21	0.08	0.01
V	5.86	0.14	1.07	0.01	2.00	0.29	-9.59	-0.26	2.93	0.05
W	23.79	11.89	-1.48	-0.74	1.00	1.00	0.55	1.11	1.03	1.03
Y	-10.24	-0.76	2.34	0.12	-0.90	-0.14	-7.82	-0.37	-3.20	-0.06
Yb	-1.39	-0.77	0.07	0.04	-0.20	-0.33	-0.22	-0.13	-0.42	-0.07
Zn	169.21	2.38	6861.21	29.32	82.00	2.05	-4.53	-0.14	64.07	0.77
PXC	3.06	4.93	0.44	0.21	1.62	3.52	1.47	1.27	0.31	0.30

Isocona	FeO, Sm, P_2O_5	Al_2O_3, Lu, Pd	P_2O_5, SiO_2, Tb	Al_2O_3, Ho, Yb	TiO_2, Gd, Nd
Correlacin	1.00	1.00	1.00	1.00	1.00
Error	0.003	0.005	0.007	0.085	0.091
ΔMasa	35.7	3.6	0.0	5.4	1.4

Δ conc: Cambio absoluto en la concentracin elemental. Δ concD^{A}: Cambio relativo en la concentracin expresado en nmero de veces con respecto a la concentracin de la roca fresca. Δ conc = (M_0/M_A) (Ea/Ef)D Δ concD^{A} = Δ conc/Ef. (M_0/M_A): Pendiente de la isocona. (Ea/Ef): Pendiente del elemento o compuesto. Ef: Concentracin original del elemento o compuesto.
Los resultados de los elementos mayores (Al_2O_3, CaO, FeO, Fe_2O_3, K_2O, MgO, MnO, Na_2O, P_2O_5, SiO_2, TiO_2, PXC) estn expresadas en %, el resto de los valores se expresan ppm. Los valores positivos indican enriquecimiento, los valores negativos indican empobrecimiento y valores en cero indican inmovilidad.
ΔMasa: Porcentaje de cambio de masa total de la roca; valores positivos indican aumento de masa y valores negativos decremento de masa.
Todos los clculos se elaboraron con el programa computacional GEOISO (Coelho, 2006).
Isocona: Elementos usados como inertes para el trazo de la línea de isocona. Correlacin y error: calculados con algoritmos de GEOISO (Coelho, 2006).

Tabla A4. Resumen de número de muestras por rango de Δ conc–C^A en orden de enriquecimiento y empobrecimiento del estudio balance de masas de las rocas encajonantes frescas y alteradas del Cinturón de Oro Orogénico Caborca, NW de Sonora, México.

Elemento	Rango-1 Δ conc–C^A (>-0.5) (x)	Rango-2 Δ conc–C^A -0.5–(<0) (x)	Δ conc–C^A 0	Rango-3 Δ conc–C^A >0–0.50 (x)	Rango-4 Δ conc–C^A >0.50–1 (x)	Rango-5 Δ conc–C^A >1–2 (x)	Rango-6 Δ conc–C^A >2 (x)	Promedio aritmético (x)* empobrecimiento	Promedio aritmético (x)* enriquecimiento
Ag		**5**(-0.11)	**1**	**2**(0.05)		**1**(1.15)	**11** (35.25)	-0.11	27.79
Al_2O_3			**12**	**7**(0.15)	**1**(0.56)			0.00	0.20
As	**6**(-0.78)	**5**(-0.24)		**2**(0.18)	**2**(0.64)	**1**(1.71)	**4**(16.83)	-0.54	7.85
Au	**5**(-0.96)	**6**(-0.09)	**2**	**3**(0.14)			**4**(79.27)	-0.49	45.35
Ba	**2**(-0.68)	**8**(-0.23)		**8**(0.14)		**2**(1.25)		-0.32	0.36
Be	**1**(-0.54)	**3**(-0.04)	**2**	**5**(0.08)	**4**(0.74)		**5**(8.80)	-0.16	3.38
Bi		**7**(-0.08)	**4**	**6**(0.12)	**3**(0.72)			-0.08	0.32
CaO	**14**(-0.81)	**4**(-0.32)		**1**(0.16)	**1**(0.58)			-0.70	0.37
Cd		**9**(-0.12)	**3**	**4**(0.08)	**3**(0.77)	**1**(1.71)		-0.12	0.55
Ce	**2**(-0.84)	**7**(-0.23)		**8**(0.16)	**1**(0.60)	**2**(1.19)		-0.37	0.39
Co	**7**(-0.72)	**9**(-0.20)		**2**(0.18)	**2**(0.80)			-0.43	0.49
Cr	**1**(-0.84)	**10**(-0.19)		**7**(0.18)	**1**(0.85)	**1**(1.99)		-0.25	0.46
Cu	**3**(-0.63)			**4**(0.20)	**1**(0.81)	**1**(1.98)	**11**(15.23)	-0.63	10.07
Dy	**4**(-0.76)	**11**(-0.24)	**1**	**4**(0.09)				-0.38	0.09
Er	**5**(-0.74)	**11**(-0.16)	**1**	**3**(0.10)				-0.34	0.10
Eu	**3**(-0.63)	**11**(-0.20)		**5**(0.11)	**1**(1.00)			-0.29	0.26
FeO	**4**(-0.86)	**3**(-0.18)	**2**	**4**(0.19)	**3**(0.72)	**1**(1.47)	**3**(371.13)	-0.57	101.62
Fe_2O_3	**3**(-0.72)	**9**(-0.17)		**5**(0.17)	**3**(0.57)			-0.31	0.32
Gd	**3**(-0.75)	**9**(-0.13)	**1**	**6**(0.11)		**1**(1.54)		-0.28	0.31
Ho	**6**(-0.71)	**11**(-0.17)		**3**(0.16)				-0.36	0.16
Ir	**3**(-0.72)	**9**(-0.17)		**5**(0.17)	**3**(0.57)			-0.31	0.32
K_2O	**1**(-0.70)	**1**(-0.04)		**7**(0.22)	**6**(0.72)	**5**(1.42)		-0.37	0.72
La	**2**(-0.81)	**9**(-0.18)	**1**	**5**(0.28)	**3**(0.85)			-0.30	0.49
Lu	**8**(-0.63)	**5**(-0.16)	**2**	**5**(0.08)				-0.45	0.08
MgO	**4**(-0.62)	**7**(-0.21)		**7**(0.15)	**1**(0.95)	**1**(1.60)		-0.36	0.40
MnO	**9**(-0.70)	**6**(-0.21)	**1**	**3**(0.17)	**1**(0.69)			-0.50	0.30
Mo		**3**(-0.19)	**2**	**3**(0.11)	**5**(0.75)	**2**(1.40)	**5**(29.69)	-0.19	10.35
Na	**9**(-0.84)	**8**(-0.27)		**2**(0.15)		**1**(1.10)		-0.57	0.47
Nd	**3**(-0.77)	**8**(-0.08)		**8**(0.17)			**1**(3.20)	-0.27	0.50
Ni	**3**(-0.75)	**6**(-0.12)		**9**(0.21)	**2**(0.71)			-0.33	0.30
Os	**1**(-0.98)	**5**(-0.09)	**13**	**1**(0.04)				-0.24	0.04
Pb	**3**(-0.93)	**2**(-0.17)	**1**		**2**(0.60)	**2**(1.90)	**10**(28.46)	-0.63	20.69
Pd	**2**(-0.19)	**9**(-0.29)		**6**(0.19)	**2**(0.78)	**1**(1.11)		-0.35	0.42
Pr	**3**(-0.74)	**8**(-0.19)		**7**(0.20)	**1**(0.64)		**1**(2.08)	-0.27	0.46
Pt	**3**(-0.76)	**7**(-0.14)	**3**	**6**(0.12)			**1**(2.85)	-0.33	0.51
P_2O_5	**5**(-0.77)	**6**(-0.22)	**3**	**5**(0.16)			**1**(4.54)	-0.47	0.89
Rh		**8**(-0.08)	**4**	**5**(0.14)	**2**(0.92)	**1**(1.07)		-0.08	0.39
Ru		**8**(-0.08)	**4**	**6**(0.12)	**2**(0.66)			-0.08	0.26
Sb	**1**(-0.75)	**4**(-0.05)	**3**	**4**(0.04)	**2**(0.56)		**6**(6.80)	-0.19	3.51
Sc	**2**(-0.65)	**11**(-0.18)		**3**(0.14)	**2**(0.70)	**2**(1.05)		-0.25	0.56
Se	**3**(-0.89)	**4**(-0.10)	**2**	**5**(0.08)	**3**(0.77)		**3**(6.04)	-0.44	1.89
SiO_2		**9**(-0.10)		**9**(0.09)	**1**(0.83)	**1**(1.24)		-0.10	0.26
Sm	**3**(-0.80)	**7**(-0.14)	**3**	**6**(0.13)			**1**(3.24)	-0.34	0.57
Sn	**3**(-0.53)	**4**(-0.11)	**2**	**6**(0.12)	**4**(0.87)		**1**(2.52)	-0.29	0.61
Sr	**10**(-0.73)	**7**(-0.28)	**1**	**1**(0.28)	**1**(0.84)			-0.54	0.56
Tb	**3**(-0.76)	**10**(-0.23)	**2**	**4**(0.08)		**1**(1.77)		-0.36	0.42
Te	**4**(-0.78)	**7**(-0.32)		**6**(0.17)	**3**(0.92)			-0.49	0.42
Th	**4**(-0.81)	**7**(-0.15)		**5**(0.22)	**1**(0.80)	**3**(1.46)		-0.39	0.70
TiO_2	**3**(-0.71)	**6**(-0.19)	**1**	**9**(0.20)	**1**(0.78)			-0.36	0.26
Tl	**1**(-0.75)	**4**(-0.30)	**1**	**2**(0.36)	**3**(0.75)	**3**(1.44)	**6**(93.09)	-0.39	40.42
Tm	**6**(-0.67)	**6**(-0.07)	**3**	**5**(0.08)				-37.00	0.08
U	**4**(-0.70)	**6**(-0.26)		**5**(0.17)	**2**(0.80)	**1**(1.47)	**2**(2.91)	-0.44	0.97
V	**1**(-0.62)	**7**(-0.14)		**10**(0.11)	**1**(0.87)	**1**(1.03)		-0.20	0.25
W	**1**(-0.74)	**2**(-0.14)		**2**(0.35)	**2**(0.86)	**2**(1.07)	**11**(18.17)	-0.34	12.02
Y	**6**(-0.74)	**11**(-0.15)		**3**(0.12)				-0.36	0.12
Yb	**6**(-0.74)	**9**(-0.20)		**5**(0.19)				-0.42	0.19
Zn	**2**(-0.59)	**6**(-0.19)		**4**(0.20)	**2**(0.84)	**1**(1.85)	**5**(44.13)	-0.29	18.75
PXC	**1**(-0.83)	**2**(-0.09)		**5**(0.23)	**4**(0.82)	**1**(1.27)	**7**(3.24)	-0.33	1.67

Δ conc–C^A: Cambio en la concentración elemental expresado en número de veces con respecto a la concentración de la roca fresca.

Ejemplo en la tabla: Arsénico (As): **6**(-0.78) = 6 muestras empobrecidas dentro del intervalo >0.5 veces de empobrecimineto (promedio aritmético del intervalo).

Datos con encabezados en azul indican empobrecimiento, y en rojo enriquecimiento.(x): Promedio aritmético de ese intervalo. (x)*: Promedio aritmético de enriquecimiento o empobrecimiento de ese elemento.

Para los cálculos en los elementos mayores (Al_2O_3, CaO, FeO, Fe_2O_3, K_2O, MgO, MnO, Na_2O, P_2O_5, SiO_2, TiO_2, PXC) se emplearon unidades de % en peso, en el resto de los valores se utilizó ppm. Los valores positivos indican enriquecimiento, los valores negativos indican empobrecimiento y valores en cero indican inmovilidad.

Tabla A5. Resultados de los rangos 1 y 6 ordenados de menor a mayor incidencia, que se muestran en la Tabla A4 del ApŽndice A, y obtenidos a partir del estudio de balance de masas de las rocas encajonantes frescas y alteradas de la mineralizaci–n del Cintur–n de Oro OrogŽnico Caborca, Sonora, MŽxico.

Elemento	Rango-1 Δ concDC[A] (>-0.5) (x)	Promedio aritmŽtico (x)* empobrecimiento	Elemento	Rango-6 Δ concDC[A] >2 (x)	Promedio aritmŽtico (x)* enriquecimiento
Be	**1**(-0.54)	-0.16	**Pr**	**1**(2.08)	0.46
V	**1**(-0.62)	-0.20	**Sn**	**1**(2.52)	0.61
K_2O	**1**(-0.70)	-0.37	**Pt**	**1**(2.85)	0.51
W	**1**(-0.74)	-0.34	**Nd**	**1**(3.20)	0.50
Sb	**1**(-0.75)	-0.19	**Sm**	**1**(3.24)	0.57
Tl	**1**(-0.75)	-0.39	**P_2O_5**	**1**(4.54)	0.89
PXC	**1**(-0.83)	-0.33	**U**	**2**(2.91)	0.97
Cr	**1**(-0.84)	-0.25	**FeO**	**3**(371.13)	101.62
Os	**1**(-0.98)	-0.24	**Se**	**3**(6.04)	1.89
Pd	**2**(-0.19)	-0.35	**As**	**4**(16.83)	7.85
Zn	**2**(-0.59)	-0.29	**Au**	**4**(79.27)	45.35
Sc	**2**(-0.65)	-0.25	**Mo**	**5**(29.69)	10.35
Ba	**2**(-0.68)	-0.32	**Zn**	**5**(44.13)	18.75
La	**2**(-0.81)	-0.30	**Be**	**5**(8.80)	3.38
Ce	**2**(-0.84)	-0.37	**Sb**	**6**(6.80)	3.51
Sn	**3**(-0.53)	-0.29	**Tl**	**6**(93.09)	40.42
Cu	**3**(-0.63)	-0.63	**PXC**	**7**(3.24)	1.67
Eu	**3**(-0.63)	-0.29	**Pb**	**10**(28.46)	20.69
TiO_2	**3**(-0.71)	-0.36	**Ag**	**11** (35.25)	27.79
Fe_2O_3	**3**(-0.72)	-0.31	**Cu**	**11**(15.23)	10.07
Ir	**3**(-0.72)	-0.31	**W**	**11**(18.17)	12.02
Pr	**3**(-0.74)	-0.27			
Gd	**3**(-0.75)	-0.28			
Ni	**3**(-0.75)	-0.33			
Pt	**3**(-0.76)	-0.33			
Tb	**3**(-0.76)	-0.36			
Nd	**3**(-0.77)	-0.27			
Sm	**3**(-0.80)	-0.34			
Se	**3**(-0.89)	-0.44			
Pb	**3**(-0.93)	-0.63			
MgO	**4**(-0.62)	-0.36			
U	**4**(-0.70)	-0.44			
Dy	**4**(-0.76)	-0.38			
Te	**4**(-0.78)	-0.49			
Th	**4**(-0.81)	-0.39			
FeO	**4**(-0.86)	-0.57			
Er	**5**(-0.74)	-0.34			
P_2O_5	**5**(-0.77)	-0.47			
Au	**5**(-0.96)	-0.49			
Tm	**6**(-0.67)	-37.00			
Ho	**6**(-0.71)	-0.36			
Y	**6**(-0.74)	-0.36			
Yb	**6**(-0.74)	-0.42			
As	**6**(-0.78)	-0.54			
Co	**7**(-0.72)	-0.43			
Lu	**8**(-0.63)	-0.45			
MnO	**9**(-0.70)	-0.50			
Na	**9**(-0.84)	-0.57			
Sr	**10**(-0.73)	-0.54			
CaO	**14**(-0.81)	-0.70			

Δ concDC[A]: Cambio en la concentraci–n elemental expresado en nœmero de veces con respecto a la concentraci–n de la roca fresca.

Datos con encabezados en azul indican empobrecimiento, y en rojo enriquecimiento.(x): Promedio aritmŽtico de ese intervalo.

(x)*: Promedio aritmŽtico de enriquecimiento o empobrecimiento de ese elemento.

Para los c‡lculos en los elementos mayores (Al_2O_3, CaO, FeO, Fe_2O_3, K_2O, MgO, MnO, Na_2O, P_2O_5, SiO_2, TiO_2, PXC) se emplearon unidades de % en peso, en el resto delos valores se utiliz—ppm. Los valores positivos indican enriquecimiento, los valores negativos indican empobrecimiento.

Tabla A6. Correlación bivariable del Au y Ag en el Cinturón de Oro Orogénico Caborca, NW Sonora, México.

Elem. Au	*Corr.	Elem. Ag	*Corr.
Pb	0.604	**Pb**	0.703
Ag	0.553	**Zn**	0.565
Zn	0.523	**Au**	0.553
Fe	0.510	**Sb**	0.522
As	0.377	**As**	0.469
Cu	0.355	**Cu**	0.432
Ni	0.296	**Mo**	0.305
Bi	0.294	**Sr**	0.274
Cr	0.278	**Fe**	0.251
Mo	0.243	**Bi**	0.241
Sr	0.236	**Ba**	0.231
Sb	0.225	**Cr**	0.219
Sc	0.178	**V**	0.145
V	0.175	**Ni**	0.140
Co	0.148	**Eu**	0.124
Ti	0.148	**U**	0.116
Nd	0.146	**W**	0.107
Ba	0.143	**Pr**	0.083
La	0.143	**K**	0.051
U	0.142	**Al**	0.039
Ce	0.137	**Nd**	0.028
K	0.128	**Ce**	0.025
Al	0.126	**P**	0.014
Mg	0.103	**Sc**	0.007
Gd	0.097	**La**	0.006
Sm	0.091	**Co**	0.005
Mn	0.090	**Sm**	-0.004
Eu	0.076	**Gd**	-0.012
Th	0.072	**Mn**	-0.036
P	0.042	**Th**	-0.061
W	0.038	**Mg**	-0.080
Ca	0.017	**Ti**	-0.124
Dy	0.001	**Dy**	-0.129
Pr	-0.022	**Yb**	-0.135
Er	-0.044	**Y**	-0.153
Yb	-0.063	**Ca**	-0.173
Y	-0.066	**Na**	-0.173
Na	-0.073	**Er**	-0.240

*Correlación de 102 muestras de cuarzo auríferas. Los coeficientes de correlación r varían entre -1 y +1. Cuando r = 0 significa una completa independencia entre dos elementos analizados; r = +1 indica una relación funcional directa y cuando r = -1 indica una correlación funcional inversa (p.ej., Davis, 1986). Elem. = Elemento, Corr = Coeficiente de correlación "r".

Capítulo 4. Geocronología $^{40}Ar/^{39}Ar$ de las vetas auríferas del COGB

El cinturón de oro orogénico Caborca Larámide del Noroeste de Sonora, México: Geocronología $^{40}Ar/^{39}Ar$ de micas blancas en vetas ricas en oro (*The Laramide Caborca Orogenic Gold Belt of northwestern Sonora, México: White mica $^{40}Ar/^{39}Ar$ geochronology from Au-rich quartz veins*) publicado: Open File Report del *U.S. Geological Survey* (2016) doi:10.3133/ofr20161008. Autores: Aldo Izaguirre, Michael J. Kunk, Alexander Iriondo, Ryan J. McAleer, Juan A. Caballero-Martínez, Enrique Espinoza-Arámburu.

• Objetivos: El objetivo de este estudio fue la determinación de nuevas edades individuales de mineralización de vetas de cuarzo aurífero muestreadas a lo largo de la extensión del COGB (Izaguirre et al., 2016). Otro objetivo fue encontrar el comportamiento del total de estas edades obtenidas de mineralización y poner a prueba la hipótesis que sugeriría un pulso de mineralización exclusivamente originada durante el periodo de la orogenia Laramídica. Por último, generar datos geocronológicos que ayudaran a elaborar un encuadre tectónico de la mineralización del COGB (Izaguirre *et al.*, en prensa).

• Estudios: Se realizó el estudio en 63 nuevas localidades distribuidas a lo largo del COGB (Figura 14) obteniendo edades de mineralización con la técnica $^{40}Ar/^{39}Ar$ en mica blanca hidrotermal.

USGS
science for a changing world

The Laramide Caborca Orogenic Gold Belt of Northwestern Sonora, Mexico: White Mica $^{40}Ar/^{39}Ar$ Geochronology from Gold-Rich Quartz Veins

Open-File Report 2016–1008

U.S. Department of the Interior
U.S. Geological Survey

The Laramide Caborca Orogenic Gold Belt of Northwestern Sonora, Mexico: White Mica $^{40}Ar/^{39}Ar$ Geochronology from Gold-Rich Quartz Veins

By Aldo Izaguirre, Michael J. Kunk, Alexander Iriondo, Ryan McAleer, Juan Antonio Caballero-Martínez, and Enrique Espinosa-Arámburu

Open-File Report 2016–1008

U.S. Department of the Interior
U.S. Geological Survey

U.S. Department of the Interior
SALLY JEWELL, Secretary

U.S. Geological Survey
Suzette M. Kimball, Director

U.S. Geological Survey, Reston, Virginia: 2016

For more information on the USGS—the Federal source for science about the Earth, its natural and living resources, natural hazards, and the environment—visit http://www.usgs.gov or call 1–888–ASK–USGS.

For an overview of USGS information products, including maps, imagery, and publications, visit http://www.usgs.gov/pubprod/.

Any use of trade, firm, or product names is for descriptive purposes only and does not imply endorsement by the U.S. Government.

Although this information product, for the most part, is in the public domain, it also may contain copyrighted materials as noted in the text. Permission to reproduce copyrighted items must be secured from the copyright owner.

Suggested citation:
Izaguirre, Aldo, Kunk, M.J., Iriondo, Alexander, McAleer, Ryan, Caballero-Martínez, J.A, and Espinosa Arámburu, Enrique, 2016, The Laramide Caborca orogenic gold belt of northwestern Sonora, Mexico; white mica $^{40}Ar/^{39}Ar$ geochronology from gold-rich quartz veins: U.S. Geological Survey Open-File Report 2016–1008, 30 p., http://dx.doi.org/10.3133/ofr20161008.

ISSN 2331-1258 (online)

Contents

1. Introduction 1
2. Methods 2
    2.1. Sample Preparation 2
    2.2. Packing and Irradiation Method 2
    2.3. Sample Analysis 2
    2.4. Isotopic Data Reduction 3
3. Results of $^{40}Ar/^{39}Ar$ Data 3
    3.1. Group 1 Plateau Ages 3
    3.2. Group 2 Isochron Ages 3
    3.3. Group 3 Average or Single-Step Ages 3
    3.4. Histogram and Cumulative Probability Diagram of Ages 4
4. Conclusions 4
5. Acknowledgments 4
6. References Cited 5

Figures

1. Sample locations for dated white micas of gold-rich quartz veins 7
2. Histogram and cumulative probability distribution diagram of $^{40}Ar/^{39}Ar$ ages determined from hydrothermal white mica samples of gold-rich quartz veins from the Caborca orogenic gold belt (COGB), northwestern Sonora, Mexico 8
3. Age spectra and inverse-isotope correlation diagrams from group 1 of white mica samples of gold-rich quartz veins, with plateau ages as best age, from the Caborca orogenic gold belt (COGB), northwestern Sonora, Mexico 9
4. Age spectra and inverse-isotope correlation diagrams from group 2 of white mica samples of gold-rich quartz veins, with isochron ages as best age, from the Caborca orogenic gold belt (COGB), northwestern Sonora, Mexico 16
5. Age spectra and inverse-isotope correlation diagrams from group 3 of white mica samples of gold-rich quartz veins, with average and (or) single-step ages as best age, from the Caborca orogenic gold belt (COGB), northwestern Sonora, Mexico 22

Tables

[Available as separate files for download in Excel format from http://dx.doi.org/10.3133/ofr20161008.]

1. Summary of 63 $^{40}Ar/^{39}Ar$ ages determined from white micas of gold-rich quartz veins of the Caborca orogenic gold belt (COGB), northwestern Sonora, Mexico.
2. $^{40}Ar/^{39}Ar$ step-heating data and plateau ages determined from white micas of gold-rich quartz veins of the Caborca orogenic gold belt (COGB), northwestern Sonora, Mexico.
3. $^{40}Ar/^{39}Ar$ step-heating data and isochron ages determined from white micas of gold-rich quartz veins of the Caborca orogenic gold belt (COGB), northwestern Sonora, Mexico.
4. $^{40}Ar/^{39}Ar$ step-heating data and average or single step ages determined from white micas of gold-rich quartz veins of the Caborca orogenic gold belt (COGB), northwestern Sonora, Mexico.

Conversion Factors

Multiply	By	To obtain
	Length	
kilometer (km)	0.6214	mile (mi)

Temperature in degrees Celsius (°C) may be converted to degrees Fahrenheit (°F) as follows:
°F=(1.8×°C)+32

The Laramide Caborca Orogenic Gold Belt of Northwestern Sonora, Mexico: White Mica $^{40}Ar/^{39}Ar$ Geochronology from Gold-Rich Quartz Veins

By Aldo Izaguirre,[1,2] Michael J. Kunk,[3] Alexander Iriondo,[2,4] Ryan McAleer,[3] Juan Antonio Caballero-Martínez,[5] and Enrique Espinosa-Arámburu[5]

1. Introduction

This report contains reduced $^{40}Ar/^{39}Ar$ geochronological data from hydrothermal white mica (63 samples) separated from orogenic quartz gold-rich veins in the Laramide Caborca orogenic gold belt (COGB) of northwestern Sonora, Mexico (fig. 1). The main objective of this report is to present the sample locations, $^{40}Ar/^{39}Ar$ experimental methodology, and $^{40}Ar/^{39}Ar$ isotopic data (tables 1–4). We also include age spectra and inverse-isotope correlation diagrams for all white mica samples (figs. 3–5). The age spectra are separated into three groups based on the type of age used for geologic interpretation, including (1) plateau ages, (2) isochron ages, and (3) average or single-step heating ages. These age spectra are interpreted to represent the time of mineralization for each sample locality, and together, all the ages help to establish the age of mineralization for the entire COGB (fig. 2). Another objective of this Open-File Report (OFR) is to organize the data in a systemic way so that they can be integrated into future scientific publications.

The COGB is approximately 600 kilometers (km) long and 60 to 80 km wide, trends northwest, and extends from west-central Sonora to southern Arizona and California (fig. 1). The COGB contains mineralized gold-rich quartz veins that contain free gold associated with white mica "sericite" and carbonate minerals (calcite and ankerite) plus sulfides such as pyrite and galena (Izaguirre and others, 2012).

Limited geochronologic studies (K-Ar, Ar-Ar (white mica), and Re-Os (magnetite)) exist for parts of the COGB, and previous work was concentrated in mining districts (Pérez-Segura, 1993; Pérez-Segura and others, 1996; Araux-Sánchez, 2000; Iriondo and Atkinson, 2000; Iriondo, 2001; Poulsen and others, 2008; Quintanar-Ruíz, 2008). These scattered studies recorded mineralization ages of approximately 70 to 40 Ma (mega-annum, or million years ago). Therefore, some workers proposed that the orogenic gold mineralization in the region occurred during a single pulse that was associated with the Laramide Orogeny that took place during Cretaceous to early Eocene in the western margin of North America (Damon and others, 1964; Coney, 1976; Dickinson and others, 1988). However, the geochronologic dataset was quite limited, making any regional interpretations tenuous. Accordingly, one of the objectives of this geochronology study was to get a better representative sampling of the COGB in order to obtain a more complete record of the mineralization history. The 63 samples presented in this work are broadly distributed throughout the area of the COGB (fig. 1) and allow us to better test the hypothesis that mineralization occurred in a single pulse.

[1]U.S. Geological Survey, Mail Stop 973, Denver Federal Center, Denver, CO 80225

[2]Centro de Geociencias, Universidad Nacional Autónoma de Mexico, Campus Juriquilla, Boulevard Juriquilla 3001, Juriquilla, 76230, Querétaro, Mexico

[3]U.S. Geological Survey, Mail Stop 926A, National Center, Reston, VA 20192

[4]Department of Geological Sciences, Jackson School of Geosciences, The University of Texas at Austin, Austin, TX 78712

[5]Servicio Geológico Mexicano, Boulevard Felipe Ángeles, km 93.50-4, Colonia Venta Prieta, 42080, Hidalgo, Mexico

2. Methods

2.1. Sample Preparation

All of the quartz vein samples were crushed, ground, and sized using 250-, 180-, and 150-micrometer (μm) sieves. White mica separations were performed using a magnetic separation instrument (Frantz™), paper shaking, and hand picking with a goal of getting greater than 99 percent purity on the white micas. The resulting separates were washed three times in acetone, alcohol, and deionized water in an ultrasonic cleaner (Branson™) to remove dust and other impurities, and then re-sieved using 250- and 180-μm sieve sizes.

2.2. Packing and Irradiation Method

The samples were irradiated in five separate irradiation packages (DD60, KD12, KD52, KD53, and KD55). Two copper packets were loaded for each white mica sample, with weights of approximately 1 milligram (mg) and 20 mg, respectively. The packets were sealed under vacuum in fused silica tubes and irradiated in the central thimble facility at the Training Reactor Isotopes General Atomics (TRIGA) reactor at the U.S. Geological Survey in Denver, Colorado. The monitor mineral used in all the irradiation packages was hornblende (sample MMhb-1) with an age of 519.4±2.5 Ma (Alexander and others, 1978; Dalrymple and others, 1981). The type of container, and the geometry of samples and standards are similar to those described by Snee and others (1988).

2.3. Sample Analysis

White mica samples were analyzed in the U.S. Geological Survey Argon Thermochronology Laboratory in Reston, Virginia. The large white mica samples (approximately 20 mg) were analyzed in a VG Isotopes, Ltd. model 1200 mass spectrometer fitted with an electron multiplier using the $^{40}Ar/^{39}Ar$ step-heating method. All samples were heated for 10 minutes per step (11–20 steps) in a small-volume, molybdenum-lined, low-blank tantalum resistance furnace similar to that described by Staudacher and others (1978). The temperature was monitored by a W5Re-W26Re thermocouple and controlled by a proportional, programmable controller. The furnace and the rear manifold were pumped between steps with a turbo molecular pump. Two isolated ion pumps evacuated the front manifold and the mass spectrometer flight-tube between each incremental step. Prior to analysis in the mass spectrometer, the gas was purified in the rear manifold by a SAES ST707 Zr-V-Fe (zirconium-vanadium-iron) getter operated at room temperature and a hot Re (rhenium) filament. Gas was equilibrated with the front manifold, then isolated and cleaned in the front manifold with a SAES ST101 Al-Zr (aluminum-zirconium) getter operated at 400°C and a Ti (titanium) getter operated at 350°C.

An activated charcoal finger submerged in a thermally equilibrated mixture of dry ice and acetone in the front manifold was used to remove gasses with a molecular weight greater than 60 or 80 (primarily other noble gasses) prior to the expansion of the Ar (argon) dominated gas into the mass spectrometer. The gas was further purified in the mass spectrometer by a second SAES ST101 getter operated at room temperature. Ar isotopes with atomic weights of 40 through 36 and CO_2 (atomic weight of 44) were analyzed as a function of time in five or six analytical cycles. ^{40}Ar, ^{39}Ar, ^{38}Ar, and ^{37}Ar peaks and their baselines were measured for five, 1.28-second integrations in each of the five cycles. ^{36}Ar and its baselines were measured for twenty, 1.28-second integrations in each cycle. After the analysis, the mass spectrometer was evacuated with an isolated ion pump. All phases of the sample heating, cleanup, equilibration, and analysis were performed under computer automation.

Smaller white mica samples (weights of approximately 1 mg) were analyzed using a MAP-216 mass spectrometer fitted with an electron multiplier using the $^{40}Ar/^{39}Ar$ step-heating dating method. Heating for 10 minutes per step followed a schedule of 11 to 20 steps. The heating schedules were designed such that the percentage of ^{39}Ar released per step was limited to less than 20 percent of the total released for most samples. The samples were heated in the same manner and in the same type of furnace as was described earlier. The furnace and the rear and front manifolds were pumped between steps with a turbo molecular pump. An isolated ion pump was used to pump the mass spectrometer. Prior to the mass spectrometer analysis, the gas was purified in the manifold by two SAES ST101 Al-Zr getters, one operated at room temperature and a second one using a hot Re filament at 400°C. The Ar-rich gas was further purified by a third SAES ST101 getter operated at room temperature in the flight tube of the mass spectrometer. Ar isotopes with atomic weights of 40 through 36 were analyzed as a function of time in six analytical cycles. Baselines were measured for ^{39}Ar and ^{36}Ar. The ^{36}Ar baselines were subtracted from the ^{40}Ar, ^{38}Ar, ^{37}Ar, and ^{36}Ar peaks. The ^{39}Ar baseline was subtracted from the ^{39}Ar peak to reduce the influence of the tail of the ^{40}Ar peak.

2.4. Isotopic Data Reduction

All the isotopic data produced on the VG-1200 spectrometer were reduced using an updated version of the computer program ArAr* (Haugerud and Kunk, 1988). Isotopic data from the MAP-216 spectrometer was reduced using the computer program Mass Spec (Deino, 2001). We used the decay constants recommended by Steiger and Jäger (1977). The isotopic measurements made in the five- or six-cycle analysis were regressed to time zero (2/3 of the inlet time) using standard linear regression techniques. These regressed peak values, and associated analytical uncertainties, were used in data reduction. For the VG-1200 and the MAP-216, full system blanks were measured prior to the suite of analyses made on each sample and then subtracted from the analytical results. Error estimates of the blanks were quadratically combined with the analytical errors.

Corrections for interfering reactor-produced Ar isotopes from Ca (calcium), K (potassium), and Cl (chlorine) in the sample were made using the production ratios given in Dalrymple and others (1981) and Roddick (1983). Errors in calculated ages or ratios include the measurement uncertainty in the analysis, decay factor uncertainties, uncertainties in measured atmospheric $^{40}Ar/^{36}Ar$ ratios, the irradiation parameter J, the production ratios of the various reactor induced Ar producing reactions, the initial $^{38}Ar/^{36}Ar$ ratio, and the age of the monitor mineral (Haugerud and Kunk, 1988).

The data in tables 2, 3, and 4 include individual step ages and total gas ages. Total gas ages represent the age calculated from the addition of all the measured Ar peaks for all steps in a single sample. The total gas ages are roughly equivalent to conventional K/Ar ages; however, no analytical precision is calculated for these total gas ages.

3. Results of $^{40}Ar/^{39}Ar$ Data

White mica $^{40}Ar/^{39}Ar$ geochronological results of 63 samples presented in this report (tables 1–4 and figs. 3–5) are subdivided into the following three age groups: plateau ages (group 1), isochron ages (group 2), and average or single-step ages (group 3). The reported ages are plotted in figure 1, and improve our knowledge of the timing of hydrothermal gold-rich quartz vein formation in the COGB.

3.1. Group 1 Plateau Ages

Group 1 is made up of 21 samples (tables 1 and 2; fig. 3) of coarse flakes of white mica separated to an optical purity of greater than 99 percent. The data from step-heating experiments on these samples meet the criteria for a plateau age defined by Fleck and others (1977) and modified by Haugerud and Kunk (1988). All of the white mica samples in this group released argon $^{39}Ar_K$ in three steps or more (accounting for a minimum of 50 percent of the total released gas) at furnace temperatures between approximately 800 to 1250°C (sample Quitovac-5; fig. 3U). In addition, isochron ages calculated for these samples, shown in inverse isotope diagrams of $^{36}Ar/^{40}Ar$ vs. $^{39}Ar/^{40}Ar$ (sample Quitovac-5; fig. 3V), support within analytical error, the more precise plateau ages (summarized in table 1). Therefore, these white mica plateau ages that range from approximately 66 to 48 Ma are interpreted to be the best approximation for the age of hydrothermal activity that resulted in this group of gold-rich quartz veins.

3.2. Group 2 Isochron Ages

Group 2 is made up of 16 samples (tables 1 and 3; fig. 4). White mica from these samples includes both coarse flakes and fine-grained aggregates, separated to an optical purity of greater than 99 percent. The flat age spectra from step-heating experiments on these samples did not meet the statistical definition of a plateau (Fleck and others; 1977). For these slightly irregular age spectra (sample Trin-10; fig. 4AC), inverse isotope correlation diagrams of $^{36}Ar/^{40}Ar$ vs. $^{39}Ar/^{40}Ar$ were generated and isochron ages calculated. A regression (and the resulting age) is considered meaningful if it includes more than three contiguous heating steps that accounts for at least 50 percent of the total $^{39}Ar_K$ released and has a MSWD (mean square weighted deviation) of ≤ 2.5.The age range determined for this group of white micas is approximately 62 to 36 Ma, and interpreted as the age interval for hydrothermal mineralization along the COGB.

3.3. Group 3 Average or Single-Step Ages

Group 3 is made up of 26 samples of white mica (tables 1 and 4; fig. 5) that consist of mostly fine-grained aggregates of white mica. These samples were prepared to a variety of purity levels (in a few instances less than 99 percent purity). It is possible that many of the impurities in the white mica separates included quartz, plagioclase, K-feldspar, or even igneous or metamorphic white micas from the quartz vein host rocks. These impurities made the $^{40}Ar/^{39}Ar$ data results more difficult to interpret.

The data for group 3 white mica samples did not meet the statistical criteria for a plateau or isochron age. However, for a group of 15 of these samples we calculated average ages for a set of contiguous steps (selected steps provided in figure 5). The selected steps define a flat portion of each age (spectrum similar to a plateau), but failed to meet one or more of the requirements established by Fleck and others (1977). This behavior is well represented in white mica sample Pit-4 (fig. 5AI) where 6 steps, representing 87 percent of the total $^{39}Ar_K$ released, were used to calculate the weighted-average age. The resulting weighted-average ages are very similar to the calculated total gas ages for the same samples. This group of 15 white micas yielded average ages in a range between approximately 65 to 39 Ma, consistent with the ages determined from groups 1 and 2.

For the remaining 11 samples from group 3 the age of a single-step was used as the preferred age (ages summarized in table 1). The resulting age spectra from these 11 samples are difficult to interpret meaningfully from the step heating results, but it is important to illustrate that not all the $^{40}Ar/^{39}Ar$ data for these gold-rich quartz veins is considered "well behaved" or "ideal," which would generally yield a flat spectrum. A good example of a "non-ideal" staircase age spectrum is shown in figure 5S (sample El Chanate) in which step C is selected as the assigned age of the sample. The single-step ages of the 11 samples are chosen by selecting the first heating step of the staircase age spectrum in which we observe a tendency of the spectrum to flatten out. The selected single-step age is interpreted as representing the maximum possible age for the formation of the white mica.

Group 3 average and single-step ages range from approximately 69 to 39 Ma. The resulting age spectrum data from group 3 are more complex than groups 1 and 2, however, the determined ages are consistent with the more reliable ages of groups 1 and 2.

3.4. Histogram and Cumulative Probability Diagram of Ages

In order to evaluate and interpret the resulting $^{40}Ar/^{39}Ar$ data of the 63 white mica samples, we generated a histogram and a cumulative probability diagram (fig. 2) of all the determined ages. The diagram shows the age range as well as apparent ages of more abundant gold mineralization along the COGB. The Late Cretaceous to late Eocene age range (69 to 36 Ma) for the quartz veins represents a mineralization event that lasted for more than 30 million years. However, in the histogram a probability peak at approximately 61 Ma is interpreted as the climax of mineralization. The climax of mineralization at 61 Ma occurred within the main pulse of mineralization between approximately 63 to 56 Ma (age range of the majority of analyzed white mica samples; 35 white micas and approximately 56 percent of the total samples). After approximately 48 Ma, only 5 scattered ages of mineralization are identified in figure 2. The youngest age is 36 Ma and represents the youngest mineralization age determined for the gold veins along the COGB.

4. Conclusions

Organization of this large $^{40}Ar/^{39}Ar$ dataset into three age groups has facilitated the interpretation of the timing of mineralization of gold-rich quartz veins in the COGB (table 1). The data presented in this report will serve as a data repository to facilitate the integration of the age data in future manuscripts for publication in scientific journals, where space restrictions are common.

We conclude that the ages between approximately 69 to 36 Ma (figs. 1 and 2), determined from the 63 white micas, represent the timing of orogenic gold mineralization in northwestern Sonora, Mexico, supporting previous interpretations that these gold-rich quartz veins are restricted to the Late Cretaceous to Eocene time. The vast majority of the sample ages (>56 percent) were determined to be between approximately 63 to 56 Ma, which we interpret as the climax of gold mineralization along the COGB. Moreover, the frequency of mineralization gradually decreased from approximately 56 to 48 Ma, followed by a final stage of vein formation that occurred between approximately 45 to 36 Ma. The end of mineralization most likely relates to the contemporaneous cessation of the Laramide orogeny along this portion of the North American Cordillera.

5. Acknowledgments

We acknowledge Consejo Nacional de Ciencia y Tecnología (CONACyT) for providing a doctoral scholarship to Aldo Izaguirre. Also we are grateful to CONACyT for supporting scientific projects CB-82518 and CB-129370 and for financing part of this work. Furthermore, we would like to thank Universidad Nacional Autónoma de Mexico grant PAPIIT IN-116709. We are thankful to the Servicio Geológico Mexicano (SGM) Gerencia Hermosillo, Sonora, for help in the logistics to undertake fieldwork, and in particular, we would like to thank Javier Hernández-Rojas (former SGM geologist) for his helpful companionship in the field while Aldo Izaguirre collected the samples of gold-rich quartz veins. Thanks to Bethany Stackhouse and Wright Horton Jr., for reviewing and improving this manuscript.

6. References Cited

Alexander, E.C., Jr., Mickelson, G.M., and Lanphere, M.A., 1978, MMhb-1–A new $^{40}Ar/^{39}Ar$ dating standard, *in* Zartman, R.E., ed., Short Papers of the Fourth International Conference, Geochronology, Cosmochronology, and Isotope Geology: U.S. Geological Survey Open-File Report 78–701, p. 6–8.

Araux-Sánchez, E., 2000, Geology and mineral deposits of the Sierra Pinta municipality of Puerto Peñasco, Sonora: Unpublished M.S. thesis, Department of Geology, University of Sonora, Mexico, 121 p.

Coney, P.J., 1976, Plate tectonics and the Laramide orogeny, *in* Woodward, L.A., and Northrop, S.A., eds., Tectonics and mineral resources of southwestern North America: New Mexico Geological Society Special Publication 6, p. 5–10.

Dalrymple, G.B., Alexander, E.C., Jr., Lanphere, M.A., and Kraker, G.P., 1981, Irradiation of samples for $^{40}Ar/^{39}Ar$ dating using the Geological Survey TRIGA reactor: U.S. Geological Survey Professional Paper 1176, 55 p. [Also available at http://pubs.er.usgs.gov/publication/pp1176.]

Damon, P.E., Mauger, R.L., and Bikerman, M., 1964, K-Ar dating of Laramide plutonic and volcanic rocks within the Basin and Range province of Arizona and Sonora, *in* Sastry, M.V.A., Bhatia, S.B., eds., Cretaceous-Tertiary boundary including volcanic activity: 22nd Indian Geotechnical Conference, New Delhi, India, Part 3 Proceedings of Section 3, p. 45–55.

Deino, A.L., 2001, User's manual for mass spec v. 5.02: Berkeley Geochronology Center Special Publication 1a, 119 p.

Dickinson, W.R., Klute, M.A., Hayes, M.J., Janecke, S.U., Lundin, E.R., McKittrick, M.A., and Olivares, M.D., 1988, Paleogeographic and paleotectonic setting of Laramide sedimentary basins in the central Rocky Mountain region: Geological Society of America Bulletin, v. 100, no. 7, p. 1023–1039.

Fleck, R.J., Sutter, J.F., and Elliot, D.H., 1977, Interpretation of discordant $^{40}Ar/^{39}Ar$ age spectra of Mesozoic tholeiites from Antarctica: Geochimica et Cosmochimica Acta, v. 41, no. 1, p. 15–32.

Haugerud, R.A., and Kunk, M.J., 1988, ArAr*; a computer program for reduction of ^{40}Ar-^{39}Ar data: U. S. Geological Survey Open-File Report 88–261, 68 p. [Also available at http://pubs.er.usgs.gov/publication/ofr88261.]

Iriondo, A., 2001, Proterozoic basements and their laramide juxtaposition in NW Sonora, Mexico; tectonic constraints on the SW margin of Laurentia: Boulder, Colorado, University of Colorado, unpublished Ph.D. thesis, 3 pls., 222 p.

Iriondo, A., and Atkinson, W.W., Jr., 2000, Orogenic gold mineralization along the proposed trace of the Mojave-Sonora megashear; evidence for the Laramide Orogeny in NW Sonora, Mexico [abs.]: Geological Society of America Abstracts with Programs, v. 32, no. 7, p. 393

Izaguirre, A., Iriondo, A., Caballero-Martínez, J.A., Moreira-Rivera, F., and Espinosa-Arámburu, E., 2012, Geochemical homogeneity of hydrothermal alteration of the orogenic gold belt in NW Sonora, Mexico; study of mass balance in host rocks of mineralization: Bulletin of the Mexican Geological Society, v. 64, p. 119–153.

Pérez-Segura, E., 1993, Deposits of gold and silver from Sonora, Mexico and its relations with the regional geology, *in* Delgado-Argote, L.A., and Barajas, M., eds., Contributions to the tectonics of western Mexico: Mexican Geophysical Union Monograph 1, p. 147–174.

Pérez-Segura, E., Cheilletz, A., Herrera-Urbina, S., and Hanes, Y.J., 1996, Geology, mineralization, hydrothermal alteration, and age of the San Francisco, Sonora gold deposit; a mesothermal deposit in northwestern Mexico: Mexican Journal of Geological Sciences, v. 13, no. 1, p. 65–89.

Poulsen, K.H., Mortensen J.K., and Walford, P.C., 2008, San Francisco gold deposit, Santa Ana region, Sonora, Mexico; Laramide orogenic, intrusion-related mineralization?, *in* Spencer, J.E., and Titley, S.R., eds., Ores and orogenesis; Circum-Pacific tectonics, geologic evolution, and ore deposits: Arizona Geological Society Digest 22, 547–559, available at http://www.azgs.az.gov/Resources/ags22_tablecontents.pdf.

Quintanar-Ruíz, F.J., 2008, La Herradura ore deposit; an orogenic gold deposit in northwestern Mexico: Unpublished M.S. thesis, Tucson, Arizona, University of Arizona, 97 p., available at http://www.geo.arizona.edu/Antevs/Theses/QuintanarMS08.pdf.

Roddick, J.C., 1983, High precision calibration of $^{40}Ar/^{39}Ar$ standards: Geochimica et Cosmochimica Acta, v. 47, no. 5, p. 887–898, available at http://www.sciencedirect.com/science/article/pii/0016703783901540.

Snee, L.W., Sutter, J.F., and Kelly, W.C., 1988, Thermochronology of economic mineral deposits; dating the stages of mineralization at Panasqueira, Portugal, by high precision $^{40}Ar/^{39}Ar$ age spectrum techniques on muscovite: Economic Geology, v. 83, no. 2, p. 335–354.

Staudacher, T., Jessberger, E.K., Dörflinger, D., and Kiko, J., 1978, A refined ultrahigh-vacuum furnace for rare gas analysis: Journal of Physics E, Scientific Instrumentation, v. 11, no. 8, p. 781–784.

Steiger, R.H., and Jäeger, E., 1977, Subcommission on geochronology; convention on the use of decay constants in geo- and cosmo-chronology: Earth and Planetary Science Letters, v. 36, no. 3, p. 359–363, available at http://citeseerx.ist.psu.edu/viewdoc/download?doi=10.1.1.456.667&rep=rep1&type=pdf.

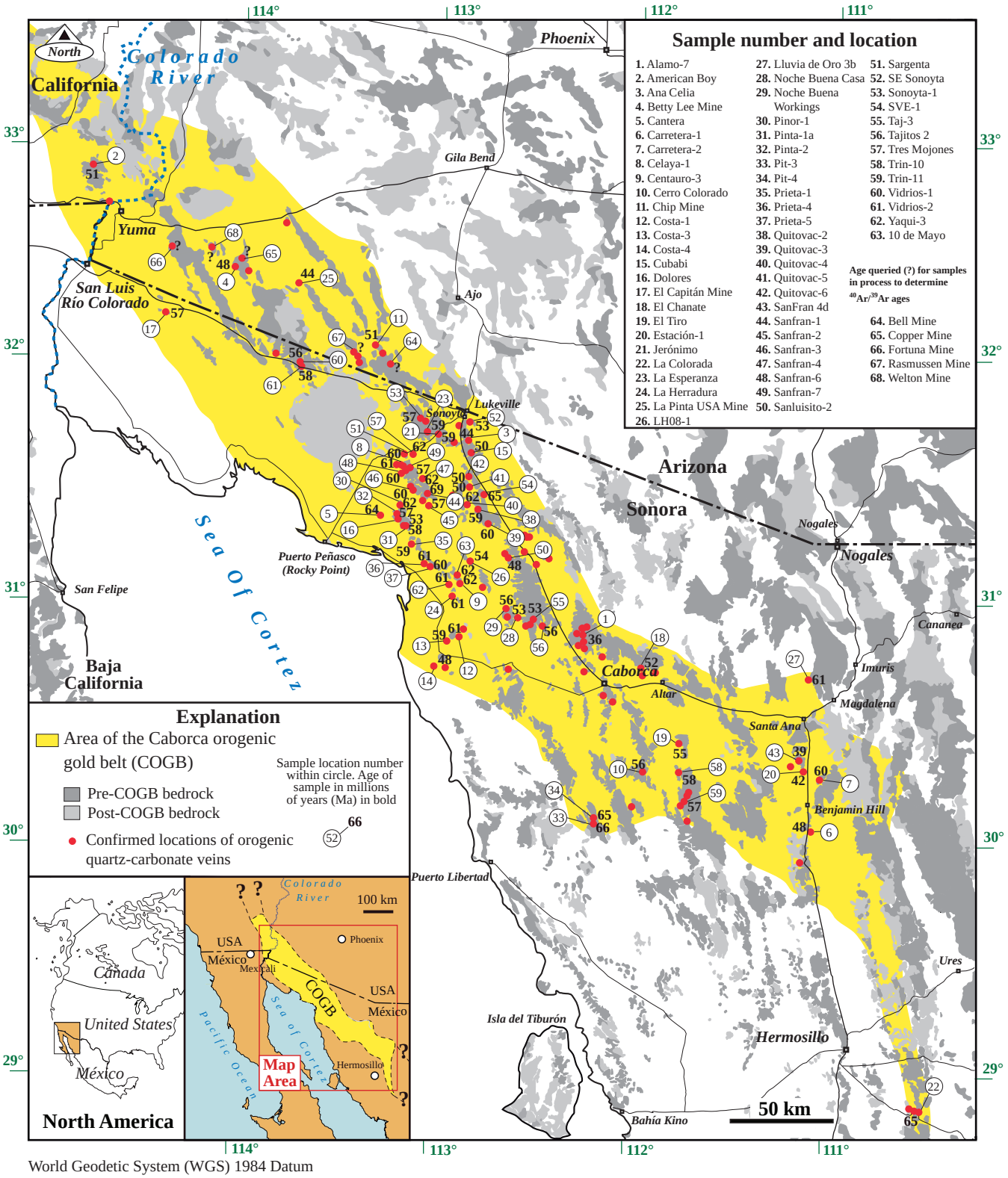

World Geodetic System (WGS) 1984 Datum

Figure 1. Sample locations for dated white micas of gold-rich quartz veins. Numbers in bold represent $^{40}Ar/^{39}Ar$ ages determined in this open-file report from the Caborca orogenic gold belt (COGB), northwestern Sonora, Mexico. Shades of gray represent pre-COGB mineralization (dark-gray) and post-COGB mineralization (light-gray) bedrock outcrops after Iriondo (2001).

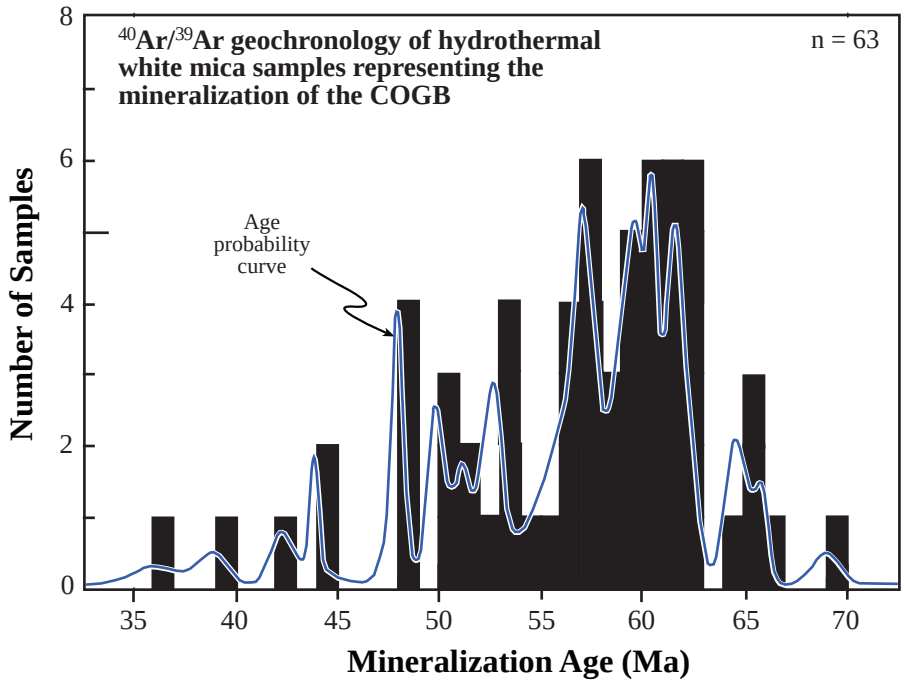

Figure 2. Histogram and cumulative probability distribution diagram (blue line) of $^{40}Ar/^{39}Ar$ ages determined from hydrothermal white mica samples of gold-rich quartz veins from the Caborca orogenic gold belt (COGB), northwestern Sonora, Mexico. Abbreviations: Ma, mega-annum; n, number of samples.

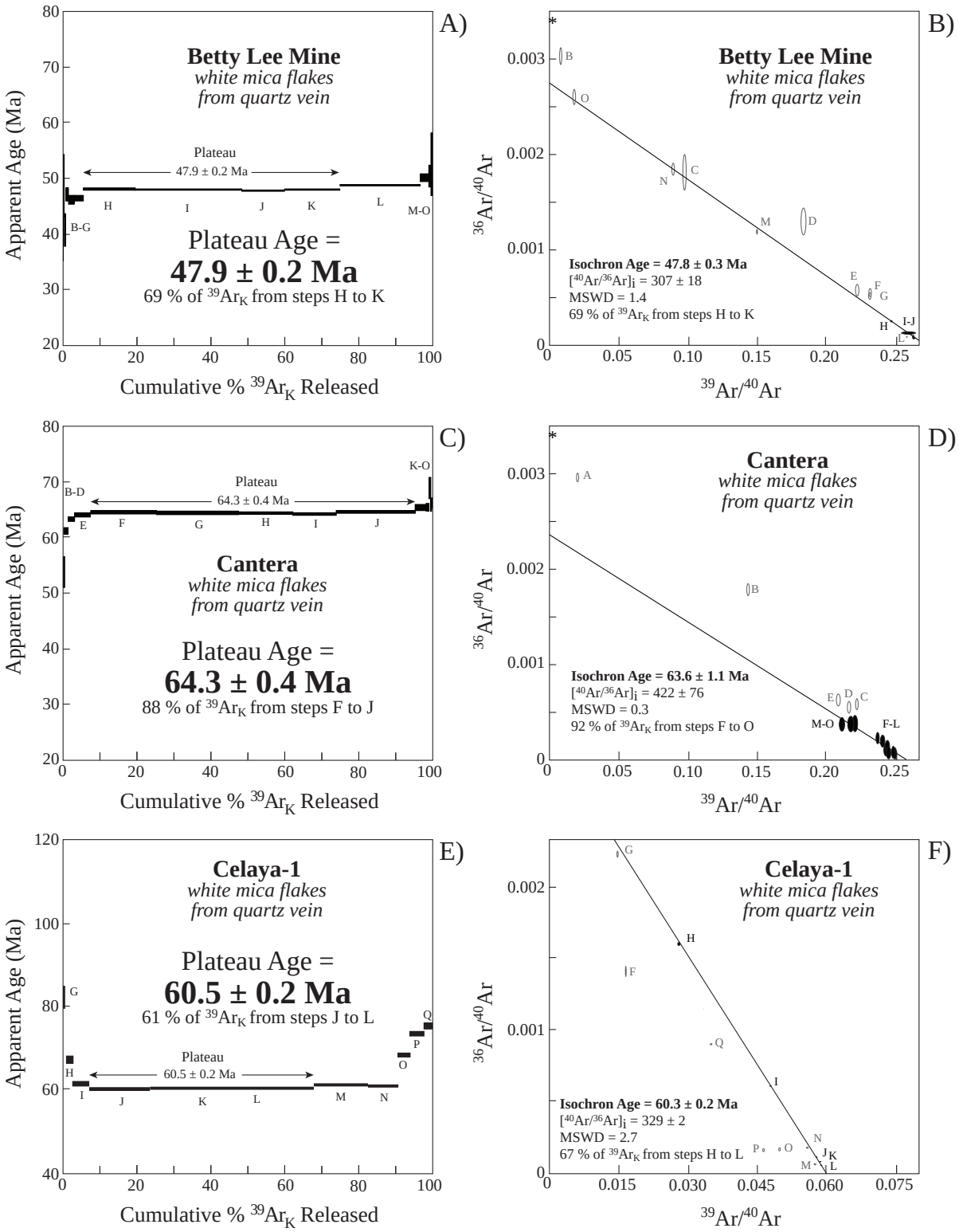

Figure 3. Age spectra (A, C, E) and inverse-isotope correlation diagrams (B, D, F) from group 1 of white mica samples of gold-rich quartz veins, with plateau ages as best age, from the Caborca orogenic gold belt (COGB), northwestern Sonora, Mexico. * is the assumed limit of the atmospheric argon ratio. Abbreviations: Ma, mega-annum; MSWD, mean square weighted deviation.

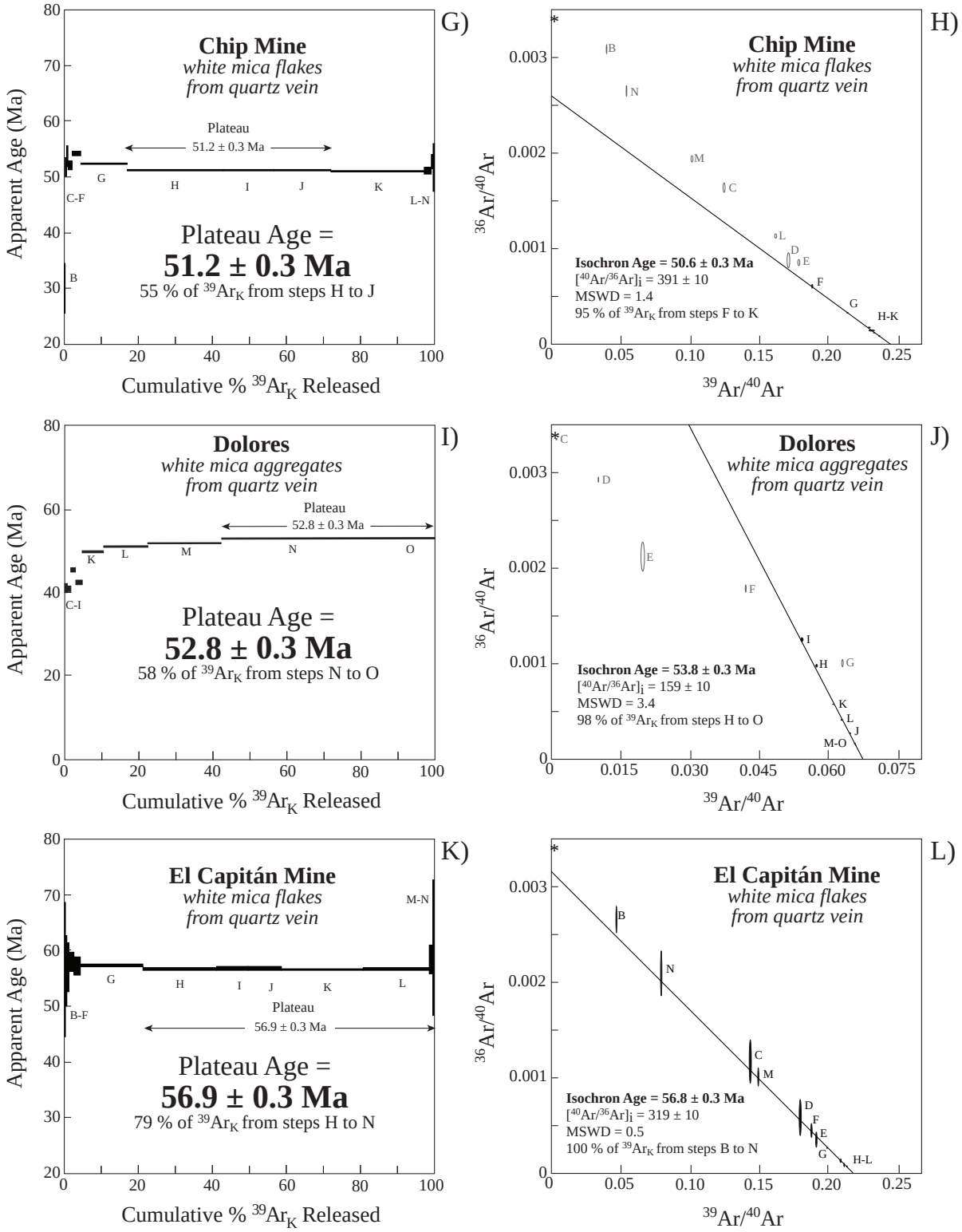

Figure 3—Continued. Age spectra (G, I, K) and inverse-isotope correlation diagrams (H, J, L) from group 1 of white mica samples of gold-rich quartz veins, with plateau ages as best age, from the Caborca orogenic gold belt (COGB), northwestern Sonora, Mexico. * is the assumed limit of the atmospheric argon ratio.

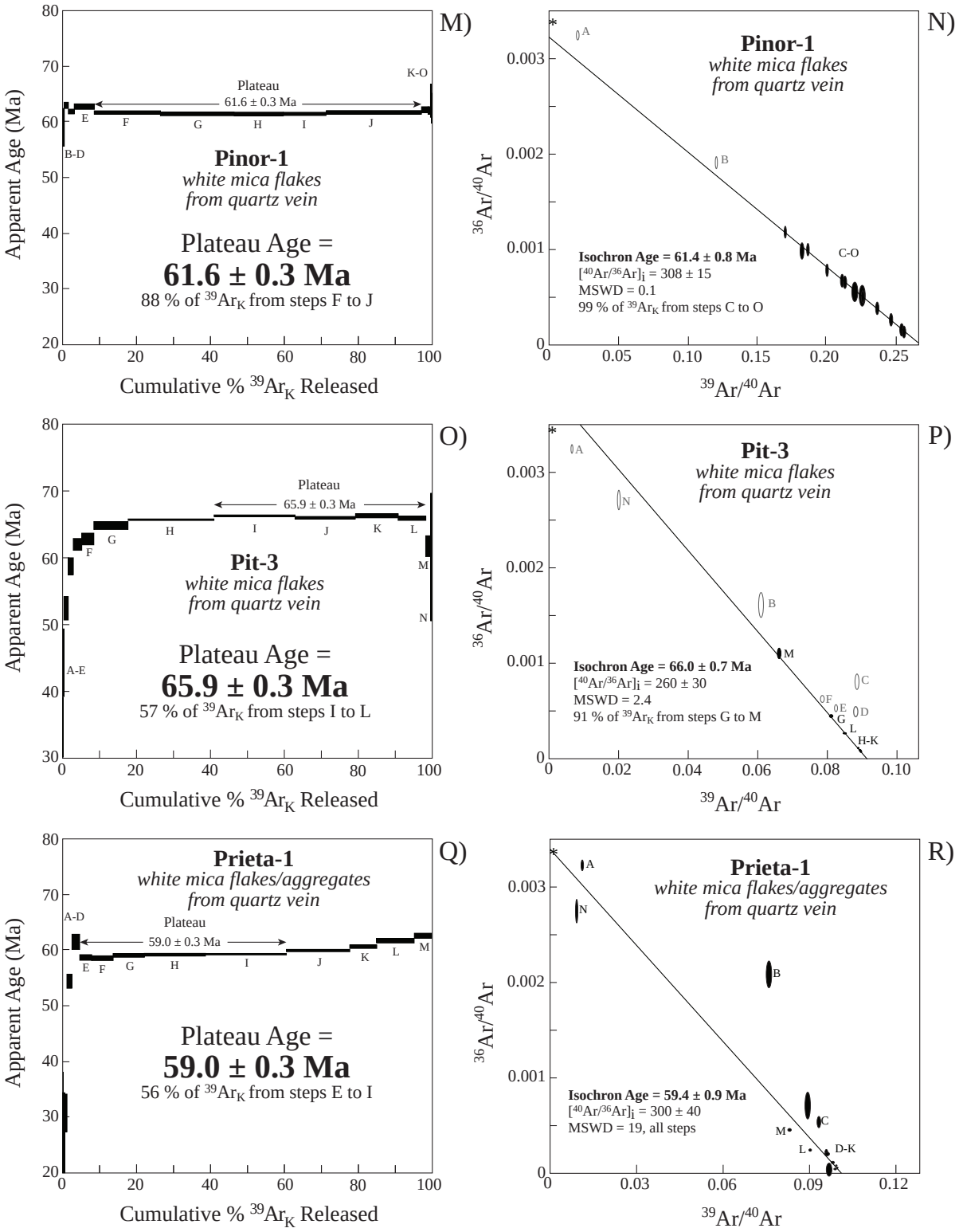

Figure 3—Continued. Age spectra (M, O, Q) and inverse-isotope correlation diagrams (N, P, R) from group 1 of white mica samples of gold-rich quartz veins, with plateau ages as best age, from the Caborca orogenic gold belt (COGB), northwestern Sonora, Mexico. * is the assumed limit of the atmospheric argon ratio.

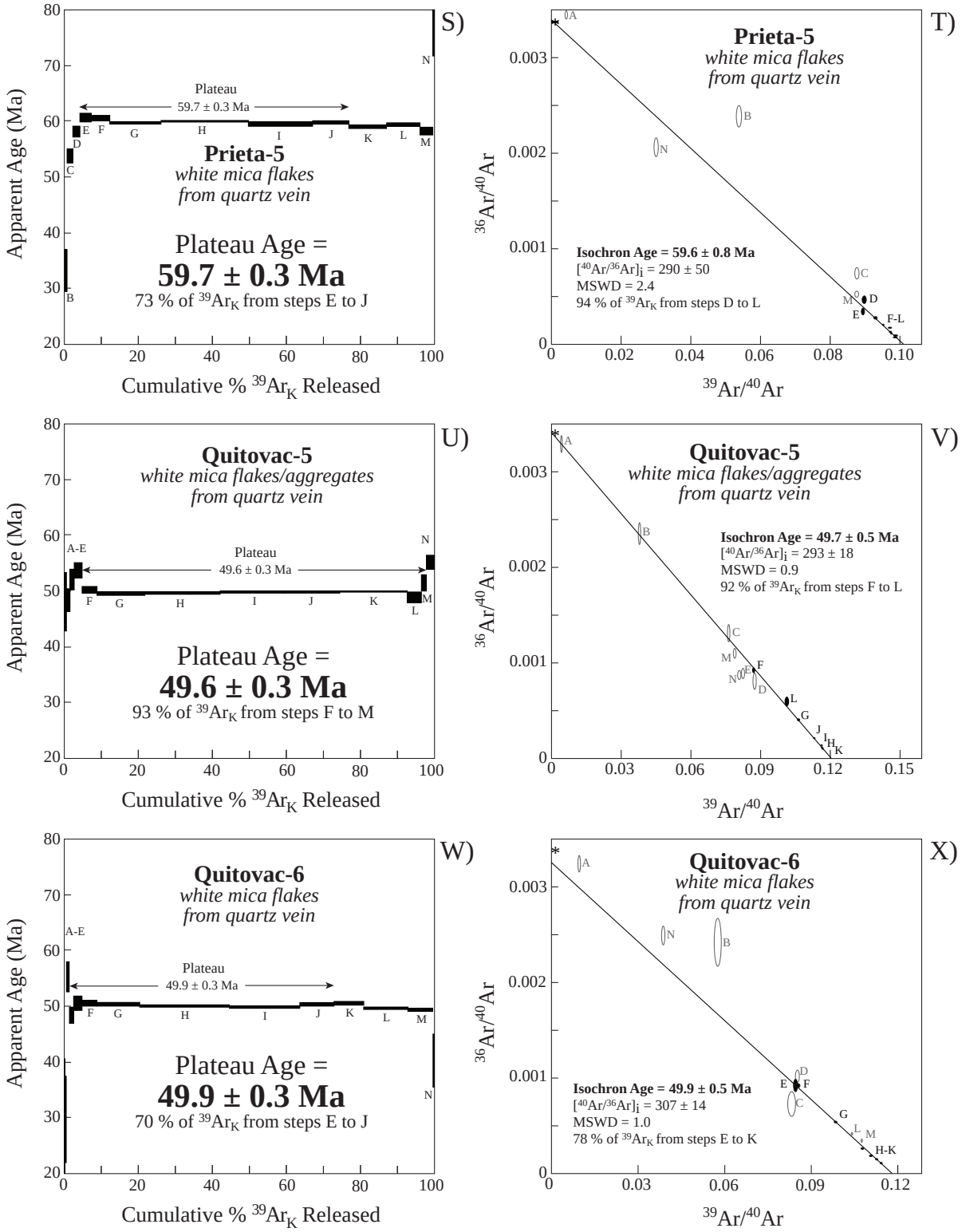

Figure 3—Continued. Age spectra (S, U, W) and inverse-isotope correlation diagrams (T, V, X) from group 1 of white mica samples of gold-rich quartz veins, with plateau ages as best age, from the Caborca orogenic gold belt (COGB), northwestern Sonora, Mexico. * is the assumed limit of the atmospheric argon ratio.

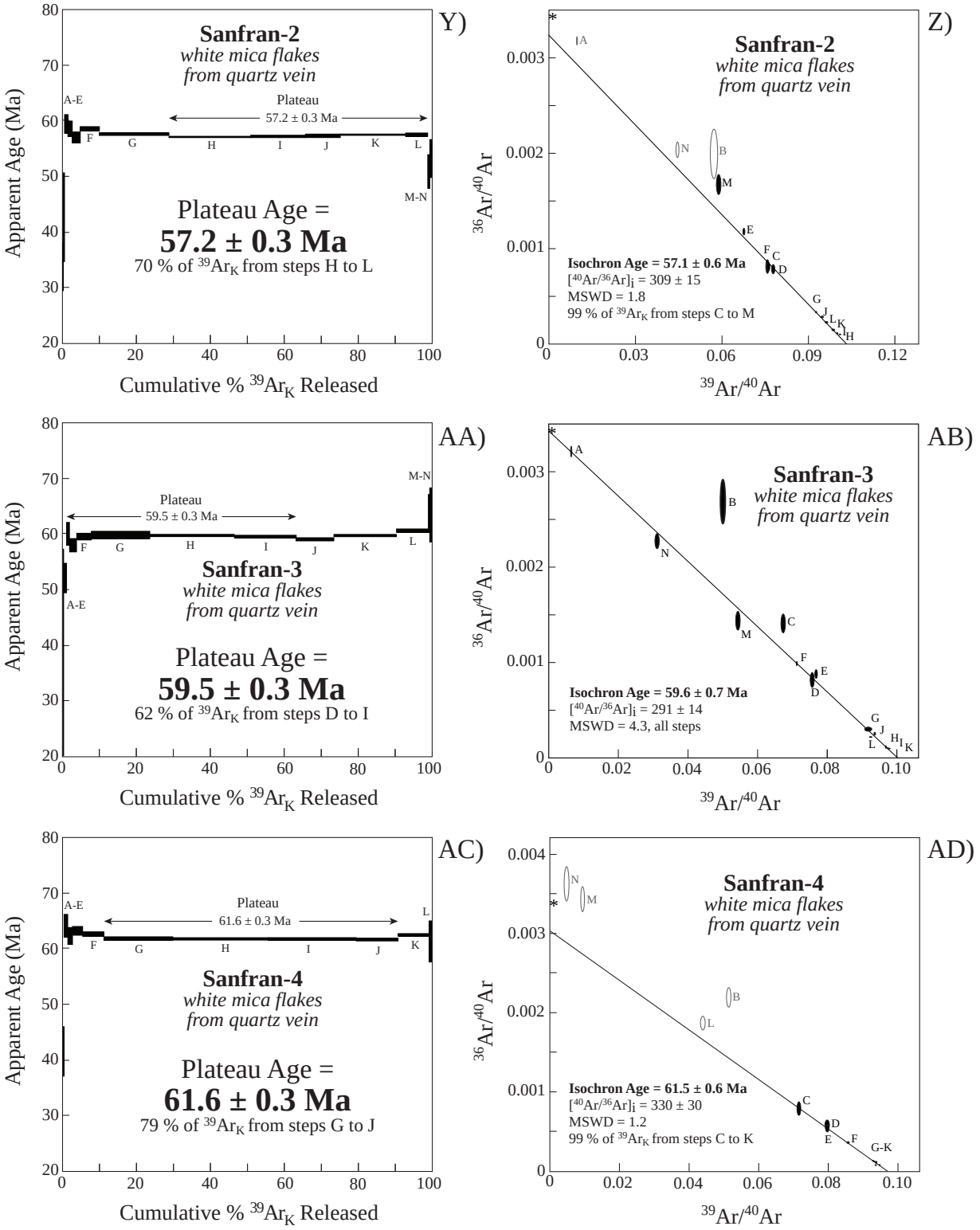

Figure 3—Continued. Age spectra (Y, AA, AC) and inverse-isotope correlation diagrams (Z, AB, AD) from group 1 of white mica samples of gold-rich quartz veins, with plateau ages as best age, from the Caborca orogenic gold belt (COGB), northwestern Sonora, Mexico. * is the assumed limit of the atmospheric argon ratio.

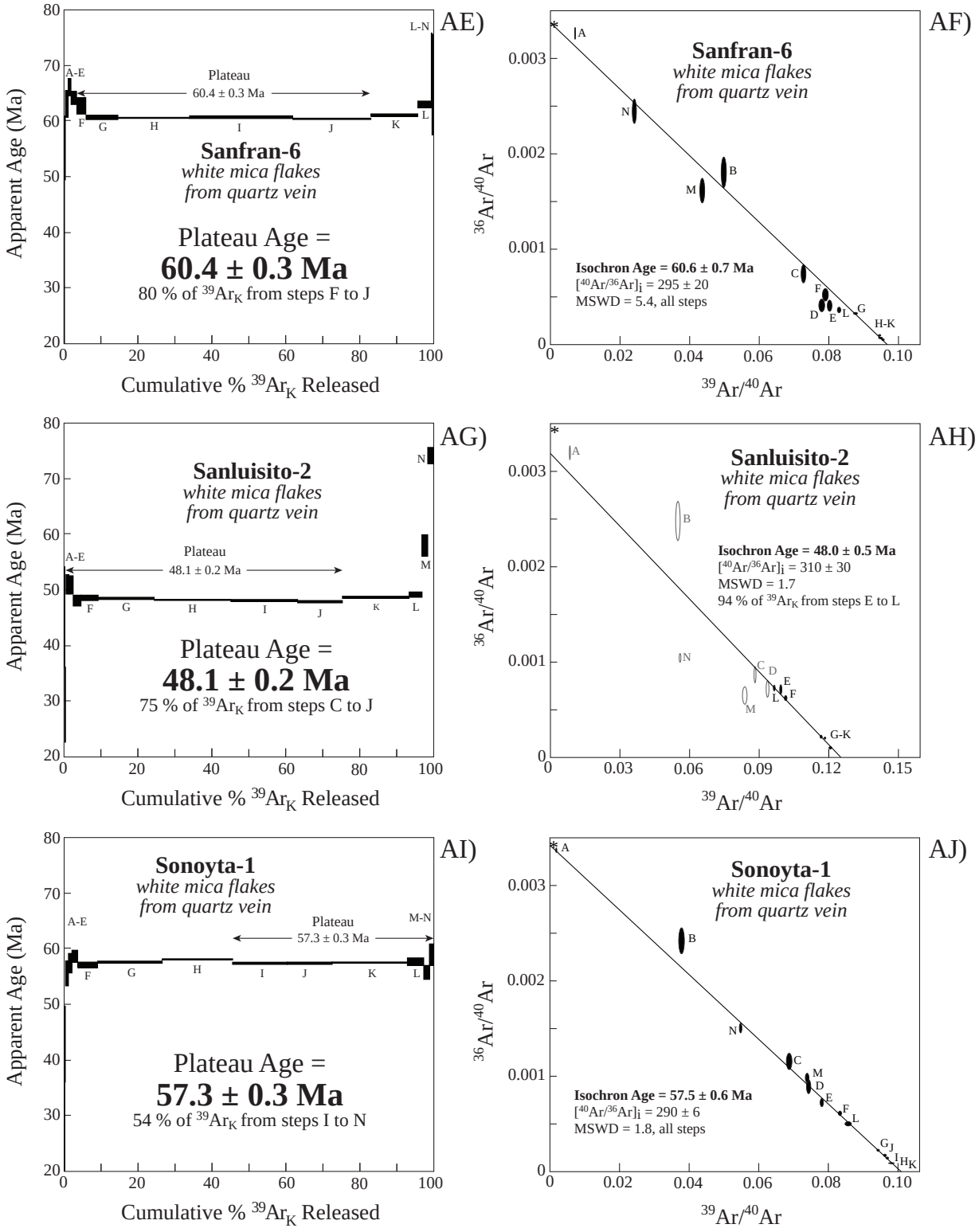

Figure 3—Continued. Age spectrum (AE, AG, AI) and inverse-isotope correlation diagrams (AF, AH, AJ) from group 1 of white mica samples of gold-rich quartz veins, with plateau age as best age, from the Caborca orogenic gold belt (COGB), northwestern Sonora, Mexico. * is the assumed limit of the atmospheric argon ratio.

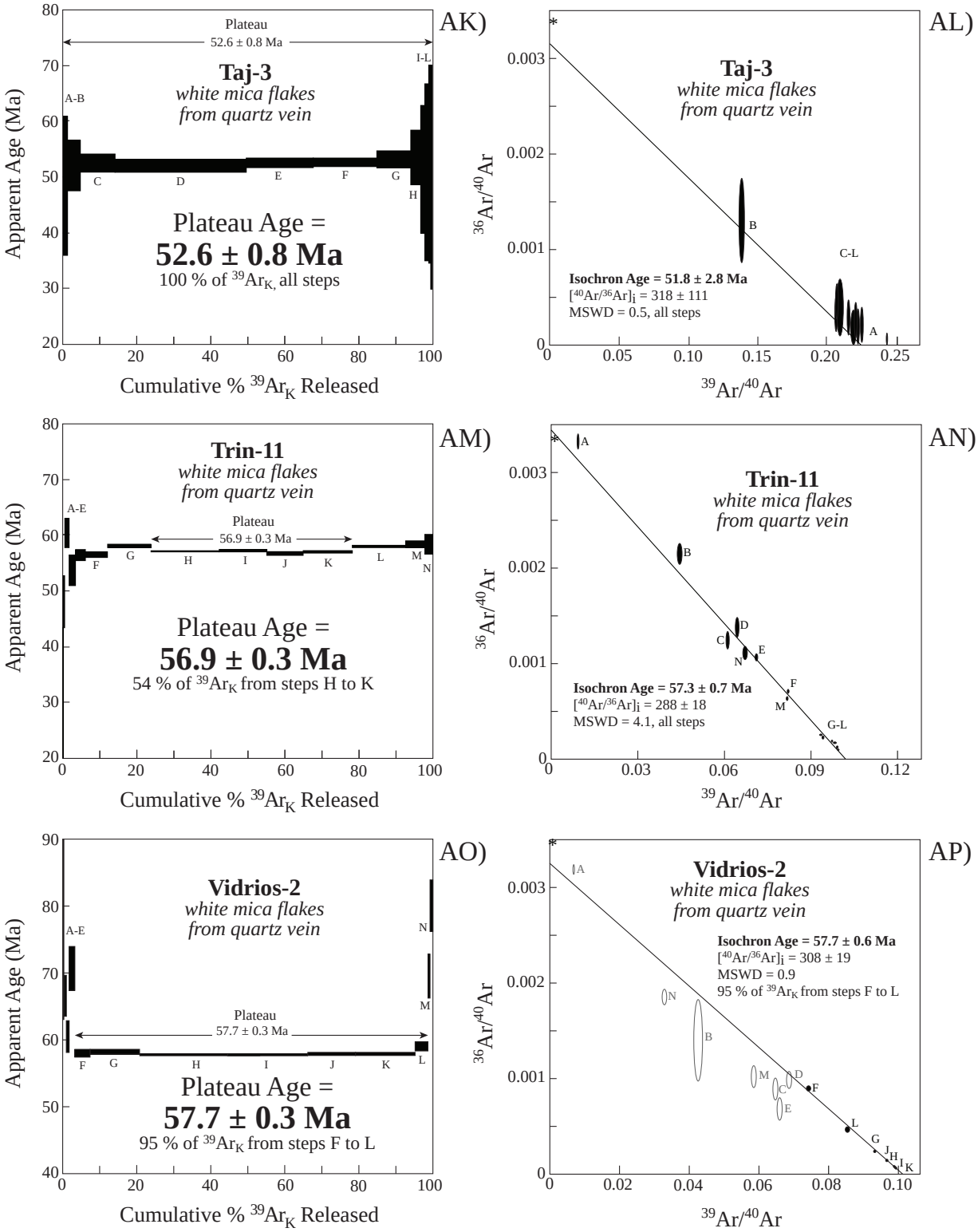

Figure 3—Continued. Age spectrum (AK, AM, AO) and inverse-isotope correlation diagrams (AL, AN, AP) from group 1 of white mica samples of gold-rich quartz veins, with plateau age as best age, from the Caborca orogenic gold belt (COGB), northwestern Sonora, Mexico. * is the assumed limit of the atmospheric argon ratio.

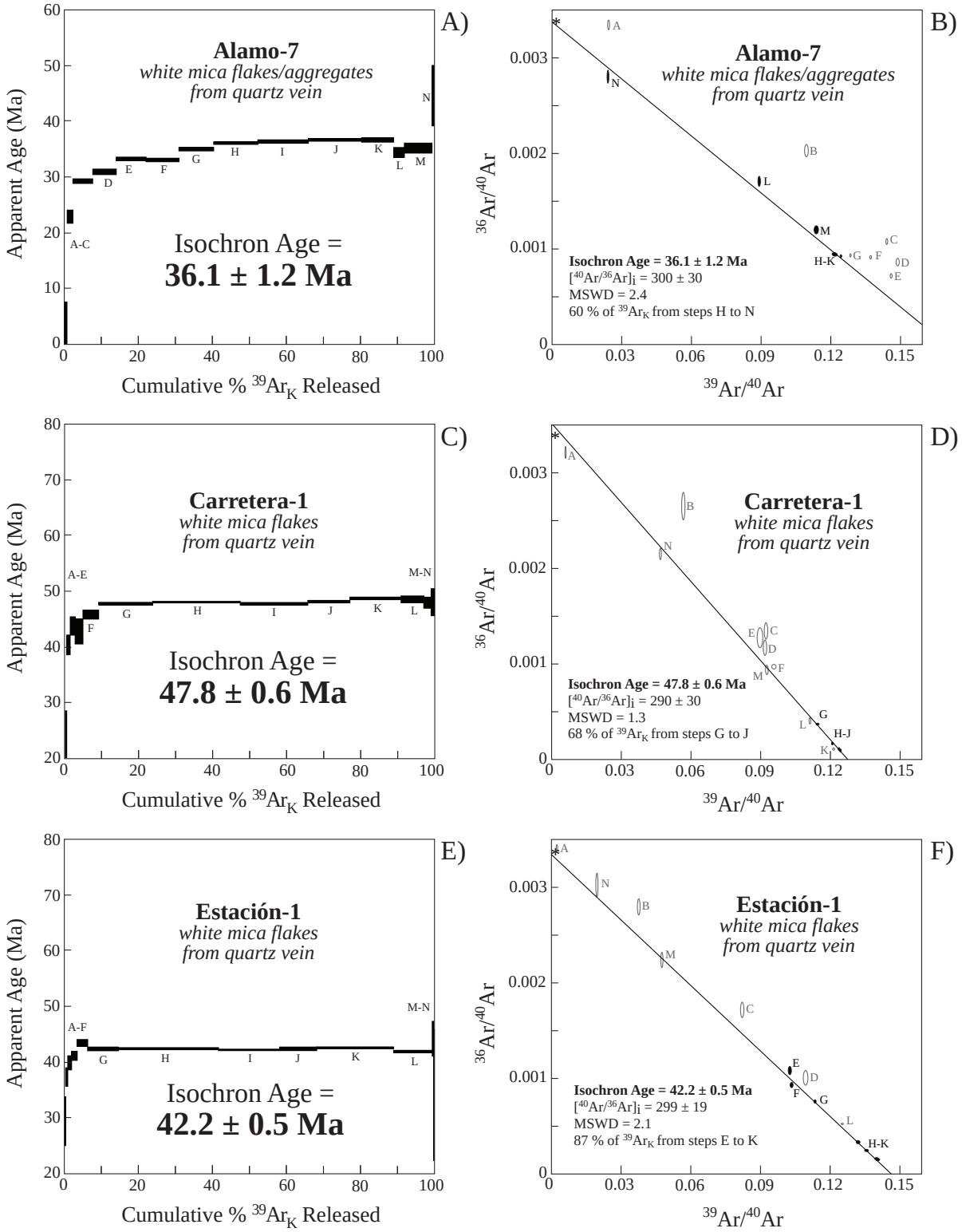

Figure 4. Age spectra (A, C, E) and inverse-isotope correlation diagrams (B, D, F) from group 2 of white mica samples of gold-rich quartz veins, with isochron ages as best age, from the Caborca orogenic gold belt (COGB), northwestern Sonora, Mexico. * is the assumed limit of the atmospheric argon ratio. Abbreviations: Ma, mega-annum; MSWD, mean square weighted deviation.

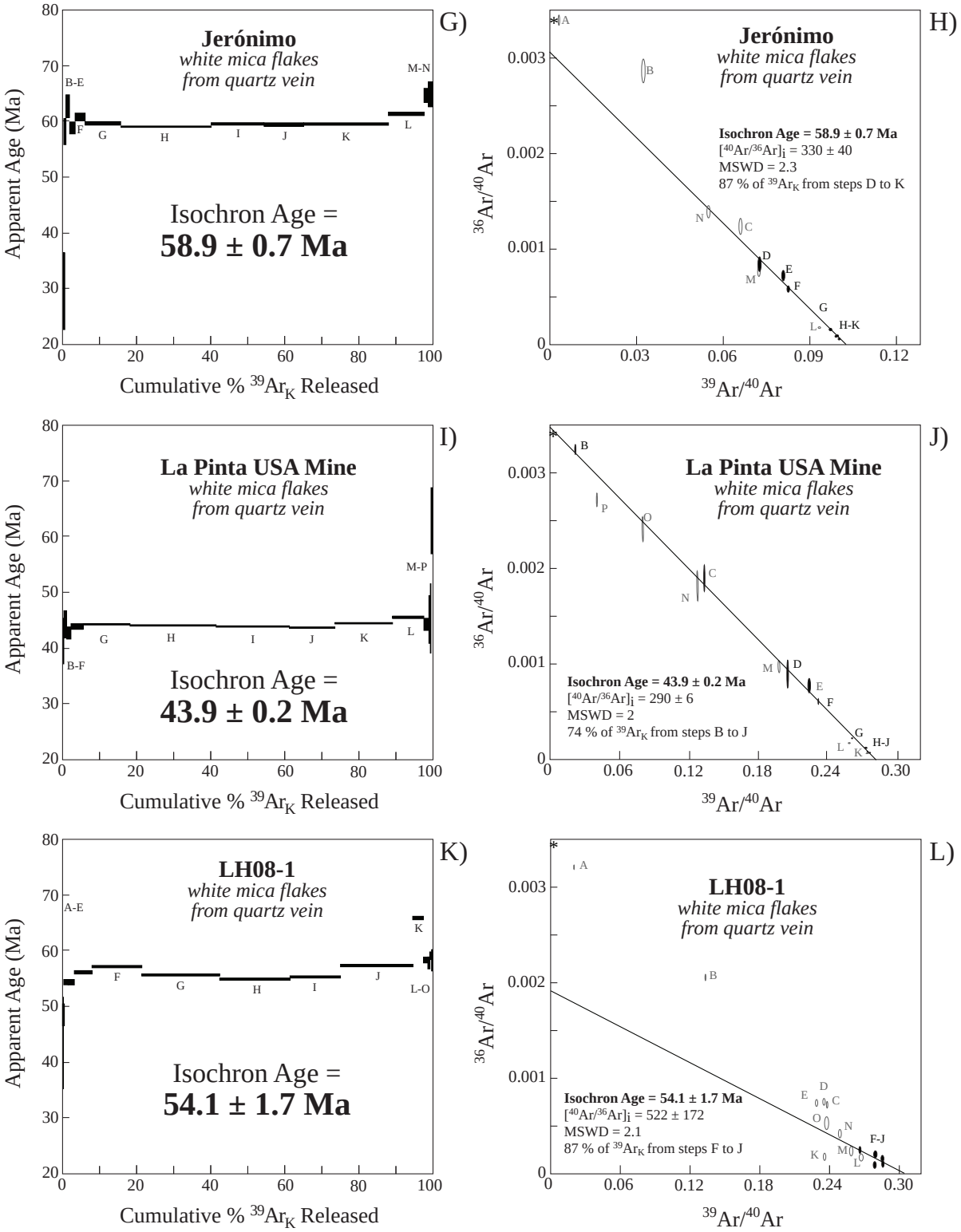

Figure 4—Continued. Age spectra (G, I, K) and inverse-isotope correlation diagrams (H, J, L) from group 2 of white mica samples of gold-rich quartz veins, with isochron ages as best age, from the Caborca orogenic gold belt (COGB), northwestern Sonora, Mexico. * is the assumed limit of the atmospheric argon ratio.

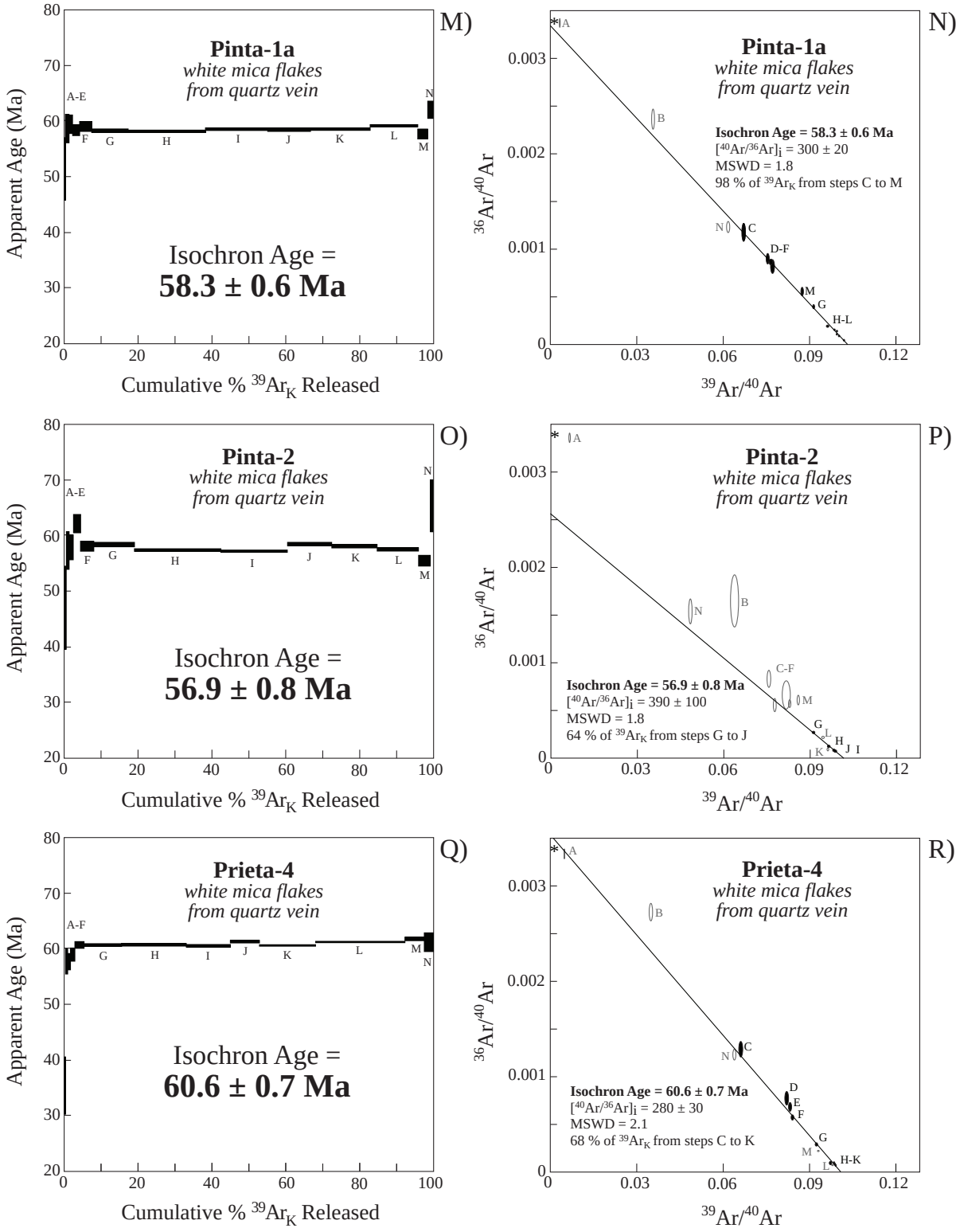

Figure 4—Continued. Age spectra (M, O, Q) and inverse-isotope correlation diagrams (N, P, R) from group 2 of white mica samples of gold-rich quartz veins, with isochron ages as best age, from the Caborca orogenic gold belt (COGB), northwestern Sonora, Mexico. * is the assumed limit of the atmospheric argon ratio.

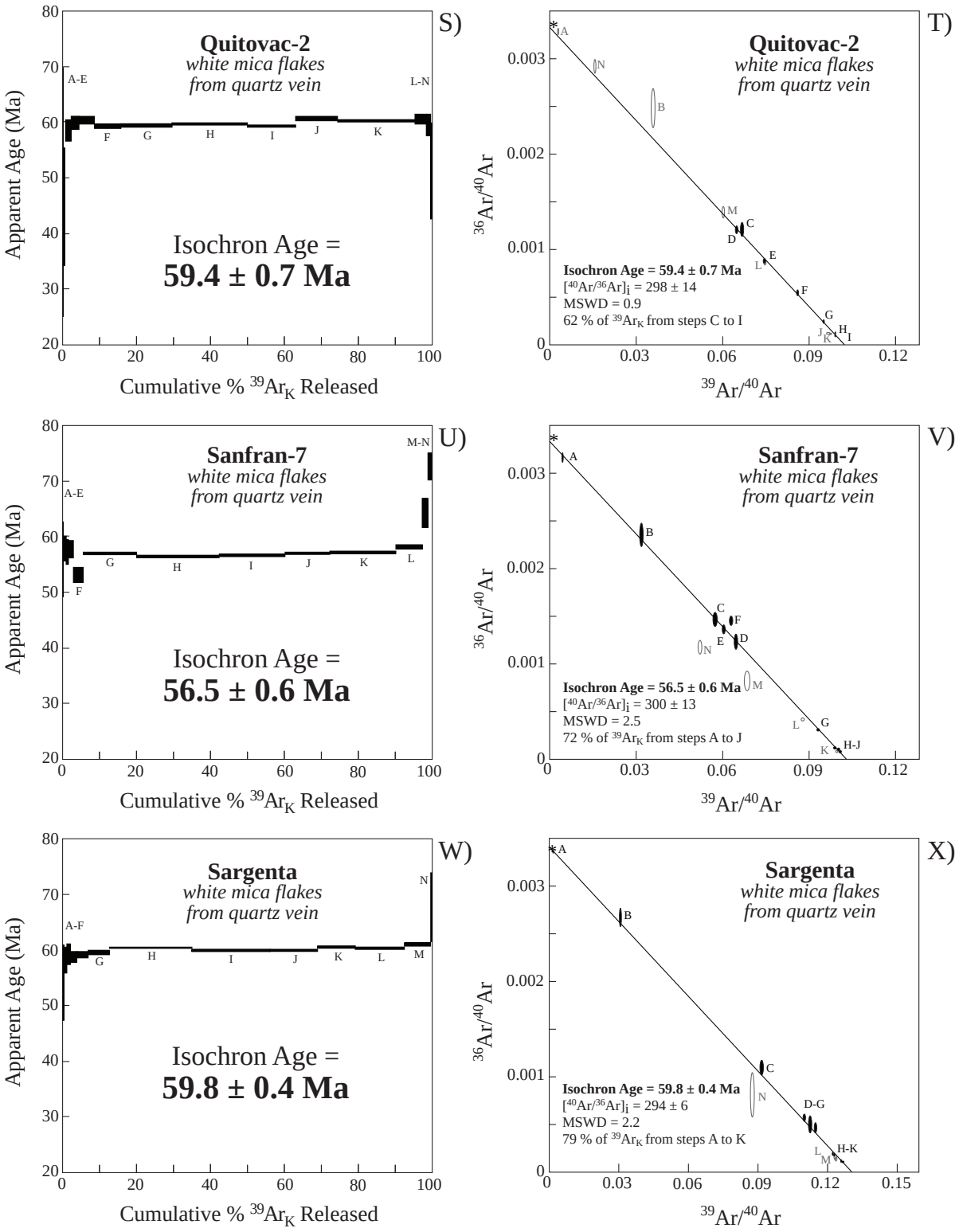

Figure 4—Continued. Age spectra (S, U, W) and inverse-isotope correlation diagrams (T, V, X) from group 2 of white mica samples of gold-rich quartz veins, with isochron ages as best age, from the Caborca orogenic gold belt (COGB), northwestern Sonora, Mexico. * is the assumed limit of the atmospheric argon ratio.

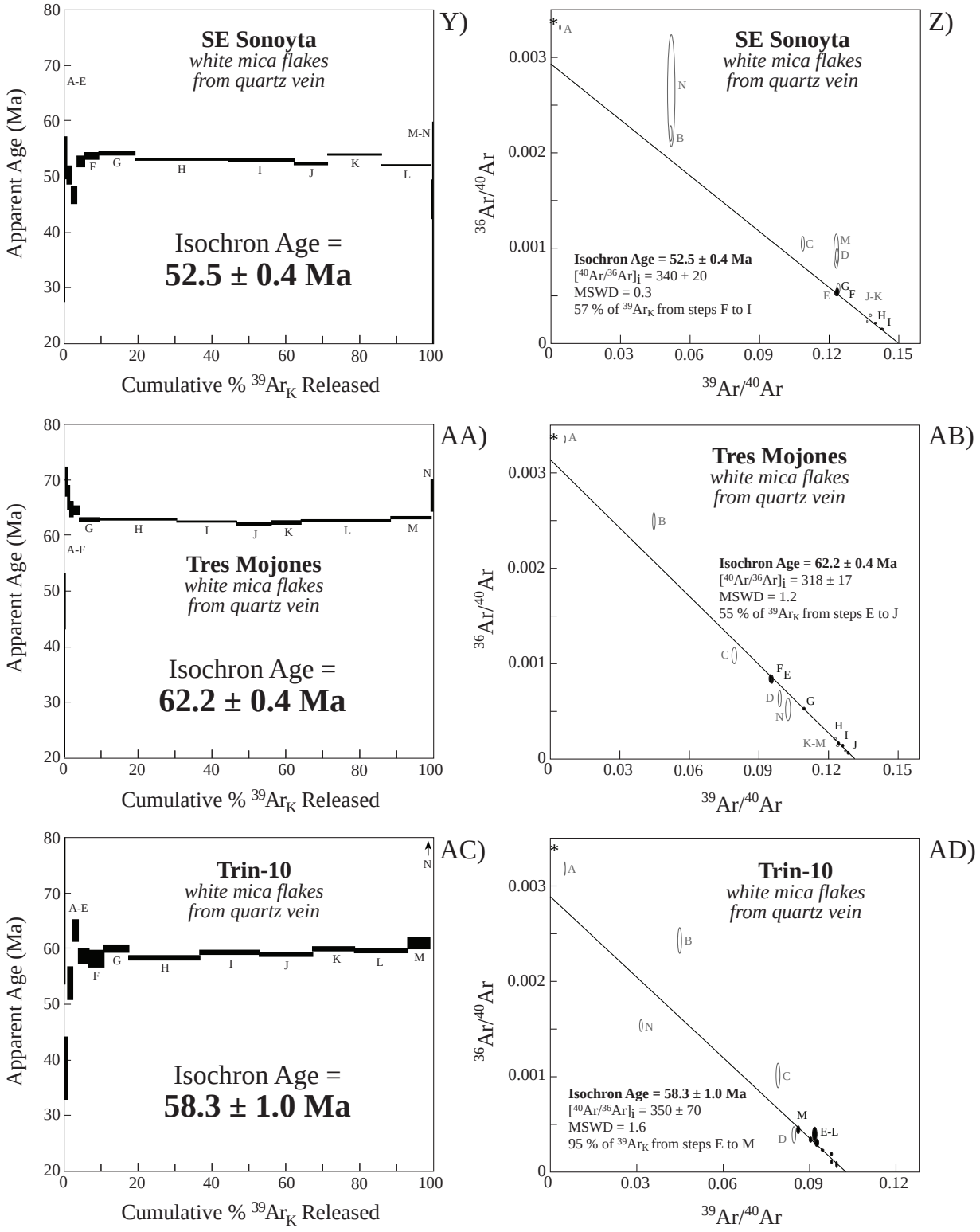

Figure 4—Continued. Age spectra (Y, AA, AC) and inverse-isotope correlation diagrams (Z, AB, AD) from group 2 of white mica samples of gold-rich quartz veins, with isochron ages as best age, from the Caborca orogenic gold belt (COGB), northwestern Sonora, Mexico. * is the assumed limit of the atmospheric argon ratio.

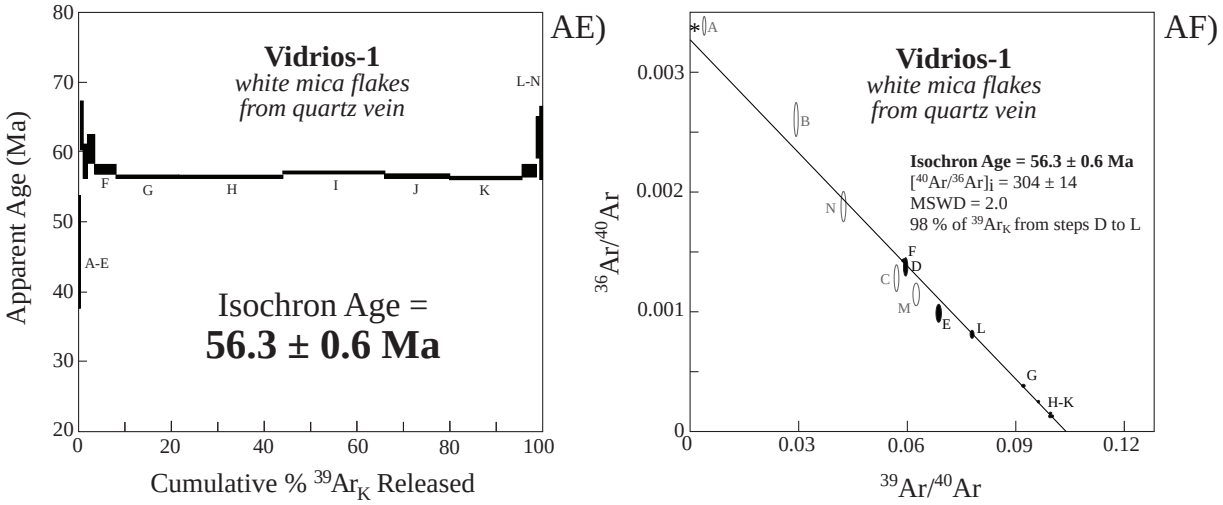

Figure 4—Continued. Age spectra (AE) and inverse-isotope correlation diagrams (AF) from group 2 of white mica samples of gold-rich quartz veins, with isochron ages as best age, from the Caborca orogenic gold belt (COGB), northwestern Sonora, Mexico. * is the assumed limit of the atmospheric argon ratio.

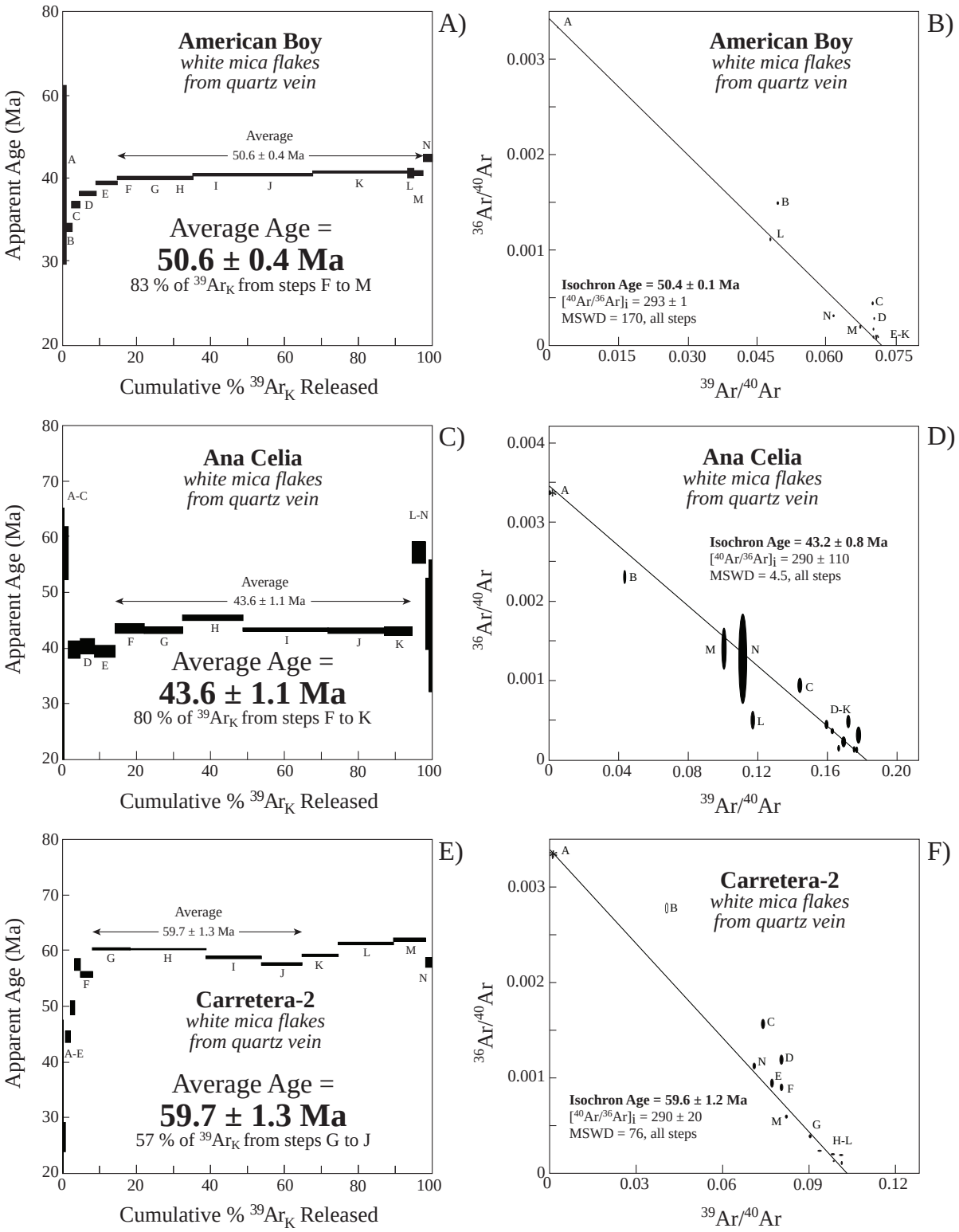

Figure 5. Age spectra (A, C, E) and inverse-isotope correlation diagrams (B, D, F) from group 3 of white mica samples of gold-rich quartz veins, with average ages as best age, from the Caborca orogenic gold belt (COGB), northwestern Sonora, Mexico. * is the assumed limit of the atmospheric argon ratio. Abbreviations: Ma, mega-annum; MSWD, mean square weighted deviation.

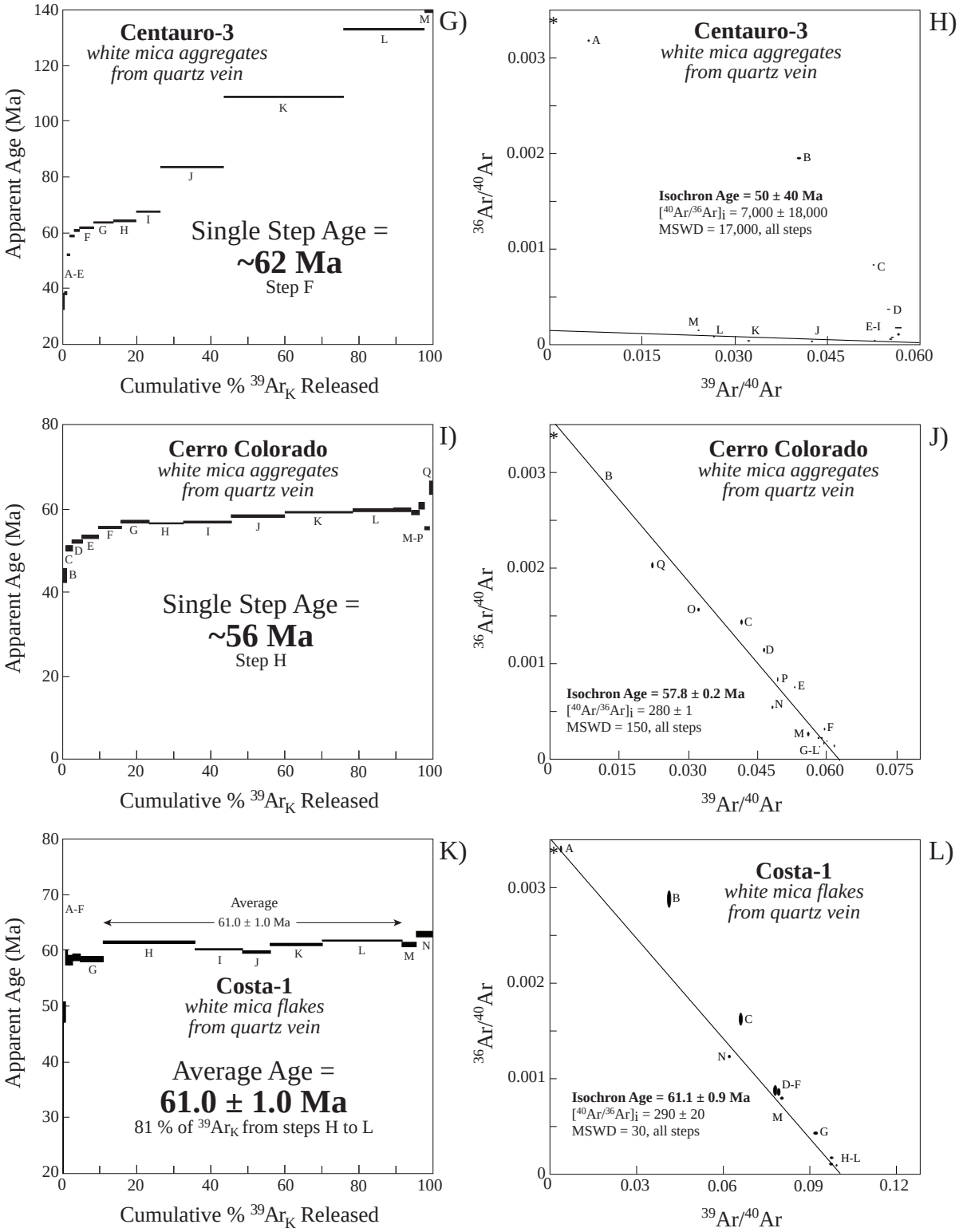

Figure 5—Continued. Age spectra (G, I, K) and inverse-isotope correlation diagrams (H, J, L) from group 3 of white mica samples of gold-rich quartz veins, with average and single-step ages as best age, from the Caborca orogenic gold belt (COGB), northwestern Sonora, Mexico. * is the assumed limit of the atmospheric argon ratio.

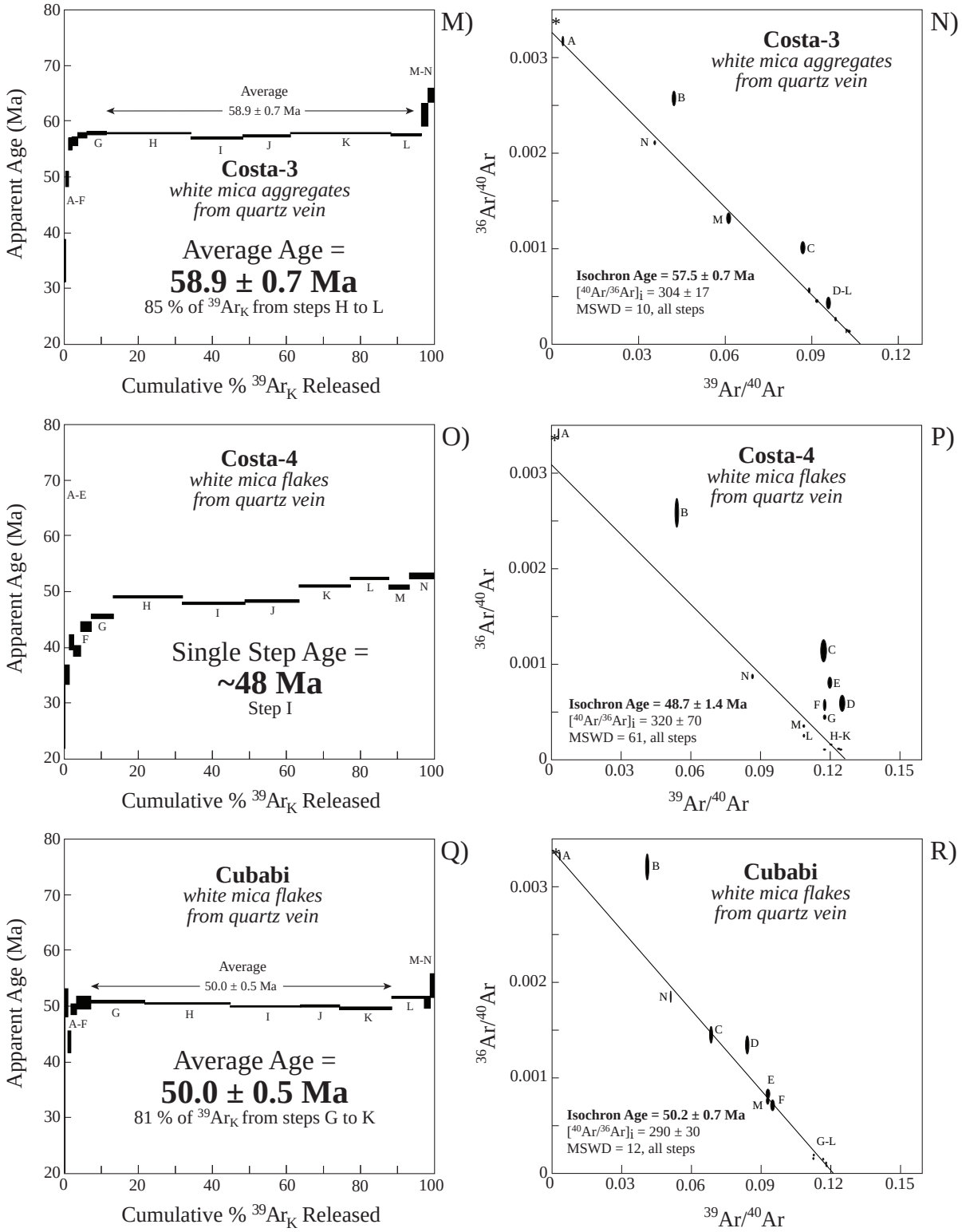

Figure 5—Continued. Age spectra (M, O, Q) and inverse-isotope correlation diagrams (N, P, R) from group 3 of white mica samples of gold-rich quartz veins, with average and single-step ages as best age, from the Caborca orogenic gold belt (COGB), northwestern Sonora, Mexico. * is the assumed limit of the atmospheric argon ratio.

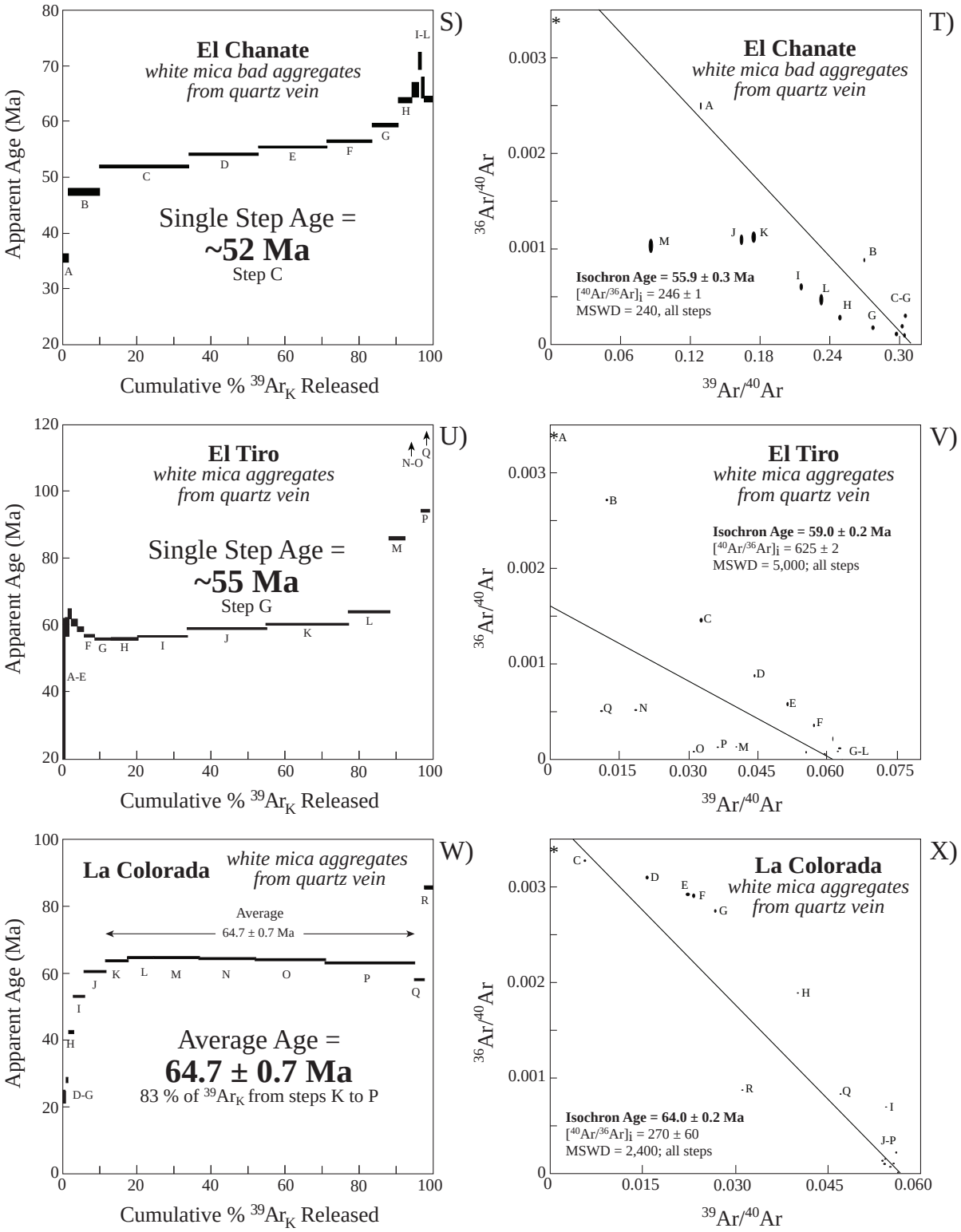

Figure 5—Continued. Age spectra (S, U, W) and inverse-isotope correlation diagrams (T, V, X) from group 3 of white mica samples of gold-rich quartz veins, with average and single-step ages as best age, from the Caborca orogenic gold belt (COGB), northwestern Sonora, Mexico. * is the assumed limit of the atmospheric argon ratio.

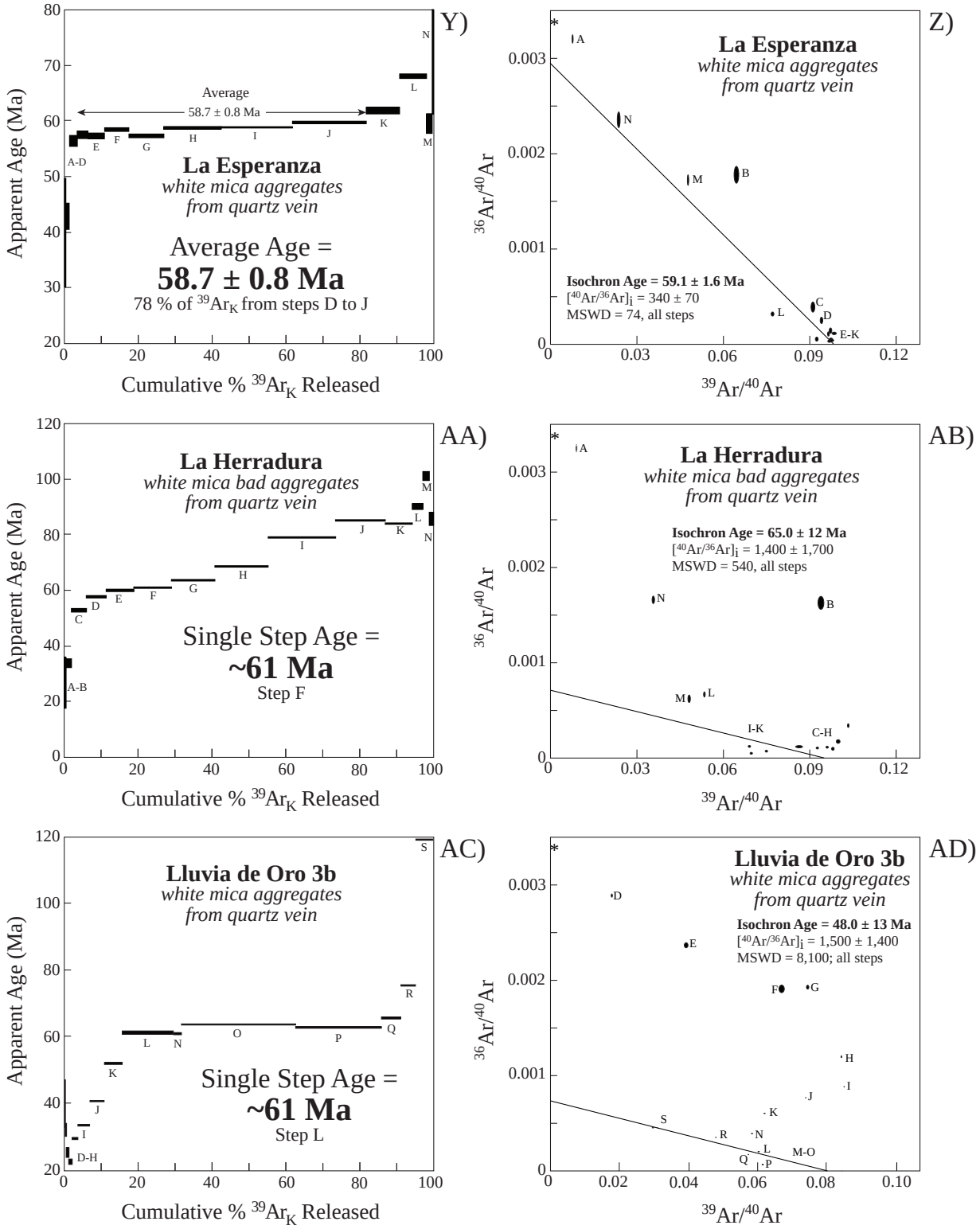

Figure 5—Continued. Age spectra (Y, AA, AC) and inverse-isotope correlation diagrams (Z, AB, AD) from group 3 of white mica samples of gold-rich quartz veins, with average and single-step ages as best age, from the Caborca orogenic gold belt (COGB), northwestern Sonora, Mexico. * is the assumed limit of the atmospheric argon ratio.

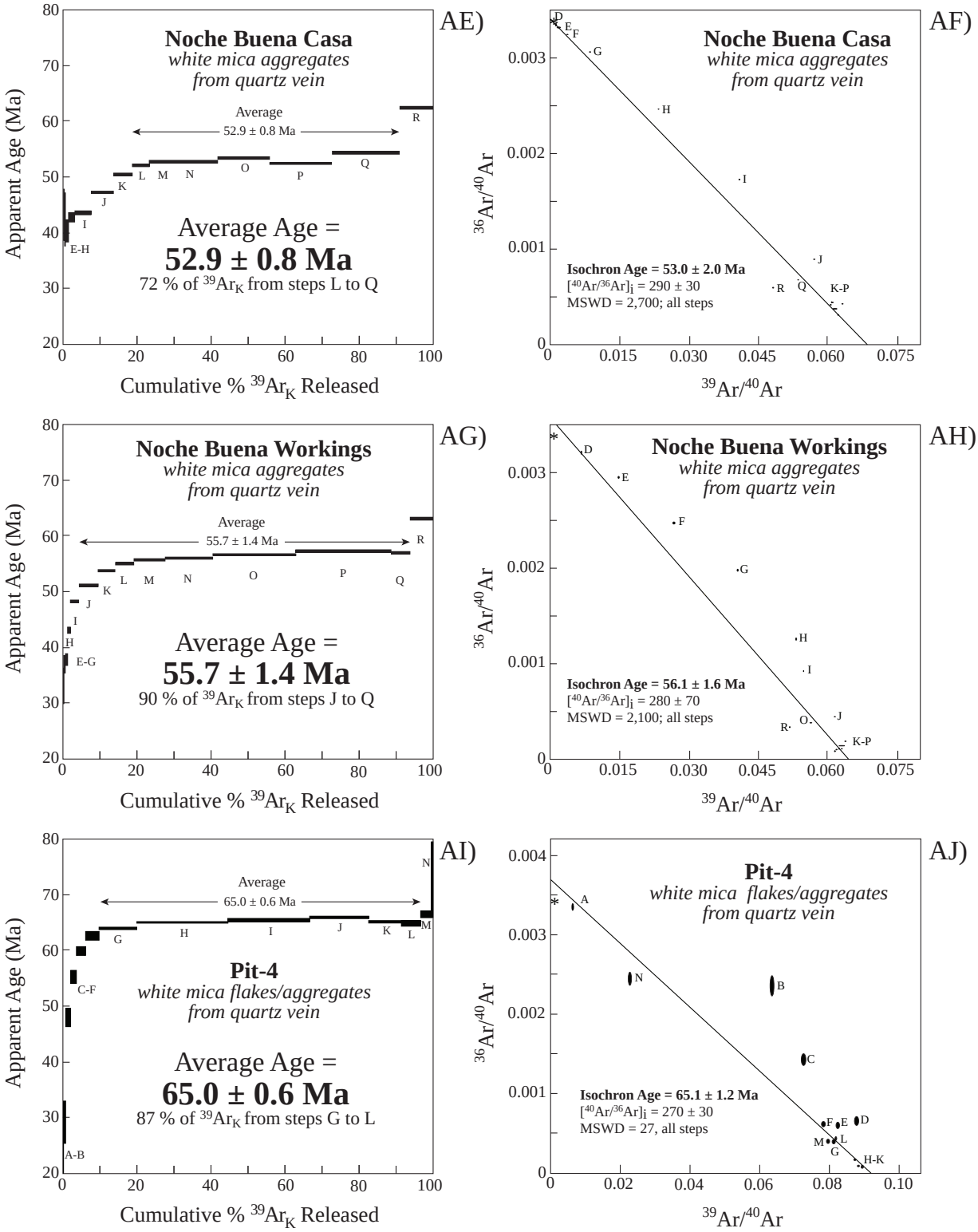

Figure 5—Continued. Age spectra (AE, AG, AI) and inverse-isotope correlation diagrams (AF, AH, AJ) from group 3 of white mica samples of gold-rich quartz veins, with average ages as best age, from the Caborca orogenic gold belt (COGB), northwestern Sonora, Mexico. * is the assumed limit of the atmospheric argon ratio.

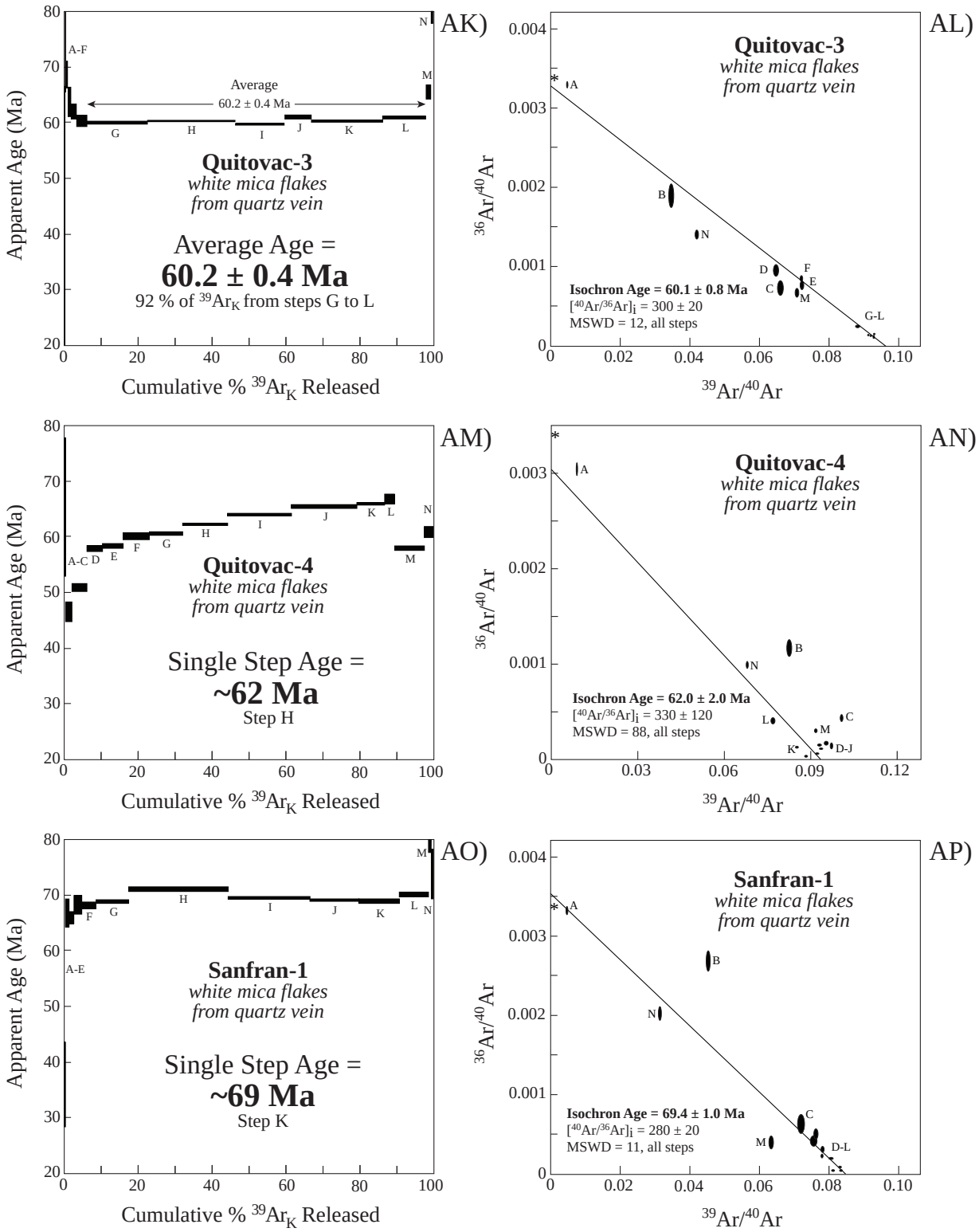

Figure 5—Continued. Age spectra (AK, AM, AO) and inverse-isotope correlation diagrams (AL, AN, AP) from group 3 of white mica samples of gold-rich quartz veins, with average and single-step ages as best age, from the Caborca orogenic gold belt (COGB), northwestern Sonora, Mexico. * is the assumed limit of the atmospheric argon ratio.

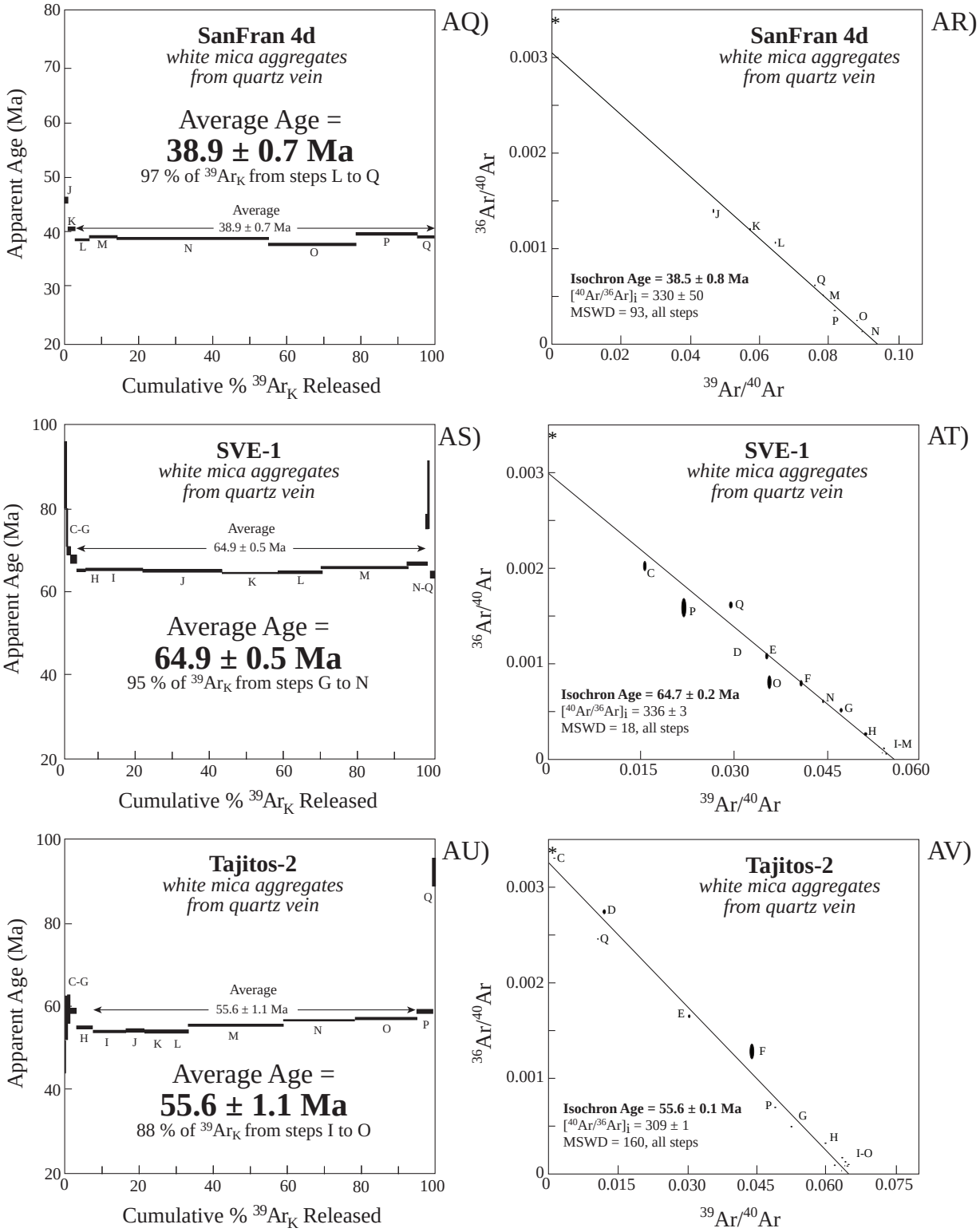

Figure 5—Continued. Age spectra (AQ, AS, AU) and inverse-isotope correlation diagrams (AR, AT, AV) from group 3 of white mica samples of gold-rich quartz veins, with average ages as best age, from the Caborca orogenic gold belt (COGB), northwestern Sonora, Mexico. * is the assumed limit of the atmospheric argon ratio.

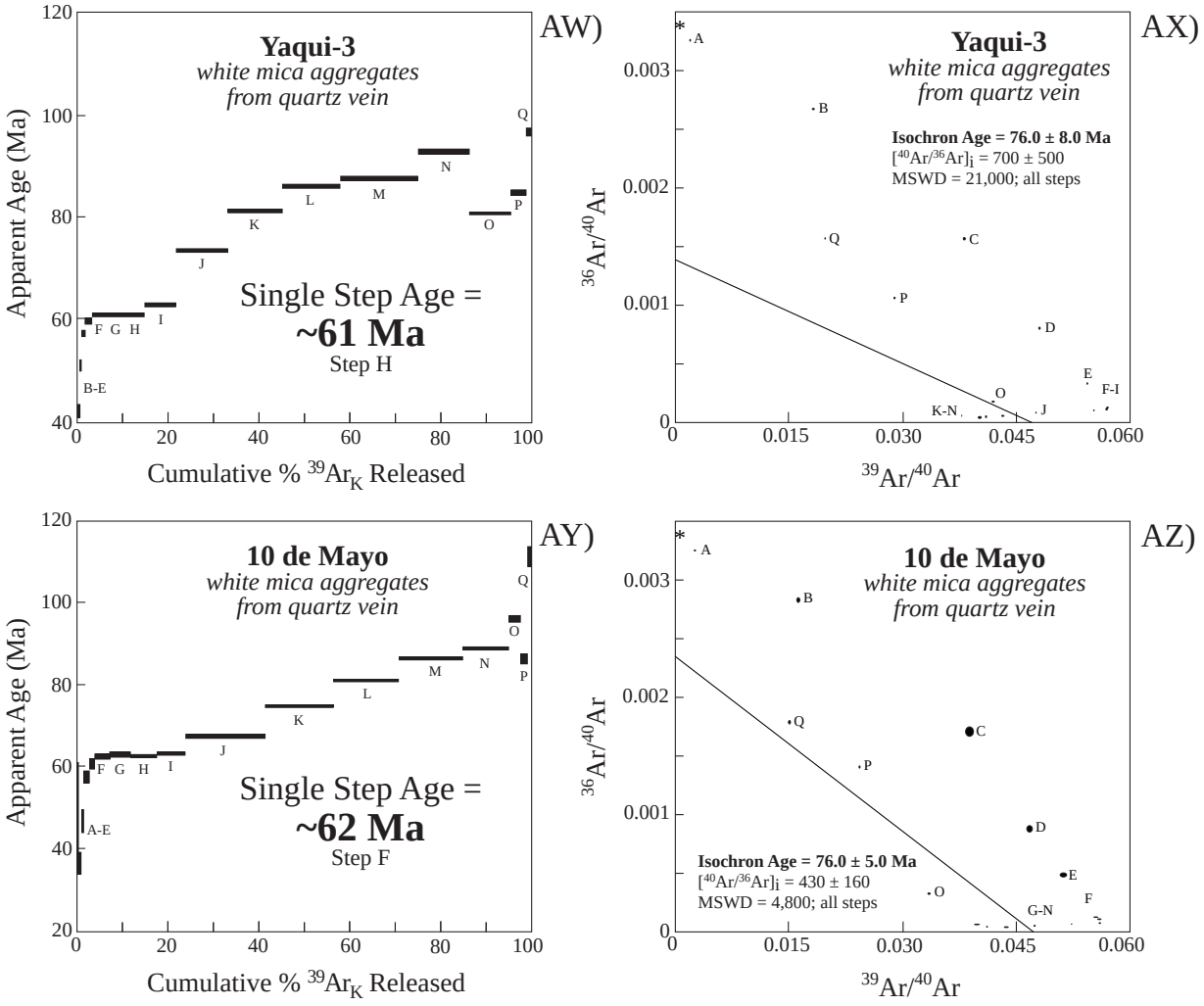

Figure 5—Continued. Age spectrum (AW, AY) and inverse-isotope correlation diagram (AX, AZ) from group 3 of white mica samples of gold-rich quartz veins, with single-step age as best age, from the Caborca orogenic gold belt (COGB), northwestern Sonora, Mexico. * is the assumed limit of the atmospheric argon ratio.

ISSN 2331-1258 (online)
http://dx.doi.org/10.3133/ofr20161008

Table 1. Summary of 63 $^{40}Ar/^{39}Ar$ ages determined from white micas of gold-rich quartz veins of the Caborca orogenic gold belt (COGB), northwestern Sonora, Mexico. [The white mica habit given for the group 3 samples La Herradura and El Chanate is described as "bad aggregates," and refers to small grain white mica used in the analysis that possibly contained impurities.]

Sample name	Location	Latitude*	Longitude*	Laboratory number	White mica habit	Type of age	Age (Ma)	Error (Ma)
Group 1-Plateau ages								
Betty Lee Mine	Copper Mountains	32° 30' 28.7"	113° 59' 41.7"	95KD60	Flakes	Plateau	**47.9**	**0.2**
Cantera	Canteras-Sierra Pinta	31° 26' 44.3"	113° 16' 29.0"	261KD52	Flakes	Plateau	**64**	**0.4**
Celaya-1	Sierra San Francisco	31° 40' 21.1"	113° 8' 11.1"	1KD12	Flakes	Plateau	**60.5**	**0.2**
Chip Mine	Papago-Sheep Area	32° 05' 47.4"	113° 21' 11.5"	98KD60	Flakes	Plateau	**51.2**	**0.3**
Dolores	Dolores Mine	31° 23' 48.1"	113° 7' 39.1"	13KD12	Aggregates	Plateau	**52.8**	**0.3**
El Capitán Mine	Ejido Aquiles Serdán	32° 18' 29.2"	114° 22' 15.5"	103KD60	Flakes	Plateau	**56.9**	**0.3**
Pinor-1	Sierra Pinta	31° 25' 23.7"	113° 7' 58.0"	267KD52	Flakes	Plateau	**61.6**	**0.3**
Pit-3	Pozos de Cerna Ranch	30° 4' 42.3"	112° 10' 48.2"	35KD55	Flakes	Plateau	**65.9**	**0.3**
Prieta-1	Sierra Prieta	31° 18' 46.5"	113° 4' 7.1"	46KD55	Flakes/aggregates	Plateau	**59.0**	**0.3**
Prieta-5	Sierra Prieta	31° 14' 2.9"	113° 0' 51.9"	40KD55	Flakes	Plateau	**59.7**	**0.3**
Quitovac-5	Bustamante Mine	31° 30' 34.2"	112° 50' 23.6"	58KD55	Flakes/aggregates	Plateau	**49.6**	**0.3**
Quitovac-6	La Negra Mine	31° 29' 54.2"	112° 51' 55.3"	71KD55	Flakes	Plateau	**49.9**	**0.3**
Sanfran-2	Sierra San Francisco	31° 31' 59.0"	113° 5' 3.7"	61KD55	Flakes	Plateau	**57.2**	**0.3**
Sanfran-3	Sierra San Francisco	31° 31' 21.7"	113° 4' 44.1"	48KD55	Flakes	Plateau	**59.5**	**0.3**
Sanfran-4	Sierra San Francisco	31° 37' 37.0"	113° 6' 42.4"	52KD55	Flakes	Plateau	**61.6**	**0.3**
Sanfran-6	Sierra San Francisco	31° 37' 57.5"	113° 6' 33.7"	63KD55	Flakes	Plateau	**60.4**	**0.3**
Sanluisito-2	Bertha Mine	31° 17' 2.0"	112° 37' 31.0"	56KD55	Flakes	Plateau	**48.1**	**0.2**
Sonoyta-1	Sierra Los Tanques	31° 53' 20.2"	113° 0' 36.5"	85KD55	Flakes	Plateau	**57.3**	**0.3**
Taj-3	Tajítos-Caborca Area	30° 57' 35.6"	112° 22' 6.4"	6DD60	Flakes	Plateau	**52.6**	**0.8**
Trin-11	Las Amarillas Mine	30° 11' 2.1"	111° 40' 57.8"	77KD55	Flakes	Plateau	**56.9**	**0.3**
Vidrios-2	La Angélica Mine	32° 5' 6.5"	113° 40' 45.5"	73KD55	Flakes	Plateau	**57.7**	**0.3**
Group 2-Isochron ages								
Alamo-7	Sierra La Gloria	30° 55' 45.8"	112° 12' 15.8"	21KD55	Flakes/aggregates	Isochron	**36.1**	**1.2**
Carretera-1	Benjamín Hill	30° 4' 54.1"	111° 5' 49.0"	32KD55	Flakes	Isochron	**47.8**	**0.6**
Estación-1	San Francisco Mine	30° 21' 4.9"	111° 7' 8.5"	16KD55	Flakes	Isochron	**42.2**	**0.5**
Jerónimo	Sierra Los Tanques	31° 47' 36.3"	112° 57' 54.1"	38KD55	Flakes	Isochron	**58.9**	**0.7**
La Pinta USA Mine	Sierra Pinta Arizona	32° 25' 23.2"	113° 40' 9.9"	101KD60	Flakes	Isochron	**43.9**	**0.2**
LH08-1	Cerro Prieto-Carina	31° 12' 48.1"	112° 47' 31.1"	265KD52	Flakes	Isochron	**54.1**	**1.7**
Pinta-1a	La Pinta Mine	31° 24' 19.3"	113° 7' 23.4"	44KD55	Flakes	Isochron	**58.3**	**0.6**
Pinta-2	Sierra Pinta	31° 24' 27.4"	113° 7' 17.3"	83KD55	Flakes	Isochron	**56.9**	**0.8**
Prieta-4	Sierra Prieta	31° 14' 46.3"	113° 1' 12.9"	25KD55	Flakes	Isochron	**60.6**	**0.7**
Quitovac-2	El Chacón Mine	31° 26' 5.9"	112° 43' 38.1"	34KD55	Flakes	Isochron	**59.4**	**0.7**
Sanfran-7	Sierra San Francisco	31° 38' 23.3"	113° 6' 34.5"	79KD55	Flakes	Isochron	**56.5**	**0.6**
Sargenta	Sargenta Mine	31° 40' 19.8"	113° 8' 11.4"	182KD53	Flakes	Isochron	**59.8**	**0.4**
SE Sonoyta	Los Misioneros Mine	31° 49' 57.7"	112° 49' 41.3"	181KD53	Flakes	Isochron	**52.5**	**0.4**
Tres Mojones	Tres Mojones Mine	31° 40' 25.3"	113° 7' 42.0"	191KD53	Flakes	Isochron	**62.2**	**0.4**
Trin-10	Sierra La Salada	30° 10' 57.9"	111° 41' 14.1"	59KD55	Flakes	Isochron	**58.3**	**1.0**
Vidrios-1	La Angélica Mine	32° 5' 6.8"	113° 40' 45.2"	75KD55	Flakes	Isochron	**56.3**	**0.6**
Group 3-Average or single step ages								
American Boy	American Boy Mine	32° 51' 20.9"	114° 47' 8.2"	33KD12	Flakes	Average	**50.6**	**0.4**
Ana Celia	Ana Cecilia Mine	31° 49' 3.5"	112° 52' 3.5"	180KD53	Flakes	Average	**43.6**	**1.1**
Carretera-2	La Jarra Mine	30° 18' 14.4"	110° 57' 3.2"	14KD55	Flakes	Average	**59.7**	**1.3**
Centauro-3	La Herradura Mine	31° 8' 40.2"	112° 51' 45.8"	20KD12	Aggregates	Single step	**~62**	
Cerro Colorado	Cerro Colorado Hills	30° 13' 27"	111° 49' 22.9"	9KD12	Aggregates	Single step	**~56**	
Costa-1	Cerro El Sahuaro	30° 56' 9.3"	112° 52' 47.8"	20KD55	Flakes	Average	**61.0**	**1.0**
Costa-3	Cerro El Sahuaro	30° 55' 0.3"	112° 53' 49.8"	18KD55	Aggregates	Average	**58.9**	**0.7**
Costa-4	Caborca Coast	30° 48' 33.2"	112° 56' 52.5"	24KD55	Flakes	Single step	**~48**	
Cubabi	Sierra Cubabi	31° 45' 48.5"	112° 49' 2.3"	28KD55	Flakes	Average	**50.0**	**0.5**
El Chanate	El Chanate Mine	30° 48' 8.8"	111° 55' 13.2"	263KD52	Bad aggregates	Single step	**~52**	
El Tiro	El Tiro Mine	30° 17' 8.9"	111° 44' 30.9"	15KD12	Aggregates	Single step	**~55**	
La Colorada	La Colorada Mine	28° 48' 1.4"	110° 34' 37.0"	7KD12	Aggregates	Average	**64.7**	**0.7**
La Esperanza	La Esperanza Mine	31° 49' 21.5"	112° 58' 18.7"	87KD55	Aggregates	Average	**58.7**	**0.8**
La Herradura	La Herradura Mine	31° 8' 41.8"	112° 51' 49.0"	29KD55	Bad aggregates	Single step	**~61**	
Lluvia de Oro 3b	Lluvia de Oro Mine	30° 43' 20.6"	111° 2' 8.9"	43KD12	Aggregates	Single step	**~61**	
Noche Buena Casa	Noche Buena Mine	31° 01' 48.9"	112° 38' 51.6"	5KD12	Aggregates	Average	**52.9**	**0.8**
Noche Buena Workings	Noche Buena Mine	31° 01' 50.3"	112° 38' 46.0"	31KD12	Aggregates	Average	**55.7**	**1.4**
Pit-4	South of Pitiquito	30° 4' 47.8"	112° 11' 2.8"	50KD55	Flakes/aggregates	Average	**65.0**	**0.6**
Quitovac-3	La Choya Mine	31° 25' 6.6"	112° 41' 51.1"	81KD55	Flakes	Average	**60.2**	**0.4**
Quitovac-4	Quitovac Mine	31° 29' 25.4"	112° 46' 6.1"	69KD55	Flakes	Single step	**~62**	
Sanfran-1	La Traición Mine	31° 32' 22.6"	113° 3' 56.0"	65KD55	Flakes	Single step	**~69**	
SanFran 4d	San Francisco Mine	30° 21' 11.4"	111° 7' 3.8"	11KD12	Aggregates	Average	**38.9**	**0.7**
SVE-1	Quitovac	31° 29' 19.5"	112° 46' 40.5"	46KD12	Aggregates	Average	**64.9**	**0.5**
Tajitos 2	Tajítos-Caborca	30° 57' 54.3"	112° 22' 28.1"	3KD12	Aggregates	Average	**55.6**	**1.1**
Yaqui-3	La Herradura Mine	31° 9' 11.6"	112° 51' 39.4"	39KD12	Aggregates	Single step	**~61**	
10 de Mayo	La Herradura Mine	31° 9' 19.9"	112° 52' 2.4"	22KD12	Aggregates	Single step	**~62**	

*World Geodetic System (WGS) 1984 Datum.

Table 2. $^{40}Ar/^{39}Ar$ step-heating data and plateau ages determined from white micas of gold-rich quartz veins of the Caborca orogenic gold belt (COGB), northwestern Sonora, Mexico.

Step	Temp. °C	%^{39}Ar of total	Radiogenic yield (%)	$^{39}Ar_k$ (moles)	$^{40}Ar^*/^{39}Ar_k$	Apparent K/Ca	Apparent K/Cl	Apparent age (Ma)	Error (Ma)
Betty Lee Mine	***white mica***	*flakes*	*J =0.006966 ± 0.50 %*	*weight = 2.3 mg*	*95KD60*				
B	700	0.2	10.5	9.85E-16	2.242	3	77	28.0	± 7.1
C	750	0.2	46.5	8.30E-16	3.915	5	763	48.5	± 5.7
D	800	0.4	61.5	1.67E-15	3.269	7	16667	40.6	± 2.8
E	850	0.9	83.1	3.80E-15	3.784	17	7143	46.9	± 1.2
F	900	1.5	84.2	6.17E-15	3.706	31	2381	46.0	± 0.8
G	950	2.5	84.7	1.07E-14	3.738	68	10000	46.4	± 0.5
H	1000	14.0	92.7	5.94E-14	3.871	319	7143	48.0	± 0.1
I	1050	28.8	97.9	1.22E-13	3.865	510	11111	47.9	± 0.1
J	1100	11.6	97.1	4.93E-14	3.848	448	16667	47.7	± 0.1
K	1150	15.0	96.5	6.37E-14	3.864	524	9091	47.9	± 0.1
L	1200	21.7	97.3	9.20E-14	3.917	741	12500	48.6	± 0.1
M	1250	2.3	64.8	9.60E-15	4.035	120	3704	50.0	± 0.6
N	1300	0.7	45.5	2.84E-15	4.054	63	14286	50.2	± 1.9
O	1350	0.2	23.2	1.05E-15	4.237	***	8333	52.5	± 5.6
Total Gas			94.4	4.24E-13	3.869	489	10830	48.0	
69 % of gas released on plateau in H (1000 ºC) through K (1150 ºC) steps							**Plateau Age =**	**47.9**	**± 0.2**
Cantera	***white mica***	*flakes*	*J = 0.009258 ± 0.50 %*	*weight = 21.7 mg*	*261KD52*				
A	600	0.1	12.1	3.24E-03	5.849	3	11	95.1	± 10.0
B	700	0.3	47	1.22E-02	3.262	10	80	53.7	± 1.3
C	800	1.1	82.8	5.32E-02	3.720	66	501	61.1	± 0.3
D	850	1.7	83.6	8.32E-02	3.852	132	1297	63.2	± 0.2
E	900	4.4	81.4	2.15E-01	3.897	427	1866	63.9	± 0.2
F	950	17.8	93.2	8.62E-01	3.926	971	15281	64.4	± 0.1
G	1000	22.2	97.7	1.07E+00	3.921	1099	0	64.3	± 0.1
H	1050	14.7	95.8	7.15E-01	3.918	886	95837	64.3	± 0.1
I	1100	11.7	94.2	5.67E-01	3.907	596	15917	64.1	± 0.1
J	1150	21.4	97.8	1.04E+00	3.930	1234	8505	64.5	± 0.1
K	1200	3.0	97.7	1.44E-01	3.984	258	242	65.3	± 0.2
L	1250	0.9	96.9	4.38E-02	3.981	90	2453	65.3	± 0.3
M	1350	0.3	88.9	1.32E-02	4.198	24	689	68.8	± 0.9
N	1450	0.1	88.8	6.77E-03	4.069	17	313	66.7	± 1.0
O	1650	0.4	88.8	1.97E-02	4.024	40	989	66.0	± 0.4
Total Gas			94.8	4.85E+00	3.921	911	20672	64.3	
88 % of gas released on plateau in F (950 ºC) through J (1150 ºC) steps							**Plateau Age =**	**64.3**	**± 0.4**
Celaya-1	***white mica***	*flakes*	*J = 0.002037 ± 0.25 %*	*weight = 5.1 mg*	*1KD12*				
F	850	0.2	58.4	7.08E-17	35.001	***	***	124.2	± 2.2
G	900	0.6	34.1	2.10E-16	22.898	***	2000	82.2	± 1.4
H	950	1.8	52.7	5.94E-16	18.646	***	131	67.3	± 0.5
I	1000	4.6	81.9	1.51E-15	17.060	***	355	61.6	± 0.2
J	1050	16.3	96.5	5.30E-15	16.710	***	1266	60.4	± 0.1
K	1100	22.6	98.1	7.37E-15	16.721	***	1667	60.4	± 0.1
L	1150	21.6	97.8	7.03E-15	16.755	***	730	60.5	± 0.1
M	1200	14.7	98.0	4.77E-15	16.990	***	568	61.4	± 0.1
N	1250	8.2	94.2	2.68E-15	16.875	***	529	61.0	± 0.1
O	1350	3.2	94.8	1.05E-15	18.995	***	224	68.5	± 0.2
P	1450	3.7	95.1	1.20E-15	20.433	***	201	73.6	± 0.2
Q	1650	2.3	73.4	7.54E-16	20.964	***	143	75.4	± 0.3
Total Gas			94.6	3.25E-14	17.211	***	918	62.2	
61 % of gas released on plateau in J (1050 ºC) through L (1150 ºC) steps							**Plateau Age =**	**60.5**	**± 0.2**
Chip Mine	***white mica***	*flakes*	*J = 0.006978 ± 0.50 %*	*weight = 2.4 mg*	*98KD60*				
B	700	0.2	9.1	1.89E-15	2.402	3	86	30.0	± 4.4
C	800	0.5	51.9	4.06E-15	4.174	6	1639	51.8	± 1.6
D	850	0.4	74.3	3.50E-15	4.330	17	1818	53.7	± 1.8
E	900	1.1	75.1	8.99E-15	4.189	32	3571	52.0	± 0.8
F	950	2.3	82.4	1.89E-14	4.366	67	3448	54.1	± 0.4
G	1000	12.5	90.6	1.04E-13	4.219	306	7143	52.3	± 0.1
H	1050	26.0	96.7	2.17E-13	4.127	877	7692	51.2	± 0.1
I	1100	13.7	95.1	1.14E-13	4.125	606	5556	51.2	± 0.1
J	1150	15.5	96.0	1.29E-13	4.125	1220	5882	51.2	± 0.1
K	1200	25.2	97.7	2.11E-13	4.103	1205	6667	50.9	± 0.1
L	1250	1.8	66.7	1.51E-14	4.111	181	5263	51.0	± 0.5
M	1300	0.7	43.0	5.62E-15	4.253	41	1852	52.8	± 1.3
N	1350	0.2	22.0	1.89E-15	4.168	17	2500	51.7	± 4.3
Total Gas			93.7	8.35E-13	4.136	847	6486	51.3	
55 % of gas released on plateau in H (1050 ºC) through J (1150 ºC) steps							**Plateau Age =**	**51.2**	**± 0.3**

Table 2. $^{40}Ar/^{39}Ar$ step-heating data and plateau ages.—Continued

Step	Temp. °C	%^{39}Ar of total	Radiogenic yield (%)	$^{39}Ar_k$ (moles)	$^{40}Ar^*/^{39}Ar_k$	Apparent K/Ca	Apparent K/Cl	Apparent age (Ma)	Error (Ma)
Dolores	***white mica***	*aggregates*	*J = 0.002037 ± 0.25 %*	*weight = 5.8 mg*	*13KD12*				
C	700	0.2	1.3	9.29E-17	10.430	***	72	37.9	± 11.6
D	750	0.3	13.8	1.39E-16	13.476	***	926	48.9	± 2.9
E	800	0.1	37.5	4.64E-17	18.857	***	505	68.0	± 8.1
F	850	0.6	47.5	2.79E-16	11.273	***	***	41.0	± 1.0
G	900	0.9	70.6	4.18E-16	11.216	***	***	40.8	± 0.6
H	950	1.3	71.3	5.86E-16	12.492	***	3846	45.3	± 0.5
I	1000	1.8	63.3	3.85E-17	11.659	***	787	42.3	± 0.5
J	1050	5.8	83.4	5.77E-17	13.672	***	2703	49.6	± 0.2
K	1100	11.9	87.9	1.92E-17	14.023	***	3030	50.8	± 0.1
L	1150	19.8	92.1	1.15E-16	14.251	***	3226	51.6	± 0.1
M	1200	44.2	95.9	8.53E-15	14.583	***	3704	52.8	± 0.1
N	1250	13.3	95.5	2.56E-15	14.566	***	1111	52.7	± 0.1
Total Gas			91.5	1.29E-14	14.259	***	3002	51.6	
58 % of gas released on plateau in N (1200 ºC) through O (1250 ºC) steps							**Plateau Age =**	**52.8**	**± 0.3**
El Capitán Mine	***white mica***	*flakes*	*J = 0.006978 ± 0.50 %*	*weight = 2.7 mg*	*103KD60*				
B	700	0.2	20.9	9.47E-16	4.583	2	59	56.8	± 10.9
C	800	0.4	65.4	1.77E-15	4.561	3	568	56.5	± 5.7
D	850	0.6	82.9	2.47E-15	4.613	25	1075	57.2	± 4.0
E	900	1.4	89.6	6.28E-15	4.682	308	1818	58.0	± 1.6
F	950	1.7	87.0	7.23E-15	4.631	0	2083	57.4	± 1.4
G	1000	17.0	92.5	7.39E-14	4.637	1031	3030	57.4	± 0.2
H	1050	20.0	98.3	8.68E-14	4.590	935	3846	56.9	± 0.1
I	1100	8.4	97.4	3.65E-14	4.600	588	3125	57.0	± 0.3
J	1150	9.0	96.0	3.90E-14	4.591	433	3030	56.9	± 0.3
K	1200	22.3	98.0	9.68E-14	4.584	971	3448	56.8	± 0.1
L	1250	17.8	96.1	7.74E-14	4.595	862	2857	56.9	± 0.2
M	1300	1.0	70.3	4.49E-15	4.716	***	12500	58.4	± 2.2
N	1350	0.2	38.4	9.18E-16	4.875	***	1613	60.4	± 11.0
Total Gas			95.5	4.35E-13	4.602	835	3295	57.0	
79 % of gas released on plateau in H (1050 ºC) through N (1350 ºC) steps							**Plateau Age =**	**56.9**	**± 0.3**
Pinor-1	***white mica***	*flakes*	*J = 0.009253 ± 0.50 %*	*weight = 20.6 mg*	*267KD52*				
A	600	0.1	3.7	4.19E-03	1.806	3	10	29.9	± 11.4
B	700	0.2	43.4	1.15E-02	3.596	9	79	59.0	± 1.6
C	800	1.1	76.8	5.38E-02	3.831	32	463	62.8	± 0.3
D	850	1.7	70.3	8.01E-02	3.766	146	833	61.8	± 0.2
E	900	5.5	65.0	2.66E-01	3.818	337	929	62.6	± 0.2
F	950	17.8	85.1	8.57E-01	3.759	994	3497	61.7	± 0.1
G	1000	19.9	95.3	9.56E-01	3.749	1073	251370	61.5	± 0.1
H	1050	13.2	92.4	6.33E-01	3.745	733	11275	61.5	± 0.1
I	1100	11.6	88.7	5.58E-01	3.749	600	5096	61.5	± 0.1
J	1150	25.9	96.1	1.24E+00	3.755	1010	0	61.6	± 0.1
K	1200	1.8	80.1	8.55E-02	3.789	76	151	62.2	± 0.3
L	1250	0.6	80.6	2.73E-02	3.784	32	163	62.1	± 0.3
M	1350	0.2	70.9	9.97E-03	3.887	16	124	63.8	± 1.4
N	1450	0.1	83.6	5.90E-03	3.788	13	102	62.1	± 1.3
O	1650	0.2	84.8	1.13E-02	3.756	21	346	61.6	± 0.8
Total Gas			89.6	4.80E+00	3.756	842	52847	61.6	
88 % of gas released on plateau in F (950 ºC) through J (1150 ºC) steps							**Plateau Age =**	**61.6**	**± 0.3**
Pit-3	***white mica***	*flakes*	*J = 0.003408 ± 0.50 %*	*weight = 1.4 mg*	*35KD55*				
A	600	0.3	3.8	3.78E-17	5.596	1	6	34.1	± 12.2
B	700	0.3	42.0	3.73E-17	7.258	***	23	44.1	± 5.1
C	800	1.0	76.4	1.32E-16	8.615	4	48	52.2	± 1.8
D	850	1.5	85.7	1.89E-16	9.685	8	113	58.6	± 1.2
E	900	2.2	84.5	2.83E-16	10.215	***	208	61.7	± 0.9
F	950	3.4	81.7	4.45E-16	10.351	7	351	62.5	± 0.9
G	1000	9.2	87.0	1.20E-15	10.712	42	676	64.7	± 0.6
H	1050	23.2	97.1	3.02E-15	10.839	42	1190	65.4	± 0.1
I	1100	21.8	98.3	2.84E-15	10.948	45	1250	66.1	± 0.1
J	1150	16.4	97.5	2.13E-15	10.897	43	980	65.8	± 0.2
K	1200	11.6	98.1	1.51E-15	10.947	***	980	66.1	± 0.3
L	1250	7.6	91.9	9.89E-16	10.869	11	39	65.6	± 0.3
M	1350	1.3	67.7	1.71E-16	10.184	45	14	61.6	± 1.5
N	1450	0.2	20.0	2.93E-17	9.906	***	8	59.9	± 9.6
Total Gas			94.1	1.30E-14	10.769	38	907	65.0	
57 % of gas released on plateau in I (1100 ºC) through L (1250 ºC) steps							**Plateau Age =**	**65.9**	**± 0.3**

Table 2. $^{40}Ar/^{39}Ar$ step-heating data and plateau ages.—Continued

Step	Temp. °C	%^{39}Ar of total	Radiogenic yield (%)	$^{39}Ar_k$ (moles)	$^{40}Ar^*/^{39}Ar_k$	Apparent K/Ca	Apparent K/Cl	Apparent age (Ma)	Error (Ma)
Prieta-1	***white mica***	*flakes/aggregates*	*J = 0.003394 ± 0.50 %*	*weight = 1.2 mg*	*46KD55*				
A	600	0.7	4.7	7.09E-17	4.159	***	38	25.2	± 9.1
B	700	0.5	38.5	5.07E-17	5.073	***	43	30.6	± 3.4
C	800	1.5	84.2	1.54E-16	9.039	***	65	54.2	± 1.2
D	850	2.0	98.9	2.09E-16	10.232	43	122	61.3	± 1.4
E	900	3.4	93.4	3.49E-16	9.760	***	312	58.5	± 0.5
F	950	5.7	93.8	5.88E-16	9.751	***	461	58.4	± 0.4
G	1000	8.5	96.7	8.80E-16	9.846	***	1087	59.0	± 0.3
H	1050	16.4	97.6	1.69E-15	9.845	22	1190	59.0	± 0.1
I	1100	21.9	98.2	2.26E-15	9.865	38	1471	59.1	± 0.1
J	1150	17.3	98.5	1.78E-15	9.979	***	1163	59.8	± 0.2
K	1200	7.3	97.5	7.53E-16	10.084	***	667	60.4	± 0.3
L	1250	10.1	92.8	1.04E-15	10.288	***	84	61.6	± 0.4
M	1350	4.7	86.5	4.83E-16	10.417	5	25	62.4	± 0.5
N	1450	0.1	19.0	9.86E-18	20.704	***	1	121.9	± 23.6
Total Gas			95.2	1.03E-14	9.896	29	909	59.3	
56 % of gas released on plateau in E (900 ºC) through I (1100 ºC) steps							**Plateau Age =**	**59.0**	**± 0.3**
Prieta-5	***white mica***	*flakes*	*J = 0.003394 ± 0.50 %*	*weight = 1.1 mg*	*40KD55*				
A	600	0.2	-2.0	1.95E-17	-4.451	***	10	-27.5	± 19.5
B	700	0.6	29.5	5.13E-17	5.460	0	23	33.1	± 3.8
C	800	1.5	78.2	1.37E-16	8.905	3	42	53.7	± 1.2
D	850	2.0	86.6	1.76E-16	9.623	5	119	58.0	± 1.0
E	900	3.2	90.0	2.83E-16	10.046	9	219	60.5	± 0.7
F	950	5.0	89.9	4.44E-16	10.030	21	386	60.4	± 0.5
G	1000	13.8	94.4	1.23E-15	9.890	20	794	59.6	± 0.2
H	1050	23.6	98.3	2.10E-15	9.936	63	1724	59.8	± 0.2
I	1100	17.2	97.7	1.53E-15	9.859	***	833	59.4	± 0.3
J	1150	9.8	96.6	8.71E-16	9.904	35	926	59.6	± 0.3
K	1200	10.2	95.3	9.03E-16	9.783	11	606	58.9	± 0.3
L	1250	9.1	92.0	8.13E-16	9.849	61	37	59.3	± 0.3
M	1350	3.4	84.7	2.99E-16	9.640	10	17	58.1	± 0.7
N	1450	0.4	39.2	3.18E-17	12.939	***	11	77.5	± 5.9
Total Gas			94.1	8.89E-15	9.823	36	846	59.1	
73 % of gas released on plateau in E (900 ºC) through J (1150 ºC) steps							**Plateau Age =**	**59.7**	**± 0.3**
Quitovac-5	***white mica***	*flakes/aggregates*	*J = 0.003358 ± 0.50 %*	*weight = 1.1 mg*	*58KD55*				
A	600	0.2	3.1	1.71E-17	6.890	***	8	41.3	± 37.0
B	700	0.4	30.6	4.23E-17	8.015	1	22	47.9	± 5.2
C	800	1.0	61.6	1.01E-16	8.061	1	39	48.2	± 2.0
D	850	1.2	76.4	1.19E-16	8.704	17	72	52.0	± 1.8
E	900	2.1	74.2	2.12E-16	8.981	1	184	53.6	± 1.3
F	950	4.1	73.2	4.16E-16	8.384	15	373	50.1	± 0.7
G	1000	12.9	88.4	1.31E-15	8.277	9	870	49.5	± 0.2
H	1050	20.4	96.4	2.08E-15	8.280	32	1124	49.5	± 0.1
I	1100	17.2	96.8	1.75E-15	8.317	***	990	49.7	± 0.2
J	1150	15.1	94.2	1.54E-15	8.311	9	1031	49.7	± 0.2
K	1200	18.4	97.5	1.88E-15	8.336	22	1370	49.8	± 0.1
L	1250	3.7	82.9	3.83E-16	8.159	5	22	48.8	± 0.9
M	1350	1.3	68.0	1.36E-16	8.612	3	9	51.4	± 1.4
N	1450	2.1	74.8	2.15E-16	9.228	13	50	55.1	± 1.2
Total Gas			91.5	1.02E-14	8.339	18	941	49.8	
93 % of gas released on plateau in F (950 ºC) through M (1350 ºC) steps							**Plateau Age =**	**49.6**	**± 0.3**
Quitovac-6	***white mica***	*flakes*	*J = 0.003300 ± 0.50 %*	*weight = 1.3 mg*	*71KD55*				
A	600	0.3	4.1	4.09E-17	4.251	1	19	25.1	± 15.3
B	700	0.3	28.8	3.15E-17	5.005	***	31	29.6	± 7.7
C	800	0.9	78.5	1.04E-16	9.410	1	39	55.2	± 2.7
D	850	1.2	70.1	1.46E-16	8.215	3	100	48.3	± 1.4
E	900	2.2	72.8	2.67E-16	8.595	7	214	50.5	± 1.2
F	950	4.2	73.1	5.06E-16	8.573	9	370	50.3	± 0.5
G	1000	11.5	84.2	1.39E-15	8.547	15	962	50.2	± 0.2
H	1050	24.2	95.9	2.94E-15	8.500	24	1613	49.9	± 0.1
I	1100	19.0	96.8	2.31E-15	8.469	14	1087	49.7	± 0.2
J	1150	9.3	94.7	1.14E-15	8.544	72	775	50.2	± 0.2
K	1200	8.0	92.5	9.72E-16	8.588	10	971	50.4	± 0.2
L	1250	12.0	87.8	1.46E-15	8.429	18	54	49.5	± 0.2
M	1350	6.6	90.0	8.06E-16	8.377	10	60	49.2	± 0.3
N	1450	0.4	26.4	4.57E-17	6.819	0	11	40.1	± 4.8
Total Gas			90.3	1.22E-14	8.474	21	889	49.8	
70 % of gas released on plateau in E (900 ºC) through J (1150 ºC) steps							**Plateau Age =**	**49.9**	**± 0.3**

Table 2. $^{40}Ar/^{39}Ar$ step-heating data and plateau ages.—Continued

Step	Temp. °C	%^{39}Ar of total	Radiogenic yield (%)	$^{39}Ar_k$ (moles)	$^{40}Ar^*/^{39}Ar_k$	Apparent K/Ca	Apparent K/Cl	Apparent age (Ma)	Error (Ma)
Sanfran-2	***white mica***	*flakes*	*J = 0.003308 ± 0.50 %*	*weight = 1.3 mg*	*61KD55*				
A	600	0.4	6.4	4.46E-17	6.347	***	19	37.5	± 8.0
B	700	0.3	41.4	3.38E-17	7.223	***	38	42.6	± 7.9
C	800	1.0	76.6	1.17E-16	10.109	***	48	59.3	± 1.7
D	850	1.2	77.6	1.45E-16	9.960	***	112	58.5	± 1.4
E	900	2.1	65.5	2.49E-16	9.684	***	237	56.9	± 1.0
F	950	5.2	75.2	6.13E-16	9.952	***	575	58.4	± 0.4
G	1000	18.8	90.5	2.25E-15	9.785	***	1282	57.5	± 0.1
H	1050	22.2	97.4	2.66E-15	9.707	***	1563	57.0	± 0.1
I	1100	14.7	95.9	1.75E-15	9.717	62	1205	57.1	± 0.2
J	1150	9.4	92.1	1.13E-15	9.726	***	1020	57.1	± 0.3
K	1200	17.8	96.1	2.13E-15	9.767	43	1205	57.4	± 0.1
L	1250	5.9	93.9	7.03E-16	9.777	***	30	57.4	± 0.3
M	1350	0.5	50.8	6.49E-17	8.640	***	7	50.8	± 3.0
N	1450	0.5	40.3	6.18E-17	9.026	***	25	53.1	± 3.4
Total Gas			91.6	1.20E-14	9.729	52	1114	57.2	
70 % of gas released on plateau in H (1050 ºC) through L (1250 ºC) steps							**Plateau Age =**	**57.2**	**± 0.3**
Sanfran-3	***white mica***	*flakes*	*J = 0.003377 ± 0.50 %*	*weight = 1.5 mg*	*48KD55*				
A	600	0.3	4.7	3.44E-17	7.279	13	14	43.8	± 13.2
B	700	0.2	21.4	2.70E-17	4.244	***	22	25.7	± 8.2
C	800	0.7	58.5	8.58E-17	8.648	***	35	51.9	± 2.6
D	850	0.9	76.1	1.18E-16	10.004	***	75	59.9	± 2.0
E	900	1.8	74.5	2.27E-16	9.654	4	143	57.9	± 1.2
F	950	4.1	70.9	5.19E-16	9.922	10	386	59.5	± 0.6
G	1000	15.8	91.6	2.01E-15	9.969	926	971	59.7	± 0.6
H	1050	22.9	97.6	2.90E-15	9.946	149	1613	59.6	± 0.1
I	1100	16.7	97.4	2.11E-15	9.907	29	1149	59.4	± 0.2
J	1150	10.3	92.6	1.30E-15	9.834	40	840	58.9	± 0.3
K	1200	16.9	96.8	2.14E-15	9.946	166	833	59.6	± 0.2
L	1250	8.5	93.9	1.08E-15	10.100	14	48	60.5	± 0.3
M	1350	0.5	58.0	6.93E-17	10.614	1	5	63.5	± 3.4
N	1450	0.4	33.0	4.99E-17	10.555	***	13	63.2	± 4.8
Total gas			92.8	1.27E-14	9.916	224	966	59.4	
62 % of gas released on plateau in D (850 ºC) through I (1100 ºC) steps							**Plateau Age =**	**59.5**	**± 0.3**
Sanfran-4	***white mica***	*flakes*	*J = 0.003343 ± 0.50 %*	*weight = 1.2 mg*	*52KD55*				
A	600	0.2	-0.3	2.31E-17	-0.754	***	9	-4.6	± 20.0
B	700	0.4	35.5	4.52E-17	6.952	***	20	41.4	± 4.4
C	800	1.0	76.8	1.09E-16	10.788	***	36	63.9	± 2.0
D	850	1.4	83.3	1.53E-16	10.483	***	92	62.1	± 1.5
E	900	2.7	84.4	2.92E-16	10.634	***	227	63.0	± 0.8
F	950	5.7	89.9	6.19E-16	10.540	***	524	62.5	± 0.5
G	1000	18.6	96.6	2.02E-15	10.404	***	893	61.7	± 0.2
H	1050	25.8	98.7	2.80E-15	10.397	***	1538	61.6	± 0.1
I	1100	23.7	98.1	2.58E-15	10.392	48	1351	61.6	± 0.1
J	1150	11.2	96.9	1.22E-15	10.369	***	725	61.5	± 0.2
K	1200	8.6	98.0	9.38E-16	10.505	***	595	62.3	± 0.2
L	1250	0.5	45.1	5.48E-17	10.318	***	2	61.2	± 3.7
M	1350	0.0	-1.5	4.95E-18	-1.629	***	0	-9.9	± 31.5
N	1450	0.0	-7.0	3.11E-18	-15.522	***	1	-96.1	± 95.6
Total gas			95.9	1.09E-14	10.386	48	1055	61.5	
79 % of gas released on plateau in G (1000 ºC) through J (1150 ºC) steps							**Plateau Age =**	**61.6**	**± 0.3**
Sanfran-6	***white mica***	*flakes*	*J = 0.003301 ± 0.50 %*	*weight = 1.3 mg*	*63KD55*				
A	600	0.3	3.3	3.08E-17	4.552	0	20	26.9	± 12.6
B	700	0.2	46.7	2.65E-17	9.376	2	24	55.0	± 5.7
C	800	0.7	78.3	7.78E-17	10.760	3	29	63.0	± 2.5
D	850	0.9	88.2	1.01E-16	11.278	***	76	65.9	± 1.6
E	900	1.4	88.0	1.67E-16	10.944	17	180	64.0	± 1.2
F	950	2.6	84.7	2.97E-16	10.695	4	239	62.6	± 1.4
G	1000	8.7	90.8	1.01E-15	10.331	21	943	60.5	± 0.4
H	1050	19.4	98.2	2.24E-15	10.332	33	1370	60.5	± 0.1
I	1100	27.8	98.8	3.22E-15	10.340	29	1299	60.6	± 0.1
J	1150	21.2	97.6	2.45E-15	10.285	21	952	60.2	± 0.1
K	1200	12.6	98.6	1.46E-15	10.411	47	847	61.0	± 0.2
L	1250	3.6	89.4	4.21E-16	10.741	23	21	62.9	± 0.5
M	1350	0.3	52.4	3.86E-17	12.040	1	3	70.3	± 5.3
N	1450	0.2	27.4	2.28E-17	11.358	1	8	66.4	± 9.0
Total gas			95.9	1.16E-14	10.366	28	1029	60.7	
80 % of gas released on plateau in F (950 ºC) through J (1150 ºC) steps							**Plateau Age =**	**60.4**	**± 0.3**

Table 2. $^{40}Ar/^{39}Ar$ step-heating data and plateau ages.—Continued

Step	Temp. °C	%^{39}Ar of total	Radiogenic yield (%)	$^{39}Ar_k$ (moles)	$^{40}Ar^*/^{39}Ar_k$	Apparent K/Ca	Apparent K/Cl	Apparent age (Ma)	Error (Ma)
Sanluisito-2	***white mica***	*flakes*	*J = 0.003363 ± 0.50 %*	*weight = 1.3 mg*	*56KD55*				
A	600	0.3	5.6	3.83E-17	6.618	1	17	39.7	± 14.2
B	700	0.3	26.8	3.34E-17	4.875	1	22	29.3	± 6.7
C	800	0.9	74.8	1.10E-16	8.506	***	36	50.9	± 1.8
D	850	1.1	79.1	1.37E-16	8.484	***	104	50.8	± 1.6
E	900	2.0	79.3	2.39E-16	8.008	3	208	47.9	± 1.0
F	950	4.7	81.9	5.69E-16	8.104	***	637	48.5	± 0.5
G	1000	15.2	93.9	1.84E-15	8.078	104	1471	48.4	± 0.2
H	1050	20.6	97.8	2.47E-15	8.024	29	1449	48.0	± 0.1
I	1100	18.1	97.0	2.19E-15	8.009	123	1449	47.9	± 0.1
J	1150	12.3	94.4	1.48E-15	7.988	29	1587	47.8	± 0.2
K	1200	17.9	97.5	2.16E-15	8.108	41	847	48.5	± 0.2
L	1250	3.6	78.9	4.38E-16	8.194	***	17	49.0	± 0.5
M	1350	1.4	81.0	1.71E-16	9.691	89	15	57.9	± 2.0
N	1450	1.5	69.5	1.76E-16	12.449	***	94	74.0	± 1.4
Total gas			93.2	1.21E-14	8.135	64	1170	48.7	
	75 % of gas released on plateau in C (800 ºC) through J (1150 ºC) steps						**Plateau Age =**	**48.1**	**± 0.2**
Sonoyta-1	***white mica***	*flakes*	*J = 0.003249 ± 0.50 %*	*weight = 1.2 mg*	*85KD55*				
A	600	0.2	0.6	2.79E-17	2.556	0	10	14.9	± 19.3
B	700	0.2	28.0	2.26E-17	7.372	0	15	42.7	± 6.7
C	800	0.8	66.2	8.63E-17	9.598	1	28	55.4	± 2.2
D	850	1.0	74.0	1.09E-16	9.928	2	81	57.3	± 1.7
E	900	1.6	79.2	1.86E-16	10.133	***	171	58.4	± 1.1
F	950	5.4	82.4	6.08E-16	9.864	8	483	56.9	± 0.5
G	1000	17.5	94.2	1.97E-15	9.965	38	917	57.5	± 0.2
H	1050	18.9	98.4	2.14E-15	10.042	***	2000	57.9	± 0.2
I	1100	14.9	96.6	1.69E-15	9.930	16	1124	57.3	± 0.2
J	1150	12.0	95.7	1.35E-15	9.919	12	1111	57.2	± 0.2
K	1200	20.4	98.2	2.30E-15	9.955	45	1149	57.4	± 0.1
L	1250	4.4	85.8	5.01E-16	9.982	***	22	57.6	± 0.7
M	1350	1.7	71.4	1.87E-16	9.627	6	17	55.6	± 1.2
N	1450	1.0	55.9	1.15E-16	10.193	1	24	58.8	± 1.9
Total gas			93.6	1.13E-14	9.938	27	1105	57.3	
	54 % of gas released on plateau in I (1100 ºC) through N (1450 ºC) steps						**Plateau Age =**	**57.3**	**± 0.3**
Taj-3	***white mica***	*flakes*	*J = 0.006499 ± 0.50 %*	*weight = 20.3 mg*	*6DD60*				
A	600	1.1	100.0	1.62E-01	4.176	***	846	48.3	± 6.2
B	700	3.4	61.4	4.84E-01	4.499	***	550	52.0	± 2.3
C	800	9.3	98.4	1.35E+00	4.538	***	0	52.4	± 0.8
D	900	35.6	99.3	5.13E+00	4.500	***	0	52.0	± 0.6
E	950	18.0	99.0	2.60E+00	4.546	***	0	52.5	± 0.4
F	1000	17.3	98.2	2.49E+00	4.562	***	0	52.7	± 0.4
G	1050	9.2	100.0	1.32E+00	4.609	***	0	53.3	± 0.8
H	1100	2.7	99.0	3.92E-01	4.637	***	7941	53.6	± 2.4
I	1150	1.3	90.8	1.80E-01	4.449	***	949	51.4	± 5.7
J	1200	1.0	90.5	1.48E-01	4.404	***	773	50.9	± 7.9
K	1250	0.6	99.9	8.72E-02	4.874	***	12534	56.3	± 10.8
L	1650	0.5	68.3	7.08E-02	4.944	***	1616	57.1	± 15.4
Total gas			91.2	9.80E-15	9.835	709	744	57.0	
	100 % of gas released on plateau, all steps						**Plateau Age =**	**52.6**	**± 0.8**
Trin-11	***white mica***	*flakes*	*J = 0.003262 ± 0.50 %*	*weight = 1.1 mg*	*77KD55*				
A	600	0.4	1.3	3.50E-17	1.330	***	21	7.8	± 14.4
B	700	0.3	36.7	3.29E-17	8.250	0	26	47.9	± 4.7
C	800	1.1	63.5	1.11E-16	10.399	5	39	60.2	± 2.6
D	850	1.6	59.4	1.61E-16	9.237	3	86	53.6	± 2.7
E	900	2.8	68.9	2.78E-16	9.725	***	228	56.3	± 1.0
F	950	5.9	79.6	5.78E-16	9.740	7	483	56.4	± 0.5
G	1000	11.8	94.0	1.16E-15	10.004	40	752	57.9	± 0.3
H	1050	18.5	97.2	1.81E-15	9.836	25	1282	57.0	± 0.2
I	1100	12.7	97.7	1.25E-15	9.844	3846	1250	57.0	± 0.2
J	1150	9.8	95.8	9.63E-16	9.777	***	862	56.6	± 0.3
K	1200	13.3	95.2	1.30E-15	9.816	***	935	56.9	± 0.2
L	1250	14.4	93.3	1.40E-15	9.985	156	67	57.8	± 0.2
M	1350	5.3	82.1	5.22E-16	10.056	10	38	58.2	± 0.5
N	1450	2.0	67.6	1.94E-16	10.065	5	47	58.3	± 1.8
Total gas			91.2	9.80E-15	9.835	709	744	57.0	
	54 % of gas released on plateau in H (1050 ºC) through K (1200 ºC) steps						**Plateau Age =**	**56.9**	**± 0.3**

Table 2. $^{40}Ar/^{39}Ar$ step-heating data and plateau ages.—Continued

Step	Temp. °C	%^{39}Ar of total	Radiogenic yield (%)	$^{39}Ar_k$ (moles)	$^{40}Ar^*/^{39}Ar_k$	Apparent K/Ca	Apparent K/Cl	Apparent age (Ma)	Error (Ma)
Vidrios-2	***white mica***	*flakes*	*J = 0.003289 ± 0.50 %*	*weight = 1.1 mg*	*73KD55*				
A	600	0.3	6.1	2.72E-17	8.872	1	11	51.9	± 13.0
B	700	0.2	58.7	1.50E-17	13.720	1	15	79.6	± 16.6
C	800	0.6	74.1	5.64E-17	11.421	3	22	66.5	± 3.0
D	850	0.8	71.3	7.63E-17	10.363	1	47	60.5	± 2.4
E	900	1.4	80.3	1.34E-16	12.142	***	85	70.6	± 3.3
F	950	4.2	73.9	3.88E-16	9.919	6	455	57.9	± 0.6
G	1000	13.4	93.3	1.25E-15	9.978	***	885	58.3	± 0.3
H	1050	24.0	98.1	2.24E-15	9.873	15	1613	57.6	± 0.1
I	1100	21.4	98.2	2.00E-15	9.873	45	1149	57.7	± 0.1
J	1150	12.8	96.0	1.20E-15	9.910	59	826	57.9	± 0.2
K	1200	16.1	98.6	1.50E-15	9.897	***	877	57.8	± 0.2
L	1250	3.5	86.4	3.25E-16	10.090	8	16	58.9	± 0.7
M	1350	0.7	70.0	6.53E-17	11.942	1	5	69.5	± 3.3
N	1450	0.6	45.5	5.56E-17	13.783	1	19	80.0	± 3.8
Total gas			94.4	9.34E-15	9.993	31	1020	58.3	
95 % of gas released on plateau in F (950 ºC) through L (1250 ºC) steps							**Plateau Age =**	**57.7**	**± 0.3**

Ages calculated assuming an initial $^{40}Ar/^{39}Ar = 295.5$.

All precision estimates are at the one sigma level of precision.

Ages of individual steps do not include error in the irradiation parameter J.

No error is calculated for the total gas age.

Data were obtained using a MAP 216 or a VG1200 spectrometer.

*** K/Ca or K/Cl not calculated.

Table 3. $^{40}Ar/^{39}Ar$ step-heating data and isochron ages determined from white micas of gold-rich quartz veins of the Caborca orogenic gold belt (COGB), northwestern Sonora, Mexico.

Step	Temp. °C	%^{39}Ar of total	Radiogenic yield (%)	$^{39}Ar_k$ (moles)	$^{40}Ar^*/^{39}Ar_k$	Apparent K/Ca	Apparent K/Cl	Apparent age (Ma)	Error (Ma)
Alamo-7	***white mica***	*flakes/aggregates*	*J = 0.003446 ± 0.50 %*	*weight = 1.6 mg*	*21KD55*				
A	600	0.8	1.4	1.04E-16	0.565	1	68	3.5	± 3.9
B	700	1.6	40.4	1.98E-16	3.672	8	146	22.7	± 1.2
C	800	5.4	68.1	6.67E-16	4.716	7	208	29.1	± 0.4
D	850	6.3	74.6	7.79E-16	4.999	16	400	30.8	± 0.5
E	900	8.0	78.8	9.96E-16	5.382	1064	613	33.2	± 0.3
F	950	8.8	73.4	1.08E-15	5.334	85	971	32.9	± 0.3
G	1000	9.5	72.7	1.18E-15	5.644	26	1493	34.8	± 0.3
H	1050	11.9	72.8	1.48E-15	5.838	43	1449	35.9	± 0.2
I	1100	13.7	72.3	1.69E-15	5.881	37	1124	36.2	± 0.2
J	1150	14.4	72.3	1.78E-15	5.923	93	1000	36.5	± 0.2
K	1200	8.7	72.2	1.08E-15	5.927	11	719	36.5	± 0.4
L	1250	2.8	49.7	3.44E-16	5.557	***	12	34.2	± 0.8
M	1350	7.5	64.9	9.31E-16	5.693	***	118	35.1	± 0.9
N	1450	0.6	17.5	6.84E-17	7.241	***	13	44.5	± 5.4
Total gas			70.3	1.24E-14	5.564	136	858	34.2	
60 % of gas released in steps H (1050 ºC) through N (1450 ºC) steps							**Isochron age =**	**36.1**	**± 1.2**
Carretera-1	***white mica***	*flakes*	*J = 0.003406 ± 0.50 %*	*weight = 1.3 mg*	*32KD55*				
A	600	0.2	5.6	2.41E-17	9.067	0	5	54.9	± 16.4
B	700	0.4	22.2	5.04E-17	3.914	1	22	23.9	± 4.6
C	800	1.1	60.9	1.27E-16	6.616	2	40	40.2	± 1.8
D	850	1.2	66.0	1.45E-16	7.192	7	95	43.7	± 1.7
E	900	2.2	62.9	2.65E-16	7.020	3	203	42.6	± 2.2
F	950	4.1	71.9	4.88E-16	7.523	0	373	45.6	± 0.8
G	1000	14.7	89.5	1.74E-15	7.843	28	971	47.6	± 0.2
H	1050	23.7	97.4	2.81E-15	7.883	66	2381	47.8	± 0.1
I	1100	18.1	97.1	2.15E-15	7.851	93	1370	47.6	± 0.1
J	1150	11.5	95.5	1.36E-15	7.910	107	917	48.0	± 0.2
K	1200	13.8	97.0	1.63E-15	8.008	40	1053	48.5	± 0.2
L	1250	6.1	88.3	7.27E-16	7.962	***	37	48.3	± 0.6
M	1350	1.9	73.0	2.30E-16	7.875	10	20	47.8	± 1.0
N	1450	0.9	36.9	1.06E-16	7.883	4	34	47.8	± 2.4
Total gas			91.3	1.19E-14	7.827	58	1231	47.5	
68 % of gas released in steps G (1000 ºC) through J (1150 ºC) steps							**Isochron age =**	**47.8**	**± 0.6**
Estación-1	***white mica***	*flakes*	*J = 0.003456 ± 0.50 %*	*weight = 1.2 mg*	*16KD55*				
A	600	0.1	-0.6	1.55E-17	-2.710	1	9	-17.0	± 21.0
B	700	0.3	17.9	3.17E-17	4.741	2	21	29.3	± 4.4
C	800	0.7	49.5	7.15E-17	6.030	2	23	37.2	± 1.7
D	850	0.9	70.6	9.63E-17	6.444	7	55	39.7	± 1.3
E	900	1.6	68.5	1.72E-16	6.648	4	111	41.0	± 0.8
F	950	2.8	73.0	3.00E-16	7.032	***	231	43.3	± 0.5
G	1000	8.2	78.0	8.72E-16	6.849	18	621	42.2	± 0.3
H	1050	27.2	93.4	2.90E-15	6.852	173	1786	42.2	± 0.1
I	1100	16.5	95.8	1.76E-15	6.825	***	1613	42.1	± 0.2
J	1150	10.1	90.7	1.08E-15	6.852	25	595	42.2	± 0.3
K	1200	20.7	93.6	2.21E-15	6.890	70	1099	42.5	± 0.1
L	1250	10.3	85.1	1.10E-15	6.780	166	64	41.8	± 0.2
M	1350	0.4	34.1	4.18E-17	7.150	6	2	44.0	± 3.1
N	1450	0.1	10.9	1.06E-17	5.522	***	8	34.1	± 11.8
Total gas			89.3	1.07E-14	6.824	103	1107	42.0	
87 % of gas released in steps E (900 ºC) through K (1200 ºC) steps							**Isochron age =**	**42.2**	**± 0.5**
Jerónimo	***white mica***	*flakes*	*J = 0.003398 ± 0.50 %*	*weight = 1.5 mg*	*38KD55*				
A	600	0.1	0.1	1.74E-17	0.261	2	9	1.6	± 30.4
B	700	0.3	15.7	3.61E-17	4.848	***	16	29.5	± 6.9
C	800	0.7	63.7	9.68E-17	9.631	1	29	58.1	± 2.4
D	850	0.9	75.5	1.21E-16	10.399	***	66	62.6	± 2.0
E	900	1.5	78.8	1.97E-16	9.736	***	205	58.7	± 1.1
F	950	2.7	83.1	3.60E-16	10.063	***	275	60.7	± 0.7
G	1000	9.7	91.4	1.31E-15	9.873	301	962	59.5	± 0.3
H	1050	24.4	97.3	3.28E-15	9.756	35	1235	58.8	± 0.1
I	1100	14.2	97.8	1.90E-15	9.859	195	952	59.5	± 0.2
J	1150	10.8	95.6	1.46E-15	9.829	60	833	59.3	± 0.3
K	1200	22.8	98.6	3.06E-15	9.855	741	1282	59.4	± 0.2
L	1250	9.7	94.9	1.30E-15	10.163	***	50	61.2	± 0.3
M	1350	1.3	77.8	1.71E-16	10.720	***	13	64.5	± 1.3
N	1450	1.0	59.1	1.30E-16	10.747	***	34	64.7	± 2.2
Total gas			94.6	1.34E-14	9.863	291	928	59.5	
87 % of gas released in steps D (850 ºC) through K (1200 ºC) steps							**Isochron age =**	**58.9**	**± 0.7**

Table 3. $^{40}Ar/^{39}Ar$ step-heating data and isochron ages.—Continued

Step	Temp. °C	%^{39}Ar of total	Radiogenic yield (%)	$^{39}Ar_k$ (moles)	$^{40}Ar^*/^{39}Ar_k$	Apparent K/Ca	Apparent K/Cl	Apparent age (Ma)	Error (Ma)
La Pinta USA Mine	***white mica***	*flakes*	*J = 0.006975 ± 0.50 %*	*weight = 2.5 mg*	*101KD60*				
B	700	0.2	4.6	9.52E-16	2.281	6	60	28.5	± 9.8
C	800	0.4	44.0	1.78E-15	3.311	26	885	41.2	± 4.0
D	850	0.6	73.3	2.94E-15	3.556	22	***	44.2	± 2.4
E	900	1.3	77.3	6.09E-15	3.428	885	14286	42.6	± 1.1
F	950	3.3	82.2	1.62E-14	3.525	214	3846	43.8	± 0.5
G	1000	12.6	93.5	6.15E-14	3.557	488	9091	44.2	± 0.2
H	1050	23.3	97.8	1.13E-13	3.537	1538	8333	44.0	± 0.1
I	1100	19.8	98.2	9.65E-14	3.528	***	11111	43.9	± 0.1
J	1150	12.3	96.6	6.00E-14	3.507	1111	7692	43.6	± 0.1
K	1200	15.5	98.2	7.53E-14	3.570	***	12500	44.4	± 0.1
L	1250	8.5	95.3	4.16E-14	3.654	***	5882	45.4	± 0.2
M	1300	1.4	70.9	6.64E-15	3.562	562	***	44.3	± 1.1
N	1350	0.3	46.1	1.66E-15	3.625	***	1724	45.0	± 4.2
O	1450	0.2	28.8	1.12E-15	3.640	161	5556	45.2	± 6.2
P	1650	0.3	19.7	1.38E-15	5.077	59	5263	62.8	± 5.9
Total gas			94.8	4.87E-13	3.549	1044	9019	44.1	
	74 % of gas released in steps B (700 ºC) through J (1150 ºC) steps						**Isochron age =**	**43.9**	**± 0.2**
LH08-1	***white mica***	*flakes*	*J = 0.009256 ± 0.30 %*	*weight = 21.2 mg*	*265KD52*				
A	600	0.1	5.0	4.55E-03	2.537	4	16	41.9	± 4.7
B	700	0.3	39.2	1.51E-02	2.948	12	99	48.6	± 1.0
C	800	1.2	78.7	5.68E-02	3.313	66	532	54.5	± 0.2
D	850	1.7	77.7	7.95E-02	3.312	117	1256	54.5	± 0.2
E	900	4.7	78.2	2.20E-01	3.421	281	1957	56.2	± 0.1
F	950	13.4	92.7	6.26E-01	3.489	778	12013	57.3	± 0.1
G	1000	21.1	97.0	9.84E-01	3.397	845	0	55.9	± 0.1
H	1050	19.0	95.4	8.88E-01	3.345	858	0	55.0	± 0.1
I	1100	13.6	94.1	6.37E-01	3.373	732	30746	55.5	± 0.1
J	1150	19.5	97.4	9.09E-01	3.497	1111	0	57.5	± 0.1
K	1200	2.9	94.8	1.35E-01	4.027	193	287	66.0	± 0.2
L	1250	1.2	95.0	5.64E-02	3.559	105	1041	58.5	± 0.3
M	1350	0.5	87.6	2.18E-02	3.526	40	521	57.9	± 0.5
N	1450	0.6	93.1	2.88E-02	3.609	57	562	59.3	± 0.4
O	1650	0.3	84.4	1.21E-02	3.559	26	422	58.5	± 1.0
Total gas			93.9	4.67E+00	3.434	785	5946	56.5	
	87 % of gas released in steps F (950 ºC) through J (1150 ºC) steps						**Isochron age =**	**54.1**	**± 1.7**
Pinta-1a	***white mica***	*flakes*	*J = 0.003380 ± 0.50 %*	*weight = 1.2 mg*	*44KD55*				
A	600	0.2	0.4	1.73E-17	1.425	***	11	8.7	± 25.1
B	700	0.4	30.3	3.92E-17	8.528	1	22	51.3	± 5.6
C	800	0.8	65.4	9.12E-17	9.757	***	38	58.5	± 2.6
D	850	1.1	75.9	1.23E-16	9.869	22	80	59.2	± 1.6
E	900	1.9	73.2	2.03E-16	9.704	***	155	58.2	± 1.0
F	950	3.3	75.1	3.65E-16	9.820	12	242	58.9	± 0.8
G	1000	9.6	88.3	1.06E-15	9.689	76	658	58.1	± 0.3
H	1050	21.1	96.2	2.31E-15	9.676	94	1408	58.1	± 0.1
I	1100	16.8	97.6	1.83E-15	9.746	100	990	58.5	± 0.2
J	1150	11.6	95.4	1.27E-15	9.723	444	1000	58.3	± 0.2
K	1200	16.2	96.8	1.77E-15	9.747	32	943	58.5	± 0.2
L	1250	13.0	94.5	1.42E-15	9.834	71	67	59.0	± 0.2
M	1350	2.6	83.6	2.86E-16	9.596	6	19	57.6	± 0.9
N	1450	1.4	63.6	1.57E-16	10.327	35	57	61.9	± 1.6
Total gas			92.6	1.09E-14	9.721	114	818	58.3	
	98 % of gas released in steps C (800 ºC) through M (1350 ºC) steps						**Isochron age =**	**58.3**	**± 0.6**
Pinta-2	***white mica***	*flakes*	*J = 0.003352 ± 0.50 %*	*weight = 1.3 mg*	*83KD55*				
A	600	0.3	1.1	2.98E-17	1.719	***	15	10.1	± 13.5
B	700	0.3	51.7	3.05E-17	8.096	***	30	46.9	± 7.4
C	800	0.9	80.9	8.63E-17	9.889	***	39	57.1	± 3.4
D	850	1.1	75.8	1.13E-16	10.010	13	105	57.8	± 2.3
E	900	1.8	83.7	1.82E-16	10.747	***	237	62.0	± 1.7
F	950	3.7	83.4	3.67E-16	10.041	***	386	58.0	± 0.9
G	1000	10.8	92.1	1.06E-15	10.081	***	758	58.2	± 0.3
H	1050	23.5	98.0	2.31E-15	9.928	83	1370	57.3	± 0.2
I	1100	18.2	97.9	1.79E-15	9.881	52	1299	57.1	± 0.2
J	1150	11.8	97.4	1.16E-15	10.111	***	893	58.4	± 0.3
K	1200	12.3	96.7	1.21E-15	10.037	***	917	57.9	± 0.2
L	1250	11.3	93.9	1.11E-15	9.936	12	55	57.4	± 0.3
M	1350	3.2	82.2	3.18E-16	9.570	13	33	55.3	± 1.0
N	1450	0.6	54.9	6.24E-17	11.323	***	25	65.2	± 4.6
Total gas			94.3	9.83E-15	9.958	54	888	57.5	
	64 % of gas released in steps G (1000 ºC) through J (1150 ºC) steps						**Isochron age =**	**56.9**	**± 0.8**

Table 3. $^{40}Ar/^{39}Ar$ step-heating data and isochron ages.—Continued

Step	Temp. °C	%^{39}Ar of total	Radiogenic yield (%)	$^{39}Ar_k$ (moles)	$^{40}Ar^*/^{39}Ar_k$	Apparent K/Ca	Apparent K/Cl	Apparent age (Ma)	Error (Ma)
Prieta-4	***white mica***	*flakes*	*J = 0.003440 ± 0.50 %*	*weight = 1.5 mg*	*25KD55*				
A	600	0.1	1.6	1.93E-17	3.181	1	9	19.6	± 17.8
B	700	0.3	20.1	3.79E-17	5.739	1	23	35.3	± 5.1
C	800	0.6	62.2	8.48E-17	9.427	***	30	57.6	± 2.3
D	850	0.8	77.4	1.12E-16	9.427	10	61	57.6	± 1.5
E	900	1.2	80.1	1.74E-16	9.630	***	151	58.8	± 1.1
F	950	2.5	83.4	3.56E-16	9.931	9	236	60.6	± 0.6
G	1000	10.2	91.7	1.44E-15	9.922	96	658	60.6	± 0.2
H	1050	17.5	97.7	2.47E-15	9.924	***	926	60.6	± 0.1
I	1100	11.8	97.5	1.67E-15	9.888	29	741	60.3	± 0.2
J	1150	8.0	97.3	1.12E-15	10.018	***	633	61.1	± 0.2
K	1200	15.2	97.5	2.14E-15	9.899	102	725	60.4	± 0.1
L	1250	24.3	98.0	3.43E-15	10.002	51	136	61.0	± 0.1
M	1350	5.1	93.9	7.26E-16	10.102	22	48	61.6	± 0.3
N	1450	2.4	63.9	3.46E-16	9.993	22	136	61.0	± 1.7
Total gas			94.8	1.41E-14	9.923	59	524	60.5	
68 % of gas released in steps C (800 ºC) through K (1200 ºC) steps							**Isochron age =**	**60.6**	**± 0.7**
Quitovac-2	***white mica***	*flakes*	*J = 0.003417 ± 0.50 %*	*weight = 1.1 mg*	*34KD55*				
A	600	0.2	2.3	2.32E-17	7.794	0	9	47.4	± 22.3
B	700	0.5	26.4	5.17E-17	7.350	1	23	44.8	± 10.5
C	800	1.5	64.2	1.50E-16	9.628	3	46	58.4	± 1.9
D	850	2.2	64.1	2.17E-16	9.867	6	112	59.8	± 1.2
E	900	4.2	74.1	4.10E-16	9.946	6	216	60.3	± 0.7
F	950	7.1	83.9	6.88E-16	9.766	***	408	59.2	± 0.4
G	1000	13.8	93.1	1.34E-15	9.783	12	690	59.3	± 0.3
H	1050	20.4	97.5	1.99E-15	9.828	75	1000	59.6	± 0.2
I	1100	13.1	96.6	1.28E-15	9.759	12	909	59.2	± 0.2
J	1150	11.3	96.5	1.10E-15	9.980	***	725	60.5	± 0.4
K	1200	20.9	96.9	2.04E-15	9.923	59	855	60.2	± 0.2
L	1250	3.1	74.3	3.04E-16	9.962	***	13	60.4	± 0.9
M	1350	1.2	59.0	1.19E-16	9.795	2	8	59.4	± 2.0
N	1450	0.3	13.1	2.46E-17	8.415	8	11	51.1	± 8.6
Total gas			91.4	9.74E-15	9.831	40	722	59.6	
62 % of gas released in steps C (800 ºC) through I (1100 ºC) steps							**Isochron age =**	**59.4**	**± 0.7**
Sanfran-7	***white mica***	*flakes*	*J = 0.003261 ± 0.50 %*	*weight = 1.4 mg*	*79KD55*				
A	600	0.1	6.7	1.63E-17	15.532	0	10	89.1	± 22.8
B	700	0.2	30.7	2.91E-17	9.624	***	16	55.7	± 6.7
C	800	0.6	57.2	6.95E-17	9.974	***	24	57.7	± 2.3
D	850	0.7	63.9	8.68E-17	9.876	***	52	57.2	± 2.2
E	900	1.2	60.2	1.48E-16	9.954	***	130	57.6	± 1.5
F	950	2.7	57.6	3.27E-16	9.138	***	321	53.0	± 1.3
G	1000	14.4	91.6	1.73E-15	9.832	117	909	56.9	± 0.2
H	1050	22.3	97.5	2.68E-15	9.719	149	1408	56.3	± 0.1
I	1100	17.9	98.4	2.15E-15	9.743	***	1515	56.4	± 0.2
J	1150	12.1	97.3	1.45E-15	9.822	***	1351	56.9	± 0.2
K	1200	17.9	98.2	2.15E-15	9.848	33	769	57.0	± 0.1
L	1250	7.1	88.1	8.56E-16	10.026	***	32	58.0	± 0.3
M	1350	1.5	76.3	1.80E-16	11.098	***	20	64.1	± 2.7
N	1450	1.0	65.8	1.24E-16	12.573	***	29	72.5	± 2.4
Total gas			93.4	1.20E-14	9.842	102	1034	57.0	
72 % of gas released in steps A (600 ºC) through J (1150 ºC) steps							**Isochron age =**	**56.5**	**± 0.6**
Sargenta	***white mica***	*flakes*	*J = 0.004398 ± 0.25 %*	*weight = 1.6 mg*	*182KD53*				
A	600	0.1	1.2	2.23E-17	6.640	***	65	51.9	± 27.4
B	700	0.3	21.3	4.39E-17	6.912	0	275	54.0	± 6.8
C	800	0.8	68.2	1.31E-16	7.430	3	2632	58.0	± 2.3
D	850	1.0	85.5	1.66E-16	7.574	3	917	59.1	± 1.8
E	900	1.7	86.5	2.91E-16	7.504	4	***	58.6	± 1.0
F	950	3.1	83.3	5.15E-16	7.560	6	1370	59.0	± 0.6
G	1000	5.9	86.5	1.00E-15	7.618	11	3030	59.5	± 0.4
H	1050	22.3	95.7	3.77E-15	7.724	1818	5556	60.3	± 0.1
I	1100	21.0	97.2	3.55E-15	7.660	28	2326	59.8	± 0.1
J	1150	13.0	95.2	2.19E-15	7.656	34	3571	59.7	± 0.2
K	1200	10.1	95.7	1.70E-15	7.734	***	2222	60.3	± 0.2
L	1250	13.4	94.8	2.26E-15	7.714	12	2778	60.2	± 0.2
M	1350	7.0	96.6	1.19E-15	7.798	29	1754	60.8	± 0.3
N	1450	0.3	76.2	4.49E-17	8.675	0	92	67.5	± 6.1
Total gas			94.1	1.69E-14	7.687	468	3164	60.0	
79 % of gas released in steps A (600 ºC) through K (1200 ºC) steps							**Isochron age =**	**59.8**	**± 0.4**

Table 3. $^{40}Ar/^{39}Ar$ step-heating data and isochron ages.—Continued

Step	Temp. °C	%^{39}Ar of total	Radiogenic yield (%)	$^{39}Ar_k$ (moles)	$^{40}Ar^*/^{39}Ar_k$	Apparent K/Ca	Apparent K/Cl	Apparent age (Ma)	Error (Ma)
SE Sonoyta	***white mica***	*flakes*	*J = 0.004408 ± 0.25 %*	*weight = 1.5 mg*	*181KD53*				
A	600	0.3	2.2	4.36E-17	5.193	1	74	40.8	± 13.3
B	700	0.6	35.2	9.58E-17	6.800	1	156	53.3	± 3.8
C	800	1.3	69.5	2.17E-16	6.405	***	513	50.2	± 1.6
D	850	1.5	73.3	2.59E-16	5.935	***	524	46.6	± 1.5
E	900	2.1	83.2	3.57E-16	6.717	***	1176	52.6	± 1.0
F	950	3.8	84.2	6.52E-16	6.830	14	1587	53.5	± 0.6
G	1000	9.9	84.7	1.69E-15	6.905	37	3226	54.1	± 0.3
H	1050	25.3	94.5	4.35E-15	6.760	32	3030	53.0	± 0.1
I	1100	17.8	96.1	3.06E-15	6.743	19	2778	52.8	± 0.1
J	1150	9.0	91.8	1.55E-15	6.664	10	1923	52.2	± 0.2
K	1200	14.7	93.7	2.53E-15	6.877	33	1818	53.9	± 0.2
L	1250	13.3	95.0	2.29E-15	6.621	17	3571	51.9	± 0.2
M	1350	0.5	71.8	8.33E-17	5.834	3	617	45.8	± 3.5
N	1450	0.1	21.9	1.13E-17	4.205	1	45	33.1	± 26.3
Total gas			91.4	1.72E-14	6.735	25	2594	52.8	
	57 % of gas released in steps F (950 ºC) through I (1100 ºC) steps						**Isochron age =**	**52.5**	**± 0.4**
Tres Mojones	***white mica***	*flakes*	*J = 0.004587 ± 0.25 %*	*weight = 1.5 mg*	*191KD53*				
A	600	0.2	0.8	4.39E-17	1.127	1	6	9.3	± 13.5
B	700	0.3	26.5	4.88E-17	5.882	2	19	48.0	± 4.9
C	800	0.5	68.1	9.22E-17	8.565	9	30	69.5	± 2.6
D	850	0.6	81.4	1.10E-16	8.224	22	58	66.8	± 2.1
E	900	1.0	75.9	1.80E-16	7.951	***	152	64.6	± 1.4
F	950	1.8	75.4	3.38E-16	7.932	***	250	64.5	± 0.8
G	1000	5.4	84.3	1.01E-15	7.724	641	599	62.8	± 0.3
H	1050	20.9	96.1	3.95E-15	7.722	3333	1587	62.8	± 0.1
I	1100	16.1	98.3	3.03E-15	7.664	83	1429	62.3	± 0.1
J	1150	9.5	96.1	1.80E-15	7.626	70	1136	62.0	± 0.3
K	1200	8.0	93.9	1.49E-15	7.647	76	735	62.2	± 0.2
L	1250	24.2	97.9	4.57E-15	7.700	142	1111	62.6	± 0.1
M	1350	11.1	96.0	2.10E-15	7.755	237	51	63.1	± 0.2
N	1450	0.4	84.7	7.83E-17	8.261	15	30	67.1	± 2.8
Total gas			94.8	1.88E-14	7.693	842	1042	62.6	
	55 % of gas released in steps E (900 ºC) through J (1150 ºC) steps						**Isochron age =**	**62.2**	**± 0.4**
Trin-10	***white mica***	*flakes*	*J = 0.003361 ± 0.50 %*	*weight = 0.6 mg*	*59KD55*				
A	600	0.3	6.5	1.66E-17	13.280	1	12	78.8	± 24.9
B	700	0.8	28.7	4.51E-17	6.378	0	26	38.3	± 5.4
C	800	1.4	70.4	8.58E-17	8.932	1	28	53.4	± 3.0
D	900	1.6	88.7	9.31E-17	10.518	***	64	62.7	± 1.9
E	950	2.7	90.0	1.62E-16	9.768	***	103	58.3	± 1.2
F	1000	4.1	88.5	2.46E-16	9.674	***	214	57.7	± 1.5
G	1050	6.6	90.2	3.95E-16	9.976	***	575	59.5	± 0.6
H	1100	19.3	94.7	1.15E-15	9.720	16	1031	58.0	± 0.4
I	1150	16.1	97.9	9.62E-16	9.870	***	1266	58.9	± 0.5
J	1200	14.6	97.4	8.68E-16	9.809	7	877	58.5	± 0.3
K	1250	11.2	97.1	6.68E-16	9.968	10	515	59.5	± 0.4
L	1650	14.5	93.5	8.64E-16	9.906	6	42	59.1	± 0.3
M	1350	5.9	87.3	3.52E-16	10.156	***	21	60.6	± 0.9
N	1450	0.9	54.8	5.47E-17	17.409	1	13	102.6	± 3.4
Total gas			93.0	5.96E-15	9.909	10	647	59.1	
	95 % of gas released in steps E (950 ºC) through M (1350 ºC) steps						**Isochron age =**	**58.3**	**± 1.0**
Vidrios-1	***white mica***	*flakes*	*J = 0.003280 ± 0.50 %*	*weight = 1.3 mg*	*75KD55*				
A	600	0.1	-0.2	1.71E-17	-0.416	1	13	-2.5	± 35.0
B	700	0.3	23.0	3.50E-17	7.789	1	19	45.5	± 8.1
C	800	0.7	62.5	7.51E-17	10.954	***	30	63.7	± 3.5
D	850	0.9	59.8	1.04E-16	10.042	***	79	58.5	± 2.5
E	900	1.6	71.3	1.87E-16	10.355	7	175	60.3	± 2.0
F	950	4.6	58.4	5.26E-16	9.851	***	341	57.4	± 0.7
G	1000	13.4	88.9	1.55E-15	9.652	***	855	56.2	± 0.2
H	1050	22.6	96.7	2.61E-15	9.664	58	1389	56.3	± 0.1
I	1100	21.9	96.8	2.53E-15	9.767	***	1587	56.9	± 0.2
J	1150	14.0	93.3	1.62E-15	9.682	***	1087	56.4	± 0.2
K	1200	15.7	96.1	1.81E-15	9.629	610	1111	56.1	± 0.2
L	1250	3.1	76.4	3.52E-16	9.803	9	15	57.1	± 0.8
M	1350	0.8	66.6	8.78E-17	10.629	***	9	61.8	± 2.9
N	1450	0.4	44.8	4.92E-17	10.514	***	15	61.2	± 5.3
Total gas			91.0	1.16E-14	9.714	252	1122	56.6	
	98 % of gas released in steps D (850 ºC) through L (1250 ºC) steps						**Isochron age =**	**56.3**	**± 0.6**

Ages calculated assuming an initial $^{40}Ar/^{39}Ar = 295.5$.

All precision estimates are at the one sigma level of precision.

Ages of individual steps do not include error in the irradiation parameter J.

No error is calculated for the total gas age.

Data were obtained using a MAP 216 or a VG1200 spectrometer.

***K/Ca or K/Cl not calculated.

Table 4. $^{40}Ar/^{39}Ar$ step-heating data and average or single step ages determined from white micas of gold-rich quartz veins of the Caborca orogenic gold belt (COGB), northwestern Sonora, Mexico.

Step	Temp. °C	%^{39}Ar of total	Radiogenic yield (%)	$^{39}Ar_k$ (moles)	$^{40}Ar^*/^{39}Ar_k$	Apparent K/Ca	Apparent K/Cl	Apparent age (Ma)	Error (Ma)
American Boy	***white mica***	*flakes*	*J = 0.002037 ± 0.25 %*	*weight = 5.2 mg*	*33KD12*				
A	650	0.6	1.5	1.77E-16	13.922	***	8	50.5	± 8.0
B	700	1.7	56.0	5.05E-16	11.306	***	168	41.1	± 0.4
C	750	2.3	87.1	6.65E-16	12.438	***	917	45.1	± 0.2
D	800	4.4	91.5	1.30E-15	12.989	***	917	47.1	± 0.1
E	850	5.7	95.1	1.67E-15	13.543	***	1408	49.1	± 0.1
F	900	6.5	97.0	1.91E-15	13.786	***	952	50.0	± 0.1
G	950	5.8	97.1	1.71E-15	13.756	***	5882	49.9	± 0.1
H	1000	8.1	98.0	2.39E-15	13.801	***	4167	50.0	± 0.1
I	1050	10.8	98.9	3.16E-15	13.951	***	0	50.6	± 0.1
J	1100	21.8	99.0	6.38E-15	13.986	***	2703	50.7	± 0.1
K	1200	25.7	98.3	7.53E-15	14.074	***	3448	51.0	± 0.0
L	1250	1.6	67.1	4.82E-16	14.020	***	148	50.8	± 0.4
M	1350	2.7	94.5	7.93E-16	14.018	***	***	50.8	± 0.2
N	1550	2.2	91.0	6.43E-16	14.782	***	***	53.5	± 0.3
Total gas			95.5	2.93E-14	13.832	***	2365	49.3	
83 % of gas released in steps F (900 ºC) through M (1350 ºC) steps							**Average age =**	**50.6**	**± 0.4**
Ana Celia	***white mica***	*flakes*	*J = 0.004398 ± 0.25 %*	*weight = 1.5 mg*	*180KD53*				
A	600	0.4	0.1	1.77E-17	2.016	***	20	15.9	± 49.0
B	700	1.2	31.8	5.06E-17	7.296	1	***	57.0	± 4.7
C	800	3.3	72.9	1.33E-16	5.044	***	***	39.6	± 1.5
D	850	3.9	91.5	1.59E-16	5.127	***	***	40.2	± 1.3
E	900	5.5	86.5	2.24E-16	5.014	***	***	39.3	± 1.1
F	950	7.8	94.2	3.17E-16	5.541	***	***	43.4	± 0.9
G	1000	10.5	90.0	4.29E-16	5.499	***	***	43.1	± 0.6
H	1050	16.3	96.6	6.64E-16	5.790	26	4167	45.4	± 0.4
I	1100	23.0	96.7	9.30E-16	5.508	***	11111	43.2	± 0.3
J	1150	15.3	97.2	6.23E-16	5.482	29	***	43.0	± 0.5
K	1200	7.4	87.6	3.00E-16	5.480	6	2778	43.0	± 0.8
L	1250	3.8	85.8	1.53E-16	7.307	***	***	57.1	± 2.0
M	1350	1.0	59.3	4.09E-17	5.876	11	3125	46.0	± 6.4
N	1450	0.6	62.7	2.38E-17	5.607	1	***	44.0	± 11.8
Total gas			91.5	4.07E-15	5.572	22	3472	43.7	
80 % of gas released in steps F (950 ºC) through K (1200 ºC) steps							**Average age =**	**43.6**	**± 1.1**
Carretera-2	***white mica***	*flakes*	*J = 0.003462 ± 0.50 %*	*weight = 1.2 mg*	*14KD55*				
A	600	0.2	0.4	2.79E-17	3.820	0	11	23.7	± 23.8
B	700	0.6	17.4	6.99E-17	4.255	1	53	26.4	± 2.5
C	800	1.3	53.7	1.45E-16	7.208	3	61	44.5	± 1.1
D	850	1.2	65.0	1.35E-16	8.047	2	83	49.6	± 1.3
E	900	1.5	72.4	1.70E-16	9.329	***	171	57.3	± 1.0
F	950	3.3	73.4	3.79E-16	9.050	6	366	55.7	± 0.5
G	1000	10.2	89.2	1.16E-15	9.800	***	781	60.2	± 0.2
H	1050	20.5	95.9	2.32E-15	9.779	30	1053	60.1	± 0.1
I	1100	15.0	97.3	1.70E-15	9.546	35	1351	58.7	± 0.2
J	1150	11.1	94.9	1.27E-15	9.337	17	962	57.4	± 0.2
K	1200	9.7	94.7	1.10E-15	9.609	15	498	59.0	± 0.2
L	1250	15.1	93.8	1.72E-15	9.963	30	178	61.2	± 0.2
M	1350	8.6	82.8	9.81E-16	10.061	14	43	61.8	± 0.2
N	1450	1.6	67.1	1.77E-16	9.402	3	125	57.8	± 0.9
Total gas			90.6	1.13E-14	9.596	24	703	58.9	
57 % of gas released in steps G (1000 ºC) through J (1150 ºC) steps							**Average age =**	**59.7**	**± 1.3**
Centauro-3	***white mica***	*aggregates*	*J = 0.002035 ± 0.25 %*	*weight = 1.3 mg*	*20KD12*				
A	550	0.4	6.2	1.53E-15	9.656	3	23	35.1	± 1.4
B	650	0.9	42.4	3.27E-15	10.461	8	41	38.0	± 0.3
C	700	0.7	75.4	2.83E-15	14.309	16	122	51.8	± 0.2
D	750	1.3	89.3	4.80E-15	16.210	30	277	58.5	± 0.1
E	800	1.3	95.0	5.23E-15	16.744	49	704	60.4	± 0.1
F	850	3.9	97.0	1.53E-14	17.106	46	794	61.7	± 0.1
G	900	5.2	97.8	2.03E-14	17.544	55	1299	63.3	± 0.1
H	950	6.3	98.3	2.46E-14	17.723	52	1316	63.9	± 0.0
I	1000	6.5	98.9	2.53E-14	18.736	62	1754	67.5	± 0.0
J	1050	17.0	99.2	6.61E-14	23.264	61	1786	83.5	± 0.1
K	1100	32.2	99.0	1.25E-13	30.496	30	885	108.6	± 0.1
L	1450	22.1	97.7	8.57E-14	37.502	28	63	132.7	± 0.1
M	1550	2.1	95.6	8.28E-15	39.403	43	213	139.2	± 0.1
Total gas			97.3	3.88E-13	27.493	40	917	98.2	
					Step F (850 ºC)		**Single step age =**	**~62**	

Table 4. $^{40}Ar/^{39}Ar$ step-heating data and average or single step ages.—Continued

Step	Temp. °C	%^{39}Ar of total	Radiogenic yield (%)	$^{39}Ar_k$ (moles)	$^{40}Ar^*/^{39}Ar_k$	Apparent K/Ca	Apparent K/Cl	Apparent age (Ma)	Error (Ma)
Cerro Colorado	***white mica***	*aggregates*	*J = 0.002037 ± 0.25 %*	*weight = 4.6 mg*	*9KD12*				
B	650	1.2	13.5	1.80E-16	12.029	***	36	43.7	± 1.6
C	700	1.5	57.6	2.18E-16	13.892	***	202	50.3	± 0.6
D	750	2.7	66.3	4.01E-16	14.319	***	917	51.9	± 0.4
E	800	4.6	77.6	6.76E-16	14.653	***	172	53.1	± 0.2
F	850	5.9	90.7	8.71E-16	15.267	***	476	55.3	± 0.2
G	900	7.5	94.2	1.11E-15	15.695	***	1923	56.8	± 0.1
H	950	9.6	95.8	1.41E-15	15.520	***	205	56.2	± 0.1
I	1000	12.9	96.5	1.90E-15	15.631	***	***	56.5	± 0.1
J	1050	14.2	95.8	2.10E-15	16.060	***	***	58.1	± 0.1
K	1100	18.5	96.2	2.74E-15	16.321	***	971	59.0	± 0.1
L	1150	10.9	96.3	1.61E-15	16.459	***	11111	59.5	± 0.1
M	1200	4.9	92.1	7.21E-16	16.466	***	1429	59.5	± 0.2
N	1250	2.0	83.0	2.94E-16	16.305	***	885	58.9	± 0.4
O	1350	1.4	53.6	2.09E-16	16.736	***	134	60.5	± 0.6
P	1450	1.5	75.3	2.27E-16	15.199	***	149	55.0	± 0.5
Q	2530	0.6	40.0	8.61E-17	17.965	***	14	64.8	± 1.4
Total gas			90.7	1.48E-14	15.810	***	1713	56.2	
					Step H (950 ºC)		**Single step age =**	**~56**	
Costa-1	***white mica***	*flakes*	*J = 0.003456 ± 0.50 %*	*weight = 1.4 mg*	*20KD55*				
A	600	0.1	-0.3	1.42E-17	-0.679	0	8	-4.2	± 16.6
B	700	0.2	15.1	3.20E-17	3.651	1	20	22.6	± 4.0
C	800	0.6	52.5	7.48E-17	7.943	1	24	48.9	± 1.8
D	850	0.7	74.6	9.26E-17	9.546	39	48	58.6	± 1.4
E	900	1.2	75.0	1.65E-16	9.466	4	111	58.1	± 0.8
F	950	2.2	77.0	2.85E-16	9.562	***	195	58.7	± 0.5
G	1000	6.0	87.6	7.98E-16	9.505	15	699	58.3	± 0.4
H	1050	24.9	97.1	3.29E-15	10.006	53	1087	61.3	± 0.1
I	1100	12.7	97.5	1.68E-15	9.803	47	1031	60.1	± 0.1
J	1150	7.7	95.2	1.01E-15	9.726	35	893	59.6	± 0.2
K	1200	13.9	97.0	1.84E-15	9.952	135	862	61.0	± 0.2
L	1250	21.6	97.5	2.86E-15	10.052	278	158	61.6	± 0.1
M	1350	3.8	80.2	4.98E-16	9.947	***	24	61.0	± 0.4
N	1450	4.3	64.0	5.69E-16	10.252	148	149	62.8	± 0.4
Total gas			93.0	1.32E-14	9.884	115	681	60.6	
	81 % of gas released in steps H (1050 ºC) through L (1250 ºC) steps						**Average age =**	**61.0**	**± 1.0**
Costa-3	***white mica***	*aggregates*	*J = 0.003454 ± 0.50 %*	*weight = 1.1 mg*	*18KD55*				
A	600	0.1	6.1	1.68E-17	14.379	***	11	87.4	± 22.3
B	700	0.3	24.0	3.91E-17	5.647	***	26	34.8	± 3.7
C	800	0.8	70.2	9.05E-17	8.053	***	36	49.5	± 1.4
D	850	1.0	87.3	1.16E-16	9.092	***	69	55.8	± 1.1
E	900	1.5	88.0	1.76E-16	9.178	***	116	56.3	± 0.7
F	950	2.5	83.6	2.95E-16	9.350	***	263	57.3	± 0.5
G	1000	5.2	86.7	6.21E-16	9.425	***	578	57.8	± 0.3
H	1050	23.0	96.5	2.72E-15	9.421	262	1351	57.8	± 0.1
I	1100	14.1	97.2	1.67E-15	9.274	81	1190	56.9	± 0.2
J	1150	12.7	96.2	1.51E-15	9.341	***	1000	57.3	± 0.1
K	1200	27.2	98.5	3.23E-15	9.410	253	1370	57.7	± 0.1
L	1250	8.2	92.5	9.77E-16	9.373	***	56	57.5	± 0.2
M	1350	1.6	61.4	1.91E-16	9.958	5	11	61.0	± 2.0
N	1450	1.7	37.7	2.00E-16	10.541	***	45	64.5	± 1.3
Total gas			93.6	1.19E-14	9.385	213	1024	57.6	
	85 % of gas released in steps H (1050 ºC) through L (1250 ºC) steps						**Average age =**	**58.9**	**± 0.7**
Costa-4	***white mica***	*flakes*	*J = 0.003449 ± 0.50 %*	*weight = 1.1 mg*	*24KD55*				
B	700	0.4	23.7	3.68E-17	4.382	14	28	27.1	± 5.2
C	800	1.1	66.7	1.04E-16	5.676	3	41	35.0	± 1.8
D	850	1.2	83.2	1.18E-16	6.626	***	79	40.8	± 1.3
E	900	1.9	76.6	1.81E-16	6.378	2857	234	39.3	± 1.0
F	950	2.9	83.6	2.80E-16	7.090	14	241	43.6	± 0.9
G	1000	6.1	87.3	5.94E-16	7.394	***	781	45.4	± 0.4
H	1050	18.6	96.1	1.80E-15	7.970	21	1389	48.9	± 0.2
I	1100	16.9	97.2	1.64E-15	7.784	***	1149	47.8	± 0.1
J	1150	14.6	97.1	1.43E-15	7.848	***	1351	48.2	± 0.1
K	1200	14.0	97.6	1.37E-15	8.277	***	813	50.8	± 0.2
L	1250	10.3	93.0	1.00E-15	8.517	***	38	52.2	± 0.3
M	1350	5.6	90.2	5.48E-16	8.256	54	67	50.7	± 0.4
N	1450	6.6	74.5	6.49E-16	8.591	***	173	52.7	± 0.4
Total gas			92.5	9.74E-15	7.931	202	842	48.7	
					Step I (1100 ºC)		**Single step age =**	**~48**	

Table 4. $^{40}Ar/^{39}Ar$ step-heating data and average or single step ages.—Continued

Step	Temp. °C	%^{39}Ar of total	Radiogenic yield (%)	$^{39}Ar_k$ (moles)	$^{40}Ar^*/^{39}Ar_k$	Apparent K/Ca	Apparent K/Cl	Apparent age (Ma)	Error (Ma)
Cubabi	***white mica***	*flakes*	*J = 0.003416 ± 0.50 %*	*weight = 1.4 mg*	*28KD55*				
A	600	0.1	1.7	1.46E-17	4.949	1	9	30.2	± 27.5
B	700	0.3	4.7	3.35E-17	1.144	1	18	7.0	± 6.2
C	800	0.6	57.3	7.63E-17	8.308	3	26	50.5	± 2.4
D	850	0.8	60.3	1.07E-16	7.148	4	62	43.5	± 2.0
E	900	1.6	75.6	2.10E-16	8.106	5	166	49.3	± 0.9
F	950	3.7	79.1	4.80E-16	8.309	49	493	50.5	± 1.1
G	1000	14.6	94.5	1.88E-15	8.348	25	1235	50.7	± 0.2
H	1050	23.1	98.1	3.00E-15	8.284	41	1429	50.3	± 0.1
I	1100	19.0	97.7	2.47E-15	8.208	47	1370	49.9	± 0.1
J	1150	10.7	96.0	1.38E-15	8.201	103	1031	49.8	± 0.2
K	1200	14.0	96.8	1.82E-15	8.151	***	952	49.5	± 0.1
L	1250	8.8	95.8	1.13E-15	8.475	***	47	51.5	± 0.2
M	1350	1.6	77.2	2.03E-16	8.313	3	14	50.5	± 1.1
N	1450	1.0	45.2	1.32E-16	8.824	***	35	53.6	± 2.1
Total gas			94.0	1.29E-14	8.238	46	1042	50.1	
81 % of gas released in steps G (1000 ºC) through K (1200 ºC) steps							**Average age =**	**50.0**	**± 0.5**
El Chanate	***white mica***	*bad aggregates*	*J = 0.009251 ± 0.50 %*	*weight = 20.8 mg*	*263KD52*				
A	600	1.7	26.3	2.69E-02	2.150	3	159	35.5	± 0.4
B	700	8.4	73.8	1.36E-01	2.883	2	830	47.5	± 0.3
C	800	24.0	91.5	3.87E-01	3.166	0	2236	52.1	± 0.1
D	850	18.8	94.7	3.03E-01	3.305	0	7304	54.3	± 0.1
E	900	18.5	97.5	2.99E-01	3.381	5	0	55.6	± 0.1
F	950	12.1	97.1	1.95E-01	3.447	6	0	56.6	± 0.1
G	1000	7.0	95.1	1.13E-01	3.627	5	8135	59.5	± 0.2
H	1050	3.8	92.0	6.12E-02	3.909	4	1676	64.1	± 0.2
I	1100	1.6	82.3	2.62E-02	4.027	2	626	66.0	± 0.6
J	1150	0.8	67.5	1.34E-02	4.352	1	226	71.2	± 0.8
K	1200	0.7	66.9	1.16E-02	4.047	1	17	66.3	± 1.0
L	1250	2.2	86.4	3.60E-02	3.916	1	422	64.2	± 0.3
M	1350	0.3	69.6	5.12E-03	8.535	0	51	137.1	± 2.5
Total gas			90.9	1.61E+00	3.350	2	2638	55.1	
					Step C (800 ºC)		**Single step age =**	**~52**	
El Tiro	***white mica***	*aggregates*	*J = 0.002037 ± 0.25 %*	*weight = 3.1 mg*	*15KD12*				
A	550	0.4	0.8	1.04E-16	8.102	***	4	29.5	± 11.0
B	650	1.1	20.1	2.96E-16	16.324	***	84	59.0	± 1.4
C	700	0.9	57.2	2.59E-16	17.403	***	186	62.8	± 0.8
D	750	1.4	74.3	3.73E-16	16.763	***	680	60.6	± 0.5
E	800	2.0	83.2	5.44E-16	16.138	***	476	58.4	± 0.4
F	850	2.9	89.3	7.88E-16	15.586	***	***	56.4	± 0.2
G	900	4.3	93.9	1.18E-15	15.299	***	424	55.4	± 0.2
H	950	7.2	96.6	1.97E-15	15.352	***	***	55.6	± 0.1
I	1000	13.4	97.4	3.66E-15	15.542	***	769	56.2	± 0.1
J	1050	21.3	98.6	5.81E-15	16.250	***	2632	58.7	± 0.1
K	1100	22.3	98.9	6.09E-15	16.602	***	680	60.0	± 0.1
L	1150	11.0	97.8	3.00E-15	17.628	***	690	63.6	± 0.1
M	1200	4.2	96.4	1.15E-15	23.863	***	694	85.6	± 0.2
N	1250	1.6	84.6	4.27E-16	45.378	***	435	159.5	± 0.6
O	1350	2.8	96.3	7.60E-16	28.388	***	283	101.4	± 0.3
P	1450	2.6	95.2	7.14E-16	26.133	***	546	93.6	± 0.3
Q	1650	0.8	84.9	2.09E-16	75.917	***	32	259.4	± 1.1
Total gas			95.0	2.73E-14	18.100	***	988	0.2	
					Step G (900 ºC)		**Single step age =**	**~55**	
La Colorada	***white mica***	*aggregates*	*J = 0.002037 ± 0.25 %*	*weight = 5.7 mg*	*7KD12*				
C	700	0.1	3.7	4.74E-16	6.427	1	20	23.5	± 2.61
D	750	0.2	8.9	7.58E-16	5.631	2	25	20.6	± 1.49
E	800	0.3	14.0	1.11E-15	6.267	2	34	22.9	± 0.91
F	850	0.5	14.5	1.64E-15	6.212	2	38	22.7	± 0.96
G	900	0.8	19.1	2.50E-15	7.112	6	56	25.9	± 0.52
H	950	1.3	44.5	4.23E-15	11.090	13	112	40.3	± 0.29
I	1000	2.7	79.7	8.63E-15	14.610	29	299	52.9	± 0.13
J	1050	5.9	93.8	1.85E-14	16.706	38	552	60.4	± 0.06
K	1075	6.0	95.7	1.88E-14	17.624	42	909	63.6	± 0.06
L	1100	6.9	96.3	2.16E-14	17.848	42	1176	64.4	± 0.06
M	1150	12.3	97.2	3.86E-14	17.921	45	1266	64.7	± 0.05
N	1200	15.3	98.0	4.83E-14	17.765	55	1111	64.1	± 0.05
O	1250	18.7	99.9	5.91E-14	17.697	37	364	63.9	± 0.06
P	1350	24.1	97.2	7.59E-14	17.431	28	610	62.9	± 0.05
Q	1450	2.7	75.5	8.56E-15	16.045	8	6	58.0	± 0.15
R	1650	2.2	74.4	6.98E-15	23.800	7	85	85.4	± 0.22
Total gas			93.7	3.16E-13	17.327	36	721	62.6	
83 % of gas released in steps K (1075 ºC) through P (1350 ºC) steps							**Average age =**	**64.7**	**± 0.7**

Table 4. $^{40}Ar/^{39}Ar$ step-heating data and average or single step ages.—Continued

Step	Temp. °C	%^{39}Ar of total	Radiogenic yield (%)	$^{39}Ar_k$ (moles)	$^{40}Ar^*/^{39}Ar_k$	Apparent K/Ca	Apparent K/Cl	Apparent age (Ma)	Error (Ma)
La Esperanza	***white mica***	*aggregates*	*J = 0.003248 ± 0.50 %*	*weight = 1.3 mg*	*87KD55*				
A	600	0.5	5.5	5.40E-17	6.882	9	20	39.9	± 9.7
B	700	0.9	47.5	8.90E-17	7.376	***	57	42.7	± 2.3
C	800	2.1	88.6	2.10E-16	9.769	***	79	56.4	± 1.0
D	850	2.9	92.9	2.89E-16	9.939	***	181	57.3	± 0.7
E	900	4.6	95.7	4.55E-16	9.912	***	341	57.2	± 0.4
F	950	6.5	97.1	6.45E-16	10.117	***	667	58.3	± 0.3
G	1000	9.4	97.0	9.28E-16	9.904	***	833	57.1	± 0.2
H	1050	15.7	98.7	1.55E-15	10.162	104	1136	58.6	± 0.2
I	1100	19.3	99.0	1.91E-15	10.182	***	1538	58.7	± 0.2
J	1150	20.0	99.3	1.98E-15	10.337	107	1099	59.6	± 0.1
K	1200	8.9	98.7	8.82E-16	10.729	***	1235	61.8	± 0.6
L	1250	7.3	90.6	7.15E-16	11.811	***	32	67.9	± 0.3
M	1350	1.6	48.9	1.59E-16	10.294	***	12	59.3	± 1.7
N	1450	0.3	30.5	3.09E-17	12.855	***	8	73.8	± 6.4
Total gas			95.6	9.90E-15	10.287	104	952	59.3	
78 % of gas released in steps D (850 ºC) through J (1150 ºC) steps							**Average age =**	**58.7**	**± 0.8**
La Herradura	***white mica***	*bad aggregates*	*J = 0.003414 ± 0.50 %*	*weight = 1.5 mg*	*29KD55*				
A	600	0.4	3.9	5.18E-17	4.367	1	20	26.7	± 9.0
B	700	1.6	52.1	1.91E-16	5.568	1	80	34.0	± 1.5
C	800	4.1	90.2	4.85E-16	8.747	3	108	53.1	± 0.5
D	850	5.3	95.2	6.16E-16	9.555	14	225	57.9	± 0.4
E	900	7.6	97.4	9.02E-16	9.943	***	495	60.2	± 0.3
F	950	10.1	96.9	1.19E-15	10.105	21	709	61.2	± 0.2
G	1000	11.7	97.3	1.39E-15	10.532	20	943	63.7	± 0.2
H	1050	14.4	97.5	1.71E-15	11.393	***	943	68.8	± 0.2
I	1100	18.3	98.4	2.17E-15	13.150	30	1042	79.2	± 0.2
J	1150	13.5	98.9	1.60E-15	14.222	99	781	85.5	± 0.2
K	1200	7.3	96.5	8.61E-16	14.031	33	368	84.4	± 0.4
L	1250	2.8	80.6	3.31E-16	15.085	78	14	90.6	± 0.8
M	1350	1.8	81.9	2.16E-16	16.971	10	13	101.6	± 1.4
N	1450	1.0	51.3	1.20E-16	14.327	3	24	86.2	± 2.3
Total gas			94.9	1.18E-14	11.854	37	698	71.6	
					Step F (950 ºC)		**Single step age =**	**~61**	
Lluvia de Oro 3b	***white mica***	*aggregates*	*J = 0.002037 ± 0.25 %*	*weight = 5.8 mg*	*43KD12*				
D	750	0.2	14.8	6.64E-16	11.757	9	11	42.7	± 1.7
E	800	0.4	30.2	1.20E-15	8.806	1	12	32.1	± 0.9
F	850	0.7	43.5	1.93E-15	6.970	1	13	25.4	± 0.6
G	900	0.9	43.1	2.53E-15	6.190	3	26	22.6	± 0.3
H	950	1.6	64.7	4.80E-15	8.091	12	83	29.5	± 0.2
I	1000	3.2	73.8	9.42E-15	9.169	25	207	33.4	± 0.1
J	1050	3.9	77.4	1.14E-14	11.178	28	300	40.6	± 0.1
K	1100	5.1	82.2	1.50E-14	14.334	45	355	51.9	± 0.1
L	1150	13.8	94.2	4.07E-14	16.919	86	258	61.1	± 0.1
N	1200	2.1	90.1	6.23E-15	16.811	46	1695	60.7	± 0.1
O	1250	31.0	101.3	9.18E-14	17.586	32	439	63.5	± 0.1
P	1300	23.3	98.1	7.56E-14	17.349	15	272	62.7	± 0.1
Q	1350	5.1	95.1	1.50E-14	18.118	14	324	65.4	± 0.1
R	1450	4.1	89.8	1.21E-14	20.893	16	8	75.2	± 0.1
S	1650	4.7	87.0	1.40E-14	33.533	12	172	119.2	± 0.2
Total gas			93.1	3.02E-13	17.274	33	333	62.5	
					Step L (1150 ºC)		**Single step age =**	**~61**	
Noche Buena Casa	***white mica***	*aggregates*	*J = 0.002037 ± 0.25 %*	*weight = 5.4 mg*	*5KD12*				
D	750	0.2	1.1	6.32E-16	8.794	1	16	32.0	± 6.1
E	801	0.3	2.2	8.53E-16	11.063	1	25	40.2	± 3.7
F	850	0.4	4.3	1.33E-15	11.586	1	35	42.1	± 2.2
G	900	0.7	9.7	2.34E-15	11.076	3	66	40.3	± 1.0
H	950	1.7	27.5	5.81E-15	11.722	8	211	42.6	± 0.3
I	1000	4.5	49.0	1.49E-14	11.958	17	448	43.4	± 0.1
J	1050	6.2	73.9	2.08E-14	12.982	24	680	47.1	± 0.1
K	1075	5.0	87.6	1.66E-14	13.910	27	893	50.4	± 0.1
L	1100	4.7	87.1	1.55E-14	14.319	28	909	51.9	± 0.1
M	1150	7.8	87.9	2.58E-14	14.523	37	1111	52.6	± 0.1
N	1200	10.5	89.2	3.51E-14	14.544	40	1075	52.7	± 0.0
O	1250	14.1	91.2	4.71E-14	14.687	43	1408	53.2	± 0.0
P	1350	16.9	87.3	5.63E-14	14.416	39	746	52.2	± 0.0
Q	1450	18.2	80.1	6.06E-14	14.993	31	47	54.3	± 0.1
R	1650	9.0	82.9	2.99E-14	17.217	28	255	62.2	± 0.1
Total gas			81.5	3.34E-13	14.502	33	708	52.6	
72 % of gas released in steps L (1100 ºC) through Q (1450 ºC) steps							**Average age =**	**52.9**	**± 0.8**

Table 4. $^{40}Ar/^{39}Ar$ step-heating data and average or single step ages.—Continued

Step	Temp. °C	%^{39}Ar of total	Radiogenic yield (%)	$^{39}Ar_k$ (moles)	$^{40}Ar^*/^{39}Ar_k$	Apparent K/Ca	Apparent K/Cl	Apparent age (Ma)	Error (Ma)
Noche Buena Workings	***white mica***	*aggregates*	*J = 0.002037 ± 0.25 %*	*weight = 4.6 mg*	*31KD12*				
D	750	0.2	5.5	6.00E-16	8.133	3	23	29.6	± 2.0
E	800	0.3	13.1	8.22E-16	8.802	2	36	32.1	± 1.1
F	850	0.4	27.2	1.23E-15	10.130	3	44	36.8	± 0.7
G	900	0.5	41.8	1.71E-15	10.307	4	43	37.5	± 0.5
H	950	0.9	62.9	3.03E-15	11.811	11	109	42.9	± 0.3
I	1000	2.2	72.8	7.27E-15	13.269	26	236	48.1	± 0.1
J	1050	5.1	87.0	1.66E-14	14.087	53	508	51.0	± 0.1
K	1075	4.7	94.6	1.51E-14	14.773	50	730	53.5	± 0.1
L	1100	5.0	95.8	1.61E-14	15.147	63	885	54.8	± 0.1
M	1150	8.4	96.9	2.72E-14	15.337	67	1111	55.5	± 0.0
N	1200	12.9	96.9	4.19E-14	15.481	54	1176	56.0	± 0.0
O	1250	22.6	97.1	7.30E-14	15.650	54	1449	56.6	± 0.0
P	1350	25.7	97.7	8.30E-14	15.831	52	885	57.3	± 0.0
Q	1450	5.2	88.7	1.85E-14	15.698	19	10	56.8	± 0.1
R	1650	6.1	90.3	1.97E-14	17.393	15	282	62.8	± 0.1
Total gas			93.8	3.26E-13	15.441	49	927	55.9	
90 % of gas released in steps J (1050 ºC) through Q (1450 ºC) steps							**Average age =**	**55.7**	**± 1.4**
Pit-4	***white mica***	*flakes/aggregates*	*J = 0.003372 ± 0.50 %*	*weight = 1.3 mg*	*50KD55*				
A	600	0.2	1.2	2.73E-17	1.839	3	19	11.2	± 12.4
B	700	0.6	30.6	7.06E-17	4.813	***	61	29.0	± 3.8
C	800	1.3	58.0	1.48E-16	7.984	2	60	47.9	± 1.6
D	850	1.6	81.0	1.78E-16	9.206	7	127	55.2	± 1.2
E	900	2.5	82.3	2.83E-16	9.977	3	238	59.7	± 0.8
F	950	3.7	81.9	4.26E-16	10.459	***	341	62.5	± 0.8
G	1000	10.1	87.4	1.16E-15	10.682	20	800	63.8	± 0.3
H	1050	24.6	96.2	2.81E-15	10.858	31	1471	64.9	± 0.1
I	1100	22.0	97.9	2.52E-15	10.935	***	2564	65.3	± 0.2
J	1150	16.0	97.4	1.83E-15	11.008	44	990	65.8	± 0.2
K	1200	8.8	95.2	1.00E-15	10.875	22	758	65.0	± 0.2
L	1250	5.2	88.4	5.97E-16	10.836	15	30	64.7	± 0.5
M	1350	3.0	88.5	3.39E-16	11.104	***	23	66.3	± 0.6
N	1450	0.3	27.9	2.86E-17	12.173	0	11	72.6	± 6.7
Total gas			92.7	1.14E-14	10.738	28	1257	64.1	
87 % of gas released in steps G (1000 ºC) through L (1250 ºC) steps							**Average age =**	**65.0**	**± 0.6**
Quitovac-3	***white mica***	*flakes*	*J = 0.003260 ± 0.50 %*	*weight = 1.4 mg*	*81KD55*				
A	600	0.2	2.7	2.88E-17	5.543	0	13	32.3	± 14.3
B	700	0.2	44.3	2.13E-17	12.698	1	18	73.2	± 7.6
C	800	0.6	78.6	7.43E-17	11.879	2	27	68.5	± 2.4
D	850	0.8	72.1	9.43E-17	11.117	***	59	64.2	± 2.1
E	900	1.5	77.4	1.78E-16	10.701	15	166	61.9	± 1.3
F	950	3.0	75.0	3.58E-16	10.401	***	295	60.2	± 1.0
G	1000	16.3	88.3	1.98E-15	10.337	37	917	59.8	± 0.2
H	1050	24.0	97.1	2.91E-15	10.415	61	1235	60.2	± 0.1
I	1100	13.2	95.9	1.60E-15	10.296	16	1266	59.6	± 0.2
J	1150	7.3	92.8	8.90E-16	10.515	***	735	60.8	± 0.4
K	1200	19.2	96.6	2.33E-15	10.407	27	769	60.2	± 0.1
L	1250	11.8	96.4	1.43E-15	10.515	54	67	60.8	± 0.2
M	1350	1.3	80.4	1.61E-16	11.332	3	12	65.4	± 1.3
N	1450	0.7	58.6	8.55E-17	13.919	6	21	80.1	± 2.4
Total gas			93.0	1.21E-14	10.454	39	834	60.4	
92 % of gas released in steps G (1000 ºC) through L (1250 ºC) steps							**Average age =**	**60.2**	**± 0.4**
Quitovac-4	***white mica***	*flakes*	*J = 0.003288 ± 0.50 %*	*weight = 1.3 mg*	*69KD55*				
A	600	0.5	10.3	4.02E-17	11.196	***	28	65.2	± 12.3
B	700	1.8	65.6	1.52E-16	7.934	2	116	46.5	± 1.8
C	800	4.1	87.4	3.53E-16	8.679	***	126	50.8	± 0.7
D	850	4.2	96.1	3.61E-16	9.891	4	292	57.7	± 0.5
E	900	5.5	95.2	4.71E-16	9.967	5	391	58.2	± 0.4
F	950	7.1	95.8	6.09E-16	10.284	12	521	60.0	± 0.5
G	1000	9.1	96.9	7.85E-16	10.355	27	943	60.4	± 0.3
H	1050	12.1	98.4	1.04E-15	10.650	46	794	62.1	± 0.2
I	1100	17.3	98.6	1.49E-15	10.943	8	1176	63.8	± 0.2
J	1150	17.6	99.1	1.51E-15	11.213	160	1042	65.3	± 0.3
K	1200	7.6	96.4	6.54E-16	11.293	6	510	65.8	± 0.3
L	1250	2.6	88.2	2.27E-16	11.452	6	12	66.7	± 0.8
M	1350	8.1	91.2	6.95E-16	9.902	28	60	57.8	± 0.4
N	1450	2.4	71.0	2.08E-16	10.415	3	155	60.7	± 0.9
Total gas			94.8	8.60E-15	10.554	44	695	61.6	
Step H (1050 ºC)							**Single step age =**	**~62**	

Table 4. $^{40}Ar/^{39}Ar$ step-heating data and average or single step ages.—Continued

Step	Temp. °C	%^{39}Ar of total	Radiogenic yield (%)	$^{39}Ar_k$ (moles)	$^{40}Ar^*/^{39}Ar_k$	Apparent K/Ca	Apparent K/Cl	Apparent age (Ma)	Error (Ma)
Sanfran-1	***white mica***	*flakes*	*J = 0.003310 ± 0.25 %*	*weight = 1.2 mg*	*65KD55*				
A	600	0.2	1.8	2.05E-17	3.682	0	12	21.9	± 17.4
B	700	0.4	20.6	3.70E-17	4.553	***	28	27.0	± 5.3
C	800	0.9	81.6	9.88E-17	11.330	1	35	66.4	± 3.0
D	850	1.3	85.0	1.31E-16	11.145	***	110	65.4	± 1.3
E	900	2.2	87.8	2.26E-16	11.621	11	185	68.1	± 1.8
F	950	3.8	90.6	4.01E-16	11.602	5	315	68.0	± 0.6
G	1000	8.8	94.6	9.24E-16	11.741	***	763	68.8	± 0.3
H	1050	27.0	99.0	2.82E-15	12.178	***	2632	71.3	± 0.4
I	1100	22.2	99.0	2.32E-15	11.873	21	1449	69.5	± 0.2
J	1150	13.2	97.9	1.38E-15	11.790	***	1149	69.1	± 0.2
K	1200	11.0	97.8	1.15E-15	11.759	27	885	68.9	± 0.4
L	1250	8.0	93.4	8.35E-16	11.977	32	34	70.1	± 0.5
M	1350	0.7	88.6	7.73E-17	13.993	5	8	81.7	± 2.6
N	1450	0.4	40.2	4.32E-17	12.761	1	22	74.6	± 5.2
Total gas			96.2	1.05E-14	11.871	22	1368	69.6	
					Step K (1200 ºC)		**Single step age =**	**~69**	
SanFran 4d	***white mica***	*flakes*	*J = 0.002037 ± 0.25 %*	*weight = 4.9 mg*	*11KD12*				
J	1050	1.0	58.8	5.86E-16	12.643	***	2941	45.9	± 0.5
K	1100	2.0	64.3	1.13E-15	11.222	***	4545	40.8	± 0.3
L	1150	3.8	68.5	2.14E-15	10.619	***	3333	38.6	± 0.2
M	1200	7.5	84.7	4.25E-15	10.799	***	3448	39.3	± 0.1
N	1250	40.9	95.9	2.31E-14	10.704	***	6667	38.9	± 0.0
O	1350	23.6	92.3	1.33E-14	10.465	***	7143	38.1	± 0.0
P	1450	16.7	89.4	9.42E-15	10.942	***	9091	39.8	± 0.1
Q	1650	4.4	81.8	2.50E-15	10.757	***	588	39.1	± 0.1
Total gas			90.5	5.64E-14	10.724	***	6469	39.0	
97 % of gas released in steps L (1150 ºC) through Q (1650 ºC) steps							**Average age =**	**38.9**	**± 0.7**
SVE-1	***white mica***	*aggregates*	*J = 0.002037 ± 0.25 %*	*weight = 4.5 mg*	*46KD12*				
C	700	0.3	40.3	3.29E-17	25.993	***	***	93.1	± 2.9
D	750	0.5	66.0	4.98E-17	22.688	***	126	81.5	± 1.9
E	800	0.9	68.0	9.00E-17	19.307	***	391	69.6	± 1.2
F	850	1.5	76.5	1.41E-16	18.793	***	459	67.8	± 0.7
G	900	2.5	85.2	2.36E-16	17.981	***	303	64.9	± 0.4
H	950	4.3	92.2	4.04E-16	17.986	***	373	64.9	± 0.3
I	1000	11.1	96.1	1.06E-15	18.013	***	662	65.0	± 0.1
J	1050	21.4	97.9	2.03E-15	17.971	***	408	64.9	± 0.1
K	1100	15.2	97.8	1.45E-15	17.790	***	355	64.2	± 0.1
L	1150	11.7	97.0	1.11E-15	17.890	***	1250	64.6	± 0.1
M	1200	23.2	98.3	2.21E-15	18.173	***	1587	65.6	± 0.1
N	1250	5.3	81.7	5.03E-16	18.489	***	***	66.7	± 0.3
O	1350	0.5	76.2	4.90E-17	21.350	***	***	76.8	± 1.8
P	1450	0.2	53.0	2.01E-17	24.174	***	1786	86.7	± 4.6
Q	1650	1.3	52.3	1.21E-16	17.680	***	328	63.8	± 1.0
Total gas			94.5	9.50E-15	18.112	***	773	70.7	
95 % of gas released in steps G (900 ºC) through N (1250 ºC) steps							**Average age =**	**64.9**	**± 0.5**
Tajitos 2	***white mica***	*aggregates*	*J = 0.002037 ± 0.25 %*	*weight = 4.8 mg*	*3KD12*				
C	700	0.2	1.5	4.39E-17	13.076	***	22	47.4	± 11.9
D	750	0.4	19.0	1.11E-16	15.517	***	45	56.1	± 2.1
E	800	0.5	50.8	1.35E-16	16.662	***	107	60.2	± 1.1
F	850	0.2	62.6	5.73E-17	14.237	***	***	51.6	± 2.0
G	900	1.9	85.3	4.99E-16	16.249	***	446	58.7	± 0.3
H	950	4.3	90.6	1.16E-15	15.158	***	412	54.9	± 0.2
I	1000	8.9	94.8	2.37E-15	14.901	***	450	53.9	± 0.1
J	1050	5.0	96.9	1.32E-15	14.956	***	952	54.1	± 0.1
K	1075	9.6	96.0	2.41E-15	14.882	***	412	53.9	± 0.1
L	1100	2.3	98.6	6.11E-16	14.908	***	245	54.0	± 0.2
M	1150	25.6	98.5	6.82E-15	15.257	***	1408	55.2	± 0.1
N	1200	19.5	99.0	5.18E-15	15.632	***	2564	56.6	± 0.1
O	1250	16.8	97.3	4.46E-15	15.719	***	543	56.9	± 0.1
P	1450	4.2	79.6	1.12E-15	16.188	***	235	58.5	± 0.2
Q	1650	0.6	27.4	1.62E-16	25.650	***	44	91.9	± 1.6
Total gas			95.1	2.65E-14	15.435	***	1122	55.9	
88 % of gas released in steps I (1000 ºC) through O (1250 ºC) steps							**Average age =**	**55.6**	**± 1.1**

Table 4. $^{40}Ar/^{39}Ar$ step-heating data and average or single step ages.—Continued

Step	Temp. °C	%^{39}Ar of total	Radiogenic yield (%)	$^{39}Ar_k$ (moles)	$^{40}Ar^*/^{39}Ar_k$	Apparent K/Ca	Apparent K/Cl	Apparent age (Ma)	Error (Ma)
Yaqui-3	***white mica***	*aggregates*	*J = 0.002037 ± 0.25 %*	*weight = 5.2 mg*	*39KD12*				
A	550	0.2	3.8	6.54E-16	18.415	1	14	66.4	± 3.6
B	650	0.6	21.2	1.74E-15	11.565	6	35	42.0	± 0.6
C	700	0.5	53.9	1.53E-15	14.092	12	103	51.1	± 0.5
D	750	0.8	76.3	2.40E-15	15.843	16	157	57.3	± 0.3
E	800	1.5	90.1	4.36E-15	16.539	16	287	59.8	± 0.1
F	850	2.5	94.8	7.41E-15	16.829	36	503	60.8	± 0.1
G	900	4.0	96.4	1.16E-14	16.853	48	719	60.9	± 0.1
H	950	5.0	96.7	1.46E-14	16.946	54	847	61.2	± 0.1
I	1000	6.8	96.8	1.98E-14	17.481	50	794	63.1	± 0.1
J	1050	11.4	97.6	3.31E-14	20.458	48	1087	73.7	± 0.1
K	1075	12.0	98.4	3.47E-14	22.649	48	1250	81.4	± 0.1
L	1100	12.8	98.7	3.73E-14	24.002	50	1250	86.1	± 0.1
M	1150	17.1	98.9	4.97E-14	24.525	46	1163	87.9	± 0.1
N	1200	11.3	98.3	3.29E-14	25.916	36	833	92.8	± 0.1
O	1250	9.0	94.9	2.62E-14	22.527	34	29	80.9	± 0.1
P	1450	3.4	68.8	1.00E-14	23.680	19	95	85.0	± 0.2
Q	1650	1.1	53.8	3.27E-15	27.082	10	223	96.9	± 0.3
Total gas			95.1	2.91E-13	22.058	43	879	79.3	
					Step H (950 ºC)		**Single step age =**	**~61**	
10 de Mayo	***white mica***	*aggregates*	*J = 0.002037 ± 0.25 %*	*weight = 5.7 mg*	*22KD12*				
A	550	0.3	3.9	8.72E-16	14.692	1	12	53.2	± 3.8
B	650	0.7	16.4	2.18E-15	9.994	5	35	36.4	± 1.3
C	700	0.6	49.6	1.74E-15	12.749	7	118	46.3	± 1.3
D	750	1.1	74.1	3.27E-15	15.814	9	253	57.2	± 0.8
E	800	1.3	85.9	3.92E-15	16.760	10	493	60.6	± 0.7
F	850	3.5	91.9	1.00E-14	17.181	12	658	62.1	± 0.2
G	900	4.4	96.4	1.31E-14	17.340	20	971	62.6	± 0.2
H	950	5.8	96.9	1.68E-14	17.261	32	1087	62.3	± 0.1
I	1000	6.3	97.9	1.83E-14	17.452	37	1351	63.0	± 0.1
J	1050	17.4	98.0	5.08E-14	18.716	48	1818	67.5	± 0.1
K	1075	15.2	98.6	4.43E-14	20.719	50	2041	74.6	± 0.1
L	1100	14.3	98.8	4.19E-14	22.483	47	1639	80.8	± 0.1
M	1150	14.0	98.6	4.10E-14	23.970	40	1449	86.0	± 0.1
N	1200	10.2	98.1	2.99E-14	24.639	33	893	88.3	± 0.1
O	1250	2.5	90.1	7.41E-15	26.793	16	9	95.9	± 0.4
P	1450	1.6	58.5	4.58E-15	24.053	2	38	86.3	± 0.6
Q	1650	0.8	47.1	2.40E-15	31.152	6	97	111.0	± 1.2
Total gas			95.1	2.92E-13	20.841	38	1381	75.0	
					Step F (850 ºC)		**Single step age =**	**~62**	

Ages calculated assuming an initial $^{40}Ar/^{39}Ar = 295.5$.

All precision estimates are at the one sigma level of precision.

Ages of individual steps do not include error in the irradiation parameter J.

No error is calculated for the total gas age.

Data were obtained using a MAP 216 or a VG1200 spectrometer.

***K/Ca or K/Cl not calculated.

Capítulo 5. Introducción a los depósitos de oro orogénico de México

Depósitos de oro orogénico Mesozoicos de México (*Mesozoic orogenic gold deposits in México*) publicado: Ore Geology Reviews (2017) doi:10.1016/j.oregeorev.2015.10.006. Autores: Aldo Izaguirre, Antoni Camprubí, Alexander Iriondo.

• Objetivos: Generar una compilación científica que estableciera el estado actual del conocimiento de los depósitos de oro orogénico en México (Izaguirre et al., 2017). Grosso modo hacer una recopilación y comparativa entre las diferentes zonas mineralizadas de México como oro orogénico y contextualizando con las que ocurren en la Cordillera de América del Norte.

• Estudios: Se hizo una recopilación del conocimiento de las características geológicas del oro orogénico en México a través del uso de textos científicos y comunicaciones personales. Sin embargo, cabe destacar que la información generada hasta el momento es precaria y con limitantes importantes. Las características más destacables son edades de mineralización (específicamente del COGB), descriptiva de minerales de las ocurrencias, control estructural y termometría.

Ore Geology Reviews 81 (2017) 1172–1183

Contents lists available at ScienceDirect

Ore Geology Reviews

journal homepage: www.elsevier.com/locate/oregeorev

Mesozoic orogenic gold deposits in Mexico

Aldo Izaguirre [a,*], Antoni Camprubí [b], Alexander Iriondo [c,d]

[a] Programa de Posgrado en Ciencias de la Tierra, Centro de Geociencias, Universidad Nacional Autónoma de México, Boulevard Juriquilla 3001, 76230 Juriquilla, Querétaro, Mexico
[b] Instituto de Geología, Universidad Nacional Autónoma de México, Ciudad Universitaria, 04510 México, D.F., Mexico
[c] Centro de Geociencias, Universidad Nacional Autónoma de México, Boulevard Juriquilla 3001, 76230 Juriquilla, Querétaro, Mexico
[d] Department of Geological Sciences, Jackson School of Geosciences, The University of Texas at Austin, Austin, TX 78712, USA

ARTICLE INFO

Article history:
Received 27 September 2014
Received in revised form 5 October 2015
Accepted 6 October 2015
Available online 20 October 2015

Keywords:
North American Cordillera
Orogenic gold deposits
Shear zones
Caborca orogenic gold belt
Arteaga metamorphic complex
Oaxacan metamorphic complex

ABSTRACT

Although orogenic gold deposits in Mexico were mostly formed during the Cenozoic, they started forming during the Late Cretaceous, or perhaps even earlier. Mylonitic zones in the Oaxacan metamorphic complex span either Permo-Triassic or Triassic-Jurassic ages, but none of these have been formally associated with the existing orogenic gold occurrences. Given the current scarcity of age data for them, any interpretation concerning the age patterns or distribution of orogenic gold deposits in Mexico other than those in the Sonoran belt is hitherto deemed to be precarious. A few known Mesozoic examples are part of the Quitovac–La Choya deposits in the Caborca Orogenic Gold Belt (COGB) in Sonora, and Los Uvares in the Los Cabos Block (southernmost part of the Baja California Peninsula). The COGB constitutes the most economically important and geologically consistent mineralized area in Mexico with respect to orogenic gold deposits. Also, the COGB arguably correlates with the Mother Lode trend in California and Nevada, whereas the cluster of deposits in the Los Cabos Block may have correspondent similarly mineralized areas in mainland southwestern Mexico (Jalisco Block). Other areas with orogenic gold deposits in Mexico, which have been traditionally overlooked or scantly mentioned, are the northernmost part of the Baja California Peninsula, and the Arteaga and Oaxacan metamorphic complexes, although no geochronological data are available from these. Besides the overly lack of such data, one of the typical problems concerning the characterization and metallogenesis of orogenic deposits in Mexico has been their inaccurate or incorrect ascription to other genetic paradigms or types of deposits, such as epithermal or porphyry Cu–Au deposits, therefore misguiding exploration efforts.

The formation of orogenic gold deposits in Mexico has been commonly associated with the Laramide orogeny, in association with cataclastic or mylonitic deformation and shear zones. Their depth of formation, under lithostatic pressure, has ben estimated at a range between ~3 and ~10 km. Alteration assemblages in them are generally dominated by quartz ± "sericite" ± pyrite, and may be carbonate-rich. The hypogene mineralogy of orogenic gold deposits in Mexico is normally dominated by sulfides like pyrite, galena, sphalerite and whereas gold normally occurs as "electrum", also known as unspecified Ag-rich gold, Au-rich silver, or as free gold. The latter may either be a hypogene or supergene mineral, in which case it is likely to be due mostly to the leaching-off of Ag from "electrum". Te-rich associations are rare and have complex parageneses that consist typically of silver and/or gold tellurides. The mineralizing fluid precipitation into quartz veins occurred at temperatures ~350 °C and are CO_2-rich deeply seated crustal brines from metamorphic sources, with salinities typically ranging between ~2 and ~10 wt.% NaCl equiv. but attaining up to ~33 wt.% NaCl equiv.

© 2015 Elsevier B.V. All rights reserved.

1. Introduction

Orogenic gold deposits formed late in the evolution of convergent margin settings during major orogenic events, and their formation requires some form of accretionary setting involving subduction or underplating of oceanic crust (Bierlein et al., 2009), and Mexican examples are no exception to this. The Mexican orogenic gold deposits are clearly linked to the geology of the North American Cordillera originated mostly in compressional conditions (Fig. 1). The majority of the known orogenic gold deposits in Mexico are located in northern Sonora (Fig. 2). This type of ore deposits has become one of the most important in terms of gold production in the country during the last decades, provided that the combined reserves and extraction in these deposits have generated resources of more than 10 Moz Au. The most important deposits in this region (Fig. 2) are La Herradura, El Chanate, San Francisco-Llano, Soledad-Dipolos, Noche Buena, La Choya, and El Boludo, a placer gold deposit most likely from Laramide orogenic veins (Radelli and Pérez-Segura, 1992). The orogenic gold deposits in Sonora cover an elongated area with ~600 km long and ~60–80 km

* Corresponding author.
E-mail address: aldoizapo@gmail.com (A. Izaguirre).

http://dx.doi.org/10.1016/j.oregeorev.2015.10.006
0169-1368/© 2015 Elsevier B.V. All rights reserved.

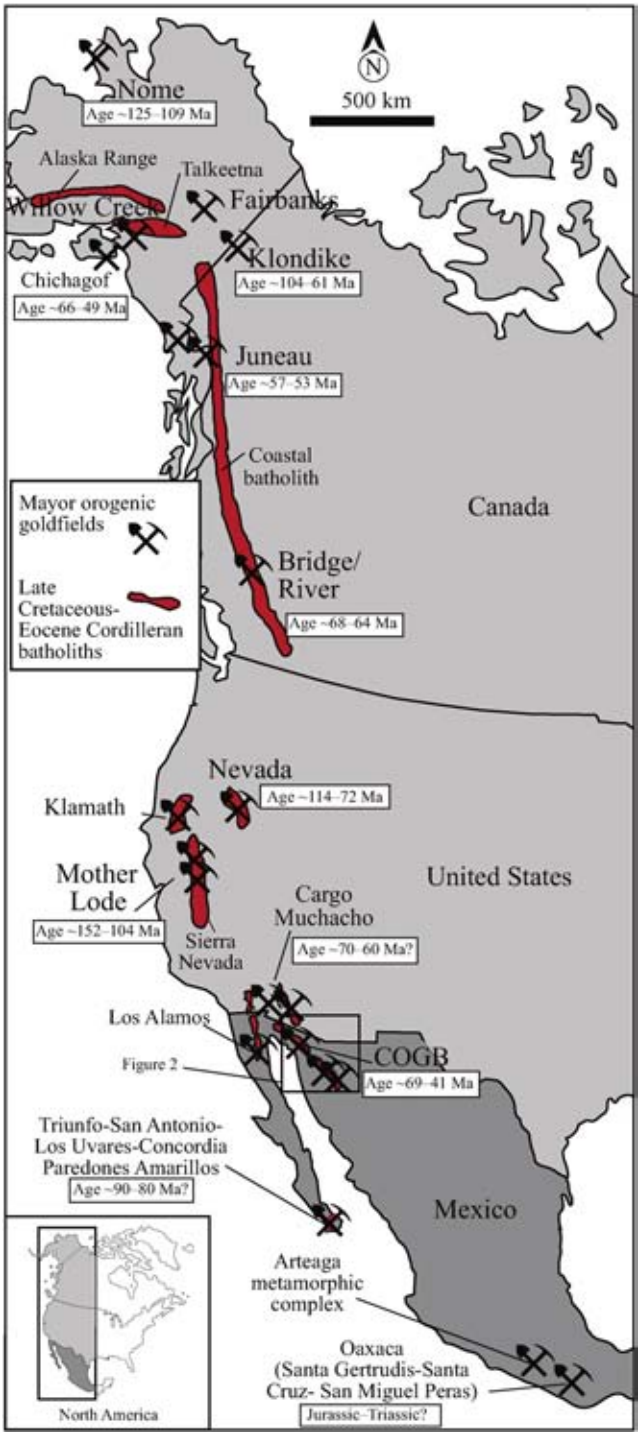

Fig. 1. Map with the distribution of the main mineralized belts that contain orogenic gold deposits in the Cordillera of Western North American (modified from Goldfarb et al., 2008), including the Mesozoic and Cenozoic orogenic gold deposits of Mexico. COGB: Caborca Orogenic Gold Belt.

across with a general NW-SE orientation, and it was labeled recently as the "Caborca Orogenic Gold Belt (COGB)" (Fig. 1) by Izaguirre et al. (2012); however, these deposits were known as the Sonora Gold Belt (Silberman et al., 1988) or Gold Deposits from the Sonoran Desert Province (Pérez-Segura, 1993); nevertheless, previous names included different mineralized areas and involve more type of gold deposits (e. g., epithermal deposits). However, those names are helpful to link previous studies with this publication. The COGB is structurally dissected by the current extensional Basin and Range province, and originated in the active North American margin, as the former Farallon plate was being consumed by subduction underneath the North American plate. Early work (Silberman et al., 1987, 1988) in the Sonoran orogenic gold deposit belt was based on structural geology and vein geochemistry studies, but these included other types of deposits, such as epithermal deposits, which certainly have nothing to do with the orogenic gold model or its associated processes. As a consequence, these studies finally described a favorable area far larger than is known to be nowadays.

Other regions in Mexico where orogenic gold deposits are known to occur are the Baja California Peninsula, the Arteaga metamorphic complex in southwestern Mexico, and the Oaxacan metamorphic complex in southern Mexico (Sánchez-Rojas et al., 1998; Clark and Fitch, 2009; Jiménez-Hernández, 2011; Fig. 1). In the case of Baja California, Concordia-Paredones Amarillos deposits are interpreted as a shear zone and mylonite-hosted deposits with calculated reserves of over 48 Mt at 1.01 g/t Au (Cendejas-Cruz and Aldana-Hernández, 2008) and for Oaxacan deposits reserves are not well documented at the moment.

Host rocks for orogenic gold mineralizations in the Sonoran belt are igneous and metamorphic rocks from the Paleoproterozoic basement, Paleozoic granitic and platform sedimentary rocks, and Mesozoic sedimentary, volcanic, volcaniclastic and granitic (Fig. 2). Iriondo and Premo (2011) suggested that the orogenic gold deposits in Sonora are associated in space with the Paleoproterozoic basement rocks and, most especially, with the province of Yavapai Paleoproterozoic granitc rocks, and therefore the ultimate source for such deposits is due to processes associated with such rock assemblages. Also, the same authors postulate that the Yavapai province represents a crustal weakness area that might have played a role as channelways for buoyant mineralizing fluids. Similarly, in the Oaxacan metamorphic complex host rocks are basically Mesoproterozoic and Neoproterozoic paragneiss and metagranites, as well as Permo-Triassic intrusive rocks (Jiménez-Hernández, 2011).

Hitherto, mineralization ages for the COGB gold belt have been obtained by means of K–Ar and Ar–Ar geochronometry in "sericite" and white micas (Pérez-Segura, 1993; Pérez-Segura et al., 1996; Iriondo and Atkinson, 2000; Araux-Sánchez, 2000; Araux-Sánchez et al., 2001; Iriondo, 2001; see Table 1), and Re–Os model ages in magnetite and pyrite (Quintanar-Ruíz, 2008). However, recently Izaguirre et al. (2013) reported new 59 ages distributed along the COGB with mineralization ages between ~69–36 Ma and an age peak of mineralization activity at ~60 Ma. So the available ages from the COGB deposits suggest a relatively long-lived formation, from the latest Mesozoic (~69 Ma) until the Eocene (~36 Ma, see Table 1). Nevertheless, the available structural models at La Herradura (de la Torre-Carlos, 2004, 2009) suggest that this deposit might be significantly older than the 61 Ma Re–Os model age obtained by Quintanar-Ruíz (2008). The host rocks at the Los Uvares deposit in the state of Baja California Sur were dated between 90 to 80 Ma (K–Ar and fission tracks; Carrillo-Chávez, 1996; Carrillo-Chávez et al., 1999). This deposit is hereby considered to belong to the orogenic gold type, following Clark and Fitch (2009) and our own criteria acquired in a recent fieldwork campaign to the El Triunfo-San Antonio mineralized trend. This case suggests a necessary re-evaluation of the time and space distribution of such type of deposits in northwestern and westernmost Mexico. The nearby Concordia-Paredones Amarillos orogenic gold deposit displays similar ages to Los Uvares, as its age is constrained by those of the underlying and crosscutting intrusive rocks between 91 and 79 Ma (referred by Cendejas-Cruz and Aldana-Hernández, 2008; Clark and Fitch, 2009). The still undated El Triunfo-San Antonio deposit also occurs in the same region and shares many geological similarities with the Los Uvares and Concordia-Paredones Amarillos deposits (Carrillo-Chávez, 1996; Clark and Fitch, 2009). In spite of well constrained Permo-Triassic (Solari, 2001) and Triassic-Jurassic (Alaníz-Álvarez et al., 1996; Alaniz-Álvarez and Nieto-Samaniego, 1997; Solari et al., 2004) ages for mylonites in the Oaxacan metamorphic complex, none of these has been properly associated to the existing orogenic gold deposits, although Jiménez-

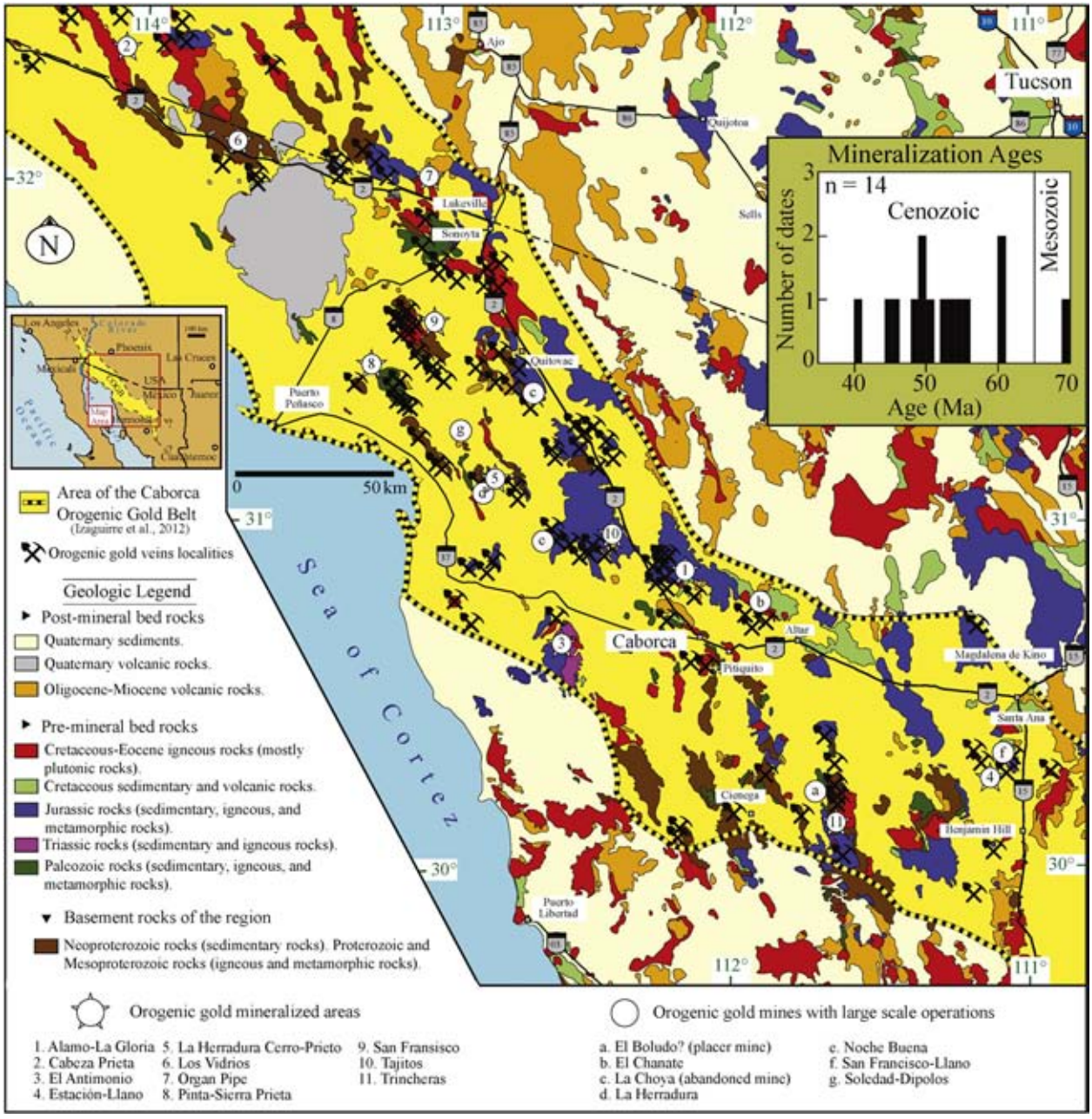

Fig. 2. Geologic map of Northwestern Sonora and Southwestern Arizona with the distribution of the Caborca Orogenic Gold Belt (Izaguirre et al., 2012). Also showing confirmed orogenic gold belt localities, orogenic gold mineralized areas, mines with large scale operations. The histogram (inset) shows the known mineralization ages reported for some localities in the Caborca Orogenic Gold Belt, with age data collected (n = 14) from Tajitos (Pérez-Segura, 1993), San Francisco-Estación Llano (Pérez-Segura et al., 1996), Sierra Pinta (Araux-Sánchez, 2000), Quitovac-La Choya (Iriondo, 2001), and La Herradura (Quintanar-Ruíz, 2008).

Hernández (2011) indicated that the observed deposits in Santa Gertrudis and Santa Cruz Mixtepec formed during two distinct stages of mineralization. Similarly, the Californian (USA) orogenic gold deposits formed between the Late Jurassic and the Cretaceous, and their timing suggests at least two regional stages of formation (Marsh et al., 2008).

2. Mineralogy and alteration

These deposits are generally constituted by quartz veins with calcium and iron carbonates, "sericite" (generally fine-grained white micas), pyrite, galena, free gold, tourmaline, magnetite, hematite, sphalerite, covellite, chlorite and epidote as hypogene minerals (Table 2 and Fig. 3), plus malachite, azurite, and several oxyhydroxide minerals due to supergene alteration. However, most of the deposits in Mexico that are ascribed to the orogenic gold type normally lack detailed mineralogical studies of either ore-bearing associations or their associated alteration halos.

The mineral parageneses in most of these deposits (COGB and Baja California) are similar to the common parageneses established around the world (Table 2). Especially those deposits containing quartz–pyrite–sericite in association with high carbonates content (~2–3%). These mineral arrangements, in combination with compressive tectonic zones, are a key to classifying these deposits as orogenic gold (Izaguirre et al., 2012).

La Herradura is the biggest gold deposit in the COGB (over 5 Moz Au) and a multi-stage deposit (it contains at least 5 mineralization events; Quintanar-Ruíz, 2008; de la Torre-Carlos, 2004, 2009) constrained by the regional D3 deformation (Re-Os model age at 61.0 ± 2.1 Ma; Quintanar-Ruíz, 2008). The typical mineral associations at La Herradura

Table 1
Mineralization ages of previous studies from the Caborca Orogenic Gold belt Area, NW Sonora, México.

Area	Mine	Method	Mineral	Age		Error	Type	Reference
Estación Llano	San Francisco	Ar–Ar	White mica	41.0			Plateau	Pérez-Segura et al. (1996)
Quitovac-La Choya	Doña Marcia	Ar–Ar	White mica	46.0			Total gas	Iriondo (2001)
Quitovac-La Choya	La Choya	Ar–Ar	White mica	46.0			Total gas	Iriondo (2001)
Quitovac-La Choya	Doña Marcia	Ar–Ar	White mica	48.5	±	0.3	Plateau	Iriondo (2001)
Tajítos	Tajítos	K–Ar	White mica	49.2	±	2.0		Pérez-Segura (1993)
Quitovac-La Choya	La Choya	Ar–Ar	White mica	50.0			Total gas	Iriondo (2001)
Quitovac-La Choya	La Negra	Ar–Ar	White mica	50.2	±	0.1	Plateau	Iriondo (2001)
Quitovac-La Choya	La Toñita	Ar–Ar	White mica	52.0			Total gas	Iriondo (2001)
Quitovac-La Choya	Bustamante	Ar–Ar	White mica	54.0			Total gas	Iriondo (2001)
Sierra Pinta	La Pinta	K–Ar	White mica	54.8	±	1.4		Araux-Sánchez (2000)
Quitovac-La Choya	El Chacón	Ar–Ar	White mica	56.0			Total gas	Iriondo (2001)
Mina La Herradura	La Herradura	Re–Os	Magnetite-pyrite	61.0	±	2.1	Isochron	Quintanar-Ruíz (2008)
Quitovac-La Choya	Quitovac	Ar–Ar	White mica	61.0			Total gas	Iriondo (2001)
Quitovac-La Choya	Quitovac	Ar–Ar	White mica	69.0			Total gas	Iriondo (2001)

are dominated by quartz, "sericite" and albite, and contain hematite, pyrite, galena, acanthite, argentite, fluorite, chalcopyrite, sphalerite, and "electrum" as hypogene minerals, either hypogene or supergene free gold, and iron oxyhydroxides (dominantly goethite), wulfenite, natrojarosite, plumbojarosite, jarosite, anglesite, chlorargyrite and iodargyrite as supergene minerals (de la Torre-Carlos, 2004, 2009). In this deposit, distinctive types of alteration assemblages (namely, carbonation, phyllic and propylitic assemblages) occur in characteristic distribution patterns, although such alteration assemblages are masked by either metamorphic and supergene overprintings (de la Torre-Carlos, 2004, 2009). Carbonation halos, or siderite–ankerite associations, are observable up to 1.5 km laterally to the deposit. Phyllic halos, or quartz–pyrite–"sericite" associations, occur virtually restricted to the contacts between the wallrocks and quartz veins/veinlets. Propylitic halos, or chlorite-epidote-calcite associations, normally occur along barren veins.

Futhermore, Izaguirre et al. (2012) demonstrated that the hydrothermal alteration assemblages around the orogenic gold deposits in the COGB are characteristically homogeneous at a regional scale, and that host rocks were hydrothermally enriched in K_2O, H_2O, CO_2, W,

Table 2
Orogenic gold characteristics of orogenic gold in the Caborca Orogenic Gold Belt NW Sonora, Mexico, versus global knowledge of orogenic gold deposits.

	Caborca Orogenic Gold Belt1	Vs.	Global orogenic gold knowledge2
Ore host rocks	North American basement rocks mostly gneisses, schists and granitoids in metamophic amphibolite-greenschist facies. Mesoproterozoic plutonic rocks. Neoproterozoic and Paleozoic sedimentary rocks. Also in rocks of the North American Cordillera (gneisses, granitoids, sedimentary and volcanics) of Permian, Triassic, Jurassic, Cretaceous and Paleocene ages.		Deformed metamorphic terranes of all ages (greenschist facies rocks) associated to convergence magmatic arcs with more prevalence of archean ages.
Temperature formation	260–370 °C; with an average of 330 °C.		300 ± 50 °C.
Pressure and cortical deep formation	0.5–1.2 kbars, ~2 to 6–8 km.		1–3 kbars, epizonal-mesozonal (2–12 km).
Ore morphology	Quartz-carbonate veins and stock-work are located in shear zones (mostly trust faults). Gold dissemination are common in big deposits. Supergene alteration occurs on sulfides and carbonates and is frequently observed like iron oxides, sulfates, halides and caliche.		Quartz-carbonate veins located in shear zones (mylonites) on ductile, ductile-brittle rocks conditions, with no significant zonation mineralogy changes.
Paragenetic minerals	Quartz, carbonates (calcite, ankerite and siderite), white mica, pyrite, galena, sphalerite, scheelite, turmaline, molybdenite, tellurides and native Au.		Dominant quartz vein systems with carbonates (calcite, siderite, ankerite), white mica, pyrite, galena, sphalerite, chalcopyrite, pyrrhotite, marcasite, arsenopyrite (mainly Fe-sulfides), albite, chlorite, scheelite and tourmaline.
Alteration minerals	Silicification, sericitization, carbonitization, pyritization, chloritization.		Carbonates (calcite, ankerite, dolomite, siderite), pyrite, quartz, pyrrhotite or arsenopyrite, sericite or fuchsite (less common), albite, K-feldespar and chlorite.
Enrichment elements	K, W, Cu, Pb, Mo, Tl, Be, Zn, V, Sb, Ag, Sn, Si, Se, Ni and Fe (As and Te is less anomalous).		As, B, Bi, Hg, Sb, Te, W, Cu, Pb and Zn (depends of regional background).
Ore fluids	Metamorphic source with low salinity (2–11% eq. wt % NaCl), rich on H2O, N2, CO2 (1–11 mol%), values of δ18O = 7 to 17‰ and δ2H about −39 to −107‰.		Typical from metamorphic source with low salinity (~3–10% eq. wt % NaCl), rich on H2O, H2O–CO2 ≥ 5 mol%, ± CH4 and N2. Values of δ18O = 5 to 8‰ and δ2H = −10 to −40‰.
Approximate value for mineral tonnage (Mt)/Au production (Moz)/Au-grade (g/t) for important mines	La Herradura: 200/6.0/1.0; El Chanate: 52/1.5/0.9; San Francisco-Llano: 113/2.4/0.7; Noche Buena: 35/0.6/0.5 and La Choya: 8.3/0.4/1.3.		Golden Mile (Yilgram Craton): 1000/64.0/2.0; Homestake: > 150/40.0/8.3; Gras-Valley-Nevada: 40/21.4/16.9; Bendingo Goldfield (Tasman Orogen): 41/17.0/12.9; Brasilia: 725/10.0/0.4 and Alaska-Juneau: 198/9.0/1.4.
Other important features (potpourri)	Low content of sulfides (~3%), structural hosted deposition related. Also supergene processes with secondary mineralization (hematite, goethite, wulfenite, jarosite, plumbojarosite, anglesite and chlorargyrite). Medium-low grade of precious metals (Au = ~3 g/tonne), Au/Ag = 1:9.		Low content of sulfides (3–5%), structural hosted deposition related, medium grade of precious metals (Au = 5–30 g/tonne), Au/Ag = 10:1.

1. Data compilated from: Albinson (1989); Pérez-Segura et al. (1996); Iriondo and Atkinson (2000); Araux-Sánchez (2000); Noriega-Martínez (2006); Quintanar-Ruíz (2008); de la Torre-Carlos (2009); Izaguirre et al. (2012); Izaguirre and Iriondo (2014).
2. Data from Groves et al. (1998) and Goldfarb et al. (2005)

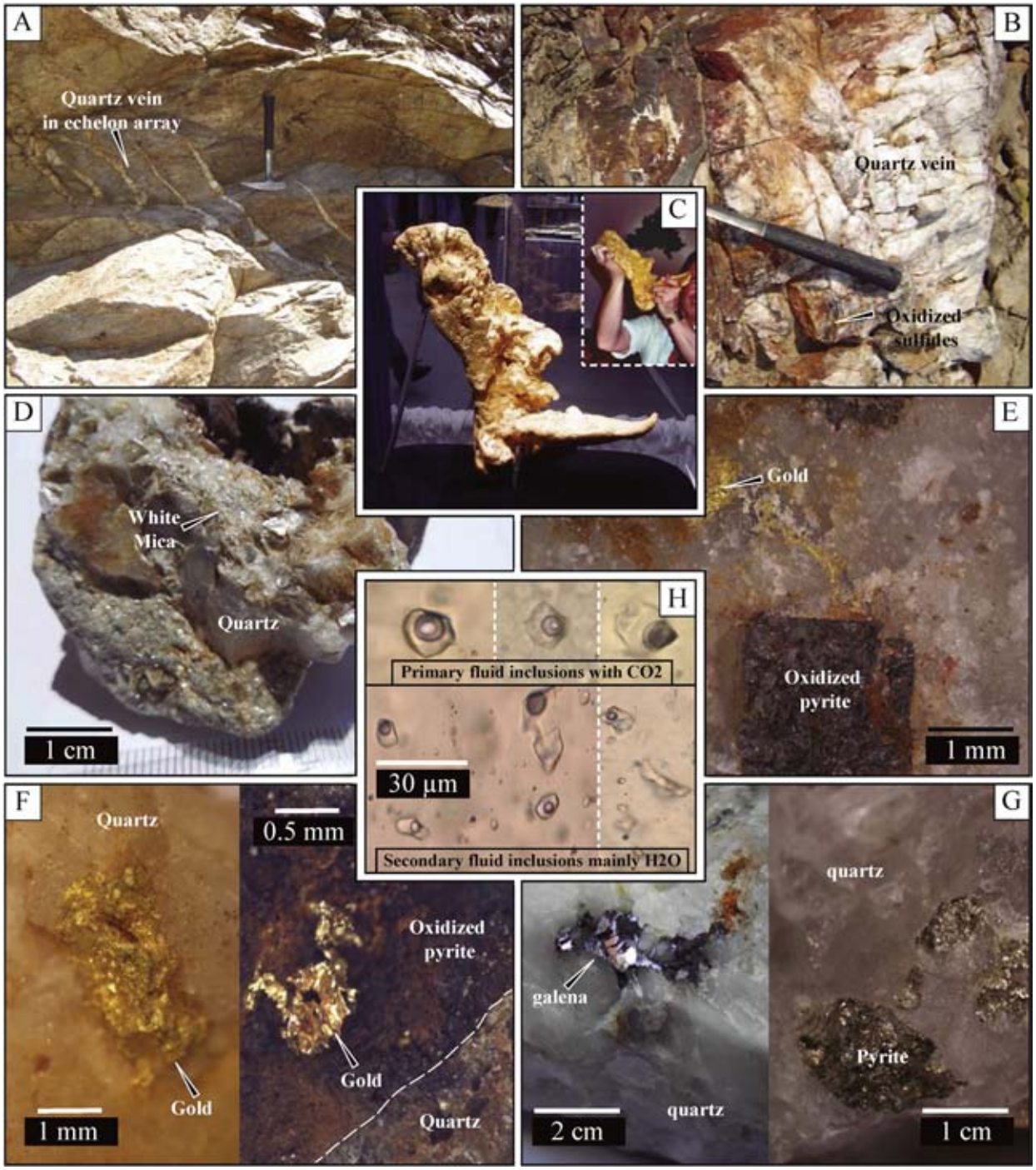

Fig. 3. Representative pictures of orogenic gold deposits in the Sonoran belt (Caborca Orogenic Gold Belt) in northwestern Mexico. (a) Mineralized en-échelon quartz veins controlled by a shear zone, La Republicana Mine, Sierra La Gloria. (b) Milky quartz vein with oxidized sulfide mineralization, Sierra Prieta mineralized zone, Puerto Peñasco. (c) The "Boot of Cortez", a >12 kg gold nugget found in alluvial placers in the Altar desert, associated with the Tajitos orogenic gold deposit, which is the largest surviving gold nugget found in the western hemisphere, see http://www.gold-classics.com/images/boot.htm. (d) Hand specimen from a quartz vein with white micas, La Angélica Mine, Sierra El Choclo Duro, close to El Pinacate Volcanic Field, Caborca. (e) Hand specimen from a quartz vein with free gold and oxidized pyrite, San Francisco Mine, Estación Llano. (f) Detail of free gold mineralization in quartz, El Capitán Mine, Ciénega. (g) Hand specimen from a quartz vein with galena, La Sargenta Mine, Sierra San Francisco, close to El Pinacate Volcanic Field, Caborca. (h) Primary CO_2-rich aqueous fluid inclusions in quartz (up), and secondary aqueous fluid inclusions in quartz (down), from the Sierra La Gloria-El Álamo and Sierra Pinta, Puerto Peñasco deposit.

Cu, Pb, Mo, Tl, Be, Zn, V, Sb, Ag, Sn, SiO_2, Se, Ni and FeO. They also found a clear link between fluid geochemistry and mineral parageneses with the observed alteration.

The San Antonio-El Triunfo deposits in Baja California Sur consist of up to 5 km long quartz fissure veins and shear zones that contain gold and silver tellurides, lead and silver sulfosalts (basically proustite–pyrargyrite), hematite, pyrite, chalcopyrite, arsenopyrite, argentian galena, realgar, stibnite, sphalerite, argentite and freibergite, whereas the supergene associations are constituted by jarosite, azurite, malachite, iron oxihydroxides, bornite, covellite, and free native gold and silver (Cendejas-Cruz and Aldana-Hernández, 2008). The shear zone of Concordia-Paredones Amarillos deposits, located near the San Antonio-El Triunfo deposits, have calculated reserves of over 48 Mt. at 1.01 g/t Au, and contain free gold, pyrite, arsenopyrite, chalcopyrite, galena, and argentite (Cendejas-Cruz and Aldana-Hernández, 2008). The mineralogy of the deposits in the Oaxacan metamorphic complex is

only succinctly described by Jiménez-Hernández (2011) and seemingly consists of base-metal sufides, free gold or "electrum" and iron oxides.

Unlike the rest of orogenic gold deposits in Mexico with available relatively detailed mineralogical characterizations, the San Francisco-Estación Llano quartz vein deposits are rich in tellurium minerals. They contain schorl-dravite, albite, "sericite" (phengite?), chlorite (ripidiolite–brungsvigite), calcite, free gold, petzite, hessite, calaverite, sylvanite, native tellurium, altaite, Ag_2TeS_3 and [Pb, Bi]Te_5 (Pérez-Segura, 2009; see Fig. 4).

A mineralogical curiosity related to Mexican orogenic gold deposits is that one of the biggest gold nuggets ever found, nicknamed "The Boot of Cortés" (or Cortez), which weighted >12 kg Au, was found at the Tajitos Area in the GOGB (Fig. 3c). This feature shows the presence of free gold crystals of megascopic scale associated to the quartz veins. Also golden nuggets between 3 and 7 kg of gold were found at the El Boludo and La Cienega mineralization zone (Fig. 2, Radelli and Pérez-Segura, 1992).

3. Fluid inclusion and stable isotope studies

Albinson (1989) determined the temperatures of ore formation, the composition of mineralizing fluids, and depths for emplacement through microthermometry of fluid inclusions in some of the COGB deposits, and characterized them as "mesothermal", an old labeling of such type of deposits that tends to fall into disuse. More recent and detailed surveys allowed characterizing the time and geochemical patterns for some mineralized areas in this belt, in order to better constrain the mineral occurrences and their parageneses (Table 2 and Fig. 5). Such deposits in Sonora (Fig. 2) are Estación–Llano (Changkuon, 1990; Pérez-Segura et al., 1996; Araiza-Martínez, 1998; Poulsen et al., 2008), Quitovac (Durgin and Terán, 1996; Iriondo and Atkinson, 2000; Iriondo, 2001), Tajitos (Noriega-Martínez, 2006; Pérez-Segura, 1993), La Pinta–Sierra Prieta (Araux-Sánchez, 2000), La Herradura–Cerro Prieto (Quintanar-Ruíz, 2008; Ornelas-Macías and Verdugo-Noriega, 2009), El Antimonio, El Álamo, Trincheras, and San Francisco. Microthermometric and stable isotope data are also available from the San Miguel Peras, Santa Gertrudis and Santa Cruz Mixtepec deposits in the Oaxacan metamorphic complex (Sánchez-Rojas et al., 1998; Jiménez-Hernández, 2011). The most relevant characteristics of mineralizing fluids in the studied Mexican orogenic gold deposits are:

(1) Average temperatures of homogenization in vein quartz range from ~260° to 370°C (Fig. 5) at San Francisco-Estación Llano (Pérez-Segura, 2009); also temperatures of homogenization for

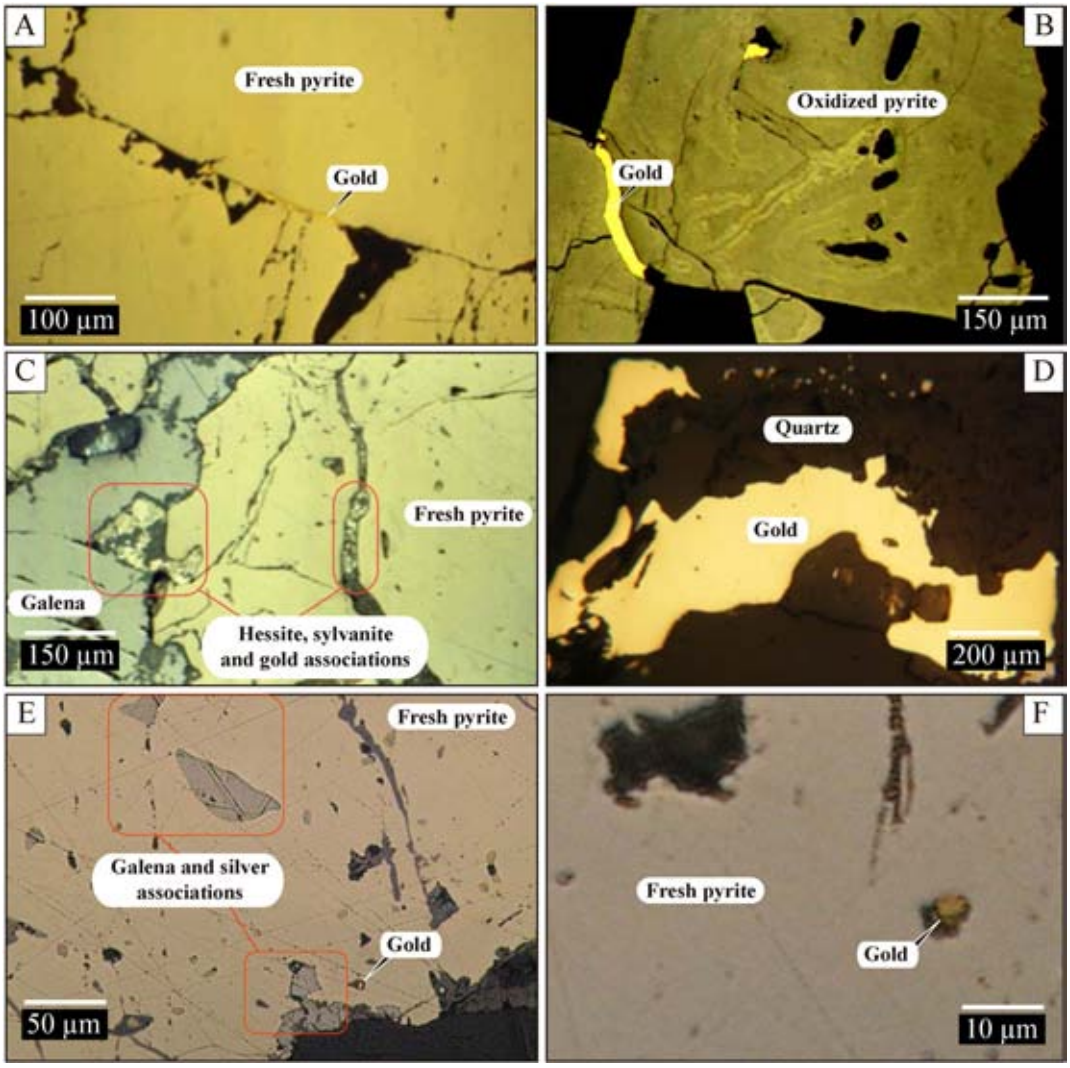

Fig. 4. From A–D photomicrographs of the San Francisco-Estación Llano telluride-rich orogenic gold deposits, Sonora. (A) Free gold along pyrite grain boundaries. (B) Free gold possibly formed after oxidation of pyrite. (D) Tellurium and gold-rich associations along sulfide grain boundaries and fractures. (D) Large free gold grains within quartz. Pictures E (El Alamo-La Gloria) and F (Pitiquito area) from COGB area. (E-F) Silver-gold minerals within pyrite. All pictures were taken under plain polarized reflected light. Pictures from A–D courtesy of Efrén Pérez-Segura. Pictures E and F after Izaguirre et al. (2012).

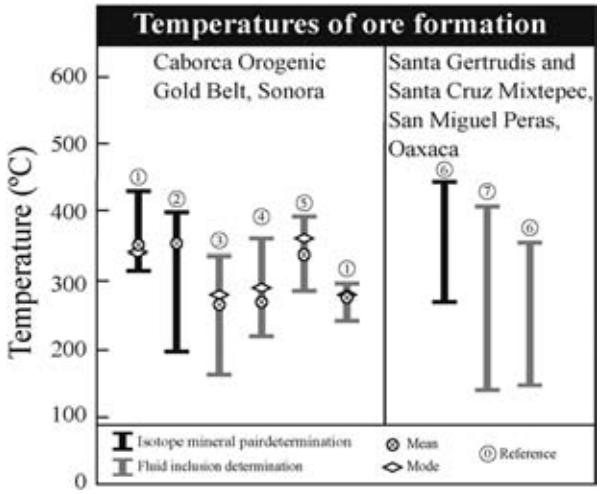

Fig. 5. Estimated temperatures of precipitation of orogenic gold deposits at the Caborca Orogenic Gold Belt, Sonora, and Santa Gertrudis, Santa Cruz Mixtepec, San Miguel Peras, Oaxaca. 1: Quintanar-Ruíz (2008); 2: Izaguirre and Iriondo (2014); 3: Albinson (1989); 4: Pérez-Segura et al. (1996); 5: Noriega-Martínez (2006); 6: Jiménez-Hernández (2011) and 7: Sánchez-Rojas et al. (1998), in order of appearance.

Tajitos quartz veins are between ~290° to 390 °C (Noriega-Martínez, 2006) and for La Herradura Mine between ~248° to 298 °C, this temperatures suggest orogenic gold ore conditions for precipitation in all cases. Similar temperatures of homogenization range from ~145° to 353 °C in Santa Gertrudis and Santa Cruz Mixtepec (Jiménez-Hernández, 2011), and from ~140° to 412 °C in San Miguel Peras (Sánchez-Rojas et al., 1998),

(2) salinities are generally low with an average of ~3 wt.% NaCl equiv. Some examples may attain up to ~7.3 wt.% NaCl equiv. at San Miguel Peras (Sánchez-Rojas et al., 1998), up to ~8.5 wt.% NaCl equiv. at La Herradura (Lang, 2003, in de la Torre-Carlos, 2004, 2009), up to ~10 wt.% NaCl equiv. at San Francisco-Estación Llano (Pérez-Segura, 2009), and an exceptional high value up to ~32.8 wt.% NaCl equiv. at Santa Gertrudis and Santa Cruz Mixtepec (Jiménez-Hernández, 2011), whereas

(3) CO_2 contents are always high between 1 to 11%, and thus liquid CO_2 is conspicuous within fluid inclusions (Fig. 3h; *e. g.*, Albinson, 1989; Pérez-Segura et al., 1996; Noriega-Martínez, 2006; Quintanar-Ruíz, 2008; Lang, 2003, in de la Torre-Carlos, 2004, 2009; Pérez-Segura, 2009; Jiménez-Hernández, 2011), This is a very particularly feature and in some way it is helpful to classify these deposits as orogenic gold,

(4) thermobarometric calculations allowed to constrain lithostatic pressure conditions generally between ~1.0 and ~2.2 kbar, which are equivalent to average formation depths between ~3.5 and ~10 km, although there are estimated to be up to 10 km at San Francisco-Estación Llano (Albinson, 1989; Noriega-Martínez, 2006; Lang, 2003, in de la Torre-Carlos, 2004, 2009; Pérez-Segura, 2009), and

(5) stable O and H isotope data of quartz and sericite, respectively, suggest that the quartz veins were derived from a fluid with strong affinity to metamorphic waters, perhaps generated at significant crustal depths (>30 km) due to a process of metamorphic dehydration of water-rich minerals (amphibole) from basement rocks. Mineralizing fluids could have come from deep crustal, likely metamorphic sources (Iriondo and Atkinson, 2000; Quintanar-Ruíz, 2008; Izaguirre and Iriondo, 2014, see Table 2), a characteristic well documented in this type of deposits (e.g., Goldfarb et al., 1991; Robert et al., 2005); also

(6) temperatures of ore formation between 200° to 400 °C (average of 350 °C, see Fig. 5) were obtained along the COGB using O and S stable technique in quartz-sericite and pyrite-galena mineral pairs, respectively (Izaguirre and Iriondo, 2014). Additionally, temperatures of S isotope between 319° to 417 °C at la Herradura Mine were reported (Quintanar-Ruíz, 2008). Furthermore in Santa Gertrudis and Santa Cruz Mixtepec, Oaxaca, temperatures for the quartz veins were obtained using the same S istope technique resulting in a range between 344 and 445 °C (Jiménez-Hernández, 2011).

4. Continuity of the known orogenic gold belts into other regions

The Sonoran orogenic gold deposits can be compared with and continued northwesterly into the state of California, where orogenic gold deposits are conspicuous (Cargo Muchacho, Mesquite and, possibly, Picacho and Copperstone deposits; Branham, 1988). A combination of recent field work, mineral parageneses descriptions and new mineralization ages were used to correlate these deposits in SW Arizona (Cabeza Prieta and Organ Pipe mineralized areas, see Fig. 2) and SE California (American Girl Mine) with the Sonoran occurrences (Izaguirre et al., 2013; Izaguirre and Iriondo, 2014). Also, in recent surveys performed in the central and northern portions of the western coast of the Baja California Peninsula, the Mexican Geological Survey located orogenic gold occurrences with similar mineral parageneses as those described in the Sonoran gold orogenic belt (E. Espinosa-Arámburu, written communication, 2011). A suspect orogenic gold deposit in the northern half of the Baja California Peninsula (state of Baja California) is Los Álamos (Fig. 1 and Fig. 5 in Camprubí, 2013). Such occurrences, plus the El Triunfo-San Antonio, Concordia-Paredones Amarillos, and Los Uvares cluster of deposits (Fig. 1) on the southernmost tip of the Baja California Peninsula, suggest that these deposits might represent the southernmost and westernmost slice of the orogenic belts along the Mexican Pacific margin, which was rifted-off towards the northwest during the opening of the Gulf of California in the latest Miocene. Orogenic gold deposits seemingly exhibit older ages in Baja California than in Sonora, although no further regional structural or metallogenic features can be ventured until orogenic gold deposits are correctly identified elsewhere, and their age patterns are sufficiently well set.

Rather interestingly, Ruiz-Marqués and Núñez-Espinal (1993) mentioned the occurrence of gold anomalies associated with shear zones hosted by metamorphic rock assemblages in the La Michoacana and Agro-Zapotillos prospects in the state of Michoacán, which occur within the Arteaga accretionary-subduction complex (Fig. 7; Camprubí, 2013). Also, besides San Miguel Peras, Santa Gertrudis and Santa Cruz Mixtepec (Sánchez-Rojas et al., 1998; Jiménez-Hernández, 2011), numerous occurrences in the Oaxacan metamorphic complex are likely to constitute examples of orogenic gold deposits, upon their geological descriptions. Such is the case of over 20 veins in Teojomulco, El Parián, Tlazoyaltepec-El Triunfo, San Martín de los Cansecos, Cerro de La Caja in San Pablo Huixtepec, Mina El Careciolo in Tlaxiaco, Mina La Soledad in San Carlos Yautepec, Buena Vista Jaltepec, San Isidro Jaltepetongo, and several occurrences in the Tlacolula district, among several other high-grade gold-bearing quartz veins hosted by metamorphic rocks. In most of these deposits "mesothermal" or "hypothermal" veins were described (Instituto Nacional para la Investigación de Recursos Minerales (INIRM), 1951; Arceo y Cabrilla, 1992, 1995; Jiménez-Hernández, 2011), albeit they were so labeled only through a descriptive approach.

5. Discussion

Orogenic gold deposits are very conspicuous in Sonora, where they form a well-defined belt where deposits started to form during the latest Cretaceous until the Eocene (the Caborca Orogenic Gold Belt; Fig. 2). The deposition of these gold deposits was controlled by shear structures (e.g. thrust faults, mylonites, strike-slip faults, Fig. 6) occurring in a regional NW-SE trend, which continues northwesterly into SW Arizona

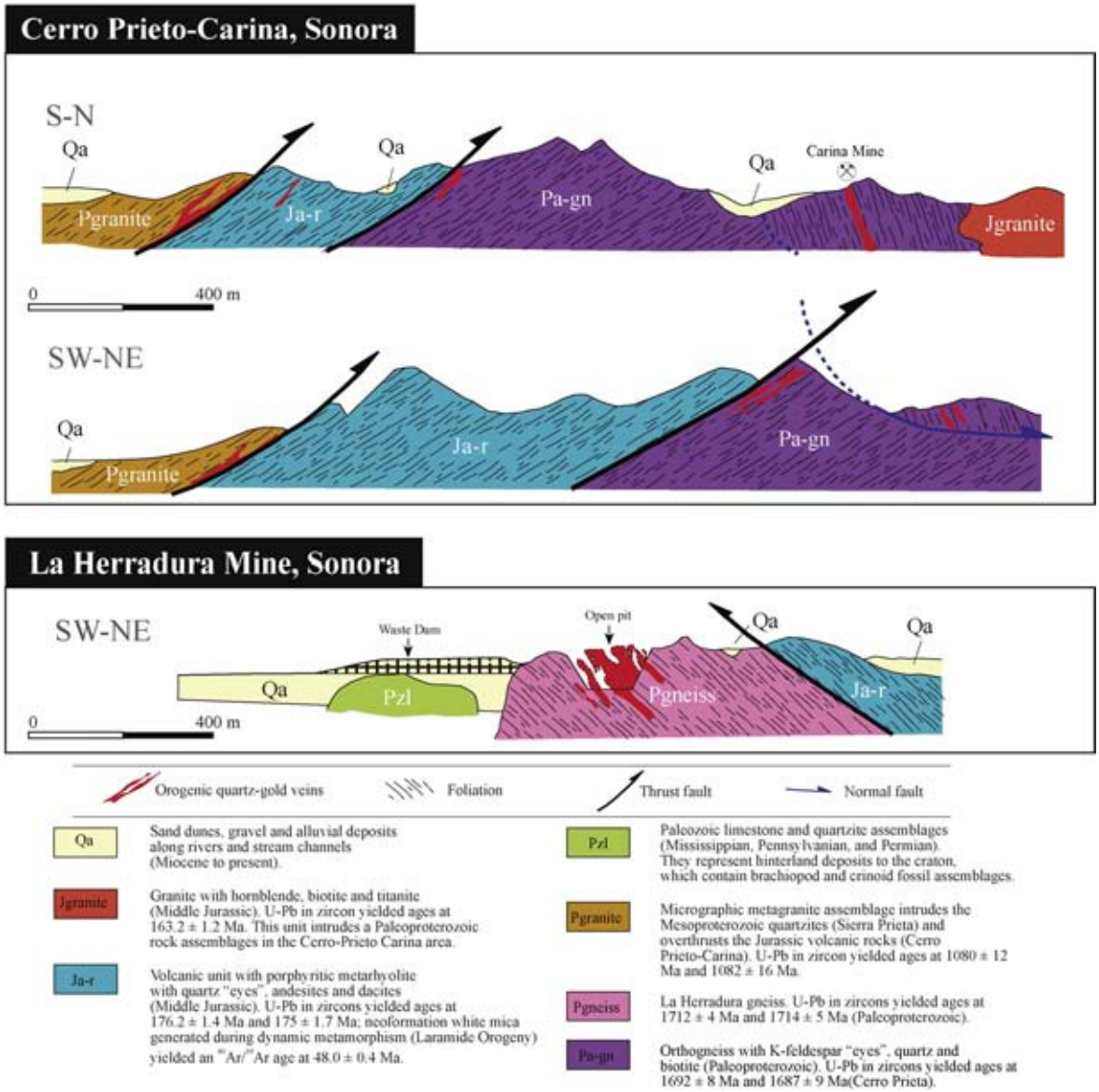

Fig. 6. Representative geologic cross sections along the mineralized zones of the Cerro Prieto-Carina and La Herradura (~6 Moz Au deposit) orogenic gold deposits, both occurring within the Caborca Orogenic Gold Belt, Sonora. Redrawn from de la Torre-Carlos (2004); Izaguirre (2009), and Ornelas-Macías and Verdugo-Noriega (2009). U–Pb zircon ages after Izaguirre (2009).

and SE California (Branham, 1988; Izaguirre et al., 2013; Izaguirre and Iriondo, 2014). The ages of such mineralized areas are comparable with those reported in the Alaskan Ranges, such as Willow Creek, Juneau and Chichagof, and in the Canadian batholiths, such as Bridge River (see Fig. 1; Goldfarb et al., 2008). However, the potential for Cretaceous deposits extends towards the Baja California Peninsula, both within the Peninsular Batholiths and in the Los Cabos Block (northernmost and southernmost regions of the peninsula, respectively). Such interpretation stems from the occurrence of the cataclasite/mylonite related disseminated gold deposit at Los Uvares (Fig. 1) in southernmost Baja California, whose age was constrained at 90–80 Ma (Carrillo-Chávez et al., 1999). Despite the unavailability of microthermometric data for this deposit and the subsequent lack of further diagnostic data for its origin, (1) the close association of this deposit with cataclasites, (2) its disseminated character, and (3) the vaguely zoned sericite-quartz-pyrite ± chlorite ± chalcopyrite alteration assemblages described by Carrillo-Chávez et al. (1999) suggest a close affinity with orogenic gold deposits. Such affinity is rather likelier than the original epithermal model invoked by Carrillo-Chávez et al. (1999), as already indicated by Camprubí (2009, 2013) and Clark and Fitch (2009). The occurrence of the neighboring Concordia-Paredones Amarillos (dated at ~91 Ma, reported by Clark and Fitch, 2009) and the El Triunfo-San Antonio orogenic gold deposits further supports the above interpretation presented (Fig. 7). Known similar deposits, albeit undated and insufficiently characterized, stretch along the Baja California Peninsula.

Besides the stand-alone interesting potential for gold in this region that the deposits mentioned above may represent, they may also constitute the starting point for further exploration southwards. The most prospective regions for orogenic gold deposits would then be those near the present continental edge in the Guerrero composite terrane and in Oaxaca, where regional deformation due to Late Cretaceous, or older, to Paleocene orogenic pulses (either contemporaneous to the Sevier or the Laramide episodes) occurs. In such areas special due attention to shear zones and cataclastic deformation should be paid. Such features are not uncommon in the Guerrero composite terrane or the adjacent terranes, although hitherto the timing and regional significance of the areas in which the above prospective deformation occurs are ill defined. The likeliness of such possibility is underlined by the occurrence of the

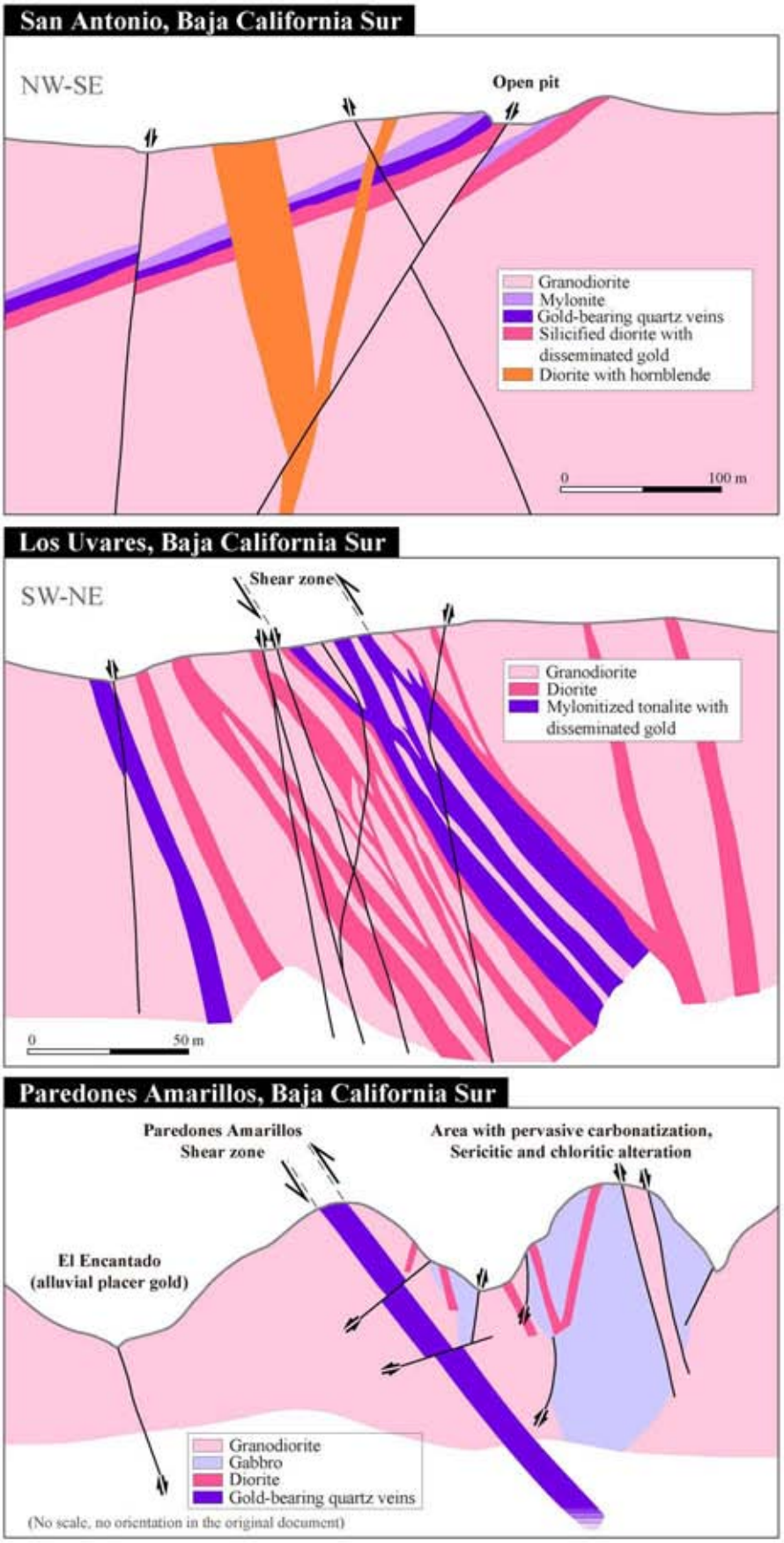

Fig. 7. Representative geologic cross sections along the mineralized zones of the San Antonio, Los Uvares, and Paredones Amarillos orogenic gold deposits, Baja California Sur. Redrawn from Casarrubias-Jiménez and Romero-Rojas (1986); Romero-Rojas (1987), and Palomares-Cortés (1984), respectively.

abovementioned deposits in the Baja California Peninsula within the Los Cabos Block. The latter was split from its 'sister' Jalisco Block in mainland Mexico by the rifting apart of the Californias during the latest Miocene, and the geology of both blocks correlates, by all accounts, until such rifting episode (e.g., Schaaf et al., 2000, and references therein). The occurrence of gold anomalies within shear zones in the Arteaga accretion complex (Fig. 7 in Camprubí, 2013), and several similar occurrences in Oaxaca, can be feasibly interpreted as indicative of the likeliness of the occurrence of orogenic gold deposits in the southern portion of the Guerrero composite terrane, the Xolapa terrane, and older terranes in Oaxaca. In such case, the Teojomulco region in Oaxaca, where over 20 gold-bearing veins have been succinctly described (Arceo y Cabrilla, 1992, 1995), seemingly constitutes an interesting case for exploration.

The Arteaga (southeastern Michoacán) and Oaxacan (western Oaxaca) metamorphic complexes are separated by about 500 km and both occur close to the present Pacific margin, within the western and southern terranes of continental Mexico. Moreover, if we restitute the Los Cabos Block in the southernmost Baja California Peninsula to its original position before the opening of the Gulf of California, it turns out to be located about 500 km northwest of the Arteaga accretion complex. Therefore, provided that similar structural events occurred all along such margin during the Mesozoic and the Cenozoic (Zanchi, 1994; Oskin et al., 2001), it would be likely that a significant portion of southwestern Mexico (at least, the states of Jalisco, Michoacán, Guerrero and Oaxaca) is prospective for orogenic gold deposits. Such region includes most of the western edge of the Guerrero composite terrane, plus the Paleozoic and Proterozoic terranes in Oaxaca.

Further studies concerning orogenic gold deposits in Mexico should also be focused on regional degrees of exhumation (cf., through high-resolution determinations of P-T trajectories of metamorphism, structural analysis, geochronological determinations, microthermometric studies of fluid inclusions, etc., at regional scales) in order to better assess the exploration endeavor. That, especially in the regions where there is an unfathomed potential for this type of ore deposits, such as the Guerrero composite terrane or keen regions in the state of Oaxaca. The polyfacetic studies mentioned above are much desirable, provided that the average depths of formation of known orogenic gold deposits in northwesternmost Sonora generally range between 3.5 and 6.5 km (up to 10 km), after thermobarometric calculations from microthermometric studies of fluid inclusion assemblages (Albinson, 1989; Noriega-Martínez, 2006; Lang, 2003, in de la Torre-Carlos, 2009; Pérez-Segura, 2009). Exhumation in the southern Guerrero composite terrane has been associated by some authors to the displacement of the Chortis block, although such feature is not a necessary requisite for significant regional exhumation of the regional metamorphic rock assemblages (see references and discussion in Pérez-Gutiérrez et al., 2009). The likeliness of exhumation of depth intervals that are favorable for the occurrence orogenic gold deposits in the Guerrero composite terrane is illustrated by an estimated minimum exhumation of ~3.3 km (Lang et al., 1999) for the metamorphic rock assemblage in the Arcelia region (state of Guerrero). The latter was remarkably described to be associated with Sevier orogenic pulses between the Cenomanian and the Campanian (94.4 to 82.8 Ma; K–Ar ages), instead of the typically invoked Laramide orogenic pulses (Lang et al., 1999).

Other estimations for exhumation of Early Cretaceous rock assemblages in the Guerrero composite terrane are the fluid inclusion-based studies of Fitz-Díaz (2004) and Fitz-Díaz et al. (2008), which account for (1) pressures under a lithostatic regime at ~3 kbar (equivalent to a ~ 12 km depth interval) for D1, and between 1.6 and 1.8 (up to 7 km deep) for D2, and (2) pressures under a hydrostatic regime for late veins at 400 bar (equivalent to a >1 km depth interval) for the metamorphic rock assemblage in the Valle de Bravo area (state of México, near the Tizapa-Santa Rosa VMS deposits). Such deformation and exhumation history illustrates a progressive uplift of the metamorphic rock assemblage, albeit no geochronological determinations are yet available for it.

The exhumation case studies mentioned above are not meant to suggest the occurrence of orogenic gold deposits in these particular areas: the intention here is to illustrate the types of studies that may help to constrain the occurrence for such deposits. Approximations of this sort are scarce in the currently available literature, and exhumation of metamorphic rock assemblages varies largely between different areas. Therefore, the dynamics of exhumation constitutes a nearly virgin ground for further research, and hitherto the regional likeliness for orogenic gold deposits in the Guerrero composite terrane remains unassessed, untested and unknown.

6. Conclusions

- Known occurrences of orogenic gold deposits occur in northwestern Sonora, the Baja California Peninsula, and in the Acatlán and Oaxacan metamorphic complexes. Currently available ages for these deposits span from the Late Cretaceous to the Early Cenozoic.
- In Sonora they feature a well-defined belt of deposits associated with metamorphic fluids, which started to form during the latest Cretaceous until the Eocene, in association with rocks of the Paleoproterozoic Yavapai province (North America craton).
- Several deposits in the Baja California Peninsula still lack geochronological data, and they may constitute the southward stretching of the Sonoran belt (once the Baja California Peninsula is restituted to its original pre-rifting position). Orogenic gold deposits in the northern part of Baja California may represent the stretching westwards of the Sonoran deposits. The Cretaceous Los Uvares, El Triunfo-San Antonio and Concordia-Paredones Amarillos deposits in southernmost Baja California are seemingly older than the Sonoran deposits, which suggests a more intrincated time pattern than it can be drawn from the latter. Also, it is likely that there is a continuity between the orogenic gold deposits in the Los Cabos Block of the Baja California Peninsula and those in the Guerrero composite terrane and Oaxaca, besides the potential for them in the Baja California Peninsula alone, but no correlation can be reasonably established so far between the Sonoran deposits and those in southernmost Baja California.
- Further exploration in the regions mentioned above should pay attention to cataclasitic or mylonitic deformation and prominent shear zones. Also, regional studies concerning the extent and timing of crustal exhumation would be particularly helpful in order to evaluate the occurrence and distribution of depth segments that are prospective for orogenic gold deposits.

Acknowledgments

Financial support for this paper was obtained through the CONACYT (grants 82518 and 129370 to A. Iriondo and grant 155662 to A. Camprubí) and PAPIIT-UNAM research programs (grant IN116709 to A. Iriondo). Additional funding was received from internal annual research budgets of the Instituto de Geología and the Centro de Geociencias (UNAM). A. Izaguirre obtained a doctoral student grant and A. Iriondo a sabbatical fellowship (147409) to visit the University of Texas at Austin, both funded by CONACYT. Enrique Espinosa-Arámburu is thanked for his fruitful comments about the current surveys concerning orogenic gold deposits in the Baja California Peninsula that are being carried out by the Servicio Geológico Mexicano. Efrén Pérez Segura kindly provided some of the pictures displayed in this paper. Finally, we are grateful to the editor José María González and the reviewers of this manuscript Daniel Moncada, Ignacio Subías and Lucas Ochoa, they helped improve the quality of the manuscript.

References

Alaniz-Álvarez, S.A., Nieto-Samaniego, A.F., 1997. Representación grÁfica de los dominios de ruptura y deslizamiento-aplicación de la falla de Oaxaca, México. Rev. Mex. Cienc. Geol. 14, 26–37.

Alaníz-Álvarez, S.A., Van der Heyden, P., Nieto-Samaniego, A.F., Ortega-Gutiérrez, F., 1996. Radiometric and kinematics evidence for Middle Jurassic strike-slip faulting in southern Mexico related to the opening of the Gulf of Mexico. Geology 24, 443–446.

Albinson, T., 1989. Vetas mesotermales auríferas del sector Norte del Estado de Sonora. Memorias técnicas, XVIII convención Nacional AIMMGM, Acapulco, Guerrero, México, asociación de ingenieros de minas. Metal. Geól. Méx. 20–40.

Araiza-Martínez, H., 1998. Geology and mineralization of the San Francisco gold deposit. In: Clark, K.F. (Ed.), Gold Deposits of Northern Sonora, México, Society of Economic Geologists Guidebook Series. 30, pp. 49–58.

Araux-Sánchez, E., 2000, Geología y Yacimientos Minerales de la Sierra Pinta, Municipio de Puerto Peñasco, Sonora. Unpublished MSc Dissertation, Departamento de Geología, Universidad de Sonora, Hermosillo, Sonora, Mexico, 121 p.

Araux-Sánchez, E., Vega-Granillo, R., Enríquez-Minjárez, E., 2001. Características Geológicas de un Yacimiento Mesotermal Asociado a Zonas de Cizalla en el Noroeste de Sonora. In: Corona-Esquivel, R., Gómez-Godoy, J. (Eds.), Asociación de Ingenieros de Minas, Metalurgistas y Geólogos de México A.C., XXIV Convención Minera, Acapulco, Guerrero, pp. 25–32.

Arceo y Cabrilla, F.A., 1992, Yacimientos de Oro del Distrito Minero de Teojomulco, Estado de Oaxaca. Unpublished report, Consejo de Recursos Minerales, Subgerencia Regional Zona Sur, Residencia Oaxaca, 12 pp.

Arceo y Cabrilla, F.A., 1995, Panorama General de la Minería en el Estado de Oaxaca. Unpublished report, Consejo de Recursos Minerales, Oficina Regional Oaxaca, 71 pp.

Bierlein, F.P., Groves, D.I., Cawood, P.A., 2009. Metallogeny of accretionary orogens–the connection between lithospheric processes and metal endowment. Ore Geol. Rev. 36, 282–292.

Branham, A.D., 1988, Gold mineralization in low angle faults American Girl Valley, Cargo Muchacho Mountains, California. Unpublished MSc Dissertation, Department of Geology, Washington State University, Pullman, Washington, USA, 144 p.

Camprubí, A., 2009. Major metallogenic provinces and epochs of Mexico. SGA News 25, 1–20.

Camprubí, A., 2013. Tectonic and Metallogenic History of Mexico. In: Colpron, M., Bissig, T., Rusk, B.G., Thompson, J.F.H. (Eds.), Tectonics, Metallogeny, and Discovery: The North American Cordillera and Similar Accretionary Settings. Soc. Econ. Geol. Spec. Pub. 17, pp. 201–243.

Carrillo-Chávez, A., 1996, Environmental Geochemistry of the San Antonio-El Triunfo Mining Area, Southernmost Baja California Peninsula, Mexico. Unpublished PhD dissertation, University of Wyoming, Laramie, Wyoming, USA, 130 p.

Carrillo-Chávez, A., Huyck, H., Zentilli, M., Griest, A., 1999. Age constraints on host rocks of Los uvares gold deposit: magmatic pulses in southernmost Baja California, Mexico. Geofis. Int. 38, 27–33.

Casarrubias-Jiménez, J.S., and Romero-Rojas, S.A., 1986, Informe Geológico Minero y Evaluativo del Tajo San Antonio Ubicado en la Reserva Minera Nacional La Perla, Municipio de La Paz, Estado de Baja California Sur. Unpublished report, Consejo de Recursos Minerales, Subgerencia Regional Zona Noroeste, Residencia Baja California Sur, 71 p.

Cendejas-Cruz, F., Aldana-Hernández, M., 2008. Monografía Geológico-Minera del Estado de Baja California Sur, Edición 2008. Servicio Geológico Mexicano (411 pp.).

Changkuon, L., 1990, Genesis of Gold Mineralization: San Francisco Mine, Sonora, Mexico. Unpublished MSc Dissertation, New Mexico Institute of Mining and Technology, Socorro, New Mexico, USA, 129 p.

Clark, K.F., Fitch, D.C., 2009. Evolución de depósitos metálicos en tiempo y espacio en México. In: Clark, K.F., Salas-Pizá, G., Cubillas-Estrada, R. (Eds.), Geología económica de México, 2nd edition Servicio Geológico Mexicano—Asociación de Ingenieros de Minas, Metalurgistas y Geólogos de México, pp. 62–133.

Durgin, D.C., Terán, P.I., 1996. La Choya Au Deposit, NW Sonora, Mexico. In: Coyner, A.R., Fahey, P.L. (Eds.), Geology and Ore Deposits of the American Cordillera, Geological Society of Nevada Symposium, Proceedings, Reno/Sparks, Nevada, pp. 1369–1373.

Fitz-Díaz, E., 2004, Historia de deformación de las rocas metasedimentarias cretÁcicas de Valle de Bravo, Edo. de México, y resultados preliminares de microtermometría de la deformación. Unpublished MSc dissertation, Programa de Posgrado en Ciencias de la Tierra, Universidad Nacional Autónoma de México, Distrito Federal, Mexico, 92 p.

Fitz-Díaz, E., Tolson, G., Camprubí, A., Rubio-Ramos, M.A., Prol-Ledesma, R.M., 2008. Deformación, vetas, inclusiones fluidas y la evolución tectónica de las rocas cretÁcicas de Valle de bravo, Estado de México, México. Rev. Mex. Cienc. Geol. 25, 59–81.

Goldfarb, R.J., Hart, C.J., Marsh, E.E., 2008. Orogenic gold and evolution of the cordilleran origen. In: Spencer, J.E., Titley, S.R. (Eds.), Ores and Orogenesis: Circum-Pacific Tectonics, Geologic Evolution, and ore Deposits, Arizona Geological Society Digest. 22, pp. 311–323.

Goldfarb, R.J., Newberry, R.J., Pickthorn, W.J., Gent, C.A., 1991. Oxygen, hydrogen, and sulfur isotope studies in the Juneau gold belt, Southeastern Alaska: constrains on the origin of hydrothermal fluids. Econ. Geol. 86, 66–80.

Goldfarb, R.J., Baker, T., Dubé, B., Groves, D.I., Hart, C.J.R., Gosselin, P., 2005. Distribution, Character, and Genesis of Gold deposits in metamorphic terranes. Econ. Geol. 100, 407–450.

Groves, D.I., Goldfarb, R.J., Grebre-Meriam, M., Hagemann, S.G., Robert, F., 1998. Orogenic gold deposits: a proposed classification in the context of their crustal distribution and relationship to other gold deposit types. Ore Geol. Rev. 13, 7–27.

Instituto Nacional para la Investigación de Recursos Minerales (INIRM), 1951, Yacimientos de Minerales Metálicos, Estado de Oaxaca. Unpublished Report, Instituto Nacional para la Investigación de Recursos Minerales, 81 p.

Iriondo, A., 2001, Proterozoic basements and their Laramide juxtaposition in NW Sonora, México: Tectonic constraints on the SW margin of Laurentia. Unpublished PhD Dissertation, Department of Geological Sciences, University of Colorado, Boulder, Colorado, USA, 222 p.

Iriondo, A., Atkinson Jr., W.W., 2000. Orogenic gold mineralization along the proposed trace of the Mojave-Sonora megashear: evidence for the laramide orogeny in NW Sonora, México. Geol. Soc. Am. Abstr. Programs 32, 393.

Iriondo, A., Premo, W.R., 2011. Las Rocas Cristalinas Proterozoicas de Sonora y su Importancia Para la Reconstrucción del Margen Continental SW de Laurencia–la Pieza Mexicana del Rompecabezas de Rodinia. In: Calmus, T. (Ed.), Panorama Sobre la Geología de Sonora, México 118. Universidad Nacional Autónoma de México, Instituto de Geología, Boletín, pp. 25–55.

Izaguirre, A., 2009, El basamento Paleoproterozoico (~1.71–1.68 Ga) Yavapai en el área Mina La Herradura en el NW de Sonora: sus implicaciones para el desarrollo del margen magmático continental Mesozoico-Cenozoico del NW de México. Unpublished MSc Dissertation, Programa de Posgrado en Ciencias de la Tierra, Universidad Nacional Autónoma de México, Juriquilla, Querétaro, México, 201 pp.

Izaguirre, A., Iriondo, A., 2014. A metamorphic origin for the hydrothermal fluids forming the gold-bearing quartz veins from the laramide caborca orogenic gold belt of NW Sonora: an oxygen, hydrogen and sulfur isotopic study: GEOS. Unión Geofís. Mex. 34, 334.

Izaguirre, A., Iriondo, A., Caballero-Martínez, J.A., Moreira-Rivera, F., Espinosa-Arámburu, E., 2012. Homogeneidad geoquímica de la alteración hidrotermal del cinturón de oro orogénico del NW de Sonora, México: estudio de balance de masas en rocas encajonantes de la mineralización. Bol. Soc. Geol. Mex. 64, 119–153.

Izaguirre, A., Iriondo, A., Kunk, M., McAleer, R., 2013. Mineralización orogénica larámide en el NW de Sonora: Una complicación adicional para la controvertida megacizalla Mojave-Sonora: GEOS. Unión Geofís. Mex. 33, 170.

Jiménez-Hernández, A., 2011, Mineralización de oro en el Complejo Oaxaqueño, sur de México. Unpublished MSc Dissertation, Universidad de Chile, Santiago de Chile, Chile, 95 pp.

Lang, J.R., 2003. Fluid Inclusion Study of the La Herradura Deposit Caborca, Sonora, Mexico: Petrography and microthermometry results. Report prepared for Minera Penmont S.A (29 pp.).

Lang, H.R., Cabral-Cano, E., Jansma, P.E., Johnson, C.A., 1999. K/Ar ages from the Guerrero transect date four thermotectonic events affecting the North America plate in Mexico from 301 Ma to 29 Ma. NASA Technical Report (39 pp.).

Marsh, E.E., Goldfarb, R.J., Kunk, M.J., Groves, D.I., Bierlein, F.P., Creaser, R.A., 2008. New constraints on the timing of gold formation in the Sierra Foothills province, central California. In: Spencer, J.E., Titley, S.R. (Eds.), Ores and orogenesis: Circum-Pacific tectonics, geologic evolution, and ore deposits. Arizona Geological Society Digest 22, pp. 369–388.

Noriega-Martínez, O., 2006, Evidencias de dos Etapas de Mineralización de oro Mesotermal en las Áreas de Tajitos, Juárez-San Francisco, en la Región de Caborca, Sonora México. Unpublished MSc Dissertation, Departamento de Geología, Universidad de Sonora, Hermosillo, Sonora, México, 85 pp.

Ornelas-Macías, A., and Verdugo-Noriega, G., 2009, Caracterización Geológica, Estructural y de Mineralización en el Área Karina, Municipio de Caborca, Sonora, México. Unpublished BSc Dissertation Departamento de Geología, Universidad de Sonora, Hermosillo, Sonora, México, 110 p.

Oskin, M., Stock, J., Martín-Barajas, A., 2001. Rapid localization of Pacific–North America plate motion in the Gulf of California. Geology 29, 459–462.

Palomares-Cortés, L., 1984, Visita de Reconocimiento a el Lote Minero "Extensión de Paredones Amarillos", San Antonio, Municipio de La Paz, Baja California Sur. Unpublished report, Consejo de Recursos Minerales, Subgerencia Regional Zona Noroeste, Residencia Baja California Sur, 25 pp.

Pérez-Gutiérrez, R., Solari, L.A., Gómez-Tuena, A., Martens, U., 2009. Mesozoic geologic evolution of the xolapa migmatitic complex north of Acapulco, southern Mexico: implications for paleogeographic reconstructions. Rev. Mex. Cienc. Geol. 26, 201–221.

Pérez-Segura, E., 1993. Los Yacimientos de oro y Plata de Sonora, México y sus Relaciones con la Geología Regional. In: Delgado-Argote, L.A., Barajas, M. (Eds.), Contribuciones a la Tectónica del Occidente de México. Unión Geofísica Mexicana, Monografía. 1, pp. 147–174.

Pérez-Segura, E., 2009. Geología y mineralización de la mina de oro de San Francisco, en la provincia del desierto de Sonora, México. In: Clark, K.F., Salas-Pizá, G., Cubillas-Estrada, R. (Eds.), Geología económica de México, 2ª edición, Servicio Geológico Mexicano—Asociación de Ingenieros de Minas. Metalurgistas y Geólogos de México, pp. 875–881.

Pérez-Segura, E., Cheilletz, A., Herrera-Urbina, S., Hanes, Y.J., 1996. Geología, mineralización, alteración hidrotermal y edad del yacimiento de oro de San Francisco, Sonora–Un depósito mesotermal en el noroeste de México. Rev. Mex. Cienc. Geol. 13, 65–89.

Poulsen, K.H., Mortensen, J.K., Walford, P.C., 2008. San Francisco gold deposit, Santa Ana region, Sonora, Mexico. Laramide orogenic, intrusion-related mineralization? In: Spencer, J.E., Titley, S.R. (Eds.), Ores and Orogenesis: Circum-Pacific Tectonics, Geologic Evolution, and ore Deposits, Arizona Geological Society Digest. 22, pp. 547–559

Quintanar-Ruíz, F.J., 2008, La Herradura ore Deposit: An Orogenic Gold Deposit in Northwestern Mexico. Unpublished MSc Dissertation, University of Arizona, Tucson, Arizona, USA, 97 pp.

Radelli, L., Pérez-Segura, E., 1992. The gold placer of El Boludo Northern Sonora. Mexico: Boletín del Departamento de Geología de la Universidad de Sonora 9(1), pp. 63–80.

Robert, F., Poulsen, K.H., Cassidy, K.F., Hodgson, C.J., 2005. Gold metallogeny of the superior and yilgarn cratons. In: Hedenquist, J.W., Thompson, J.F.H., Goldfarb, R.J., Richards, J.P. (Eds.), Economic Geology 100th Anniversary Volume, pp. 1001–1033.

Romero-Rojas, S.A., 1987, Informe geológico minero-evaluativo del sector los Uvares, (Reserva Minera Nacional El Triunfo), subdelegación El Rosario, municipio de La Paz, B.C.S. Unpublished report, Consejo de Recursos Minerales, Subgerencia Regional Zona Noroeste, Residencia Baja California Sur, 63 p.

Ruiz-Marqués, A., Núñez-Espinal, J., 1993, Informe final por áreas, proyecto zona costa de Michoacán. Unpublished report, Consejo de Recursos Minerales, Gerencia Regional Zona Centro, Residencia Michoacán, 115 p.

SÁnchez-Rojas, L.E., Aranda-Osorio, J.N., Castro-Rodríguez, M.G., ZÁrate-López, J., ZÁrate-Barradas, G.R., 1998, Informe geológico-minero y geoquímico carta Zaachila, Escala 1:250,000. Unpublished report, Consejo de Recursos Minerales, 50 p.

Schaaf, P., Böhnel, H., Pérez-Venzor, J.A., 2000. Pre-Miocene palaeogeography of the Los Cabos block, Baja California Sur: geochronological and palaeomagnetic constraints. Tectonophysics 318, 53–69.

Silberman, M.L., Giles, D.A., Graubard, C., 1988. Characteristics of gold deposits in northern Sonora, Mexico. A preliminary report. Econ. Geol. 83, 1966–1974.

Silberman, M.L., Staude, J.M., Cox, D.P., 1987. Reconnaissance of gold prospects in northern Sonora, Mexico. U.S. Geological Survey, Administrative Report (23 pp.).

Solari, L., 2001, La Porción Norte del Complejo Oaxaqueño, Estado de Oaxaca: Estructuras, Geocronología y Tectónica. Unpublished PhD Dissertation, Programa de Posgrado en Ciencias de la Tierra, Universidad Nacional Autónoma de México, México D.F., 192 p.

Solari, L.A., Keppie, J.D., Ortega-Gutiérrez, F., 2004. Phanerozoic structures in the grenvillian northern oaxacan complex, southern Mexico: result of thick-skinned tectonics. Int. Geol. Rev. 46, 1–15.

de la Torre-Carlos, J., 2004. Geología del yacimiento mina La herradura. Proceedings VI Seminario Minero Internacional Sonora 2004 (8 pp.).

de la Torre-Carlos, J., 2009. Geología del yacimiento mina La herradura. In: Clark, K.F., Salas-Pizá, G., Cubillas-Estrada, R. (Eds.), Geología económica de México, 2ª edición Servicio Geológico Mexicano – Asociación de Ingenieros de Minas, Metalurgistas y Geólogos de México, pp. 844–851.

Zanchi, A., 1994. The opening of the Gulf of California near Loreto, Baja California, Mexico: from basin and range extension to transtensional tectonics. J. Struct. Geol. 16, 1619–1639.

Capítulo 6. Encuadre tectónico de la mineralización aurífera del COGB

Encuadre tectónico de la mineralización Cretácico tardío-eocena de vetas de cuarzo-oro del cinturón de oro orogénico Caborca en el Noroeste de México (*Tectonic framework for Late Cretaceous to Eocene quartz-gold vein mineralization from the Caborca orogenic gold belt in northwestern Mexico*) aceptado: Economic Geology (2017). Autores: Aldo Izaguirre, Alexander Iriondo, Michael J. Kunk, Ryan J. McAleer, William W. Atkinson Jr., Luis M. Martínez-Torres.

• Objetivos: Lograr un encuadre tectónico útil para encontrar el origen del oro orogénico del COGB (Izaguirre *et al*., en prensa).

• Estudios: Utilizando la combinación de resultados de los estudios anteriores y empleando el conocimiento geológico de la región se elaboró un modelo de encuadre tectónico que propone una explicación al origen del COGB.

View Letter

Close

Date: Mar 21 2017 2:36PM
To: "Aldo Izaguirre" aldoizapo@gmail.com
From: "Economic Geology" econgeol@segweb.org
Subject: Your Submission

Ref.: Ms. No. SEG-D-16-00163R2

Dear Aldo,

I am pleased to inform you that your manuscript entitled Tectonic framework for Late Cretaceous to Eocene quartz-gold vein mineralization from the Caborca orogenic gold belt in northwestern Mexico has been accepted for publication in Economic Geology. Please send all Figures, Text, and Tables in their original format (e.g., Illustrator, CorelDraw, Word, Excel etc.) to the production editor, Alice Bouley (alicebouley@segweb.org); large files can be uploaded to the ftp site (ftp://ftp.segweb.org, username: seguser; password: publish): contact alicebouley@segweb.org to confirm any ftp upload. You will hear directly from the publications editor regarding page proofs, etc.

Thank you for your hard work in making this an excellent contribution to Economic Geology.

Sincerely,

Larry Meinert
Editor - Economic Geology

Close

Manuscript
Click here to download Manuscript Manuscript Izaguirre et al. March 19.pdf

Tectonic framework for Late Cretaceous to Eocene quartz-gold vein mineralization from the Caborca orogenic gold belt in northwestern Mexico

Aldo Izaguirre
Centro de Geociencias, Universidad Nacional Autónoma de México, Campus Juriquilla, Boulevard Juriquilla 3001, Juriquilla, 76230, Querétaro, México
Universidad Autónoma de Ciudad Juárez, Departamento de Ingeniería Civil y Ambiental Instituto de Ingeniería y Tecnología, Av. del Charro 450, 32310, Cd. Juárez, Chihuahua, México

Alexander Iriondo
Centro de Geociencias, Universidad Nacional Autónoma de México, Campus Juriquilla, Boulevard Juriquilla 3001, Juriquilla, 76230, Querétaro, México

Michael J. Kunk and Ryan J. McAleer
U.S. Geological Survey, Mail Stop 926A, National Center, Reston, 20192, Virginia, USA

William W. Atkinson Jr.
Department of Geological Sciences, University of Colorado at Boulder, Boulder, 80309, Colorado, USA
Department of Geology and Geology Museum, Colorado School of Mines, Golden, 80401, Colorado, USA

Luis M. Martínez-Torres
Departamento de Geodinámica, Universidad del País Vasco, Apartado 644, E-48080 Bilbao, Spain

e-mail corresponding author: aldoizapo@gmail.com, aldo.izaguirre@uacj.mx

Abstract

The Caborca orogenic gold belt (COGB) is a large gold metallogenic province located in the North American Cordillera that hosts orogenic gold-bearing quartz veins and extends from northwestern Mexico into southwestern United States. The COGB includes a number of deposits currently in production (e.g., La Herradura, San Francisco-Llano, El Chanate, Soledad-Dipolos, and Noche Buena) that combined contain gold reserves and resources over 10 million ounces.

Extensive new $^{40}Ar/^{39}Ar$ geochronology of white micas associated with gold-bearing quartz veins along the COGB suggests that mineralization developed rapidly after ~69 Ma, peaked at ~61 Ma and decreased more slowly from 58 to 36 Ma, when it ceased. Triggering of mineralization is closely related to an increase in the rate of convergence and the subsequent shallowing of the subducted Farallon slab that resulted in rapid eastward migration of the magmatic arc toward the continent during the Late Cretaceous-Eocene Laramide orogeny. Mineralization within the COGB formed contemporaneously with some other orogenic gold deposits along the North American Cordillera, including districts in Alaska (e.g., Chichagof, Juneau, and Port Wells) and Canada (e.g., Bridge River).

After a process of crustal shortening/thickening during the early compressive stage (~90–70 Ma) of the Laramide orogeny, also a time for generation of mineralizing fluids, a process of synconvergent crustal extension started at ~70 Ma and affected the Cordillera forearc region in northwestern Mexico as a response to the flat subduction and the eastward Laramide arc migration. This Laramide synconvergent extension produce a marked cooling of the thinned crust which in turn generated regional brittle conditions that facilitated the ascent and precipitation of metal-laden metamorphic fluids that formed the quartz-gold vein mineralization along the COGB.

Another consequence of the eastward arc migration during the Laramide orogeny was the generation of contemporaneous Late Cretaceous-Eocene Cu-Mo porphyry deposits in northwestern Mexico and southwestern United States. In this scenario, orogenic gold deposits would have formed in the amagmatic forearc region, whereas the porphyries were generated further to the east in the magmatic arc region.

In this mineralization model, we interpret that the COGB area was more uplifted, and suffered higher degrees of denudation (veins formed at depths of ~4–6 km), than the region of Cu-Mo porphyries that formed at shallower crustal depths (~1–2 km). In other words, both coeval mineral belts were exposed next to each other even though they represent very different crustal levels. This crustal level disparity could be explained by a period of intense Eocene to Oligocene tectonic/crustal denudation that preferentially affected the previously over thickened forearc region. Perhaps due to isostatic rebound, at least 4–6 km of crustal material from the forearc region were removed until the final exhumation of the COGB veins occurred, most likely, by the Oligocene.

Soon after this period of intense crustal denudation, Oligocene-Miocene epithermal mineralization overprinted both the COGB and the porphyry Cu-Mo belt. In addition, supergene alteration of hypogene orogenic mineralization, and supergene enrichment of the porphyry deposits (enriched layers of secondary copper minerals), increased mineral concentrations due to groundwater level fluctuations (oxidation-reduction cycles) in an arid desert environment that prevailed since the Miocene. The combination of all these tectonic and climatic factors makes northwestern Mexico a unique and attractive place in the North American Cordillera to undertake mineral exploration endeavours.

Introduction

The Caborca orogenic gold belt (COGB) is a gold metallogenic province located in the North American Cordillera that hosts orogenic gold-bearing quartz veins and extends from northwestern Mexico into southwestern United States (Izaguirre et al., 2017; Fig. 1A). The COGB is more than 600 km long, 60–80 km wide (Fig. 1B), and contains a number of deposits currently in production (e.g., La Herradura, San Francisco-Llano, El Chanate, Soledad-Dipolos, and Noche Buena). The majority of the mines are open pits, although some are small underground operations. The mines in operation contain combined gold reserves and resources of more than 10 million ounces (Izaguirre et al., 2017), but this figure could be double (~22 million ounces) with current exploration surveys.

In this article, we present the results of $^{40}Ar/^{39}Ar$ dating of hydrothermal white mica (flakes and sericite) deposited together with quartz and gold within the COGB (Table 1). The 63 samples dated in this study define an extended period of mineralization between ~69 and 36 Ma that was associated with a regional-scale orogenic hydrothermal mineralization event (Figs. 1B and 2). The aim of this study is to determine the overall timing of deposition, and the spatial-temporal relations of the COGB mineralization occurrences. Another goal is to present a tectonic model for the gold mineralization that occurred during the Late Cretaceous to Eocene Laramide orogeny (~90–40 Ma).

On the basis of our new $^{40}Ar/^{39}Ar$ geochronological data, we propose a coherent tectonic framework for the COGB which is consistent with several regional geologic observations including: (1) the orogenic gold-bearing quartz veins are located solely in the cordillera Laramide forearc; (2) the age of mineralization decreases slightly moving eastward indicating an overall younging to the east-northeast; (3) there is a magmatic gap in the COGB area during the

time of mineralization; (4) the orogenic mineralization within the COGB was contemporaneous with the formation of the porphyry copper-molybdenum belt oriented parallel to the COGB (Fig. 1B); and (5) the orogenic mineralization formed contemporaneously with a decrease in the subduction angle of the Farallon plate, which evolved from a high-angle subduction to a sub-horizontal one during the Laramide orogeny (Coney and Reynolds, 1977; Dickinson and Snyder, 1978; Usui et al., 2003).

Our new geochronologic results also indicate that mineralization within the COGB formed contemporaneously with some other orogenic gold deposits along the North American Cordillera (Fig. 1A), including districts of Alaska (e.g., Chichagof, Juneau, and Port Wells; Goldfarb et al., 1991, 1997; Adams et al., 1992; Miller et al., 1994; Taylor et al., 1994; Hauessler et al., 1995; Selby et al., 2002) and Canada (e.g., Bridge River; Hart et al., 2008). This age correlation suggests that similar tectonic conditions could have prevailed in different segments of the North American Cordillera, all of which are associated with the formation of orogenic Au mineralization.

Geological setting of the COGB mineralization

Previous geochronological studies

Previous geochronological research on the orogenic gold deposits present in northwestern Sonora have focused on a few individual ore deposits rather than taking a regional perspective (Table A1). These studies used K-Ar and $^{40}Ar/^{39}Ar$ analyses of hydrothermal white mica collected in mines and/or mining districts, including Tajítos (Pérez-Segura, 1993), San Francisco-Llano (Pérez-Segura et al., 1996), La Pinta (Araux-Sánchez et al., 2001), and Quitovac (Iriondo and Atkinson, 2000; Iriondo, 2001). These data are supplemented by Re-Os

geochronology of pyrite and magnetite in samples from the world-class La Herradura deposit (Quintanar-Ruíz, 2008; see Table A1 and Fig. 1B). All of the geochronologic data yield ages of mineralization between ~69 and 41 Ma. However, the areas sampled by these previous studies are very small and is not representative of the entire COGB.

Host rocks

The mineralization in the study area is hosted by a large variety of lithologies with various ages. Gold-bearing quartz veins within the COGB are commonly hosted by igneous and metamorphic basement rocks (green schist-low amphibolite facies) of northwestern Sonora. These rocks are dominated by orthogneiss, paragneiss, banded gneiss, schist, and meta-granite units that formed during the Paleoproterozoic (~1800–1600 Ma) and Mesoproterozoic plutonic rocks that intruded them at ~1400 and ~1100 Ma (Damon et al., 1961; Anderson and Silver, 1979, 2005; Iriondo et al., 2004; Nourse et al., 2005; Arvizu-Gutiérrez, 2008; Iriondo and Premo, 2011). Less abundant are veins hosted by Neoproterozoic and Paleozoic calcareous platform and basinal units (Stewart, 1988; Dickinson and Lawton, 2001; Poole et al., 2005). Gold-bearing veins are also found in Jurassic and Cretaceous clastic and calcareous rocks (González-León, 1994; Dickinson and Lawton, 2001). Regionally, quartz veins of the COGB are also abundant in outcropping granites, volcanic and volcaniclastic rocks, gneisses and schists that formed along the active Cordilleran margin apparently intermittently from the Permian to the Paleocene (Tosdal et al., 1989; McDowell et al., 2001; Arvizu et al., 2009; Mauel et al., 2011; Rodríguez-Castañeda and Anderson, 2011; Valencia-Moreno and Ortega-Rivera, 2011).

The rocks we consider to be post-mineralization are principally Oligocene-Miocene lavas and pyroclastic rocks, and Pliocene-Quaternary basalt flows (Fig. 2; Gans, 1997; McDowell et

al., 1997; Grijalva-Noriega and Roldán-Quintana, 1998; Vidal-Solano et al., 2008). The region also contains significant volumes of post-mineralization sedimentary rocks filling intermontane basins. These sediments were formed by the erosion of uplifted blocks during the late extension of the Basin-and-Range event in the Late Cenozoic (Stewart and Roldán-Quintana, 1994; Henry and Aranda-Gómez, 2000). However, it is worth mentioning that these basins host historic and actively mined placer gold deposits (e.g., El Boludo Mine, Tajitos; Fig. 1B) that were likely sourced by orogenic gold quartz veins of the COGB (e.g., Wilson et al., 2009).

Structural control of the gold mineralization

The prevailing structural model for the COGB is that mineralization is associated with the hypothetical Mojave-Sonora Megashear (hMSM) and associated faults (Fig. 3; Anderson and Silver, 1979, 2005; Campbell and Anderson, 2003), a model that has become the most influential among mining companies and exploration geologists (Silberman et al., 1988; Quintanar-Ruíz, 2008; De la Torre-Carlos, 2009). The hMSM is supposed to have accommodated a sinistral displacement of ~800–1000 km during the Late Jurassic, and has been used to interpret the origin and location of mineralization along a northwest-southeast axis within the study area. This fault would have affected Paleoproterozoic crystalline basement and overlying supracrustal rocks. Numerous studies, however, question its existence principally because the majority of deformation in the region did not occur during the Jurassic (Molina-Garza and Geissman, 1999; Iriondo et al., 2004; Poole et al., 2005; Iriondo and Premo, 2011; Izaguirre et al., 2013; Jacques-Ayala and García-Barragán, 2014). The hMSM, however, continues to be a controversial and contentious issue in Sonoran geology.

Another genetic model for the COGB is that the mineralization was controlled by low-angle shear zones, thrusting, and schistose bands of Laramide age, and by the reactivation of ancient zones during the Laramide orogeny (Iriondo and Atkinson, 2000; Iriondo et al., 2005; Poulsen et al., 2008; Nourse and Irwin, 2010; Izaguirre et al., 2017). The quartz veins are commonly hosted by Precambrian metamorphic and igneous basement rocks located in a belt known as the Paleoproterozoic Yavapai Province (Fig. 3). This belt includes Paleoproterozoic crustal rocks that record a high degree of structural weakening and likely acted as preferential conduits for channeling fluids through the crust, including the hydrothermal fluids that formed the orogenic gold veins within the COGB (Iriondo and Premo, 2011).

Characteristics of orogenic gold veins

The general characteristics of orogenic veins within the COGB are similar to those of orogenic gold deposits worldwide (Table 2; Groves et al., 1998; Goldfarb et al., 2005, 2008; Goldfarb and Groves, 2015). Typical massive hydrothermal quartz veins within the COGB contain megascopic calcium-iron carbonate minerals (mostly calcite, siderite, and ankerite), white mica (sericite and locally larger crystals of muscovite), pyrite, galena, and native gold (Fig. 4), as well as significant microscopic inclusions of sphalerite, covellite, tourmaline, scheelite, and Au-Ag tellurides in quartz and pyrite (Pérez-Segura, 2009; Izaguirre et al., 2012). The hydrothermal fluids that passed through the host rocks led to intense alteration within stockwork areas but alteration is less pervasive in areas hosting single veins. This alteration consists of silicification, carbonatization, sericitization, pyritization and chloritization, as well as hydrothermally altered areas throughout the belt that are enriched in K, W, Cu, Pb, Mo, Zn, Sb, Ag, Si, Se, Ni, Fe, As, and Th, and unusual elements like Tl, Be, V, and Sn (Izaguirre et al.,

2012). Most of these enriched elements demonstrate a good correlation between alteration zones and the paragenesis of minerals within the ore deposits (Izaguirre et al., 2012). Thermometric studies of fluid inclusions in quartz, and stable isotope analysis of mineral pairs in the veins, indicate formation temperatures of ~260°C to ~370°C (mean ~330°C; Albinson, 1989; Pérez-Segura et al., 1996; Araux-Sánchez et al., 2001; Noriega-Martínez, 2006; Izaguirre and Iriondo, 2014). Fluid inclusion studies also indicate that the hydrothermal fluids forming these deposits were aqueous, low salinity (~2–11 wt % NaCl equivalent), and were enriched in N_2 and CO_2 (1–11 mol %). In general, the gold-bearing veins within the belt contain few sulfides (average modal abundance of ~3%) that correlate a roughly low average gold grade, and have an Au/Ag ratio of 1:9 (Izaguirre et al., 2012). In addition, stable isotope analysis indicates that the hydrothermal fluids that produced the mineralization had $\delta^{18}O$ values of 7–17‰ and δD values from –39‰ to –107‰, as recorded by quartz and white mica, respectively (Iriondo and Atkinson, 2000; Quintanar-Ruíz, 2008; Izaguirre and Iriondo, 2014). This suggests that the fluids were derived from metamorphic dehydration reactions that possibly occurred in deep basement rocks (>20 km).

The Laramide orogeny in southwestern United States and northwestern Mexico

The Laramide orogeny began in northwestern Mexico and the southwestern United States at ~90 Ma (Damon et al., 1983), sometime after the accretion of the Alisitos island arc to the western edge of the cordillera (~110–100 Ma), in a region that now forms the western regions of Baja and southwestern California (Johnson et al., 1999; Wetmore et al., 2003). Late Cretaceous subduction was initially characterized by a steeply dipping oceanic Farallon plate, and resulted in both magmatic activity and Andean-style deformation in the North American plate (Damon et

al., 1983; Valencia-Moreno and Ortega-Rivera, 2011). Shortly after, at ~70 Ma, the subduction angle apparently shallowed (Coney and Reynolds, 1977; Bird, 1998; Usui et al., 2003; Wells and Hoisch, 2008) resulting in rapid migration of the magmatic arc toward the continent with the arc eventually reaching a maximum distance from the trench of ~700 km (Coney and Reynolds, 1977; Bird, 1998; Usui et al., 2003). This change in subduction angle explains the presence of both thick- and thin-skin style deformation along the COGB area (Dickinson and Snyder, 1978; Haxel et al., 1984; Allmendinger, 1992; DeCelles, 2004; Iriondo et al., 2005) and has also been proposed as a cause of uplift far to the north in the Colorado Plateau and Rocky Mountain regions (Spencer, 1996; Flowers, 2010).

The Laramide orogeny was also associated with voluminous calc-alkaline magmatism and the formation of the Sonoran batholith which is comprised of abundant granitic, volcanic, and subvolcanic rocks of intermediate to felsic composition (Damon et al., 1983; Valencia-Moreno et al., 2001; Valencia-Moreno and Ortega-Rivera, 2011). These silicic rocks include deposits of the copper-molybdenum porphyry belt of United States and Mexico (CMPB US-MEX; Fig. 1B). This belt formed at ~75–40 Ma and is a northwest to southeast trending group of mineral deposits that extends from northern Arizona in the United States to the southern part of Sinaloa in Mexico (Barra et al., 2005). This copper-molybdenum metallogenic belt or province has been the subject of many investigations that have contributed significantly to the understanding of this type of ore deposit worldwide (Shafiqullah et al., 1980; Damon et al., 1983; McCandless et al., 1993; Titley, 2001; Barra et al., 2005; Valencia et al., 2006; and references therein).

Sample collection for $^{40}Ar/^{39}Ar$ geochronology

Quartz veins containing hydrothermal white mica were sampled at 63 locations throughout the COGB for $^{40}Ar/^{39}Ar$ dating (Fig. 2 and 5). All of these samples contained quartz and white mica, and the majority contained other hydrothermal minerals such as carbonates, pyrite, galena and gold (Fig. 4 and 5).

The quartz veins usually occur as en echelon arrays (Figs. 4A, 4B, and 4D) or are braided (Figs. 4C and 4E). Fieldwork revealed that many of the veins are located along shear structures that are typically associated with reverse faults and/or intensely foliated bands. Measured attitudes of the veins indicate they are predominantly steeply dipping (~70°) and strike northwest-southeast (330°–340°; Fig. 6). However, it is unclear if the distribution observed in Figure 6 is an original feature, or was caused by post-mineralization tectonic processes such as unrecognized tilting or vertical-axis rotations.

Analytical techniques and results for $^{40}Ar/^{39}Ar$ geochronology of hydrothermal white mica

The $^{40}Ar/^{39}Ar$ analyses of 63 hydrothermal white mica samples for this study were carried out at the U.S. Geological Survey Argon Thermochronology Laboratory in Reston, Virginia. The details of the analytical techniques used and the isotopic data obtained during this study are reported in an Open-File Report of the U.S. Geological Survey (Izaguirre et al., 2016). A summary of the $^{40}Ar/^{39}Ar$ data is presented in Table 1, including mineralization ages of each sample, localities, latitude and longitude, white mica habit (flakes or aggregates), and the 'age type' of each sample. 'Age type' refers to the groups of $^{40}Ar/^{39}Ar$ ages that were graphically categorized based on their characteristics as follows: Group 1 plateau-type ages (n = 21), Group 2 isochron-type ages (n = 16), and Group 3 average age/single step ages (n = 26). A

representative example of each group is shown in Figure 7. It should be noted that the most reliable $^{40}Ar/^{39}Ar$ geochronology data were generated from white mica flakes. Those micas separated from aggregates, in general may have included impurities in addition to the white mica (such as quartz, feldspar, and bedrock fragments), which can complicate the $^{40}Ar/^{39}Ar$ analysis and data interpretation.

A total of 21 plateau-type ages (Group 1; Table 1) were obtained from step-heating experiments on pure white mica flake separates (optical purity >99%) with sizes between 177–250 microns. Plateau ages are defined here as containing gas from at least three contiguous steps that overlap at the 2σ confidence level and contain > 50% of the $^{39}Ar_K$ (Fleck et al., 1977). Sample Dolores is an exception for this group with two steps building a plateau age but including 58% of the $^{39}Ar_K$ (Table 1). An example from Group 1 is given in Figure 7A (sample Quitovac-5).

Sixteen isochron-type ages (Group 2, Table 1) were obtained from flakes (optical purity >99%) and microcrystalline aggregates of white mica. This age was reported for samples that did not yield plateau ages but did yield statistically meaningful regressions on an isotope correlation diagram (Fig. 7B). The regression was considered meaningful if it included 3 or more consecutive heating steps containing >50% of the $^{39}Ar_K$ and had an MSWD ≤ 2.5 (e.g., Kunk et al., 2005; MSWD–Mean square weighted deviation).

The isotopic data from 26 separates containing white mica in fine-grained aggregates failed to produce plateau or isochron ages (Group 3; Table 1). The white mica in these veins was too fine to separate as individual flakes and was instead concentrated in white mica rich aggregates (typically 150–250 μm) that included variable amounts of quartz, plagioclase, potassium feldspar, or even fragments of rock that encased the quartz veins. These impurities likely

contributed to the complexity of the $^{40}Ar/^{39}Ar$ isotopic data and made these analyses more challenging to interpret. Also, it is possible that these isotopic data were distorted as a result of largely effects of 39Ar recoil in both into impurities phases in these mica aggregates and into the atmosphere (39Ar lost) during irradiation.

Although Group 3 samples failed to provide plateau-type or isochron-type ages, 15 of the 26 samples produced relatively "flat" age spectra. For these samples a weighted average of contiguous steps from the flat portion of the age spectrum is reported in Table 1 and is interpreted to reflect the time of mineralization (Fig. 7C). For the other 11 samples the age spectra typically showed a gradual climb in age across most of the age spectrum (Fig 7D). For these age spectra, the age of the heating step that follows a change in concavity of the age spectrum is interpreted to be a possible formation age (best age) of the gold-bearing quartz veins. Clearly these samples record the least reliable ages and so no uncertainty is included in Table 1. These samples highlight the difficulty in obtaining precise ages of gold-bearing veins with only fine-grained muscovite and with impurity mineral phases.

Discussion

Age of mineralization

Our 63 new $^{40}Ar/^{39}Ar$ ages of white mica associated with mineralization of gold-bearing veins along the Caborca orogenic gold belt (COGB) allow us to set limits on the timing of mineralization between the Late Cretaceous and the Eocene (~69–36 Ma; Table 1). The ages from these white micas represent formation ages and not cooling ages because most of the country rocks are much older than COGB gold veins. So, we estimated that white micas grew

below the closure temperature and are not cooling ages. For this reason, we interpret the hydrothermal ages of white micas to reflect the time of gold mineralization (Table 1).

Ages are displayed in a histogram with a probability curve (Fig. 8A), along with published mineralization ages (Table A1). These data indicate that there was a long period of mineralization in this region (time-span of ~33 m.y.; Fig. 8A), and that its end is coincident with the final phase of the Laramide orogeny in northwestern Mexico (e.g., Haxel et al., 1984; Iriondo et al., 2005; Poulsen et al., 2008). The temporal age distribution suggests that mineralization developed rapidly after ~69 Ma, and decreased more slowly from 58 to 36 Ma, when it ceased. The geochronological data also indicate that the peak of gold-bearing vein formation in the COGB occurred around 61 Ma (Fig. 8A). As discussed below, we interpret this peak in terms of measurable quantity of samples as rise of mineralization activity. Also, that this peak of mineralization is closely associated with tectonic changes that occurred during the Laramide orogeny, followed by a period of gradual decrease in deposition until cessation of mineralization within the COGB in the Eocene (~36 Ma).

A gold grade curve, created using gold concentrations (Fig. 8A) from dated quartz-rich veins of the COGB (Izaguirre et al., 2012), suggests that gold endowment is not dependent upon an evolution of the fluids after they are generated at depth, and rich gold deposits were formed throughout the entire time-span of deposit formation. This view is supported by the presence of several clusters of important gold deposits that formed at the beginning, middle, and end of the time-span of mineralization (e.g., La Herradura, El Chanate, and San Francisco-Estación Llano; Fig. 2), rather than gold mineralization being concentrated in a single pulse of time. However, areas containing high concentrations of gold veins, or greater gold endowments (i.e., greater economic potential), are commonly found in areas that record multiple generations of gold-rich

quartz veins (e.g., Quitovac at ~60 and ~50 Ma, Sierra San Francisco at ~69 and ~60 Ma, and Sierra Cubabi at ~50 and ~43 Ma; Table 1; Fig. 2). The presence of multiple age veins indicates that several pulses of mineralization were superimposed at the same locality and suggests that tectonic activity may have continued to provide fluids through the same crustal conduits. In other locations, gold mineralization was generated in a single pulse, perhaps indicating that these areas have less economic potential (e.g., Trincheras at 58–57 Ma, Los Vidrios at 58–56 Ma, and Los Tanques at 59–57 Ma; Table 1; Fig. 2).

Our geochronologic study helps to extend the area of the COGB (Fig. 2) and the number of new mineral occurrences in northwestern Sonora (e.g., El Chanate, Noche Buena, La Colorada, Cerro Colorado, Lluvia de Oro, El Tiro, La Sargenta, El Capitán, La Republicana, and Los Vidrios) and southern California and Arizona (e.g., American Boy, Betty Lee, and Sheep). Some dated mineral occurrences in this study have been new discovers and others were abandoned mines with unimportant mining activity and without mineral classification type. Hence one of the important points of this study was to find new mineral occurrences with orogenic characteristics to investigate their mineralization type. As a result, we can see a better panorama for the size of the COGB (Fig. 2).

In summary, the ages of mineralization along the COGB are limited to the Late Cretaceous-Eocene, and the mineralization is geochemically homogeneous (Izaguirre et al., 2012), providing additional evidence that this mineralization was associated with a single regional orogenic event, the Laramide orogeny.

Comparing the timing and tectonic regime between the COGB and the North American Cordillera orogenic gold belts

The orogenic gold provinces of the North American Cordillera, including the COGB, were formed during the relatively recent Phanerozoic (Fig. 9; Böhlke and Kistler, 1986; Böhlke et al., 1989; Elder and Cashman, 1992; Goldfarb et al., 2005; Marsh et al., 2008; Snow et al., 2008; Izaguirre et al., 2017; this study), in most cases due to the accretion of crustal blocks or terranes onto the mountainous Pacific margin (Goldfarb et al., 2008). However, the COGB differs from this geological setting because it was established in an active continental margin. This particular feature avoids a relationship to accreted terranes that typically suffer large displacements along suture zones due to changes in subduction plate motions. For this reason, we propose that the COGB is rather geologically similar to Phanerozoic orogenic gold deposits reported within cratonal margins in China (Goldfarb et al., 2014) than to other deposits within the North American Cordillera.

The geochronological data from the COGB (Fig. 9) suggest that the mineralization was coeval with some of the orogenic gold deposits present in the North American Cordillera like the ones in Alaska (e.g., Juneau, Chichagof, Valdez, Bearners, Willow Creek, Nuka, Hope-Sunrise, Girdwood, Port Wells, and Sitka) and with the Bridge River orogenic deposit in Canada. However, the apparent peak age for orogenic gold in Alaska is slightly younger (~55 Ma) than the peak time of gold mineralization within the COGB (~61 Ma). Nevertheless, the long interval of mineralization established for the COGB (time-span ~33 m.y.) places these occurrences among the youngest in the North American Cordillera.

Temporal correlation of orogenic gold and porphyry copper-molybdenum mineralization in northwestern Mexico and the southwestern United States

A comparison of mineralization ages for the COGB (~69–36 Ma) with available ages for the copper-molybdenum porphyry belt of United States and Mexico (CMPB US-MEX; ~77–40 Ma) confirms that these belts of mineralization formed contemporaneously during the Late Cretaceous-Eocene (Fig. 8A and 8B). We interpret that both metallogenic events are caused by the eastward migration of the magmatic arc as a result of a sudden shallowing of the subducted Farallon slab as proposed by Coney and Reynolds (1977). This led to arc development at a considerable distance from the Laramide Baja California trench (up to ~700 km), and produced voluminous, primarily volcanic, igneous rocks in regions as far as Chihuahua and New Mexico (Clark et al., 1982; McDowell and Mauger, 1994; Valencia-Moreno and Ortega-Rivera, 2011). Migration of the continental magmatic arc was followed by the generation of the COGB quartz veins, and is responsible for the formation of contemporaneous mineralized porphyry Cu-Mo deposits of the CMPB US-MEX. In this scenario, orogenic gold deposits formed in the forearc region and porphyries in the arc region of northwestern Sonora and southwestern United States (Fig. 10B). This differs significantly, on a global level, from typical metallogenic models proposed for the formation of orogenic gold (Groves et al., 1998; Goldfarb et al., 2005) that are commonly related to terrane accretion and subsequent displacement along shear zones due to shifts in subduction plate motions.

A consequence of the eastward arc migration during the Laramide orogeny was the generation of a magmatic gap within the forearc region in parts of the North American Cordillera. In particular, the absence of magmatism is well documented along coastal California between ~70 and ~45 Ma (Lipman et al., 1972; Armstrong, 1974; Dickinson and Snyder, 1978;

Ward, 1991). This gap in magmatism is also present in the forearc region in northwestern Sonora where there is an absence of igneous activity between ~60 and ~25 Ma (Fig. 8C). Furthermore, this magmatic gap temporally coincides with the ages of the majority of the orogenic gold veins dated in this study, which suggests that the area of the COGB records the nearly complete migration of the magmatic arc toward the east during the formation of the orogenic gold mineralization within the COGB.

A comparative analysis of the mineralization ages along the COGB, and the estimated distances to the paleo-subduction trench of Baja California (Fig. 10B), provides useful insights into the relationship between the magmatic gap and the timing of gold and copper-molybdenum mineralization in this region. An eastward shift in ages of gold mineralization with time is clearly apparent (Fig. 10A). A similar shift in age is observed in the 106 samples of porphyry copper deposits dated along the copper-molybdenum porphyry belt of United States and Mexico (CMPB US-MEX; Fig. 10A). We interpret these eastward shifts, or overall younging to the east, as a pattern of migration and evolution in the generation of both the orogenic gold and porphyry copper deposits (Figs. 10B and 10C), similar to the recently suggested migration for the CMPB US-MEX, documented by geochronological studies of Cu-Mo mineralization (Barra and Valencia, 2014). This apparent eastward migration of gold mineralization occurred at an estimated rate of displacement of ~1.5 km/Ma (red arrow in Fig. 10A).

Superposition of epithermal mineralization and supergene alteration and possible extent of the COGB

After the magmatic gap ended, episodes of volcanic activity, as evidenced by the presence of calc-alkaline lavas within the COGB, occurred in the retreat of the magmatic arc

since the Oligocene due to slab rollback of the Farallon plate (Grijalva-Noriega and Roldán-Quintana, 1998; Vidal-Solano et al., 2008; Fig. 8C). As a consequence, this magmatism triggered hydrothermal activity that generated epithermal, low temperature, base metal Au- and Ag-quartz vein mineralization that formed deposits across a broad region of northwestern Sonora, southwestern California, and southwestern Arizona (Staude and Barton, 2001; Zawada et al., 2001; Ochoa-Landín et al., 2011; Camprubí, 2013). The age bracketing of these epithermal deposits is between the Oligocene to Miocene (~32–17 Ma) but most of them were formed at ~26 Ma (Table A5). Their occurrences are located within the COGB region and overprint the orogenic gold deposits (e.g., La Colorada, Lluvia de Oro, and Quitovac; Fig. 2), as well as in parts of southwestern Arizona and southeastern California, especially in the area near Yuma (e.g., Mesquite, American Girl, and Fortuna deposits). This mineralization overprinting has made it difficult to develop useful models for ore genesis that could aid gold exploration in the region. At the same time, epithermal mineralization in the area of the porphyry copper-molybdenum belt in southwestern United States and northwestern Mexico has also produced significant gold-bearing deposits, in addition to silver and base metals (e.g., El Tigre, Mulatos, El Alamo, Santa Teresa, and Lampazos; Ochoa-Landín et al., 2011).

Supergene alteration of hypogene orogenic mineralization along the COGB is characterized by ~80–90% (by volume) destruction of sulfides and carbonates within the gold-rich quartz veins in this region (e.g., pyrite, galena, and calcite; Figs. 4B and 4L). This supergene alteration produced iron oxides, sulfates, and residual carbonates or caliche (Nourse and Irwin, 2010; Izaguirre et al., 2017) and is thought to have resulted from fluctuations in groundwater levels (oxidation-reduction cycles) that typically occur in the arid desert climate that has prevailed in the study area since the Miocene (Noguez-Alacátara et al., 2007; Ochoa-Landín et

al., 2011). This supergene alteration generates free gold and makes more affordable the process of gold mining as occur at La Herradura mine (Quintanar-Ruíz, 2008; De la Torre-Carlos, 2009). However, there is not yet a consensus of how much upgrade the gold content from the upper oxidized portions versus to the lower unoxidized and sulfitic ore.

In some ways, this supergene alteration is similar to supergene enrichment that has been widely documented in copper-molybdenum porphyry deposits that is characterized by the generation of enriched layers of secondary copper minerals associated directly with changes in groundwater levels (Chávez, 2000). The Oligocene-Miocene post-mineralization Basin-and-Range crustal extension (Gans, 1997; Grijalva-Noriega and Roldán-Quintana, 1998; Henry and Aranda-Gómez, 2000; Dickinson, 2002), and the development of metamorphic core complexes (Coney and Harms, 1984; Nourse et al., 1994; Vega-Granillo and Calmus, 2003), may have favored the aforementioned oxidation-reduction processes observed in this region. This Tertiary extension would have controlled the groundwater level and would have also exposed Au-bearing veins at shallower crustal levels to encounter more oxidizing environments. However, some orogenic veins in the study area do not record this type of supergene alteration (e.g., El Chanate and Estación Llano-San Francisco; Fig. 2), possibly because these occurrences represent areas with different denudation rates or just, encapsulated ore bodies out of the range of oxidizing agents.

Finally, it is important to mention that the COGB may extend beyond its current proposed boundaries (Fig. 2). Reconstruction of the Baja California peninsula suggests that the COGB could extend farther into the area around north-central Baja California. The continuation may also extend today to the mountains near Mexicali (e.g., Sierra Cucapah or Sierra El Mayor; Fig. 1B); a possible orogenic gold occurrence known as El Alamo has been reported in the

northern part of Baja California peninsula (Camprubi, 2013). The possible extension of the COGB to the northeast is truncated abruptly by areas dominated by porphyry copper deposits (Izaguirre et al., 2012). The search for an east-southeast extension of the COGB was hampered largely by post-mineralization Oligocene and Miocene volcanic rocks that make up the western Sierra Madre Occidental volcanic province (e.g., Ferrari et al., 2002).

In addition, apparent occurrences of orogenic mineralization crop out in the southernmost part of the Baja California peninsula, particularly to the south of La Paz in the El Triunfo, Los Uvares, Paredones Amarillos, and San Antonio gold deposits (Izaguirre et al., 2017). However, these deposits appear to be older than, and may be unrelated to, the COGB mineralization, possibly as old as ~90–80 Ma according to reports of mineralization in the region by Carrillo-Chávez et al. (1999).

The Laramide orogeny: driver for the generation of metamorphic ore-forming fluids

In this study, we suggest that plate convergence during the Laramide orogeny was the main tectonic process that help generating the mineralizing fluids within the COGB region. The established convergent regime led to crustal thickening caused an elevated geothermal gradient in northwest Sonora. Therefore, the time suitable for formation of these hydrothermal fluids was some time before mineralization process (~90–70 Ma; Fig. 11A; Dickinson and Sneyder, 1978; Damon et al., 1983; English and Johnston, 2004). Stable isotope data obtained from quartz and white mica from gold-bearing veins along the COGB show that the precursor fluids have a strong affinity to metamorphic waters (Iriondo and Atkinson, 2000; Quintanar-Ruíz, 2008; Izaguirre and Iriondo, 2014). Hence, the mineralizing fluids were likely generated by devolatization (e.g., H_2O and CO_2; see Table 2) at significant crustal depths (>20 km) due to

metamorphic dehydration reactions occurring in the over thickened orogen that achieved greenschist-amphibolite conditions or even higher granulite facies like it has been proposed by experimental studies (Fu and Touret, 2014). Also, a metamorphic origin for the COGB mineralizing fluids matches with an extended period of tectonic compression like it has been suggested in other orogenic fields globally (e.g., Gaboury, 2013).

Tectonic framework for the COGB mineralization

It has been proposed that the Laramide orogeny led to the orogenic mineralization within the COGB (Iriondo and Atkinson, 2000; Ocho-Landín et al., 2011; Izaguirre and Iriondo, 2014), although to this point, no tectonic framework has been proposed to explain the process for generating these deposits. Here, we propose a tectonic framework in which the factors that triggered the orogenic mineralization are closely related to a sudden decrease in the subduction angle (up to ~15º) of the Farallon plate during the Laramide orogeny (Fig. 11B). This tectonic shift had to occur after the regional metamorphic peak for the orogeny and could have resulted from a still unexplained increase in the rate of subduction that began between ~75 and ~70 Ma and peaked between ~60 and ~40 Ma (Coney and Reynolds, 1977; Ward, 1991). Other effects associated with this tectonic shift could have included isostatic uplift during the Laramide orogeny (Hodges and Walker, 1992; Wells and Hoisch, 2008), a process that may have been caused by mantle erosion and/or delamination (Wells and Hoisch, 2008; Fig. 11B).

As a result, these tectonic changes are suggested to have caused a later regional Laramide crustal extension event over the Cordilleran forearc, where Early Cenozoic compressive deformation on reverse faults and thrusts and crustal shortening occurred simultaneously during this event defined as synconvergent crustal extension (Applegate et al., 1992; Wells et al., 2005;

Jacobson et al., 2007). In addition, a possible consequence of this synconvergent crustal extension in the Cordillera forearc region is a marked cooling of the thinned crust, which in turn generated regional brittle conditions (Dumitru et al., 1991; Livaccari, 1991; Applegate et al., 1992).

These tectonic changes should have favored the ascent and channeling of orogenic hydrothermal fluids that were rich in volatiles and had the capacity of leaching and carrying significant quantities of gold and other precious and base metals (e.g., Ag, Cu, Pb, W, and Zn; Table 2). The fluids rose to depths of 4–6 km in the crust, a level that represents the ideal ductile-brittle limit to host the gold-bearing quartz veins in the COGB (Fig. 11B; Iriondo and Atkinson, 2000; Noriega-Martínez, 2006; Izaguirre and Iriondo, 2014). The quartz vein fillings are estimated to have precipitated from hydrothermal fluids at an average temperature of ~330°C (Albinson, 1989; Pérez-Segura et al., 1996; Noriega-Martínez, 2006; Izaguirre and Iriondo, 2014).

In summary, most of the mineralization within the COGB formed around 61 Ma (Fig. 8A), a period that matches with an increase in convergence (Ward, 1991), and with the shallowing of the Farallon subducting plate from its originally more steeply dipping angle (Coney and Reynolds, 1977). In addition, this maximum peak of mineralization appears to coincide with the internal decoupling of the middle crust (Wells and Hoisch, 2008), which may have allowed the ascent of significant volumes of hydrothermal fluids. Overall, the proposed tectonic shift that could explain gold mineralization along the COGB appear to be somehow more complicated than mechanisms suggested for the formation of orogenic mineralization belts in other parts of the North American Cordillera (e.g., Goldfarb et al., 1991, 2008).

Differential uplift and denudation/exhumation of mineralized belts and final dismissal for the hMSM as the tectonic cause for gold mineralization

Differential uplift and denudation must be interpreted between the Caborca orogenic gold belt area and the copper-molybdenum porphyry belt of United States and Mexico (CMPB US-MEX). The COGB area shows a level of exhumation ~2–4 times greater than the CMPB US-MEX region. Field observations show that gold-bearing quartz vein mineralization is overlain by Oligocene-Miocene volcanic rocks (~25–22 Ma). This indicates that the veins, which formed at estimated depths of 4–6 km (Albinson, 1989; Noriega-Martínez, 2006), were exhumed at least by the Miocene. In our model, we interpret that the COGB was more denuded and possibly more uplifted than the Laramide copper-molybdenum porphyry region (Fig. 11C) that formed at shallower crustal depths (~1–2 km). In other words, both coeval mineral belts are exposed next to each other even though they represent very different crustal levels.

This exposure of different crustal levels can be explained by the period of synconvergent crustal extension, discussed above, which caused preferential tectonic denudation of the previously thickened forearc region. This preferential denudation can be also a result of large uplift during the early shortening that produced crustal thickening (~90–70 Ma). Furthermore, the COGB preferential denudation and exhumation has been associated due to a greater uplift and exhumation of the Yavapai crustal province, with respect to the adjacent Mojave and Mazatzal province (Iriondo and Izaguirre, 2016). The Yavapai crustal province overlaps in area with the COGB (Fig. 3) and represent deeper crustal rocks levels.

Finally, it should be noted that our tectonic model does not invoke the hypothetical Mojave-Sonora Megashear (hMSM; Fig. 3) to explain the occurrence of orogenic gold mineralization along the COGB because it differs significantly in both timing and structural

style. A model with a hypothetical Late-Jurassic megashear is not coherent with our field observations and with age data presented in this study that indicate an origin by an initial stage of compressional Laramide tectonism that caused crustal thickening and generation of deep metamorphic volatile-rich hydrothermal fluids. In addition, a period of synconvergent crustal extension, which represents the later stage of the Laramide orogeny, affected the forearc region and produce a marked cooling of the thinned crust which in turn generated regional brittle conditions that triggered the multi-stage dewatering process and the final precipitation of mineralizing fluids that formed the quartz-gold vein deposits along the COGB during the Late Cretaceous-Eocene (~69–36 Ma).

Conclusions

New $^{40}Ar/^{39}Ar$ geochronology of gold-bearing quartz veins along the Caborca orogenic gold belt (COGB) suggests that mineralization developed rapidly after ~69 Ma, peaked at ~61 Ma and decreased more slowly from 58 to 36 Ma, when it ceased (time-span ~33 m.y.). It is common that pulses of mineralization were superimposed at the same locality suggesting that tectonic activity may have continued to provide fluids through the same crustal conduits. Mineralization within the COGB formed contemporaneously with some other orogenic gold deposits along the North American Cordillera, including districts in Alaska and Canada but under different tectonic settings since the deposits in northwestern Mexico were formed in an active continental arc environment.

Initial crustal thickening during the early compressive stage (~90–70 Ma) of the Laramide orogeny was the primary reason to generate the mineralizing fluids due to metamorphic dehydration reactions of deep-seated basement rocks (>20 km). Later Laramide

synconvergent upper crustal extension in the forearc region triggered the multi-stage crustal dewatering using reactivated compressional shear structures and newly created brittle structures. Synconvergent extension began when flat slab subduction started at ~70 Ma as result of a sudden shallowing of the subducted Farallon slab that caused a rapid eastward migration of the magmatic arc toward the continent.

Eastward arc migration also facilitated the generation of contemporaneous Late Cretaceous-Eocene porphyry Cu-Mo mineralization in northwestern Mexico and southwestern United States; perhaps a unique place around the world where there is evidence that orogenic gold deposits would have formed in the amagmatic forearc region, whereas the porphyries were simultaneously generated in the magmatic arc region.

The COGB area was more uplifted, and suffered higher degrees of denudation (veins formed at depths of ~4–6 km) than the region of Cu-Mo porphyries that formed at shallower crustal depths (~1–2 km). This crustal level disparity is explained by a period of intense Eocene to Oligocene crustal denudation that preferentially affected the forearc region until final exhumation of the COGB veins occurred, most likely, by the Late Oligocene.

Post exhumation Oligocene-Miocene epithermal mineralization overprinted both the COGB and the porphyry Cu-Mo belt making it more difficult developing useful genetic exploration models. Additionally, supergene alteration of hypogene orogenic mineralization and supergene enrichment of the porphyry deposits both led to increased mineral concentrations as a result of groundwater level fluctuations.

The combination of all these tectonic and climatic factors makes northwestern Mexico a unique and attractive place in the North American Cordillera to undertake precious and base metals exploration endeavours.

Acknowledgements

We acknowledge the *Consejo Nacional de Ciencia y Tecnología* (CONACyT) and UNAM/PAPIIT for providing support to Iriondo that partially financed this work (CB-82518, CB-129370 and IN-116709). We also acknowledge CONACyT for providing a doctoral scholarship to Izaguirre and for giving complementary funds in a mobility scholarship program (*Becas mixtas*) for supporting academic scientific research at the U.S. Geological Survey, Denver, Colorado. Special thanks goes to Dan Miggins for his help and friendship during the stay in Denver. Also thanks to Erin Marsh, Richard Goldfarb, Leonid Neymark, Craig Johnson and many other friendly people for their unconditional support and advice to undertake scientific research while in Denver. We wish to thank the *Servicio Geológico Mexicano* (SGM) *Gerencia* Hermosillo, Sonora, for logistics and for helping with the fieldwork, and in particular, we would like to thank Javier Hernández-Rojas (SGM geologist) for his helpful companionship in the field while Izaguirre collected quartz vein samples along the Caborca orogenic gold belt. We are grateful to Roberto Molina-Garza (UNAM researcher) for reviewing the manuscript making constructive and thoughtful comments. Thanks to Edward du Bray for performing an internal U.S. Geological Survey review of the manuscript that significantly improved it. Nancy Stamm, a technical specialist reviewer from the U.S. Geological Survey, is greatly acknowledged for making observations related to the correct usage of geological terminology. Finally we are grateful to the Economic Geology reviewers Ryan Taylor, Dan Barfod and Dave Selby for valuable contributions resulting in improvements in the manuscript. Any use of trade, product, or firm names is for descriptive purposes only and does not imply endorsement by the U.S. Government.

References Cited

Adams, D.D., Freeman, C.J., Goldfarb, R.J., Gent, C.A., and Snee, L.W., 1992, Age and geochemical constrains on mesothermal gold mineralization, Valdez Creek district, Alaska [abs.]: Geological Society of America Abstracts with Programs, Cordilleran Section, v. 24, p. 2.

Albinson, T.F., 1989, Vetas mesotermales auríferas del sector norte del Estado de Sonora: Memorias, XVIII Convención Nacional AIMMGM, Acapulco, Guerrero, México, Asociación de Ingenieros de Minas, Metalurgistas y Geólogos de México, p. 20–40.

Allmendinger, R.W., 1992, Fold and thrust tectonics of the western United States exclusive of the accreted terranes, *in* Burchfiel, B.C., Lipman, P.W., and Zoback, M.L., eds., The Cordilleran Orogen: Conterminous U.S.: Boulder, Colorado, Geological Society of America, Geology of North America, v. 3, p. 583–607.

Anderson, T.H., and Silver L.T., 1979, The role of the Mojave-Sonora megashear in the tectonic evolution of northern Sonora, *in* Anderson, T.H., and Roldán-Quintana, J., eds., Geology of northern Sonora Guidebook, University of Pittsburgh and Universidad Nacional Autónoma de México, Instituto de Geología, Geological Society of America Annual Meeting, Hermosillo, Sonora, v. 27, p. 59–68.

Anderson, T.H., and Silver L.T., 2005, The Mojave-Sonora megashear-Field and analytical studies leading to the conception and evolution of the hypothesis, *in* Anderson, T.H., Nourse, J.A., McKee, J.W., and Steiner, M.B., eds., The Mojave-Sonora Megashear Hypothesis: Development, Assessment, and Alternatives: Geological Society of America Special Paper 393, p. 1–50.

Applegate, J.D.R., Walker, J.D., and Hodges, K.V., 1992, Late Cretaceous extensional unroofing in the Funeral Mountains metamorphic core complex, California: Geology, v. 20, p. 519–522.

Araux-Sánchez, E., Vega-Granillo, R., and Enríquez-Minjárez, E., 2001, Características geológicas de un yacimiento mesotermal asociado a zonas de cizalla en el noroeste de Sonora, *in* Corona-Esquivel, R., and Gómez-Godoy, J., eds., Asociación de Ingenieros de Minas, Metalurgistas y Geólogos de México A.C., XXIV Convención Minera, Acapulco, Guerrero, p. 25–32.

Armstrong, R.L., 1974, Geochronometry of the Eocene volcanic-plutonic episode of Idaho: Northwest Geology, v. 3, p. 1–15.

Arvizu-Gutiérrez, H.E., 2008, El basamento paleoproterozoico Yavapai-Mazatzal en los alrededores de la Sierra Pinta, NW de Sonora: Su importancia para el entendimiento del magmatismo Pérmico y el inicio del margen continental activo del SW de Norte América: Unpublished B.Sc. thesis, Linares, Nuevo León, México, Universidad Autónoma de Nuevo León, 181 p.

Arvizu, H.E., Iriondo, A., Izaguirre, A., Chávez-Cabello, G., Kamenov, G.D., Solís-Pichardo, G., Foster, D.A., and Lozano-Santa Cruz, R., 2009, Rocas graníticas pérmicas en la Sierra Pinta, NW de Sonora, México: Magmatismo de subducción asociado al inicio del margen continental activo del SW de Norteamérica: Revista Mexicana de Ciencias Geológicas, v. 26, p. 709–728.

Barra, F., and Valencia, V.A., 2014, Late Cretaceous porphyry copper mineralization in Sonora, Mexico: Implications for the evolution of the Southwest North America porphyry copper province: Mineralium Deposita, v. 49, p. 879–884.

Barra, F., Ruiz, J., Valencia, V.A., Ochoa-Landín, L., and Chesley, J., 2005, Laramide Porphyry Cu-Mo Mineralization in Northern Mexico: Age Constraints from Re-Os Geochronology in Molybdenite: Economic Geology, v. 100, p. 1605–1616.

Bird, P., 1998, Kinematic history of the Laramide orogeny in latitudes 35°–49°, western United States: Tectonics, v. 17, p. 780–801.

Böhlke, J.K., and Kistler, R.W., 1986, Rb-Sr, K-Ar, and stable isotope evidence for the ages and sources of fluid components of gold-bearing quartz veins in the northern Sierra Nevada Foothills Metamorphic Belt, California: Economic Geology, v. 81, p. 296–322.

Böhlke, J.K., Kirshbaum, C., and Irwin, J.J., 1989, Simultaneous analyses of noble gas isotopes and halogens in fluid inclusions in neutron irradiated quartz veins using a laser microprobe noble gas mass spectrometer: U.S. Geological Survey Bulletin 1890, p. 61–80.

Campbell, P.A., and Anderson, T.H., 2003, Structure and kinematics along a segment of the Mojave-Sonora megashear: A strike-slip fault that truncates the Jurassic continental magmatic arc of southwestern North America: Tectonics, v. 22, p. 1–21.

Camprubí, A., 2013, Tectonic and metallogenic history of Mexico, *in* Colpron, T., Bissig, T.,

Rusk, B.G., and Thompson, J.F.H., eds., Tectonics, metallogeny, and discovery: The North American Cordillera and similar accretionary settings: Society of Economic Geologists Special Publication 17, p. 201–243.

Carrillo-Chávez, A., Huyck, H., Zentilli, M., and Griest, A., 1999, Age constraints on host rocks of Los Uvares gold deposit: Magmatic pulses in southernmost Baja California, Mexico: Geofísica Internacional, v. 38, p. 27–33.

Chávez, W.X., Jr., 2000, Supergene oxidation of copper deposits: Zoning and distribution of copper oxide minerals: Society of Economic Geologist, Newsletter April, p. 10–22.

Clark, K.F., Foster, C.T., and Damon, P.E., 1982, Cenozoic mineral deposits and subduction-related magmatic arcs in Mexico: Geological Society of American Bulletin, v. 93, p. 533–544.

Coney, P.J., and Harms, T.A., 1984, Cordilleran metamorphic core complexes: Cenozoic extensional relics of Mesozoic compression: Geology, v. 12, p. 550–554.

Coney, P.J., and Reynolds, S.J., 1977, Cordilleran Benioff zones: Nature, v. 270, p. 403–406.

Damon, P.E., Livingston, D.E., and Giletti, B.J., 1961, Extension of the older Precambrian of the southwest into Sonora, Mexico [abs.]: Geological Society of America, Abstracts with Programs, v. 68, p. 158–159.

Damon, P.E., Shafiqullah, M., and Clark, K.F., 1983, Geochronology of the porphyry copper deposits and related mineralization of Mexico: Canadian Journal of Earth Sciences, v. 20, p. 1052–1071.

DeCelles, P.G., 2004, Late Jurassic to Eocene evolution of the Cordilleran thrust belt and Foreland basin system, western USA: American Journal of Science, v. 304, p. 105–168.

De la Torre-Carlos, J., 2009, Geología del yacimiento mina La Herradura, *in* Clark, K.F., Salas-Pizá, G., and Cubillas-Estrada, R., eds., Geología económica de México 2ª edición: Servicio Geológico Mexicano-Asociación de Ingenieros de Minas, Metalurgistas y Geólogos de México, p. 844–851.

Dickinson, W.R., 2002, The Basin and Range Province as a composite extensional domain: International Geology Review, v. 44, p. 1–38.

Dickinson, W.R., and Lawton, T.F., 2001, Carboniferous to Cretaceous assembly and fragmentation of Mexico: Geological Society of America Bulletin, v. 113, p. 1142–1160.

Dickinson, W.R., and Snyder, W.S., 1978, Plate tectonics of the Laramide orogeny, *in* Matthews, V., ed., Laramide folding associated with basement block faulting in the western United States, Geological Society of America Memoir 151, p. 355–366.

Dumitru, T.A., Gans, P.B., Foster, D.A., and Miller, E.L., 1991, Refrigeration of the western Cordillera lithosphere during Laramide shallow-angle subduction: Geology, v. 19, p. 1145–1148.

Elder, D., and Cashman, S.M., 1992, Tectonic controls and fluid evolution in the Quartz Hill, California, lode gold deposits: Economic Geology, v. 87, p. 1795–1812.

English, J.M., and Johnston, S.T., 2004, The Laramide orogeny: What were the driving forces?: International Geology Review, v. 40, p. 833–838.

Ferrari, L., López-Martínez, M., and Rosas-Elguera, J., 2002, Ignimbrite flare-up and deformation in the southern Sierra Madre Occidental, western Mexico: Implications for the late subduction history of the Farallon plate: Tectonics, v. 21, p. 1–24.

Fleck, R.J., Sutter, J.F., and Elliot, D.H., 1977, Interpretation of discordant $^{40}Ar/^{39}Ar$ age spectra of Mesozoic tholeiites from Antarctica: Geochimica et Cosmochimica Acta, v. 41, p. 15–32.

Flowers, R.M., 2010, The enigmatic rise of the Colorado Plateau: Geology, v. 38, p. 671–672.

Fu, B., and Touret, J.L.R., 2014, From granulite fluids to quartz-carbonate megashear zones: The gold rush: Geociencies Frontiers, v. 5, p. 743–758.

Gaboury, D., 2013, Does gold in orogenic deposits come from pyrite in deeply buried carbon-rich sediments?: Insight from volatiles in fluid inclusions: Geology, v. 41, p. 1207–1210.

Gans, P.B., 1997, Large-magnitude Oligo-Miocene extension in southern Sonora: Implications for the tectonic evolution of northwest Mexico: Tectonics, v. 16, p. 388–408.

Grijalva-Noriega, F.J., and Roldán-Quintana, J., 1998, An Overview of the Cenozoic tectonic and magmatic evolution of Sonora, northwestern México: Revista Mexicana de Ciencias Geológicas, v. 15, p. 145–156.

Goldfarb, R.J., and Groves, D.I., 2015, Orogenic gold: Common or evolving fluid and metal sources through time: Lithos, v. 233, p. 2–26.

Goldfarb, R.J., Snee, L.W., Miller, L.D., and Newberry, R.J., 1991, Rapid dewatering of the crust deduced from ages of mesothermal gold deposits: Nature, v. 354, p. 296–298.

Goldfarb, R.J., Miller, L.D., Leach, D.L., and Snee, L.W., 1997, Gold deposits in metamorphic rocks in Alaska, *in* Goldfarb, R.J., and Miller, L.D., eds., Mineral Deposits of Alaska: Economic Geology Monograph 9, p. 151–190.

Goldfarb, R.J., Baker, T., Dubé, B., Groves, D.I., Hart, C.J.R., and Gosselin, P., 2005, Distribution, Character, and Genesis of Gold deposits in metamorphic terranes: Economic Geology, v. 100, p. 407–450.

Goldfarb, R.J., Hart, C.J.R., and Marsh, E.E., 2008, Orogenic gold and evolution of the Cordilleran orogen, *in* Spencer, J.E., and Titley S.R., eds., Ores and orogenesis: Circum-Pacific tectonics, geologic evolution, and ore deposits: Arizona Geological Society Digest 22, p. 311–323.

Goldfarb, R.J., Taylor, R.D., Collins, G.S., Goryachev, N.A., and Orlandini, O.F., 2014, Phanerozoic continental growth and gold metallogeny of Asia: Gondwana Research, v. 25, p. 48–102.

González-León, C.M., 1994, Early Cretaceous tectono-sedimentary evolution of the southwestern margin of the Bisbee Basin: Revista Mexicana de Ciencias Geológicas, v. 11, p. 139–146.

Groves, D.I., Goldfarb, R.J., Grebre-Meriam, M., Hagemann, S.G., and Robert, F., 1998, Orogenic gold deposits: A proposed classification in the context of their crustal distribution and relationship to other gold deposit types: Ore Geology Reviews, v. 13, p. 7–27.

Haeussler, P.J., Bradley, D., Goldfarb, R.J., Snee, L.W., and Taylor, C., 1995, Link between ridge subduction and gold mineralization in southern Alaska: Geology, v. 23, p. 995–998.

Hart, C.J.R., Goldfarb, R.J., Ullrich, T.D., and Friedman, R., 2008, Gold, Granites, and Geochronology: Timing of Formation of the Bralorne-Pioneer Gold Orebodies and the Bendor Batholith, Southwestern British Columbia: Geoscience BC, Summary of Activities 2007, Report 2008-1, p. 47–54.

Haxel, G.B., Tosdal, R.M., May, D.J., and Wright, J.E., 1984, Latest Cretaceous and early Tertiary orogenesis in south-central Arizona: Thrust faulting, regional metamorphism, and granitic plutonism: Geological Society of America Bulletin, v. 95, p. 631–653.

Henry, C.D., and Aranda-Gomez, J.J., 2000, Plate interactions control middle-Late Miocene, proto-Gulf and Basin and Range extension in the southern Basin and Range: Tectonophysics, v. 318, p. 1–26.

Hodges, K.V., and Walker, J.D., 1992, Extension in the Cretaceous Sevier orogen, North American Cordillera: Geological Society of America Bulletin, v. 104, p. 560–569.

Iriondo, A., 2001, Proterozoic basements and their laramide juxtaposition in NW Sonora, Mexico: Tectonic constraints on the SW margin of Laurentia: Unpublished Ph.D. thesis, Boulder, Colorado, USA, University of Colorado at Boulder, 222 p.

Iriondo, A., and Atkinson, W.W., Jr., 2000, Orogenic gold mineralization along the proposed trace of the Mojave-Sonora megashear: Evidence for the Laramide Orogeny in NW Sonora, Mexico [abs.]: Geological Society of America, Abstracts with Programs, v. 32, p. 393.

Iriondo, A., and Premo, W.R., 2011, Las rocas cristalinas proterozoicas de Sonora y su importancia para la reconstrucción del margen continental SW de Laurencia-la pieza mexicana del rompecabezas de Rodinia, *in* Calmus, T., ed., Panorama sobre la geología de Sonora, México: Instituto de Geología, Universidad Nacional Autónoma de México, v. 118, p. 25–55.

Iriondo, A., and Izaguirre, A., 2016, Paleoproterozoic Yavapai igneous rocks with late Cretaceous to Early Cenozoic Ar-Ar ages: Thermal disturbance “resetting” due to widespread Laramide magmatism in Sonora, Mexico [abs.]: GEOS, Unión Geofísica Mexicana, v. 35.

Iriondo, A., Premo, W.R., Martínez-Torres, L.M., Budahn, J.R., Atkinson, W.W., Jr., Siems, D.F., and Guarás-González, B., 2004, Isotopic, geochemical and temporal characterization of Precambrian basement rocks in the Quitovac region, northwestern Sonora, Mexico: Its implications for the tectonic reconstruction of southwestern North America: Geological Society of America Bulletin, v. 116, p. 154–170.

Iriondo, A., Martínez-Torres, L.M., Kunk, M.J., Atkinson, W.W., Jr., Premo, W.R., and McIntosh W.C., 2005, Northward Laramide thrusting in the Quitovac region, northwestern Sonora, Mexico: Implications for the juxtaposition of Paleoproterozoic basement blocks and the Mojave-Sonora megashear hypothesis, *in* Anderson, T.H., Nourse, J.A., McKee, J.W.,

Steiner, M.B., eds., The Mojave-Sonora megashear hypothesis: Development, assessment, and alternatives: Geological Society of America Special Paper 393, p. 631–669.

Izaguirre, A., Iriondo, A., Kunk, M., and McAleer, R., 2013, Mineralización orogénica larámide en el NW de Sonora: Una complicación adicional para la controvertida megacizalla Mojave-Sonora [abs.]: GEOS, Unión Geofísica Mexicana, v. 33, p. 170.

Izaguirre, A., and Iriondo, A., 2014, A metamorphic origin for the hydrothermal fluids forming the gold-bearing quartz veins from the Laramide Caborca Orogenic Gold Belt of NW Sonora [abs]: An oxygen, hydrogen and sulfur isotopic study: GEOS, Unión Geofísica Mexicana, v. 34, p. 334.

Izaguirre, A., Iriondo, A., Caballero-Martínez, J.A., Moreira-Rivera, F., and Espinosa-Arámburu, E., 2012, Homogeneidad geoquímica de la alteración hidrotermal del cinturón de oro orogénico del NW de Sonora, México: Estudio de balance de masas en rocas encajonantes de la mineralización: Boletín de la Sociedad Geológica Mexicana, v. 64, p. 119–153.

Izaguirre, A., Iriondo, A., Kunk, M.J., McAleer, J.R., Caballero-Martínez, J.A., and Espinosa-Arámburu, E., 2016, The Laramide Caborca orogenic gold belt of northwestern Sonora, México: White mica $^{40}Ar/^{39}Ar$ geochronology from Au-rich quartz veins: U.S. Geological Survey Open-file Report 2016–1008, 30 p., http://dx.doi.org/10.3133/ofr20161008.

Izaguirre, A., Camprubí, A., and Iriondo, A., 2017, Mesozoic orogenic gold deposits in Mexico: Ore Geology Reviews, v. 81, 1172–1183, doi: 10.1016/j.oregeorev.2015.10.006.

Jacobson, C.E., Grove, M., Vućić, A., Pedrick, J.N., and Ebert, K.A., 2007, Exhumation of the Orocopia Schist and associated rocks of southeastern California: Relative roles of erosion, synsubduction tectonic denudation, and middle Cenozoic extension, *in* Cloos, M., Carlson, W.D., Gilbert, M.C., Liou, J.G., and Sorensen, S.S., eds., Convergent Margin Terranes and Associated Regions: A Tribute to W.G. Ernst: Geological Society of America Special Paper 419, p. 1–37.

Jacques-Ayala, C., and García-Barragán, J.C., 2014, Deletion of the Caborca Terrane and renaming the Papago Terrane [abs.]: GEOS, Unión Geofísica Mexicana, v. 34, p. 330.

Johnson, S.E., Tate, M.C., and Fanning, C.M., 1999, New geologic mapping and SHRIMP U-Pb zircon data in the Peninsular Ranges batholith, Baja California, Mexico: Evidence for a suture?: Geology, v. 27, p. 743–746.

Kunk, M.J., Wintsch, R.P., Naeser, C.W., Naeser, N.D., Southworth, C.S., Drake A.A., Jr., and Becker J.L., 2005, Contrasting tectonothermal domains and faulting in the Potomac terrane, Virginia-Maryland—discrimination by $^{40}Ar/^{39}Ar$ and fission-track thermochronology: Geological Society of America Bulletin, v. 117, p. 1347–1366.

Lipman, P.W., Prostka, J.H., and Christiansen, R.L., 1972, Cenozoic volcanism and plate-tectonic evolution of the Western United States: Part 1, Early and middle Cenozoic: Royal Society of London Philosophical Transactions, Series A, v. 271, p. 217–248.

Livaccari, R.F., 1991, Role of crustal thickening and extensional collapse in the tectonic evolution of the Sevier-Laramide orogeny, western United States: Geology, v. 19, p. 1104–1107.

Ludwig, K.R., 2003, ISOPLOT; A geochronological toolkit for Microsoft Excel, Version 3.00: Berkeley Geochronology Center Special Publication, v. 4, 70 p.

Marsh, E.E., Goldfarb, R.J., Kunk, M.J., Groves, D.I., Bierlein, F.P., and Creaser, R.A., 2008, New constraints on the timing of gold formation in the Sierra Foothills province, central California, *in* Spencer, J.E., and Titley, S.R., eds., Ores and orogenesis: Circum-Pacific tectonics, geologic evolution, and ore deposits: Arizona Geological Society Digest 22, p. 369–388.

Mauel, D.J., Lawton, T.F., González-León, C., Iriondo, A., and Amato, J.M., 2011, Stratigraphy and age of Upper Jurassic strata in north-central Sonora, Mexico: Southwestern Laurentian record of crustal extension and tectonic transition: Geosphere, v. 7, p. 390–414.

McCandless, T.E., Ruiz, J., and Campbell, A.R., 1993, Rhenium behavior in molybdenite in hypogene and near-surface environments: Implications for Re-Os geochronology: Geochimica et Cosmochimica Acta, v. 57, p. 889–905.

McDowell, F.W., and Mauger, R.L., 1994, K-Ar and U-Pb zircon chronology of Late Cretaceous and Tertiary magmatism in central Chihuahua State, Mexico: Geological Society of America Bulletin, v. 106, p. 118–132.

McDowell, F.W., Roldán-Quintana, J., and Amaya-Martínez, R., 1997, Interrelationship of sedimentary and volcanic deposits associated with Tertiary extension in Sonora, Mexico: Geological Society of America Bulletin, v. 109, p. 1349–1360.

McDowell, F.W., Roldán-Quintana, J., and Connelly, J.N., 2001, Duration of Late Cretaceous-

early Tertiary magmatism in east-central Sonora, Mexico: Geological Society of America Bulletin, v. 113, p. 521–531.

Miller, L.D., Goldfarb, R.J., Gehrels, G.E., and Snee, L.W., 1994, Genetic links among fluid cycling, vein formation, regional deformation, and plutonism in the Juneau gold belt, southeastern Alaska: Geology, v. 22, p. 203–206.

Molina-Garza, R.S., and Geissman, J.W., 1999, Paleomagnetic data from the Caborca terrane, Mexico: Implications for the Cordilleran tectonics and the Mojave-Sonora megashear hypothesis: Tectonics, v. 18, p. 293–325.

Noguez-Alcántara, B., Valencia-Moreno, M., and Calmus, T., 2007, Enriquecimiento supergénico y analisis de balance de masa en el yacimiento de pórfido cuprífero Milpillas, Distrito Cananea, Sonora, México: Revista Mexicana de Ciencias Geológicas, v. 24, p. 368–388.

Noriega-Martínez, O., 2006, Evidencias de dos etapas de mineralización de oro mesotermal en las áreas de Tajitos, Juárez-San Francisco, en la región de Caborca, Sonora México: Unpublished M.Sc. thesis, Hermosillo, Sonora, México, Universidad de Sonora, 85 p.

Nourse, J.A., and Irwin, J.J., 2010, Tectonic and structural setting of gold mineralization in the Sonora-Mojave Belt: Example from the Juarez-Tajitos area [abs.]: American Association of Petroleum Geologists, Geological Society of America, Cordilleran Section, Abstracts with Programs, Annual Meeting, v. 42, p. 108.

Nourse, J.A., Anderson, T.H., and Silver, L.T., 1994, Tertiary metamorphic core complexes in Sonora, northwestern Mexico: Tectonics, v. 13, p. 1161–1182.

Nourse, J.A., Premo, W.R., Iriondo, A., and Stahl, E.R., 2005, Contrasting Proterozoic basement complexes near the truncated margin of Laurentia, northwestern Sonora-Arizona international border region, *in* Anderson, T.H., Nourse, J.A., McKee, J.W, and Steiner, M.B., eds., The Mojave-Sonora Megashear Hypothesis: Development, Assessment, and Alternatives: Geological Society of America Special Paper 393, p. 123–182.

Ochoa-Landín, L., Pérez-Segura, E., Del Río-Salas, R., and Valencia-Moreno, M., 2011, Depósitos Minerales de Sonora, México, *in* Calmus, T., ed., Panorama sobre la geología de Sonora, México: Instituto de Geología, Universidad Nacional Autónoma de México, v. 118, p. 299–331.

Oskin, M., Stock, J., and Martín-Barajas, A., 2001, Rapid localization of Pacific–North America plate motion in the Gulf of California: Geology, v. 29, p. 459–462.

Pérez-Segura, E., 1993, Los yacimientos de oro y plata de Sonora, México y sus relaciones con la geología regional, *in* Delgado-Argote, L.A., and Martín-Barajas, A., eds., Contribuciones a la tectónica del occidente de México: Monografía, Unión Geofísica Mexicana, v. 1, p. 147–174.

Pérez-Segura, E., 2009, Geología y mineralización de la mina de oro de San Francisco, en la provincia del Desierto de Sonora, México, *in* Clark, K.F., Salas-Pizá, G., and Cubillas-Estrada, R., eds., Geología económica de México, 2ª edición, Servicio Geológico Mexicano-Asociación de Ingenieros de Minas, Metalurgistas y Geólogos de México, p. 875–881.

Pérez-Segura, E., Cheilletz, A., Herrera-Urbina, S., and Hanes, Y.J., 1996, Geología, mineralización, alteración hidrotermal y edad del yacimiento de oro de San Francisco, Sonora-Un depósito mesotermal en el Noroeste de México: Revista Mexicana de Ciencias Geológicas, v. 13, p. 65–89.

Poole, F.G., Perry, W.J., Jr., Madrid, R.J., and Amaya-Martínez, R., 2005, Tectonic synthesis of the Ouachita-Marathon-Sonora orogenic margin of southern Laurentia: Stratigraphic and structural implications for timing of deformational events and plate-tectonic model, *in* Anderson, T.H., Nourse, J.A., McKee, J.W., and Steiner, M.B., eds., The Mojave-Sonora megashear hypothesis: Development, assessment, and alternatives: Geological Society of America Special Paper 393, p. 543–596.

Poulsen, K.H., Mortensen J.K., and Walford, P.C., 2008, San Francisco gold deposit, Santa Ana region, Sonora, Mexico: Laramide orogenic, intrusion-related mineralization?, *in* Spencer, J.E., and Titley, S.R., eds., Ores and orogenesis: Circum-Pacific tectonics, geologic evolution, and ore deposits: Arizona Geological Society Digest 22, p. 547–559.

Quintanar-Ruíz, F.J., 2008, La Herradura ore deposit: An orogenic gold deposit in northwestern Mexico: Unpublished M.Sc. thesis, Tucson, Arizona, USA, University of Arizona, 97 p.

Rodriguez-Castañeda, J.L., and Anderson, T.H., 2011, El arco magmático jurásico en Sonora, México—Distribución, edades y ambiente tectónico, *in* Calmus, T., ed., Panorama de la geología de Sonora, México: Universidad Nacional Autónoma de México, Instituto de Geología, v. 118, p. 81–111.

Selby, D., Creaser, R.A., Hart, C.J.R., Rombach, C.S., Thompson, J.F.H., Smith, M.T., Bakke, A.A, and Goldfarb, R.J., 2002, Absolute timing of sulfide and gold mineralization: A comparison of Re-Os molybdenite and Ar-Ar mica methods from the Tintina Gold Belt, Alaska: Geology, v. 30, p. 791–794.

Shafiqullah, M., Damon, P.E., Lynch, D.J., Reynolds, S.J., Rehring, W.A., and Raymond, R.H., 1980, K-Ar Geochronology and Geologic History of southwestern Arizona and adjacent areas: Arizona Geological Society Digest 7, p. 201–260.

Silberman, M.L., Giles D.A., and Graubard, C., 1988, Characteristics of gold deposits in Northern Sonora, Mexico: A preliminary report: Economic Geology, v. 83, p. 1966–1974.

Snow, C.A., Bird, D.K., Metcalf, J., and McWilliams, M., 2008, Chronology of gold mineralization in the Sierra Nevada Foothills from $^{40}Ar/^{39}Ar$ dating of mariposite: International Geology Review, v. 50, p. 503–518.

Spencer, J.E., 1996, Uplift of the Colorado Plateau due to lithosphere attenuation during Laramide low-angle subduction: Journal of Geophysical Research, v. 101, p. 13,595–13,609.

Staude, J.M.G., and Barton, M.D., 2001, Jurassic to Holocene tectonics, magmatism, and metallogeny of northwestern Mexico: Geological Society of America Bulletin, v. 133, p. 1357–1374.

Stewart, J.H., 1988, Latest Proterozoic and Paleozoic southern margin of North America and the accretion of Mexico: Geology, v.16, p. 186–189.

Stewart, J.H., and Roldán-Quintana, J., 1994, Map showing late Cenozoic extensional tilt patterns and associated structures in Sonora and adjacent areas, Mexico: United States Geological Survey, Miscellaneous Field Studies, map MF-2238.

Taylor, C.D., Goldfarb, R.J., Snee, L.W., Gent, C.A., Karl, S.M., and Haeussler, P.J., 1994, New age data for gold deposits and granites, Chichagof mining district, SE Alaska: Evidence for a common origin [abs.]: Geological Society of America, Abstracts with Programs, v. 26, p. 140.

Tosdal, R.M., Haxel, G.B., and Wright, J.E., 1989, Jurassic geology of the Sonoran Desert region, southern Arizona, southeastern California, and northernmost Sonora: Construction of a continental-margin magmatic arc, *in* Jenney, J.P., and Reynolds, S.J.,

eds., Geologic evolution of Arizona: Tucson, Arizona Geological Society Digest 17, p. 397–434.

Titley, S.R., 2001, Crustal Affinities of Metallogenesis in the American Southwest: Economic Geology, v. 96, p. 1323–1342.

Usui, T., Nakamura, E., Kobayashi, K., Maruyama, S., and Helmstaedt, H., 2003, Fate of the subducted Farallon plate inferred from eclogite xenoliths in the Colorado Plateau: Geology, v. 31, p. 589–592.

Valencia, V.A., Noguez-Alcántara, B., Barra, F., Ruiz, J., Gehrels, G.E., Quintanar, F.J., and Valencia-Moreno, M., 2006, Re-Os molybdenite and LA-ICPMS-MC U-Pb zircon geochronology for the Milpillas porphyry copper deposit: insights for the timing of mineralization in the Cananea District, Sonora, Mexico: Revista Mexicana de Ciencias Geológicas, v. 23, p. 39–53.

Valencia-Moreno, M., and Ortega-Rivera, M.A., 2011, Cretácico Tardío-Eoceno Medio en el noroeste de México—Evolución del arco magmático continental y su contexto geodinámico (orogenia Laramide), *in* Calmus, T., ed., Panorama de la geología de Sonora, México: Universidad Nacional Autónoma de México, Instituto de Geología, v. 118, p. 201–226.

Valencia-Moreno, M., Ruiz, J., Barton, M.D., Patchett, P.J., Zürcher, L., Hodkinson, D., and Roldán-Quintana, J., 2001, A chemical and isotopic study of the Laramide granitic belt of northwestern Mexico: Identification of the southern edge of the North American Precambrian basement: Geological Society of America Bulletin, v.113, p. 1409–1422.

Vega-Granillo, R., and Calmus, T., 2003, Mazatan metamorphic core complex (Sonora, Mexico): structures along the detachment fault and its exhumation evolution: Journal of South American Earth Sciences, v. 16, p. 193–204.

Vidal-Solano, J.R., Demant, A., Paz-Moreno, F.A., Lapierre, H., Ortega-Rivera, M.A., and Lee, J.K., 2008, Insights into the tectonomagmatic evolution of NW Mexico: Geochronology and geochemistry of the Miocene volcanic rocks from the Pinacate area, Sonora: Geological Society of America Bulletin, v. 120, p. 691–708.

Ward, P.L., 1991, On plate tectonics and the geologic evolution of Southwestern North America: Journal of Geophysical Research, v. 96, p. 12,479–12,496.

Wells, M.L., and Hoisch, T.D., 2008, The role of mantle delamination in widespread Late Cretaceous extension and magmatism in the Cordilleran orogen, western United States: Geological Society of America Bulletin, v. 120, p. 515–530.

Wells, M.L., Beyene, M.A., Spell, T.L., Kula, J.L., Miller, D.M., and Zanetti, K.A., 2005, The Pinto Shear zone; a Laramide synconvergent extensional shear zone in the Mojave Desert region of the southwestern United States: Journal of Structural Geology, v. 27, p. 1697–1720.

Wetmore, P.H., Herzig, C., Alsleben, H., Sutherland, M., Schmidt, K.L., Schultz, P.W., and Paterson, S.R., 2003, Mesozoic tectonic evolution of the Peninsular Ranges of Southern and Baja California, *in* Johnson, S.E., Paterson, S.R., Fletcher, J.M., Girty, G.H., Kimbrough, D.L., and Martin-Barajas, A., eds., Tectonic Evolution of Northwestern Mexico and the Southwestern United States: Geological Society of America Special Paper 374, p. 93–116.

Wilson, P.D., Sullivan, K., Piggott, K., Marín-Payán, M., and Clark, K.F., 2009, Oro en depósitos de placer de El Boludo, Sonora, Méxco, *in* Clark, K.F., Salas-Pizá, G.A., and Cubillas-Estrada, R., eds., Geología Económica de México, p. 817–830.

Zawada, R.D., Albinson, T.F., and Aneyta, R., 2001, Geology of the El Crestón Gold Deposit, Sonora State Mexico: Economic Geology Special Publication 8, New Mines and Discoveries in Mexico and Central America, p. 187–197.

Figure Captions

Figure 1. Distribution of orogenic gold provinces in the North American Cordillera. A) Mesozoic and Cenozoic major orogenic gold fields and the main Late Cretaceous to Eocene batholitic bodies from the North American Cordillera (modified from Goldfarb et al., 2008); including the Caborca orogenic gold belt (COGB). B) Close up of northwestern

Mexico and southwestern United States showing the main orogenic gold prospects and mines along the COGB; the copper-molybdenum porphyry belt of United States and Mexico (CMPB US-MEX) and related mine sites and prospects in the United States and Mexico are also shown.

Figure 2. Map of northwestern Sonora and southwestern Arizona showing 63 sample locations for the $^{40}Ar/^{39}Ar$-dated Au-rich quartz veins from the Caborca orogenic gold belt (COGB). Red localities indicate orogenic gold sites confirmed by mineral paragenesis. Yellow shaded area represents the estimated area of orogenic Au-rich quartz veins. Shades of dark grey represent pre-mineral bedrock outcrops with ages older than ~60 Ma and post-mineral bedrock outcrops with younger ages (~25 Ma) than the gold mineralization, are represented in light grey.

Figure 3. Distribution of Paleoproterozoic basement provinces of southwestern Laurentia in northwestern Sonora and southwestern United States (modified from Iriondo and Premo, 2011). Red dotted line delimits the Caborca orogenic gold belt (COGB) and the blue dashed line shows the trace of the hypothetical Mojave-Sonora Megashear (hMSM) as proposed by Anderson and Silver (1979, 2005) and Campbell and Anderson (2003). Outcrops in dark brown represent Proterozoic basement rocks.

Figure 4. Examples of quartz veins and associated mineral textures for the Caborca orogenic gold belt (COGB). A-D) Orogenic quartz veins with en echelon array, mostly related to shear zones; several of them showing milky quartz with reddish to yellowish patches related to oxidation of sulfides (mostly pyrite) that occurred during supergene alteration. E) Quartz vein structure in anastomosed arrangement. F) White mica flakes in quartz. G) Brown carbonate (Cb) in quartz. H) Unaltered pyrite in clear quartz. I) Unaltered galena

in milky quartz. J) Chunk of gold in clear quartz. K) Nuggets of gold from quartz concentrated using heavy liquids (San Francisco-Llano Mine sample, vein with ~134 g/t of Au). L) Clear quartz with free gold and goethite pseudomorph after pyrite. Au = Gold; Cb = Carbonate mineral (commonly calcite); Gn = Galena; Py = Pyrite; Py* = Pyrite pseudomorph; Qtz = Quartz; Wmca = White mica.

Figure 5. Examples of dated Au-rich quartz veins from the Caborca orogenic gold belt. A) Quartz Vein from San Francisco-Llano Mine (vein with ~134 g/t of Au) with intergrowths of white mica crystallized between pyrite (now goethite pseudomorph after pyrite). B) Quartz vein with high content of white and goethite. C) Example of quartz vein plus white mica and large crystals of goethite. D) A view under optical microscope of a thin section (microphotograph) of quartz vein with white mica intergrowths and some sulfides (opaque minerals). E) Microphotograph showing a close view of the quartz and white mica. Gt = Goethite; Op = Opaque mineral; Py = Pyrite; Qtz = Quartz; Wmca = White mica.

Figure 6. Rose diagram showing orientation planes of 113 quartz veins measured along the Caborca orogenic gold belt in northwestern Sonora, Mexico. The main trend for these quartz veins is north-northwest oriented.

Figure 7. Four representative $^{40}Ar/^{39}Ar$ spectra and inverse-isotope correlation diagrams (inverse isochrons) for the white mica samples along the Caborca orogenic gold belt (COGB; see figure 2 for sample locations of dated quartz-gold veins). All $^{40}Ar/^{39}Ar$ analytical data and tables for the 63 white mica samples in this study are available in an U.S. Geological Survey Open-File Report (Izaguirre et al., 2016). A) Example of a plateau age spectrum and inverse isochron obtained from fresh white mica flakes separated to an optical purity

of >99%. B) Example of an isochron age obtained from fresh white mica flakes. C) Example of an average age calculated by picking a coherent group of heating steps out of the age spectrum diagram from white mica aggregates. D) Example of a single step age type from a step heating experiment on a polycrystalline aggregate rich in white mica. The first step in the climbing age spectrum in which a flattening in the age is observed is interpreted to be a minimum estimate for the time of white mica growth.

Figure 8. Histogram and age probability plots of A) mineralization ages of quartz-gold veins (n = 77) from the Caborca orogenic gold belt (COGB; Table A1) showing a mineralization age peak at ~61 Ma (middle Paleocene). B) Plot of mineralization ages (n = 106) of the copper-molybdenum porphyry belt of United States and Mexico (CMPB US-MEX) (Table A2). C) Plot of crystallization ages of pre-mineralization Laramide igneous rocks and post-mineralization (Oligocene to present) rocks along the COGB area (Table A3 and A4). Age plots were created using Isoplot 3.0 add-in for Microsoft Excel (Ludwig, 2003).

Figure 9. Histogram and probability plots of mineralization ages compiled from all major orogenic gold fields in the North American Cordillera (Table A1) including data of the Caborca orogenic gold belt (COGB) in northwestern Mexico. Plots were created using Isoplot 3.0 add-in for Microsoft Excel (Ludwig, 2003).

Figure 10. A) Scatter plot of mineralization ages of the Caborca orogenic gold belt (COGB) and the copper-molybdenum porphyry belt of United States and Mexico (CMPB US-MEX) versus distance from Baja California paleotrench after removing the effects of Cenozoic extension. Dashed red and gray arrows show paths of general rejuvenation trends for the orogenic gold and the porphyry mineralization ages. B) Paleogeography of northwestern Mexico and southwestern United States at ~50 Ma with Baja California Peninsula

restored (Oskin et al., 2001) and including the restoration of Cenozoic extension (Henry and Aranda-Gómez, 2000). This figure shows a scenario of the COGB forming in the forearc domain and the CMPB US-MEX in the magmatic arc region further away from the trench. C) Present day position of the COGB and CMPB US-MEX with respect to the paleotrench. Mineralized quartz veins along the COGB are differentiated in grades of yellow and gray to show rejuvenation and/or migration towards the East. The CMPB US-MEX is subdivided between an A trend (closer from the paleotrech) and a B trend (farther from the paleotrench); both showing a complicated age distribution of porphyry bodies.

Figure 11. Proposed tectonic framework of the Caborca orogenic gold belt (COGB) for this portion of the North American Cordillera. Illustration shows cross sections of the paleoposition localities of Ensenada (Baja California), Caborca (Sonora) and Tucson (Arizona) during the Early Cretaceous to Eocene tectonic convergence. A) Tectonic cross section showing the environment of formation of deep metamorphic fluids during high-angle subduction of the Farallon oceanic slab beneath the North American continental plate and shortening in the forearc and arc domains. Additionally, this figure shows the suture of the earlier accretion of the Baja California-California terranes against the North American continental plate, which ended at ~110 Ma (Aptian-Albian). Magmatic activity was established near the current Sonoran coast between ~96 and ~85 Ma. B) Orogenic hydrothermal vein formation began when flat slab subduction started at ~70–65 Ma and synconvergent upper crustal extension triggered the multi-stage dewatering process on the forearc domain. Orogenic mineralization occurs during this period of time with a peak of activity at ~61 Ma (middle Paleocene); ore forming process occurred mostly in the

ductile-brittle transition zone (4–6 km deep) in preexisting compressional Laramide shear structures reactivated during this period of synconvergent crustal extension. An observed eastward migration of magmatism is suggested by the age analysis of the dated rocks from the copper-molybdenum porphyry belt. C) An eastward rejuvenation of the orogenic gold belt is interpreted as representing migration of the source of the remaining orogenic fluids. The final stage of orogenic gold and copper-molybdenum mineralization occurred prior to ~36 Ma, which is the estimated time for cessation of the orogenic quartz-gold mineralization in this part of the North American Cordillera.

Figure

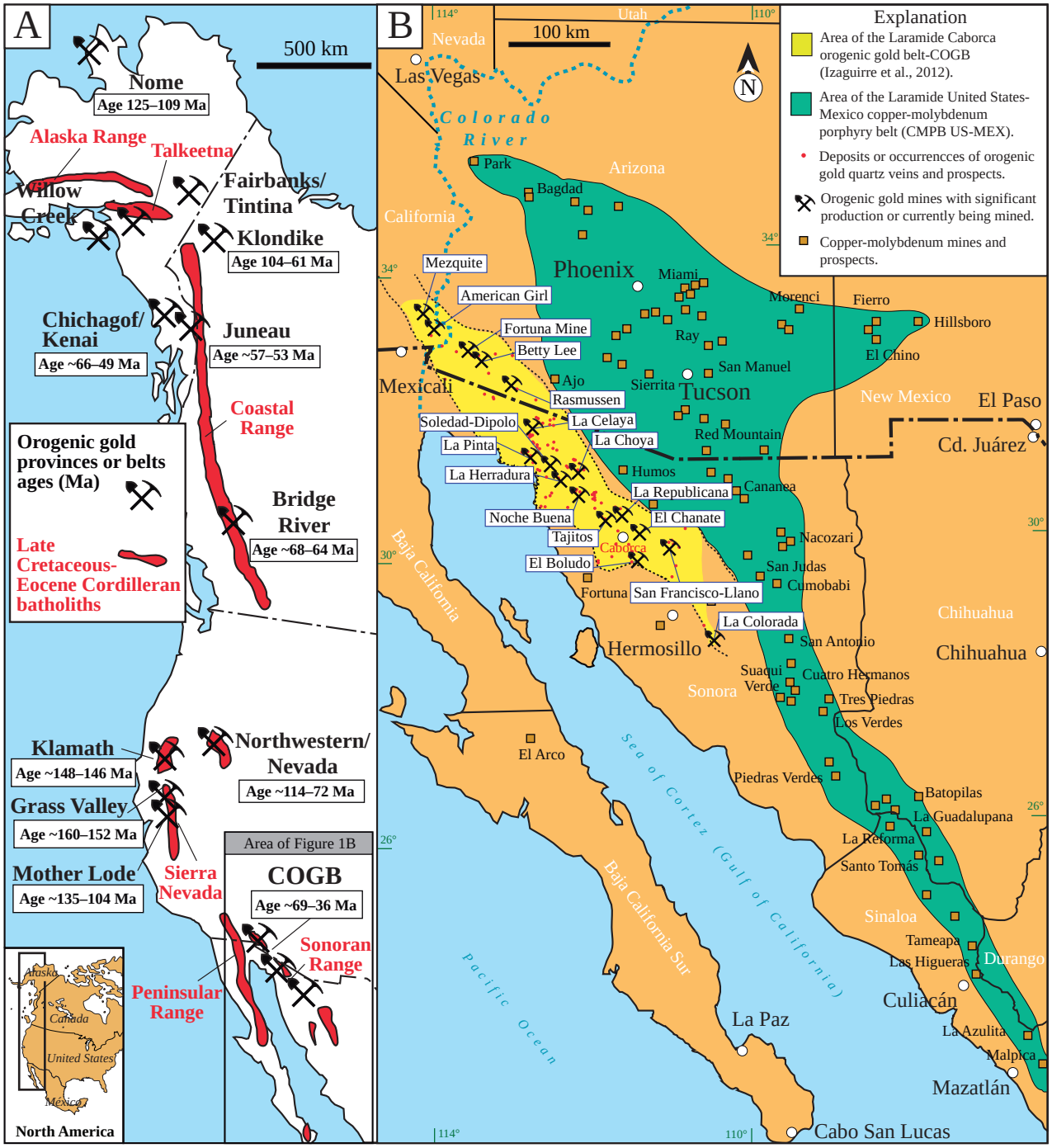
A
500 km
Nome
Age 125–109 Ma
Alaska Range
Talkeetna
Willow Creek
Fairbanks/ Tintina
Klondike
Age 104–61 Ma
Chichagof/ Kenai
Age ~66–49 Ma
Juneau
Age ~57–53 Ma
Coastal Range
Orogenic gold provinces or belts ages (Ma)
Late Cretaceous-Eocene Cordilleran batholiths
Bridge River
Age ~68–64 Ma
Klamath
Age ~148–146 Ma
Northwestern/ Nevada
Age ~114–72 Ma
Grass Valley
Age ~160–152 Ma
Mother Lode
Age ~135–104 Ma
Sierra Nevada
Area of Figure 1B
COGB
Age ~69–36 Ma
Sonoran Range
Peninsular Range
Alaska
Canada
United States
Mexico
North America
B
100 km
Nevada
Utah
Las Vegas
Colorado River
Arizona
California
Park
Bagdad
Phoenix
Miami
Morenci
Fierro
Hillsboro
El Chino
Ray
San Manuel
Sierrita
Tucson
New Mexico
El Paso
Cd. Juárez
Mezquite
American Girl
Fortuna Mine
Betty Lee
Ajo
Rasmussen
Soledad-Dipolo
La Celaya
La Choya
La Pinta
La Herradura
Humos
La Republicana
Cananea
Red Mountain
Noche Buena
El Chanate
Tajitos
Caborca
El Boludo
Nacozari
San Judas
Cumobabi
Fortuna
San Francisco-Llano
La Colorada
Hermosillo
San Antonio
Chihuahua
Chihuahua
Suaqui Verde
Cuatro Hermanos
Tres Piedras
Los Verdes
Sonora
El Arco
Piedras Verdes
Batopilas
La Guadalupana
La Reforma
Santo Tomás
Sinaloa
Tameapa
Las Higueras
Durango
Culiacán
La Azulita
Malpica
Mazatlán
La Paz
Cabo San Lucas
Baja California
Baja California Sur
Sea of Cortez (Gulf of California)
Pacific Ocean
Explanation
Area of the Laramide Caborca orogenic gold belt-COGB (Izaguirre et al., 2012).
Area of the Laramide United States-Mexico copper-molybdenum porphyry belt (CMPB US-MEX).
Deposits or occurrencces of orogenic gold quartz veins and prospects.
Orogenic gold mines with significant production or currently being mined.
Copper-molybdenum mines and prospects.
N

Fig. 1

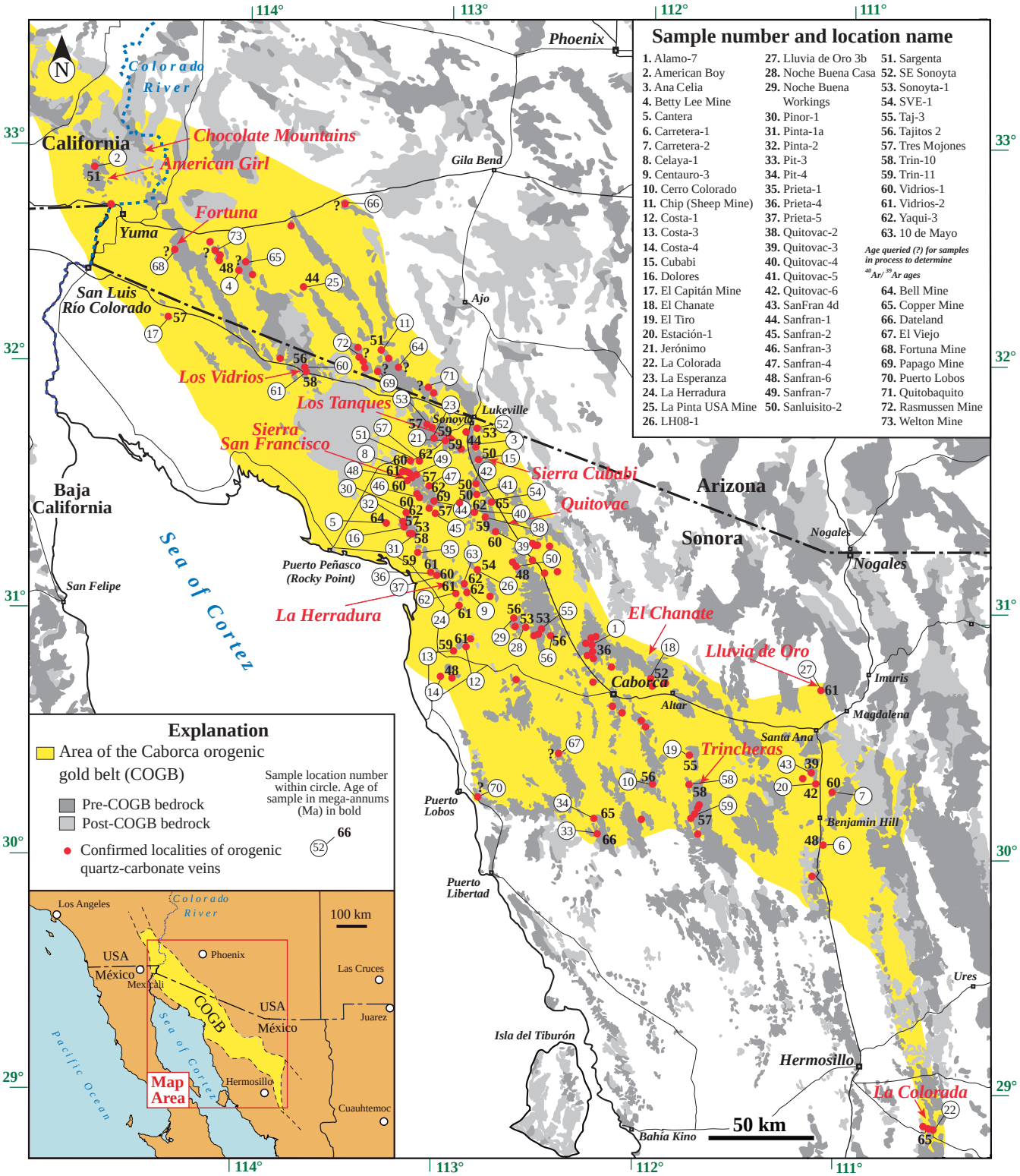
Sample number and location name
1. Alamo-7
2. American Boy
3. Ana Celia
4. Betty Lee Mine
5. Cantera
6. Carretera-1
7. Carretera-2
8. Celaya-1
9. Centauro-3
10. Cerro Colorado
11. Chip (Sheep Mine)
12. Costa-1
13. Costa-3
14. Costa-4
15. Cubabi
16. Dolores
17. El Capitán Mine
18. El Chanate
19. El Tiro
20. Estación-1
21. Jerónimo
22. La Colorada
23. La Esperanza
24. La Herradura
25. La Pinta USA Mine
26. LH08-1
27. Lluvia de Oro 3b
28. Noche Buena Casa
29. Noche Buena Workings
30. Pinor-1
31. Pinta-1a
32. Pinta-2
33. Pit-3
34. Pit-4
35. Prieta-1
36. Prieta-4
37. Prieta-5
38. Quitovac-2
39. Quitovac-3
40. Quitovac-4
41. Quitovac-5
42. Quitovac-6
43. SanFran 4d
44. Sanfran-1
45. Sanfran-2
46. Sanfran-3
47. Sanfran-4
48. Sanfran-6
49. Sanfran-7
50. Sanluisito-2
51. Sargenta
52. SE Sonoyta
53. Sonoyta-1
54. SVE-1
55. Taj-3
56. Tajitos 2
57. Tres Mojones
58. Trin-10
59. Trin-11
60. Vidrios-1
61. Vidrios-2
62. Yaqui-3
63. 10 de Mayo
Age queried (?) for samples in process to determine 40Ar/39Ar ages
64. Bell Mine
65. Copper Mine
66. Dateland
67. El Viejo
68. Fortuna Mine
69. Papago Mine
70. Puerto Lobos
71. Quitobaquito
72. Rasmussen Mine
73. Welton Mine
Explanation
Area of the Caborca orogenic gold belt (COGB)
Pre-COGB bedrock
Post-COGB bedrock
Confirmed localities of orogenic quartz-carbonate veins
Sample location number within circle. Age of sample in mega-annums (Ma) in bold
66
52
Colorado River
California
Chocolate Mountains
American Girl
Fortuna
Yuma
San Luis
Río Colorado
Los Vidrios
Los Tanques
Sierra San Francisco
Baja California
Sea of Cortez
San Felipe
Puerto Peñasco (Rocky Point)
La Herradura
Phoenix
Gila Bend
Ajo
Lukeville
Sonoyta
Sierra Cubabi
Quitovac
Arizona
Sonora
Nogales
Nogales
El Chanate
Lluvia de Oro
Caborca
Altar
Imuris
Magdalena
Santa Ana
Trincheras
Benjamin Hill
Puerto Lobos
Puerto Libertad
Isla del Tiburón
Hermosillo
Ures
La Colorada
Bahía Kino
50 km
114°
113°
112°
111°
33°
32°
31°
30°
29°
Los Angeles
Colorado River
100 km
USA
México
Mexicali
Phoenix
Las Cruces
Juarez
COGB
Sea of Cortez
Pacific Ocean
Hermosillo
Cuauhtemoc
Map Area

Fig. 2

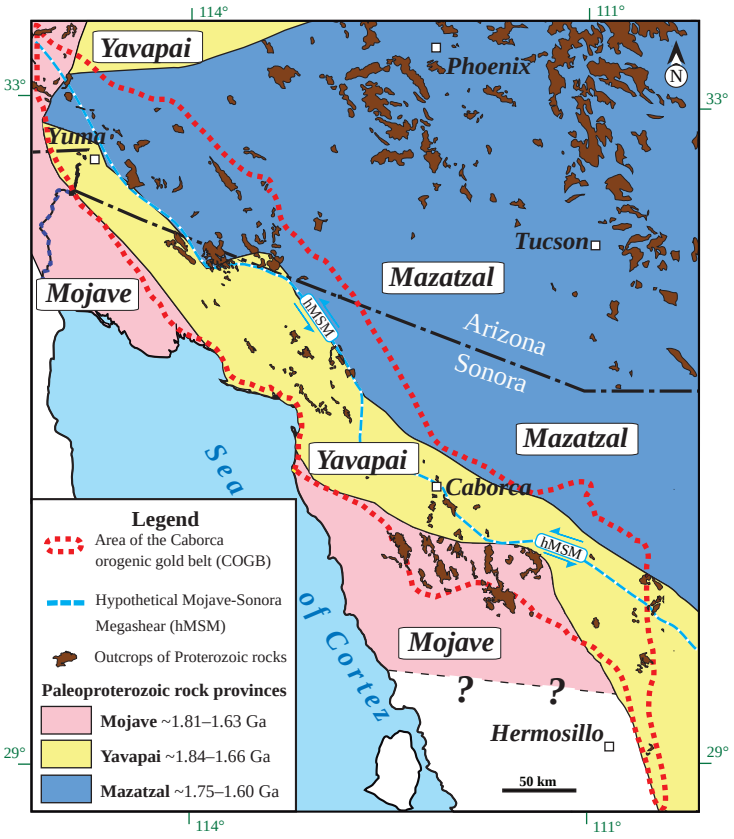
114°
111°
33°
29°
Yavapai
Phoenix
N
Yuma
Tucson
Mazatzal
Mojave
hMSM
Arizona
Sonora
Mazatzal
Yavapai
Caborca
Sea of Cortez
hMSM
Mojave
? ?
Hermosillo
50 km
Legend
Area of the Caborca orogenic gold belt (COGB)
Hypothetical Mojave-Sonora Megashear (hMSM)
Outcrops of Proterozoic rocks
Paleoproterozoic rock provinces
Mojave ~1.81–1.63 Ga
Yavapai ~1.84–1.66 Ga
Mazatzal ~1.75–1.60 Ga

Fig. 3

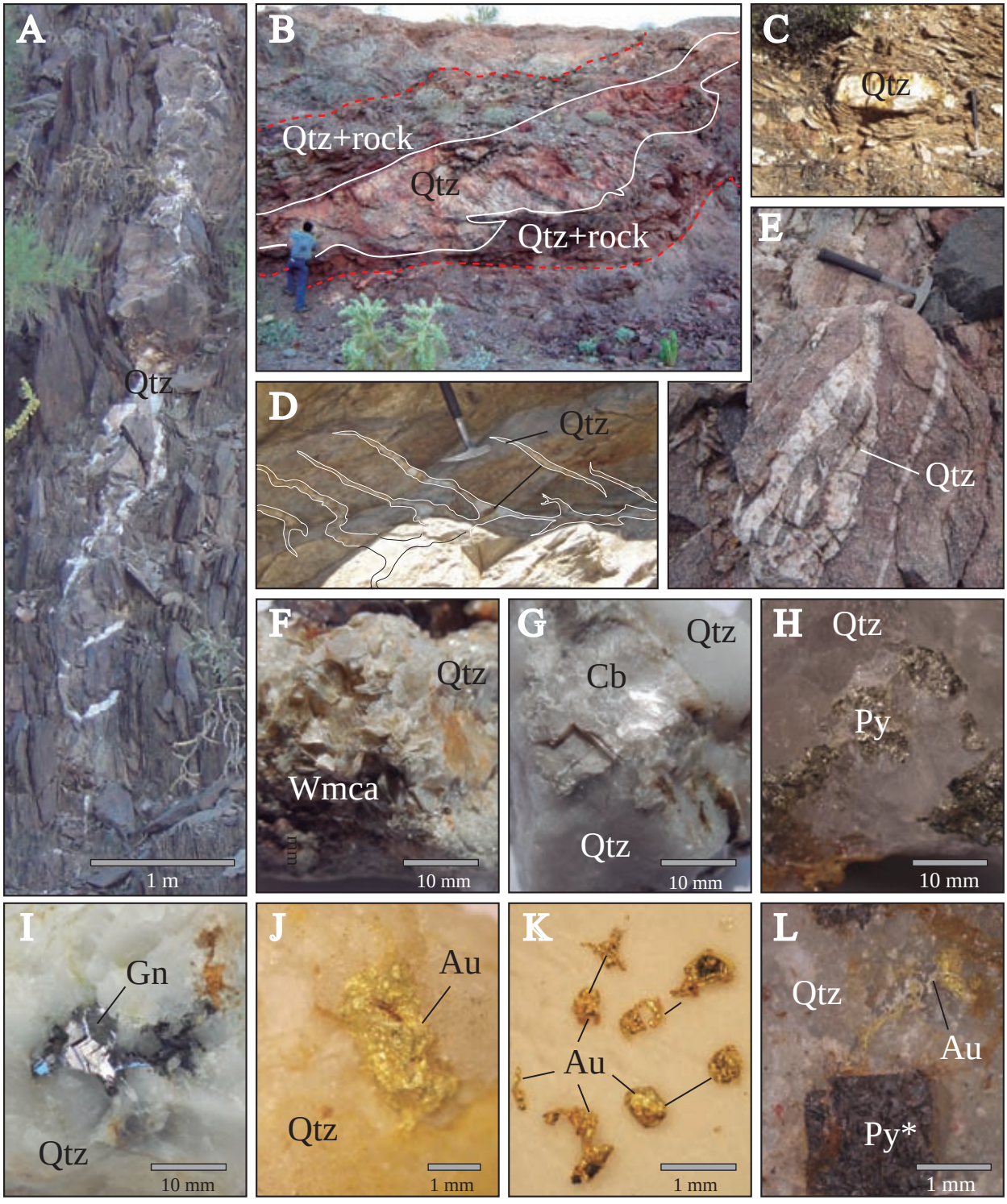
A
Qtz
1 m
B
Qtz+rock
Qtz
Qtz+rock
C
Qtz
D
Qtz
E
Qtz
F
Qtz
Wmca
10 mm
G
Qtz
Cb
Qtz
10 mm
H
Qtz
Py
10 mm
I
Gn
Qtz
10 mm
J
Au
Qtz
1 mm
K
Au
1 mm
L
Qtz
Au
Py*
1 mm

Fig. 4

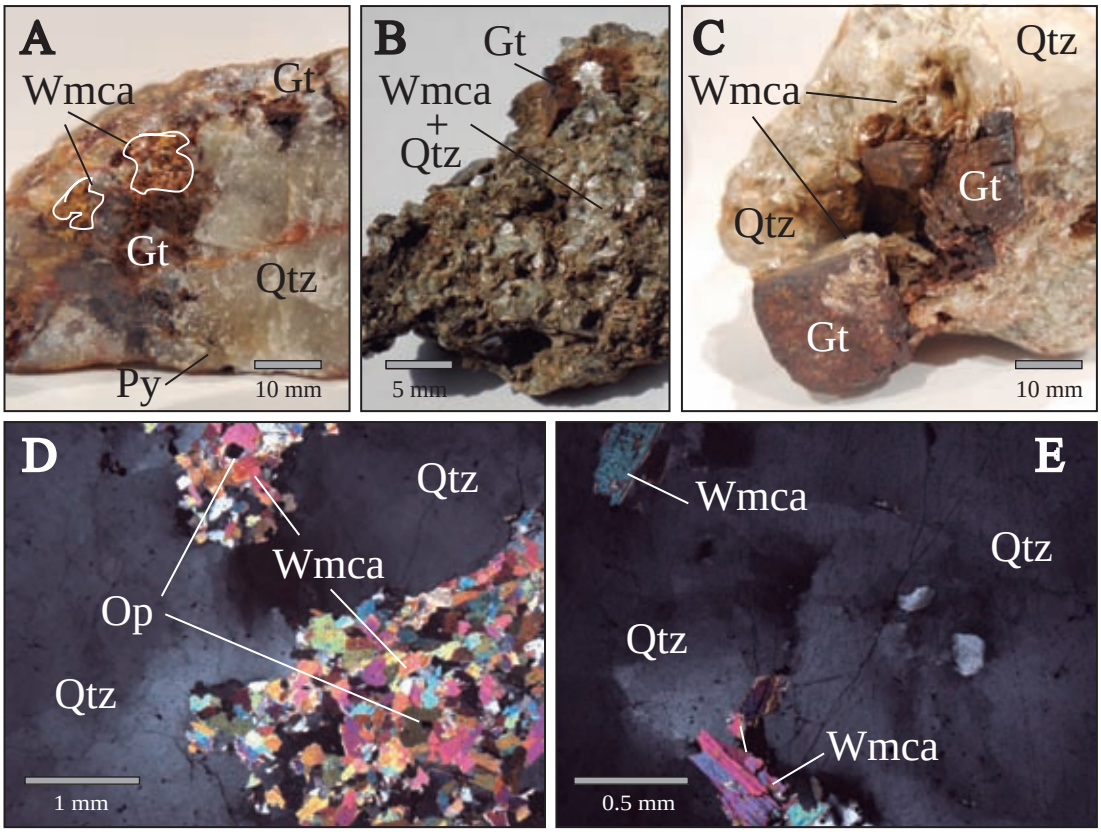
A
Wmca
Gt
Gt
Qtz
Py
10 mm
B
Gt
Wmca
+
Qtz
5 mm
C
Qtz
Wmca
Gt
Qtz
Gt
10 mm
D
Qtz
Wmca
Op
Qtz
1 mm
E
Wmca
Qtz
Qtz
Wmca
0.5 mm

Fig. 5

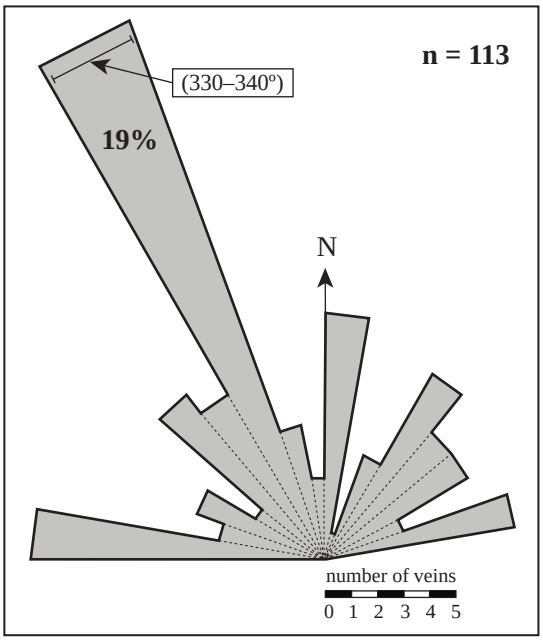

Fig. 6

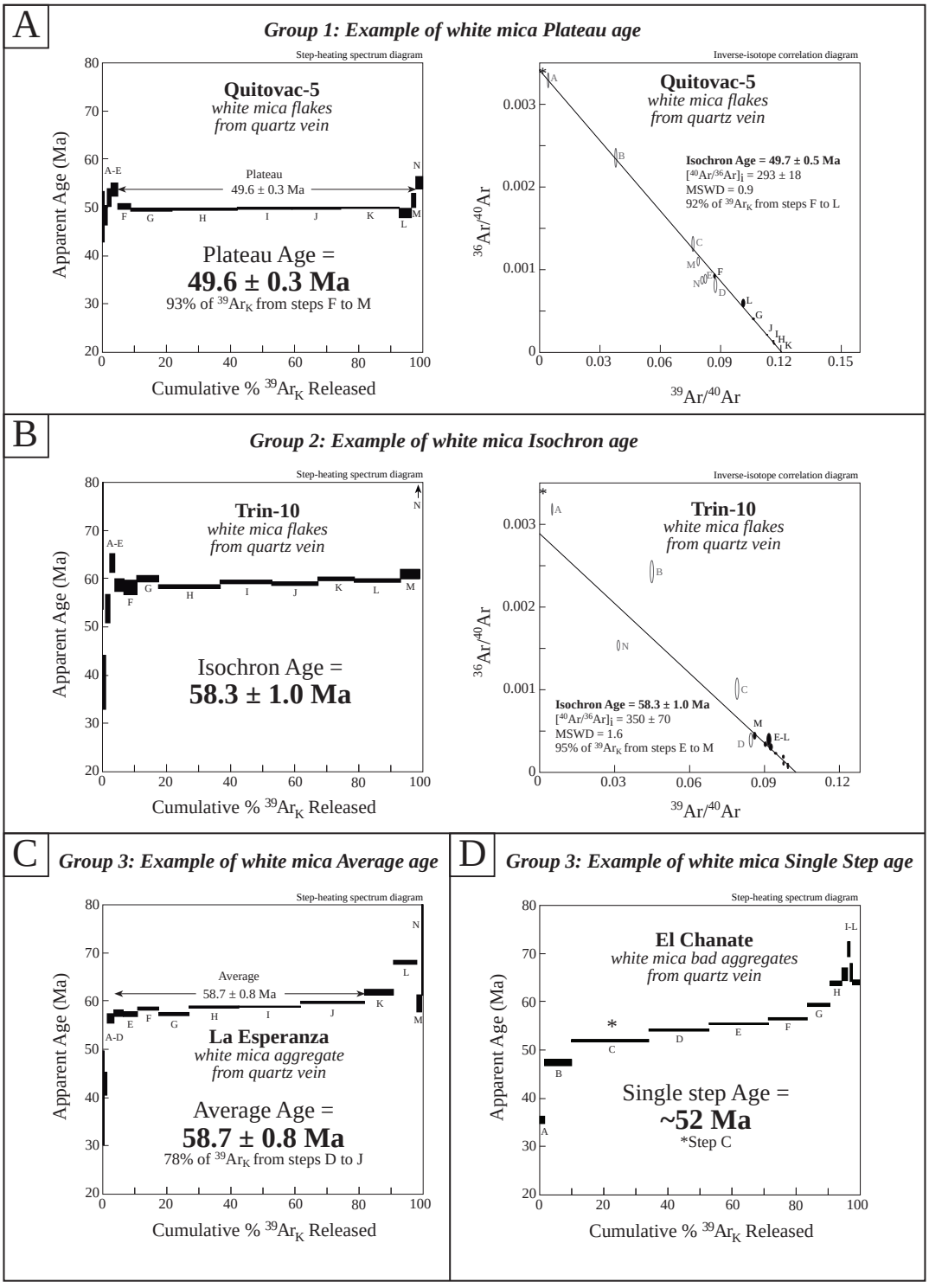
A
Group 1: Example of white mica Plateau age
Step-heating spectrum diagram
Quitovac-5
white mica flakes
from quartz vein
Plateau
49.6 ± 0.3 Ma
Plateau Age =
49.6 ± 0.3 Ma
93% of 39ArK from steps F to M
Apparent Age (Ma)
Cumulative % 39ArK Released
Inverse-isotope correlation diagram
Quitovac-5
white mica flakes
from quartz vein
Isochron Age = 49.7 ± 0.5 Ma
[40Ar/36Ar]i = 293 ± 18
MSWD = 0.9
92% of 39ArK from steps F to L
36Ar/40Ar
39Ar/40Ar
B
Group 2: Example of white mica Isochron age
Step-heating spectrum diagram
Trin-10
white mica flakes
from quartz vein
Isochron Age =
58.3 ± 1.0 Ma
Apparent Age (Ma)
Cumulative % 39ArK Released
Inverse-isotope correlation diagram
Trin-10
white mica flakes
from quartz vein
Isochron Age = 58.3 ± 1.0 Ma
[40Ar/36Ar]i = 350 ± 70
MSWD = 1.6
95% of 39ArK from steps E to M
36Ar/40Ar
39Ar/40Ar
C
Group 3: Example of white mica Average age
Step-heating spectrum diagram
Average
58.7 ± 0.8 Ma
La Esperanza
white mica aggregate
from quartz vein
Average Age =
58.7 ± 0.8 Ma
78% of 39ArK from steps D to J
Apparent Age (Ma)
Cumulative % 39ArK Released
D
Group 3: Example of white mica Single Step age
Step-heating spectrum diagram
El Chanate
white mica bad aggregates
from quartz vein
Single step Age =
~52 Ma
*Step C
Apparent Age (Ma)
Cumulative % 39ArK Released

Fig. 7

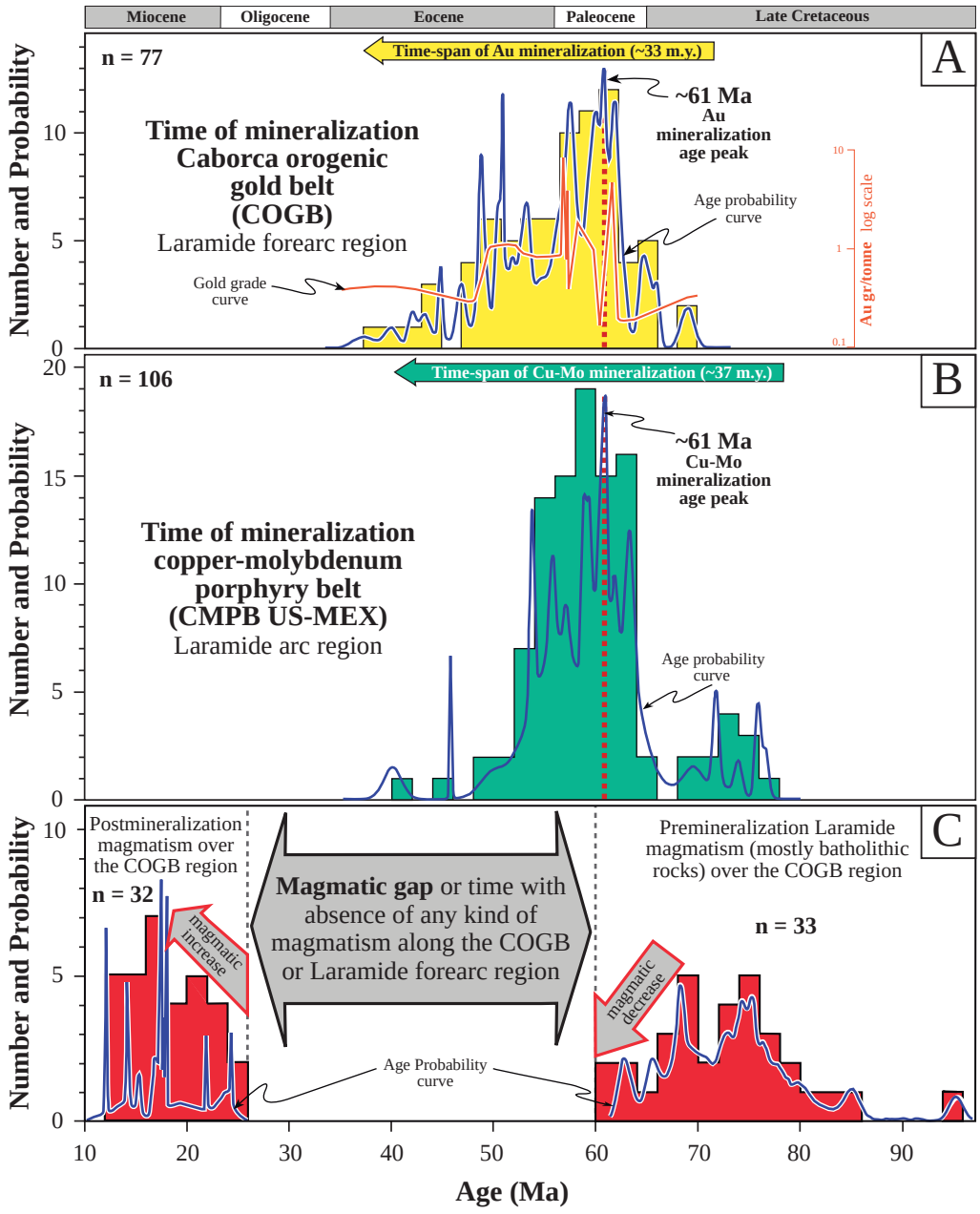
Miocene
Oligocene
Eocene
Paleocene
Late Cretaceous
A
n = 77
Time-span of Au mineralization (~33 m.y.)
~61 Ma
Au
mineralization
age peak
Time of mineralization
Caborca orogenic
gold belt
(COGB)
Laramide forearc region
Age probability
curve
Gold grade
curve
Au gr/tonne log scale
Number and Probability
B
n = 106
Time-span of Cu-Mo mineralization (~37 m.y.)
~61 Ma
Cu-Mo
mineralization
age peak
Time of mineralization
copper-molybdenum
porphyry belt
(CMPB US-MEX)
Laramide arc region
Age probability
curve
C
Postmineralization
magmatism over
the COGB region
n = 32
magmatic
increase
Magmatic gap or time with
absence of any kind of
magmatism along the COGB
or Laramide forearc region
Premineralization Laramide
magmatism (mostly batholithic
rocks) over the COGB region
n = 33
magmatic
decrease
Age Probability
curve
Age (Ma)

Fig. 8

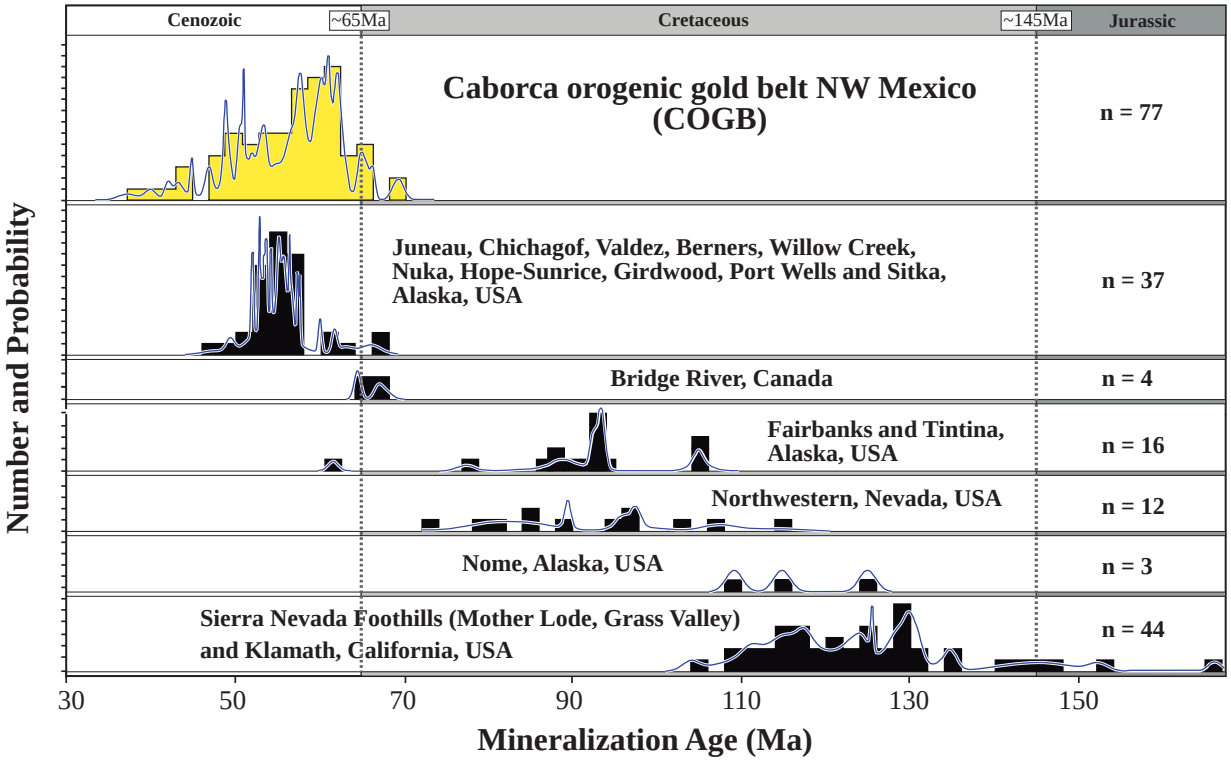
Cenozoic
~65Ma
Cretaceous
~145Ma
Jurassic
Caborca orogenic gold belt NW Mexico (COGB)
n = 77
Juneau, Chichagof, Valdez, Berners, Willow Creek, Nuka, Hope-Sunrice, Girdwood, Port Wells and Sitka, Alaska, USA
n = 37
Bridge River, Canada
n = 4
Fairbanks and Tintina, Alaska, USA
n = 16
Northwestern, Nevada, USA
n = 12
Nome, Alaska, USA
n = 3
Sierra Nevada Foothills (Mother Lode, Grass Valley) and Klamath, California, USA
n = 44
Number and Probability
30
50
70
90
110
130
150
Mineralization Age (Ma)

Fig. 9

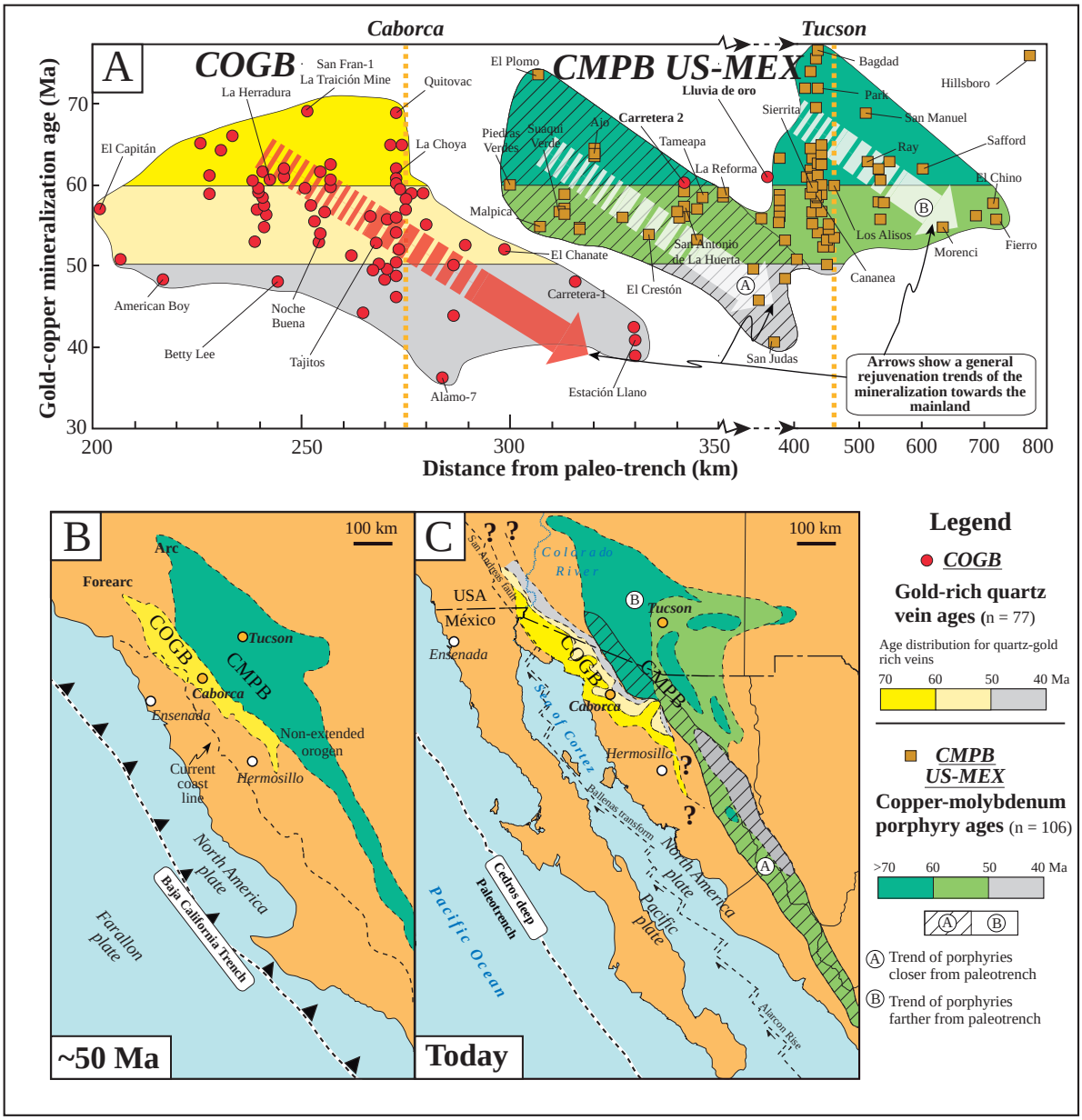
A
COGB
CMPB US-MEX
Caborca
Tucson
Gold-copper mineralization age (Ma)
Distance from paleo-trench (km)
San Fran-1
La Traición Mine
La Herradura
Quitovac
La Choya
El Capitán
American Boy
Noche Buena
Betty Lee
Tajitos
Alamo-7
El Chanate
Carretera-1
Estación Llano
El Plomo
Piedras Verdes
Suaqui Verde
Ajo
Carretera 2
Tameapa
La Reforma
Malpica
San Antonio de La Huerta
El Crestón
San Judas
Lluvia de oro
Sierrita
Bagdad
Hillsboro
Park
San Manuel
Ray
Safford
El Chino
Los Alisos
Morenci
Fierro
Cananea
Arrows show a general rejuvenation trends of the mineralization towards the mainland
B
100 km
Arc
Forearc
COGB
CMPB
Tucson
Caborca
Ensenada
Non-extended orogen
Current coast line
Hermosillo
North America plate
Baja California Trench
Farallon plate
~50 Ma
C
100 km
San Andreas fault
Colorado River
USA
México
Ensenada
Tucson
Caborca
Hermosillo
Sea of Cortez
Ballenas transform
North America plate
Pacific plate
Cedros deep
Paleotrench
Pacific Ocean
Alarcon Rise
Today
Legend
COGB
Gold-rich quartz vein ages (n = 77)
Age distribution for quartz-gold rich veins
70 60 50 40 Ma
CMPB US-MEX
Copper-molybdenum porphyry ages (n = 106)
>70 60 50 40 Ma
A Trend of porphyries closer from paleotrench
B Trend of porphyries farther from paleotrench

Fig. 10

Early Cretaceous to Eocene convergence along the North American Cordillera
(cross section along NW Mexico-SW United States)

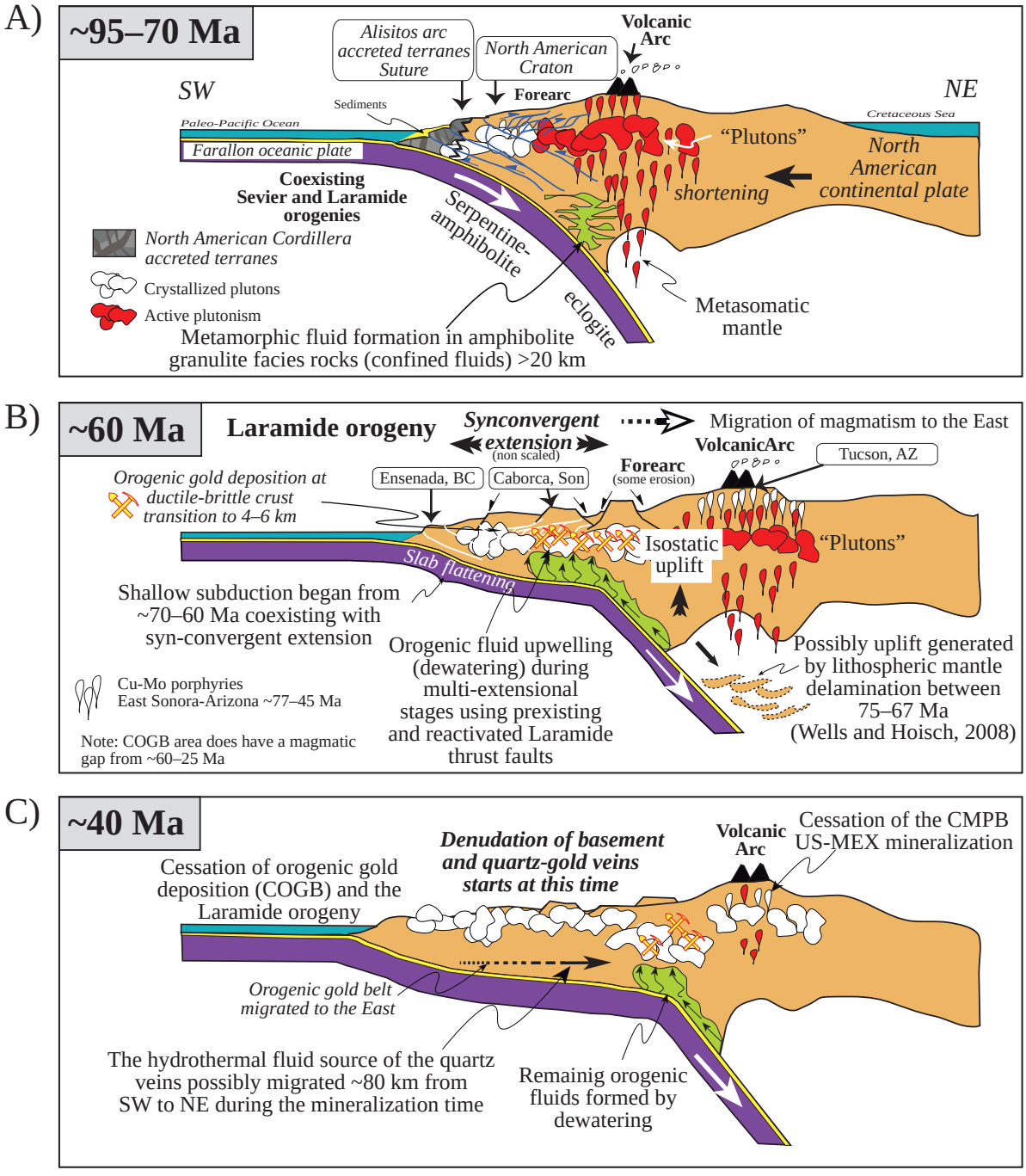

Fig. 11

Table Click here to download Table Tables Izaguirre et al.,.pdf

Table 1. Summary of sixty-three $^{40}Ar/^{39}Ar$ ages obtained from white micas of Au-rich quartz veins of the Caborca orogenic gold belt of northwestern Sonora, Mexico.

Sample name	Locality	Latitude*	Longitude*	Laboratory number	White mica habit	Type of age	Trench distance (km)	Age (Ma)	Error (Ma)
Group 1-Plateau ages	n = 21								
Pit-3	Pozos de Cerna Ranch	30° 4' 42.3"	112° 10' 48.2"	35KD55	Flakes	Plateau	233	**65.9**	± **0.3**
Cantera	Canteras-Sierra Pinta	31° 26' 44.3"	113° 16' 29.0"	261KD52	Flakes	Plateau	231	**64.3**	± **0.4**
Sanfran-4	Sierra San Francisco	31° 37' 37.0"	113° 6' 42.4"	52KD55	Flakes	Plateau	255	**61.6**	± **0.3**
Pinor-1	Sierra Pinta	31° 25' 23.7"	113° 7' 58.0"	267KD52	Flakes	Plateau	241	**61.6**	± **0.3**
Celaya-1	Sierra San Francisco	31° 40' 21.1"	113° 8' 11.1"	1KD12	Flakes	Plateau	257	**60.5**	± **0.2**
Sanfran-6	Sierra San Francisco	31° 37' 57.5"	113° 6' 33.7"	63KD55	Flakes	Plateau	257	**60.4**	± **0.3**
Prieta-5	Sierra Prieta	31° 14' 2.9"	113° 0' 51.9"	40KD55	Flakes	Plateau	240	**59.7**	± **0.3**
Sanfran-3	Sierra San Francisco	31° 31' 21.7"	113° 4' 44.1"	48KD55	Flakes	Plateau	251	**59.5**	± **0.3**
Prieta-1	Sierra Prieta	31° 18' 46.5"	113° 4' 7.1"	46KD55	Flakes/aggregates	Plateau	240	**59.0**	± **0.3**
Vidrios-2	La Angélica Mine	32° 5' 6.5"	113° 40' 45.5"	73KD55	Flakes	Plateau	241	**57.7**	± **0.3**
Sonoyta-1	Sierra Los Tanques	31° 53' 20.2"	113° 0' 36.5"	85KD55	Flakes	Plateau	241	**57.3**	± **0.3**
Sanfran-2	Sierra San Francisco	31° 31' 59.0"	113° 5' 3.7"	61KD55	Flakes	Plateau	253	**57.2**	± **0.3**
El Capitán Mine	Ejido Aquiles Serdán	32° 18' 29.2"	114° 22' 15.5"	103KD60	Flakes	Plateau	201	**56.9**	± **0.3**
Trin-11	Las Amarillas Mine	30° 11' 2.1"	111° 40' 57.8"	77KD55	Flakes	Plateau	275	**56.9**	± **0.3**
Dolores	Dolores Mine	31° 23' 48.1"	113° 7' 39.1"	13KD12	Aggregates	Plateau	239	**52.8**	± **0.3**
Taj-3	Tajítos-Caborca Area	30° 57' 35.6"	112° 22' 6.4"	6DD60	Flakes	Plateau	268	**52.6**	± **0.8**
Chip Mine	Papago-Sheep Mine Area	32° 05' 47.4"	113° 21' 11.5"	98KD60	Flakes	Plateau	262	**51.2**	± **0.3**
Quitovac-6	La Negra Mine	31° 29' 54.2"	112° 51' 55.3"	71KD55	Flakes	Plateau	269	**49.9**	± **0.3**
Quitovac-5	Bustamante Mine	31° 30' 34.2"	112° 50' 23.6"	58KD55	Flakes/aggregates	Plateau	268	**49.6**	± **0.3**
Sanluisito-2	Bertha Mine	31° 17' 2.0"	112° 37' 31.0"	56KD55	Flakes	Plateau	271	**48.1**	± **0.2**
Betty Lee Mine	Copper Mountains	32° 30' 28.7"	113° 59' 41.7"	95KD60	Flakes	Plateau	244	**47.9**	± **0.2**
Group 2-Isochron ages	n = 16								
Tres Mojones	Tres Mojones Mine	31° 40' 25.3"	113° 7' 42.0"	191KD53	Flakes	Isochron	257	**62.2**	± **0.4**
Prieta-4	Sierra Prieta	31° 14' 46.3"	113° 1' 12.9"	25KD55	Flakes	Isochron	239	**60.6**	± **0.7**
Sargenta	Sargenta Mine	31° 40' 19.8"	113° 8' 11.4"	182KD53	Flakes	Isochron	257	**59.8**	± **0.4**
Quitovac-2	El Chacón Mine	31° 26' 5.9"	112° 43' 38.1"	34KD55	Flakes	Isochron	274	**59.4**	± **0.7**
Jerónimo	Sierra Los Tanques	31° 47' 36.3"	112° 57' 54.1"	38KD55	Flakes	Isochron	279	**58.9**	± **0.7**
Pinta-1a	La Pinta Mine	31° 24' 19.3"	113° 7' 23.4"	44KD55	Flakes	Isochron	241	**58.3**	± **0.6**
Trin-10	Sierra La Salada	30° 10' 57.9"	111° 41' 14.1"	59KD55	Flakes	Isochron	276	**58.3**	± **1.0**
Pinta-2	Sierra Pinta	31° 24' 27.4"	113° 7' 17.3"	83KD55	Flakes	Isochron	240	**56.9**	± **0.8**
Sanfran-7	Sierra San Francisco	31° 38' 23.3"	113° 6' 34.5"	79KD55	Flakes	Isochron	256	**56.5**	± **0.6**
Vidrios-1	La Angélica Mine	32° 5' 6.8"	113° 40' 45.2"	75KD55	Flakes	Isochron	242	**56.3**	± **0.6**
LH08-1	Cerro Prieto-Carina	31° 12' 48.1"	112° 47' 31.1"	265KD52	Flakes	Isochron	255	**54.1**	± **1.7**
SE Sonoyta	Los Misioneros Mine	31° 49' 57.7"	112° 49' 41.3"	181KD53	Flakes	Isochron	290	**52.5**	± **0.4**
Carretera-1	Benjamín Hill	30° 4' 54.1"	111° 5' 49.0"	32KD55	Flakes	Isochron	316	**47.8**	± **0.6**
La Pinta USA Mine	Sierra Pinta Arizona	32° 25' 23.2"	113° 40' 9.9"	101KD60	Flakes	Isochron	265	**43.9**	± **0.2**
Estación-1	San Francisco Mine	30° 21' 4.9"	111° 7' 8.5"	16KD55	Flakes	Isochron	330	**42.2**	± **0.5**
Alamo-7	La Republicana area	30° 55' 45.8"	112° 12' 15.8"	21KD55	Flakes/aggregates	Isochron	284	**36.1**	± **1.2**
Group 3-Average or single step ages	n = 26								
Sanfran-1	La Traición Mine	31° 32' 22.6"	113° 3' 56.0"	65KD55	Flakes	Single step	252	**~69**	
Pit-4	South of Pitiquito	30° 4' 47.8"	112° 11' 2.8"	50KD55	Flakes/aggregates	Average	226	**65.0**	± **0.6**
SVE-1	Quitovac	31° 29' 19.5"	112° 46' 40.5"	46KD12	Aggregates	Average	272	**64.9**	± **0.5**
La Colorada	La Colorada Mine	28° 48' 1.4"	110° 34' 37.0"	7KD12	Aggregates	Average	274	**64.7**	± **0.7**
Centauro-3	La Herradura Mine	31° 8' 40.2"	112° 51' 45.8"	20KD12	Aggregates	Single step	246	**~62**	
Quitovac-4	Quitovac Mine	31° 29' 25.4"	112° 46' 6.1"	69KD55	Flakes	Single step	273	**~62**	
10 de Mayo	La Herradura Mine	31° 9' 19.9"	112° 52' 2.4"	22KD12	Aggregates	Single step	246	**~62**	
Costa-1	Cerro El Sahuaro	30° 56' 9.3"	112° 52' 47.8"	20KD55	Flakes	Average	228	**61.0**	± **1.0**
La Herradura	La Herradura Mine	31° 8' 41.8"	112° 51' 49.0"	29KD55	Dirty aggregates	Single step	243	**~61**	
Lluvia de Oro 3b	Lluvia de Oro Mine	30° 43' 20.6"	111° 2' 8.9"	43KD12	Aggregates	Single step	363	**~61**	
Yaqui-3	La Herradura Mine	31° 9' 11.6"	112° 51' 39.4"	39KD12	Aggregates	Single step	246	**~61**	
Quitovac-3	La Choya Mine	31° 25' 6.6"	112° 41' 51.1"	81KD55	Flakes	Average	273	**60.2**	± **0.4**
Carretera-2	La Jarra Mine	30° 18' 14.4"	110° 57' 3.2"	14KD55	Flakes	Average	342	**59.7**	± **1.3**
Costa-3	Cerro El Sahuaro	30° 55' 0.3"	112° 53' 49.8"	18KD55	Aggregates	Average	228	**58.9**	± **0.7**
La Esperanza	La Esperanza Mine	31° 49' 21.5"	112° 58' 18.7"	87KD55	Aggregates	Average	277	**58.7**	± **0.8**
Cerro Colorado	Cerro Colorado Hills	30° 13' 27"	111° 49' 22.9"	9KD12	Aggregates	Single step	267	**~56**	
Noche Buena Workings	Noche Buena Mine	31° 01' 50.3"	112° 38' 46.0"	31KD12	Aggregates	Average	254	**55.7**	± **1.4**
Tajitos 2	Tajítos-Caborca	30° 57' 54.3"	112° 22' 28.1"	3KD12	Aggregates	Average	271	**55.6**	± **1.1**
El Tiro	El Tiro Mine (placer)	30° 17' 8.9"	111° 44' 30.9"	15KD12	Aggregates	Single step	280	**~55**	
Noche Buena Casa	Noche Buena Mine	31° 01' 48.9"	112° 38' 51.6"	5KD12	Aggregates	Average	255	**52.9**	± **0.8**
El Chanate	El Chanate Mine	30° 48' 8.8"	111° 55' 13.2"	263KD52	Dirty aggregates	Single step	299	**~52**	
American Boy	American Boy Mine	32° 51' 20.9"	114° 47' 8.2"	33KD12	Flakes	Average	207	**50.6**	± **0.4**
Cubabi	Sierra Cubabi	31° 45' 48.5"	112° 49' 2.3"	28KD55	Flakes	Average	287	**50.0**	± **0.5**
Costa-4	Caborca Coast	30° 48' 33.2"	112° 56' 52.5"	24KD55	Flakes	Single step	217	**~48**	
Ana Celia	Ana Cecilia Mine	31° 49' 3.5"	112° 52' 3.5"	180KD53	Flakes	Average	287	**43.6**	± **1.1**
SanFran 4d	San Francisco Mine	30° 21' 11.4"	111° 7' 3.8"	11KD12	Aggregates	Average	330	**38.9**	± **0.7**

*Latitude-Longitude Northern Hemisphere; DATUM WGS-84.

Trench distances were calculated from the Baja California paleo-trench to each of the dated occurrences by subtracting ~200 km to eliminate the effects of Cenozoic extension.

Table 2. Orogenic gold characteristics in the Caborca orogenic gold belt of northwestern Sonora, Mexico, versus global knowledge of orogenic gold deposits.

	Caborca orogenic gold belt[1] vs. ***Global orogenic gold***[2]	
Ore host rocks	North American ore hosts include amphibolite-greenschist facies gneisses, schists and granitoids, Mesoproterozoic plutonic rocks, Neoproterozoic and Paleozoic sedimentary rocks, and Permian, Triassic, Jurassic, Cretaceous, and Paleocene rocks (gneisses, granitoids, and sedimentary and volcanic rocks) of the North American Cordillera.	Deformed metamorphic terranes of all ages (greenschist facies rocks) associated with convergent arcs; Archean-age deposits are most prevalent.
Ore formation temperature	260–370ºC; with an average of 330°C.	300 ± 50ºC.
Pressure and crustal deep formation	0.5–1.2 kbars, ~2 to 4–6 km.	1–3 kbars; epizonal-mesozonal (2–12 km).
Ore morphology	Quartz-carbonate veins and stock-work are located in shear zones (mostly thrust faults). Gold dissemination is common in large deposits. Supergene alteration occurs on sulfides and carbonates and is frequently observed as iron oxides, sulfates, halides, and caliche.	Quartz-carbonate veins located in shear zones (mylonites) formed in ductile, ductile-brittle conditions, mineral assemblages not significantly zoned.
Hydrothermal minerals	Quartz, carbonates (calcite, ankerite, and siderite), white mica, pyrite, galena, sphalerite, scheelite, tourmaline, molybdenite, tellurides, and native Au.	Quartz, carbonates (calcite, siderite, ankerite), white mica, pyrite, galena, sphalerite, chalcopyrite, pyrrhotite, marcasite, arsenopyrite (mainly Fe-sulfides), albite, chlorite, scheelite, and tourmaline.
Alteration type and alteration minerals in the host rock	Silicification, carbonatization, sericitization, pyritization, chloritization.	Carbonates (calcite, ankerite, dolomite, siderite), pyrite, quartz, pyrrhotite or arsenopyrite, sericite or fuchsite (less common), albite, K-feldespar, and chlorite.
Geochemical elements of enrichment	K, W, Cu, Pb, Mo, Tl, Be, Zn, V, Sb, Ag, Sn, Si, Se, Ni, and Fe (As and Te are less anomalous).	K, As, B, Bi, Hg, Sb, Te, W, Cu, Pb, and Zn.
Ore fluids	Metamorphic source with low salinity (2–11% eq. wt % NaCl), rich in H_2O, N_2, CO_2 (1–11 mol %), values of $\delta^{18}O$ = 7 to 17‰ and δ^2H about -39 to -107‰.	Metamorphic source with low salinity (~3–10% eq. wt % NaCl), rich in H_2O, H_2O–$CO_2 \geq$ 5mol%, ± CH_4 and N_2. Values of $\delta^{18}O$ = 5 to 8‰ and δ^2H = -10 to -40‰.
Approximate value for mineral tonnage (Mt)/Au production (Moz)/Au-grade (g/t) for important mines	La Herradura: 200/6.0/1.0; El Chanate: 52/1.5/0.9; San Francisco-Llano: 113/2.4/0.7; Noche Buena: 35/0.6/0.5, and La Choya: 8.3/0.4/1.3.	Golden Mile (Yilgram Craton): 1000/64.0/2.0; Homestake: > 150/40.0/8.3; Grass-Valley-Nevada: 40/21.4/16.9; Bendingo Goldfield (Tasman Orogen): 41/17.0/12.9; Brasilia: 725/10.0/0.4, and Alaska-Juneau: 198/9.0/1.4.
Other important features	Low sulfide content (~3%), structural hosted deposition, and supergene processes with secondary mineralization (hematite, goethite, wulfenite, jarosite, plumbojarosite, anglesite, and chlorargyrite). Medium-low grade of precious metals (Au = ~3 gr/tonne), Au/Ag = 1:9. Deposition controlled by regional structures and local shears.	Low sulfide content (3–5%), structurally-controlled ore deposition, medium grade of precious metals (Au = 5–30 gr/tonne), Au/Ag = 10:1. Deposition focused in open-space fillings within shear structures.

1. Data compiled from: Albinson (1989); Pérez-Segura et al. (1996); Iriondo and Atkinson (2000); Araux-Sánchez et al. (2001); Noriega-Martínez (2006); Quintanar-Ruíz (2008); De la Torre-Carlos (2009); Izaguirre et al. (2012); Izaguirre and Iriondo (2014).
2. Data from Groves et al. (1998) and Goldfarb et al. (2005).

Appendix (electronic)

Economic Geology

Tectonic framework for Late Cretaceous to Eocene quartz-gold vein mineralization from the Caborca orogenic gold belt in northwestern Mexico

Aldo Izaguirre; Alexander Iriondo; Michael J. Kunk, Ryan J. McAleer, William W. Atkinson Jr., and Luis M. Martínez-Torres

This appendix contains four tables of geochronological data compiled from published scientific literature. These geochronological data were used to construct age–frequency histograms shown in Figures 7 and 8 and the plots in Figure 9.

1. Table A1. Ages of orogenic gold mineralization within the North American Cordillera including white mica $^{40}Ar/^{39}Ar$ ages obtained in this study (Fig. 1A), as detailed in a *U.S. Geological Survey Open File Report* (Izaguirre et al., 2016).

2. Table A2. Ages of porphyry copper–molybdenum deposits in Arizona, Sonora, Sinaloa, and New Mexico (listed in order of economic importance; see Fig. 1B).

3. Table A3. Ages of Late Cretaceous and Paleocene pre-mineralization igneous rocks within the COGB region.

4. Table A4. Ages of Oligocene to Quaternary post-mineralization igneous rocks within the COGB region.

Table A1. Mineralization ages of orogenic gold localities from the North American cordillera orogen, including data of this study.

Locality	Occurrence or mine	Method	Dated mineral	Age	Error	Author references
Caborca Orogenic Gold Belt, Mexico						
Alamo-7	Sierra La Gloria	Ar-Ar	White mica	36.1	± 1.2	This study
SanFran 4d	San Francisco Mine	Ar-Ar	White mica	38.9	± 0.7	This study
Estación-1	San Francisco Mine	Ar-Ar	White mica	42.2	± 0.5	This study
Ana Celia	Ana Cecilia Mine	Ar-Ar	White mica	43.6	± 1.1	This study
La Pinta USA Mine	Sierra Pinta Arizona	Ar-Ar	White mica	43.9	± 0.2	This study
Carretera-1	Benjamín Hill	Ar-Ar	White mica	47.8	± 0.6	This study
Betty Lee Mine	Copper Mountains	Ar-Ar	White mica	47.9	± 0.2	This study
Costa-4	Caborca Coast	Ar-Ar	White mica	48		This study
Sanluisito-2	Bertha Mine	Ar-Ar	White mica	48.1	± 0.2	This study
Quitovac-5	Bustamante Mine	Ar-Ar	White mica	49.6	± 0.3	This study
Quitovac-6	La Negra Mine	Ar-Ar	White mica	49.9	± 0.3	This study
Cubabi	Sierra Cubabi	Ar-Ar	White mica	50.0	± 0.5	This study
American Boy	American Boy Mine	Ar-Ar	White mica	50.6	± 0.4	This study
Chip Mine	Papago-Sheep Area	Ar-Ar	White mica	51.2	± 0.3	This study
El Chanate	El Chanate Mine	Ar-Ar	White mica	52		This study
SE Sonoyta	Los Misioneros Mine	Ar-Ar	White mica	52.5	± 0.4	This study
Taj-3	Tajítos-Caborca Area	Ar-Ar	White mica	52.6	± 0.8	This study
Dolores	Dolores Mine	Ar-Ar	White mica	52.8	± 0.3	This study
Noche Buena Casa	Noche Buena Mine	Ar-Ar	White mica	52.9	± 0.8	This study
LH08-1	Cerro Prieto-Carina	Ar-Ar	White mica	54.1	± 1.7	This study
El Tiro	El Tiro Mine	Ar-Ar	White mica	55		This study
Tajitos 2	Tajítos-Caborca	Ar-Ar	White mica	55.6	± 1.1	This study
Noche Buena Working	Noche Buena Mine	Ar-Ar	White mica	55.7	± 1.4	This study
Cerro Colorado	Cerro Colorado Hills	Ar-Ar	White mica	56		This study
Vidrios-1	La Angélica Mine	Ar-Ar	White mica	56.3	± 0.6	This study
Sanfran-7	Sierra San Francisco	Ar-Ar	White mica	56.5	± 0.6	This study
El Capitán Mine	Ejido Aquiles Serdán	Ar-Ar	White mica	56.9	± 0.3	This study
Trin-11	Las Amarillas Mine	Ar-Ar	White mica	56.9	± 0.3	This study
Pinta-2	Sierra Pinta	Ar-Ar	White mica	56.9	± 0.8	This study
Sanfran-2	Sierra San Francisco	Ar-Ar	White mica	57.2	± 0.3	This study
Sonoyta-1	Sierra Los Tanques	Ar-Ar	White mica	57.3	± 0.3	This study
Vidrios-2	La Angélica Mine	Ar-Ar	White mica	57.7	± 0.3	This study
Pinta-1a	La Pinta Mine	Ar-Ar	White mica	58.3	± 0.6	This study
Trin-10	Sierra La Salada	Ar-Ar	White mica	58.3	± 1.0	This study
La Esperanza	La Esperanza Mine	Ar-Ar	White mica	58.7	± 0.8	This study
Jerónimo	Sierra Los Tanques	Ar-Ar	White mica	58.9	± 0.7	This study
Costa-3	Cerro El Sahuaro	Ar-Ar	White mica	58.9	± 0.7	This study
Prieta-1	Sierra Prieta	Ar-Ar	White mica	59.0	± 0.3	This study
Quitovac-2	El Chacón Mine	Ar-Ar	White mica	59.4	± 0.7	This study
Sanfran-3	Sierra San Francisco	Ar-Ar	White mica	59.5	± 0.3	This study
Prieta-5	Sierra Prieta	Ar-Ar	White mica	59.7	± 0.3	This study
Carretera-2	La Jarra Mine	Ar-Ar	White mica	59.7	± 1.3	This study
Sargenta	Sargenta Mine	Ar-Ar	White mica	59.8	± 0.4	This study
Quitovac-3	La Choya Mine	Ar-Ar	White mica	60.2	± 0.4	This study
Sanfran-6	Sierra San Francisco	Ar-Ar	White mica	60.4	± 0.3	This study
Celaya-1	Sierra San Francisco	Ar-Ar	White mica	60.5	± 0.2	This study
Prieta-4	Sierra Prieta	Ar-Ar	White mica	60.6	± 0.7	This study
Costa-1	Cerro El Sahuaro	Ar-Ar	White mica	61.0	± 1.0	This study
La Herradura	La Herradura Mine	Ar-Ar	White mica	61		This study
Lluvia de Oro 3b	Lluvia de Oro Mine	Ar-Ar	White mica	61		This study
Yaqui-3	La Herradura Mine	Ar-Ar	White mica	61		This study
Pinor-1	Sierra Pinta	Ar-Ar	White mica	61.6	± 0.3	This study
Sanfran-4	Sierra San Francisco	Ar-Ar	White mica	61.6	± 0.3	This study
Centauro-3	La Herradura Mine	Ar-Ar	White mica	62		This study
Quitovac-4	Quitovac Mine	Ar-Ar	White mica	62		This study
10 de Mayo	La Herradura Mine	Ar-Ar	White mica	62		This study
Tres Mojones	Tres Mojones Mine	Ar-Ar	White mica	62.2	± 0.4	This study
Cantera	Canteras-Sierra Pinta	Ar-Ar	White mica	64.3	± 0.4	This study
La Colorada	La Colorada Mine	Ar-Ar	White mica	64.7	± 0.7	This study
SVE-1	Quitovac	Ar-Ar	White mica	64.9	± 0.5	This study
Pit-4	South of Pitiquito	Ar-Ar	White mica	65.0	± 0.6	This study
Pit-3	Pozos de Cerna Ranch	Ar-Ar	White mica	65.9	± 0.3	This study
Sanfran-1	La Traición Mine	Ar-Ar	White mica	69		This study
Previous geochronology from the COGB						
Estación Llano	San Francisco	Ar-Ar	White mica	41		Pérez-Segura et al. (1996)
Quitovac-La Choya	Doña Marcia	Ar-Ar	White mica	46		Iriondo (2001)
Quitovac-La Choya	La Choya	Ar-Ar	White mica	46		Iriondo (2001)
Quitovac-La Choya	Doña Marcia	Ar-Ar	White mica	48.5	± 0.3	Iriondo (2001)
Tajítos	Tajítos	K-Ar	White mica	49.2	± 2.0	Pérez-Segura (1993)
Quitovac-La Choya	La Choya	Ar-Ar	White mica	50		Iriondo (2001)
Quitovac-La Choya	La Negra	Ar-Ar	White mica	50.2	± 0.1	Iriondo (2001)

continued on the next page

Table A1.-continued.

Locality	Occurrence or mine	Method	Dated mineral	Age	Error	Author references
Quitovac-La Choya	La Toñita	Ar-Ar	White mica	52		Iriondo (2001)
Quitovac-La Choya	Bustamante	Ar-Ar	White mica	54		Iriondo (2001)
Sierra Pinta	La Pinta	K-Ar	White mica	54.8	± 1.4	Araux-Sánchez et al. (2001)
Quitovac-La Choya	El Chacón	Ar-Ar	White mica	56		Iriondo (2001)
Mina La Herradura	La Herradura	Re-Os	Magnetite-pyrite	61.0	± 2.1	Quintanar-Ruíz (2008)
Quitovac-La Choya	Quitovac	Ar-Ar	White mica	61		Iriondo (2001)
Quitovac-La Choya	Quitovac	Ar-Ar	White mica	69		Iriondo (2001)
Juneau, Chichagof, Valdez, Berners, Willow Creek, Nuka, Hope-Sunrise, Girdwood and Port Wells and Sitka, Alaska, USA						
Berners Bay	Kesington	Rb-Sr		47.6	± 1.6	Kistler et al. (1983)
Sitka	Lucky Chance	Ar-Ar	Muscovite	49.4	± 0.5	Haeussler et al. (1995)
Chichagof	Apex	Ar-Ar	Fuchsite	51.9	± 0.1	Taylor et al. (1994)
Chichagof	El Nido	Ar-Ar	Muscovite	51.9	± 1.1	Taylor et al. (1994)
Chichagof	Apex	Ar-Ar	Muscovite	52.1	± 0.1	Taylor et al. (1994)
Hope-Sunrise	Kenai Star	K-Ar	Altered zone	52.7	± 1.6	Silberman et al. (1981)
Juneau	Treadwell	Ar-Ar	Muscovite	52.8	± 0.1	Miller et al. (1994)
Nuka Bay	Thunder Bay	Ar-Ar	Muscovite	52.9	± 0.1	Goldfarb et al. (1997)
Berners Bay	Jualin	Ar-Ar	Muscovite	53.2	± 0.1	Miller et al. (1994)
Hope-Sunrise	Bear Creek	K-Ar	Muscovite	53.2	± 1.6	Silberman et al. (1981)
Berners Bay	Kesington	Ar-Ar	Muscovite	53.5	± 0.1	Miller et al. (1994)
Port Wells	Homestake	Ar-Ar	Muscovite	53.7	± 0.1	Haeussler et al. (1995)
Juneau	Lemon Creek	Ar-Ar	Muscovite	54		Goldfarb et al. (1997)
Juneau	Alaska-Juneau	Ar-Ar	Muscovite	54.2	± 0.1	Goldfarb et al. (1991)
Girdwood	Jewel	Ar-Ar	Muscovite	54.3	± 1.6	Haeussler et al. (1995)
Port Wells	Granite	Ar-Ar	Muscovite	54.3	± 1.6	Haeussler et al. (1995)
Port Valdez	Rough Tough	Ar-Ar	Muscovite	54.3	± 1.6	Haeussler et al. (1995)
Juneau	Lemon Creek	Ar-Ar	Fuchsite	55		Goldfarb et al. (1997)
Juneau	Treadwell	Ar-Ar	Muscovite	55.1	± 0.2	Goldfarb et al. (1991)
Windham Bay	Sumdum Chief	Ar-Ar	Muscovite	55.1	± 0.2	Goldfarb et al. (1991)
Berners Bay	Jualin	Ar-Ar	Muscovite	55.5	± 0.3	Goldfarb et al. (1991)
Nuka Bay	Little Creek	Ar-Ar	Muscovite	55.7	± 0.2	Borden et al. (1992)
Windham Bay	Marty	Ar-Ar	Muscovite	56		Goldfarb et al. (1997)
Juneau	Alaska-Juneau	Ar-Ar	Muscovite	56.1	± 0.3	Miller et al. (1994)
Juneau	Alaska-Juneau	Ar-Ar	Biotite	56		Goldfarb et al. (1997)
Juneau	Treadwell	Rb-Sr		56.1	± 3.1	Kistler et al. (1983)
Berners Bay	Kesington	Ar-Ar	Muscovite	56.4	± 0.1	Goldfarb et al. (1991)
Willow Creek	Gold Bullion	K-Ar	Muscovite	56.6	± 1.7	Madden-McGuire et al. (1989)
Juneau	Alaska-Juneau	Rb-Sr		56.7	± 3.7	Newberry and Brew (1987)
Nuka Bay	Little Creek	Ar-Ar	Muscovite	56.7	± 0.2	Goldfarb et al. (1997)
Nuka Bay	Port Dick	Ar-Ar	Muscovite	57.3	± 0.1	Goldfarb et al. (1997)
Valdez Creek	Timberline Creek	Ar-Ar	Muscovite	57.6	± 0.1	Adams et al. (1992)
Valdez Creek	Placer pit	Ar-Ar	Muscovite	60.0	± 0.2	Adams et al. (1992)
Valdez Creek	Lucky Hill	Ar-Ar	Muscovite	61.7	± 0.3	Adams et al. (1992)
Valdez Creek	Surprise Creek	Ar-Ar	Muscovite	63		Goldfarb et al. (1997)
Willow Creek	Indepencence	Ar-Ar	Muscovite	66		Goldfarb et al. (1997)
Willow Creek	Lucky Shot	K-Ar	Muscovite	66.3	± 2.0	Madden-McGuire et al. (1989)
Bridge River, Canada						
Bralorne-Pioneer	Pioneer vein	Ar-Ar	Muscovite	64.4	± 0.4	Hart et al. (2008)
Bralorne-Pioneer	Pioneer vein	Ar-Ar	Muscovite	64.4	± 0.4	Hart et al. (2008)
Bralorne-Pioneer	Peter vein	Ar-Ar	Fuchsite	66.8	± 0.5	Hart et al. (2008)
Bralorne-Pioneer	King vein	Ar-Ar	Fuchsite	67.7	± 0.7	Hart et al. (2008)
Fairbanks and Tintina Alaska, USA						
Tintina Belt	Liese zone	Ar-Ar	Sericite	61.5	± 0.6	Selby et al. (2002)
Fairbanks	Christina	Ar-Ar	Muscovite	77		Goldfarb et al. (1997)
Fairbanks	Democrat	K-Ar	K-feldespar	86.9	± 2.6	Bundtzen and Reger (1977)
Fairbanks	Fort Knox	Ar-Ar	Muscovite	87.5	± 5.0	McCoy et al (1997)
Fairbanks	Ryan	Ar-Ar	Muscovite	88		McCoy et al. (1997)
Fairbanks	Ryan	Ar-Ar	Muscovite	89		McCoy et al. (1997)
Tintina Belt	Fort Knox	Re-Os	Molybdenite	91.8	± 0.3	Selby et al. (2002)
Bommifield	Liberty Bell	K-Ar	Muscovite	92.0	± 1.0	Suleyman (1994)
Tintina Belt	Fort Knox	Re-Os	Molybdenite	92.2	± 0.5	Selby et al. (2002)
Tintina Belt	Fort Knox	Re-Os	Molybdenite	92.6	± 0.4	Selby et al. (2002)
Tintina Belt	Fort Knox	Re-Os	Molybdenite	92.9	± 0.4	Selby et al. (2002)
Tintina Belt	Fort Knox	Re-Os	Molybdenite	92.9	± 0.4	Selby et al. (2002)
Tintina Belt	Fort Knox	Re-Os	Molybdenite	93.0	± 0.4	Selby et al. (2002)
Tintina Belt	Pogo-Liese zone	Re-Os	Molybdenite	104.2	± 0.5	Selby et al. (2002)
Tintina Belt	Pogo-Liese zone	Re-Os	Molybdenite	104.2	± 1.0	Selby et al. (2002)
Tintina Belt	Pogo-Liese zone	Re-Os	Molybdenite	104.5	± 1.5	Selby et al. (2002)
Northwestern Nevada, USA						
Nevada	Ten Mile	Ar-Ar	Sericite	72.0	± 5.4	Cheong (1999)
Nevada	Nevada Packard	K-Ar	Sericite	78.8	± 2.4	Vikre (1981)

continued on the next page

Table A1.-continued.

Locality	Occurrence or mine	Method	Dated mineral	Age	Error	Author references
Nevada	Stalin's Present	K-Ar	White mica	81.7	± 2.4	Vikre and McKee (1985)
Nevada	Starlight	K-Ar	Muscovite	85.3	± 2.5	Russell et al. (1989)
Nevada	Nenzel Hill	K-Ar	Sericite	85.7	± 4.3	Vikre (1981)
Nevada	Antelope Siding	Ar-Ar	Sericite	89.2	± 0.4	Cheong (1999)
Nevada	Pine Forest Range	Ar-Ar	Sericite	95.8	± 0.9	Cheong (1999)
Nevada	Santa Rosa	Ar-Ar	Sericite	97.4	± 0.6	Cheong (1999)
Nevada	Nenzel Hill	K-Ar	Biotite	97.6	± 3.0	Vikre and McKee (1985)
Nevada	Hollywood	K-Ar	Clinochlore	103.4	± 10.0	Vikre and McKee (1985)
Nevada	Slumbering	Ar-Ar	Sericite	107.2	± 1.9	Cheong (1999)
Nevada	Nenzel Hill	K-Ar	White mica	114.1	± 4.0	Vikre and McKee (1985)
Nome Alaska, USA						
Nome	Bluff	Ar-Ar	Muscovite	109		Ford and Snee (1996)
Nome	Mount Distin	Ar-Ar	Muscovite	115		Ford (1993)
Nome	McDuffee	Ar-Ar	Muscovite	125		Ford (1993)
Sierra Nevada Foothills (Mother Lode) and Klamath, California, USA						
Allegheny	Oriental	Ar-Ar	Mica	104		Böhlke et al. (1989)
Mother Lode	Mary Harrison	K-Ar	Mariposite	108.0	± 3.0	Kistler et al. (1983)
Allegheny	Gold crown	Rb-Sr	Carbonate	109.6	± 3.0	Böhlke and Kistler (1986)
Allegheny	Oriental	Ar-Ar	Mica	111		Böhlke et al. (1989)
Allegheny	Rainbow Extension	K-Ar	Mariposite	111.6	± 3.0	Böhlke and Mckee (1984)
Allegheny	Plumbago	K-Ar	Mica	112.5	± 3.0	Böhlke and Kistler (1986)
Allegheny	Irelan	K-Ar	Mariposite	112.9	± 3.0	Böhlke and Mckee (1984)
Mother Lode	Garibaldi	Rb-Sr	Mariposite	114.6	± 3.0	Kistler et al. (1983)
Allegheny	Sixteen to One	Ar-Ar	Mariposite	114.7	± 1.4	Marsh et al. (2008)
Allegheny	Irelan	Rb-Sr	Carbonate	115.0	± 3.0	Böhlke and Kistler (1986)
Bagby	Pine Tree/Josephine	Ar-Ar	Mariposite	115.6	± 1.3	Marsh et al. (2008)
Mother Lode	Mary Harrison	K-Ar	Mariposite	116.0	± 3.0	Kistler et al. (1983)
Allegheny	Irelan	Rb-Sr	Quartz	116.3	± 3.0	Böhlke and Kistler (1986)
Mother Lode	Garibaldi	K-Ar	Mariposite	116.3	± 3.0	Kistler et al. (1983)
Allegheny	Oxford	Ar-Ar	Mariposite	117.3	± 0.8	Marsh et al. (2008)
Allegheny	Oriental	Ar-Ar	Mica	118		Böhlke et al. (1989)
Washington	Red Ledge	Rb-Sr	Carbonate	119.4	± 3.0	Böhlke and Kistler (1986)
Mother Lode	Couterville road cut	Ar-Ar	Mariposite	120.8	± 1.5	Snow et al. (2008)
Washington	Red Ledge	K-Ar	Mica	120.9	± 4.0	Böhlke and Kistler (1986)
Mother Lode	Garibaldi	Ar-Ar	Mariposite	121.2	± 4.7	Snow et al. (2008)
Coulterville	McAlpine	Ar-Ar	Mariposite	123		Marsh et al. (2008)
Mother Lode	Quartz Hill, Placerville	Ar-Ar	Mariposite	123.5	± 1.1	Marsh et al. (2008)
Allegheny	Kate Hardy	Rb-Sr	Quartz	124.2	± 3.0	Böhlke and Kistler (1986)
Mother Lode	Jack Adit	Ar-Ar	Mariposite	124.3	± 0.7	Marsh et al. (2008)
Allegheny	Kate Hardy	Rb-Sr	Carbonate	124.5	± 3.0	Böhlke and Kistler (1986)
Mother Lode	Royal Mountain King	Ar-Ar	Mariposite	125.4	± 0.2	Marsh et al. (2008)
Mother Lode	Harvard/Jamestown	K-Ar	Mariposite	127.0	± 3.0	Kistler et al. (1983)
Allegheny	Sixteen to One	Ar-Ar	Mariposite	127.5	± 1.4	Snow et al. (2008)
Confidence	Confidence	Ar-Ar	Muscovite	128.2	± 0.7	Marsh et al. (2008)
Mother Lode	Quartz Mountain, Jamestown	Ar-Ar	Mariposite	128.5	± 1.3	Marsh et al. (2008)
Mother Lode	Quartz Mountain, Jamestown	Ar-Ar	Mariposite	129.7	± 0.7	Marsh et al. (2008)
Mother Lode	Sutter Hill	Ar-Ar	Muscovite	129.8	± 2.3	Marsh et al. (2008)
Mother Lode	Harvard Pit	Ar-Ar	Mariposite	129.8	± 0.8	Marsh et al. (2008)
Mother Lode	Harvard Pit	Ar-Ar	Mariposite	129.9	± 0.7	Marsh et al. (2008)
Mother Lode	Alameda	Ar-Ar	Mariposite	130.4	± 1.5	Marsh et al. (2008)
Mother Lode	Harvard	Ar-Ar	Mariposite	130.9	± 0.6	Snow et al. (2008)
Mother Lode	Carson Hill Pit	Ar-Ar	Mariposite	134.3	± 1.0	Marsh et al. (2008)
Mother Lode	Carson Hill	Ar-Ar	Mariposite	134.8	± 0.7	Snow et al. (2008)
Grass Valley	Brunswick	Rb-Sr	Quartz	140.9	± 3.0	Böhlke and Kistler (1986)
Grass Valley	Brunswick	K-Ar	Mica	143.7	± 3.0	Böhlke and Kistler (1986)
Klamath	Morrison-Carlock	K-Ar	Sericite	145.8	± 3.0	Elder and Cashman (1992)
Klamath	Morrison-Carlock	K-Ar	Sericite	147.7	± 2.8	Elder and Cashman (1992)
Grass Valley	Idaho-Maryland	Ar-Ar	Mariposite	152.2	± 1.2	Snow et al. (2008)
Grass Valley	Empire-North Star	U-Pb	Xenotime	162.0	± 5.0	Taylor et al., 2015

Table A2. Copper-molybdenum phorphyry ages from Sonora, NW, Mexico and, SW Arizona, USA.

Locality	Method	Dated mineral	Trench distance (km)	Age	Error	Author references
Sonora, NW, Mexico						
San Judas	K-Ar	Biotite	386	40.0	± 0.9	Damon et al. (1983)
La Washington	K-Ar	Sericite	375	45.7	± 0.1	Damon et al. (1983)
San Nicolas	K-Ar	Biotite	372	49.6	± 1.2	Barton et al. (1995)
La Caridad	K-Ar	Biotite	452	50.0	± 1.2	Damon et al. (1983)
Florida Barrigon	K-Ar	Sericite	447	52.4	± 1.1	Damon et al. (1983)
La Caridad	K-Ar	Biotite	452	52.5	± 1.3	Damon et al. (1983)
El Crestón	K-Ar	Sericite	333	53.5	± 1.1	Damon et al. (1983)
La Caridad	Re-Os	Molybdenite	452	53.6	± 0.2	Valencia et al. (2005)
El Crestón	Re-Os	Molybdenite	333	53.6	± 0.2	Barra et al. (2005)
La Caridad	Re-Os	Molybdenite	452	53.8	± 0.2	Valencia et al. (2005)
La Caridad	K-Ar	Biotite	452	54.3	± 1.2	Damon et al. (1983)
La Caridad	K-Ar	Sericite	452	54.5	± 0.9	Livingston (1973)
Cumobabi	K-Ar	Whole rock	390	55.6	± 0.3	Scherkenbach et al. (1985)
Cuatro Hermanos	Re-Os	Molybdenite	327	55.7	± 0.3	Barra et al. (2005)
Tres Piedras	Ar-Ar	Muscovite	378	55.7	± 0.8	Wodzicki (2001)
Aurora	K-Ar	Biotite	340	55.8	± 1.8	Damon et al. (1983)
Bella Esperanza	K-Ar	Biotite	435	55.9	± 1.2	Damon et al. (1983)
Cumobabi	K-Ar	Biotite	390	56.0	± 5.1	Scherkenbach et al. (1985)
Suaqui Verde	K-Ar	Biotite	313	56.4	± 1.2	Damon et al. (1983)
María	Re-Os	Molybdenite	431	56.5	± 3.2	McCandless et al., (1993)
El Alacrán	K-Ar	Biotite	431	56.7	± 1.2	Damon et al. (1983)
Cumobabi	K-Ar	Biotite	390	56.7	± 1.3	Scherkenbach et al. (1985)
Suaqui Verde	K-Ar	Sericite	313	56.7	± 1.1	Damon et al. (1983)
Batamote	K-Ar	Biotite	443	56.8	± 1.2	Damon et al. (1983)
Suaqui Verde	Re-Os	Molybdenite	313	57.0	± 0.3	Barra et al. (2005)
San Antonio de La Huerta	K-Ar	whole rock	342	57.4	± 1.4	Damon et al. (1983)
María	K-Ar	Biotite	431	58.2	± 2.0	Wodzicki (2001)
Cumobabi	Re-Os	Molybdenite	390	58.7	± 0.2	Barra et al. (2005)
Cumobabi	Re-Os	Molybdenite	390	58.7	± 0.2	Barra et al. (2005)
Suaqui Verde	K-Ar	Hornblende	313	58.8	± 1.3	Damon et al. (1983)
La Aurora	K-Ar	Biotite	342	58.8	± 1.8	Damon et al. (1983)
Cananea	U-Pb	Zircon	435	58.9	± 1.4	Del Río-Salas (2011)
Mariquita	Re-Os	Molybdenite	431	59.2	± 0.3	Del Río-Salas (2011)
Cananea	Re-Os	Molybdenite	435	59.2	± 0.3	Barra et al. (2005)
Mariquita	Re-Os	Molybdenite	431	59.3	± 0.3	Del Río-Salas (2011)
Cananea	Re-Os	Molybdenite	435	59.3	± 0.3	Barra et al. (2005)
La Colorada	K-Ar	Phlogopite	435	59.9	± 2.0	Damon and Mauger (1966)
Piedras Verdes	Re-Os	Molybdenite	300	~60		Espinosa-Perea (1999)
Los Alisos	U-Pb	Zircon	464	60.2	± 0.8	Rascón-Heimpel et al. (2012)
María	Re-Os	Molybdenite	431	60.4	± 0.3	Barra et al. (2005)
Mariquita	U-Pb	Zircon	435	60.4	± 1.1	Del Río-Salas (2011)
El Alacrán	Re-Os	Molybdenite	431	60.8	± 0.2	Barra et al. (2005)
El Alacrán	Re-Os	Molybdenite	431	60.9	± 0.2	Barra et al. (2005)
Cananea	U-Pb	Zircon	435	61.3	± 1.4	Del Río-Salas (2011)
Lucy	Re-Os	Molybdenite	425	61.6	± 0.3	Del Río-Salas (2011)
Lucy	Re-Os	Molybdenite	425	61.8	± 0.3	Del Río-Salas (2011)
Mariquita	U-Pb	Zircon	435	62.7	± 1.3	Del Río-Salas (2011)
Milpillas	Re-Os	Molybdenite	435	63.1	± 0.3	Valencia et al. (2006)
Cumobabi	K-Ar	whole rock	390	63.1	± 1.7	Scherkenbach et al. (1985)
Milpillas	Ar-Ar	Whole rock	435	63.7	± 8.0	Noguez-Alcántara (2008)
Lucy	U-Pb	Zircon	425	63.8	± 1.1	Del Río-Salas (2011)
Milpillas	U-Pb	Zircon	435	63.9	± 1.3	Valencia et al. (2006)
Pilar	Re-Os	Molybdenite	424	73.9	± 0.4	Del Río-Salas (2011)
El Plomo	Re-Os	Molybdenite	307	~74		Barra and Valencia (2014)
La Fortuna del Cobre	Re-Os	Molybdenite	204	~75		Barra and Valencia (2014)
Sinaloa, NW, Mexico						
Tameapa	Re-Os	Molybdenite	344	~53		Barra et al. (2003)
Malpica	K-Ar	Biotite	307	54.1	± 0.3	Damon et al. (1983)
Las Higueras	K-Ar	Biotite	316	54.9	± 1.2	Damon et al. (1983)
Tameapa	Re-Os	Molybdenite	344	~57		Barra et al. (2003)
Santo Tomás	K-Ar	Biotite	340	57.2	± 1.2	Damon et al. (1983)
Cosalá	K-Ar	Biotite	346	59.0	± 1.2	Damon et al. (1983)
La Reforma	K-Ar	Biotite	360	59.2	± 1.3	Damon et al. (1983)
La Azulita	K-Ar	Biotite	342	59.5	± 1.2	Damon et al. (1983)
La Reforma	K-Ar	Biotite	360	59.9	± 1.3	Damon et al. (1983)

continued on the next page

Table A2. Continued.

Locality	Method	Dated mineral	Trench distance (km)	Age	Error	Author references
Chihuahua, NW, Mexico						
Batopilas	K-Ar	Biotite	406	51.6	± 1.1	Wilkerson et al. (1988)
La Guadalupana	K-Ar	Biotite	393	54.9	± 1.2	Damon et al. (1983)
Cerro Colorado	K-Ar	Biotite	393	48.0	± 1.2	Shafiqullah et al. (1980)
Arizona, SW, USA						
Twin Buttes	K-Ar	Biotite	435	~54		Damon and Mauger (1966)
Morenci	Re-Os	Molybdenite	639	54.9	± 1.8	McCandless et al. (1993)
Morenci	K-Ar	Biotite	639	~55		McDowell (1966)
Sierrita	Re-Os	Molybdenite	426	55.3	± 3.6	McCandless et al. (1993)
Copper Creek	Re-Os	Molybdenite	538	56.1	± 1.8	McCandless et al. (1993)
Pima-Mission	Re-Os	Molybdenite	430	57.0	± 2.8	McCandless et al. (1993)
Copper Creek	Re-Os	Molybdenite	538	58.0	± 3.0	McCandless et al. (1993)
Inspiration	K-Ar	Biotite	533	~58		McDowell (1966)
Mission	K-Ar	Biotite	440	~59		Damon and Mauger (1966)
Sierrita	Re-Os	Molybdenite	426	60.0	± 0.3	Jensen (1998)
Bagdad	Re-Os	Molybdenite	436	60.2	± 0.3	Barra et al. (2003)
Copper Creek	Re-Os	Molybdenite	538	60.7	± 0.3	Barra et al. (2005)
Sierrita	Re-Os	Molybdenite	426	60.7	± 0.3	Jensen (1998)
Sierrita	Re-Os	Molybdenite	426	60.8	± 0.3	Jensen (1998)
Esperanza	K-Ar	Phlogopite	424	~61		Damon and Mauger (1966)
Castle Dome	K-Ar	Biotite	535	~62		Creasey and Kistler (1962)
Safford	K-Ar	Biotite	607	~63		Damon and Mauger (1966)
Ajo	K-Ar	Whole rock	320	62.9	± 1.9	Hagstrum et al. (1987)
Esperanza	K-Ar	Muscovite	431	~63		Damon and Mauger (1966)
New Cornelia	K-Ar	Biotite	320	~63		Creasey (1965)
Copper Cities Hill's	K-Ar	Biotite	551	~63		Creasey (1965)
Ray	K-Ar	Biotite	517	~63		Creasey and Kistler (1962)
Silverbell	Re-Os	Molybdenite	428	63.2	± 0.3	Barra et al. (2005)
Sierrita	Re-Os	Molybdenite	426	63.5	± 0.3	Jensen (1998)
Ajo	K-Ar	Whole rock	320	63.8	± 1.9	McDowell (1971)
Ajo	K-Ar	Whole rock	320	64.2	± 1.9	McDowell (1971)
Ajo	K-Ar	Whole rock	320	65.2	± 1.9	McDowell (1971)
San Manuel	K-Ar	Biotite	514	~69		Rose and Cook (1965)
Bagdad	Re-Os	Molybdenite	436	69.7	± 0.8	McCandless et al. (1993)
Bagdad	Re-Os	Molybdenite	436	71.7	± 0.3	Barra et al. (2003)
Bagdad	Re-Os	Molybdenite	436	71.7	± 0.3	Barra et al. (2003)
Mineral Park	K-Ar	Phlogopite	415	~72		Damon and Mauger (1966)
Bagdad	Re-Os	Molybdenite	436	75.8	± 0.3	Barra et al. (2003)
Bagdad	Re-Os	Molybdenite	436	75.8	± 0.3	Barra et al. (2003)
Bagdad	Re-Os	Molybdenite	436	76.6	± 0.3	Barra et al. (2003)
New Mexico, SW, USA						
Tyrone Mine	K-Ar	Whole rock	688	56.2	± 1.7	McDowell (1971)
Fierro-Hanover	Ar-Ar	K-feldespar	726	57.6	± 0.1	McLemore et al. (1999)
Chino Copper Mine	K-Ar	Whole rock	724	58.0	± 1.8	McDowell (1971)
Hillsboro district	Ar-Ar	Hornblende	777	74.9	± 0.7	McLemore et al. (1999)

Trench distances, from the Cedros deep to each mineral occurrence, were calculated for Cretaceous–Eocene. Approximately 200 km was subtract each distance to compensate for Cenozoic extension. (~): Indicates an average of two or more ages for multiple samples dated from the same location.

Table A3. U-Pb zircon ages of premineralization batholiths granitoids from the Caborca orogenic gold belt region, NW, Sonora, Mexico.

Sample	Rock or mineral	Age (Ma)	Error	Author references
Quitovac				
SA-3	Diorite	76.1	± 3.7	Iriondo et al. (2005)
KZ-3	Granite	79.4	± 1.3	Iriondo et al. (2005)
KZ-4	Granite	~80		Iriondo et al. (2005)
Sierra Los Alacranes-Cerros Los Ojos				
TJA # 21	Quartzdiorite	72.8	± 1.8	Nourse et al. (2005)
CD-16-99	Quartzdiorite	73.4	± 3.3	Nourse et al. (2005)
Caborca y Pitiquito				
Andesite porphyry	Subvolcanic	70.5	± 5.6	Nourse et al. (2007)
Proveedora Granite	Granite	~74		Jacques-Ayala et al. (2008)
Pitiquito Granite	Granite	~74		Jacques-Ayala et al. (2008)
Sierrita Blanca				
SB07-3	Quartzdiorite	69.7	± 1.0	Enríquez-Castillo et al. (2009)
SB07-5	Quartzdiorite	72.6	± 1.2	Enríquez-Castillo et al. (2009)
Sierra Pinta				
PIN-07-6	Granite	67.0	± 1.3	Arvizu et al. (2009)
PIN-07-14	Monzogranite	68.3	± 0.7	Arvizu et al. (2009)
La Herradura mine area				
LH06-42, Sierrita Blanca	Granite	69.7	± 1.3	Izaguirre-Pompa (2009)
04FP-37, Coastal Batholith	Granitoid	76.3	± 0.4	Izaguirre-Pompa (2009)
San Francisco Llano				
El Durazno	Biotite Granodiorite	65.5	± 0.5	Poulsen et al. (2008)
El Durazno	Biotite Granite	66.0	± 2.0	Poulsen et al. (2008)
La Barajita	Quartz monzonite	68.3	± 3.2	Poulsen et al. (2008)
Tanques NW Sonoyta				
Los Tanques, Cipriano area	Granitoid	58.2	± 0.9	Ishiki-Pérez et al. (2013)
Los Tanques, Cipriano area	Granitoid	59.8	± 0.7	Ishiki-Pérez et al. (2013)
Los Tanques, Jerónimo area	Granitoid	63.2	± 0.6	Arvizu-Gutiérrez (2012)
Los Tanques, Jerónimo area	Granitoid	67.5	± 1.5	Arvizu-Gutiérrez (2012)
Los Tanques, Cipriano area	Granitoid	70.6	± 1.0	Arvizu-Gutiérrez (2012)
Los Tanques, Cuate Gray area	Granitoid	72.7	± 0.6	Arvizu-Gutiérrez (2012)
Los Tanques, Cuate Gray area	Granitoid	75.4	± 0.3	Arvizu-Gutiérrez (2012)
Los Tanques	Granitoid	78.0	± 0.6	Arvizu-Gutiérrez (2012)
Other localities in NW Sonora				
La soledad Caborca Coast	Granite	62.6	± 0.5	A. Iriondo, pers. commun. (2015)
Benjamín Hill	Granite	68.3	± 0.3	A. Iriondo, pers. commun. (2015)
Sierra San Francisco	Granite	74.3	± 0.4	A. Iriondo, pers. commun. (2015)
San Antonio Diorite	Diorite	75.0	± 0.5	A. Iriondo, pers. commun. (2015)
El Chanate	Quartz latite dike	77.0	± 0.6	A. Iriondo, pers. commun. (2015)
Cerro Colorado	Rhyolite porphyry	83.0	± 1.8	A. Iriondo, pers. commun. (2015)
Puerto Peñasco	Granite	85.1	± 0.7	A. Iriondo, pers. commun. (2015)
Monument Hill's-border USA-Mexico	Granite	96.5	± 1.2	Ruiz-Segoviano et al. (2013)

Table A4. Radiometric ages of postmineralization volcanic rocks (Oligocene to present day) on the Caborca orogenic gold belt area, NW, Sonora, Mexico.

Sample	Rock or mineral	Method	Age (Ma)	Error	Author references
Quitovac region, volcanic flows and pyroclastics de Caldera El Pilar					
Andesite	Whole rock	Ar-Ar	17.0	± 0.2	Iriondo (2001)
	Hornblende	Ar-Ar	17.4	± 0.1	Iriondo (2001)
Basalt	Biotite	Ar-Ar	17.5	± 0.1	Iriondo (2001)
	Biotite	Ar-Ar	17.7	± 0.1	Iriondo (2001)
Ignimbrite	Sanidine	Ar-Ar	~18		Iriondo (2001)
	Biotite	Ar-Ar	18.0	± 0.1	Iriondo (2001)
North of Caborca					
CA03-11	Tuff/sanidine	Ar-Ar	16.7	± 0.2	Izaguirre-Pompa (2006)
CA03-8	Basalt/matrix	Ar-Ar	17.4	± 0.3	Izaguirre-Pompa (2006)
CA99-1	Plagioclase	Ar-Ar	20.9	± 1.2	Izaguirre-Pompa (2006)
CA99-1	Andesite/matrix	Ar-Ar	21.9	± 0.1	Izaguirre-Pompa (2006)
CA03-13	Andesite/matrix	Ar-Ar	24.1	± 0.5	Izaguirre-Pompa (2006)
CA03-01	Andesite/matrix	Ar-Ar	24.3	± 0.1	Izaguirre-Pompa (2006)
	Hornblende	Ar-Ar	24.6	± 0.1	Nourse et al. (2007)
Pinacate Pre-pinacate volcanic event					
JR99-83	Dacite/plagioclase	Ar-Ar	12.0	± 1.4	Vidal-Solano et al. (2008)
PO2-8	Rhyolite/whole rock	Ar-Ar	12.1	± 0.1	Vidal-Solano et al. (2008)
	Rhyolite/Obsidian	Ar-Ar	12.1	± 0.1	Vidal-Solano et al. (2008)
	Rhyolite/Obsidian	Ar-Ar	12.2	± 0.1	Vidal-Solano et al. (2008)
JR98-20	Dacite/plagioclase	Ar-Ar	13.5	± 1.2	Vidal-Solano et al. (2008)
PO3-22	Volcanic glass/obsidian	Ar-Ar	14.2	± 1.2	Vidal-Solano et al. (2008)
Volcanic	Riolite/zircon	U-Pb	14.2	± 0.1	Arvizu-Gutiérrez (2012)
JR98-23	Rhyolite/whole rock	Ar-Ar	14.2	± 0.2	Vidal-Solano et al. (2008)
	Volcanic glass/obsidian	Ar-Ar	14.3	± 0.9	Vidal-Solano et al. (2008)
PO3-27	Volcanic glass/obsidian	Ar-Ar	15.3	± 0.2	Vidal-Solano et al. (2008)
JR98-21	Basalt/Plagioclase	Ar-Ar	19.0	± 0.9	Vidal-Solano et al. (2008)
91-30	Basalt/Plagioclase	Ar-Ar	20.1	± 2.2	Vidal-Solano et al. (2008)
JR97-23	Basalt/Plagioclase	Ar-Ar	20.6	± 1.7	Vidal-Solano et al. (2008)
Sierrita Blanca					
SB07-1	Plagioclase	Ar-Ar	17.3	± 0.1	Enríquez-Castillo et al. (2009)
	Volcanic matrix	Ar-Ar	18.3	± 1.3	Enríquez-Castillo et al. (2009)
La Herradura mine district					
Soledad-Dipolo	Dacite/matrix	Ar-Ar	23.2	± 0.8	Izaguirre-Pompa (2009)
Soledad-Dipolo	Andesite/matrix	Ar-Ar	23.6	± 4.2	Izaguirre-Pompa (2009)
Soledad-Dipolo	Basalt/matrix	Ar-Ar	23.8	± 0.6	Izaguirre-Pompa (2009)
Sierra El Carnero					
Granodiorite-milonitized	Zircon	U-Pb	21.2	± 0.2	Nourse et al. (2007)

References Cited

Adams, D.D., Freeman, C.J., Goldfarb, R.J., Gent, C.A., and Snee, L.W., 1992, Age and geochemical constrains on mesothermal gold mineralization, Valdez Creek district, Alaska [abs.]: Geological Society of America Abstracts with Programs, Cordilleran Section, v. 24, p. 2.

Araux-Sánchez, E., Vega-Granillo, R., and Enríquez-Minjárez, E., 2001, Características geológicas de un yacimiento mesotermal asociado a zonas de cizalla en el noroeste de Sonora, *in* Corona-Esquivel, R., and Gómez-Godoy, J., eds., Asociación de Ingenieros de Minas, Metalurgistas y Geólogos de México A.C., XXIV Convención Minera, Acapulco, Guerrero, p. 25–32.

Arvizu-Gutiérrez, H.E., 2012, Magmatismo permo-triásico en el NW de Sonora, México: Inicio de la subducción y maduración de un margen continental activo: Unpublished M.Sc. thesis, Juriquilla, Querétaro, México, Universidad Nacional Autónoma de México, 248 p.

Arvizu, H.E., Iriondo, A., Izaguirre, A., Chávez-Cabello, G., Kamenov, G.D., Solís-Pichardo, G., Foster, D.A., and Lozano-Santa Cruz, R., 2009, Rocas graníticas pérmicas en la Sierra Pinta, NW de Sonora, México: Magmatismo de subducción asociado al inicio del margen continental activo del SW de Norteamérica: Revista Mexicana de Ciencias Geológicas, v. 26, p. 709–728.

Barra, F., and Valencia, V.A., 2014, Late Cretaceous porphyry copper mineralization in Sonora, Mexico: Implications for the evolution of the Southwest North America porphyry copper province: Mineralium Deposita, v. 49, p. 879–884.

Barra, F., Ruiz, J., Mathur, R., and Titley, S., 2003, A Re-Os study on sulfide minerals from the Bagdad porphyry Cu-Mo deposit, northern Arizona, United States: Mineralium Deposita, v. 38, p. 585–596.

Barra, F., Ruiz, J., Valencia, V.A., Ochoa-Landín, L., and Chesley, J., 2005, Laramide Porphyry Cu-Mo Mineralization in Northern Mexico: Age Constraints from Re-Os Geochronology in Molybdenite: Economic Geology, v. 100, p. 1605–1616.

Barton, M.D., Staude, J.M., Zürcher, L., and Megaw, P.K.M., 1995, Porphyry copper and other intrusion-related mineralization in Mexico, *in* Pierce, F.W., and Bolm, J.G., eds.,

Porphyry copper deposits of the American Cordillera: Arizona Geological Society Digest 20, p. 487–524.

Borden, J.C., Goldfarb, R.J., Gent, C.A., Burruss, R.C., and Roushey, B.H., 1992, Geochemistry of lode-gold deposits, Nuka Bay district, southern Kenai peninsula: U.S. Geological Survey Bulletin 2041, p. 13–22.

Böhlke, J.K., and Kistler, R.W., 1986, Rb-Sr, K-Ar, and stable isotope evidence for the ages and sources of fluid components of gold-bearing quartz veins in the northern Sierra Nevada Foothills Metamorphic Belt, California: Economic Geology, v. 81, p. 296–322.

Böhlke, J.K., and McKee, E.H., 1984, K-Ar ages relating to metamorphism, plutonism, and gold-quartz vein mineralization near Alleghany, Sierra County, California: Isochron-West, v. 39, p. 3–7.

Böhlke, J.K., Kirshbaum, C., and Irwin, J.J., 1989, Simultaneous analyses of noble gas isotopes and halogens in fluid inclusions in neutron irradiated quartz veins using a laser microprobe noble gas mass spectrometer: U.S. Geological Survey Bulletin 1890, p. 61–80.

Bundtzen, T.K., and Reger, R.D., 1977, The Richardson lineament: A structural control for gold deposits in the Richardson mining district, interior Alaska: Alaska Division of Geological and Geophysical Surveys Report, v. 55, p. 29–34.

Cheong, S., 1999, Structural setting and fluid characteristics of metamorphic gold-quartz veins in northwest Nevada: Unpublished Ph.D. thesis, Reno, Nevada, USA, University of Nevada, 332 p.

Creasey, S.C., 1965, Geology of the San Manuel area, Pinal County, Arizona: U.S. Geological Survey Professional Paper 471, 64 p.

Creasey, S.C., and Kistler, R.W., 1962, Age of some copper-bearing porphyries and other igneous rocks in southeastern Arizona: U.S. Geological Survey Professional Paper 450–D, p. 1–5.

Damon, P.E., and Mauger, R.L., 1966, Epeirogeny-orogeny viewed from the Basin and Range province: Transactions of the American Institute of Mining, Metallurgical, and Petroleum Engineers, v. 235, p. 99–112.

Damon, P.E., Shafiqullah, M., and Clark, K.F., 1983, Geochronology of the porphyry copper deposits and related mineralization of Mexico: Canadian Journal of Earth Sciences, v. 20, p. 1052–1071.

Del Río-Salas, R.E., 2011, Metallogenesis for the Boléo and Cananea copper mining districts: A contribution to the understanding of copper ore deposits in northwestern México: Unpublished Ph.D. thesis, Tucson, Arizona, USA, University of Arizona, 259 p.

Elder, D., and Cashman, S.M., 1992, Tectonic controls and fluid evolution in the Quartz Hill, California, lode gold deposits: Economic Geology, v. 87, p. 1795–1812.

Enríquez-Castillo, M.A., Iriondo, A., Chávez-Cabello, G., and Kunk, M.J., 2009, Interacción termal entre magmas graníticos laramídicos y rocas encajonantes mesoproterozoicas: Historia de enfriamiento de intrusivos de la Sierrita Blanca, NW Sonora: Boletín de la Sociedad Geológica Mexicana, v. 61, p. 451–483.

Espinosa-Perea, V.J., 1999, Magmatic evolution and geochemistry of the Piedras Verdes deposit, Sonora, Mexico: Unpublished M.Sc. thesis, Tucson, Arizona, USA, University of Arizona, 114 p.

Ford, R.C., 1993, Geology, geochemistry, and age of gold lodes at Bluff and Mt. Distin, Seward Peninsula, Alaska: Unpublished Ph.D. thesis, Golden, Colorado, USA, Colorado School of Mines, 302 p.

Ford, R.C., and Snee, L.W., 1996, $^{40}Ar/^{39}Ar$ thermochronology of white mica from the Nome district, Alaska: The first ages of lode sources to placer gold deposits in the Seward Peninsula: Economic Geology, v. 91, p. 213–220.

Goldfarb, R.J., Snee, L.W., Miller, L.D., and Newberry, R.J., 1991, Rapid dewatering of the crust deduced from ages of mesothermal gold deposits: Nature, v. 354, p. 296–298.

Goldfarb, R.J., Miller, L.D., Leach, D.L., and Snee, L.W., 1997, Gold deposits in metamorphic rocks in Alaska, *in* Goldfarb, R.J., and Miller, L.D., eds., Mineral Deposits of Alaska: Economic Geology Monograph 9, p. 151–190.

Haeussler, P.J., Bradley, D., Goldfarb, R.J., Snee, L.W., and Taylor, C.D., 1995, Link between ridge subduction and gold mineralization in southern Alaska: Geology, v. 23, p. 995–998.

Hagstrum, J.T., Cox, D.P., and Miller, R.J., 1987, Structural reinterpretation of the Ajo mining district, Pima County, Arizona, based on paleomagnetic and geochronologic studies: Economic Geology, v. 82, p. 1348–1361.

Hart, C.J.R., Goldfarb, R.J., Ullrich, T.D., and Friedman, R., 2008, Gold, Granites, and Geochronology: Timing of Formation of the Bralorne-Pioneer Gold Orebodies and the Bendor Batholith, Southwestern British Columbia: Geoscience BC, Summary of Activities 2007, Report 2008-1, p. 47–54.

Iriondo, A., 2001, Proterozoic basements and their laramide juxtaposition in NW Sonora, Mexico: Tectonic constraints on the SW margin of Laurentia: Unpublished Ph.D. thesis, Boulder, Colorado, USA, University of Colorado at Boulder, 222 p.

Iriondo, A., Martínez-Torres, L.M., Kunk, M.J., Atkinson, W.W., Jr., Premo, W.R., and McIntosh, W.C., 2005, Northward Laramide thrusting in the Quitovac region, northwestern Sonora, Mexico: Implications for the juxtaposition of Paleoproterozoic basement blocks and the Mojave-Sonora megashear hypothesis, *in* Anderson, T.H., Nourse, J.A., McKee, J.W., and Steiner, M.B., eds., The Mojave-Sonora megashear hypothesis: Development, assessment, and alternatives: Geological Society of America Special Paper 393, p. 631–669.

Ishiki-Pérez, N.H., Ruiz-Segoviano, S.A., Iriondo, A., Paz-Moreno, F.A., Izaguirre, A., and Arvizu, H., 2013, Acotamiento temporal de la deformación dúctil en Sierra Cipriano, NW de Sonora: Estudios Geocronológicos U-Pb en zircones de rocas graníticas [abs.]: GEOS, Unión Geofísica Mexicana, v. 33, p. 266.

Izaguirre-Pompa, A., 2006, Estudio petrológico y geocronológico del volcanismo orogénico intermedio-ácido de edad Oligo-Mioceno del Norte de Caborca, Sonora, México: Unpublished B.Sc. thesis, Hermosillo, Sonora, México, Universidad de Sonora, 84 p.

Izaguirre-Pompa, A., 2009, El basamento Paleoproterozoico (~1.71–1.68 Ga) Yavapai en el área Mina La Herradura en el NW de Sonora: sus implicaciones para el desarrollo del margen magmático continental Mesozoico-Cenozoico del NW de México: Unpublished M.Sc. thesis, Juriquilla, Querétaro, México, Universidad Nacional Autónoma de México, 201 p.

Jacques-Ayala, C., Barth, A.P., Jacobson, C.E., and Roldán-Quintana, J., 2008, Tectonically trasported Laramide granitoids in the Caborca area [abs.], *in* Valencia-Moreno, M., and Vega-Granillo, E.L., eds., Primer congreso sobre la evolución geológica y ecológica del Noroeste de México, 141 p.

Jensen, P.W., 1998, A structural and geochemical study of the Sierrita porphyry copper system, Pima County, Arizona: Unpublished M.Sc. thesis, Tucson, Arizona, USA, University of Arizona, 136 p.

Kistler, R.W., Newberry, R.J., and Brew, D.A., 1983, Rubidium-strontium isotopic systematics of vein minerals in the Juneau gold belt, Alaska, *in* Dusel-Bacon, C., and Till A.B., eds., Geologic studies in Alaska by the U.S. Geological Survey: U.S. Geological Survey Bulletin 2068, p. 236–240.

Livingston, D.E., 1973, A plate tectonic hypothesis for the genesis of porphyry copper deposits of the southern Basin and Range province: Earth and Planetary Science Letters, v. 20, p. 171–179.

Madden-McGuire, D.J., Silberman, M.L., and Church, S.E., 1989, Geologic relationships, K-Ar ages, and isotopic data from the Willow Creek gold mining district, southern Alaska, *in* Keays, R.R., Ramsay, W.R., and Groves, D.I., eds., The geology of gold deposits: Economic Geology Monograph 6, p. 242–251.

Marsh, E.E., Goldfarb, R.J., Kunk, M.J., Groves, D.I., Bierlein, F.P., and Creaser, R.A., 2008, New constraints on the timing of gold formation in the Sierra Foothills province, central California, *in* Spencer, J.E., and Titley, S.R., eds., Ores and orogenesis: Circum-Pacific tectonics, geologic evolution, and ore deposits: Arizona Geological Society Digest 22, p. 369–388.

McCandless, T.E., Ruiz, J., and Campbell, A.R., 1993, Rhenium behavior in molybdenite in hypogene and near-surface environments: Implications for Re-Os geochronology: Geochimica et Cosmochimica Acta, v. 57, p. 889–905.

McCoy, D., Newberry, R.J., Layer, P., DiMarchi, J.J., Bakke, A., Masterman, J.S., and Minehand, D.L., 1997, Plutonic-related gold deposits of interior Alaska, *in* Goldfarb, R.J., and Miller, L.D., eds., Mineral Deposits of Alaska: Economic Geology Monograph 9, p. 191–241.

McDowell, F.W., 1966, Potassium-argon dating of Cordilleran intrusives: Unpublished Ph.D. thesis, New York, New York, USA, Columbia University, 246 p.

McDowell, F.W., 1971, K-Ar ages of igneous rocks from the western United States: Isochron/ West, v. 2, p. 1–16.

McLemore, V.T., Munroe, E.A., Heizler, M.T., and McKee, C., 1999, Geochemistry of the Copper Flat porphyry and associated deposits in the Hillsboro mining district, Sierra County, New Mexico, USA: Journal of Geochemical Exploration, v. 67, p. 167–189.

Miller, L.D., Goldfarb, R.J., Gehrels, G.E., and Snee, L.W., 1994, Genetic links among fluid cycling, vein formation, regional deformation, and plutonism in the Juneau gold belt, southeastern Alaska: Geology, v. 22, p. 203–206.

Newberry, R.J., and Brew, D.A., 1987, The Alaska-Juneau gold deposit: A remobilized syngenetic vs. epigenetic origen: U.S. Geological Survey Circular 998, p. 128–131.

Noguez-Alcántara, B., 2008, Reconstrucción del modelo genético y evolución tectónica del yacimiento tipo pórfido cuprífero Milpillas, Distrito de Cananea, Sonora, México: Unpublished Ph.D. thesis, Hermosillo, Sonora, México, Universidad Nacional Autónoma de México, 390 p.

Nourse, J.A., Premo, W.R., Iriondo, A., and Stahl, E.R., 2005, Contrasting Proterozoic basement complexes near the truncated margin of Laurentia, northwestern Sonora-Arizona international border region, *in* Anderson, T.H., Nourse, J.A., McKee, J.W, and Steiner, M.B., eds., The Mojave-Sonora Megashear Hypothesis: Development, Assessment, and Alternatives: Geological Society of America Special Paper 393, p. 123–182.

Nourse, J.A., Oskin, M.E., Iriondo, A, and Premo, W.R., 2007, Laramide fold-thrust belt overprinted by Middle Miocene detachment faults, Caborca region, Sonora, Mexico [abs.]: Ores and Orogenesis, Arizona Geological Society, Program with Abstracts, p. 96–97.

Pérez-Segura, E., 1993, Los yacimientos de oro y plata de Sonora, México y sus relaciones con la geología regional, *in* Delgado-Argote, L.A., and Barajas, M., eds., Contribuciones a la tectónica del occidente de México: Monografía, Unión Geofísica Mexicana, v. 1, p. 147–174.

Pérez-Segura, E., Cheilletz, A., Herrera-Urbina, S., and Hanes, Y.J., 1996, Geología, mineralización, alteración hidrotermal y edad del yacimiento de oro de San Francisco, Sonora–Un depósito mesotermal en el Noroeste de México: Revista Mexicana de Ciencias Geológicas, v. 13, p. 65–89.

Poulsen, K.H., Mortensen J.K., and Walford, P.C., 2008, San Francisco gold deposit, Santa Ana region, Sonora, Mexico: Laramide orogenic, intrusion-related mineralization?, *in*

Spencer, J.E., and Titley, S.R., eds., Ores and orogenesis: Circum-Pacific tectonics, geologic evolution, and ore deposits: Arizona Geological Society Digest, v. 22, p. 547–559.

Quintanar-Ruíz, F.J., 2008, La Herradura ore deposit: An orogenic gold deposit in northwestern Mexico: Unpublished M.Sc. thesis, Tucson, Arizona, USA, University of Arizona, 97 p.

Rascón-Heimpel, M.A., Valencia-Moreno, M., Ochoa-Landín, L., and Calmus, T., 2012, Geología y geoquímica del pórfido cuprífero Los Alisos, distrito minero de La Caridad, Sonora, México: Revista Mexicana de Ciencias Geológicas, v. 29, p. 355–383.

Rose, A.W., and Cook, D.R., 1965, Radioactive age dates of porphyry copper deposits in the western United States [abs.]: Geological Society of America Special Paper 87, p. 139.

Ruiz-Segoviano, S.A., Ishiki-Pérez N.H., Iriondo A., Paz-Moreno, F.A., Arvizu, H., and Izaguirre, A., 2013, Brechamiento cataclástico de granitos del cretácico tardío (~96 Ma) en San Luis Río Colorado, NW de Sonora: Ejemplo de metamorfismo dinamotérmico asociado a la orogenia Larámide [abs.]: GEOS, Unión Geofísica Mexicana, v. 33, p. 266.

Russell, P.C., McKee, E.H., and Vikre, P.G., 1989, K-Ar ages from Nevada and eastern California: Isochron/West, no. 52, p. 12–14.

Selby, D., Creaser, R.A., Hart, C.J.R., Rombach, C.S., Thompson, J.F.H., Smith, M.T., Bakke, A.A, and Goldfarb, R.J., 2002, Absolute timing of sulfide and gold mineralization: A comparison of Re-Os molybdenite and Ar-Ar mica methods from the Tintina Gold Belt, Alaska: Geology, v. 30, p. 791–794.

Scherkenback, D.A., Sawkins, F.J., and Seyfried, W.E., 1985, Geologic, fluid inclusions, and geochemical studies of the mineralized breccias at Cumobabi, Sonora, Mexico: Economic Geology, v. 80, p. 1566–1592.

Shafiqullah, M., Damon, P.E., Lynch, D.J., Reynolds, S.J., Rehring, W.A., and Raymond, R.H., 1980, K-Ar Geochronology and Geologic History of southwestern Arizona and adjacent areas: Arizona Geological Society Digest 7, p. 201–260.

Silberman, M.L., Mitchell, P.A., and O'Neil, J.R., 1981, Isotopic data bearing on the origin and age of the epithermal lode gold deposits in the Hope-Sunrise northern Kenai peninsula, Alaska: U.S. Geological Survey Circular 823-B, p. 81–84.

Snow, C.A., Bird, D.K., Metcalf, J., and McWilliams, M., 2008, Chronology of gold mineralization in the Sierra Nevada Foothills from $^{40}Ar/^{39}Ar$ dating of mariposite: International Geology Review, v. 50, p. 503–518.

Suleyman, Y., 1994, Geology, geochemistry, and mineralization of the Liberty Bell gold mine, Alaska: Unpublished M.Sc. thesis, Corvallis, Oregon, USA, Oregon State University, 189 p.

Taylor, C.D., Goldfarb, R.J., Snee, L.W., Gent, C.A., Karl, S.M., and Haeussler, P.J., 1994, New age data for gold deposits and granites, Chichagof mining district, SE Alaska: Evidence for a common origin [abs.]: Geological Society of America, Abstracts with Programs, v. 26, p. 140.

Taylor, R.D., Goldfarb, R.J., Monecke, T., Fletcher, I.A., Cosca, M.A., and Kelly, N.M., 2015, Application of U-Th-Pb Phosphate Geochronology to Young Orogenic Gold Deposits: New Age Constraints on the Formation of the Grass Valley Gold District, Sierra Nevada Foothills Province, California: Economic Geology, v. 110, p. 1313–1337.

Valencia, V.A., Ruiz, J., Barra, F., Gehrels, G., Ducea, M., Titley, S.R., and Ochoa-Landin, L., 2005, U-Pb zircon and Re-Os molybdenite geochronology from La Caridad porphyry copper deposit: Insights for the duration of magmatism and mineralization in the Nacozari district, Sonora, Mexico: Mineralium Deposita, v. 40, p. 175–191.

Valencia, V.A., Noguez-Alcántara, B., Barra, F., Ruiz, J., Gehrels, G., Quintanar, F., and Valencia-Moreno, M., 2006, Re-Os molybdenite and LA-ICP-MS-MC U-Pb zircon geochronology for the Milpillas porphyry copper deposit: insights for the timing of mineralization in the Cananea District, Sonora, Mexico: Revista Mexicana de Ciencias Geológicas, v. 23, p. 39–53.

Vidal-Solano, J.R., Demant, A., Paz-Moreno, F.A., Lapierre, H., Ortega-Rivera, M.A., and Lee, J.K., 2008, Insights into the tectonomagmatic evolution of NW Mexico: Geochronology and geochemistry of the Miocene volcanic rocks from the Pinacate area, Sonora: Geological Society of America Bulletin, v. 120, p. 691–708.

Vikre, P.G., 1981, Silver mineralization in the Rochester district, Pershing County, Nevada: Economic Geology, v. 76, p. 580–609.

Vikre, P.G., and McKee, E.H., 1985, Zoning and chronology of hydrothermal events in the Humboldt Range, Pershing County, Nevada: Isochron/West, v. 44, p. 17–24.

Wilkerson, G., Deng, Q., Llavona, R., and Goodell, P., 1988, Batopilas mining district, Chihuahua, Mexico: Economic Geology, v. 83, 1721–1736.

Wodzicki, W.A., 2001, The Evolution of Magmatism and Mineralization in the Cananea District, Sonora, Mexico, *in* Albinson, T., and Nelson, C.E., eds., New Mines and Discoveries in Mexico and Central America: Economic Geology Special Publication 8, p. 241–261.

Capítulo 7. Conclusiones

Este trabajo de tesis presenta varios estudios con resultados analíticos generados a partir de un muestreo regional representativo del cinturón de oro orogénico Caborca (COGB). Además, en este se plantea un encuadre tectónico regional novedoso que expone el origen de la mineralización del COGB utilizando los estudios realizados y el conocimiento geológico actual de la región. A continuación, se presentan las conclusiones más importantes del trabajo de tesis:

• Los resultados obtenidos del estudio geoquímico de balance de masas sugieren que los fluidos que generaron la alteración hidrotermal y las vetas auríferas a lo largo del COGB fueron altamente homogéneos. Esta homogeneidad ocurre a pesar de existir grandes distancias de centenares de kilómetros entre las muestras estudiadas. Los elementos K_2O, W, Cu, Pb, Mo, Tl, Be, Zn, V, Sb, Ag, Sn, SiO_2, Se, Ni y FeO representan enriquecimiento geoquímico y caracterizan al fluido; su presencia parcial o total puede servir como guía para la exploración mineral de Au en la región.

• La geocronología $^{40}Ar/^{39}Ar$ en 63 muestras de micas blancas hidrotermales a lo largo del COGB permitió encontrar un periodo de mineralización considerable de ~33 millones de años (69–36 Ma). Los datos siguieren un inicio súbito y rápido de la mineralización (~69 Ma) con un clímax de mineralización a los ~61 Ma y un declive paulatino entre 58–36 Ma. Este estudio geoquímico detallado descarta mineralización aurífera orogénica previa o posterior al periodo Cretácico tardío-Eoceno y asocia la mineralización exclusivamente al periodo orogénico larámide. Cabe destacar que la homogeneidad

geoquímica de los fluidos es coherente con la existencia de un único pulso de mineralización.

• Los resultados obtenidos con isotopía estable ($\delta^{18}O$ y $\delta^{34}S$) de pares minerales (cuarzo-mica blanca, pirita-galena) ayudaron a determinar una temperatura promedio de formación (~327ºC) de las vetas de cuarzo hidrotermal a lo largo del COGB. Considerando esta temperatura general de precipitación, el modelado de isótopos de $\delta^{18}O$ (cuarzo) y δD (mica blanca) permitió encontrar que el agua asociada al fluido mineralizante es afín al generado por reacciones metamórficas; típico por originarse por metamorfismo y deshidratación de rocas profundas (>20 km) en facies de anfibolita y posiblemente de rocas en facies metamórficas de mayor grado y menos hidratadas (*e.g.*, granulita).

• El COGB hasta el momento se convierte en la referencia de mineralización de oro orogénico mejor caracterizada con respecto a otras zonas auríferas postuladas como mineralización orogénica de México (*e.g.*, Oaxaca, Michoacán, Guerrero, Baja California). A pesar de disponer de un escaso conocimiento en general entre estas zonas de oro orogénico en México, se puede destacar que las ocurrencias de oro orogénico mexicanas presentan temperaturas de formación del rango de temperaturas mesotermales (200–400ºC). Entre estas se puede observar similitud en el control estructural de formación (cataclástico-milonítico) con profundidades mesotermales típicas (~3–6 km); además la existencia de una paragénesis (cuarzo, mica blanca, y pirita) mineral en común de algunas de estas regiones. Sin embargo, debido a las grandes distancias que separan a estas ocurrencias minerales orogénicas se recomendaría hacer primero reconstrucciones

continentales al momento de hacer comparativas o interpretar extensiones minerales, y se pone en evidencia que existe un gran campo de estudio en las ocurrencias de oro orogénico mexicanas.

• El encuadre tectónico del COGB sugiere que un engrosamiento cortical ocurrió durante la etapa temprana (~70 Ma) de la orogénia Larámide y fue la causa principal de generación de los fluidos mineralizantes. Después, a causa de la repentina subducción plana, un evento de extensión cortical sinconvergente sobre el antearco desencadenó episodios de ascenso de fluidos a través de conductos principales formados previamente durante la compresión y, quizás, por nuevos conductos creados en el proceso de estensión.

Una migración del arco magmático hacia el este del COGB permitió la generación contemporánea del cinturón de pórfidos Cu-Mo en el noroeste de México y suroeste de Estados Unidos, generando, quizás, una situación única en el mundo donde coexisten dos diferentes tipos de mineralización, una formada en el antearco y sin presencia de magmatismo (COGB) y otra en el arco (pórfidos Cu-Mo). La actual exposición de estos cinturones minerales es producto de una diferencia de denudación que afectó mayormente al COGB.

Por último, la combinación de diversos factores como son la presencia de: (1) mineralización aurífera orogénica, (2) pórfidos Cu-Mo, (3) mineralización epitermal (Oligoceno-Mioceno) y (4) una componente de alteración supergénica regional, quizá sea la causa de que el noroeste de México sea considerado como uno de los lugares más

atractivos, a nivel mundial, para llevar a cabo prospección por metales preciosos y metales base.

Apéndices

Apéndice A. Poster de estudios de isotopía estable δD, $\delta^{18}O$ y $\delta^{34}S$ de vetas auríferas del COGB

Un origen metamórfico de los fluidos hidrotermales para las vetas de cuarzo aurífero del cinturón de oro orogénico Caborca de edad Larámide, en el NW Sonora: Estudios isotópicos de oxígeno, hidrógeno y azufre (*A metamorphic origin for the hydrothermal fluids forming the gold-bearing quartz veins from the Laramide Caborca Orogenic Gold Belt of NW Sonora: An oxygen, hydrogen and sulfur isotopic study*) publicado: GEOS (Unión Geofísica Mexicana) (2014) 35-poster, 334 p. Autores: Aldo Izaguirre, Alexander Iriondo.

• Objetivos: Determinar el origen del fluido hidrotermal generador de las vetas de cuarzo aurífero a lo largo del COGB (Izaguirre e Iriondo, 2014, Apéndice A). También obtener la temperatura de formación de la mineralización en su conjunto.

• Estudios: Un estudio de isótopos estables de deuterio, oxígeno y azufre (δD, $\delta^{18}O$ y $\delta^{34}S$) se planteó para estudiar en el mayor número posible de ocurrencias minerales del COGB. Se utilizaron pares minerales de la paragénesis de las vetas de cuarzo aurífero (*e.g*., pirita, galena, cuarzo, mica blanca, turmalina). Primero, se calcularon las temperaturas de formación de las ocurrencias individuales usando cálculos termométricos de equilibrio isotópico (Figura 7). Además, se estimó una temperatura media ponderada (~327ºC). Después, se usó la temperatura para estimar gráficamente (Figura 8) el origen del agua que probablemente constituyó el fluido hidrotermal generador de las vetas de cuarzo aurífero del COGB.

UNIVERSIDAD NACIONAL AUTÓNOMA DE MÉXICO

Centro de Geociencias
http://www.geociencias.unam.mx/geociencias/index.html

Reunión Anual Unión Geofísica Mexicana
2-7 de Noviembre, 2014, Puerto Vallarta, Jalisco

Cartel: SE12-10

Resumen: 0786

Presentan:

Aldo Izaguirre
(aldoizapo@gmail.com)
Estudiante de doctorado

Alexander Iriondo
(iriondo@geociencias.unam.mx)
Investigador y tutor

A metamorphic origin for the hydrothermal fluids forming the gold-bearing quartz veins from the Laramide Caborca Orogenic Gold Belt of NW Sonora: An oxygen, hydrogen and sulfur isotopic study

1. Resumen

An oxygen, hydrogen, and sulfur isotopic study was undertaken on a variety of hydrothermal minerals aiming to determine the origin of the mineralizing fluid that formed the gold-bearing quartz veins of the Caborca Orogenic Gold Belt (COGB). The COGB forms an elongated area in northwestern Sonora of ~600 km long and ~60 to 80 km a cross with a general NW-SE orientation; furthermore, the northernmost portion of the belt includes parts of southwestern Arizona and southeasternmost California.

Hypogene mineralization consists mostly of quartz, carbonates, white mica, pyrite and galena. The mineralizing fluid altered host rocks causing pervasive silicification, sericitization, chloritization, epidotization and pyritization. Younger, possible Miocene, supergene alteration is also observed in some locations (e.g., oxidation of pyrite). The age of hypogene mineralization for the COGB veins has been previously established between ~70 to 36 Ma (Late Cretaceous-Eocene) with a main age peak at ~61 Ma. This age has been interpreted as representing the time of fluid migration from confined sources deep in the middle crust into more surficial levels (4 to 10 km) to finally precipitate as quartz veins during the last stages of the Laramide Orogeny for this section of the North American Cordillera.

A representative sampling of quartz veins along the entire COGB was used to determinate quartz isotopic $\delta^{18}O$ values between 16.5 to 7.2 ‰ (n = 42), indicating that the mineralizing fluid in equilibrium with the quartz ranged from 10.0 to 0.7 ‰ at an estimated temperature of 327° C. In the same way, hydrothermal white micas were analyzed for hydrogen isotopes and δD values between −107 to −39 ‰ (n = 39) were obtained, with an estimated fluid value between −65 and 3 ‰. Moreover, sulfides from the quartz veins were analyzed to obtain $\delta^{34}S$ values between 7.3 and −5.7 ‰ on pyrite and between 5.2 and −9.5 ‰ on galena. Using stable isotopic data on coexisting mineral pairs of sulfides (pyrite-galena; n = 15) as well as pairs of silicates (quartz-white mica; n = 27) we calculated vein formation temperatures between ~200 to 400°C, with an average of ~327°C.

Isotopic data for the fluid, calculated at ~327°C and plotted in a δD vs. $\delta^{18}O$ discrimination diagram, suggest that the quartz veins were derived from a fluid with strong affinity to metamorphic waters, perhaps generated at significant crustal depths (>30 km) due to a process of metamorphic dehydration of water-rich minerals (e.g., amphibole) from basement rocks. This basement dehydration was most likely triggered by a significant crustal thickening due to Laramide compression in this section of the North America Cordillera.

Finally, some isotopic data patterns slightly change spatially from West to East in the COGB area. This feature could be caused by a progressive migration of the source of the hydrothermal fluids while the subducting oceanic plate was flattening in the Sonoran section of the North American Cordillera; the metamorphic fluids could have been modified by passing through different basement rocks in the easternmost area of the COGB.

2. Mapa regional del COGB

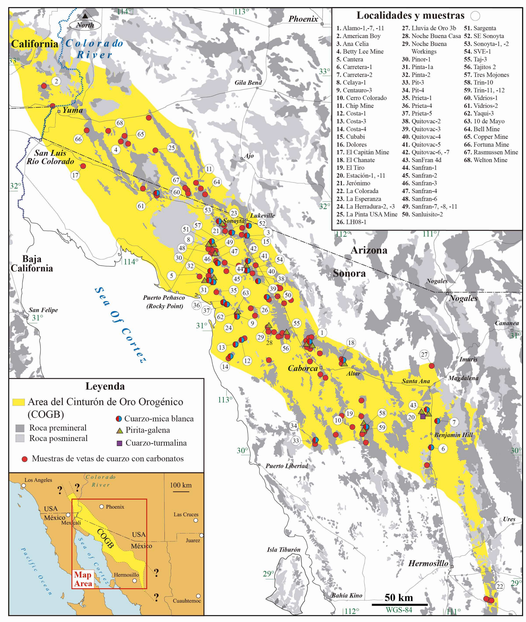

3. Geología del COGB

Edad Laramide COGB

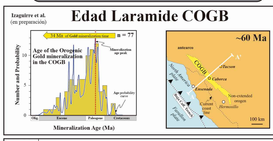

Encuadre tectónico COGB

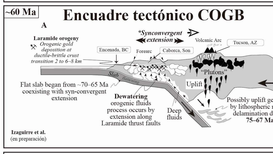

Homogeneidad Geoquímica a nivel COGB

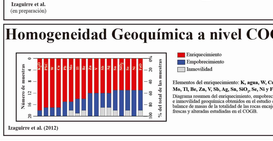

4. Paragénesis mineral, alteraciones y oro del COGB

Qtz = Veta de cuarzo
Bt = Biotita
Kfs = Feldespato potásico
Wm = Mica blanca

Vetas cuarzo-carbonato

Minerales primarios comunes

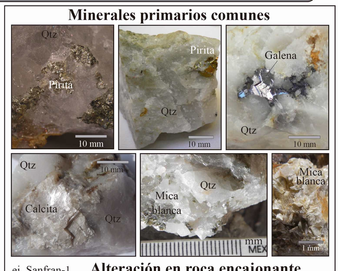

Alteración en roca encajonante

ej. Sanfran-1

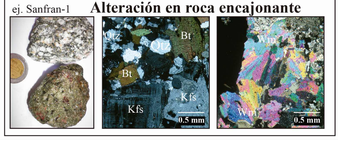

Oro

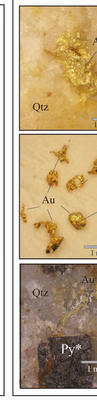

5. Separación mineral y métodos analíticos

Seperación mineral

Métodos analíticos

^{18}O por fluorinización usando BrF_5

• Para la obtención de los isótopos de oxígeno se utilizó una mezcla mineral + pentafluoruro de bromo (BrF_5) para fluorinizar en una línea de extracción con viales de níquel (Clayton and Mayeda, 1963); en los laboratorios del U.S. Geological Survey en Denver, Colorado.
• Cuarzo (7.0 mg); mica blanca (8.5 mg); turmalina (9.0 mg).
• Se generó CO_2 calentando a ~600° C por ~12 horas.

Línea-fluorinización

• Para medir los isótopos de O se utilizó un espectrómetro *FinniganMAT 252* multicolector.

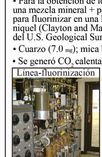

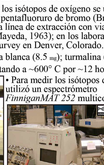

Deuterio (D) por TC/EA

• En la obtención de isótopos de hidrógeno se usó un instrumento *Thermo TC/EA* para producir H_2 y se medió según la técnica descrita por Sharp et al. (2001).
• Se utilizó 5–7 mg de mica blanca calentando a ~1425° C.
• La mica blanca previamente se peso y empaquetó en cápsulas de plata.

Cápsulas

Empaquetado

^{34}S por combustión continua usando V_2O_5

• Los isótopos de azufre se obtuvieron por medio de la combustión continua de una mezcla de pirita (0.1 mg) y la galena (0.4 mg) con pentóxido de vanadio (V_2O_5).
• Se utilizaron cápsulas de *zinc* al empacar.
• Se utilizó un equipo *Costech* para obtener SO_2 y un espectrómetro de masas *Micromass Optima*.

Pesado

6. Resultados de isótopos estables de O, D, S

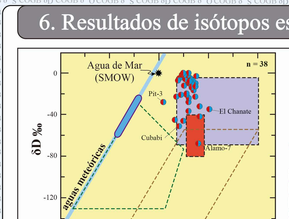

Datos isotópicos de las vetas de cuarzo del Cinturón de Oro Orogénico Caborca (COGB) utilizando el par mineral cuarzo-mica blanca (n = 38). Los datos fueron recalculados a la temperatura del fluido hidrotermal a ~327° C usando las ecuaciones de Zhang *et al.* (1989) para el oxigeno y Suzuoki and Epstein (1976) para el deuterio.

Aguas meteóricas en el NW de Sonora durante el Paleogeno (Taylor, 1974).

Campos de aguas naturales

Aguas metamórficas (Sheppard, 1986).
Aguas magmáticas (Taylor, 1974).
Aguas derivadas de andesitas (Giggenbach, 1992).
Aguas de mineralización de tipo epitermal (compo a partir de Barnes, 1997).
Aguas de mineralización de tipo pórfido cuprífero (compo a partir de Barnes, 1997).

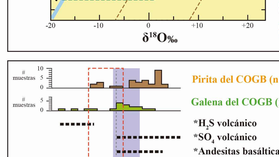

*H_2S volcánico
*SO_4 volcánico
*Andesitas basálticas de arcos de islas
*Granitoides

Rango de azufre reportado para la mayoría de los sulfuros en la tipología de oro orogénico alrededor del mundo (Taylor, 1986).

Rango de azufre reportado para los sulfuros de pórfidos cupríferos de Arizona (Ajo, Twin Butts, Sierrita) (Ohmoto y Rye, 1979).

***Rangos de valores de azufre de fuentes naturales.**

7. Temperaturas de formación de las vetas del COGB

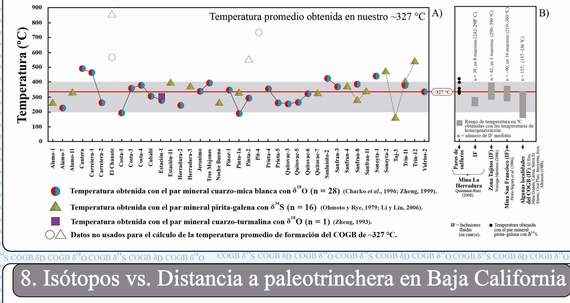
Temperatura promedio obtenida en nuestro ~327 °C
A)
B)
Temperatura (°C)
~327°C
Alamo-1
Alamo-7
Cantera
Carretera-1
Carretera-2
El Chanate
Costa-1
Costa-3
Costa-4
Cubabi
Estación-1
Herradura-1
Herradura-2
Herradura-3
Jerónimo
Noche Buena
Pinta-1a
Pinta-2
Pinta-4
Pinta-5
Quitovac-2
Quitovac-3
Quitovac-5
Quitovac-7
Sanfran-2
Sanfran-3
Sanfran-4
Sanfran-6
Sonoyta-1
Sonoyta-2
Trin-11
Trin-12
Vidrios-1
Mina La Herradura (Sonora, México) (2008).
Mina San Francisco (Sonora, México) (2008).
Mina La Herradura (Sonora, México) (2008).
Mina La Herradura (Sonora, México) (2008).
Mina La Herradura

Apéndice B. Técnicas empleadas en los estudios analíticos del COGB

A continuación, se presentan las diferentes técnicas analíticas y métodos de preparación de muestras empleados en los diferentes estudios del Cinturón de oro orogénico Caborca (COGB). Los estudios se realizaron con distintos minerales provenientes de las vetas hidrotermales del COGB y estos fueron procesados en el laboratorio de separación de minerales (SepLab) del Centro de Geociencias, UNAM, Querétaro, utilizando los procedimientos convencionales de separación mineral. También se usaron las instalaciones de la Instituto de Geología UNAM, Estación Regional Noroeste (ERNO) en Hermosillo.

B.1. Preparación de muestras y análisis geoquímico en rocas encajonantes y vetas de cuarzo

Para el estudio geoquímico de balance de masas utilizando rocas encajonantes (fresca y alterada) y vetas de cuarzo se usaron ~5 kg de muestra representativa de cada localidad del área de estudio (Izaguirre *et al.*, 2012). Para el triturado se empleó una quebradora de gran capacidad marca *Chipmuck* que fue previamente limpiada con cada una de las muestras para evitar al máximo la contaminación entre muestras. Del material quebrado resultante se realizó un cuarteo para obtener ~150 g de gravilla que se utilizó en el proceso final de pulverizado usando el sistema de pulverizado *Shatter Box* con contenedor de alúmina para evitar contaminación metálica. Sin embargo, para el pulverizado de las muestras de vetas de cuarzo se utilizó un contenedor de carburo de tungsteno con anillo interno para agilizar el proceso. De cada muestra se obtuvieron ~100 g de polvo con un tamaño de partícula inferior a las ~74 micras, el cual se envió para su análisis a los

laboratorios del Centro Experimental Chihuahua pertenecientes al Servicio Geológico Mexicano.

Las muestras se analizaron por medio de diferentes técnicas analíticas para determinar las concentraciones de elementos mayores, traza y preciosos. Se usaron las técnicas analíticas de espectrometría de emisión atómica con fuente de plasma de acoplamiento inductivo (ICP–AES, por sus siglas en inglés) para analizar Al, Al_2O_3, As, Ba, Be, Bi, CaO, Co, Cr, Cu, FeO, Fe_2O_3, K_2O, MgO, MnO, Mo, Na_2O, Ni, P_2O_5, Pb, Sb, SiO_2, Se, Sn, Sr, Te, TiO_2, Tl, V, W, Zn. También se empleó la espectrometría de masas con fuente de plasma de acoplamiento inductivo (ICP–MS, por sus siglas en inglés) para obtener Ag, Ce, Dy, Eu, Gd, Ho, Ir, La, Lu, Nd, Os, Pd, Pr, Pt, Rh, Ru, Sc, Sm, Tb, Th, Tm, U, Y, Yb. Por otro lado, la pérdida por calcinación (probablemente, y en mayor medida, se componga de H_2O, contenidos orgánicos, carbonato de calcio y dióxido de carbono) se obtuvo al calentar la muestra a 950º C. Para el caso de la medición del Au, en vetas de cuarzo, se realizó copelación al fuego (*fire assay*) para obtener mejores resultados. Esto debido a que el oro de esta región se caracteriza por ser de grano fino, o criptocristalino, esta característica lo hace invisible, e inclusive cuando se emplea lupa de aumento.

B.2. Método de balance de masas

El estudio de balance de masas se elaboró utilizando el método de isocona propuesto por Grant (1986, 2005), técnica basada en los estudios pioneros de Gresens (1967). Esta consiste en emplear un simple gráfico binario “x–y” donde, por costumbre universal, el eje “x” es igual a la concentración de elementos químicos medidos en la roca

fresca y el eje “y” es igual a la concentración de elementos medidos en la roca alterada. Sobre este gráfico, se busca visualmente, o por medios estadísticos, una correlación entre los elementos que han tenido inmovilidad o que fueron inertes (argumento principal del método) durante el fenómeno geológico de alteración. De esta forma se elige la línea de isocona que se traza a través del origen (0,0) y los elementos inertes elegidos. El campo por encima de la línea de isocona incluye o abarca los elementos que sufrieron enriquecimiento elemental, mientras que los del campo inferior a la isocona indican empobrecimiento. Este método ha sido útil en los estudios de balance de masas y de movilidad de elementos mayores, traza y preciosos en depósitos minerales de oro orogénico en Nueva Zelanda (Pitcairn *et al*., 2006) y China (Wei *et al*., 2001). En estos estudios, se han determinado los elementos característicos de la alteración hidrotermal que han servido como una guía de exploración y en el cálculo de predicción de volúmenes de roca mineralizada de Au. Así mismo, otras tipologías de yacimientos (*p.e*., skarn) también han sido estudiadas con este método, en donde se ha tratado de determinar los mismos aspectos antes mencionados (Lentz, 2005).

El estudio de balance de masas se realizó enteramente con el programa computacional GEOISO (Coelho, 2006) y se generaron gráficos binarios de la geoquímica de la roca fresca versus la roca alterada para cada par de las muestras estudiadas. En la elaboración de estos gráficos, las concentraciones químicas de los elementos expresadas en diferentes unidades (*p.e*., ppm; % en peso) se escalaron de forma arbitraria para conseguir treinta unidades en cada eje, multiplicando cada elemento por factores de normalización incluidos en el programa computacional. Cabe aclarar que cuando los valores de las concentraciones elementales de las muestras se encontraron por

debajo del nivel de detección, se utilizó la mitad de ese valor (N.D.) para poder incluirlos en los diagramas de isocona. Con ayuda de los algoritmos del programa se seleccionó la mejor isocona posible (línea de inmovilidad elemental), según los parámetros de correlación y error. Por medio de estos algoritmos se obtuvieron las estimaciones de empobrecimiento, enriquecimiento e inmovilidad

B.3. Método de correlación geoquímica bivariable

Con los datos geoquímicos obtenidos de las vetas se realizó un estudio de análisis de correlación geoquímica bivariable utilizando el paquete computacional *Statistical Package for Social Sciencies* (SPSS v19) para determinar el coeficiente de correlación "r" entre el elemento clave Au y los otros elementos traza y preciosos. Los coeficientes de correlación varían entre -1 y +1, y cuando r = 0, significa una completa independencia entre dos elementos analizados; o bien, cuando r = +1, indica una relación funcional directa. Por último, cuando r = -1 representa una correlación funcional inversa (***p.e.***, Davis, 1986). Cabe aclarar que, al momento de realizar los cálculos para algunas de las muestras, se utilizó el valor del límite de detección de los elementos.

B.4. Técnica de SEM-EDS

Los estudios de microscopía electrónica de barrido con detector de espectroscopía de rayos X de energía dispersiva (SEM-EDS, por sus siglas en inglés) se realizaron en granos milimétricos de pirita, oro y galena de algunas muestras de vetas de cuarzo del cinturón de oro orogénico Caborca (COGB). El procedimiento consistió en la elaboración de probetas de resina epóxica, montando cristales de pirita y galena de algunas de las

muestras estudiadas en cinta doble cara, para posteriormente verter la resina epóxica en un molde y capturar los granos. Después del endurecimiento de las probetas se desbastó y pulió hasta llegar aproximadamente a la mitad de los granos para obtener un área máxima de exposición de los mismos. Por otro lado, los granos de oro de las muestras observadas se adhirieron con pintura de carbón conductora de electrones en unas pequeñas pastillas metálicas que sirven para su transporte y análisis dentro del SEM.

Para la obtención de imágenes y espectros de energía dispersiva por medio de análisis puntual de las muestras de pirita y galena se utilizó un SEM-EDS de marca *JEOL5800LV*. Para las muestras de oro se empleó un equipo *FEI Quanta 450 FEG*, ambos, equipos del laboratorio de microsonda y microscopia electrónica del *U.S. Geological Survey, Federal Center*, en Denver, Colorado, Estados Unidos. Los datos fueron reducidos con el paquete computacional NSS 2.3 *Microbeam X-ray analysis* de *Thermo Scientific*, del cual se obtuvieron espectros de elementos químicos y composiciones de los análisis puntuales realizados sobre las superficies de los minerales.

B.5. Técnicas analíticas utilizadas para estudios de isótopos estables de azufre en sulfuros y oxígeno–hidrógeno en silicatos

Los procedimientos y análisis instrumentales para obtener isotopos de azufre ($\delta^{34}S$) utilizando sulfuros (galena y pirita) de las vetas hidrotermales del COGB son equivalentes a las técnicas reportas por Johnson *et al.* (2004). En primera estancia, se seleccionaron cristales de galena (~0.4 mg ± 0.10 %) y pirita (~0.1 mg ± 0.10 %) con 99.9% de pureza para ser empaquetados en cápsulas de estaño de tamaño 4x6 mm (relación ancho–largo) y añadiendo ~1–2 mg de pentaóxido de vanadio (V_2O_5). Las

cápsulas se analizaron directamente para obtener isótopos de azufre en un espectrómetro de masas *Micromass Optima Delta X* de flujo continuo del *U.S. Geological Survey, Federal Center,* en Denver, Colorado, Estados Unidos; transformando la mezcla de sulfuro más V_2O_5 en SO_2 (Giesemann *et al*., 1994). También, se analizó un blanco y un estándar NBS123 ($\delta^{34}S$ = 21 por mil) alternando cada 4 muestras desconocidas para realizar las correcciones pertinentes en la reducción de los datos finales.

Para obtener isótopos de oxígeno ($\delta^{18}O$) en los silicatos provenientes de las vetas auríferas del COGB (cuarzo, mica blanca y turmalina) se hizo reaccionar BrF_5 con cuarzo (~7 mg), mica blanca (~8.5 mg) y turmalina (~9 mg) en un contenedor de níquel a ~600° C por 12 horas. La mezcla mencionada se transformó en CO_2 utilizando una línea de purificación enfriada con nitrógeno líquido (Clayton y Mayeda, 1963). El procedimiento se realizó en las instalaciones de *U.S. Geological Survey*, en Denver, Estados Unidos. Posteriormente, se analizó el CO_2 en un espectrómetro de masas multicolector *Finnigan MAT 252.* Durante la preparación de las muestras se incluyó un estándar de sílice conocido como AGS ($\delta^{18}O$ = 10 por mil) por cada 5 muestras desconocidas, de esta manera, se verificó el comportamiento del procedimiento analítico del laboratorio. Al momento de analizar en el espectrómetro se usó un gas de referencia interno de laboratorio (TSF2) con un valor de $\delta^{18}O$ = 17 por mil en cada bloque de 5 muestras desconocidas.

Por último, la obtención de isótopos de hidrógeno (δD) en micas blancas, de las vetas auríferas, se hizo en las instalaciones del *U.S. Geological Survey,* en Denver, Estados Unidos. Para esto se encapsularon cristales de mica blanca (5–7 mg) usando envolturas de plata (4x4 mm) y se analizaron a alta temperatura (~1425° C) para liberar

H_2 directamente en un espectrómetro *Thermo TC/EA-Delta plus XL* según la técnica descrita por Sharp *et al*., (2001). El sistema fue calibrado por el estándar NBS 30 (Biotita) aprobado por la Agencia Internacional de Energía Atómica (IAEA, por sus siglas en inglés).

B.6. Métodos analíticos utilizados para estudios de geocronología por el método $^{40}Ar/^{39}Ar$ en mica blanca hidrotermal

Sesenta y tres muestras de mica blanca hidrotermal de vetas de cuarzo aurífero provenientes del COGB fueron estudiadas en cinco paquetes diferentes (DD60, KD12, KD52, KD53 y KD55). Cada muestra de mica blanca fue encapsulada dentro de paquetes individuales de cobre con un peso aproximado de 1 miligramo (mg) y en otro con 20 mg. Los paquetes fueron puestos al vacío en tubos de cuarzo y posteriormente fueron irradiados en un reactor nuclear *Training Reactor Isotopes General Atomics* (TRIGA) del *U.S. Geological Survey* en Denver, Colorado. Conjuntamente dentro de los paquetes se colocó un mineral estándar (hornblenda MMhb-1) con una edad de 519.4 ± 2.5 Ma (Alexander *et al*., 1978; Dalrymple *et al*., 1981). El tipo de contenedor y la geometría de las muestras/estándar se realizaron usando los métodos de Snee *et al*., (1988).

Las muestras de mica blanca fueron analizadas en el *U.S. Geological Survey Argon Thermochronology Laboratory* en Reston, Virginia. Las muestras con 20 mg fueron analizadas en un espectrómetro *VG Isotopes, Ltd. model 1200 mass* equipado con un detector (multiplicador de electrones) para analizar $^{40}Ar/^{39}Ar$ usando la técnica de calentamiento por pasos. Todas las muestras fueron calentadas por 10 minutos cada paso (11–20 pasos) en un horno compacto con una resistencia de molibdeno-tántalo, similar a

como se describe en Staudacher *et al*., (1978). La temperatura fue controlada por un control termopar electrónico programable (W5Re-W26Re). La línea de extracción, horno y un dedo de cuarzo donde se manipularon las muestras fueron limpiados internamente usando un sistema de extracción por bombas turbomoleculares entre cada paso de calentamiento. Se usaron dos bombas iónicas para generar un vació para limpiar el espectrómetro de masas y una línea que conecta entre el espectrómetro cada paso de calentamiento. Antes de cada análisis el sistema fue purificado usando un dispositivo *SAES ST707 Zr-V-Fe* (*zirconium-vanadium-iron*) a temperatura ambiente y a alta temperatura usando un filamento de Re (renio).

En el sistema de colector, un dedo de carbón activado fue sumergido en una mezcla de hielo seco y acetona con el objetivo de remover los gases con pesos moleculares mayores a 60 y 80 (gases nobles) antes de introducir el gas argón de las muestras al espectrómetro. Durante cada paso el gas fue purificado por segunda vez antes de ser analizado usando un dispositivo *SAES ST101* operando a temperatura ambiente. Los isotopos del gas con pesos atómicos de 40 a 36 (^{40}Ar, ^{39}Ar, ^{38}Ar, y ^{37}Ar) y el CO_2 (peso atómico de 44) fueron analizados durante 5 o 6 ciclos. Todas las fases del proceso analítico, calentamiento de las muestras, blanqueo, calibración y análisis, fueron realizados usando un control por medio de un computador.

Las muestras empaquetadas de un 1 mg fueron analizadas usando un espectrómetro de gases MAP-216 equipado con un detector (multiplicador de electrones) de ^{40}Ar/^{39}Ar y usando el método de calentamiento por pasos. El proceso consistió en una rutina de incrementos de temperatura usando de 11 a 20 pasos. La rutina de calentamiento por pasos fue diseñada de tal manera que el porcentaje de argón ^{39}Ar liberado de cada

paso fuera limitado a menos del 20% del total del gas liberado para la mayoría de las muestras. Las muestras fueron calentadas de la misma manera como se describió anteriormente en las muestras de mayor tamaño (20 mg). De igual forma, el horno y los colectores fueron limpiados cada paso usando una bomba turbomolecular. Por separado, una bomba iónica fue usada para limpiar el espectrómetro de masas. Antes de analizar con el espectrómetro de masas el gas de cada muestra fue purificado usando dos dispositivos eléctricos (*SAES ST101 Al-Zr getters*), uno operando a temperatura ambiente y el otro usando a 400°C con un filamento de Re. Después, el gas (mayormente argón) fue purificado una tercera vez usando un tercer dispositivo (*SAES ST101 getter*) acoplado al espectrómetro y operado a temperatura ambiente.

Los datos generados en el espectrómetro VG-1200 fueron reducidos en una versión actualizada de un programa de computadora llamado *ArAr** (Haugerud y Kunk, 1988). Los datos generados en el espectrómetro MAP-216 fueron reducidos usando un programa computacional llamado *Mass Spec* (Deino, 2001). Se usaron las constantes de decaimiento de Steiger y Jäger (1977).

Se realizaron correcciones debido a la presencia de isótopos de Ar a partir de Ca (calcio), K (potasio) y Cl (cloro) usando las proporciones isotópicas sugeridas por Dalrymple *et al*., (1981) y Roddick (1983). Los errores de las edades calculadas incluyen la incertidumbre de la medición en el análisis, las incertidumbres del factor de desintegración, las incertidumbres en las relaciones atmosféricas medidas $^{40}Ar/^{36}Ar$, el parámetro de irradiación J, las generadas durante el proceso de irradiación nuclear, las de la relación inicial $^{38}Ar/^{36}Ar$ y la incertidumbre del mineral estándar (Haugerud y Kunk, 1988).

Referencias

Albinson, T.F., 1989, Vetas mesotermales auríferas del sector norte del Estado de Sonora: Memorias, XVIII Convención Nacional AIMMGM, Acapulco, Guerrero, México, Asociación de Ingenieros de Minas, Metalurgistas y Geólogos de México, 20–40.

Alexander, E.C., Jr., Mickelson, G.M., Lanphere, M.A., 1978, MMhb-1–A new $^{40}Ar/^{39}Ar$ dating standard, *en* Zartman, R.E., (ed), Short Papers of the Fourth International Conference, Geochronology, Cosmochronology, and Isotope Geology: U.S. Geological Survey Open-File Report 78–701, 6–8.

Anderson, T.H., Silver, L.T., 1979, The role of the Mojave-Sonora megashear in the tectonic evolution of northern Sonora, *en* Anderson, T.H., Roldán-Quintana, J., (eds), Geology of northern Sonora Guidebook, University of Pittsburgh and Universidad Nacional Autónoma de México, Instituto de Geología, Geological Society of America Annual Meeting, Hermosillo, Sonora, 27, 59–68.

Anderson, T.H., Silver, L.T., 2005, The Mojave-Sonora megashear—Field and analytical studies leading to the conception and evolution of the hypothesis, *en* Anderson, T.H., Nourse, J.A., McKee, J.W., Steiner, M.B., (eds), The Mojave-Sonora Megashear Hypothesis: Development, Assessment, and Alternatives: Geological Society of America Special Paper 393, 1–50.

Araux-Sánchez, E., Vega-Granillo, R., Enríquez-Minjárez, E., 2001, Características geológicas de un yacimiento mesotermal asociado a zonas de cizalla en el noroeste de Sonora, *en* Corona-Esquivel, R., Gómez-Godoy, J., (eds), Asociación de Ingenieros de Minas, Metalurgistas y Geólogos de México A.C., XXIV Convención Minera, Acapulco, Guerrero, 25–32.

Arvizu, H.E., Iriondo, A., Izaguirre, A., Chávez-Cabello, G., Kamenov, G.D., Solís-Pichardo, G., Foster, D.A., Lozano-Santa Cruz, R., 2009, Rocas graníticas pérmicas en la Sierra Pinta, NW de Sonora, México: Magmatismo de subducción asociado al inicio del margen continental activo del SW de Norteamérica: Revista Mexicana de Ciencias Geológicas, 26, 709–728.

Bennett, S.E.K., Oskin, M.E., Iriondo, A., 2013, Transtensional rifting in the proto–Gulf of California near Bahía Kino, Sonora, México: Geological Society of America Bulletin, 125(11), 1752–1782.

Bierlein, F.P., Groves, D.I., Cawood, P.A., 2009, Metallogeny of accretionary orogens–the connection between lithospheric processes and metal endowment: Ore Geology Reviews 36, 282–292.

Bird, P., 1998, Kinematic history of the Laramide orogeny in latitudes 35°–49°, western United States: Tectonics, 17, 780–801.

Campbell, P.A., Anderson, T.H., 2003, Structure and kinematics along a segment of the Mojave-Sonora megashear: A strike-slip fault that truncates the Jurassic continental magmatic arc of southwestern North America: Tectonics, 22, 1–21.

Chacko, T., Hu, X., Mayeda, T.M., Clayton, R.N., Goldsmith, J.R., 1996, Oxygen isotope fractionations in muscovite, phlogopite, and rutile: Geochimica et Cosmochimica Acta, 60, 2595–2608.

Changkuon, L., 1990, Genesis of gold mineralization: San Francisco Mine, Sonora, Mexico: New Mexico Institute of Mining and Technology, Socorro, New Mexico, tesis de maestría, 129 p.

Clayton, R.N., Mayeda, T.K., 1963, The use of bromine pentafluoride in the extraction of oxygen from oxides and silicates for isotopic analysis: Geochimica et Cosmochimica Acta, 27, 43–52.

Coelho, J., 2006, GEOISO–A Windows program to calculate and plot mass balances and volume changes occurring in a variety of geologic processes: Computers and Geosciences, 32, 1523–1528.

Coney, P.J., Reynolds, S.J., 1977, Cordilleran Benioff zones: Nature, 270, 403–406.

Damon, P.E., Shafiqullah, M., Clark, K.F., 1983, Geochronology of the porphyry copper deposits and related mineralization of Mexico: Canadian Journal of Earth Sciences, 20, 1052–1071.

Dalrymple, G.B., Alexander, E.C., Jr., Lanphere, M.A., Kraker, G.P., 1981, Irradiation of samples for $^{40}Ar/^{39}Ar$ dating using the Geological Survey TRIGA reactor: U.S. Geological Survey Professional Paper 1176, 55 p.

Davis, J.C., 1986, Statistics and Data Analysis in Geology: Jonh Wiley & Sons Inc., New York, 2646 p.

Deino, A.L., 2001, User's manual for mass spec v. 5.02: Berkeley Geochronology Center Special Publication 1a, 119 p.

De la Torre-Carlos, J., 2009, Geología del yacimiento mina La Herradura, *en* Clark, K.F., Salas-Pizá, G., Cubillas-Estrada, R., (eds), Geología Económica de México 2ª edición: Servicio Geológico Mexicano-Asociación de Ingenieros de Minas, Metalurgistas y Geólogos de México, 844–851.

Fu, B., Touret, J.L.R., 2014, From granulite fluids to quartz-carbonate megashear zones: The gold rush: Geociencies Frontiers, 5, 743–758.

Gastil, R.G., 1975, Plutonic zones in the Peninsular Ranges of southern California and northern Baja California: Geology, 3, 361–363.

Giesemann, A., Jager, H.J., Norman, A.L., Krouse, H.R., Brand, W.A., 1994, On-line sulfur isotope determination using an elemental analyzer coupled to a mass spectrometer: Analytical Chemistry, 66, 2816–2819.

Goldfarb, R.J., Groves, D.I., 2015, Orogenic gold: Common or evolving fluid and metal sources through time: Lithos, 233, 2–26.

Grant, J.A., 1986, The isocon diagram–a simple solution to Gresens' ecuation for metasomatic alteration: Economic Geology, 81, 1976–1982.

Grant, J.A., 2005, Isocon analysis: A brief review of the method and applications: Physics and Chemistry of the Earth, 30, 997–1004.

Gresens, R.L., 1967, Composition–volume relationships of metasomatism: Chemical Geology, 2, 47–65.

Haugerud, R.A., Kunk, M.J., 1988, ArAr*; a computer program for reduction of ^{40}Ar-^{39}Ar data: U. S. Geological Survey Open-File Report 88–261, 68 p.

Henry, C.D., Aranda-Gomez, J.J., 2000, Plate interactions control middle-Late Miocene, proto-Gulf and Basin and Range extension in the southern Basin and Range: Tectonophysics, 318, 1–26.

Iriondo, A., 2001, Proterozoic basements and their laramide juxtaposition in NW Sonora, Mexico: Tectonic constraints on the SW margin of Laurentia: Boulder, Colorado, University of Colorado at Boulder, tesis de doctorado 222 p.

Iriondo, A., Atkinson, W.W., Jr., 2000, Orogenic gold mineralization along the proposed trace of the Mojave-Sonora megashear: Evidence for the Laramide Orogeny in NW Sonora, Mexico: Geological Society of America, Abstracts with Programs, 32, 393.

Iriondo, A., Premo, W.R., 2011, Las rocas cristalinas proterozoicas de Sonora y su importancia para la reconstrucción del margen continental SW de Laurencia-La pieza mexicana del rompecabezas de Rodinia, *en* Calmus, T., (ed), Panorama sobre la geología de Sonora, México: Instituto de Geología, Universidad Nacional Autónoma de México, 118, 25–55.

Iriondo, A., Izaguirre, A., 2016, Paleoproterozoic Yavapai igneous rocks with late Cretaceous to Early Cenozoic Ar-Ar ages: Thermal disturbance “resetting” due to widespread Laramide magmatism in Sonora, Mexico: GEOS, Unión Geofísica Mexicana, 35.

Iriondo, A., Martínez-Torres, L.M., Kunk, M.J., Atkinson, W.W., Jr., Premo, W.R., McIntosh W.C., 2005, Northward Laramide thrusting in the Quitovac region, northwestern Sonora, Mexico: Implications for the juxtaposition of Paleoproterozoic basement blocks and the Mojave-Sonora megashear hypothesis, *en* Anderson, T.H., Nourse, J.A., McKee, J.W., Steiner, M.B., (eds), The Mojave-Sonora megashear hypothesis: Development, assessment, and alternatives: Geological Society of America Special Paper 393, 631–669.

Izaguirre-Pompa, A., 2009, El basamento Paleoproterozoico (~1.71–1.68 Ga) Yavapai en el área Mina La Herradura en el NW de Sonora: Sus implicaciones para el desarrollo del margen magmático continental Mesozoico-Cenozoico del NW de México: Querétaro, Qro., Universidad Nacional Autónoma de México, tesis de maestría, 201 p.

Izaguirre, A., Iriondo, A., 2014, A metamorphic origin for the hydrothermal fluids forming the gold-bearing quartz veins from the Laramide Caborca Orogenic Gold Belt of NW Sonora: An oxygen, hydrogen and sulfur isotopic study: GEOS, Unión Geofísica Mexicana, 34, 334.

Izaguirre, A., Iriondo, A., Caballero-Martínez, J.A., Moreira-Rivera, F., Espinosa-Arámburu, E., 2012, Homogeneidad geoquímica de la alteración hidrotermal del

cinturón de oro orogénico del NW de Sonora, México: Estudio de balance de masas en rocas encajonantes de la mineralización: Boletín de la Sociedad Geológica Mexicana, 64, 119–153.

Izaguirre, A., Iriondo, A., Kunk, M.J., McAleer, J.R., Caballero-Martínez, J.A., Espinosa-Arámburu, E., 2016, The Laramide Caborca orogenic gold belt of northwestern Sonora, México: White mica $^{40}Ar/^{39}Ar$ geochronology from Au-rich quartz veins: U.S. Geological Survey Open-file Report 2016–1008, 30 p., http://dx.doi.org/10.3133/ofr20161008.

Izaguirre, A., Camprubí, A., Iriondo, A., 2017, Mesozoic orogenic gold deposits in Mexico: Ore Geology Reviews, 81, 1172–1183, doi: 10.1016/j.oregeorev.2015.10.006.

Izaguirre, A., Iriondo, A., Kunk., M.J., McAleer, R.J., Atkinson, W.W., Jr., Martínez-Torres, L.M., 2017, Tectonic framework for Late Cretaceous to Eocene quartz-gold vein mineralization from the Caborca orogenic gold belt in northwestern Mexico: Economic Geology, en prensa.

Jacques-Ayala, C., García-Barragán, J.C., 2014, Deletion of the Caborca Terrane and renaming the Papago Terrane: GEOS, Unión Geofísica Mexicana, 34, 330.

Johnson, C.A., Kelley, K.D., Leach, D.L., 2004, Sulfur and Oxygen Isotopes in Barite Deposits of the Western Brooks Range, Alaska, and Implications for the Origin of the Red Dog Massive Sulfide Deposits: Economic Geology, 99, 1435–1448.

Johnson, S.E., Tate, M.C., Fanning, C.M., 1999, New geologic mapping and SHRIMP U-Pb zircon data in the Peninsular Ranges batholith, Baja California, Mexico: Evidence for a suture?: Geology, 27, 743–746.

Lentz, D.R., 2005, Mass-balance analysis of mineralized skarn systems: Implications for replacement processes, carbonate mobility, and permeability evolution, *en* Mao, J., Bierlein, F.P., (eds), Mineral Deposit Research: Meeting the Global Challenge, Proceedings of the Biennial SGA Meeting, Beijing, China, 4, 421–424.

Li, Y.B., Liu J.M., 2006, Calculation of sulfur isotope fractionation in sulfides: Geochimica et Cosmochimica Acta, 70, 1789–1795.

Mauel, D.J., Lawton, T.F., González-León, C., Iriondo, A., Amato, J.M., 2011, Stratigraphy and age of Upper Jurassic strata in north-central Sonora, Mexico:

Southwestern Laurentian record of crustal extension and tectonic transition: Geosphere, 7, 390–414.

McDowell, F.W., Roldán-Quintana, J., Connelly, J.N., 2001, Duration of Late Cretaceous-early Tertiary magmatism in east-central Sonora, Mexico: Geological Society of America Bulletin, 113, 521–531.

Molina-Garza, R.S., Geissman, J.W., 1999, Paleomagnetic data from the Caborca terrane, Mexico: Implications for the Cordilleran tectonics and the Mojave-Sonora megashear hypothesis: Tectonics, 18, 293–325.

Molina-Garza, R.S., Iriondo, A., 2005, La megacizalla Mojave-Sonora: la hipótesis, la controversia y el estado actual de conocimiento del problema, *en* Alaniz-Álvarez, S.A., Nieto-Samaniego, A.F., (eds), Volumen Centenario SGM—Grandes Fronteras Tectónicas de México: Boletín de la Sociedad Geológica Mexicana, 57(1), 1–26.

Noriega-Martínez, O., 2006, Evidencias de dos etapas de mineralización de oro mesotermal en las áreas de Tajitos, Juárez-San Francisco, en la región de Caborca, Sonora México: Departamento de Geología, Universidad de Sonora, tesis de maestría, 85 p.

Nourse, J.A., Irwin, J.J., 2010, Tectonic and structural setting of gold mineralization in the Sonora-Mojave Belt: Example from the Juarez-Tajitos area: American Association of Petroleum Geologists, Geological Society of America, Cordilleran Section, Abstracts with Programs, Annual Meeting, 42, 108.

Ohmoto, H., Rye, R.O., 1979, Isotope of sulfur and carbon, *en* Barnes, H.L., (ed), Geochemistry of hydrothermal ore deposits, John Wiley & Sons, 509–567.

Ornelas-Macías, A., Verdugo-Noriega, G., 2009, Caracterización geológica, estructural y de mineralización en el área Karina, municipio de Caborca, Sonora, México: Hermosillo, Sonora, Departamento de Geología, Universidad de Sonora, tesis de licenciatura, 110 p.

Pérez-Segura, E., 1993, Los yacimientos de oro y plata de Sonora, México y sus relaciones con la geología regional, *en* Delgado-Argote, L.A., Martín-Barajas, A., (eds), Contribuciones a la tectónica del occidente de México: Monografía, Unión Geofísica Mexicana, 1, 147–174.

Pérez-Segura, E., 2009, Geología y mineralización de la mina de oro de San Francisco, en la provincia del Desierto de Sonora, México, *en* Clark, K.F., Salas-Pizá, G., Cubillas-Estrada, R., (eds), Geología Económica de México, 2ª edición, Servicio Geológico Mexicano-Asociación de Ingenieros de Minas, Metalurgistas y Geólogos de México, 875–881.

Pérez-Segura, E., Cheilletz, A., Herrera-Urbina, S., Hanes, Y.J., 1996, Geología, mineralización, alteración hidrotermal y edad del yacimiento de oro de San Francisco, Sonora-Un depósito mesotermal en el Noroeste de México: Revista Mexicana de Ciencias Geológicas, 13, 65–89.

Pitcairn, I.K., Teagle, D.A., Craw, D., Olivo, G.R., Kerrich, R., Brewer, T.S., 2006, Sources of metals and fluids in orogenic gold deposits: Insights from the Ontago and Alpine Schists, New Zealand: Economic Geology, 101, 1525–1546.

Poole, F.G., Perry, W.J., Jr., Madrid, R.J., Amaya-Martínez, R., 2005, Tectonic synthesis of the Ouachita-Marathon-Sonora orogenic margin of southern Laurentia: Stratigraphic and structural implications for timing of deformational events and plate-tectonic model, *en* Anderson, T.H., Nourse, J.A., McKee, J.W., Steiner, M.B., (eds), The Mojave-Sonora megashear hypothesis: Development, assessment, and alternatives: Geological Society of America Special Paper 393, 543–596.

Poulsen, K.H., Mortensen J.K., Walford, P.C., 2008, San Francisco gold deposit, Santa Ana region, Sonora, Mexico: Laramide orogenic, intrusion-related mineralization?, *en* Spencer, J.E., Titley, S.R., (eds), Ores and orogenesis: Circum-Pacific tectonics, geologic evolution, and ore deposits: Arizona Geological Society Digest 22, 547–559.

Quintanar-Ruíz, F.J., 2008, La Herradura ore deposit: An orogenic gold deposit in northwestern Mexico: Department of Geosciences, University of Arizona, tesis de maestría, 97 p.

Roddick, J.C., 1983, High precision calibration of $^{40}Ar/^{39}Ar$ standards: Geochimica et Cosmochimica Acta, 47(5), 887–898.

Sharp, Z., Atudorei, V., Durakiewicz, T., 2001, A rapid method for determination of hydrogen and oxygen isotope ratios from water and hydrous minerals: Chemical Geology 178, 197–210.

Sheppard, S.M.F., 1986, Characterization and isotopic variations in natural waters, *en* Valley, J.W., Taylor, H.P. Jr., O'Neil, J.R., (eds), Stable isotopes in high temperature geological processes, Mineralogical Society of America, Reviews in Mineralogy, 16, 165–183.

Silberman, M.L., Giles D.A., Graubard, C., 1988, Characteristics of gold deposits in Northern Sonora, Mexico: A preliminary report: Economic Geology, 83, 1966–1974.

Suzuoki, T., Epstein, S., 1976, Hydrogen isotope fractionation between OH-bearing minerals and water: Geochimica et Cosmochimica Acta: 40, 1229–1240.

Snee, L.W., Sutter, J.F., Kelly, W.C., 1988, Thermochronology of economic mineral deposits; dating the stages of mineralization at Panasqueira, Portugal, by high precision $^{40}Ar/^{39}Ar$ age spectrum techniques on muscovite: Economic Geology, 83(2), 335–354.

Staudacher, T., Jessberger, E.K., Dörflinger, D., Kiko, J., 1978, A refined ultrahigh-vacuum furnace for rare gas analysis: Journal of Physics E, Scientific Instrumentation, 11(8), 781–784.

Steiger, R.H., Jäeger, E., 1977, Subcommission on geochronology; convention on the use of decay constants in geo- and cosmo-chronology: Earth and Planetary Science Letters, 36(3), 359–363.

Taylor, H.P. Jr., 1974, The application of oxygen and hydrogen studies to problems of hydrothermal alteration and ore deposition, Economic Geology, 69, 843–883.

Taylor, H.P. Jr., 1997, Oxygen and hydrogen isotope relationships in hydrothermal mineral deposits, *en* Barnes, H.L., (ed), Geochemistry of hydrothermal ore deposits, John Wiley & Sons, 229–302.

Tomkins, A.G., 2013, On the source of orogenic gold: Geology: 41(12), 1255–1256,

Usui, T., Nakamura, E., Kobayashi, K., Maruyama, S., Helmstaedt, H., 2003, Fate of the subducted Farallon plate inferred from eclogite xenoliths in the Colorado Plateau: Geology, 31, 589–592.

Valencia-Moreno, M., Ortega-Rivera, M.A., 2011, Cretácico Tardío-Eoceno Medio en el noroeste de México—Evolución del arco magmático continental y su contexto geodinámico (orogenia Laramide), *en* Calmus, T., (ed), Panorama de la geología de Sonora, México: Universidad Nacional Autónoma de México, Instituto de Geología, 118, 201–226.

Wells, M.L., Hoisch, T.D., 2008, The role of mantle delamination in widespread Late Cretaceous extension and magmatism in the Cordilleran orogen, western United States: Geological Society of America Bulletin, 120, 515–530.

Wetmore, P.H., Herzig, C., Alsleben, H., Sutherland, M., Schmidt, K.L., Schultz, P.W., Paterson, S.R., 2003, Mesozoic tectonic evolution of the Peninsular Ranges of Southern and Baja California, *en* Johnson, S.E., Paterson, S.R., Fletcher, J.M., Girty, G.H., Kimbrough, D.L., Martin-Barajas, A., (eds), Tectonic Evolution of Northwestern Mexico and the Southwestern United States: Geological Society of America Special Paper 374, 93–116.

Wei, J.H., Liu, C.Q., Li, Z.D., Zhao, Y.X., 2001, Simulation of rock mass balance of two typical altered rocks in Wulong gold deposit of Liaoning, China: Journal of Central South University of Technology, China, 8, 197–202.

Wilson, P.D., Sullivan, K., Piggott, K., Marín-Payán, M., Clark, K.F., 2009, Oro en depósitos de placer de El Boludo, Sonora, Méxco, *en* Clark, K.F., Salas-Pizá, G.A., Cubillas-Estrada, R., (eds), Geología Económica de México, 817–830.

Zhang, Y.X., Walker, D., Lesher, C.E., 1989, Diffusive crystal dissolution: Contributions to Mineralogy and Petrology, 102, 492–513.

Zheng, Y.F., 1993, Calculation of oxygen isotope fractionation in anhydrous silicate minerals: Geochemica et Cosmochimica Acta, 57, 1079–1091.

Zheng, Y.F., 1999, On calculations of Oxygen isotope fractionation in minerals. Episodes, 22, 99–126.